

*INTERNATIONAL SERIES OF MONOGRAPHS ON*  
**ELECTROMAGNETIC WAVES**

EDITORS: A. L. CULLEN, V. A. FOCK AND J. R. WAIT

---

VOLUME 2

IONOSPHERIC SPORADIC *E*

*OTHER TITLES IN THE SERIES ON*

**ELECTROMAGNETIC WAVES**

Vol. 1 *Diffraction by Convex Surface*—FOCK

Vol. 2 *Ionospheric Sporadic E*—SMITH AND MATSUSHITA (Editors)

Vol. 3 *Electromagnetic Waves in Stratified Media*—WAIT

Vol. 4 *The Scattering of Electromagnetic Waves from Rough Surfaces*—BECKMANN  
AND SPIZZICHINO



# IONOSPHERIC SPORADIC *E*

Edited by

ERNEST K. SMITH, Jr., Ph.D.

*Central Radio Propagation Laboratory  
U.S. National Bureau of Standards  
Boulder, Colorado*

and

SADAMI MATSUSHITA, Dr. Sc.

*High Altitude Observatory  
also  
Astro-Geophysics Department  
University of Colorado  
and  
U.S. National Bureau of Standards  
Boulder, Colorado*

PERGAMON PRESS

OXFORD · LONDON · NEW YORK · PARIS

1962

**IIA LIB.**

PERGAMON PRESS LTD.  
*Headington Hill Hall, Oxford*  
*4 & 5 Fitzroy Square, London, W.1.*

PERGAMON PRESS INC.  
*122 East 55th Street, New York 22, N.Y.*

GAUTHIER-VILLARS  
*55 Quai des Grands-Augustins, Paris 6<sup>e</sup>*

PERGAMON PRESS G.m.b.H.  
*Kaiserstrasse 75, Frankfurt am Main*

Copyright

©

1962

PERGAMON PRESS INC.

Library of Congress Card Number 62-12346

*Set in Imprint 101, 11 on 12pt. by*  
SANTYPE LTD., SALISBURY

*and printed in Great Britain by*  
COX AND WYMAN LTD., READING

*Dedicated to*

*Capt. MARY P. CONVERSE*

# Contents

	<i>page</i>
Preface	
E. K. SMITH, JR. and S. MATSUSHITA	ix
Introductory remarks	
E. K. SMITH, JR. and S. MATSUSHITA	xi
Chapter I	
1. The occurrence of sporadic $E$	
E. K. SMITH, JR.	3
2. Reflection mechanisms for sporadic $E$	
K. TAO	13
3. Final remarks of 1957 AGARD conference on sporadic- $E$ ionization	
J. A. RATCLIFFE	28
Chapter II	
PART A	
1. The reflection coefficient and fading characteristics of signals returned from the $E_s$ layer at Ibadan	
N. J. SKINNER and R. W. WRIGHT	37
2. A study of radio wave scattering from sporadic $E$ near the magnetic equator	
K. L. BOWLES and R. COHEN	51
3. Sporadic $E$ as observed with rockets	
J. C. SEDDON	78
4. Backscatter observations of sporadic $E$	
R. D. EGAN and A. M. PETERSON	89
5. Sporadic $E$ as observed from Mayaguez, P. R. by backscatter sounders	
B. DUEÑO	110
6. Report on recent $E_s$ work in Brisbane	
J. A. THOMAS	123
7. Recent sporadic- $E$ experimental work in the United States	
J. F. DEGREGORIO, J. W. FINNEY, K. KILDAHL and E. K. SMITH, JR.	131
8. Sporadic- $E$ propagation with 3 $\mu$ sec pulses	
G. R. OCHS, R. J. CARPENTER and E. K. SMITH, JR.	143
PART B	
1. Definitions of frequency parameters of $E_s$ -layers and their accuracy	
K. RAWER	151
2. The occurrence of sporadic $E$ during the IGY	
H. I. LEIGHTON, A. H. SHAPLEY and E. K. SMITH, JR.	166
3. A note on the heights of the different IGY types of $E_s$	
S. C. GLADDEN	178

	page
4. Variations in frequency of occurrence of sporadic $E$ , 1949–1959 W. B. CHADWICK	182
5. Lunar tidal variations of sporadic $E$ S. MATSUSHITA	194
6. On the width of the equatorial $E_s$ belt R. W. KNECHT and R. E. McDUFFIE	215
7. The night- $E$ layer G. A. M. KING	219
PART C	
1. A theoretical study of sporadic- $E$ structure in the light of radio measurements K. TAO	235
2. The turbulence criterion in stably stratified shear flow and the origin of sporadic $E$ D. LAYZER	258
3. The formation of a sporadic- $E$ layer from a vertical gradient in horizontal wind J. D. WHITEHEAD	276
4. Structure of $E_s$ at temperate latitudes K. RAWER	292
5. Interrelations of sporadic $E$ and ionospheric currents S. MATSUSHITA	344
Concluding remarks S. MATSUSHITA and E. K. SMITH, JR.	376
Name Index	381
Subject Index	385

## Preface

THE idea for a volume such as this had two sources. Several years ago I. R. Maxwell, Publisher at Pergamon Press, suggested to the editors that he would welcome a monograph on the subject of sporadic *E*. Later, one of us (E. K. Smith) had a contract from the National Science Foundation to organize the vertical-incidence results coming from the IGY measurements. Some of these results are reflected in the contributions in this monograph; but more important, as a result of work on this project it became apparent that the best way of satisfying the need for the compilation of IGY results was to consolidate papers from the various workers who had carried out programs during that period. In addition to these two reasons, it is the feeling of the editors that the field of sporadic *E* has progressed to a point where a volume of this nature serves a useful purpose. There are several recent theoretical advances and many new experimental observations which it is useful to present in the same volume.

We would like to thank all of the authors for their excellent contributions which make up this volume. We also wish to thank them for their forbearance with the editorial process.

We gratefully acknowledge the assistance provided by the Boulder Laboratories of the National Bureau of Standards and the High Altitude Observatory. We particularly wish to thank Miss Alice McRae of NBS and Miss Clara Mae Place of HAO.

E. K. SMITH, JR.  
and  
S. MATSUSHITA



## Introductory Remarks

E. K. SMITH, JR.  
and  
S. MATSUSHITA

THE material in this volume is organized into two chapters. The first chapter includes introductory and survey material and is rather modest in length. Chapter II contains most of the meat of the volume and is organized into three parts. In Part A, the emphasis is on the experimental work which is an integral part of the contribution. Included in Part A are specialized measurements on the ionosphere, backscatter determinations, cw recordings at v.h.f., and rocket measurements. In Part B, the emphasis is primarily on the analysis of routine data. These data are in all cases vertical-incidence ionograms scaled in accordance with standardized international practice. In Part C, we have gathered together papers that are primarily theoretical in their approach. Theoretical implications of different structures are discussed, different physical mechanisms are considered. The concluding remarks contain the Editors' view of the status of the sporadic- $E$  field at present, particularly in the light of material in this volume.

The first chapter of this volume contains three contributions. The first one, "The Occurrence of Sporadic  $E$ ", is an updated version of part of the paper delivered by E. K. Smith at the 1960 URSI General Assembly in London, and is largely concerned with vertical-incidence observations. The following contribution, entitled "Reflection Mechanisms for Sporadic  $E$ " by K. Tao, is a theoretical survey of the various suggested mechanisms to explain the observed sporadic- $E$  results. The last contribution in this chapter is a reprint of J. A. Ratcliffe's final remarks at the Advisory Group on Aeronautical Research and Development (AGARD) Symposium on Sporadic- $E$  Ionization held at the Cavendish Laboratories in 1957.

In Part A of Chapter II we have eight contributions from eight quite separate groups in seven different laboratories. The first paper by Skinner and Wright, entitled "The Reflection Coefficient and Fading Characteristics of Signals Returned from the  $E_s$  Layer at Ibadan", covers vertical incidence measurements in the lower h.f. band made in West Africa. Bowles and Cohen in the second contribution, entitled "A Study of the Radio Wave Scattering from Sporadic  $E$  near the Magnetic Equator", present experimental evidence at oblique and vertical incidence in the h.f.



to low v.h.f. band on equatorial sporadic  $E$  as observed on the West Coast of South America. The third contribution, entitled "Sporadic  $E$  as Observed with Rockets", by Seddon, is a discussion of the results of measurements of electron density profiles as they apply to sporadic  $E$  made by using rockets flown over New Mexico, U.S.A., and Manitoba, Canada. In the fourth contribution, entitled "Backscatter Observations of Sporadic  $E$ " by Egan and Peterson, we find a survey of recent Stanford backscatter results with particular emphasis on the IGY data. In the fifth paper: "Sporadic  $E$  as Observed from Mayaguez, P. R. by Backscatter Sounders", Dueño presents observations made at Puerto Rico on about 22 and 41 Mc/s using backscatter techniques. In "Report on Recent  $E_s$  Work at Brisbane", Thomas highlights several areas of developing sporadic- $E$  work at Brisbane. The seventh contribution by DeGregorio, Finney, Kildahl, and Smith reviews some of the recent work on relating vertical to oblique incidence conditions at CRPL and also some multiple station measurements. The final contribution in Part A entitled, "Sporadic- $E$  Propagation with 3  $\mu$ sec Pulses", by Ochs, Carpenter, and Smith, presents some 50 Mc/s short pulse recordings made by CRPL over a v.h.f. oblique path.

The first contribution of Part B by Rawer is appropriately entitled, "Definitions of Frequency Parameters of  $E_s$  Layers and their Accuracy". This contribution is a critical review of the significance of regularly scaled sporadic- $E$  parameters. The following paper by Leighton, Shapley, and Smith, entitled "The Occurrence of Sporadic  $E$  during the IGY", is a survey of both total incidence of sporadic  $E$  during the IGY in the form of world maps and of  $E_s$  types at selected stations around the world. Contribution number three by Gladden, titled "A Note on the Heights of the Different IGY Types of  $E_s$ " contains a brief look at the variations in height of the different types around the world. Variation of sporadic  $E$  with sunspot number is then treated by Chadwick, in which data over the past sunspot cycle are considered. The fifth contribution, entitled "Lunar Tidal Variations of Sporadic  $E$ " by Matsushita, contains both a presentation of data and the theoretical consideration of the results. The sixth contribution, "On the Width of the Equatorial  $E_s$  Belt" by Knecht and McDuffie, presents the most recent determination on the width of this belt. The seventh and final contribution of Part B consists of a study by King of the night- $E$  layer which is frequently observed at auroral latitudes.

The first contribution in Part C is a study by Tao of v.h.f. oblique-incidence sporadic- $E$  results in the light of expectations from the different structures which have been suggested. This is followed by a paper by Layzer of the Harvard College Observatory which considers the possibility that sporadic  $E$  may be a result of turbulent strata in the  $E$  region. The third contribution by Whitehead of the University of Sydney treats the exciting new theory of sporadic  $E$  produced by wind shear. The next

contribution in Part C is entitled, "Structure of  $E_s$  at Temperate Latitudes", and presents a wealth of material which leads Rower to his feeling that sporadic  $E$  is made up of intense blobs of ionization. The final paper, by Matsushita, treats the question of interrelations of sporadic  $E$  and ionospheric currents.



# CHAPTER I



# The Occurrence of Sporadic *E*

ERNEST K. SMITH, JR.

Boulder Laboratories, National Bureau of Standards, Boulder, Colorado, U.S.A.

**Abstract**—A brief review is presented of the principal temporal and geographic variations in the occurrence of sporadic *E* based on knowledge prior to the International Geophysical Year. The occurrence statistics used for this purpose are for vertical-incidence reflections by sporadic *E* at frequencies above 5 Mc/s. A bibliography of recent papers on sporadic *E* is included.

## 1. INTRODUCTION

The aim of this paper is to survey briefly the principal features in the occurrence of sporadic *E* largely to afford a background and point of departure for some of the following papers in this book. Attention is focused on the state of our knowledge of the geographical and temporal variations of sporadic *E* as it stood before the International Geophysical Year. A bibliography of sporadic-*E* papers which have appeared since the survey of *E*<sub>s</sub> published by Thomas and Smith (1959) is included at the end of this paper and can be used as an appendix to the earlier survey in order to bring it up to date.

## 2. GEOGRAPHIC OCCURRENCE OF SPORADIC *E*

The frequency of occurrence of sporadic *E* as observed at vertical incidence at 5 Mc/s is shown in Fig. 1. This particular chart is for day time and June solstice conditions. It is seen that sporadic-*E* occurrence is high in the northern hemisphere, peaking between 10° to 30° in latitude, while in the southern hemisphere it is greatly depressed. This situation, of course, reverses itself for the December solstice. Also observable is the fact that the "E-Zone" stations (those in the Far East and in Australia) are distinctly higher than those in the "W-Zone" (North and South America.). It should be mentioned that the strictly equatorial-zone stations do not show up on this chart. Figure 2 shows the same data plotted on a map of the world with the auroral and the equatorial zones blocked out. The distinct peak between the Philippines and Japan shows up quite markedly and was the object of a special experiment utilizing v.h.f. oblique-incidence circuits which was

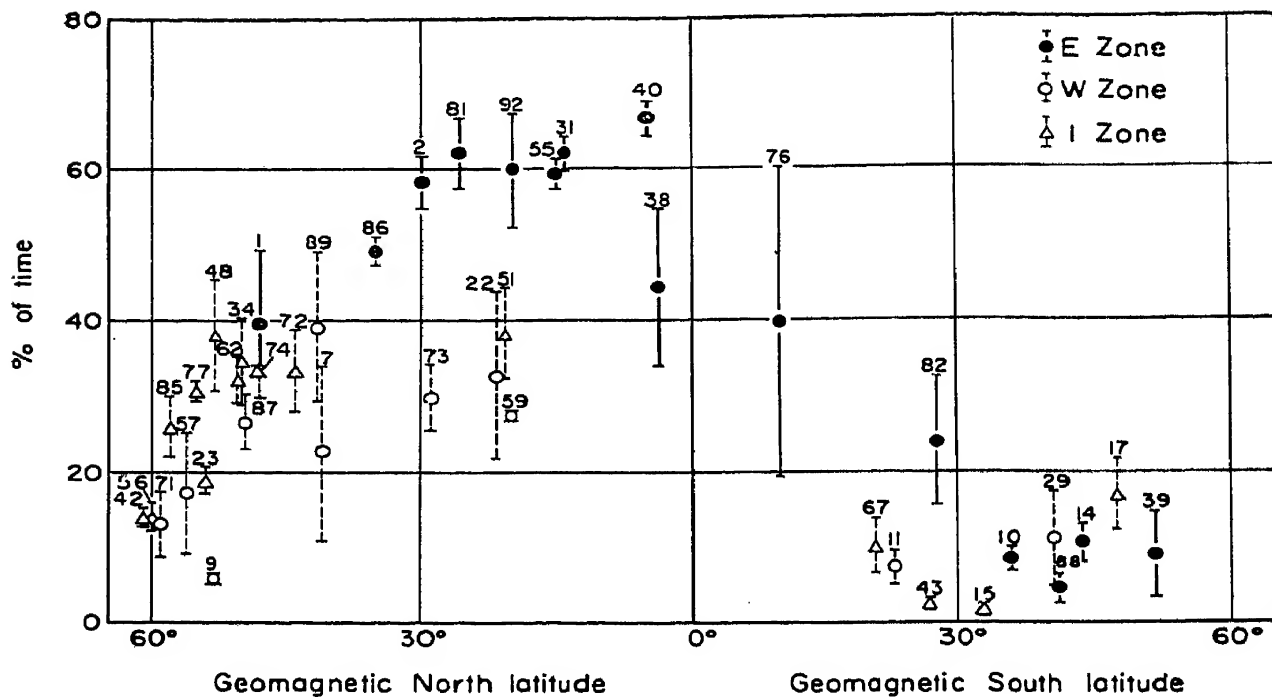


Fig. 1.  $E_s$  Occurrence vs Latitude—June Solstice, Daytime.

JUNE SOLSTICE, DAYTIME  
 MAP OF TEMPERATE ZONE  $E_s$  OCCURRENCE  
 May, June, July and August; 0600–1800 Local Time  
 $fEs > 5$  Mc, 1948–1954

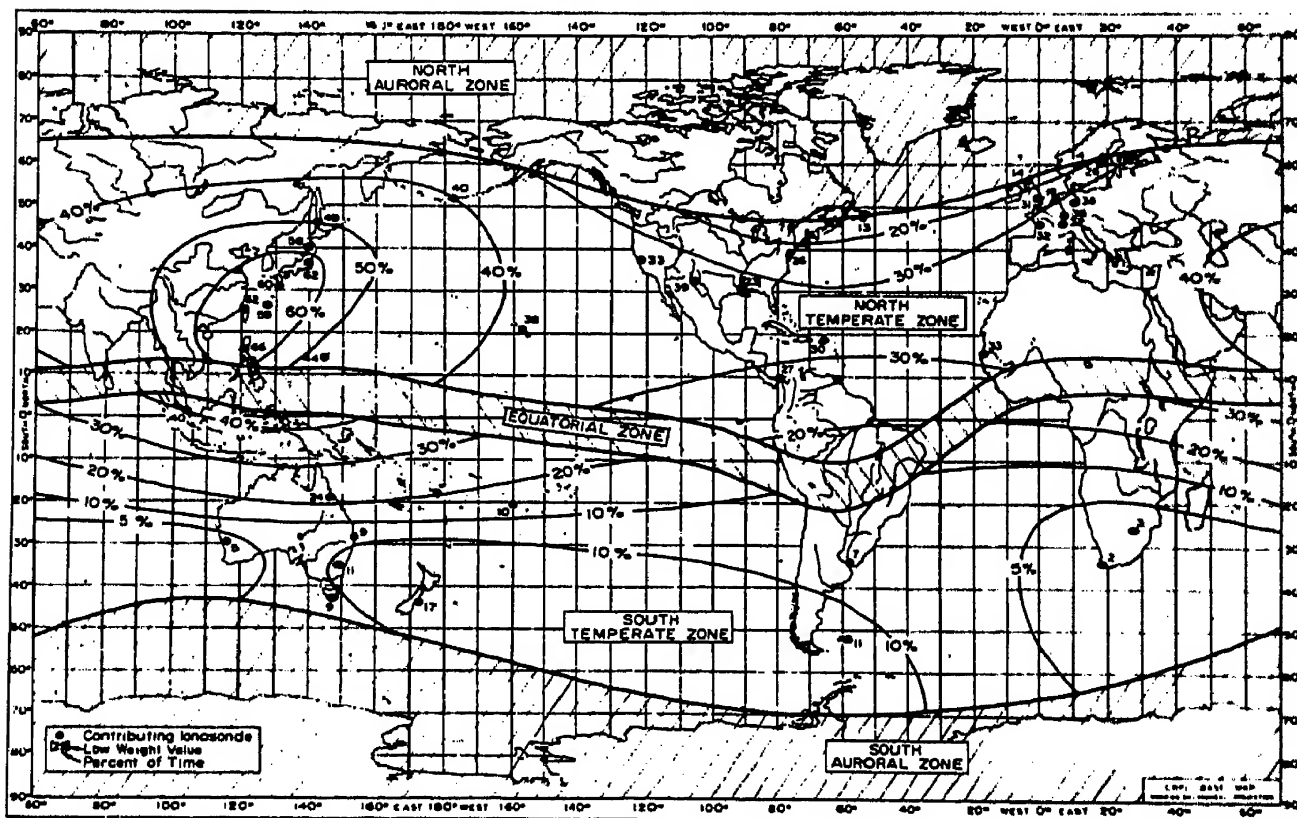


Fig. 2. Map of June Solstice, Daytime.

carried out cooperatively by the United States and Japan during the IGY (Smith and Finney, 1960) and served to confirm the ionosonde results.

A close-spaced chain of stations was available in South America bridging the magnetic equator during the IGY. Knecht and McDuffie studied the distribution of *q*-type sporadic *E* for these stations and have arrived at a half-occurrence width of  $\pm 5\frac{1}{2}^\circ$  in magnetic dip for *q*-type sporadic *E* and, by association, the equatorial electrojet.

Sporadic-*E* distribution for the year as a whole in the temperate zone is shown in Fig. 3. The main features of the total annual distribution of

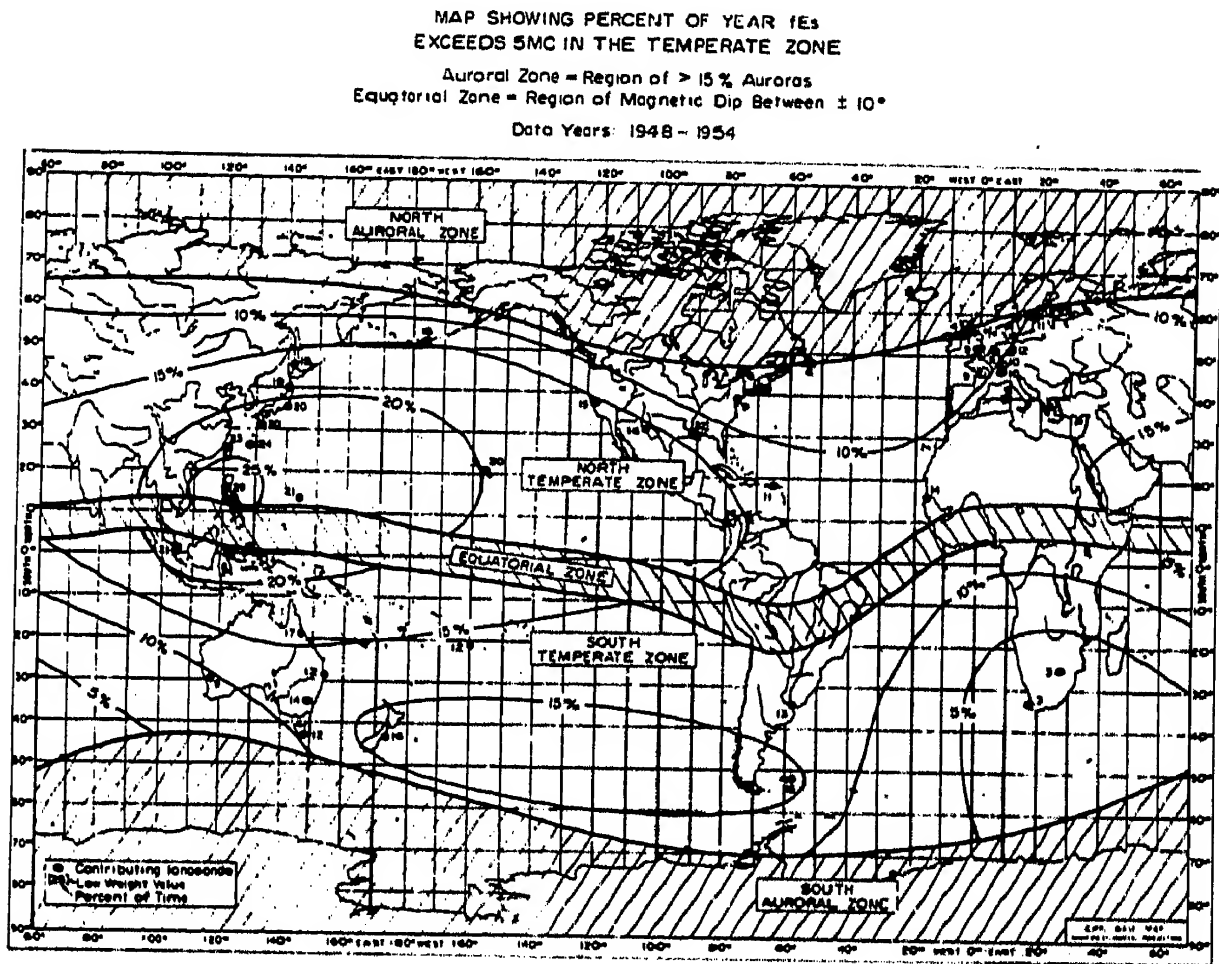


Fig. 3. Map of  $E_s > 5$  for the year.

sporadic *E* are still the peak in the Far East, which has now descended in latitude to around the Philippines, and a minimum in sporadic *E* which shows up for South Africa. It should be pointed out that when these charts were drawn no adequate sporadic-*E* data were available between the Far East and Europe. Therefore it is quite reasonable to suppose that the extension of this peak all the way to the Mediterranean for the IGY (Leighton, Shapley, and Smith) holds for the average year. The corresponding presentation for the auroral zone and polar cap is shown in



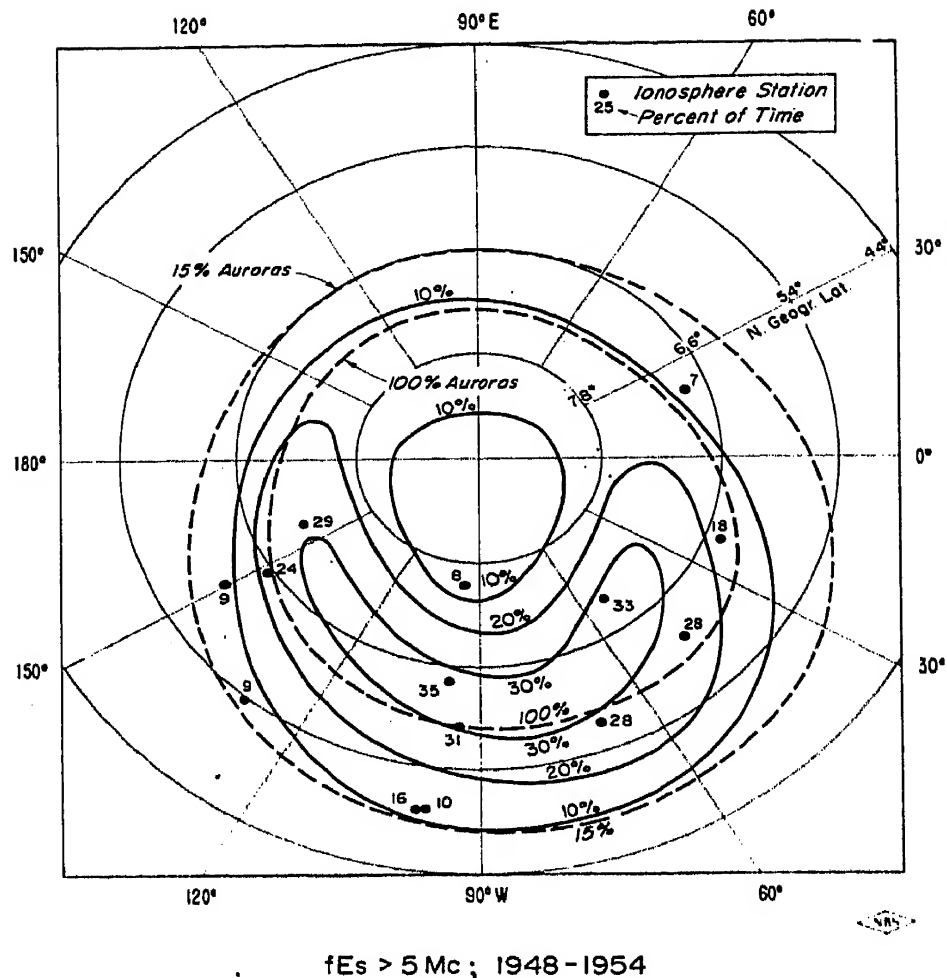


Fig. 4. Mean Annual Occurrence in the Auroral Zone.

Fig 4 and obviously suffers from lack of data.  $E_s$  can be seen to be most intense over Canada and at the peak of the auroral zone and to die off southward and also inside the polar cap. No data were then available for Siberia but the IGY results (Leighton, Shapley and Smith) confirm the three-to-one difference in occurrence between the Canadian and Siberian side of the auroral zone. Bellchambers and Piggott (1960) have offered an interesting explanation of this effect. Many efforts have been made to see spirals in sporadic- $E$  distributions in the auroral zone and polar cap. The most recent one is by Hagg, Muldrew and Warren (1959).

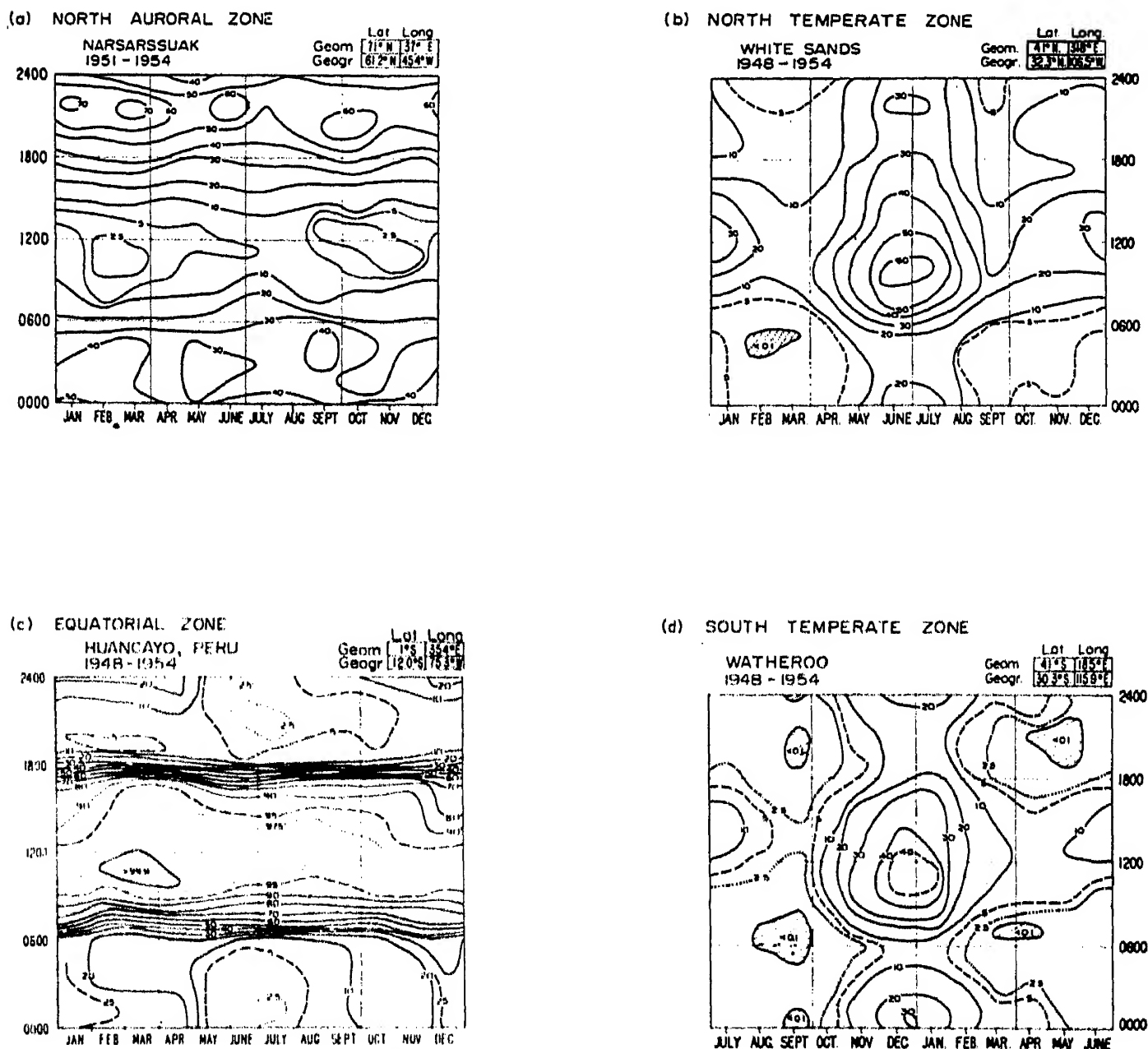
### 3. TEMPORAL VARIATIONS OF SPORADIC $E$

Let us now consider the diurnal and seasonal variations of sporadic  $E$  (observed on 5 Mc/s at vertical incidence). These are the dominant variations in sporadic  $E$ . Sunspot cycle variations (see also Chadwick), con-

sidered in this section, have been perhaps the most contentious of any of the temporal variations.

### *Diurnal and Seasonal Variations of Sporadic E*

One of the strongest indications that the spectrum of observations classed as sporadic *E* must, in fact, contain quite distinct phenomena comes from a consideration of the temporal variations of sporadic *E* as a function of



SAMPLE TEMPORAL VARIATION IN  $E_s$  IN TERMS OF PERCENT OF TIME FOR WHICH  $fE_s$  EXCEEDS 5 Mc

Fig. 5. Sample temporal variations in  $E_s$  (4 charts).

zone. In Fig. 5 we see a series of four contour charts representing long-term averages of the occurrence of sporadic  $E$  as observed at stations located in four principal zones (i.e. the north- and south-temperate zones, the equatorial zone, and the north-auroral zone). The north- and south-temperate zones, as exemplified by the distributions for White Sands and Watheroo, are characterized by a summer solstice maximum occurring slightly before noon, a secondary summer evening maximum, and a much smaller maximum which shows up during the daytime around the winter solstice. The abscissa scale on the chart for Watheroo has been shifted by six months to bring the seasons into the same relationship in the top and bottom charts. In the auroral zone, as illustrated by Narsarssuak in the top left-hand corner, it can be seen that sporadic  $E$  is distinctly a night-time phenomenon with very little apparent seasonal variation. For Huancayo, in the lower left-hand chart, we see that the  $E_s$  now occurs almost completely in the daytime, again with very little seasonal variation apparent. In the case of Huancayo the sporadic- $E$  incidence is completely dominated by  $q$ -type sporadic  $E$  which is autochthonous to the equatorial zone. An interesting feature of Knecht and McDuffie's recent work on equatorial sporadic  $E$  which is substantiated by Bowles and Cohen is that, in addition to the high incidence of  $q$ -type sporadic  $E$  which occurs there in the daytime, there is a narrower zone right at the equator where the blanketing-type of sporadic  $E$  is forbidden.

The auroral-temperate zone boundary is a very interesting one. The general characteristics of sporadic  $E$  in these two zones are quite different. In the temperate zone the dominant temporal features are the strong seasonal maximum in the vicinity of the summer solstice, the secondary maximum near the winter solstice and the minima in the equinoctial periods. At the maximum of the auroral zone there is very little seasonal variation and the dominant temporal characteristic is in the diurnal occurrence, where there is a distinct night-time peak.

### *Sunspot Cycle Variation of Sporadic E*

The year-to-year variability of sporadic  $E$ , together with the relatively short period for which we have observations, makes the delineation of a sunspot variation quite difficult. Generally speaking, the correlation is positive in the auroral zone (this is probably largely a magnetic correlation), slightly negative in the temperate zone, and rather indeterminate on the magnetic equator where the  $q$ -type sporadic  $E$  shows somewhat greater power sensitivity than the other types. An interesting recent study by Kasuya (1958) shows that the occurrence of  $E_s$  in Japan was almost constant over the last sunspot cycle. Chadwick provides very comprehensive data for the stations he has selected.

## A. PUBLICATIONS 1957-1961\*

- AIDA, K., KOSEKI, T. and UCHIKURA, K. (1961) *J. Rad. Res. Lab. (Japan)* 8, No. 35, 69 "Effect of Es on V.H.F. Pulse Wave Propagation".
- ALBRECHT, H. J., (1960) *Proc. Inst. Radio. Engrs. Austr.* 21, 345-347 "Technical Corrections to Measurements of the sporadic-E layer".
- BATES, H. F. (1961) *J. Geophys. Res.* 66, 447-454, "The Slant Es Echo—A High-Frequency Auroral Echo".
- BECKER, W. (1958) *Arch. Elekt. Übertragung* 12, 481-487 "Sporadic-E Ionization over Lindau/Harz during Last Year".
- BECKER, W. (1957) *Arch. Elekt. Übertragung* 11, 101-104 "Sporadic-E Ionization in the E Region of the Ionosphere at Medium Latitudes".
- BELLCHAMBERS, W. H., and PIGGOTT, W. R. (1960) *Proc. Roy. Soc. A* 25x, 200 "The Ionosphere over Halley Bay".
- BENNINGTON, T. W., *Wireless World* (1959) 65, 262-263 "Sporadic E and the F2 Layer".
- BIBL, K., (1960) *Ann. Geophys. (France)* 16, 148-151 "On the Mechanism of Ionization of the Sporadic Es Layer in the Ionosphere".
- BIBL, K., PAUL, A., and RAWER, K. (1959) *J. Atmosph. Terr. Phys.* 16, 324-339 "The Frequency Dependence of Ionospheric Absorption".
- BOSSALASCO, M., ELENA, A. (1959) *Planetary and Space Science* 1, 205-212 "On Some Characteristics of the Es Layer".
- BOWLES, K. L., COHEN, R., OCHS, G. R., and BALSLEY, B. B. (1960) *J. Geophys. Res.*, 65, 1835-1855 "Radio Echoes from Field-Aligned Ionization above the Magnetic Equator and Their Resemblance to Auroral Echoes".
- BOWMAN, G. G. (1960) *Planetary and Space Science* 2, 195-211 "Some Aspects of Sporadic E at Middle Latitudes".
- DAVIS, R. M., SMITH, E. K., and ELLYETT, C. D. (1959) *Proc. Inst. Radio. Engrs.* 47, 762-769, "Sporadic E at v.h.f. in the USA".
- DIEMINGER, W. E. (1959) *Ann. Geophys. (France)* 15, 23-30, "Clouds in the Sporadic-E Layer".
- DUNGEY, J. W. (1959) *J. Geophys. Res.* 64, 2188-9, "Effect of a Magnetic Field on Turbulence in an Ionized Gas".
- ELLIS, G. R. A. (1960) *J. Atmosph. Terr. Phys.* 18, No. 1, 20-28, "Gyro-splitting of Ionospheric Echoes".
- FOOKS, G. F. (1961) *Nature (London)* 190, 707-708, "Irregularities in the Es Layer of the Ionosphere".
- GAZZARD, A. D. (1958) *Aust. J. Phys.* 11, 272, "Lunar Tides in E2s at Brisbane".
- GERSON, N. C. (1957) *J. Atmosph. Terr. Phys.* 16, 189-191, "Annual Distribution of Sporadic E".
- GOODWIN, G. L., *J. Atmosph. Terr. Phys.* 11, 177-186, "The Movement of Sporadic-E Clouds".
- HAGG, E. L., MULDREW, D., and WARREN, E. (1959) *J. Atmosph. Terr. Phys.* 14, 345-347, "Spiral Occurrence of Sporadic E".
- HARNISCHMACKER, E., and RAWER, K. (1957) *Beiträge Zur Physik der Atmosph.* Bd. 29, s. 253-268 "Ergebnisse Ionosphärischer Windmessungen in der E-Region".
- HEISLER, L. H. (1958) *Austr. J. Physics* 11, 79, "Anomalies in Ionosonde Records due to Travelling Ionospheric Disturbances".
- HEISLER, L. H. (1959) *Nature (London)*, 184, No. 4701, Supple. No. 23, 1788-1789, "A Relation Between Giant Travelling Disturbances and Sporadic-E Ionization".
- HEISLER, L. H., and WHITEHEAD, J. D. (1960) *J. Geophys. Res.* 65, 2767-2773, "F-region Travelling Disturbances and Sporadic-E Ionization".
- HEISLER, L. H. and WHITEHEAD, J. D. (1960) *Nature (London)* 187, 676-677, "Longitude Effect in the Temperate Zone Sporadic E and the Earth's Magnetic Field".

\* For earlier published work, see THOMAS and SMITH (1959).

- HINES, C. O. (1960) *Canad. J. Phys.* **38**, 1441-1481, "Internal Atmospheric Gravity Waves at Ionospheric Heights".
- JACKSON, J. E. and SEDDON, J. C. (1958) *J. Geophys. Res.* **63**, 197-218, "Ionosphere Electron-Density Measurements with the Navy Aerobee-Hi Rocket".
- KASUYA, I., (1958) *J. Rad. Res. Labs. (Japan)* **5**, 117-125, "Long Term Variations of Sporadic E in Japan".
- KNECHT, R. W. (1959) *J. Atmosph. Terr. Phys.* **14**, 348-349, "An Additional Lunar Influence on Equatorial Es at Huancayo".
- KOTADIA, K. M., *J. Sci. and Industr. Res. (India)* **17A**, 46-49, "Meteors and Es Ionization".
- MARTYN, D. F. (1959) *J. Geophys. Res.*, **64**, 2178-2179, "Large Scale Movements of Ionization in the Ionosphere".
- MARTYN, D. F. (1959) *Nature (London)* **183**, 1382-1383, "Sporadic E Region Ionization, 'Spread F' and the Twinkling of Radio Stars".
- MATSUSHITA, S. (1957) *J. Atmosph. Terr. Phys.* **10**, 163-165, "Lunar Effects on the Equatorial Es".
- MIYA, K., SASAKI, T. and ISHIKAWA, M. (1961) *J. Res. NBS* **65D**, 92-99, "Observation of F-layer and Sporadic-E Scatter at v.h.f. in the Far East".
- NICOLET, M. (1959) *J. Geophys. Res.* **64**, 2092-2101, "Constitution of the Atmosphere at Ionospheric Level".
- PENNDORF, R. and CORONITI, S. C. (1958) *J. Geophys. Res.* **63**, 789, "Polar Es".
- PETERSON, A. M. EGAN, R. D. and PRATT, D. S. (1959) *Proc. Inst. Radio. Engrs.* **47**, 300, "The IGY Three-Frequency Backscatter Sounder".
- POINCELOT, P. (1959) *Ann. Telecommun.* **14**, 54-58, "Influence of Absorption on the Reflection Coefficient of the Ionosphere".
- PRESSMAN, J., MARMO, F. F. and ASCHENBRAND, L. M. (1959) *Planet. and Space Sci.* **2**, 17-25, "Artificial Electron Clouds-IV: Thermal Ionization Study, Night Time Cesium Release at 101 km".
- RAO, M. S. (1959) *Canad. J. Physics* **37**, 557-568, "Size of Irregularities in the E-Region of the Ionosphere".
- RATCLIFFE, J. A. (1959) *J. Geophys. Res.* **64**, 2102-2111, "Ionizations and Drifts in the Ionosphere".
- RAWER, K. (1960) *Comptes Rendus* **250**, 1517-1519, "Étude des propriétés de transparence de la couche ionosphérique Es dite sporadique".
- SHAW, J. (1959) *Planet. and Space Sci.* **2**, 56-59, "A Theory of the Origin and Geomagnetic Control of Two Types of High Latitude Es".
- SHEARMAN, E. D. R. and HARWOOD, J. (1960) *J. Atmosph. Terr. Phys.* **18**, 29-42, "Sporadic E as Observed by Backscatter Techniques in the United Kingdom".
- SHIMAZAKI, T. (1959) *J. Radio Res. Labs. (Japan)* **6**, No. 28 *Report of Ionos. and Space Res. in Japan* **8**, No. 1, 21-47 (1959), "Worldwide Measurements of Horizontal Ionospheric Drifts".
- SKINNER, N. J. and WRIGHT, R. W. (1957) *Proc. Phys. Soc.* **70**, No. 453B, 833-839, "The Effect of the Equatorial Electrojet on the Ionospheric Es and F2 Layers".
- SMITH, E. K. and KNECHT, R. W. (1957) *J. Atmosph. Terr. Phys.* (Special Supplement on Polar Symposium) **195**, "Some Implications of Slant Es".
- SMITH, E. K. and FINNEY, J. W. (1960) *J. Geophys. Res.* **65**, 855-892, "Peculiarities of the Ionosphere in the Far East: Sporadic E and F-Region Scatter".
- TAMAOKA, M. (1960) *J. Rad. Res. Labs. (Japan)* **7**, 599-613, "Relationships between foE and Field Intensity Depending on Sporadic-E Propagation in the 50 Mc/s Band".
- THOMAS, J. A. and SMITH, E. K. (1959) *J. Atmosph. Terr. Phys.* **13**, 295-314, "A Survey of the Present Knowledge of Sporadic-E Ionization".
- VENKATESWARLU, P. and SATYANARAYANA, R. (1961) *J. Sci. Industr. Res. (India)*, **20B**, No. 1, 8-10, "Some Studies on Sporadic E".
- WHITEHEAD, J. D., *J. Atmosph. Terr. Phys.* **16**, 99-102, "Sudden Changes in the Virtual Height of Radio Waves Reflected From the E-Region of the Ionosphere".
- WHITEHEAD, J. D. (1960) *Nature (London)* **188**, 567, "The Formation of the Sporadic-E Layer in the Temperate Zones".

- WRIGHT, J. W. and GAUTIER, T. N. (1960) *J. Res. NBS* **64D**, 347–348, “Note on a Test of the Equivalence Theorem for Sporadic-*E* Propagation”.
- WRIGHT, R. W., and SKINNER, N. J. (1959) *J. Atmosph. Terr. Phys.* **13**, 217–221, “Lunar Tides in the Sporadic-*E* Layer at Ibadan”.
- ZHEKULIN, L. (1960) *Planet. and Space Sci.* **2**, 110–120, “Radio Wave Propagation Characteristics of a Simple Ionospheric Model Based on Rocket Data”.

## B. TABLE OF CONTENTS FROM AGARDOGRAPH 34:

Proceedings of the Cambridge, 1958 Conferences on Sporadic-*E* Ionization

	Page
Foreword	ii
Opening Address by Mr. J. A. RATCLIFFE, O.B.E., F.R.S.	v
PART I	
Temporal and World-wide Variation of Sporadic <i>E</i> by E. K. SMITH, JR.	1
Outline of Suggested Theories of Sporadic <i>E</i> by J. A. THOMAS	23
Summary of Discussion	31
PART II	
Classification of Sporadic <i>E</i> by J. A. THOMAS	33
Slant <i>E<sub>s</sub></i> Disturbance at Godhavn and Its Correlation with Magnetic Activity by J. K. OLESEN and J. RYBNER	37
Sporadic Ionization of the <i>E</i> -Region of the Ionosphere Above Lindau-Harz During the Last Year by W. BECKER	59
Correlation of <i>E<sub>s</sub></i> Characteristics in Time and Space by K. RAWER	67
Latitude Effects in Sporadic- <i>E</i> Observations by N. C. GERSON	81
De L'Origine des Echos <i>E</i> Sporadique: Quelques Données Experimentales Recueillies en France per D. LEPENCHINSKY	97
Summary of Discussion	108
PART III	
Sporadic <i>E</i> as Observed by Backscatter Techniques in the United Kingdom by E. D. R. SHEARMAN and J. HARWOOD	111
Sporadic <i>E</i> Observed on v.h.f. Oblique-Incidence Circuits by E. K. SMITH, JR.	129
Summary of Discussion	146
PART IV	
Evidence About <i>E<sub>s</sub></i> from N(h) Profiles by K. WEEKES	149
Some Characteristics of Sporadic- <i>E</i> Ionization as Determined by a Rapid Frequency-Sweep Experiment by B. H. BRIGGS	151
Anisotetry in the Fading Pattern of Sporadic <i>E</i> as Observed Near the Auroral Zone by B. MAHLUM	163
Summary of Discussion	169

PART V	Page
High Electron Density Gradients in the Ionosphere as Observed With Rockets	171
by J. C. SEDDON	
Measurement of Ionospheric Fine Structure by High Altitude Rockets	183
by W. PFISTER	
Summary of Discussion	193
PART VI	
Introduction to Discussion on Theoretical Explanation of Sporadic <i>E</i>	195
by K. WEEKES	
Summary of Discussion	197
FINAL REMARKS: (A Summary of the <i>E</i> <sub>s</sub> Conference)	201
by Mr. J. A. RATCLIFFE, O.B.E., F.R.S.	

# Reflection Mechanisms for Sporadic *E*

K. TAO\* and J. R. WAIT†

## 1. THIN LAYER MODEL

A sporadic-*E* patch indicates relatively sharp variations in the gradient of electron density in both the horizontal and vertical directions. Nevertheless, the horizontal extent of sporadic *E* is often great enough for it to be regarded as a definite layer capable of producing reflection. At first we shall consider the thin layer model. The theory of reflection from a thin ionized layer has been developed by Hartree (1929), Booker (1938), Rydbeck (1942)(1946), Rawer (1938) and Millington (1945). These authors obtained the reflection coefficient from an exact wave equation. We shall briefly outline their theories.

### (a) *Rydbeck's Theory*

The distribution of electron density is assumed to be parabolic, so that the dielectric constant  $\epsilon(z)$  is expressed as follows:

$$\epsilon(z) = 1 - \frac{f_N^2}{f^2} \left\{ 1 - \left( \frac{z}{\Delta h} \right)^2 \right\}, \quad (1.1)$$

where

$\Delta h$  : half-thickness of the layer

$f_N$  : critical frequency

$z$  : vertical distance

From this distribution of dielectric constant, the wave equation can be written

$$\frac{d^2 \Pi}{dz^2} + \frac{\omega^2}{c^2} \left[ 1 - \frac{f_N^2}{f^2} \left\{ 1 - \left( \frac{z}{\Delta h} \right)^2 \right\} \right] \Pi = 0.$$

If we put  $\rho \equiv \pi \frac{\Delta h}{\lambda_N} \frac{f_N^2 - f^2}{f_N^2}$  and  $V = \left( \frac{4\pi\Delta h}{\lambda_N} \right)^{1/2} \left( \frac{z}{\Delta h} \right) e^{i\pi/4}$ , the above

wave equation is transformed as follows:

$$\frac{d^2 \Pi}{dV^2} + \left[ i\rho - \frac{V^2}{4} \right] \Pi = 0. \quad (1.2)$$

\* Radio Research Laboratory, Kokubunji, Tokyo, Japan.

† National Bureau of Standards, Boulder, Colo., U.S.A.



This equation is satisfied by Weber's parabolic cylinder functions.

$$\begin{aligned}\Pi &= D_{i\rho-1/2}(V \cdot e^{i\pi/4}) \\ &= \frac{(i\rho + \frac{1}{2})!}{(2\pi)^{1/2}} e^{(\pi\rho/2) + (i\pi/4)} D_{-i\rho-1/2}(V \cdot e^{-i\pi/4}) \\ &\quad + \frac{(i\rho + \frac{1}{2})!}{(2\pi)^{1/2}} e^{-(\pi\rho/2) - (i\pi/4)} D_{-i\rho-1/2}(V \cdot e^{i3/4\pi}).\end{aligned}$$

In the above solution, according to Rydbeck, first term on the right-hand side represents a reflected wave and the second term a refracted wave. From this relation, the reflection coefficient  $R$  is obtained by the following equation.

$$\frac{R^2}{T^2} = \frac{R^2}{1 - R^2} = e^{2\pi\rho} = \exp\left[\left(4\pi^2 \frac{\Delta h}{\lambda_N} \frac{f_N^2 - f^2}{2f_N}\right)\right], \quad (1.3)$$

where  $T$  is a transmission coefficient.

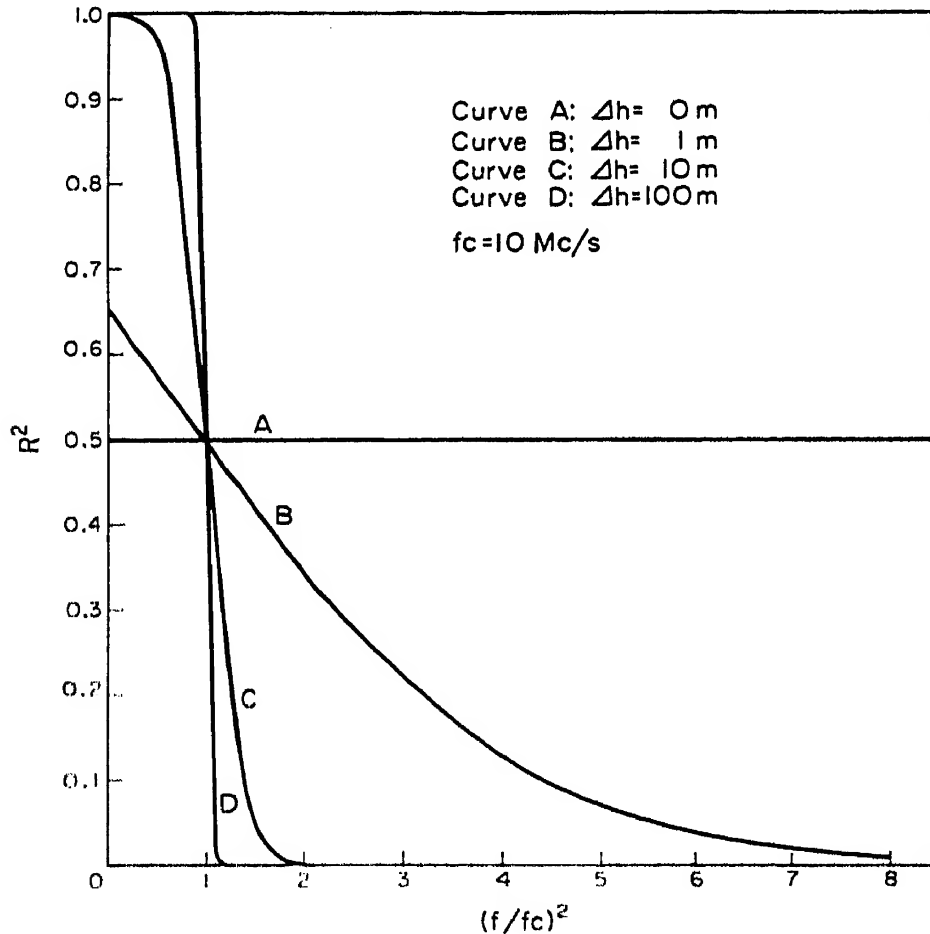


Fig.1. Reflection coefficient for a parabolic layer.

(It is possible that the calculations in this figure are in error because, as pointed out by Northover (1962), the value of  $R$  defined above is not always equal to the actual reflection coefficient.)

Figure 1 shows several plots of the reflection coefficient squared as a function of  $f/f_N$ . In this figure, the critical frequency is assumed to be 10 Mc/s.

(b) *Rawer's Investigation*

Rawer investigated the reflection from the so-called Epstein layer. In this layer, the dielectric constant is expressed as follows:

$$\varepsilon(z) = 1 - N \frac{e^{\kappa z}}{(1 + e^{\kappa z})} - M \frac{4e^{\kappa z}}{(1 + e^{\kappa z})^2}. \quad (1.4)$$

The second term represents a monotonic transition of the dielectric constant and the third term represents a symmetrical layer. If we assume a symmetrical layer, the dielectric constant within a layer becomes, neglecting collisional frequency:

$$\varepsilon(z) = 1 - \frac{f_N^2}{f^2} \frac{4e^{\kappa z}}{(1 + e^{\kappa z})^2}. \quad (1.5)$$

The wave equation is

$$\frac{d^2 \Pi}{dz^2} + \frac{\omega^2}{c^2} \left[ 1 - \frac{f_N^2}{f^2} \frac{4e^{\kappa z}}{(1 + e^{\kappa z})^2} \right] \Pi = 0.$$

He transformed this equation into the hypergeometric differential equation and after complicated calculation obtained the reflection coefficient

$$|R|^2 = \frac{\cosh^2 \frac{\pi}{2} \sqrt{\left[ 4S^2 \left( \frac{f_N^2}{f^2} \right) - 1 \right]}}{\cosh \pi \left\{ \frac{1}{2} \sqrt{\left[ 4S^2 \left( \frac{f_N^2}{f^2} \right) - 1 \right]} + S \right\} \cosh \pi \left\{ \frac{1}{2} \sqrt{\left[ 4S^2 \left( \frac{f_N^2}{f^2} \right) - 1 \right]} - S \right\}}, \quad (1.6)$$

where  $S = 4\pi/\lambda\kappa$  (relative layer thickness).

From this reflection coefficient, reflection curves are drawn as shown in Fig. 2.

(c) *Millington's Theory*

Millington considered a sine-squared layer. In this case, the dielectric constant is given

$$\varepsilon(z) = 1 - \frac{f_N^2}{f^2} \sin^2 \pi z. \quad (1.7)$$

The total thickness of the layer is taken as  $p$  wave lengths,  $\lambda_0$  corresponding to the critical frequency. If the distance  $z$  in the layer is measured in terms of a unit of  $\lambda/2\pi$ , actual distance is  $\lambda z/2\pi$ . If the layer extends from 0 to  $z_0$ , then

$$\frac{\lambda}{2\pi} z_0 = p \cdot \lambda_0.$$

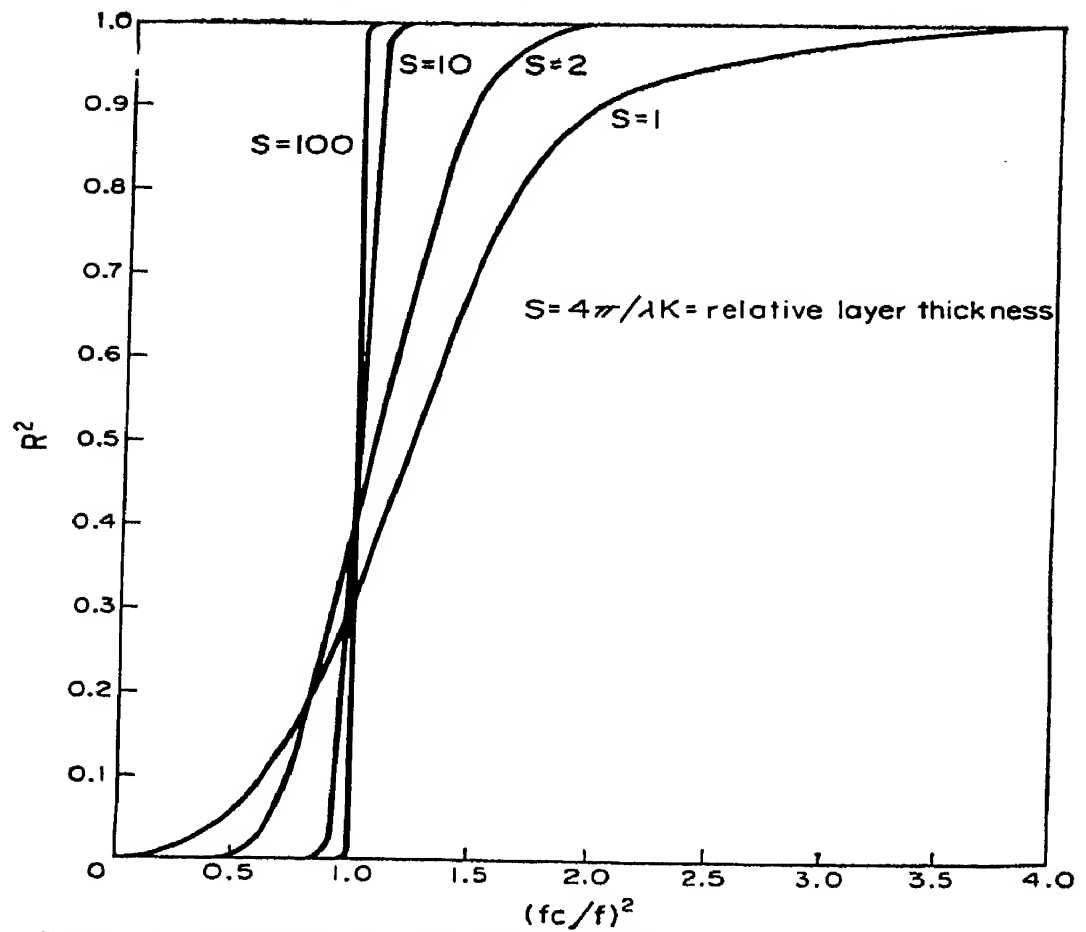


Fig. 2. Reflection coefficient for the Epstein layer.

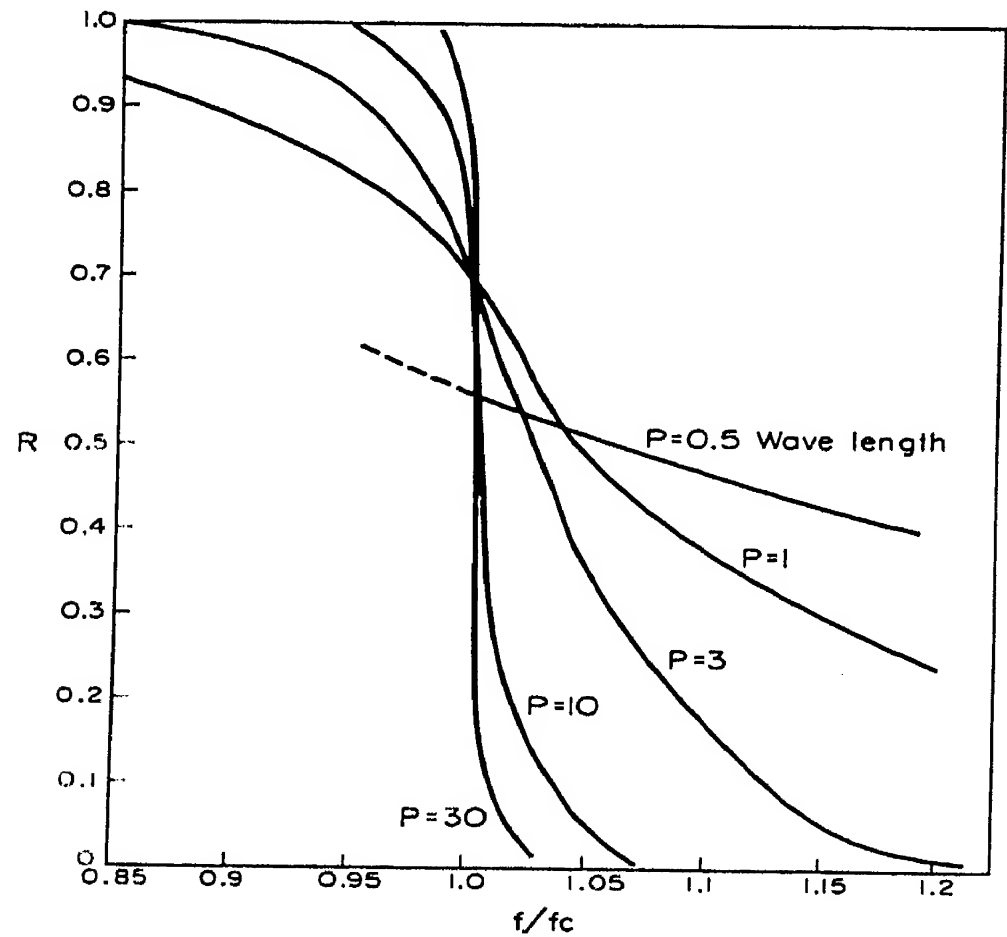


Fig. 3. Reflection coefficient for a sine squared layer.

The wave equation in this case becomes

$$\frac{d^2\Pi}{dz^2} + \frac{\omega^2}{c^2} \left[ 1 - \frac{f_N^2}{f^2} \sin^2 \pi z \right] \Pi = 0.$$

If we substitute  $\frac{1}{\Pi} \frac{d\Pi}{dz} \equiv \nu = \nu_R + i\nu_I$ , the above equation is transformed to:

$$\frac{d\nu}{dz} + \nu^2 + \frac{\omega^2}{c^2} \left[ 1 - \frac{f_N^2}{f^2} \sin^2 \pi z \right] \Pi = 0.$$

Millington obtained the reflection coefficient by a different method which he defines as follows :

$$|R| = \frac{|\nu_R|}{\sqrt{(\nu_R^2 + \nu_I^2)}}. \quad (1.9)$$

Curves of reflection coefficient are given in Fig. 3.

The theories, mentioned above, strictly apply only for normal incidence and some modification is required for oblique incidence (Wait 1962).

Besides the rigorous treatments, Tao (1961) has postulated a simple model of a thin layer in order to account for oblique  $E_s$  measurement. The basic idea for this model was developed by Friis, Crawford and Hogg (1957) in order to explain the persistent tropospheric field intensity beyond the horizon. According to their single theory, if a layer has a reflection coefficient  $\rho$ , the received power is given in the form :

$$P_r = P_t \frac{A_r A_t}{\lambda^2 d^2} \rho^2, \quad (1.10)$$

where  $P_t$  is the transmitted power,  $A_t$  and  $A_r$  are the effective areas of transmitting and receiving antennas, and  $d$  is the distance between the transmitter and receiver. This relation is appropriate when the following conditions are satisfied,

$$b > \frac{\sqrt{(\lambda d)}}{\theta}, \quad a > \sqrt{(\lambda d)},$$

where  $\theta$  is the grazing angle to the layer and  $a$  and  $b$  are horizontal dimensions of sporadic  $E$ . If the dielectric constant in the layer is assumed to have the form

$$\varepsilon(z) = 1 - \frac{f_N^2}{f^2} \left\{ 1 - \left( \frac{z}{\Delta h} \right)^{2n} \right\}, \quad n = 1, 2, 3, \dots \quad (1.11)$$

the reflection coefficient is given by (Tao 1961)

$$\rho^2 = \left( \frac{E_r}{E_i} \right)^2 = \frac{f_N^4 n^2 [(2n-1)!]^2}{f^4 \theta^4 L^{4n}} \times \left[ (-1)^n \sum_{k=0}^{n-1} \frac{L^{2k}}{2k!} (-1)^k \left( \cos L + \frac{L \sin L}{2k+1} \right) + 1 \right]^2, \quad (1.12)$$

where

$E_i$  : incident electric field

$E_r$  : reflected electric field

$L = (4\pi \sin \theta \Delta h)/\lambda$

$\Delta h$  : half-thickness

$k = n - m$ .

Therefore, the received power is obtained by combining formulas (1.10) and (1.12). Figure 4 shows a comparison between the theoretical calculation from this theory and the statistical analysis of measured data carried out by Yamaoka (1960). Measured results agree with the theoretical curve

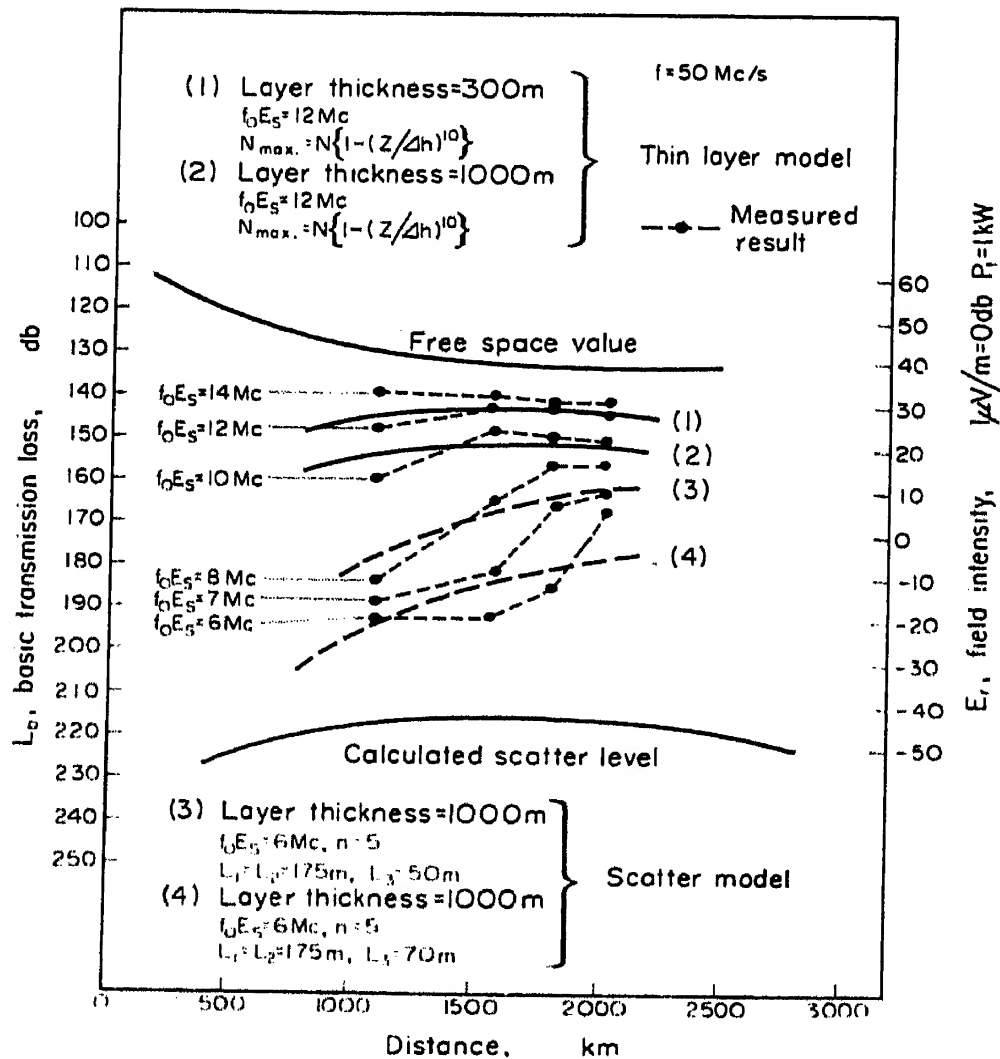


Fig. 4. Comparison of measured field intensities with theoretical models.

at comparatively high values of  $f_o E_s$ , so that high field intensity of sporadic- $E$  enhancement corresponding to comparatively high plasma frequency may be explained by reflection from a thin ionized layer.

## 2. SCATTERING MODEL

Next we shall consider a scattering model for sporadic  $E$ . Some types of sporadic  $E$  have many features of scattering phenomena. Many authors have tried to explain sporadic  $E$  from the standpoint of scattering theory.

The outline of scattering theory will be described. Among various theoretical works, the following three treatments have been proposed. The first treatment is an auto-correlation method of dielectric constant (or electron density fluctuations), which was derived by Booker and Gordon (1950) and was used for an exponential auto-correlation. Staras (1952) derived the scattering cross-sections more rigorously by using various correlation functions; i.e. Gaussian and generalized Cauchy correlation functions, in addition to the exponential type. Recently the modified exponential and modified Bessel correlation functions have been proposed in order to explain observed scattered fields. The second method was obtained by Villars and Weisskopf (1954) using the statistical theory of isotropic homogeneous turbulence. The third treatment was proposed for the first time by Villars and Weisskopf (1955) and Gallet (1955) and these theories suggest that the fluctuation mechanism of electron density is produced by turbulent mixing. This concept has also been developed by Silverman (1956), Bolgiano (1958), Wheelon (1957) and others.

### (a) *Scattering Theory expressed by an Auto-correlation Function*

We shall consider an intersecting region of the atmosphere where the transmitting and receiving beams overlap. Let  $\varepsilon$  be the average dielectric constant of the atmosphere in the region under consideration and let  $\Delta\varepsilon$  be the departure of the dielectric constant from its average value at a point  $P$ . Similarly, let us define  $\Delta\varepsilon'$  to be the departure at a neighbouring point  $P'$ . We shall define an auto-correlation function in the following form:

$$\rho = \frac{1}{v \langle (\Delta\varepsilon)^2 \rangle} \int_v (\Delta\varepsilon)(\Delta\varepsilon')^* dv, \quad (2.1)$$

where the asterisk denotes the complex conjugate and

$$\langle (\Delta\varepsilon)^2 \rangle = \frac{1}{v} \int_v |\Delta\varepsilon|^2 dv.$$

Therefore a macroscopic volume  $v$  is regarded as the sum of many microscopic elements of volume  $dv$ . Denoting  $C(0)$  for the time variance

$\langle(\Delta n)^2\rangle$  of the refractive index  $n$  of the atmosphere, we can put  $C(r) = C(0)\rho$ , so the scattering cross-section is given by:

$$\sigma(q) = \frac{k^4 \sin^2 \chi l^3}{\pi q} \int_0^\infty \rho C_n(\rho) \sin(q\rho) d\rho, \quad (2.2)$$

where

$$q = 2kl \sin \frac{\theta}{2} \cong kl\theta, \quad \rho = \frac{r}{l},$$

$\theta$  : scattering angle.

Booker and Gordon adopted an exponential auto-correlation function

$$C(r) = C(0)e^{-r/l},$$

and the following scattering cross-section was obtained in this case:

$$\sigma = \frac{\langle(\Delta \varepsilon/\varepsilon)^2\rangle (2\pi l/\lambda)^3 \sin^2 \chi}{\lambda [1 + \{(4\pi l/\lambda) \sin \theta/2\}^2]^2}. \quad (2.3)$$

This scattering cross-section is transformed into the following form when the scale of turbulence is large compared with the wave length.

$$\sigma = \frac{\langle(\Delta \varepsilon/\varepsilon)^2\rangle \sin^2 \chi}{32\pi l \sin^4 \theta/2}. \quad (2.4)$$

#### (b) *Scattering Theory by means of Turbulent Energy*

Villars and Weisskopf (1954) obtained a new scattering theory using the statistical theory of isotropic homogeneous turbulence. As this theory is based on the pressure fluctuations of the ionospheric neutral fluid which accompanies its velocity pulsation, it is called the pressure fluctuation theory.

Let us consider the scattering of radio waves from the region containing a medium whose dielectric constant is:

$$\varepsilon = \varepsilon_0 + \Delta \varepsilon,$$

where  $\Delta \varepsilon$  is the variation of dielectric constant from average value. The scattering field at a distance  $R$  from the scattering volume is given in the form:

$$E_s = \frac{E_0}{4\pi R} \left(\frac{\omega}{c}\right)^2 \left| \int \Delta \varepsilon(\vec{r}) e^{ik\vec{r}} dv \right| \sin \chi. \quad (2.5)$$

Here  $E_0$  is the electric field of the incident wave and  $\chi$  the angle between the directions of incident and scattered fields. In this case, the scattering cross-section is given as follows:

$$\sigma = \frac{\pi^2}{\lambda^4 v} |M|^2 \sin^2 \chi, \quad (2.6)$$

where

$$M = \int \Delta \epsilon(\vec{r}) e^{ik\vec{r}} d\vec{r}.$$

As the fluctuation of dielectric constant  $\Delta \epsilon$  is related to the density fluctuation  $\Delta \rho$  in the following form,  $\Delta \epsilon$  may be expressed by:

$$\Delta \epsilon = - \frac{\omega_N^2}{\omega^2} \frac{\Delta N}{N} = - \frac{\omega_N^2}{\omega^2} \frac{\Delta \rho}{\rho}, \quad (2.7)$$

where  $N$  indicates the free electron density and  $\omega_N$  the plasma angular frequency. We shall now connect the density fluctuation with the velocity fluctuations by means of Bernoulli's law. Since the local velocity fluctuation  $v_{ln}$  will be produced by the local pressure fluctuation  $p_{ln}$ , the density fluctuation will be given by the equation:

$$\rho_{ln} = \frac{1}{\gamma} \frac{\rho}{p} p_{ln} \cong \rho \frac{v_{ln}^2}{v_M^2},$$

where  $\gamma$  is the adiabatic exponent,  $v_M$  the molecular velocity and  $v_{ln}$  is defined as follows:

$$v_{ln}^2 = \langle (v - \langle v \rangle_{ln-1})^2 \rangle_{ln}.$$

Villars and Weisskopf derived the following relation from the Weizsäcker's theory of the homogeneous turbulence

$$\rho_{ln}^2 = \rho^2 \left( \frac{S_0}{\rho} \right)^{4/3} \frac{l_n^{4/3}}{v_M^4},$$

where  $S_0 \cong \rho \frac{v_0^3}{l_0}$  expresses turbulent energy. The scattering cross-section is obtained:

$$\sigma = N^2 r_e^2 \left( \frac{S_0}{\rho} \right)^{4/3} \frac{l_n^{13/3}}{v_M^4} \sin^2 \chi, \quad (2.8)$$

where  $l_0$  indicates the largest scale of turbulence and  $l_n$  means effective scale of turbulence. As described above, although the Villars-Weisskopf's theory is expressed in terms of energy of turbulence, in some problems the analysis by energy spectrum is more convenient (Wheelon 1957, Gallet 1956, Tao 1958). However, the theory of pressure fluctuations has been abandoned at the present time.

### (c) *Scattering Theory by means of Turbulent Mixing*

In 1955, Gallet (1955) showed that the mechanism of pressure fluctuations which was proposed by Villars and Weisskopf is too small, by a



factor of about  $10^{-4}$ , to produce the observed density fluctuations. He proposed a new idea of stratification of the sporadic- $E$  layer by considering the turbulent mixing process. In a nonadiabatic atmosphere, the vertical transport of air masses produces fluctuations of temperature which give rise to air density fluctuations. He showed that fluctuations of the electron density is produced by air density fluctuations and also from transport in the presence of the gradient of electron density. From the considerations mentioned above he obtained the following relation :

$$\left\langle \left( \frac{\Delta N}{N} \right)^2 \right\rangle \cong \frac{1}{3} l_0^2 \left( \frac{\text{grad } N}{N} \right)^2. \quad (2.9)$$

By combining this relation with the maximum of the gradient of electron density existing above and below the maximum of the  $E$ -region electron density and the effect of temperature fluctuations, he suggested a stratification tendency of the sporadic- $E$  layer in three levels which can be explained by a turbulent mixing process. Gallet has also suggested that the spectra of temperature and density fluctuations in the inertia subrange of turbulence varies as  $K^{-3}$   $\left( K = \frac{2\pi}{l_n} \right)$ , while the Kolmogoroff's spectrum which describes energy contained in the velocity fluctuations is  $K^{-5/3}$ . He obtained the scattering cross-section as follows:

$$\sigma = - \frac{(f_N/f)^4 (\Delta N/N)^2 \sin^2 \chi k^3 \partial G_1(K_1)}{\overline{\Delta_1^2} 8 \cdot 2 \sin \theta/2 \partial K_1},$$

where

$$\overline{\Delta_1^2} = \frac{2^3 \pi^2}{3} \frac{1}{K_0^2} (\text{grad } N), \quad K_0 = \frac{2\pi}{l_0}, \quad (2.10)$$

$$G_1(K_1) = \frac{2^3 \pi^2}{3} (\text{grad } N)^2 \frac{1}{K_0^3} \frac{1}{[1 + (K_1/K_0)^2]^{3/2}} \cdot \frac{1}{[1 + (K_1/K_s)^4]^{4/3}},$$

$$K_1 = \frac{2\pi}{l_n}, \quad K_s = \frac{2\pi}{l_s}.$$

The theory of turbulent mixing was also proposed by Villars and Weisskopf (1955). Let us consider a region where the electron density has an average gradient in one direction:

$$N(z) = N_0 + (z - z_0) \left( \frac{dN}{dz} \right) + \dots \quad (2.11)$$

If a distribution expressed as (2.11) is embedded in a turbulent medium, electron density fluctuations  $\Delta N_{l_n}$  will be produced by eddies of size  $l_n$ :

$$\Delta N_{l_n} \sim \left( \frac{dN}{dz} \right) l_n.$$

In this case, the scattering cross-section is expressed in the form:

$$\sigma = \left( \frac{dN}{dz} \right)^2 r_e^2 l_n^5 \sin^2 \chi. \quad (2.12)$$

Other scattering cross-sections have been obtained by Silverman (1956) and Wheelon (1957) from the turbulent mixing theory.

$$\sigma \sim \frac{r_e^2 \langle N^2 \rangle}{6\pi l_0^{2/3}} l_n^{11/3} \quad (\text{Silverman}). \quad (2.13)$$

$$\sigma = 2\pi^2 r_e^2 \left( \frac{dN}{dz} \right)^2 \left[ \frac{4\pi}{\lambda} \sin \frac{\theta}{2} \right]^{-5} \quad (\text{Wheeler}). \quad (2.14)$$

As indicated above, many theories have been proposed from the scattering model. Most often these have been applied to v.h.f. forward scatter propagation. Recently a scattering theory has been developed by Tao (1961), specifically to explain frequency and distance dependences of oblique sporadic- $E$  propagation. This is outlined in what follows.

As the phenomenon of sporadic  $E$  generally appears to have a denser concentration of electron density than the normal scattering phenomenon, it seems inappropriate to use the auto-correlation functions which are used to account for the normal scattering phenomenon. So we shall take the following correlation function:

$$C_n(\rho) = C(0) \left[ \frac{2^{1-n}}{\Gamma(n)} \right] \rho^n K_n(\rho), \quad \rho = \frac{r}{l}, \quad (2.15)$$

where  $K_n(\rho)$  is the modified Bessel function of the second kind of order  $n$  and  $\Gamma$  is the gamma function. This correlation function was derived by Muchmore and Gallet (private communication). The calculated curves of this correlation function are shown in Fig. 5. In addition to these curves, the exponential and the Gaussian models are plotted in this figure.

Models of the exponential, the Gaussian and the modified Bessel function of the first order have been used so far in order to explain both the ionospheric and tropospheric scattering cases. Although these correlation functions are proper for the phenomena of normal scattering, they may not be appropriate for the scattering model of sporadic  $E$  which appears to have denser concentration of electrons. Another trouble occurs because the frequency dependence of sporadic- $E$  propagation may be difficult to explain from the correlation function normally used in scattering theory. A correlation function of the modified Bessel function of higher order, however, seems appropriate for the sporadic- $E$  model.

We shall consider a model wherein a sporadic- $E$  path which has a large horizontal dimension contains a large number of small irregularities. In this analysis, it is necessary to note that the scale of turbulence which is

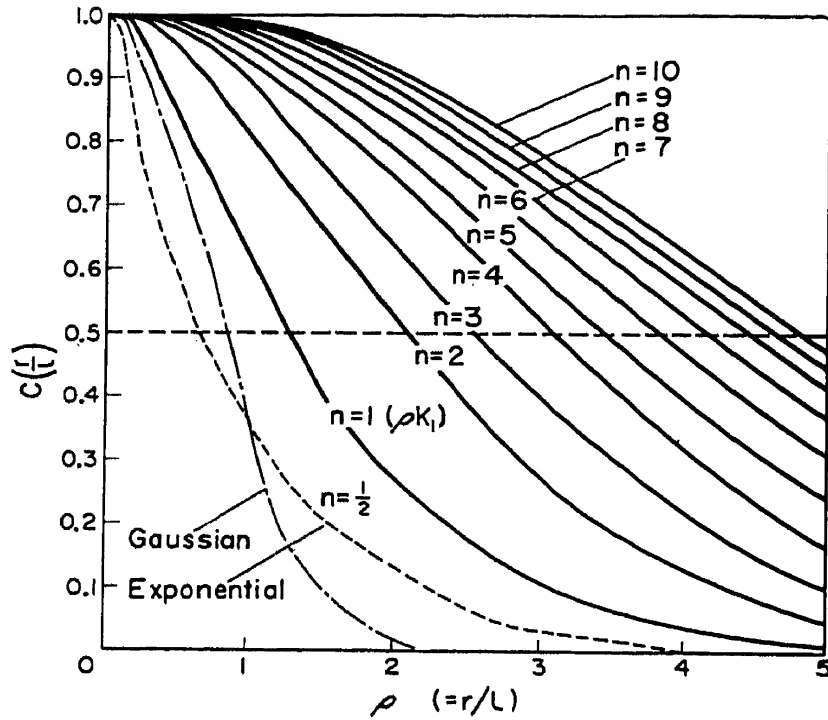


Fig. 5. Autocorrelation function of the modified Bessel function  $[2^{1-n}\Gamma(n)]\rho^n K_n(\rho)$ .

represented in the correlation function (2.15) does not describe the scale of irregularities of sporadic  $E$ , but expresses the usual scale of turbulence responsible for normal scattering. Although some confusion exists concerning the use of the word "scale" to describe the size of irregularities of electron density in the ionosphere, we shall define the "scale" of irregularities to mean the distance in which the correlation is reduced to a specified value, such as 0.5, according to Booker's (1958) definition. Following the theory of turbulence, the turbulent motion is considered to consist of superposition of a large number of different-sized component motions in which a large eddy distinegrates into smaller eddies after its life time. Thus the energy is transferred from the largest eddy to the smallest eddy in which the energy is transformed into heat by viscosity.

There exists a scale of irregularities which has the following relationship concerning an operated frequency and a scattering angle:

$$l = \frac{\lambda}{2 \sin \theta/2}.$$

The scattering process thus acts like a narrow band filter on the spectrum. The scale of the small sporadic- $E$  irregularities may be given as:

$$L = ml,$$

where  $l$  is the scale of normal turbulence and  $m$  is an arbitrary multiplication factor.

From the correlation curves, the scale of the small sporadic-*E* irregularities has dimensions of  $m$  times (3–4 times) the scale of the normal turbulence.

The generalized scattering cross-section in the case of anisotropic irregularities is given in the form:

$$\sigma_n = \frac{\left(\frac{\Delta N}{N}\right)^2 \left(\frac{f_N}{f}\right)^4 \Gamma\left(n + \frac{3}{2}\right) (m)^{2n} \sin^2 \chi L_1 L_2 L_3 \left(1 + \frac{1}{q^2}\right)^{-(n+3/2)}}{2^{2n+4} \sqrt{(\pi) \Gamma(n)} k^{2n-1} \left(\sin \frac{\theta}{2}\right)^{2n+3} [(L_1^2 \sin^2 \gamma + L_2^2 \cos^2 \gamma) \sin^2 \phi + L_3^2 \cos^2 \phi]^{n+3/2}} \quad (2.16)$$

where

$$q \cong \frac{2k \sin \theta/2}{m} [(L_1^2 \sin^2 \gamma + L_2^2 \cos^2 \gamma) \sin^2 \phi + L_3^2 \cos^2 \phi]^{1/2},$$

and  $L_1$ ,  $L_2$ ,  $L_3$  are different scales of the sporadic-*E* irregularities in directions parallel, normal and vertical to the mean horizontal drift.  $\gamma$  is the angle between the mean drift and the great circle plane. The angle between the plane containing the scattering blob under consideration and the great-circle plane is denoted by  $\phi$ . This generalized scattering cross-section has been also obtained by Norton (1960) for the tropospheric scattering case. If the sporadic-*E* irregularities exist near the great-circle plane, we can get the scattering cross-section available for sporadic-*E* scatter, by putting  $n = 5$

$$\sigma_5 \cong 1.03 \times 10^2 \frac{\left(\frac{\Delta N}{N}\right)^2 \left(\frac{f_N}{f}\right)^4 L_1 L_2 \left[1 + \left(\frac{3.5\lambda}{4\pi L_3 \sin \theta/2}\right)^2\right]^{-13/2}}{\left(\frac{2\pi L_3}{\lambda}\right)^9 L_3^3 \left(\sin \frac{\theta}{2}\right)^{13}}. \quad (2.17)$$

Theoretical curves calculated from the above formula are compared with some measured field intensities in Fig. 6. From this figure, the scale of small irregularities of the sporadic-*E* patch responsible for these experimental observations may be considered to have a horizontal scale of the order of 200 m and a vertical scale of 50 m. If we take a high-order value of  $n$  in the correlation function, i.e.,  $n = 4 \sim 7$ , we obtain

$$P_r \propto \frac{1}{f^{13}} \sim \frac{1}{f^{19}}. \quad (2.18)$$

Therefore, we can explain the frequency dependence of sporadic *E* by considering an auto-correlation function of higher order (cf. Section 5 in my other article in this book). In Figs. 7 and 8 in my other article (p. 235)

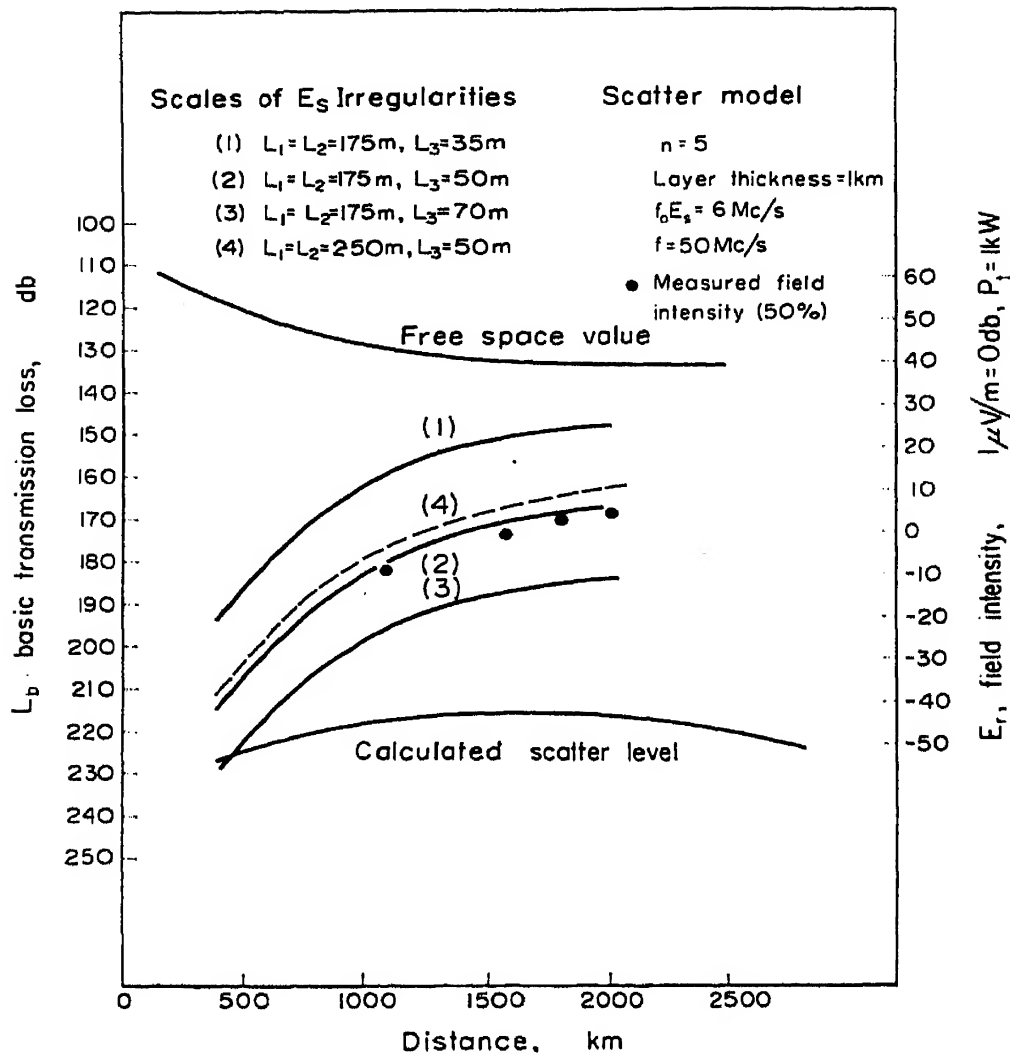


Fig. 6. Distance dependence of sporadic- $E$  propagation (scatter model).

are drawn families of curves with various values of  $n$  of this function. From these figures, the auto-correlations of the modified Bessel function with  $n = 4 \sim 7$  seem to be responsible for the scattering model of sporadic  $E$ . Also, we can examine the distance dependence of field intensity corresponding to comparatively low value of  $f_o E_s$  from this scattering model. Relatively low sporadic- $E$  field may be explained by the scattering model, as indicated in Fig. 4.

#### REFERENCES

- BOLGIANO, R. (1958) *Trans. Inst. Radio. Engrs.* PGAP, AP-6, 159.  
 BOOKER, H. G. (1938) *Proc. Phys. Soc. Lond.* **51**, 81.  
 BOOKER, H. G. (1958) *Proc. Inst. Radio. Engrs.* **46**, 298.  
 BOOKER, H. G. and GORDON, W. E. (1950) *Proc. Inst. Radio. Engrs.* **38**, 401.  
 FRIIS, H. T., CRAWFORD, A. B. and HOGG, D. C. (1957) *Bell. Sys. Tech. J.* **36**, 627.  
 GALLET, R. M. (1955) *Proc. Inst. Radio. Engrs.* **43**, 1240.  
 GALLET, R. M. (1956) *Polar Atmos. Symp.*, Pt. 2, Pergamon Press, p. 165.  
 HARTREE, D. R. (1929) *Proc. Camb. Phil. Soc.* **25**, 97.  
 MILLINGTON, G. (1945) *Air Ministry Great Baddow Res. Rep.* T. R. 508.  
 NORTHOVER F. H. (1962) *Jour. Res. Natl. Bur. Stds.* **66D**, 73-80.  
 NORTON, K. (1960) *J. Geophys. Res.* **65**, 2029.

- RAWER, K. (1938) *Ann d. Physik.* 35, 385.
- RYDBECK, O. E. H. (1942) *J. Appl. Phys.* 13, 577.
- RYDBECK, O. E. H. (1946) *Trans. Chalmers. Univ. Tech.* 34.
- SILVERMAN, R. A. (1956) *J. Appl. Phys.* 27, 699.
- STARAS, H. (1952) *J. Appl. Phys.* 23, 1152.
- TAO, K. (1958) *J. Radio Res. Lab.* 5, 20.
- TAO, K. (1961) *NBS Tech.*, Note 87.
- VILLAS, F. and WEISSKOPF, V. F. (1954) *Phys. Rev.* 94, 232.
- VILLAS, F. and WEISSKOPF, V. F. (1955) *Proc. Inst. Radio. Engrs.* 43, 1231.
- WAIT, J. R. (1962) *Electromagnetic Waves in Stratified Media.* Pergamon Press.
- WHEELON, A. D. (1957) *Phys. Rev.* 105, 1706.
- YAMAOKA, M. (1960) *J. Radio Res. Lab.* 7, 599.

# Final Remarks of 1957 AGARD Conference of Sporadic- $E$ Ionization

J. A. RATCLIFFE

Department of Scientific and Industrial Research, Radio Research  
Section, Slough, Bucks, England

**Abstract**—In this paper I shall not attempt to summarize everything that has been said at the conference, but instead, I shall present, in outline, a reasoned account of what I, as one member of the conference, consider to be the main points which have arisen. I shall consider, in turn, the facts, deductions from them about electron distributions, theories about the production of these distributions, and gaps in our knowledge and suggestions for future work.

## 1. THE FACTS

### 1.1 *Statistics of Occurrence in Different Parts of the World*

There are three major zones in which the temporal variation of the occurrence of sporadic  $E$  is markedly different. The *auroral zone* in which  $E_s$  is predominantly a night time phenomenon which shows little seasonal variation. A *middle latitude zone* in which  $E_s$  is predominantly a summer-time phenomenon, occurring both by day and by night, but more intensely by day. An *equatorial zone* in which  $E_s$  is a daytime phenomenon with little seasonal variation. Observations in both Europe and Australia seem to show that observers in middle latitudes find more  $E_s$  nearer the equator.

Although there is not a very strong correlation with magnetic disturbances, it seems clear that on disturbed days there is a likelihood that, in the auroral zone, more  $E_s$  will be present, and that in the middle latitude zone there will be less. There is no clearly established variation with the solar cycle, although there is some evidence to show that in winter there may be more in the decreasing phase than in the increasing.

### 1.2 *The Character of $E_s$ Echoes Observed at One Place*

The presence of  $E_s$  shows on the  $h'(f)$  trace in different ways, which have been classified by the World-Wide Sounding Committee as explained in the papers by Smith and Thomas. Although this classification is useful for correlating observations made all over the world as a routine, more detailed information about the echoes is needed before useful theories can be properly tested.

Surprisingly little is known about the reflection coefficient of  $E_s$  echoes.

This magnitude is determined partly by absorption below the level of reflection and partly by the process of reflection itself. It is not of much interest to know, for example, that  $E_s$  is stronger at night than by day, because presumably this difference results mainly from the ordinary diurnal change in the  $D$ -region absorption. A most significant quantity, if it were available, would be the ratio of the strengths of  $E_s$  echoes to the strengths of  $E$  or  $F$  echoes on the same or on neighbouring frequencies. This should not be difficult to determine, and it is to be hoped that more extensive measurements of it will be available before long.

As with the ordinary  $E$  and  $F$  echoes, it would be valuable to know the form of the function  $\rho(f, t, d)$  which describes how the reflection coefficient  $\rho$  depends on wave-frequency  $f$ , time  $t$  and distance between observing points  $d$  for small changes of these three quantities. Briggs and Chatterjee have investigated how  $\rho$  depends on  $f$  for a limited number of examples. It would be interesting to investigate the function  $\rho(f)$  for several different types of  $E_s$ , so that average curves were available for comparison with theory. In particular, not much is known about how the mean, smoothed value of  $\rho$  varies with frequency between the blanketing frequency  $f_b E_s$  and the end frequency  $f_o E_s$  of the type of  $E_s$  in which there is a large  $E$ - $F$  overlap. The fact that  $f_o E_s$  is not dependent on the sensitivity of the apparatus suggests that  $\rho$  decreases rapidly as  $f$  approaches  $f_o E_s$ . It appears that the difference  $f_o E_s - f_b E_s$  can change quite rapidly mainly through changes of  $f_b E_s$ .

Investigations of the fading at three close-spaced receivers have led to determination of the size and shape of the irregularities in the radio wave pattern at the ground. It is found, in general, to be such that its correlation function falls to 0.5 in the order of one or two wavelengths, just as for  $E$  and  $F$  echoes. The auroral type of  $E_s$  gives rise to a ground pattern which is somewhat anisotropic and in which the ellipses of constant correlation have an axis ratio of the order of 4 : 1 and are aligned with their major axes E-W. In the intermediate zone the pattern is statistically isotropic, while in the equatorial zone there is a marked anisotropy with axis ratio about 10 : 1, with the major axis along the N-S direction.

When  $E_s$  and  $F$  echoes are present simultaneously, there are occasions when the phase of the  $E_s$  echo is altering rapidly and by several multiples of  $2\pi$ , while that of the  $F$  echo shows no rapid variations comparable with  $2\pi$ . It would be useful to know whether the appearance of an  $E_s$  echo corresponds, on the average, to a change in the mean phase of an  $F$  echo detectable at the same time, but the information is difficult to obtain because the phase of any  $F$  echo always changes considerably in a time corresponding to the growth of an  $E_s$  echo.

Radio stars observed vertically, by day, when  $E_s$  echoes are present, do not scintillate, but when observed obliquely they often do.



### 1.3 *Spatial Distribution and Movement of $E_s$ Echoes*

$E_s$  echoes occur on the average in "patches" having extensions of the order of 200 km. When the echoes are observed at one place they last for a time which is very variable, but has a mean of the order of one hour.

It is not yet clear whether these patches move about much, or whether they grow and decay roughly in the same position. There is some evidence that they do *not* move much, on the average. Inside the patches small "clouds" of  $E_s$  are sometimes observed to pass overhead with a well-defined steady drift.

As with echoes from the  $E$ - and  $F$ -layers, the  $E_s$  echoes consist of an irregular pattern of amplitude on the ground, which alters randomly and also drifts with an average overall velocity. Ionospheric drift movements have been deduced from observations of this pattern at close-spaced receivers and, in the Arctic region, at times of ionosphere disturbance, the velocities have been as great as 1000 m/s. They most probably represent movements of electrons produced by electro-magnetic forces. It is worthy of note that auroral electrons have also been observed to move in the E-W direction with velocities of this order.

## 2. ELECTRON DISTRIBUTIONS

The first step in making deductions from the observations is to decide what distributions of electrons could produce the observed echoes. Since there are many types of echo, each with its own special characteristics, it would not be surprising if there were a corresponding number of electron distributions. The ones that have been suggested include:—

Horizontally irregular distributions	$\begin{cases} \Delta N/N \text{ small} \\ \Delta N/N \text{ large} \end{cases}$
Horizontally stratified distributions	$\begin{cases} \text{thin layers} \\ \text{sharp gradients} \end{cases}$

Horizontally irregular distributions, with  $\Delta N/N$  small, would be expected to produce comparatively weak partial reflections over a wide range of frequencies. It seems probable that they are the cause of the "meteoric"  $E_s$  of Naismith, the equatorial  $E_s$ , and the partially-reflecting type of auroral  $E_s$ . Slant auroral  $E_s$  could be produced by a horizontally irregular layer of this type situated a short distance below the level of reflection in the  $E$ -layer.

Horizontally irregular distributions, in which  $\Delta N/N$  was large, could be the cause of the type of  $E_s$  which shows "blanketing" up to a frequency  $f_b E_s$  and partial transparency between  $f_b E_s$  and a "top" frequency  $f_o E_s$ .  $f_b E_s$  would then correspond to the smallest electron densities and  $f_o E_s$  to

the greatest. It is desirable that reflection from this kind of distribution should be investigated more fully theoretically.

There seems to be little doubt that, on some occasions,  $E_s$  reflections are produced by horizontally stratified thin layers of electrons. The  $\rho(f)$  results of Briggs and Chatterjee demonstrate this by experiments on the ground, and the most common thickness seems to be about 5 km. On two occasions rockets have demonstrated the existence of thin layers of this kind. It has sometimes been said that measurements of  $M$ -type echoes can be used to measure the thickness of thin layers, but there has been no detailed discussion of how reflection can occur from different heights for the up-going and down-coming wave. A discussion on a full wave theory would be interesting.

The only evidence that sharp gradients of electron density, as distinct from thin layers, might be responsible comes from the results of rocket soundings. It appears, however, that spurious gradients might appear in the electron density profiles if the rocket traversed a region where there were marked inhomogeneities in the horizontal direction, so that this evidence is unreliable.

### 3. THE ULTIMATE CAUSES OF $E_s$

If the types of electron distribution responsible for  $E_s$  were known, it would next be necessary to consider how they could be produced. They might result from (a) redistribution of existing electrons or (b) changes in the rates of production or loss of electrons.

There is possibly a little evidence that thin layers of electrons are sometimes produced by vertical re-distribution, for it has been noticed that the shape of the remainder of the  $N(h)$  curve, determined on one occasion by vertical sounding, and on another by a rocket experiment, changed when a thin layer was formed.

It seems that the only type of force which could reasonably be expected to re-distribute electrons into a thin layer would be an electro-magnetic one, and would involve a loop of current which ought to be detectable by a magnetometer sent through the layer.

The recombination time (the "sluggishness" of Appleton) in the  $E$ -layer is known to be about 10 min, so that, if a thin layer were to be kept in being for one hour (the average duration of an  $E_s$  patch) the forces redistributing the electrons would have to continue for nearly the whole of that time.

A re-distribution of electrons to produce irregularities in the horizontal plane could be the result of turbulence. It has to be remembered, however, that recent work has shown that turbulence is insufficient to produce even the weaker irregularities in the normal  $E$ -region by simple compression and dilation. A vertical gradient of electron density is first required, so

that turbulent whirls can move denser and less dense parts up and down to produce the irregularities required. Enhancement of these irregularities to produce an  $E_s$  echo might result from an increased gradient, or increased turbulence, or both.

To account for large values of  $\Delta N/N$  in an irregular layer would require a steep gradient for the turbulent whirls to work upon. But a gradient of the necessary steepness would almost certainly be sufficient to produce an  $E_s$  echo by itself.

The electron distributions responsible for  $E_s$  echoes could be the result of modifications to the rates of production or loss of electrons. Direct increases of the production rate by incoming particles may well be the cause of the irregular ionization responsible for the "meteoric"  $E_s$ -layer and the auroral  $E_s$ . It is less likely to be responsible for the equatorial  $E_s$ , because of the difficulty which incoming charged particles experience in reaching the equator. It is difficult to see how smooth thin layers, having the extent of  $E_s$  patches, could be produced at any part of the earth by any incoming ionizing agency.

Patches of increased ionization, either smooth or irregular, could be produced by modifications of the atmosphere in one or other of the following ways.

The presence of a minor atmospheric constituent, more easily ionizable by the sun's radiation, could be responsible for extra ionization during the day. A similar constituent which modified the recombination rate could be effective either by day or by night. It has been suggested that minor constituents of these kinds might collect near a height of 100 km by the diffusion of matter from meteor trails.

Another mechanism by which extra electrons might be produced is through the transport upwards of some atmospheric constituent which carried stored energy, ready to be released in the production of free electrons. The most likely constituent of this kind appears to be negative ions. The precise mechanism for detaching the electrons has not been suggested, and it is difficult to see why it should be most efficient near 100 km.

The fact that the equatorial zone of  $E_s$  coincides approximately with the zone of the equatorial electrojet has suggested that the current in the electrojet might be directly responsible for the  $E_s$  ionization. Another suggestion might be that the ions in the electrojet experience a force which carries them up to a level where the electrons are, for some reason or other, more easily detached.

#### 4. FUTURE INVESTIGATIONS

When the IGY is over a mass of data will have been collected from routine ionospheric observatories. It is highly desirable that it should be

supplemented by some detailed *ad hoc* experiments made at a few key places. The most valuable observations would seem to be those made with powerful ionosondes having good resolution. The ratios of the amplitude of the  $E_s$  echo to the amplitude of the  $E$  and  $F$  echoes should be determined at one frequency, and the way in which the reflection coefficient of  $E_s$  varies with frequency should be examined. The fading of  $E_s$  should be studied at close-spaced receivers and analysed to show the size of the irregularities and their movements. Attention should be paid to observation and theory of  $M$ -type echoes. The lower frequency radiations from artificial satellites should be used to investigate the passage of waves through patches of  $E_s$ . Detailed  $N(h)$  curves should be computed to show the distribution of electron density in the  $E_s$ -layer and in the  $E$ -layer before, and after, the  $E_s$ -layer has formed. The growth and decay, and movement, of patches of  $E_s$  should be studied. Investigations should continue with rockets which, when possible, should carry magnetometers and mass spectrographs through the reflecting region. It is important that, when rockets are used, ionograms of the very highest quality should be simultaneously recorded.



# CHAPTER II

## Part A



# The Reflection Coefficient and Fading Characteristics of Signals Returned from the $E_s$ Layer at Ibadan

N. J. SKINNER

University College, Ibadan, Nigeria

R. W. WRIGHT

University College, Legon, Ghana

**Abstract**—Some of the characteristics of echoes from the two principal daytime types of  $E_s$  at Ibadan have been investigated by means of vertical incidence pulse transmissions in the frequency range 4 to 8 Mc/s. For the equatorial  $q$ -type  $E_s$  it is found that the fraction of the incident power reflected back varies with frequency  $f$  approximately as  $1/f^{0.4}$ . The fading rates are of the order of 4 c/s and increase almost linearly with wave frequency. Spaced receiver experiments indicate that the irregularities in the diffraction pattern on the ground are elongated along the geomagnetic field lines with scale sizes of about 20 metres and 300 metres in the east–west and north–south directions respectively. Blanketing  $E_s$  is observed only occasionally at Ibadan and it is found that its fading characteristics are very similar to those of the normal  $E$  layer with fading rates of about 0.8 c/s. The ground amplitude pattern has scale sizes of 60 metres and 500 metres transverse and parallel to the field lines respectively and the fading at midday is consistent with the picture that the irregularities in the ionosphere are moving westwards with a steady horizontal drift velocity of about 60 m/s superimposed upon a random velocity of 30 m/s. The amplitude distributions of the signals reflected or scattered from both types of  $E_s$  are predominantly of the Rayleigh type.

## 1. INTRODUCTION

Two principal types of  $E_s$  are observed during daylight hours at Ibadan, (1) the normal equatorial or “ $q$ ” type  $E_s$  and occasionally (2) an “ $h$ ” or “ $c$ ” type blanketing  $E_s$ . Equatorial  $E_s$  is observed only at stations in a narrow belt about  $7^\circ$  wide along the magnetic equator (Matsushita, 1951). The signal strength received at vertical incidence by scattering from this type of  $E_s$  is very strongly dependent upon the strength of the electrojet current flowing at  $E$ -layer heights in the ionosphere as is shown by the very close correlation between  $fE_s$  and the geomagnetic field components at the earth’s surface, both for large variations (Skinner and Wright, 1957) and for small variations (Bowles and Cohen, 1960). This type of  $E_s$  is almost completely transparent over the whole sounding frequency range and echoes are scattered from a constant altitude of about 100 km. In section (2) the results of some measurements of the partial reflection coefficient of equatorial type  $E_s$  in the frequency range 4–7.5 Mc/s are



presented and discussed. In sections (3) and (4) the fading characteristics and amplitude distribution of these reflections are discussed and from measurements made on spaced receiving aerials some deductions are made as to the size and shape of the amplitude pattern on the ground.

Blanketing  $E_s$  occurs much less frequently than the equatorial type at Ibadan and as yet its origin is not known. It usually lies above the equatorial  $E_s$  layer at an altitude of about 115–125 km. It shows group retardation near  $f_oE$  and it may be partially transparent at higher frequencies. The fading characteristics of reflections from this type of  $E_s$  are similar to those of the normal  $E$ -layer and completely different to those of “ $q$ ” type  $E_s$ . Some characteristics of this type of  $E_s$  are discussed in section 5. Recent work reported by Smith (1960) suggests that there is a narrow zone at the magnetic equator where the blanketing type of  $E_s$  is forbidden. In Nigeria, blanketing  $E_s$  is observed both at Ibadan (magnetic latitude  $3^\circ\text{S}$ ) and Maiduguri (magnetic latitude  $2^\circ\text{N}$ ) so that the forbidden zone, if it exists here, is less than  $5^\circ$  wide in latitude.

## 2. THE PARTIAL REFLECTION COEFFICIENT FOR EQUATORIAL TYPE $E_s$

### 2.1 *The Measurement of the Reflection Coefficient*

Midday measurements of ionospheric absorption at vertical incidence have been made at Ibadan since December 1953, using manually operated equipment of the type described by Piggott (1953). Briefly, this consists of a pulse transmitter of about 1 kW peak power, operating at a series of frequencies in the range 2–8 Mc/s, together with a stable receiver and associated display units. On a series of frequencies greater than the normal  $E$ -layer critical frequency  $f_oE$ , the amplitudes of the reflected signals from the  $E_s$  layer,  $A_E$ , and from the  $F$ -layer,  $A_F$ , are measured.

Then

$$A_E = \frac{A_o \rho_D r}{2h'E_s} \quad (2.1)$$

$$A_F = \frac{A_o \rho_D \rho_E \rho_F (1 - r^2)}{2h'F} \quad (2.2)$$

where  $r$  is the “effective” amplitude reflection coefficient of the  $E_s$  layer (assumed to be the same for rays incident from below or above), and  $\rho_D$ ,  $\rho_E$ ,  $\rho_F$  represents the absorption taking place in the double passage through the  $D$ ,  $E$ , and  $F$  layers.  $A_o$  is a constant depending upon the equipment power and frequency and  $h'E_s$ ,  $h'F$  are the virtual heights of the  $E_s$  and  $F$  layers.

In equation (2.1) no allowance is made for  $E$  layer absorption, an assumption which may be justified since  $E_s$  lies very near the bottom of the normal  $E$  layer.

From equations (2.1) and (2.2)

$$\frac{A_E}{A_F} \cdot \frac{h'E_s}{h'F} = \frac{r}{(1-r^2)} \frac{1}{\rho_E \rho_F} = R'E_s \quad (2.3)$$

Thus  $R'E_s$  can be found from the relative amplitudes and heights of the  $E_s$  and  $F$  layer echoes.

A more convenient parameter,  $RE_s$  would be one independent of  $\rho_E$  and  $\rho_F$ , for instance

$$RE_s = \frac{r}{(1-r^2)} = R'E_s \rho_E \rho_F \quad (2.4)$$

and since  $r$  is usually small,  $RE_s \approx r$ .

Reasonable estimates of  $\rho_E \rho_F$  can be made throughout the sunspot cycle from the normal absorption measurements so that values of  $R'E_s$  can be converted to corresponding values of  $RE_s$ .

## 2.2 Variation with Frequency of $RE_s$

The year of sunspot minimum, 1954, is particularly useful to study since absorption conditions were steady and reasonably confident estimates of  $RE_s$  can be made for frequencies of 4.0, 5.0, 5.8 and 6.5 Mc/s, each value being based on over 300 individual daily noon measurements. These four frequencies were chosen to avoid the critical frequencies of the  $E$ ,  $F_1$  and  $F_2$  layers by as wide a margin as possible.

Table 1—Mean values of  $RE_s$  on four frequencies for the year of sunspot minimum, 1954

Frequency Mc/s	4.0	5.0	5.8	6.5
$RE_s$	0.063	0.030	0.013	0.0072

Booker (1959) has shown that the ratio of the back-scattered power to the incident power is

$$\sigma_B \propto \exp \left[ -\frac{8\pi^2 L^2}{\lambda^2} \right] \quad (2.5)$$

for a Gaussian auto-correlation function of the irregularities, where  $L$  is the scale size of the irregularities along the direction of sounding and  $\lambda$  is the wavelength. For some other auto-correlation functions Booker shows that

$$\sigma_B \propto \left[ 1 + \left( \frac{4\pi L}{\lambda} \right)^2 \right]^{-n/2} \quad (2.6)$$

where  $n$  takes values of 4, 5, or 6. In these cases when  $4\pi L/\lambda$  is large the formula becomes  $\sigma_B \propto \lambda^n$ .

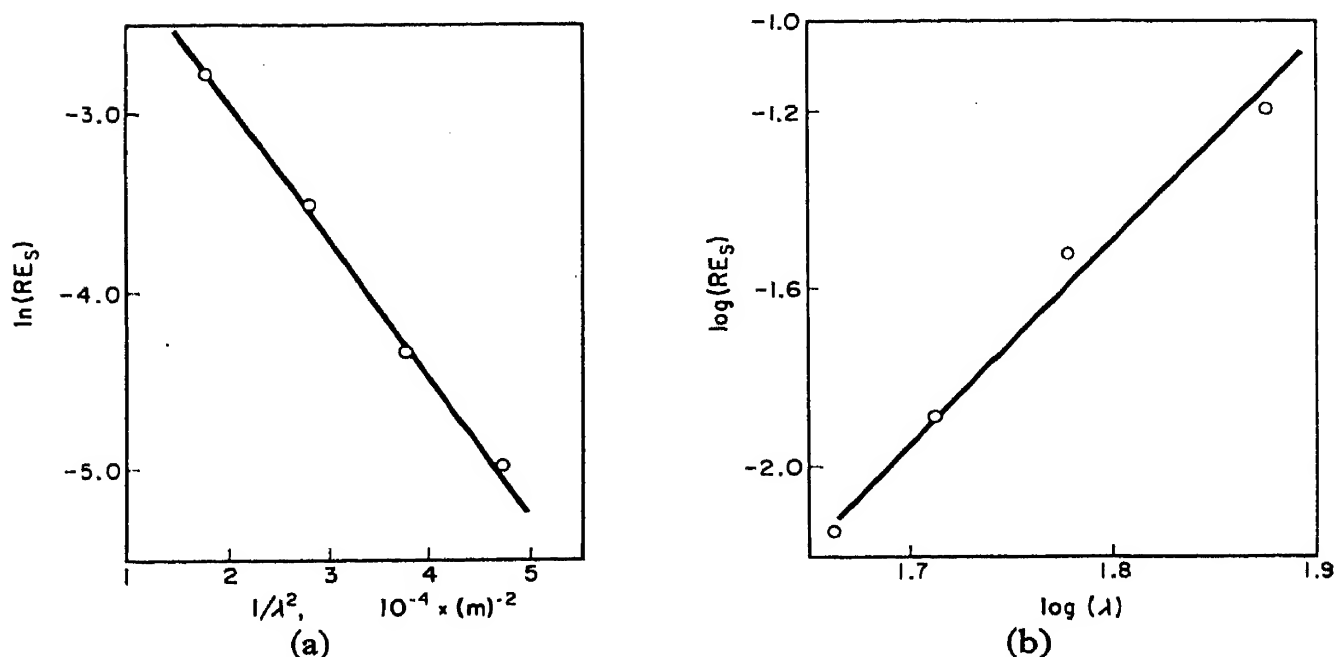


Fig. 1. The mean dependence of the partial reflection coefficient of  $q$ -type  $E_s$  on frequency at midday in 1954.

Figure 1(a) shows that a graph of  $\ln(RE_s)$  against  $1/\lambda^2$  is a reasonable straight line whose slope from equation (2.5) gives a value for  $L$  of 14 metres. Figure 1(b) shows that a graph of  $\log(RE_s)$  against  $\log(\lambda)$  is also fairly linear and gives a value for  $n$  in equation (2.6) of about 9.4. This is rather larger than the values deduced using the auto-correlation functions discussed by Booker. This value of  $n$  may be compared to the results obtained by other workers for scattering from  $E_s$ . Booker (1959) quotes measurements on oblique transmissions at frequencies of 30 to 100 Mc/s which gave a value of  $n$  equal to 18. Davis, Smith and Ellyett (1959) obtained values of  $n$  in the range zero to 27 also on oblique paths. Since, however, allowance must be made for the oblique trajectory and for the fact that these other observations were not on equatorial type  $E_s$ , no real comparison can be made.

A possible source of error in our experiments arises from the fact that the same rhombic transmitting aerial is used for all frequencies. The width of the main vertical lobe will vary with frequency so that oblique scattering from irregularities not directly overhead will contribute unequally at different sounding frequencies. We do not consider however that oblique scattering seriously affects the peak amplitude of the signal as measured at the lowest virtual height.

### 3. FADING OF PARTIAL REFLECTIONS FROM EQUATORIAL 'TYPE $E_s$

#### 3.1

Fading records of signals from  $q$ -type  $E_s$  have been taken over a range of frequencies using both single and spaced receiving aerials. By using a

recording film speed of about 2.6 cm/sec, it is possible to measure the amplitude of each reflected pulse so that with a single aerial amplitude measurements can be made every .02 sec, and with three spaced aerals measurements can be made at every .06 sec, on each trace.

The variation of amplitude with time has been investigated in three ways:

(a) by counting the number of maxima,  $N$ , per sec. The fading period  $T_2$  is then  $1/N$ .

(b) by calculating the "speed of fading"  $S$  from

$$S = \left| \frac{dR}{dt} \right| / R \quad (3.1)$$

where  $R$  is the instantaneous amplitude of the received signal.

(c) by computing the auto-correlation function of the fading.

### 3.2 The Number of Maxima/sec $N$

The fading rate of echoes from equatorial  $E_s$  is very much more rapid than that for the types of  $E_s$  experienced in temperate latitudes. Fading rates in the range 2–5 per sec are normally experienced at Ibadan, the fading rate increasing almost linearly with increasing wave frequency. This is illustrated by Fig. 2 in which the number of peaks/sec,  $N$ , is plotted against wave frequency for two typical days at about noon.

### 3.3 Speed of Fading $S$

The speed of fading  $S$  has been calculated using equation (3.1) above and Fig. 3 shows again that the fading speed  $S$  increases almost linearly with increasing wave frequency.

It can be shown from the statistical work of Rice (1945), Ratcliffe (1948) and McNicol (1949) that

$$\frac{S}{N} = 1.6 \text{ approximately} \quad (3.2)$$

Table 2 shows measured values of  $S$ ,  $N$  and  $\frac{S}{N}$  on a typical day and it is seen that the relationship (7) is obeyed approximately by the  $E_s$  fading.

### 3.4 The Auto-correlation Function of Fading

For a signal of amplitude  $R(t)$  the auto-correlogram of  $R(t)$  is defined by

$$\rho_R(\tau) = \frac{\overline{R(t) \cdot R(t + \tau)} - (\overline{R(t)})^2}{\overline{R^2(t)} - (\overline{R(t)})^2} \quad (3.3)$$

When this function is Gaussian in form

$$\rho_R(\tau) = e^{-\tau^2/2b^2} \quad (3.4)$$

Table 2.

$\lambda$	Frequency in Mc/s	$S$	$N$	$\frac{S}{N}$
70 m	4.3	4.6/sec	2.45/sec	1.88
61 m	4.9	5.2/sec	2.95/sec	1.76
53 m	5.7	5.43/sec	3.35/sec	1.68
46 m	6.5	7.41/sec	4.17/sec	1.78
40 m	7.5	9.4/sec	4.6/sec	2.04
35 m	8.5	11.6/sec	5.2/sec	2.23

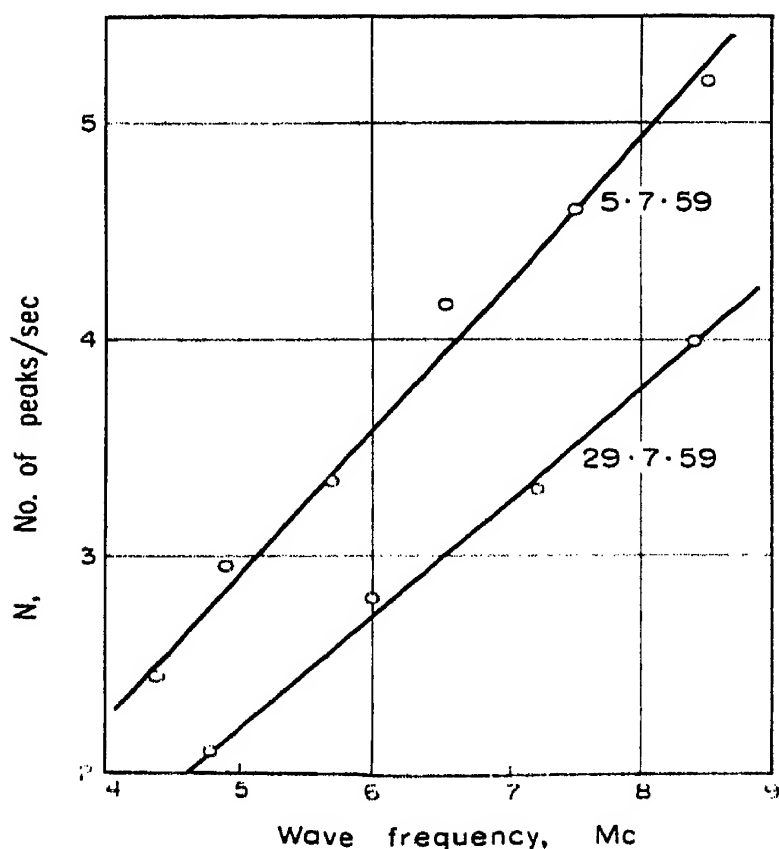


Fig. 2. The variation of fading speed (as measured by the number of peaks/sec) with frequency at noon on 5th July 1959 and 29th July 1959.

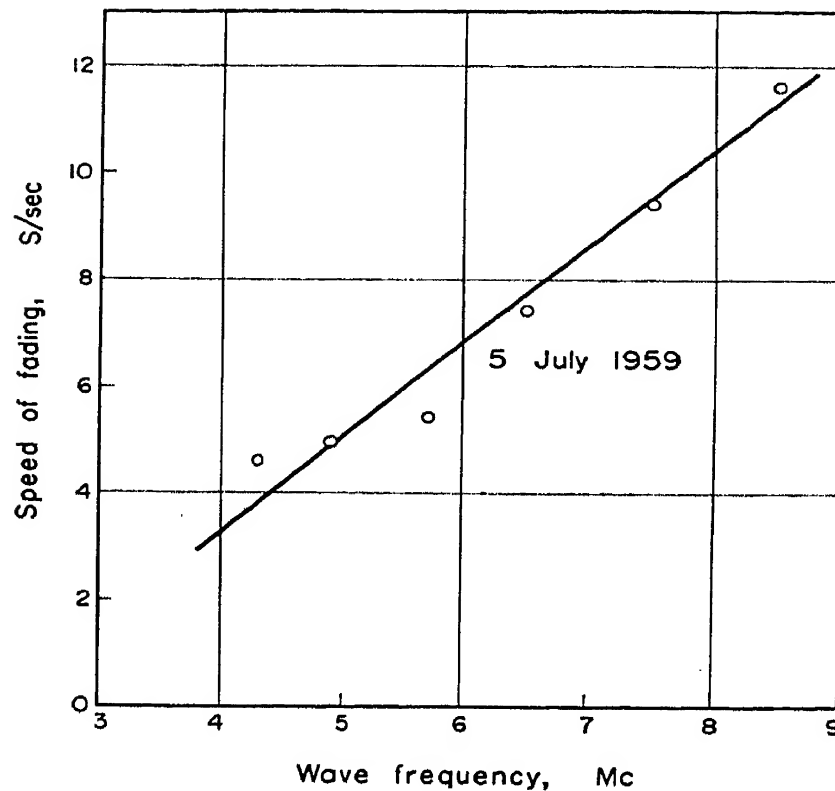


Fig. 3. The variation of the speed of fading,  $S$ , with frequency on 5th July 1959.

where  $b$  is the time displacement for which  $\rho_R(\tau) = 0.61$  and if  $R(t)$  has a Rayleigh probability distribution

$$\frac{1}{N} = 3.52b \quad (3.5)$$

Values of  $b$  have been calculated from equation (a) from auto-correlograms for signals received on 4.8, 6.0, and 7.2 Mc/s. From these values of  $b$ , equation (10) is used to calculate a value of  $N$ . Table 3 shows a direct comparison of these calculated values with those actually measured directly from the fading records.

Table 3.

$f$ (Mc/s)	Wavelength (m)	$N$ calculated	$N$ measured	North-South correlation at 180 m separation
4.8	62	2.3	2.2	0.86
6.0	50	4.4	3.6	0.70
7.2	42	5.4	3.9	0.56

### 3.5 Spaced Aerial Measurements

Simultaneous fading records have been taken using three receiving aerials spaced at the corners of the right angled triangle whose hypotenuse is in the North–South direction. The sides of the triangle are 180 m, 127 m and 127 m and the equipment is that normally used for the measurement of horizontal drifts. The transmitted pulse repetition frequency is 50 c/s so that with the aerial switching system used, pulses are received on each aerial at intervals of 0.06 sec, and the amplitude of each received pulse can be measured directly from the film record. Some of these fading records have been subjected to a full correlation analysis, a typical example of which is given in Fig. 4. This shows the mean auto-correlation function for  $E_s$  fading at a single aerial (curve I) together with the cross-correlation functions for fading at the North–South aeralis, the North–West aeralis and the South–West aeralis (curves II, III and IV respectively). There is seen to be a high cross correlation of 0.75 at zero time delay for the North–South pair of aeralis but very low correlation at all time delays for the other pairs of aeralis.

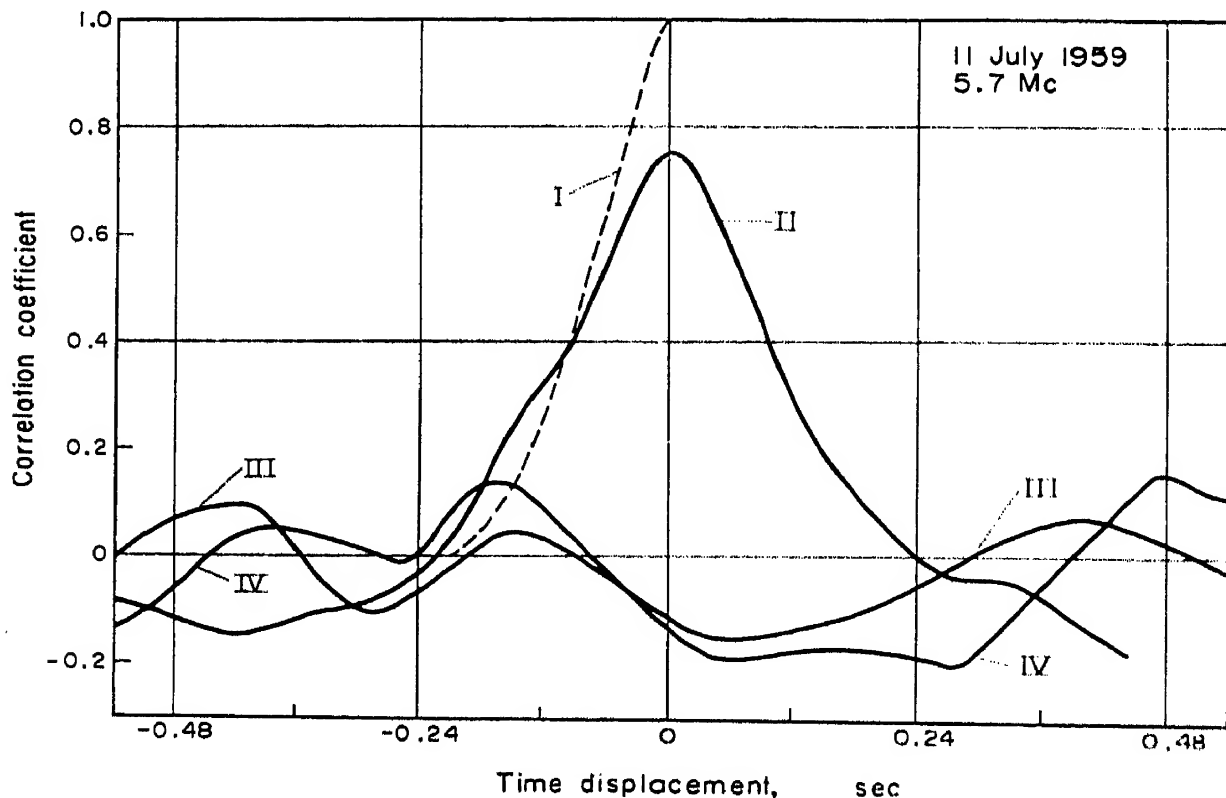


Fig. 4. Curve I—The mean auto-correlation function for fading at 3 spaced aeralis.

Curve II—The cross correlation function for fading at the north and south aeralis.

Curves III and IV—The cross-correlation functions for fading at the north and west aeralis and at the south and west aeralis respectively.

Considering the above example further, if the amplitude pattern on the ground is represented by an auto-correlation ellipse (Phillips and Spencer, 1955), the "size" of the pattern, defined as the distance for which the auto-correlation drops to 0.5, is about 20 metres in an east-west direction and about 350 metres in a north-south direction for a frequency of 5.7 Mc/s. The correlation in a north-south line decreases almost linearly with decreasing radio wavelength as shown by the last column of Table 3, so that, as would be expected, the "size" of the diffraction pattern is roughly proportional to the wavelength. Because of the relatively large wavelength used, no deductions about the "size" of the irregularities in the ionosphere can be made from the size of the diffraction pattern on the ground, although the E-W size deduced here for the amplitude pattern on the ground is of the same order as that deduced in section 2.2 above for the vertical dimension of scattering centres in the ionosphere.

The highly elliptical shape of the amplitude patterns on the ground suggests that the irregularities responsible for  $E_s$  fading are elongated along the geomagnetic field lines. We have previously observed similar effects (Skinner, Hope and Wright, 1958) with fading from normal  $E$  and  $F$  layer reflections and Egan (1959), using backscatter equipment at Huancayo, has also obtained evidence of field-aligned irregularities in the equatorial  $E_s$  region. It has recently been pointed out by Bowles, *et al.* (1960) that these results may also be interpreted in terms of a rather different model for the ionospheric irregularities. They suggest, with convincing experimental evidence, that the irregularities consist of a family of plane wavefronts (perhaps longitudinal hydromagnetic waves of electron density), whose wave normals are distributed in a plane normal to the geomagnetic field lines.

#### 4. AMPLITUDE DISTRIBUTION

##### 4.1 *The Theory of Amplitude Analysis*

An examination of the amplitude distribution of the received signals from  $E_s$  is helpful in determining the exact process by which "reflection" takes place. If the downcoming wave consists of a large number of scattered waves with phase paths differing from one another by random fractions of a wavelength the probability distribution of the resultant amplitude  $R$  will be given by the Rayleigh distribution

$$p(R) = \frac{R}{\psi} \exp\left(\frac{-R^2}{2\psi}\right)$$



where  $\psi$  is a parameter related to the average value  $\bar{R}$  by the expression

$$\bar{R} = \left( \frac{\pi\psi}{2} \right)^{1/2}$$

If, in addition, there is a steady component in the received signal due to specular reflection in the ionosphere, the probability distribution of the resultant amplitude  $Q$  is

$$p(Q) = \frac{Q}{\psi} \exp\left(-\frac{Q^2 + B^2}{2\psi}\right) I_0\left(\frac{QB}{\psi}\right)$$

where  $B$  is the amplitude of the steady signal and  $I_0$  is the Bessel function of zero order and imaginary argument.

The above expressions have been given by McNicol (1949) following the work of Rice (1945). McNicol has given a series of curves showing the amplitude distribution for various values of a parameter  $d$  which is a measure of the signal-to-noise ratio and is defined as

$$d = B/(\phi^{1/2})$$

and when  $d < 1$ ,  $p(Q)$  is approximately a Rayleigh distribution and for  $d > 3$  the distribution is almost purely Gaussian. Thus an analysis of the amplitude distribution of the signals received from  $E_s$  allows an estimate of the ratio of scattered to specularly reflected signal to be made.

## 4.2 Experimental Results

Fading records of signals received from  $q$ -type  $E_s$  in the frequency range 4.3–8.5 Mc/s have been analysed by plotting the amplitude distribution curves and comparing them with the series given by McNicol (1949). It is found that, for the higher frequencies in this range, the returned signal is almost entirely random phased with a Rayleigh amplitude distribution, whereas at the lower frequencies near 4.5 Mc/s there is often a considerable component due to specular reflection. This is illustrated in Figs. 5a and 5b which show typical amplitude distributions at radio frequencies of 4.3 and 8.5 Mc/s respectively. In Fig. 5a the experimental values (shown as circled points) are compared with the broken curve which represents the Rice–McNicol function for  $d = 2$  and it appears that there is a considerable specular component in the reflected signal. On the other hand at 8.5 Mc/s, Fig. 5b shows that a theoretical Rayleigh distribution fits the experimental measurements very closely.

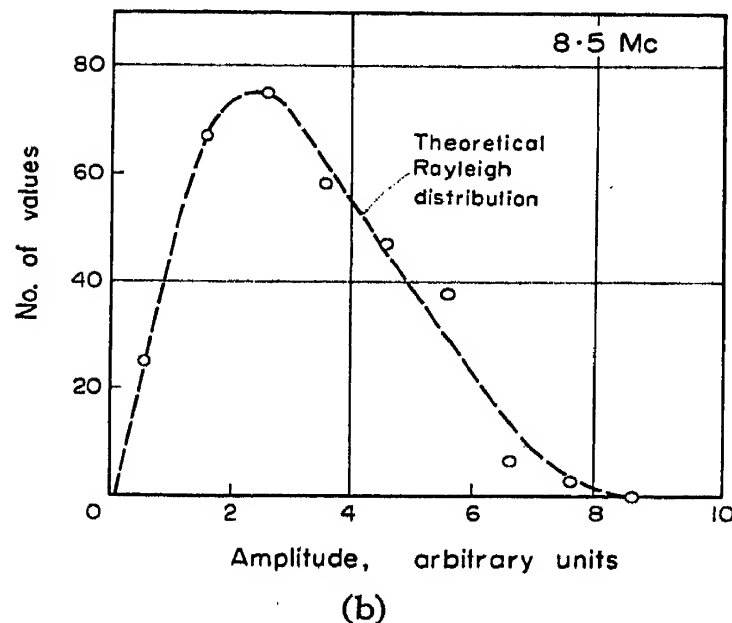
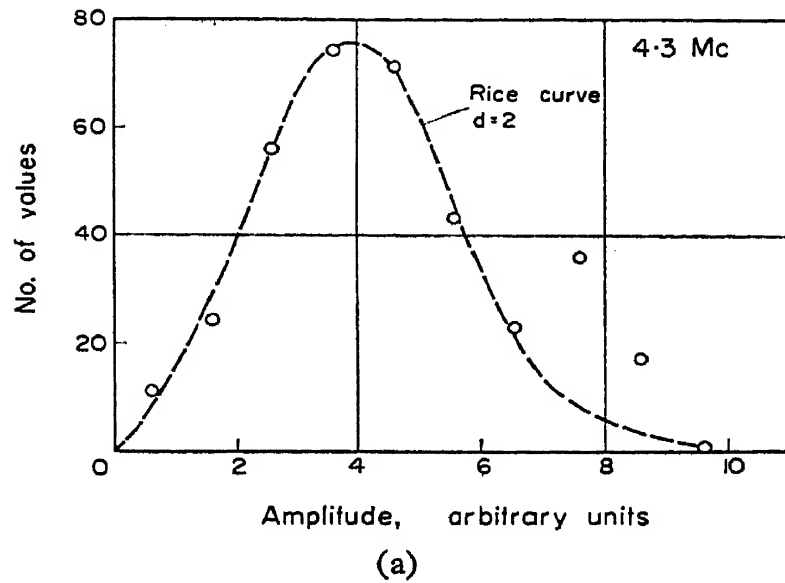


Fig. 5. (a.) The amplitude distribution at a frequency of 4.3 Mc/s. The circled points are experimental values and the broken curve shows the Rice-McNicol function  $d = 2$ . (b.) The amplitude distribution at a frequency of 8.5 Mc/s. The broken curve shows a theoretical Rayleigh distribution.

## 5. FADING CHARACTERISTICS OF ECHOES FROM BLANKETING TYPE $E_s$

### 5.1 Fading Rate

Blanketing type  $E_s$  echoes occur at Ibadan at midday on average about once per month. The fading rate of these signals is noticeably smaller than that of equatorial type  $E_s$  and to demonstrate this, values of  $N$  have been calculated from the auto-correlation function using equation (3.5). Mean values of  $N = 0.74$  per sec at 5.7 Mc/s and  $N = 0.81$  per sec at 7.5 Mc/s were obtained from six separate occurrences of blanketing  $E_s$ .

compared to values of between 3 and 5 per sec for the same frequencies with equatorial type  $E_s$ . The fading rate for blanketing  $E_s$  is thus about five times slower than that for  $q$ -type  $E_s$ .

### 5.2 *Spaced Aerial Measurements*

Fading records have also been taken on echoes from blanketing  $E_s$  using the spaced receiving aerial system and once again it is found that the irregularities in the ground amplitude pattern are strongly field aligned. It is usually possible to measure the east-west drift component from these records by using the full correlation analysis of Phillips and Spencer (1955) and twelve such records have been analysed in full. It is found from this analysis that the fading of the signal at midday is due to a combination of a steady westward drift velocity of about 60 metres per sec together with a random velocity ( $V_c$ ) of movement of the irregularities of about 30 metres per sec. The characteristic "size" of the diffraction pattern irregularities on the ground in an east-west direction is about 60 metres, which is similar to the pattern size for reflections from the normal  $E$ -layer and about three times greater than that for  $q$ -type  $E_s$ . The "size" in a north-south direction is of the order of 500 metres.

### 5.3 *Amplitude Distribution*

An analysis of several fading records from blanketing  $E_s$  shows that the amplitude distribution is of the Rayleigh type. The records analysed have been for frequencies of 5.7 and 7.5 Mc/s only and there is little evidence for the presence of a specularly reflected component at these frequencies. However, with blanketing  $E_s$  the transparent equatorial type is invariably present also and it is likely that some of the fading is due to the double passage of the reflected wave through the  $q$ -type  $E_s$ .

## 6. CONCLUSIONS

Our experimental findings may be summarized as follows.

### 6.1 *Equatorial Type $E_s$*

(a) The ratio of power scattered back through  $180^\circ$  to the incident power is proportional to  $f^{9.4}$  in frequency range 4 to 6.5 Mc/s and the scale size of the irregularities in the direction of sounding is about 14 metres.

(b) In this frequency range, fading rates of about 4 cycles per sec are experienced, and it is found that the fading rate increases almost linearly with increasing wave frequency.

(c) The irregularities in the amplitude pattern on the ground are highly elongated along the magnetic field lines. The scale "size" of the ground

pattern is about 20 metres in an east-west direction and about 300 metres in a north-south direction.

(d) The amplitude distribution of the scattered signal is of the Rayleigh type at the higher frequencies but there is some evidence for the presence of a considerable specular component at the lower frequencies.

## 6.2 Blanketing Type $E_s$

(a) Fading rates are much smaller than those for  $q$ -type  $E_s$  and are of the order 0.8 cycles per sec.

(b) The amplitude pattern on the ground is similar to that obtained with reflections from the normal  $E$ -layer, i.e. the scale size is about 60 metres in an east-west direction and about 500 metres in a north-south direction.

(c) The fading of the signal at midday is due to a steady westward drift velocity of about 60 metres per sec superimposed upon a random velocity of movement of the irregularities of about 30 metres per sec.

(d) The amplitude distribution is mainly of the Rayleigh type.

## REFERENCES

- BOOKER, H. G. (1959) *J. Geophys. Res.* **64**, 2164.  
BOWLES, K. L., and COHEN, R. (1960) *J. Geophys. Res.* **65**, 2476.  
BOWLES, K. L., COHEN, R., OCHS, G. R. and BALSLEY, B. B. (1960) *J. Geophys. Res.* **65**, 1853.  
DAVIS, R. M., SMITH, E. K. and ELLYETT, C. D. (1959) *Proc. Inst. Radio. Engrs.* **47**, 767.  
EGAN, R. D. (1960) *J. Geophys. Res.* **65**, 2343.  
MATSUSHITA, S. (1951) *J. Geomag. Geoelec. Kyoto* **3**, 44.  
McNICOL, R. W. E. (1949) *Proc. Inst. Elec. Eng.* **III** **96**, 517.  
PHILLIPS, G. J. and SPENCER, M. (1955) *Proc. Phys. Soc. B*, **68**, 481.  
PIGGOTT, W. R. (1953) *Proc. Inst. Elec. Eng.* **III** **100**, 61.  
RATCLIFFE, J. A. (1948) *Nature* **162**, 9.  
RICE, S. O. (1945) *Bell Syst. Tech. J.* **23**, 317 and **24**, 73.  
SKINNER, N. J., HOPE, J. and WRIGHT, R. W. (1958) *Nature*, **182**, 1363.  
SKINNER, N. J. and WRIGHT, R. W. (1957) *Proc. Phys. Soc. B*, **70**, 833.  
SMITH, E. K. (1960) *XIII Gen. Assembly, URSI. London.*



# A Study of Radio Wave Scattering from Sporadic *E* near the Magnetic Equator

KENNETH L. BOWLES and ROBERT COHEN

Central Radio Propagation Laboratory, National Bureau of Standards, Boulder, Colorado, U.S.A.

**Abstract**—Sporadic-*E* irregularities in the equatorial ionosphere have been simultaneously studied with an ionosonde located at Huancayo, Peru and by means of radio-wave scattering at 50 Mc/s. The latitude dependence of oblique scattering has been observed over paths in the vicinity of the magnetic equator. A close relationship has been established between the strength of the scattering irregularities associated with equatorial sporadic *E* and the intensity of the equatorial electrojet current. Radar studies at Huancayo suggest that the equatorial sporadic *E* irregularities in the electrojet are plane wave fronts parallel to the earth's magnetic lines of force. On this model, the wave normals to these planar irregularities are distributed at various angles in a surface normal to the magnetic field lines, and the planes move westward at velocities which are a function of these inclination angles. The slanted trace heretofore described as "equatorial slant sporadic *E*" is demonstrated to be a configuration arising from echoes in the east-west plane from the equatorial sporadic *E*-layer.

## 1. THE IGY EXPERIMENT

### *Background*

In order to study the behavior of v.h.f. ionospheric scattering in the vicinity of the magnetic equator, oblique scatter paths were established in South America during the International Geophysical Year. There was considerable interest, in designing these experiments, in the extension of knowledge regarding scattering effects in the ionospheric *D*-region to include the equatorial zone, and it was realized that the oblique scatter technique could provide useful information about many of the phenomena in the equatorial ionosphere due to electron density irregularities in the *E* and *F*-layers. (The terms "equator" or "equatorial" are understood in this paper to refer to the vicinity of the magnetic equator.)

One of these irregularity-phenomena is equatorial sporadic *E*. This is a daytime configuration (Fig. 1) on equatorial ionograms, such as those obtained in Huancayo, Peru (12°3'S, 75°20'W). The triangular configuration at *E*-region heights on this ionogram includes strong but not blanketing reflections at the 100 km level, and a slanted region where scattered echoes are being received at ranges increasing with frequency. These portions of the ionogram are defined as "Equatorial sporadic *E*" or "*E*<sub>s</sub>-q", and

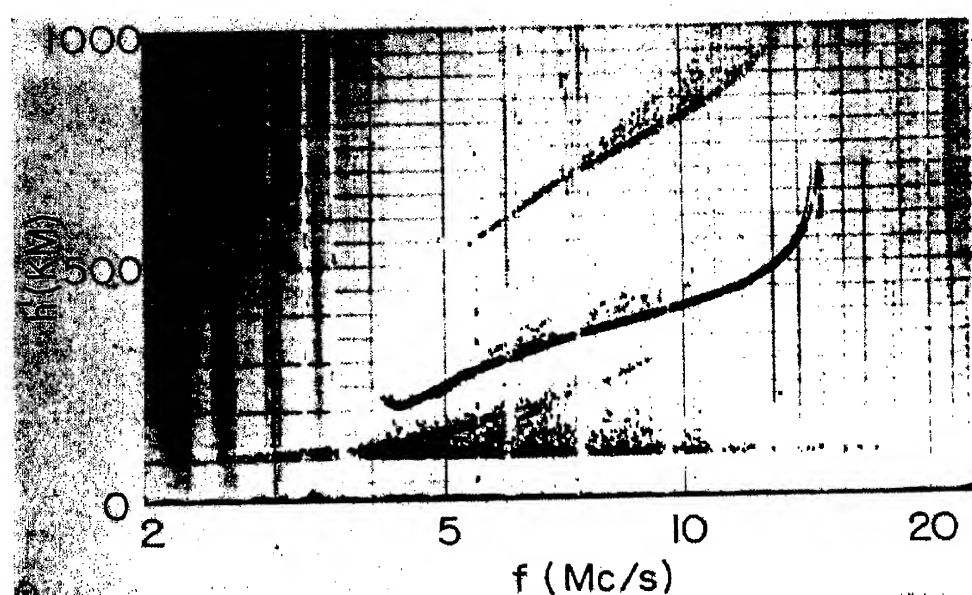


Fig. 1. The configuration of "Equatorial sporadic  $E$ " and "Equatorial slant sporadic  $E$ " observed at Huancayo, Peru at 1229 EST, 19 April 1960.

"Equatorial slant sporadic  $E$ " or " $E_s$ -s", respectively, and they usually occur simultaneously. The wedge-shaped configuration of scattered echoes bounded by these phenomena appears with them and has not been assigned an official designation.

The "critical frequency" of the equatorial sporadic  $E$ , or the highest frequency to which it extends on ionograms, has been utilized heretofore as a parameter characterizing the intensity of this scatter phenomenon. The daytime current stream known as the "equatorial electrojet" flows along the magnetic equator at the 100 km level, and an association has been noted (Matsushita 1951) between the variations in this current and those of the "critical frequency" of the  $E_s$ - $q$ . (The strength of ionospheric current systems of this sort is usually deduced from an interpretation of magnetograms obtained at points on the earth's surface situated beneath the current system under observation.)

### Instrumentation

The deployment of transmitting and receiving stations used in these experiments is shown in Fig. 2, together with the magnetic isoclines. Figure 3 is a schematic diagram of various antenna beam intersections in the vertical plane. Three of these scatter paths among those illustrated were for studies of radio wave scattering in the  $E$ -region of the equatorial ionosphere. These studies were conducted by means of transmissions from Arequipa, Peru ( $16^{\circ}44'S$ ,  $71^{\circ}53'W$ ) to Trujillo, Peru ( $8^{\circ}6'S$ ,  $79^{\circ}5'W$ ), from Antofagasta, Chile ( $23^{\circ}44'S$ ,  $70^{\circ}15'W$ ) to Huancayo, Peru, and from Huancayo to Guayaquil, Ecuador ( $2^{\circ}36'S$ ,  $80^{\circ}24'W$ ). These paths are henceforth referred to as the "basic", "southern" and "northern" paths, respectively.

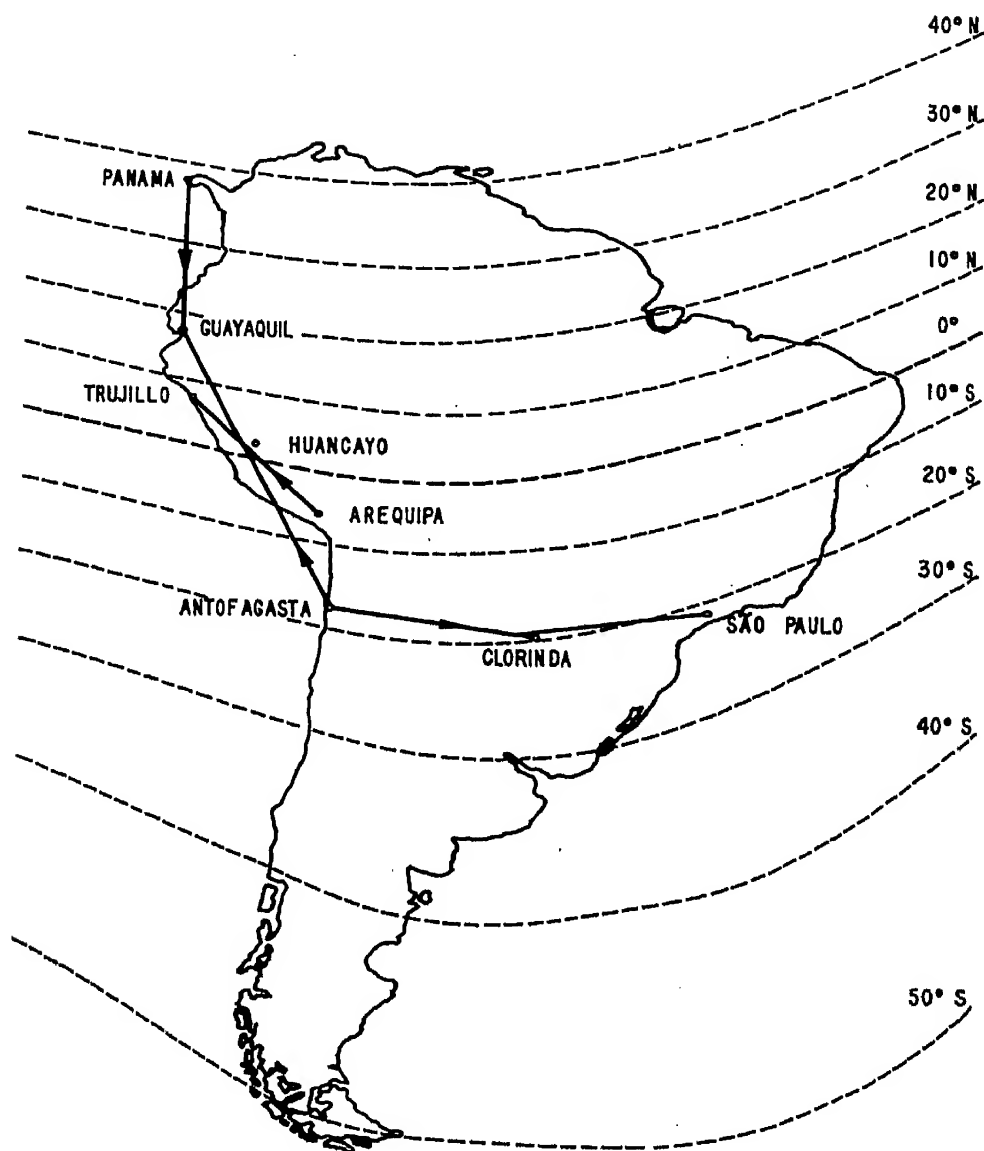


Fig. 2. The deployment of IGY forward scatter stations in South America relative to the magnetic isoclines.

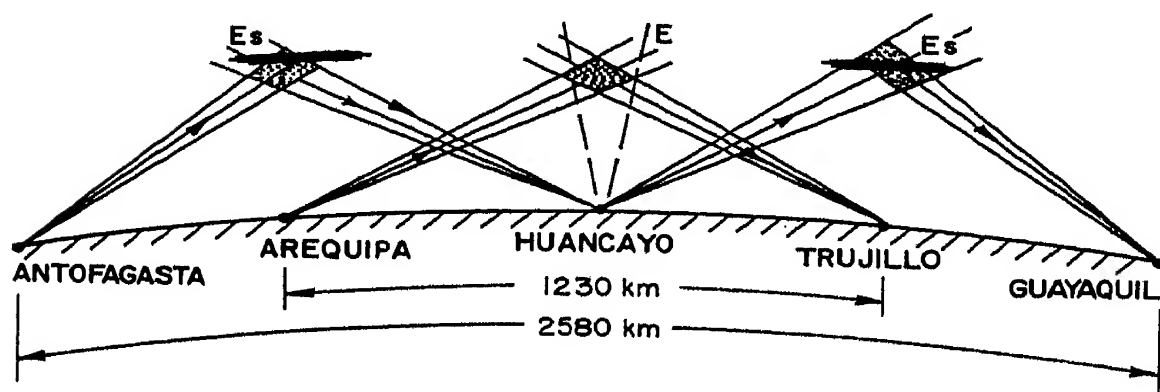


Fig. 3. Schematic diagram of the vertical cross-sections of antenna beam intersections along the west coast of South America, indicating the propagation paths referred to in this paper. (This figure does not preserve angles.)



A description of the design and instrumentation of these experiments has been published (Bowles and Cohen 1957). Research regarding ionospheric scattering in the equatorial  $F$ -region has been reported separately (Cohen and Bowles 1961).

The technique used in the oblique scatter experiments was to transmit a steady "continuous wave" (CW) signal and to monitor the variation in amplitude of the signal received at a certain distance from the transmitter, usually about 1300 km. The transmitting and receiving antennas were designed, as in previous experiments of this kind (Bailey, Bateman and Kirby 1955) so as to intersect in the 80 km region. Thus, the temporal variations of the received signal could be related to changes in the propagating medium within the ionospheric volume defined by the antenna beam intersection. Some idea as to the extent of this volume for the several paths can be gleaned from Fig. 4, which is a diagram of cross-sections

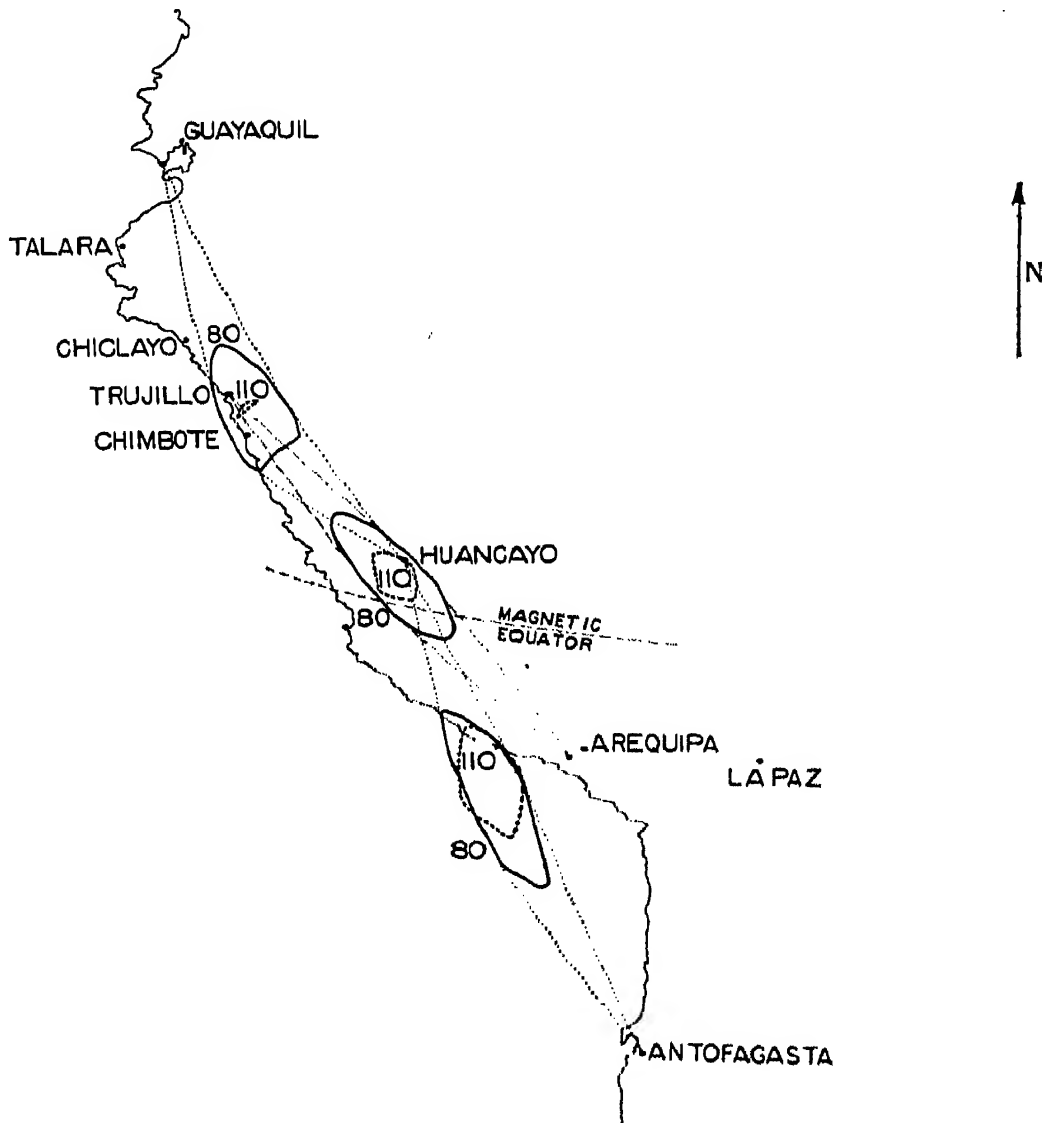


Fig. 4. The approximate loci of antenna beam intersections computed for the height (in kilometers) adjacent to each locus for the portions of ionosphere observed on the three propagation paths. (Talara, Chiclayo, Chimbote and La Paz are the locations of other ionosondes.)

obtained by passing horizontal surfaces through the antenna-beam intersections. The contours are the loci of points in the product antenna pattern that are 20 db weaker than the maximum "product-beam" sensitivity. The ionospheric regions under observation are centered at magnetic dips of about  $8^{\circ}\text{N}$ ,  $1^{\circ}\text{N}$ , and  $8^{\circ}\text{S}$ , and are concentrated around 85 km in height, with an upper cutoff height or "ceiling" of about 120 km. This latitudinal separation of the ionospheric regions being studied enabled some delimitation of the extent of the equatorial scattering effects and provided some idea as to the symmetry about the magnetic equator of the electron-irregularity strength.

The basic scatter path, as well as the other two paths referred to above, were almost identical in length and instrumentation to similar forward scatter circuits studied earlier (Bailey, Bateman and Kirby 1955) in temperate and arctic latitudes. (The transmitters were operated at frequencies near 50 Mc/s with about 3 kilowatts of power, and rhombic antennas were employed for both transmission and reception.)

### *Signal Intensities*

The strength of the forward scatter signals obtained over these three paths in the equatorial region was considerably greater than that observed and utilized for communications in temperate latitudes. On the basic path, the minimum signal during most 24 hour periods was comparable to the maximum diurnal signal (usually attained at noon) observed in temperate latitudes. It was soon apparent that the scattering in the equatorial ionosphere was usually arising from effects at heights in the ionosphere greater than the 85 km heights associated with the familiar turbulent scatter in temperate latitudes. However, at times when there was an appreciable weakening of the normally predominant equatorial scatter signals, the underlying signals scattered from the 85 km turbulent region were detectable.

The observation that strong scatter propagation (which is established in this paper as due in the daytime to equatorial sporadic *E*) is supported by the *E*-region of the equatorial ionosphere suggests that a great natural resource for communications is potentially available to nations located in equatorial zones. This propagation is, however, usually characterized by fading rates higher than those observed for ionospheric scattering in temperate latitudes.

### *Correlation with the Equatorial Electrojet*

A close relationship has frequently been noted during these oblique experiments between: (a) the magnetic manifestations of the equatorial electrojet current above Huancayo; (b) the occurrence on Huancayo ionograms of equatorial sporadic *E*; and (c) the intensity of scatter-propagated

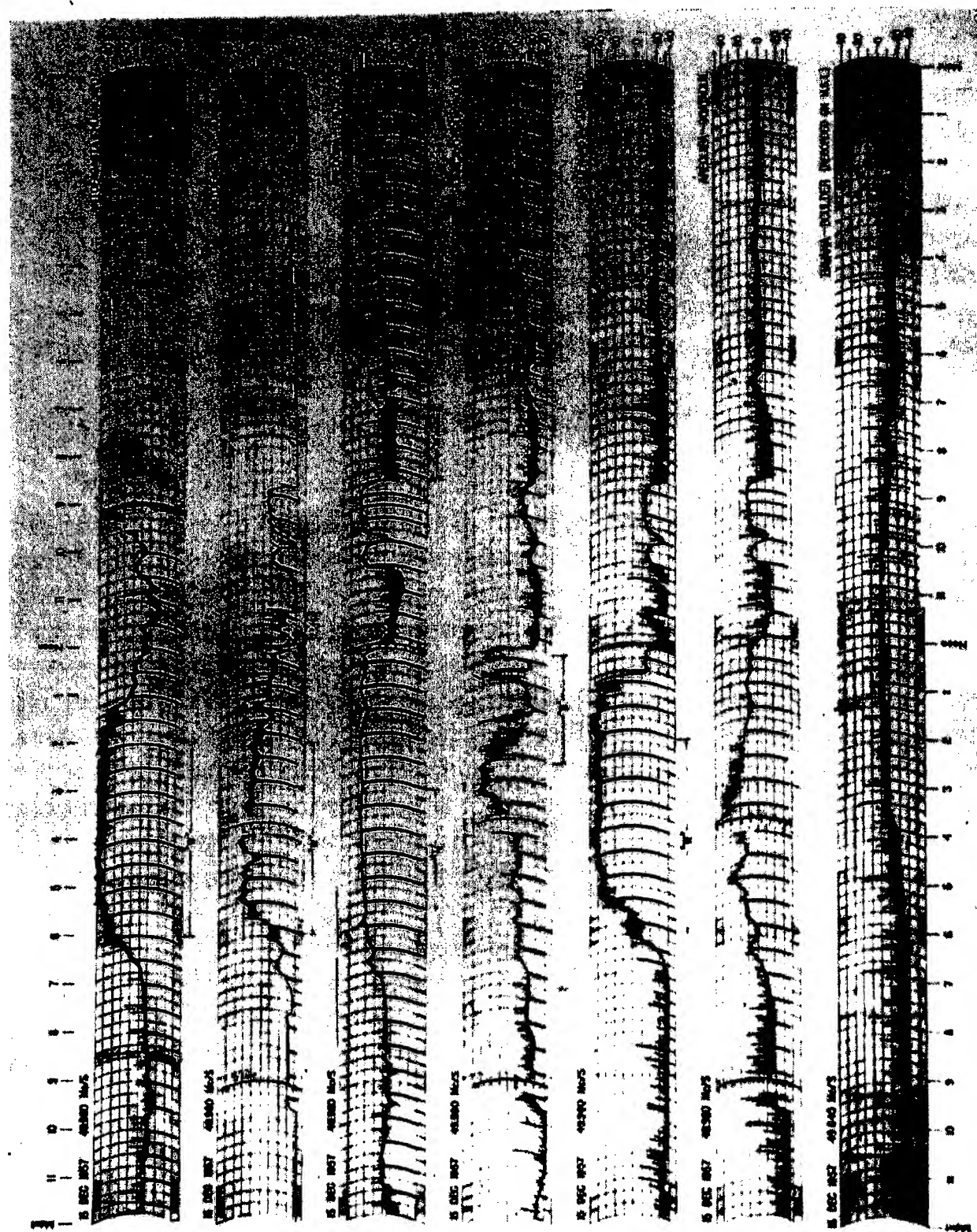


Fig. 5. A comparison of signal strength records over six South American scatter circuits on 15 December 1957, along with the record for similar transmissions from Havana, Illinois to Boulder, Colorado.

50 Mc/s signals. This correlation has been observed on all three paths under discussion here, indicating that the zone of *E*-region scattering effects associated with the equatorial electrojet extends at least  $5^\circ$  of latitude north and south of the magnetic equator.

Figure 5 consists of records for certain IGY scatter circuits during a representative 24 hour period, with the Havana, Illinois  $\rightarrow$  Boulder, Colorado signal variation shown for comparison. On this date a simultaneous modulation of all the equatorial scatter signals occurred from 0900 to 1100 hours, and it correlated well with the variations of the horizontal component of the earth's magnetic field as observed at Huancayo. The signal strength on the basic scatter path for a daytime period is compared with the magnetic field strength in Fig. 6. These correlations are discussed further in Part 2.

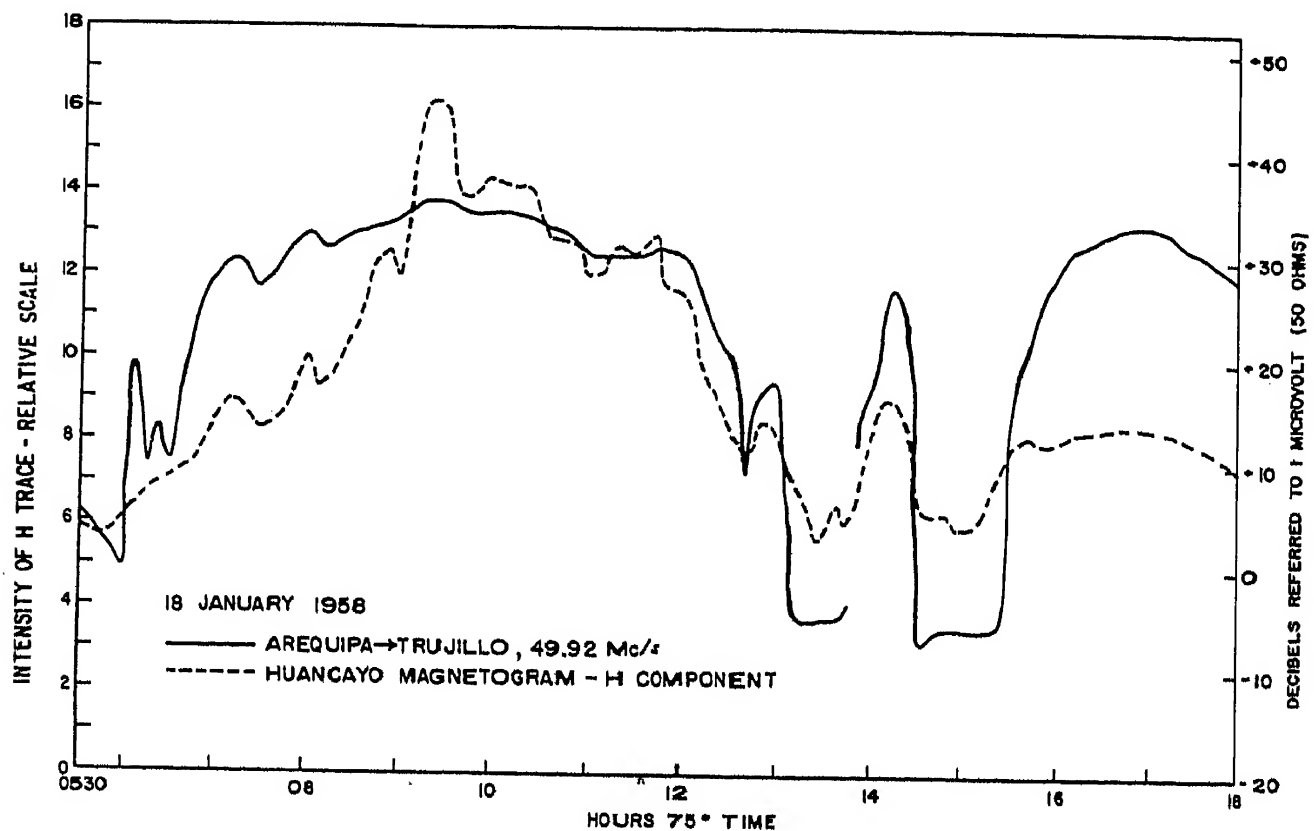


Fig. 6. Correlation of the forward scatter signal intensity for the Arequipa  $\rightarrow$  Trujillo path with the Huancayo magnetogram for 18 January 1958.

### *Blanketing $E_s$*

There were frequent daytime occurrences on the north and south paths of strong scatter propagation similar to that associated with blanketing  $E_s$  at temperate latitudes. However, such occurrences were completely absent on the basic scatter path. This means that there must be a zone in the immediate vicinity of the magnetic equator where the blanketing  $E_s$

phenomenon does not occur. Recent studies (Matsushita 1962) may explain its absence, which has also been noted from an analysis of ionograms (Knecht and McDuffie 1962).

### *Diurnal and Latitudinal Effects*

Certain systematic characteristics of the portions of ionosphere under observation may be determined from hourly median signal-strength distributions (of which Fig. 7 is a representative example) for the three

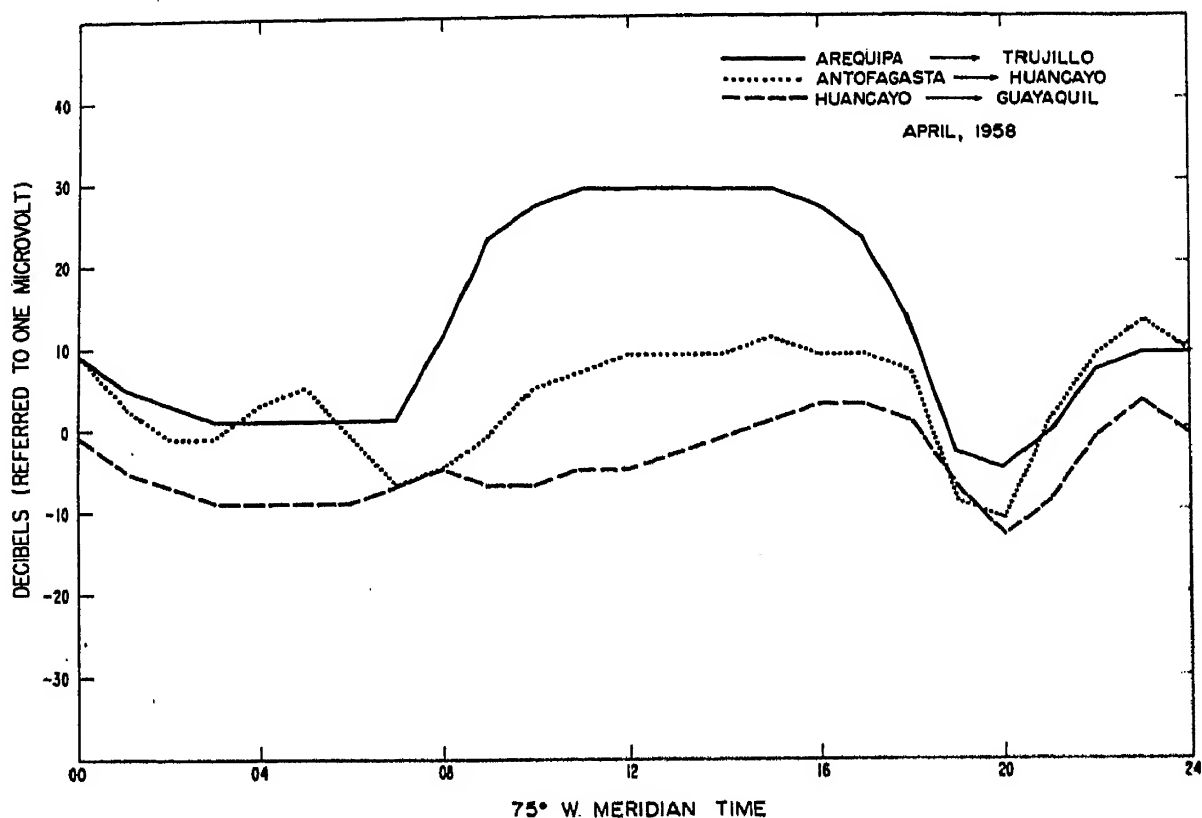


Fig. 7. Diurnal hourly median signal strength distributions for the three *E*-region scatter paths for April, 1958.

*E*-scatter paths. For one thing, all three paths have minimum diurnal signal intensity at about 2000 hours local time. This minimum occurs rather uniformly during the period studied and is a familiar characteristic of ionospheric scatter circuits located in temperate latitudes. Signal strengths observed by scattering from  $E_s$ - $q$  on the basic path exhibit a tendency to decay quite smoothly just after sunset, but their growth in the morning is quite erratic by comparison. On the southern and northern paths there is a tendency for the nighttime signal strength to attain its diurnal maximum near midnight, while on the basic path, the signal strength generally displays a semi-maximum around midnight. There is a strong indication of asymmetry on comparing signal-strength statistics for the paths with midpoints north and south of the magnetic equator, in

that the scatter signal over the southern path is almost always considerably stronger than that over the northern path. There is intense and continuous propagation at night over all of these paths by scattering from varieties of sporadic- $E$  irregularities that are different from  $E_s-q$  and that are not readily apparent on normal ionograms. Further research on these kinds of  $E_s$  seems to be indicated.

### *Height of the Irregularities*

During the course of the oblique scatter experiments, pulse measurements were conducted over the basic path for a ten day period, with a view to establishing the relative height of the scattering medium. The reference for this determination was the minimum time delay at which meteors were observed, and this delay was assumed to correspond to a height of 90 km. Relative to this reference height, the daytime  $E_s-q$  scatter-signal was interpreted as corresponding to heights ranging from 90 to about 110 km. (Absolute scatter heights could not be obtained solely from these unidirectional pulse measurements, nor was there sufficient time-resolution to determine the thickness of the scattering layer.)

### *Seasonal Effects*

From the nine months of statistical distributions available to date, it appears that the median noontime signal strengths were relatively independent of season to within 6 decibels on the basic and southern paths, while they tended to approach a peak in July on the northern path.

### *SID Effects*

There is evidence in the equatorial data that sudden ionospheric disturbances (SID's) produce increased absorption of the 50 Mc/s signals but do not enhance the strength of oblique scattering associated with sporadic  $E$  effects. (This is in contrast to the net enhancement of 50 Mc/s signals obtained at temperate latitudes during SID's, which results from increased scattering due to an augmentation in strength of the ionospheric irregularities that more than compensates for the greater absorption.)

## 2. THE ASSOCIATION OF EQUATORIAL SPORADIC $E$ WITH THE EQUATORIAL ELECTROJET

### *Oblique Scatter Intensity compared to Huancayo Magnetograms*

As has been discussed in Part 1, earlier workers have noted an association of the critical frequencies of  $E_s-q$  and the intensity of the equatorial electrojet current stream, while in the oblique scatter experiments, a more quantitative relationship has been found between the current strength and

that of the oblique scatter signals. However, this latter relationship is not always in evidence and seems to be a variable function of the amplitude of the current (as measured by the horizontal magnetic field at Huancayo). It has been found that there is a high correlation between the intensity of the daytime\* scatter signal and the horizontal component of magnetic field strength ( $H$ ) over a certain range of values of  $H$ . The rough limits of this range of variation in  $H$  could be described physically as a threshold value and a saturation value. The threshold value,  $H_t$ , is characterized by that value of  $H$  associated with the time at which  $E_s$ - $q$  propagation is first established in the morning, while the saturation value,  $H_s$ , is defined as the value of  $H$  beyond which there is no further correlation between  $H$  and the scatter signal intensity.

In general, when there are daytime features common to the records from all three oblique scatter paths under discussion, corresponding features can be found on the Huancayo magnetogram. This correlation usually occurs at intermediate values of the diurnal range of  $H$  variation. On the other hand, when the magnetic field is fluctuating about relatively high values, its modulation characteristics are not found in the time variation of the scatter signals. The fact that a correlation is present at moderate values of  $H$  but not at high values suggests that the electrojet current may be more uniform within the scattering volume at lower values of  $H$  than it is at higher values. Thus for high values of  $H$ , due to averaging over the large ionospheric volume within which the signal is being scattered, the total scattered signal strength would not be expected to vary appreciably with the  $H$  measured at Huancayo. However, on this explanation it would be expected that there should always be a good correlation if a sufficiently small portion of the electrojet above Huancayo were being examined with radio waves.

#### *Radar Echoes at 50 Mc/s from the $E_s$ - $q$ Irregularities*

That this is indeed the case is suggested by some observations taken at Huancayo during a period limited to about four hours on 17 March 1960. The amplitude of the radar echo at 49.96 Mc/s from the equatorial electrojet region immediately above Huancayo was recorded, along with the variation of  $H$ . (The fact that a direct echo could be obtained at v.h.f. would suggest, as discussed in Part 3, that the concept of a "critical frequency" of  $E_s$ - $q$  at h.f. is not particularly meaningful.) For this period there was excellent correlation between the echo strength and the  $H$  field, as illustrated in Fig. 8. In view of this correlation during the entire interval for which observations of the two quantities were recorded, it is tempting

---

\*It has been pointed out (GIESECKE 1959) that sometimes at night during magnetic disturbances there is a close correlation noticeable between the oblique scatter records and the  $H$ -field.



to infer, pending further measurements of this kind, that there would always be such a correlation.

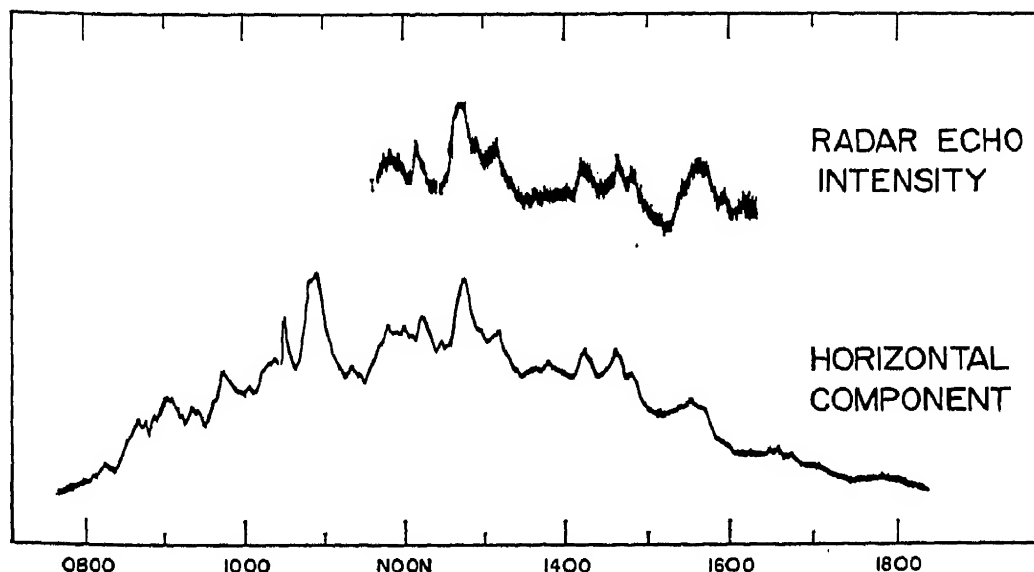


FIG. 8. Correlation of the radar echo at Huancayo from the equatorial electrojet at 49-960 Mc/s with the Huancayo magnetogram; 17 March 1960. The ordinates are nearly linear, in microvolts and gammas, respectively.

### Interpretation of the Correlations

These relationships have demonstrated the close identification of the  $E_s$ - $q$  phenomenon with the equatorial electrojet. The equatorial sporadic- $E$  irregularities are thus a manifestation of the electrojet current, much as waves are an aspect of the ocean. This identification is strengthened by radar measurements at Huancayo and by the oblique pulse observations, both of which have established that the scatter echoes arise from the same region through which the electrojet is known to flow.

Not only is there the indicated correlation of signal strength with  $H$ , but also the band width of fading of the radio signals is often closely correlated with  $H$ . This is apparent both in the fading rate of the signal scattered over the Arequipa  $\rightarrow$  Trujillo path and in the Doppler spread of the radar echoes from  $E_s$ - $q$  above Huancayo. In fact, the fading rate of the oblique scatter signal is usually more sensitively correlated with the magnetic field than is the signal amplitude itself.

It is interesting to examine the implications of these correlations, considered in conjunction with the radio measurement (cf. Part 3) of the velocity of flow of the irregularities. The intensity of scattered signal is resumed to be a function of the root-mean-square fluctuation (defined as  $\Delta N$ ) in electron density ( $N$ ), while the magnetic field variations ( $H - H_0$ ), which are a measure of the electrojet current strength ( $I$ ), correspond to the product of the density of electrons and their effective velocity of flow ( $v$ ). Thus,  $H - H_0 \propto I \propto Nv$ , where  $H_0$  is a nighttime reference



level. There has been noted a correlation of  $v$  and  $H$ , as well as a correlation of  $\Delta N$  and  $H$ , and the above linear relationship exists between  $H$  and  $Nv$ . Furthermore, it is expected that  $\Delta N$  is correlated with  $N$ , and possibly with  $v$  as well, both relations being consistent with the observations. Based upon further study and clarification of this family of cyclic relationships, and insofar as the velocity of the irregularities corresponds to the average velocity of the electrons in the equatorial electrojet, it may be possible by radio techniques to resolve the variation in current flow into its constituents, changes in velocity and/or charge density.

### *Bifurcation of the $E_s$ - $q$ Layer*

Another feature of the radar measurements (cf. Part 3) was an occasional bifurcation of the  $E_s$ - $q$  echo. The normal echo occupied the range interval from 100–107 km or so, and gave rise upon bifurcation to two contiguous echo intervals, extending between about 96–102 km and 102–108 km. This result is to be compared with some observations of the equatorial electrojet, using a magnetometer in a rocket (Cahill 1959), from which two layers were reported, extending between about 97–110 km and 122–128 km. So far no direct radio evidence has been found for the existence of an upper scattering layer this high.

## 3. ON THE NATURE OF EQUATORIAL SPORADIC $E$

### *Characteristics of the $E_s$ - $q$ Irregularities*

While the continuous-wave recordings obtained in the course of the IGY experiment revealed the presence of an intense scattering phenomenon, effective at v.h.f., near the magnetic equator, these recordings provided little information regarding the actual nature of the scattering centers. During the CW recording program some short term experiments were conducted with spaced receiving antennas on the Arequipa → Trujillo path in the same fashion described by Bailey, Bateman and Kirby (1955), in the hope of determining the dimensions and shape of the irregularities.

In one of these experiments the receiving antennas were deployed along a line oriented normal to the great circle bearing of the transmission path. Simultaneous recordings were taken for pairs of dipoles at various separations (ranging from one wavelength to twelve wavelengths) along this line. During the presence of equatorial sporadic- $E$  irregularities above the path midpoint, an excellent correlation was often found between antennas separated by as much as twelve wavelengths, while at other times during the occurrence of this phenomenon, the correlation was poor for as little as three wavelengths separation. A complete explanation of these results

has yet to be found, but the high degree of correlation is partially explained on the basis of the large scale sizes of the irregularities observed in the radar experiments to be described.

### *Field Alignment of the $E_s$ - $q$ Irregularities*

Meanwhile, and also during the IGY, Egan of the Stanford University group was operating a fixed frequency backscatter equipment at Huancayo, in cooperation with the Instituto Geofísico de Huancayo. From the results of this program Egan (1960) concluded that in the equatorial  $E$ -region there exist magnetic-field-aligned irregularities similar to those observed with the backscatter technique in the presence of auroral disturbances. (Egan's results were obtained at oblique incidence at frequencies of about 13, 18 and 30 Mc/s.) Following the IGY, the authors performed several brief experiments at Huancayo, using the C-4 equipment near 10 Mc/s in conjunction with a dipole-antenna array. Based upon split-lobe operation of this antenna it was confirmed that the  $E_s$ - $q$  irregularities are indeed magnetic field aligned.

### *Radar Echoes at 50 Mc/s from the $E_s$ - $q$ Irregularities*

Several additional experiments were conducted at that time, using relatively low-powered radar equipment at 50 Mc/s located near Huancayo and Lima, Peru, which are at the same magnetic latitude. It was found that direct scatter echoes of considerable intensity could be obtained at vertical incidence on a regular basis from irregularities at a height of about 105 km, during periods when equatorial sporadic  $E$  was also observed on a conventional ionosonde. Consequently, experiments to determine the characteristics of the irregularities in the  $E_s$ - $q$  were carried out at 50 Mc/s, in view of the lower interference levels and the relative ease of handling antennas associated with that frequency compared to h.f. The parameters of the 50 Mc/s radar which obtained a 20 decibel signal-to-noise ratio were as follows:

Peak transmitted power	5 kW
Pulse duration	100 $\mu$ sec
Receiver bandwidth	10 kc/s
Antenna	Five-element Yagi, having a measured plane wave gain of 9 decibels over an isotropic radiator.

The experiments to be discussed were conducted using a variety of antenna configurations and other instrumentation, but with system sensitivities roughly comparable to that described above. Radar echoes were obtained from the equatorial electrojet from all points where a plane normal

to the earth's magnetic field and passing through Huancayo intersects the 105 km layer. At Huancayo this plane is almost vertical, and oriented in the east-west direction. For a given antenna gain, the strongest echoes were obtained at vertical incidence. After allowing for inverse distance attenuation, the scattering cross section of the  $E_s$ - $q$  layer was found to be approximately uniform at all angles of incidence.

There is no doubt that these echoes are from irregularities directly associated with both the v.h.f. forward scatter propagation discussed in Part 1, and with equatorial sporadic  $E$  as observed on a conventional ionosonde. Both of these scattering phenomena have been closely identified with each other by the similarity of their time variations, as discussed in Part 2 above.

### *Polarization of the Radar Echoes*

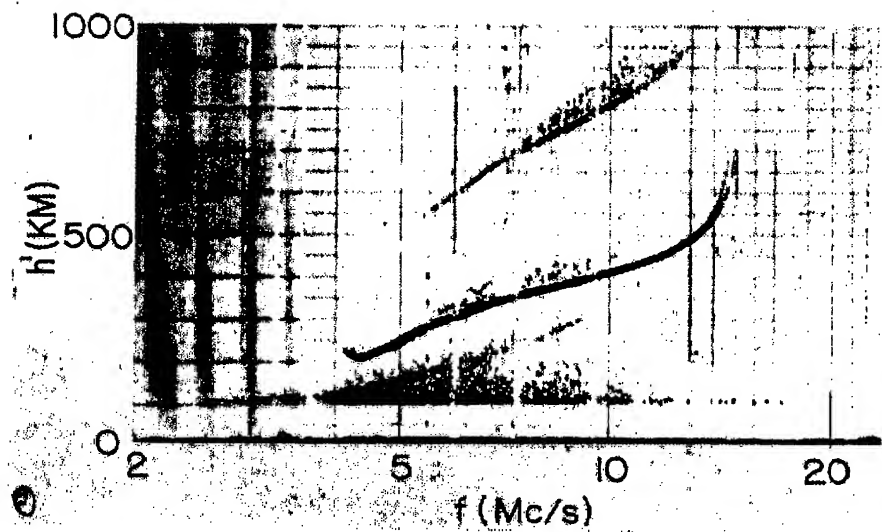
The polarization characteristics of the echoes were examined at vertical incidence at 50 Mc/s. The antenna polarization required to maximize the received echoes was always parallel to that of the transmitting antenna. The signal received on a cross-polarized antenna of the same gain was of the order of twenty decibels weaker, and one may infer that this weak signal was received due to imperfect polarization of the transmitting and receiving antennas. This behavior was observed independent of the relative orientation of the transmitting polarization and the direction of the earth's magnetic field. Similar polarization effects were exhibited throughout the equatorial sporadic  $E$  configuration on the C-4 ionograms when linearly polarized antennas were employed with the sounder. The lack of any ionospheric modification of the polarization transmitted implies that the scattering phenomenon does not involve magnetoionic cross-coupling, Faraday rotation or plasma resonance effects (Herlofson 1951).

### *Increase in Ionosonde Sensitivity*

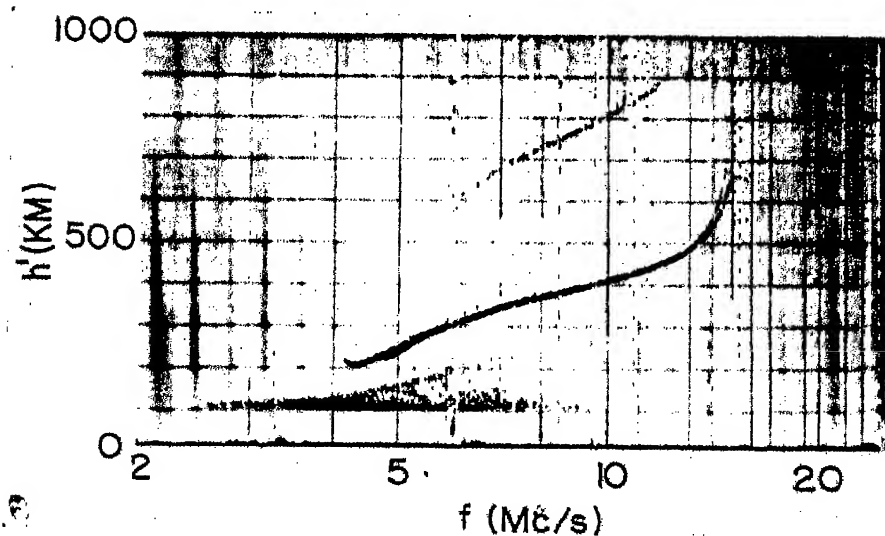
The antennas used with the C-4 ionosonde were simple log-periodic structures designed from data published by DuHamel and Berry (1958). In addition to the property of radiating and receiving linearly polarized signals, these antennas have an average design gain of about seven decibel relative to an isotropic radiator.

### *Frequency Dependence of $E_s$ - $q$ Intensity*

It was found that when using parallel-polarized log-periodic antennas for both transmitting and receiving with the C-4, the  $E_s$ - $q$  trace on the ionograms frequently extended to above 20 Mc/s. This compares with a maximum "critical frequency" of about 11 Mc/s realized when using the customary delta antennas in conjunction with the ionosonde. Figure 9 is a nearly simultaneous comparison of the traces obtained using the north-

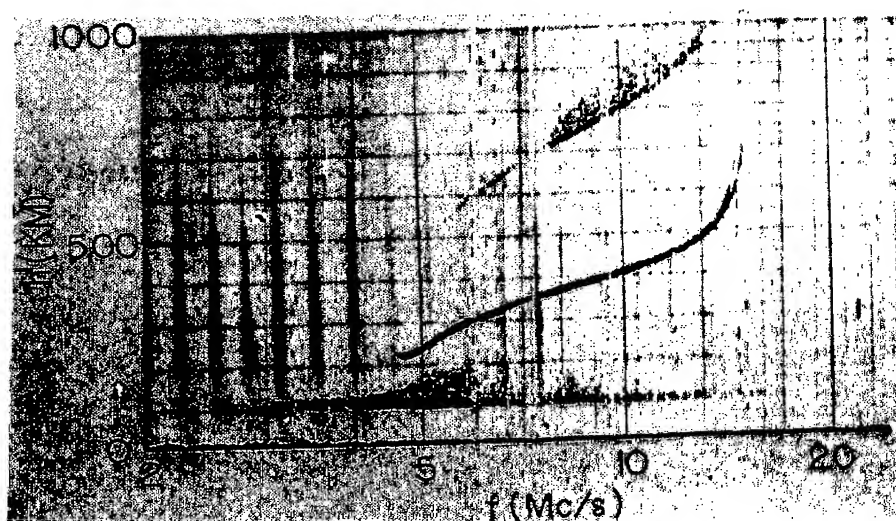


(a) 1229 EST; north-south polarized log-periodic antenna for transmitting and receiving.

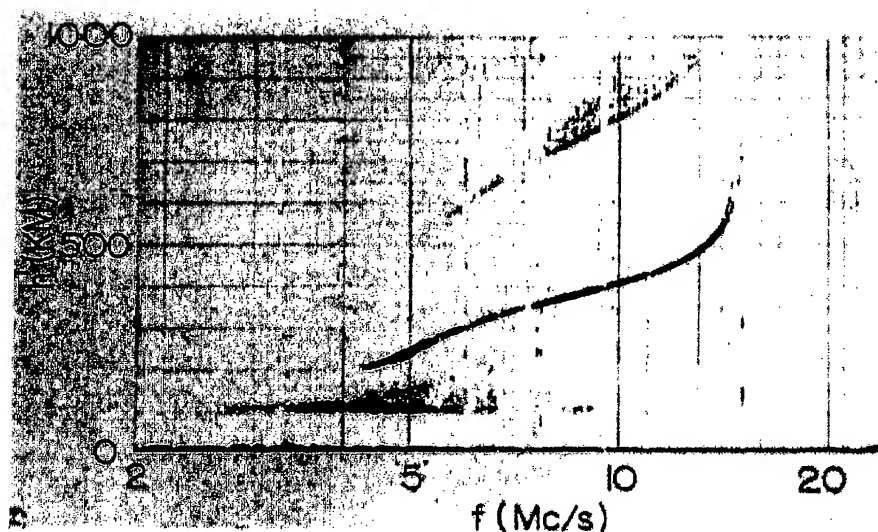


(b) 1230 EST; delta antenna for transmitting and receiving.

Fig. 9. The 'Equatorial sporadic *E*' and 'Equatorial slant sporadic *E*' configuration observed at Huancayo with various antenna combinations on 19 April 1960.



(c) 1231 EST; east-west polarized log-periodic antenna for transmitting and receiving.



(d) 1232 EST; oppositely polarized log-periodic antennas for transmitting and receiving.

Fig. 9. The 'Equatorial sporadic *E*' and 'Equatorial slant sporadic *E*' configuration observed at Huancayo with various antenna combinations on 19 April 1960.

south polarized log-periodic antennas, the delta antennas, the east-west polarized log-periodic antennas, and oppositely polarized log-periodic antennas for transmitting and receiving. These results and the observations of strong vertical-incidence echoes at 50 Mc/s make it apparent that the  $E_s$ - $q$  has no "critical frequency" (although this parameter is often utilized). Instead,  $E_s$ - $q$  is a scattering phenomenon which probably exhibits some power-law dependence of scattering cross section upon the sounding frequency. Skinner and Wright (1962) obtained scattered powers at vertical incidence varying with frequency to the exponent  $-9.4$ . How much higher in frequency than 50 Mc/s the  $E_s$ - $q$  echoes are observable has not yet been determined, but it does not seem likely from the scattered powers observed at 50 Mc/s that the Skinner and Wright result could be applicable at frequencies much higher than their range of measurements, which extended from 4 to 8 Mc/s.

### *Frequency Spectrum of the $E_s$ - $q$ Echoes*

In addition to their aspect sensitivity, the 50 Mc/s echoes display a rapid fading reminiscent of auroral echoes obtained at that frequency (Bowles 1954; Nichols 1959; Bowles *et al.* 1960). The frequency spectrum of these echoes was measured with a panoramic spectrum analyser, not only at vertical incidence, but also at various oblique angles east and west of the vertical. The method of analysis was a combination of the techniques used by Bowles (1954) and of McNamara (1955). By pulsing the transmitter with a high duty factor, at a repetition frequency of approximately 500 c/s, a spectrum was generated consisting of a number of carrier frequencies mutually displaced at multiples of the repetition frequency. As in a conventional radar, the echoes were received in the time interval between pulses. One of these carriers was chosen as a reference frequency for the spectrum analysis, and the echo frequency spectrum was then compared with this reference. The result of such a spectrum analysis is presented in Fig. 10, in which appear the echo spectrum at  $30^\circ$  east of the zenith, the transmitter frequency, and the echo spectrum at  $30^\circ$  west of the zenith.

There is some variability in the width and characteristics of the echo spectra. In general, however, the spectrum at vertical incidence is symmetrical and about 100 c/sec wide. Looking  $30^\circ$  off-vertical toward the east, the spectrum is ordinarily shifted upward in frequency by about 125 c/s, and looking symmetrically toward the west, it is ordinarily shifted downward by an equal amount. This observation could presumably be interpreted as evidence of a horizontal drift of electron density irregularities from east to west at velocities of the order of 750 m/s. To check this interpretation, the spectra obtained at  $30^\circ$  west of the zenith were compared with those obtained at  $60^\circ$  west of the zenith. If the Doppler shift were due

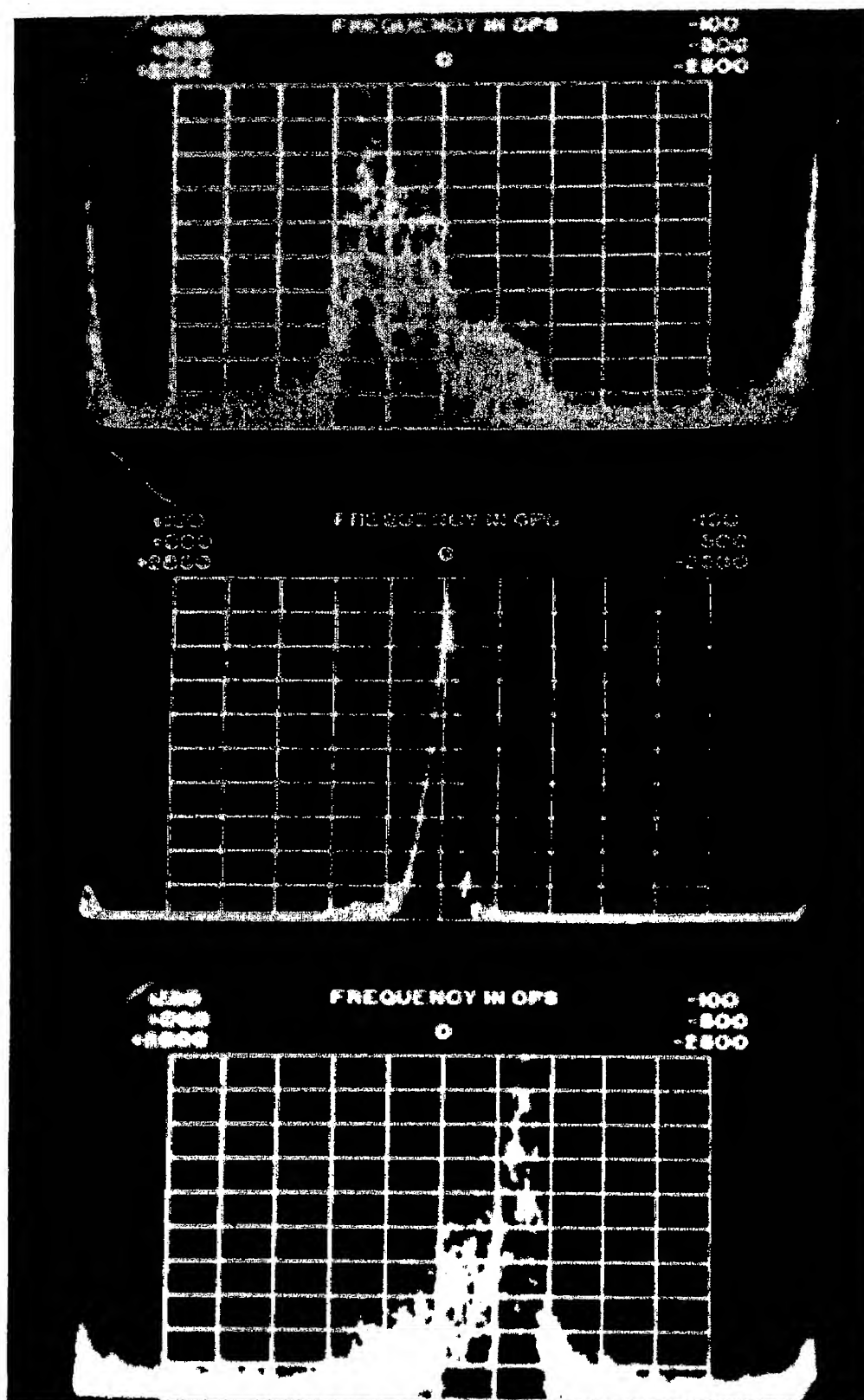


Fig. 10. Spectrum analysis of 49-960 Mc/s radar echoes from the equatorial electrojet at Huancayo on 14 March 1960. Top, 0934 EST, looking  $30^\circ$  east from the vertical; center, reference spectrum at the transmitter frequency; bottom, 0936 EST, looking  $30^\circ$  west from the vertical. (The frequency axis markers correspond to 100 c/s.)



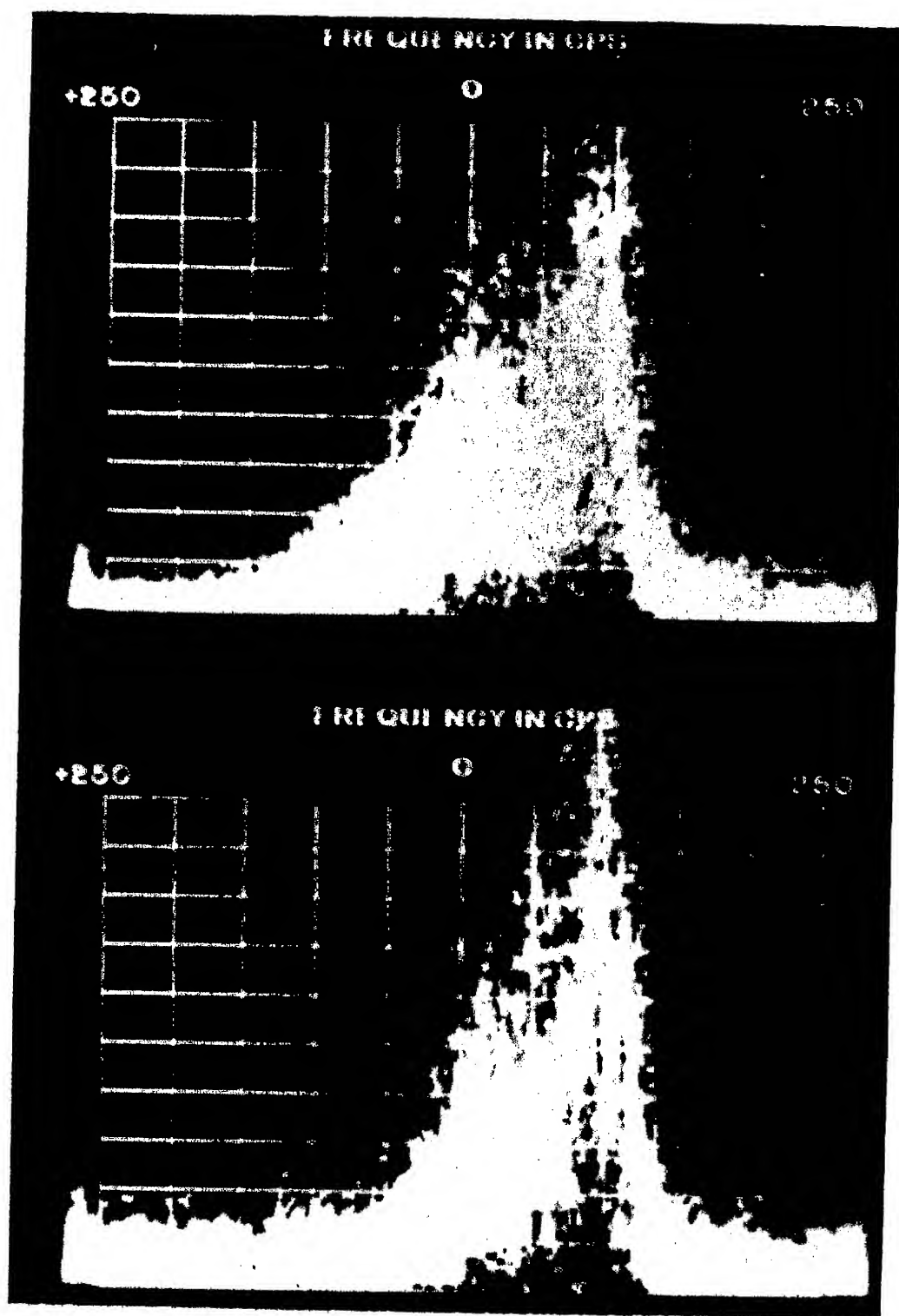


Fig. 11. Spectrum analysis of 49.960 Mc/s radar echoes from the equatorial electrojet at Huancayo on 16 March 1960. Top, 1406 EST, looking  $30^\circ$  west from the vertical; bottom, 1412 EST, looking  $60^\circ$  west from the vertical. (The frequency axis markers correspond to 50 c/s.)



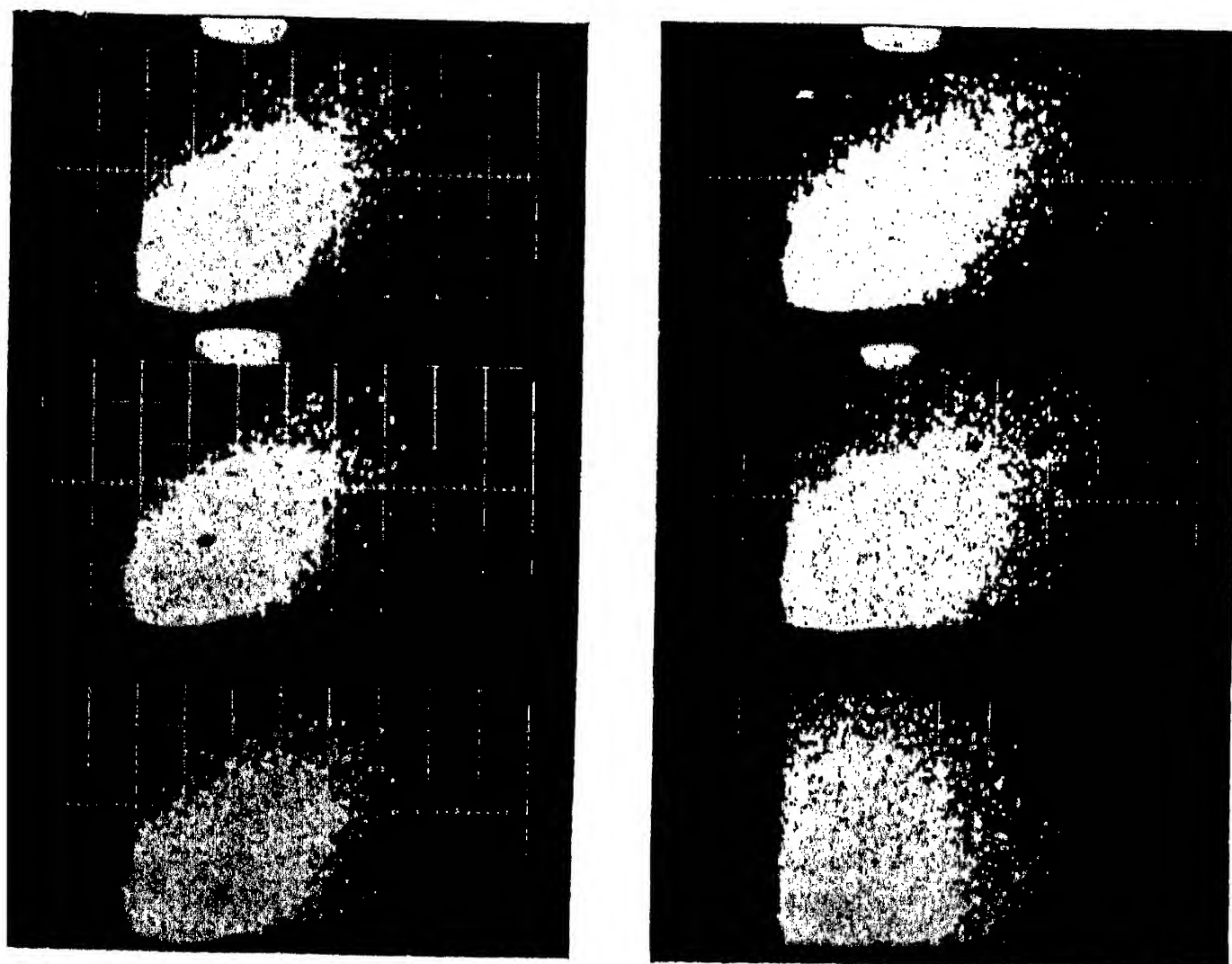
to a horizontal drift of the pattern of irregularities, the shift of frequency at  $60^\circ$  west would be in the ratio  $0.86/0.50$  to that at  $30^\circ$  west of the zenith, this ratio relating the line of sight components of the horizontal velocity at the two angles. As is evident from a typical example as shown in Fig. 11, the observations were at variance with this hypothesis, in that the Doppler shifts obtained nearly simultaneously at the two zenith angles are essentially identical.

*Correlation of Signals received on Spaced Antennas along an East-West baseline*

This result suggested that the shift in frequency is not due to a simple horizontal drift of irregularities. Hence another series of experiments was performed to discover the reason for the unexpected Doppler shift behavior. These experiments were based upon the technique of correlating the fading of signals received separately on spaced receiving antennas (Briggs and Spencer 1954). For each observation a cross-correlation coefficient relating the fading for a pair of antennas was obtained by the method of scatter diagrams (Sugar 1954). Figure 12 is an example of the correlograms produced in this way. In the observation the receiving antennas were separated about  $\frac{1}{2}$  wavelength (2 meters) in the east-west direction. (These antennas were also separated about 2 wavelengths in the north-south direction for convenience, since it had previously been established that the correlation is essentially unity for  $E_s$ - $q$  echoes received with a north-south separation of that amount, and no corresponding east-west separation.)

Figure 12b indicates a reference correlation of about 70% for the signal from a single antenna compared with the same signal delayed 1.6 msec. Figure 12a shows that the correlation is only about 50% when the sample from the east antenna was delayed relative to the west antenna by about 1.6 msec, while Fig. 12c shows a similar result when the west antenna was delayed relative to the east antenna by the same amount. The left-hand portion of Fig. 12 was photographed when the narrow-beam transmitting antenna was concentrated within a  $7^\circ$  beam centered on the zenith. The right-hand portion of Fig. 12 was photographed when the narrow beam of the transmitting antenna was split into two  $7^\circ$  lobes, one at an angle of  $30^\circ$  west of the zenith, the other aimed symmetrically toward the east. The receiving antennas were directed vertically in all cases.

Analysis of the photographs of Fig. 12, as confirmed by similar analyses for other time delays, shows clearly that the right-hand scatter plots demonstrate the presence of an east  $\rightarrow$  west drift of the fading pattern, while the left-hand scatter plots do not show a drift. Had the fading been due to a single, irregular fading pattern, both sets of photographs would have yielded identical results. The equivalent drift velocity of about



(a-c)

(d-f)

FIG. 12. Statistical scatter diagrams for receiving dipoles spaced 2 meters in the east-west direction at Huancayo, using radar echoes from the equatorial electrojet at 49.960 Mc/s on 14 March 1960. The sequence of photographs at the left is for vertical transmission, with (a) 1040 EST, east antenna delayed 1.6 msec; (b) reference correlogram for the signal of one antenna delayed 1.6 msec and compared with the original signal; and (c) 1042 EST, west antenna delayed 1.6 msec. The sequence of photographs on the right is for a split-lobe transmitting antenna, with (d) 1051 EST, east antenna delayed 1.6 msec; (e) reference correlogram for a delay of 1.6 msec (as in (b)); and (f) 1053 EST, west antenna delayed 1.6 msec.

10 m/s implied by the Doppler shift observed at oblique incidence suggests that there should be a delay of about 3 msec between the antennas at this east-west separation. On the other hand, the width of the fading spectrum, which is of the order of 100 c/s, implies that the fading on a single antenna would be auto-correlated for a period of about 3.5 msec. Thus the lack of evidence of a drift at vertical incidence using this method of observation cannot be explained on the basis of a decay of correlation due to internal rearrangement of the fading pattern.

*A Model for the Equatorial Sporadic-E Irregularities*

The authors and their collaborators (Bowles *et al.*, 1960) have sought to explain the apparent inconsistency of these two sets of experimental results in the following way: The structure of the irregularities must be such as to produce variable results as a function of the angle of incidence on the layer. A simple way of describing this is to say that the scattering centers viewed at one angle of incidence in the east-west plane differ in some way from the irregularities viewed at another angle.

Therefore it is suggested that the commonly accepted model of thin, ellipsoidal field-aligned irregularities (Booker 1956) does not explain the observed echoes, since these irregularities would be isotropic in the east-west plane. A model consistent with the results described is one in which the irregularities are plane wave fronts, the wave normals of which are distributed in a plane normal to the magnetic field lines. While the model of irregularities having cylindrical symmetry is not specifically excluded, the motions and fluctuations in density of such irregularities would have to be correlated over distances large compared with a wavelength, as in the case of an angular spectrum of wavelike disturbances. The wave fronts are perhaps longitudinal plasma waves or hydromagnetic waves of electron density. The correlation distances of these wave fronts would have to be several hundred meters or more to account for the observations described. The authors are aware that plasma and hydromagnetic waves are likely to be highly damped in the *E*-region of the ionosphere due to the high collisional frequency of the charged particles with the neutrals. The fact that such waves may be observed does not preclude the possibility that they are severely damped. The presence of a strong excitation mechanism, such as the flow of electric current in the equatorial electrojet, would very likely be a sufficient condition for the observation of these waves.

*Correlation of Signals received on Spaced Antennas along a North-South baseline*

An additional series of correlation measurements was taken along a north-south baseline. The antenna separation at 50 Mc/s required for a correlation of  $1/e$  was of the order of 35 wavelengths. For a fixed separation of about 15 wavelengths, the percentage correlation varied with time between the limits of about 40% and 80%. Comparison of nearly simultaneous spaced-receiver measurements at 50 and 21.8 Mc/s indicated that the correlation was identical at the two frequencies for the same antenna separation measured in wavelengths. The degree of correlation between simultaneous measurements on spaced receivers is a direct measurement of the width of the angular spectrum of plane waves approaching the receiver, provided that certain simple conditions are met (Booker and

Clemmow 1950; Booker, Ratcliffe and Shinn 1950). Thus the measurements at 21.8 and 50 Mc/s indicate that the angular width of the echoing region, viewed in the north-south direction, is the same at both frequencies when measured nearly simultaneously (within one minute). This result would be consistent with the model of a power spectrum of irregularities, as in the case of scattering due to turbulent irregularities (Booker 1959), if the turbulent spectrum were proportional to some power of the exploring wavelength. However, the result is not consistent with the results of a second set of measurements along a north-south baseline. These measurements were made using a wide-spaced interferometer with a pulse resolution of about 2 km. The results, which are to be described more fully elsewhere, suggest that the north-south correlation distance for the irregularities is of the order of one kilometer or more. The width of the north-south angular spectrum of the echoes is probably explained in terms of a distortion of the earth's magnetic field in the vicinity of the equatorial electrojet due to the intense flow of electric current therein.

#### *Similarity between $E_s$ -q and Auroral Echoes*

The v.h.f. echoes described in this section bear a striking resemblance to v.h.f. echoes from auroral  $E$ -region ionization. Both classes of echoes occur at about the same height range of the ionosphere. Both have about the same bandwidth of fading and similar Doppler shift characteristics. Both kinds of echo exhibit an aspect sensitivity corresponding to the influence of the earth's magnetic field, although in both instances strong echoes can be observed along propagation paths which are not precisely orthogonal to the lines of force of the main magnetic field of the earth. Strong currents are observed to flow horizontally, normal to the lines of force of the earth's magnetic field, both at the magnetic equator and in auroral forms such as the homogeneous arc and rayed band. Because of these similarities it is tempting to infer that the conditions creating the irregularities responsible for radio wave scattering might be identical in origin and description in both cases.

### 4. ON THE NATURE OF EQUATORIAL SLANT SPORADIC $E$

#### *Description of the Equatorial Slant Sporadic- $E$ Configuration*

For some years, observers have noted on ionograms for stations near the magnetic equator the prevalence of a slanted trace known as "equatorial slant sporadic  $E$ " or " $E_s$ -s". This is a daytime phenomenon and always occurs in association with equatorial sporadic  $E$ . The  $E_s$ -s trace appears at about the critical frequency of the regular  $E$ -layer trace and at a height of about 100 km, then gradually increases in height with increasing frequency, as illustrated in Fig. 1. The shape of the slanted trace

is approximately a straight line on the conventional ionograms, which have a presentation with a logarithmic frequency scale and a linear virtual height scale. (Actually, this trace has been demonstrated to be a straight line which would pass through the origin when plotted on linear frequency and virtual height coordinates (Agy reference in Smith and Knecht 1957).)

### *Explanation of the Equatorial Slant Sporadic E Configuration*

The source of the equatorial slant sporadic *E*-trace has not heretofore been explained. There has been some speculation that the trace could arise from a scattering layer located below the reflecting stratum in the *E*-layer (Smith 1955; Smith and Knecht 1957). Several special ionograms have been analysed under the hypothesis that the equatorial slant sporadic *E* is attributable to echoes from the field-aligned irregularities of equatorial sporadic *E*, located at a height of about 105 km, within the equatorial *E*-layer. This assumption follows logically from the results discussed in the preceding sections of this paper.

The ionograms in question were produced with a conventional Model C-4 ionosonde whose transmitter and receiver were sequentially connected to each of four selected antenna combinations during consecutive one minute sweeps. One antenna combination utilized the conventional delta antenna, as used with most C-4 ionosondes. The other modes involved linearly polarized log-periodic antenna structures polarized either in the north-south direction or in the east-west direction (DuHamel and Berry 1958). It was possible to transmit on a north-south polarized antenna and receive on a north-south polarized antenna, transmit east-west and receive east-west, or to transmit either east-west or north-south, receiving on the oppositely polarized antenna. Compared with the delta antenna, the log-periodic antennas have a rather restricted beam pattern mainly concentrated within a zone  $\pm 30^\circ$  from the zenith, similar to the pattern of a three or four element Yagi antenna. The east-west polarized antenna is quite insensitive to radiation near the horizon in the east-west direction, since this represents propagation off the ends of the equivalent linearly polarized dipole antenna. The north-south polarized antenna discriminates to a lesser degree against radiation in the east-west direction but is quite insensitive near the horizon in the north-south direction.

Field aligned echoes originating in the 105 km height region would appear at ranges greater than 105 km if they came from all angles of observation within the equatorial (east-west) plane. Accordingly, one should expect on this hypothesis to observe much better developed equatorial slant sporadic *E* on the north-south polarized log-periodic antennas than on the east-west polarized log-periodics. As for the equatorial sporadic-*E* trace, there should be little or no equatorial slant sporadic *E* apparent on ionograms obtained using cross-polarization for

transmitting and receiving. These predictions are generally borne out at Huancayo, as illustrated in Fig. 9, a montage of four ionograms taken almost simultaneously using the four antenna configurations.

Based upon the hypothesis stated, the authors interpret the well defined upper edge of the slant trace and the scatter echoes between that trace and the  $E_s$ - $q$  trace as arising by the following mechanism: The field-aligned irregularities in question must be located at a height slightly greater than that of the base of the regular  $E$ -layer coexisting over Huancayo, resulting in frequency-dependent delays produced by refraction in the lower-lying  $E$ -layer. This is because echoes due to scattering irregularities are obtained at a given frequency only if the waves penetrate the regular  $E$ -layer up to the scatterer. Assuming an antenna omnidirectional in the equatorial (east-west) plane, this penetration can be achieved, at that frequency, for all angles from the zenith down to a limiting or critical angle of incidence, below which the waves are totally reflected back toward the earth's surface. At any given frequency, the range to the slanted trace is the limiting range attained for total reflection upon reaching the 105 km irregularities. As may be seen from the ionograms of Fig. 9, there are apparently echoes present at all ranges between 100 km and the maximum range of the equatorial slant sporadic  $E$ . (In this figure, comparison of the record obtained with the delta antennas with that for the north-south polarized log-periodic antennas suggests that the lack of echo intensity between the  $E_s$ - $q$  and  $E_s$ - $s$  traces when using the delta antennas probably results from the difference in the radiation patterns of the antennas.)

If there were indeed irregularities above the  $E_s$ - $q$  layer, the east-west polarization mode, which is constrained to observe nearly overhead at Huancayo, would exhibit scattering effects at ranges greater than those actually obtained. Consequently, the writers would question the interpretation (Egan 1960) that the slant  $E_s$  traces on equatorial ionograms could indicate the presence of sporadic- $E$  irregularities in the 120 to 200 km height-region. Instead, it is suggested that the time delays associated with the equatorial slant sporadic- $E$  configuration are imparted due to refraction in the  $E$ -layer en route to  $E_s$ - $q$  layer irregularities in the equatorial plane. By means of calculations of these time delays it is possible to synthesize ionograms reproducing many features of the equatorial sporadic  $E$ /equatorial slant sporadic  $E$  complex observed on Huancayo ionograms, and through this process to determine certain characteristics of the regular equatorial  $E$ -layer and of the equatorial sporadic- $E$  layer (Cohen, Bowles and Calvert 1961). This treatment also accounts for the earlier observation that the  $E_s$ - $s$  trace is a straight line that would pass through the origin on a graphical presentation with linear frequency and virtual height coordinates. Finally, the fact that no partial  $E_s$ - $s$  trace is ever observed in the absence of  $E_s$ - $q$  suggests that the variations of current in the equatorial



electrojet are relatively coherent over distances of hundreds of kilometers along the magnetic equator.

## 5. CONCLUSIONS

Information has been obtained by radio techniques regarding irregularities appearing in the *E*-region of the equatorial ionosphere. Experimental evidence has been presented that:

- (1) These irregularities support strong oblique scatter propagation of 50 Mc/s radio waves during both the daytime and nighttime.
- (2) The irregularities are at a height of about 100 km.
- (3) There is an asymmetry in the scatter effects about the magnetic equator along the 75th meridian, with irregularities of greater strength occurring to the south.
- (4) During a year of scatter observations, daytime blanketing sporadic-*E* irregularities occurred at latitudes to either side of the magnetic equator, but were not present in its immediate vicinity.
- ✓ (5) The equatorial sporadic-*E* configuration on equatorial ionograms is produced by irregularities in the equatorial electrojet.
- ✓ (6) The electrojet irregularities occur in a layer extending from about 100 to 107 km in height, which bifurcates into two layers from time to time.
- (7) Radio techniques for observing the electrojet offer a possible means for resolving changes in this current into their charge and velocity constituents.
- (8) The equatorial sporadic-*E* irregularities are plane wave fronts parallel to the magnetic lines of force, drifting westward with wave normals at various angles in the equatorial plane.
- (9) These irregularities are at least 200 meters in length, measured along the magnetic field lines, with at least one transverse dimension of the order of 6 meters or less.
- (10) The concept of a "critical frequency" of equatorial sporadic *E* has little significance.
- (11) The "equatorial slant sporadic-*E*" configuration is really another manifestation of the "equatorial sporadic-*E*" irregularities, and results from echoes in the equatorial plane.

*Acknowledgments*—The experimental collaboration of G. R. Ochs and B. B. Balsley of NBS, and of A. A. Giesecke, Jr., Director-Técnico, M. Tábara, J. Lanat and H. Goller of the Instituto Geofísico del Perú is gratefully acknowledged. Suggestions by M. L. V. Pitteway of Slough and W. Calvert of NBS were of considerable help. The cooperation of all of the persons and organizations cited earlier (Cohen and Bowles 1961) was invaluable. Support for this research was provided by the

U.S. National Committee for the IGY through a grant from the National Science Foundation, by the Voice of America (U.S. Information Agency), and by funds of the National Bureau of Standards.

# REFERENCES

- BAILEY, D. K., BATEMAN, R. and KIRBY, R. C. (1955) *Proc. I.R.E.* **43**, 1181.
- BOOKER, H. G. (1956) *J. Geophys. Res.* **61**, 673.
- BOOKER, H. G. (1959) *J. Geophys. Res.* **64**, 2164.
- BOOKER, H. G. and CLEMMOW, P. C. (1950) *Proc. IEE.* **97**, 11.
- BOOKER, H. G., RATCLIFFE, J. A. and SHINN, D. H. (1950) *Phil. Trans. Roy. Soc.* **242**, 579.
- BOWLES, K. L. (1954) *J. Geophys. Res.* **59**, 553.
- BOWLES, KENNETH and COHEN, ROBERT, (1957) *QST* **41**, 11.
- BOWLES, K. L., COHEN, R., OCHS, G. R. and BALSLEY, B. B. (1960) *J. Geophys. Res.* **65**, 1853.
- BRIGGS, B. H. and SPENCER, M. (1954) "Reports on Progress in Physics," **17**, p. 245. The Physical Society, London.
- CAHILL, LAURENCE J., JR. (1959) *J. Geophys. Res.* **64**, 489.
- COHEN, ROBERT and BOWLES, KENNETH L. (1961) *J. Geophys. Res.* **66**, 1081.
- COHEN, ROBERT, BOWLES, KENNETH L. and CALVERT, WYNNE (1962) *J. Geophys. Res.* **67**, 965.
- DUHAMEL, R. H. and BERRY, D. G. (1958) *IRE WESCON Convention Record*, Part 1, 161.
- EGAN, R. D. (1960) *J. Geophys. Res.* **65**, 2343.
- GIESECKE, ALBERTO A., JR. (1959) (Private communication).
- HERLOFSON, N. (1951) *Ark. Fys.*, **3**, 247.
- KNECHT, R. W. and McDUFFIE, R. E. (1962). This volume, p. 215.
- MCNAMARA, A. G. (1955) *J. Geophys. Res.* **60**, 257.
- MATSUSHITA SADAMI (1951) *J. Geomagn. Geoelect., Kyoto*, **3**, 44.
- MATSUSHITA, S. (1962). This volume, p. 194.
- NICHOLS, BENJAMIN (1959) *Proc. IRE*, **47**, 245.
- SKINNER, N. J. and WRIGHT, R. W. (1962). This volume, p. 37.
- SMITH, ERNEST K., JR. (1955) National Bureau of Standards report, issued in 1957 as National Bureau of Standards Circular 582, "Worldwide Occurrence of Sporadic *E*," U.S. Government Printing Office, Washington.
- SMITH, E. K. and KNECHT, R. W. (1957) "Polar Atmosphere Symposium" Part II Ionospheric Section, p. 195 (Editor, K. Weekes), Pergamon Press, London.
- SUGAR, GEORGE R. (1954) *J. Applied Physics* **25**, 354.



# Sporadic *E* as Observed with Rockets

J. CARL SEDDON

Goddard Space Flight Center, Greenbelt, Maryland, U.S.A.

**Abstract**—Data concerning sporadic *E* obtained with rockets flown over New Mexico, U.S.A. and Manitoba, Canada have always shown the sporadic-*E* layer to be a thin layer with a large electron density gradient. The vertical electron density profiles and the horizontal uniformity of the sporadic-*E* layer are discussed. These layers have a strong tendency to form at preferential altitudes separated by approximately 6 kilometers and a striking correlation exists with wind-shears and magnetic field variations. In two cases where comparisons with ionograms were possible, it was found that the minimum frequency of the *F*-region echoes was approximately equal to the plasma frequency of the sporadic-*E* layer reduced by one-half the gyro frequency. On the other hand, the maximum frequency of the sporadic-*E* echoes as noted on ionograms was sometimes as much as 1 to 2 megacycles greater than the plasma frequency.

Although sporadic *E* has been intensively studied all over the world for the past two decades, it is one of the most difficult of ionospheric phenomena to explain on theoretical grounds. Beginning in 1946, the sounding rocket has provided a new means of making measurements. The most accurate measurements of sporadic *E* to date have been by means of a radio propagation technique devised by Seddon (1953). Two CW harmonic frequencies (either 4.27 or 7.75 Mc/s and the 6th harmonic) were radiated from the rocket to ground stations nearly underneath the rocket where the lower frequency was frequency-multiplied by a factor of six and mixed with the higher frequency. The result obtained is simply a constant voltage unless the rocket traverses a medium containing free electrons, whereupon a low frequency variation of the output voltage is obtained, the frequency of which depends upon the radio frequencies, rocket velocity and electron density. Certain assumptions are necessary, the most important of which are (1) the angle of arrival of the signals does not change; (2) there is no time variation of electron density along the propagation path; and (3) the index of refraction of the medium in the vicinity of the rocket does not change rapidly in a distance of  $\lambda/2\pi$  where  $\lambda$  is the vacuum wave length. Both magneto-ionic components of the lower frequency are utilized which provide a check on the results obtained.

Except during radio black-out conditions, the ground ionograms taken during the time of all but one of the flights during these experiments showed sporadic-*E* reflections to be present. On one of the flights under black-out conditions, sporadic *E* would probably have been present if the

ionogram could have shown it. Nine flights made measurements of sporadic  $E$ , but three flights were not detailed enough to provide much information. Two of these three flights resulted in signal loss because the plasma frequency of the sporadic  $E$  considerably exceeded the lower frequency used. Poor rocket attitude on the other flight caused the data to be discontinuous and not as accurate as usual. The remaining six flights, however, provided information not attainable by other means. Of these six flights, three were flown over New Mexico and the other three were flown over Ft. Churchill, Manitoba, Canada.

### 1. GRADIENTS

In all cases, both over New Mexico and Ft. Churchill, Manitoba, Canada, it was found that the sporadic- $E$  reflections observed on the ionograms were due to thin, high-gradient electron density regions superimposed upon the normal ionosphere profile. Within the accuracy of reading the ionogram records, the altitude of these layers was identical with that of the virtual height measured on the ionograms. In three out of six cases, the increase in electron density in these layers above a smooth profile was approximately 10 to 20 per cent. In one case, the increase was a factor of 2. The thickness of the layers in the  $E$ -region varied from 500 to 2000 meters. The electron density gradients of these thin layers are amazingly large, being in general about  $10^5$  to  $10^6$  el/cm<sup>3</sup>/km. The ionograms showed constant-height reflections up to frequencies 2 Mc/s greater than the plasma frequency of the thin layer. This is not unreasonable, for if one assumes that the layer has a boundary that is sharp with respect to the radio wavelength, the extraordinary ray 2 Mc/s higher than the plasma frequency has a reflection coefficient of about 5 per cent. The highest-frequency  $E_s$  echo noted during a rocket flight was 8 Mc/s.

### 2. UNIFORMITY OF THE $E_s$ LAYER

One question which has remained unanswered is whether the sporadic- $E$  layer is uniform in electron density or whether it consists of many pancake-shaped high-density clouds. The rocket data have indicated consistently that the whole sporadic- $E$  region remains uniformly enhanced in density throughout. If one examines the ionograms taken at the same time at a station 10 to 80 km distant horizontally, one finds that the minimum frequency of the  $F$ -region reflections increased by one-half the gyro-frequency agrees fairly closely with the plasma frequency measured by the rocket in the sporadic- $E$  region. An excellent example of this was described by Jackson and Seddon (1958) for the flight of Aerobee-50. The penetration frequency was 5 Mc/s which agreed with the electron density

at the rocket within 17 to 30 per cent. The 17 per cent value would apply if the penetrating ray was the Z-mode, and the 30 per cent value if it were the ordinary ray.

A previous flight over New Mexico (Seddon 1954a) showed that the signal from the rocket immersed in an electron density whose plasma frequency was greater than that of the radiation frequency (but by an amount less than one-half the gyrofrequency) was able to transmit the signal to the ground by way of the Z-mode. Additional evidence was also afforded by the presence of a reflected ray from the bottom of the sporadic-*E* region when the rocket was below it. These reflections occurred immediately upon penetration of the sporadic-*E* region on the descent and during the period of the remainder of the descent. By geometry, it was computed that the reflection point must have moved 20 km horizontally along the bottom of the layer. During this time there was a small variation in amplitude but never any cessation of the reflected signal. Further, due to differential refraction, the ordinary and extraordinary rays would have a horizontal separation at the bottom of the *E*-region up to 1 km during the rocket descent. If, then, there were clouds of 1 km or so vertical thickness present in this layer with lower electron densities between them, there would have been a substantial difference in the computed electron density around the rocket using the two magneto-ionic components due to the different electrical path lengths. There seems to be no definite evidence that this was happening. A possible explanation could be, however, that there were numerous small clouds very close together which would thus tend to average out this sort of effect and thus maintain the agreement between the two magneto-ionic component results.

Still further evidence of the approximate continuity of the ionization can be found in the V-2 flight of January 22, 1948 (Seddon 1953). The 4.274 Mc/s signal abruptly disappeared at 100 km altitude. For the remainder of the flight, there were only five short occasions when a very weak signal could be detected. These signals were received only during a few seconds of the time the rocket was above the layer (about 4 minutes). These signals could have been due to a modest decrease in the electron density in the layer which apparently has a plasma frequency slightly greater than the signal frequency. Comparison with measurements made on the ascent could not be made because of the fact that the rocket record was very irregular at this time, due apparently to rocket out-gassing. This situation has been considerably improved in recent rockets by using propellant shut-off valves. However, an interesting comparison can be made with measurements made by a probe technique over Australia, as reported by Massey (1958). Figure 1 shows the similarity between sporadic *E* over New Mexico at midday with that over Australia at night. The difference in altitude is only about  $\frac{1}{2}$  km.

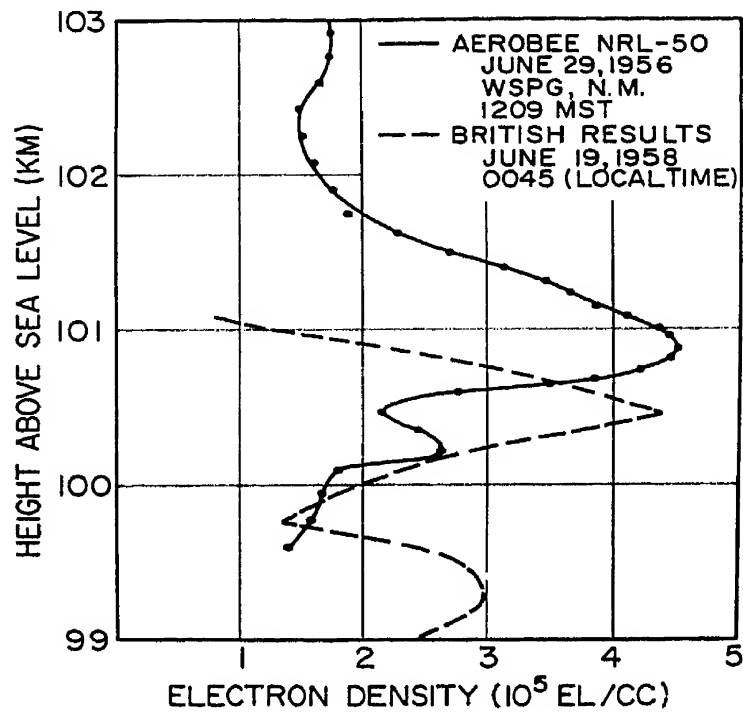


Fig. 1. Comparison of sporadic *E* at noon over New Mexico, U.S.A. with that over Woomera, Australia at midnight.

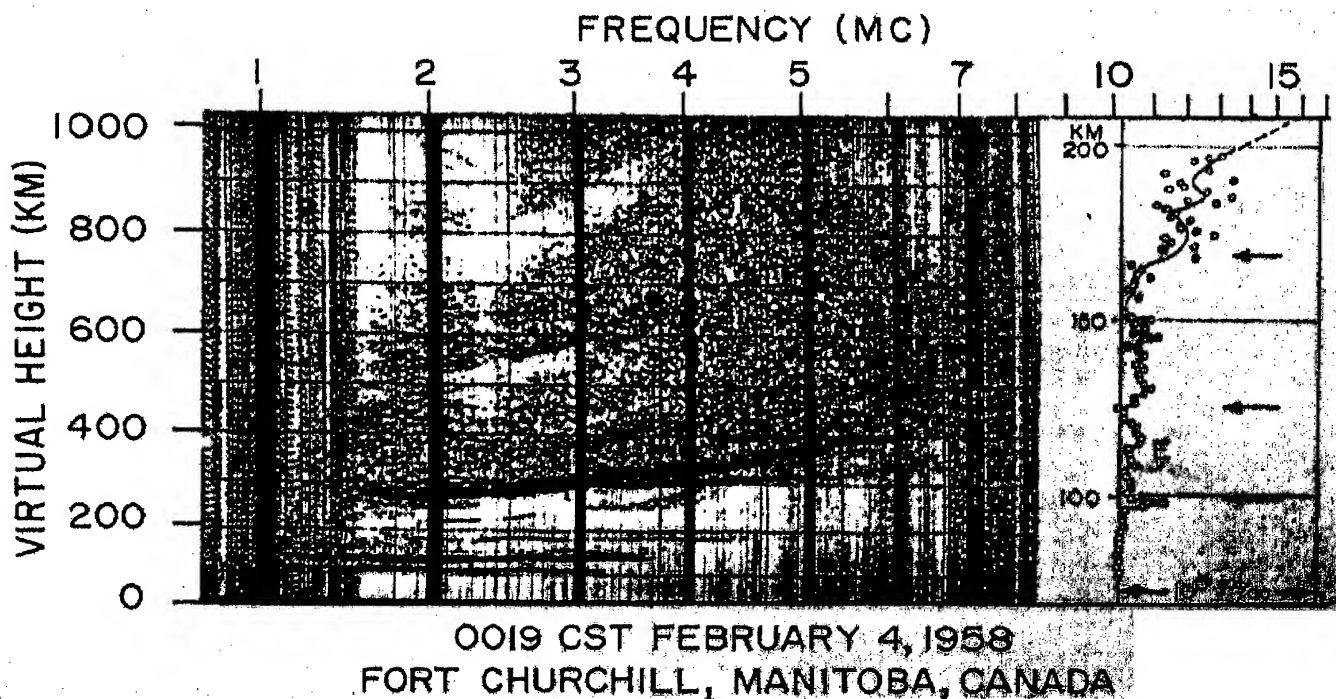
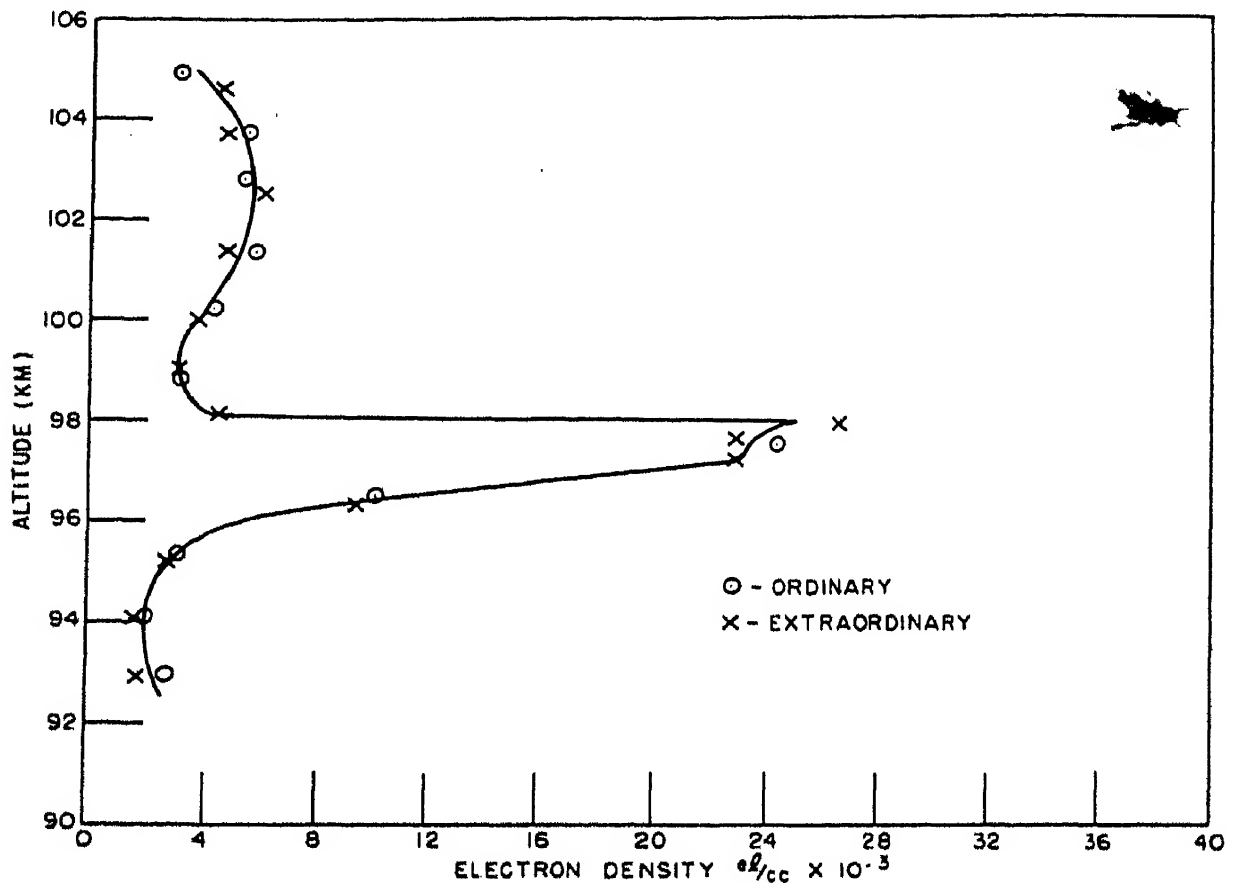


Fig. 2. Ionogram and electron density profile for a night flight over Ft. Churchill, Manitoba, Canada.

Figure 2 shows the data obtained from a rocket flight at Ft. Churchill, Canada at night, along with the corresponding ionograms. The grid placed over the ionogram at the ionosphere station is incorrectly placed. It is nearly 10 km too low. This could be verified from other ionograms where multiple echoes were present. The electron density was quite low up to an altitude of about 170 km with no trace of an *E*-region except for sporadic layers. The critical frequency of the lowest layer was approximately  $1\frac{1}{2}$  Mc/s, but the ionogram shows sporadic echoes up to  $3\frac{1}{2}$  Mc/s at this same altitude. The rocket data (Fig. 3) showed the layer to have a high electron



SPORADIC -E FEB 4, 1958 0018 HOURS CST  
 IGY ROCKET NN3.11F FT. CHURCHILL, CANADA

Fig. 3. Detailed profile of sporadic *E* over Ft. Churchill.

density gradient. This is the only case ever observed with rockets where the electron density gradient was much higher on the topside of the layer. Here a change in electron density occurred from 25,000  $\text{el/cm}^3$  to 5000  $\text{el/cm}^3$  in a vertical distance of not more than 80 meters. The thickness of the layer is about 2 km. The 129 km echoes came from a layer 600 m thick with a maximum density less than that of the lowest layer. The echoes from the lowest layer were persistent but the higher altitude echoes showed considerable variability, sometimes disappearing entirely. When the rocket

descended through the lowest layer, the gradient on the topside of the layer had decreased considerably. Thus the data indicate that this night-time ionosphere consisted of maximum ionization between 90 and 160 km of the order of a very few thousand electrons per cubic centimeter except for more dense layers at intervals which in one case reached 25,000 el/cm<sup>3</sup>. These superimposed layers vary a little in electron density with time but their gradients vary considerably and rapidly, at times reaching values unbelievably high. When the gradients become high, sporadic echoes are evident on the ground ionogram. At times the ionograms showed sporadic echoes at five different levels between 100 and 170 km. The ionosonde was located more than 30 km distant horizontally, so that the sporadic layers covered at least this distance. However, the rocket data showed a very large gradient at 200 km which persisted while the rocket travelled 12 km horizontally, then abruptly disappeared. Assuming that this gradient was due to a motionless cloud, the dimensions thus were about 12 km in extent. Although the gradient was so large that the 7.75 Mc/s signal decrease due to the partial reflection was greater than 20 db, the ionosonde does not show sporadic echoes from this altitude. Therefore, it seems that this was actually a cloud of dimensions less than 30 km that did not pass over the ionosonde and is probably associated with spread *F*. These observations are in agreement with the results reported by Prenatt (1960). At higher altitudes, other large gradients were observed of small horizontal extent which also did not show on the ionograms.

### 3. HEIGHT PREFERENCE

It was first noted by Helliwell and later by Pfister (1958) that there is a strong tendency for the sporadic-*E* layers to occur at certain specific altitudes and that, while these altitudes may show some variations, the difference in the altitudes of the sporadic-*E* layers is remarkably constant at a value of approximately 6 km. Table 1 shows the altitudes at which sporadic-*E* gradients were noted on the rocket records. The ionograms showed the usual sporadic-*E* echoes at these same altitudes. The altitudes thus seem to be near 100, 105, 111, 117 and 129 km. Pfister, using his rocket-borne pulse delay experiment, noted gradients at 94, 106, 112, 118, and 128 km. Careful scaling of the small graphs published by Gringauz (1958), (Fig. 4) shows high gradients at 101, 106, 109, 122, and 128 km. Examination of the Viking 10 results by Seddon, Pickar and Jackson (1954b) also show gradients at 142, 153 and 184 km. The difference between these altitudes and the 129 km altitude (the highest shown in Table 1), shows a difference of 13, 23, and 55 km. These differences are all close to multiples of 6 kilometers.

Observations by Millman (1959) on meteor trails has shown strong wind-shears to exist with an altitude separation of 6 km. Greenhow and

Table 1—Altitudes of high electron density gradients

Rocket	Date	Launch Time (hrs.-LMT)	Place	Altitude in Km.			
V-2 No. 34	Jan. 22, '48	1314	WSPG, N.M.	100			
Viking 5	Nov. 21, '50	1018	WSPG, N.M.			109	
Viking 10	May 7, '54	1000	WSPG, N.M.	100	105	112	129
Aerobee-Hi NRL-50	June 29, '56	1209	WSPG, N.M.	101			117
Aerobee-Hi IGY NN3.08F	July 4, '57	1216	Ft. Churchill		105		
Aerobee-Hi IGY NN3.10F	Feb. 3 '58	1202	Ft. Churchill			110	
Aerobee-Hi IGY NN3.11F	Feb. 4, '58	0017	Ft. Churchill	98			129

Neufeld (1959) have also found from meteor studies that the vertical extent of irregularities is 6 km with a horizontal extent of 100 to 200 km. Observations of rocket vapor trails and artificially-generated sodium clouds (Blamont 1959; Manring, Bedinger, Pettit and Moore 1959) frequently show a 6 km difference between wind currents, and the altitudes at which the wind gradients are the largest occur at these same altitudes in the *E*-region. Recent data by Manring, Bedinger, Knafllich and Lynch (1961) shows that large wind-shears at altitudes of 92, 100, 107, 110, 115 and 130 km. There thus seems to be a strong suspicion that the high electron density gradients are associated with wind-shear. This condition has been examined theoretically by Whitehead (1961).

Accurate but unpublished measurements of the earth's magnetic field utilizing a proton precessional magnetometer over Ft. Churchill, Canada by Meredith, Davis, Heppner and Berg (1958) shows a number of maxima between 70 and 140 km. The average separation between these maxima is approximately 6.5 km. The altitudes at which the magnetic field was a minimum correspond to the altitudes of sporadic *E*.

Measurements of temperature in the *E*-region are very difficult to make, but the pitot-static measurements of Ainsworth, Fox and Lagow (1961)



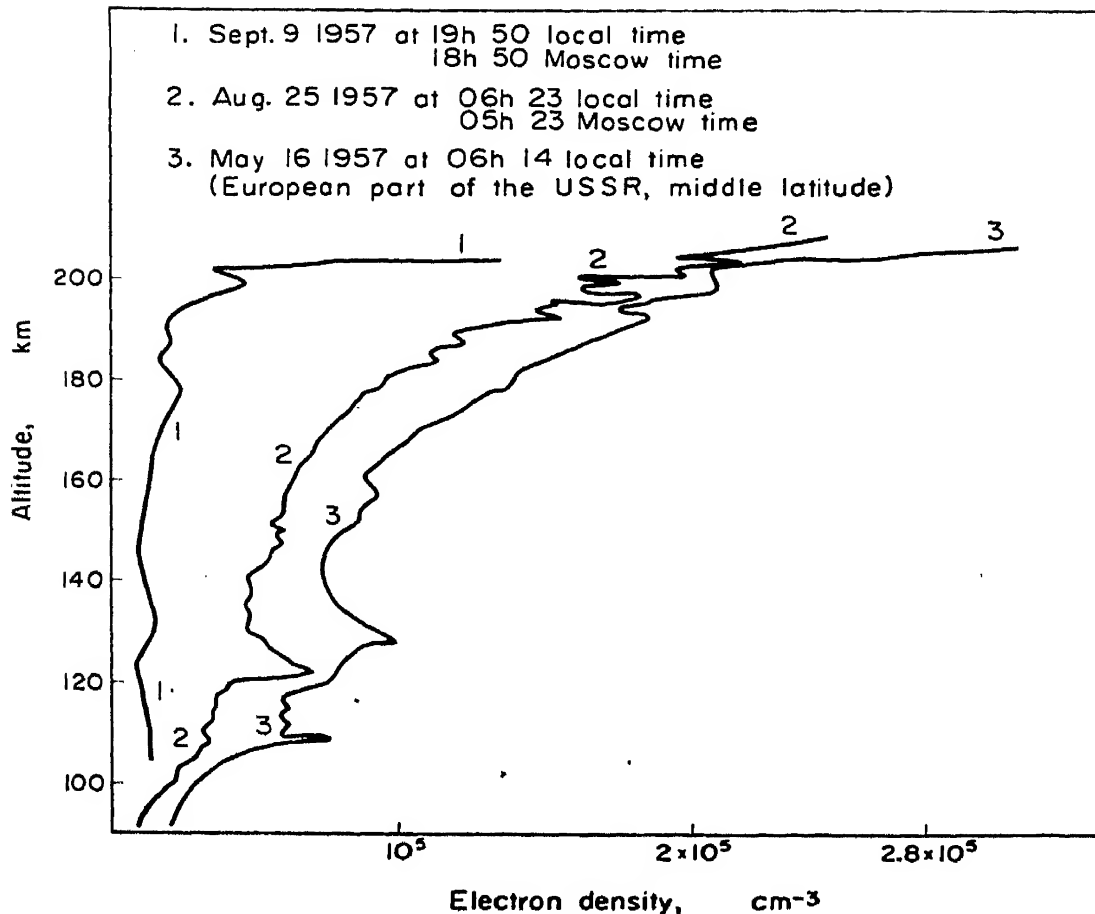


FIG. 4. Russian results using a CW technique (From *Dokl. Akad. Nauk. SSSR* and *Proc. Inst. of Radio Engrs.* 1959).

show definite minima at 73 and 92 km. At lower levels, between 30 and 70 km, there are small variations in the temperature profile with approximately 6 km separation between the peaks except for one case of 13 km separation. Ainsworth (1961) found that the vector wind gradient  $|\overline{d\vec{v}}/dh|$  had maxima at altitudes of 81, 87, 96, 103, 108, 113, 121, 126 and 131 km. The average difference is 6.25 km with an average deviation from the mean of 1.2 km. The data of Stroud, Nordberg, Bandeen, Bartman and Titus (1960) also show similar variations between 30 and 70 km. Many of these variations can be seen in their published results even though they have averaged their data. Gallet (1955) has considered the possibility that sporadic  $E$  may be associated with meteorological turbulence. His calculations, based upon the never-observed Chapman  $E$ -layer electron density distribution, shows that an increase in electron density gradient is possible one scale height below and one scale height above the maximum density of this  $E$ -layer. This separation of two scale heights exceeds the 6 km separation by a factor of slightly more than two. Further, it is difficult to see how this mechanism can account for separate, distinct layers of ionization as observed at night where these layers have a maximum electron density 5 times greater than a more or less constant electron density throughout the  $E$ -region. Wind-shear seems a more likely mechanism.



#### 4. GRADIENTS IN ELECTRON DENSITY

Rockets carrying the CW propagation experiment have penetrated 13 sporadic- $E$  layers with an electron density gradient large enough to cause echoes to show on the ground ionograms. On only one flight (Seddon, Pickar and Jackson 1954b) (Viking 10) were the gradients measured on both the ascent and descent of the rocket. On this flight, two gradients were found on both ascent and descent to be at the same level but two additional gradients developed during the rocket flight, which therefore showed only on the descent. They appeared on the proper ionogram. In all cases except three, the layer densities were less than 25 per cent above that of a smooth profile. The three remaining cases were those where a large increase in electron density occurred in the layer. In two cases, the minimum frequency of the  $F$ -region echoes was appreciably above the gyrofrequency and this minimum frequency, measured 30 km and more distant, was close to the plasma frequency of the sporadic- $E$  layer reduced by one-half the gyrofrequency. In the other case, no check was possible due to high absorption near and below the gyrofrequency. In all three of these later flights, the maximum frequency of the sporadic- $E$  echoes as noted on the ionograms was from 1 to 2 Mc/s greater than the plasma frequency.

#### 5. COMPARISON WITH THE PULSE TECHNIQUE

The rocket data show a consistent picture of sporadic- $E$  echoes being caused by high electron density gradients at the boundaries of thin horizontal layers of high density but with little evidence of an appreciable variation in electron density in a horizontal direction up to distances of 80 or more km. Unfortunately, the data are not sufficiently numerous to state that sporadic  $E$  is never any different. Even though the results have been consistent thus far, doubt has been expressed regarding the accuracy of the measurements. Some of this doubt may have been encouraged by the results obtained using a different radio propagation technique involving the time delay of pulses transmitted between the rocket and the ground. In some cases, negative numbers of electrons were obtained at some altitudes. This result may possibly occur because of the way in which the data were taken. As the delay is measured to the leading edge of the ordinary pulse, an error is introduced if this first received pulse is not the ordinary magneto-ionic component. It has been found during measurements utilizing the CW technique that additional components are present in the received signal besides the usual magneto-ionic components. This is especially true between 100 and 130 km altitude. These components consist of one or two additional frequencies which, strangely enough, may at times exceed the amplitude of the magneto-ionic component. If the

apparent index of refraction is computed for each of these components, it is usually found that the indices of refraction of the additional components are larger than those of the magneto-ionic components, but this is not invariably true. If the electron density of the medium is then computed, it is found that agreement is obtained between one ordinary component and one extraordinary component, but there is no agreement between the others. Thus it would seem reasonable that, under these conditions, pulse transmission may result in several pulses being received at slightly different time intervals. As the apparent index of refraction of the undesired components are usually greater than those of the magneto-ionic components, this would result in too small a delay being measured at times. Thus the appearance of these additional components could cause a decrease in the total delay time, resulting in computed negative electron densities.

## 6. TIME VARIATION

Another objection that has been raised to all radio propagation measurements is that the profile so obtained can be seriously in error because of either time variation of the ionosphere below the rocket, or due to inhomogeneities in the ionosphere in a horizontal direction resulting in changes in the electron content along the propagation path as a result of the horizontal motion of the rocket. It is true that some error can be introduced by these mechanisms. However, two stations 10 km apart give data that agree within about 5 per cent. In addition, the ordinary and extraordinary components at each station are in similar agreement with each other. Still further, the computation of the virtual height at various frequencies shows good agreement with the ionograms taken at the same time. In order to account for the high electron densities in the sporadic-*E* layer measured during the flight of Aerobee-50 where large electron densities were observed, one might consider the error introduced by having all the ionization between 75 and 100 km double in value in a period of  $1\frac{1}{2}$  sec, the transit time of the rocket through the layer. This extremely improbable situation is still a factor of about 5 below that needed to account for the observed results. In addition, it can be pointed out that even when these thin, high gradient layers do not increase greatly in electron density, invariably sporadic echoes are found on the ionograms at these exact heights. The rocket results obtained thus far on sporadic *E* by the CW propagation technique simply cannot be explained by either time variation of electron density or by interception of irregularities due to the horizontal motion of the rocket.

## REFERENCES

- AINSWORTH, J. A., FOX, W. F. and LAGOW, H. E. (1961a) *NASA Tech. Note D-670*.

- AINSWORTH, J. A. (1961b) Private Communication.
- BLAMONT, J. E. (1959) *Comptes Rendus* 249, 14, 1248.
- GALLET, R. M. (1955) *Proc. Inst. of Radio Engrs.* 43, 10, 1240.
- GREENHOW, J. S. and NEUFELD, E. L. (1959) *J. Geophys. Res.* 64, 12, 2129.
- GRINGAUZ, K. I. (1958) *Dokl. Akad. Nauk. SSSR*, 120, 6, 1234.
- JACKSON, J. E. and SEDDON, J. C. (1958) *J. Geophys. Res.* 63, 1, 197.
- MANRING, E., BEDINGER, J. F., PETITT, H. B. and MOORE, C. B. (1959) *J. Geophys. Res.* 64, 6, 587.
- MANRING, E., BEDINGER, J. F., KNAFLICH, H. and LYNCH, R. (1961) *Geophys. Corp. of Amer.* (Bedford, Mass.) Tech. Rept. 61-1-N.
- MASSEY, H. S. W. (1958). To be publ., *Annals of the IGY*, Pergamon Press, London, Eng.
- MEREDITH, L. H., DAVIS, L. R., HEPPNER, J. P. and BERG, O. E. (1958) *IGY Rocket Report 1*, Rockets and Satellites p. 173.
- MILLMAN, P. M. (1959) *J. Geophys. Res.* 64, 12, 2122.
- PFISTER, W. H. and ULWICK, J. C. (1958) *J. Geophys. Res.* 63, 2, 315.
- PRENATT, R. E. (1960) *J. Amer. Rocket Soc.* 30, 8, 763.
- SEDDON, J. C. (1953) *J. Geophys. Res.* 58, 3, 323.
- SEDDON, J. C. (1954a) *J. Geophys. Res.* 59, 4, 463.
- SEDDON, J. C., PICKAR, A. D. and JACKSON, J. E. (1954b) *J. Geophys. Res.* 59, 4, 513.
- STROUD, W. G., NORDBERG, W., BANDEEN, W. R., BARTMAN, F. L. and TITUS, P. (1960) *J. Geophys. Res.* 65, 8, 2307.
- WHITEHEAD, J. D. (1961) *J. Atmosph. Terr. Phys.* 20, 1, 49.

# Backscatter Observations of Sporadic *E*

R. D. EGAN and A. M. PETERSON

Radioscience Laboratory, Stanford University, Stanford,  
California, U.S.A.

**Abstract**—Backscatter sounding of the ionosphere provides information on the growth, drift and appearance of sporadic-*E* clouds over a wide region about the sounding station. Sweep-frequency backscatter sounding has been especially useful for observing certain types of auroral forms of sporadic *E*, while the fixed-frequency, swept-azimuth backscatter sounder has provided valuable information on sporadic-*E* characteristics at temperate and equatorial latitudes. Observations near the magnetic equator have revealed the presence of field-aligned irregularities in the *E*-region which are responsible for the equatorial type of sporadic *E*. Temperate latitude observations have shown that there is a marked difference in the amount of sporadic *E* observed over water and over land at a coastal observing station. In addition to these effects, sporadic-*E* drift motions as well as other observations (by backscatter techniques) made during the International Geophysical Year are summarized.

## 1. INTRODUCTION

Backscatter sounding of the ionosphere is an oblique pulsed radar method for the study of the regular layers, sporadic *E*, and a variety of irregularities which occur within the ionosphere. Whereas vertical incidence soundings record in considerable detail only those events occurring overhead, oblique backscatter sounding permits surveillance of a considerable region of the ionosphere, from a single location, though in lesser detail. Sporadic-*E* patches are regularly observed with backscatter sounders by virtue of ground backscattering. The appearance, growth, and drift of these patches can be studied in an area having a radius of roughly 1000 km about the observing station.

A wide variety of sounders with markedly different characteristics have been used successfully for scatter sounding. Two distinct types of sounders have been developed; the "fixed-frequency" sounder and the "sweep-frequency" sounder. Fixed-frequency sounders have normally been operated with transmissions at one or more fixed frequencies, making use of rotatable directive antenna systems and some suitable means of data display and recording. While a simple range-time or A-scope presentation will suffice when one is interested in measuring conditions over one particular path, for most convenient display of conditions over a large number of paths a plan-position-indicator or PPI display is desirable. With a PPI

display, as the directive antenna is rotated, a range-azimuth polar plot is traced out on the cathode ray tube screen. This display can then be photographed to provide a permanent record.

Sweep-frequency sounders are similar in many respects to the familiar vertical-incidence sweep-frequency ionosphere recorder. Modifications to the antenna system and frequency sweep rates are generally required for successful backscatter sounding. In addition, longer pulses and narrower receiver bandwidths often prove useful. Sweep-frequency sounder data display is generally in the form of a raster scan of range-versus-frequency on a cathode ray tube, which may be photographed to provide a permanent record.

Historically, backscatter echoes were first observed while monitoring high power transmissions at a short distance from the transmitter. Since 1950, when it was shown by Dieminger (1951) and Peterson (1951) that backscattering occurred primarily at the ground and not in the  $E$ -region, backscatter signals have been extensively studied. In particular, work has been carried out in the United States, England, Germany and Japan, with specialized equipment of both the fixed-frequency and sweep-frequency variety developed to facilitate ionospheric research.

During the International Geophysical Year extensive oblique-incidence backscatter studies were carried out at thirteen widely separated stations by Stanford University with additional work of this type continuing at other centers in the United States, England, Germany and Japan. Backscatter sounding efforts have also begun in Italy and Puerto Rico since the beginning of the IGY. While much of the above work deals primarily with  $F$ -region propagation, sporadic- $E$  observations are scattered throughout the reports since both forms of propagation appear on the same records simultaneously. The  $F$ -region propagated backscatter is, however, the most dominant feature of most backscatter records.

## 2. DEFINITION AND IDENTIFICATION

Proper identification of sporadic  $E$  on backscatter records requires considerable experience. In contrast to vertical-incidence  $E_s$  observations which are rather easily interpreted for sporadic- $E$  identification, oblique observations of  $E_s$  are often confused by a number of factors. Because of the height at which  $E_s$  occurs, one-hop backscatter echoes are not obtained at ranges greater than about 2200 km. However, if the oblique sounding frequency is less than about two times the critical frequency of the  $F$ -region, then  $F$ -region propagated echoes will appear at ranges less than 2000 km. In fixed-frequency soundings these  $F$ -region echoes may be mistaken for  $E_s$  or vice versa unless continuous observations are available so that hour by hour (or even minute by minute) trends may be observed.

Equally serious is the obscuring effect that  $F$ -region propagated echoes have on  $E_s$  observations. When sounding near the critical-frequency the range interval out to 2000 km and beyond may be completely filled with  $F$ -region propagated ground backscatter echoes. With oscilloscope intensity recording (e.g. PPI or range-time) all  $E_s$  information is lost. If simultaneous range-amplitude recordings are also available,  $E_s$  may sometimes be seen through the  $F$ -region propagated echoes. Sweep-frequency sounding materially reduces the problem of identification since the  $E_s$  echo may frequently be traced through the  $F$ -region propagated echo.

Inasmuch as the normal definitions of  $E_s$  are based primarily on their appearance on vertical ionograms (c.f. Smith 1957) it is necessary to group the oblique backscatter echoes into slightly different classifications unless the echo can be positively identified with one of the vertical incidence types. A detailed examination of  $E_s$  by oblique sweep-frequency sounding has not been done, although Silberstein (1953, 1954) has commented on  $E_s$  observed obliquely and vertically simultaneously and Bates (1960) has studied high latitude  $E_s$ . A much more comprehensive study has been possible with the IGY network of fixed-frequency oblique-incidence sounders (Peterson, Egan and Pratt 1959). Echoes observed on this equipment may be grouped into three categories. At sub-auroral and auroral latitudes a type of  $E_s$  is frequently observed on the PPI records which is definitely associated with auroral disturbances and will henceforth be called auroral  $E_s$ . It is characterized on the oblique sounding records by a fine grained structure with smooth edges; in contrast to the patchy appearance of other sporadic- $E$  echoes, which suggests a scattering process for the reflection mechanism.

A second type of oblique  $E_s$  is seen near the magnetic equator. Sporadic  $E$  is an unfortunate term to apply to these echoes inasmuch as the echoes are produced by scattering within the  $E$ -region and not at the ground, and the echoes appear on well over 90 per cent of the days. However, this oblique equatorial  $E_s$  is directly related to the "equatorial  $E_s$ " seen on vertical sounders.

The third category of oblique  $E_s$  is a general grouping that is predominant at temperate latitudes. In this latter category there is a marked seasonal variation with the maximum activity occurring during the summer months.

### 3. INTERPRETATION AND OBSERVATION LIMITATIONS

Originally it was thought that ionospherically propagated backscatter signals were due to backscattering in the  $E$ -region. However, Dieminger (1951) and Peterson (1951) have shown that backscattering usually occurs at the ground even in the case of  $F$ -region propagated signals. Experimental

sweep-frequency backscatter measurements made by Silberstein in 1952 and reported in 1954 indicated a number of instances where pulse signals were directly returned from sporadic- $E$  patches during disturbed periods. However, in each of the cases reported, the ground backscatter echo was also readily apparent. An analysis of early Stanford backscatter records indicated that direct backscattering from sporadic- $E$  patches occurred in less than 10 per cent of the cases. Very few instances were identified when only direct backscatter was observed without ground backscatter also being apparent.

As further proof of ground backscattering, a review of the tremendous mass of sporadic- $E$  data acquired during the IGY by the thirteen fixed-frequency backscatter sounders reveals that the centroid of the sporadic- $E$  echoes observed on the PPI recordings tend to occur at a median slant range of about 1000 km. If the sporadic- $E$  propagated ground-backscatter mode is assumed, then these patches would be seen most frequently when they were at a range of about 500 km from the observing station. However, if backscattering is assumed to take place within the  $E$ -region, then the  $E_s$  patches would be observed with the median range of 1000 km. The known vertical-plane antenna pattern of the IGY sounders is highly discriminatory against the latter case which requires a vertical take-off angle of about one degree. However, the  $E_s$  propagated ground-backscatter mode is such that the maximum radiation in the vertical plane passes through the  $E$ -region at a range of 300 to 500 km. Further study shows that the  $E_s$  patch occurrence distribution in range is essentially a reproduction of the antenna pattern when proper adjustment is made for the secant- $\phi$  factor. Thus, it will be assumed for the discussion of temperate latitude sporadic  $E$  that backscattering does not occur in the  $E$ -region unless specifically noted. The small number of instances where backscattering does occur in the  $E$ -region will not materially affect the overall statistics.

In contrast, however, most of the equatorial sporadic- $E$  observations and many of the auroral sporadic- $E$  observations result from direct backscattering from the ionosphere.

The position and size of sporadic- $E$  patches that are recorded on an oblique backscatter sounder are strongly influenced by equipment parameters, the state of the ionosphere, and geometrical ray path considerations. In particular, from purely geometrical considerations, the maximum range of  $E$ -region (110 km) observation is limited by the earth curvature. This maximum range is approximately 1180 km to the  $E$ -region, or 2360 km range to the ground backscattering point. The minimum range would, of course, be the height of the region overhead. However, the 2 millisecc pulses commonly utilized for the IGY sounders, and a maximum 1 millisecc system recovery time following the transmitted pulse, limit the minimum range to 225 km to the  $E$ -region, or 450 km to the ground backscattering point.



The vertical directivity of the three element Yagi antennas further restricts the optimum range interval from about 250 km to 750 km in the *E*-region case, or 500 to 1500 km in the ground scattering case.

Assuming a height of 110 km and that the classical "secant- $\phi$ " relation between vertical-incidence critical frequency and oblique-incidence critical frequency is valid for sporadic *E* (cf. Wright and Gautier 1960); then an *E<sub>s</sub>* patch with a vertical-incidence critical frequency of 5 Mc/s may be observed at oblique incidence at 250 km on a frequency of 11.8 Mc/s. Table 1 lists some other typical values for comparison purposes.

Table 1—Frequencies below which *E<sub>s</sub>* patches with given critical frequencies may be observed at various ranges.

$f_o E_s$	Range—km.		
	250	500	750
3	7.1	11.6	14.4
5	11.8	19.3	24.0
7	16.6	27.0	33.6
9	21.3	34.8	43.3

An exception to the minimum range limit occurs when the patch is large enough to extend partially or completely around the PPI center—in which case the centroid of match may be estimated quite closely in to zero range (overhead).

The apparent azimuthal extent of *E<sub>s</sub>* patches, when observed on PPI recordings, is the result of the convolution of the actual patch characteristics with the horizontal antenna pattern. The three-element Yagi used for the rotating antenna system in the IGY sounder has a beam width of approximately 60 degrees to the half-power points or approximately 40 degrees to the half-power points when used for both transmitting and receiving. Thus, the usual echo will be at least 40 degrees wide in azimuth, but the centroid of the patch may still be determined quite accurately—a feature that is useful in studying *E<sub>s</sub>* motion.

#### 4. AURORAL *E<sub>s</sub>*

Using the fixed-frequency backscatter sounder technique at sub-auroral latitudes, sporadic-*E* echoes that are strongly correlated with magnetic activity and echoes from field aligned irregularities may frequently be seen to the north. A typical time sequence of echoes, at sub-auroral latitudes (Fig. 1) begins with the appearance of *E*-region field-aligned echoes. These are followed, a short time later, by a ground scatter echo at twice the range—presumably the result of a formation of an *E<sub>s</sub>* patch in the *E*-region





Fig. 1. Sequence of PPI photographs (18 Mc/s) illustrating the appearance of a field-aligned irregularity echo in the north (top of PPI's) at 900 km and the subsequent appearance of an  $E_s$  propagated ground backscatter echo. June 3, 1960.

by corpuscular bombardment. Some time later, possibly minutes or hours, the field-aligned irregularity echoes will disappear, leaving only the sporadic- $E$  propagated ground-backscatter echo. This sporadic- $E$  patch may last for several hours beyond the cessation of the field-aligned irregularity echoes. The close relation between the field aligned irregularity echoes and  $E_s$  was graphically illustrated (Fig. 2) by an experiment per-

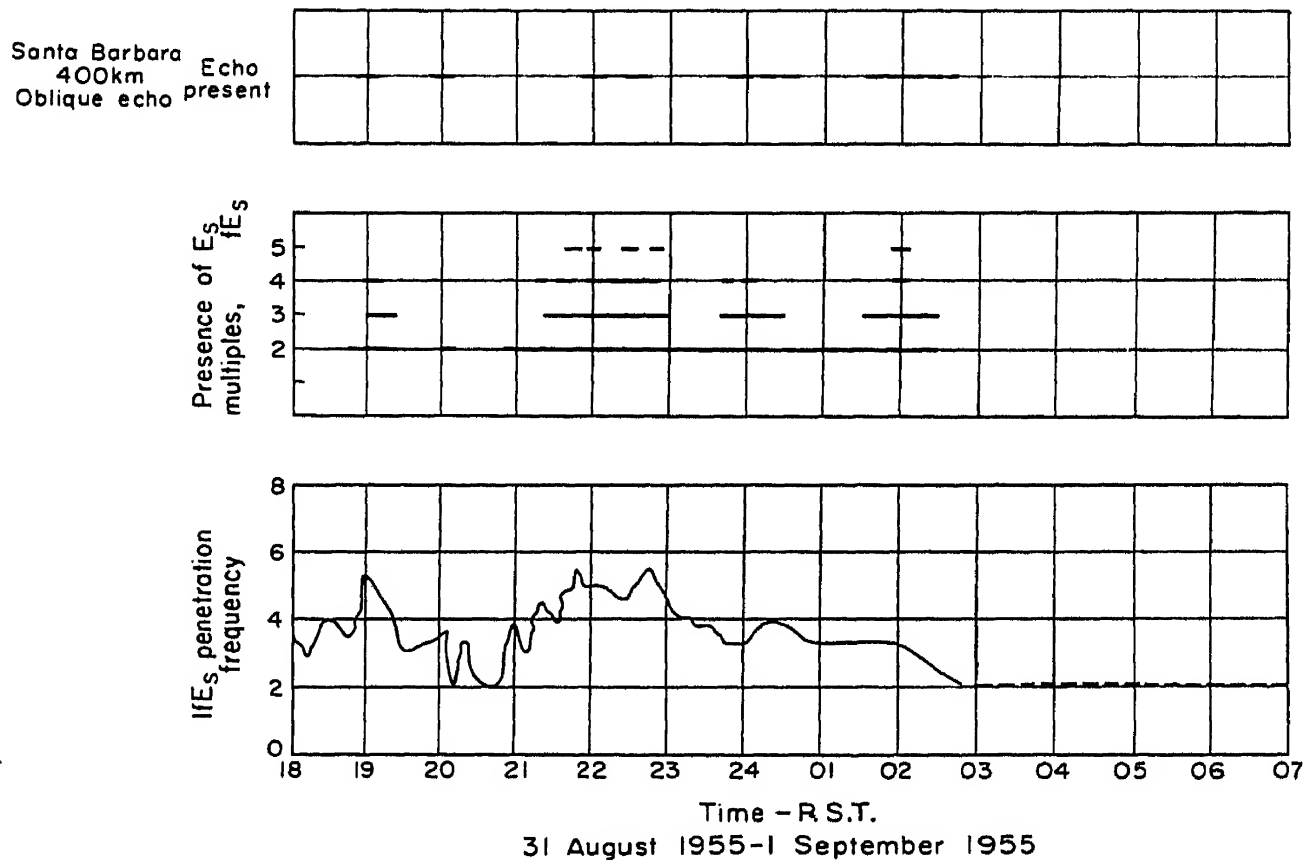


Fig. 2. Plot of occurrence of  $E$ -region field-aligned irregularity echo overhead at Stanford as seen from Santa Barbara, California, and  $E_s$  critical frequency and numbers of multiples observed simultaneously at Stanford.

formed at Stanford (Leadabrand 1955). The  $E$ -region overhead at Stanford was sounded with a vertical-incidence sounder and simultaneously with a backscatter radar approximately 400 km south of Stanford.

This same type of  $E_s$  is also observed in the auroral zone, although the aspect-sensitive field-aligned irregularity echo may not always be observed because of geometry limitations between the observing radar and the magnetic field.

At auroral latitudes, using the oblique sweep-frequency backscatter sounding technique, Bates (1960) has recently shown that auroral  $E_s$  (as observed on vertical sounders) is very likely the result of scattering from field-aligned irregularities — a possible mechanism suggested earlier by Smith (1957). At these high latitudes a perpendicular intersection between

the magnetic field lines and a line of sight from the observing radar is not always possible, even to the north. Therefore, a certain amount of ionospheric refraction is required to cause the radio energy to be incident normally on the scattering irregularities. In contrast to the lower latitude  $E_s$ , the auroral  $E_s$  always emanates from the high frequency end of the normal vertical-incidence  $E_s$  trace (Fig. 3). Bates describes the slanting portion of the echo as being a natural consequence of "least time focusing" of an oblique echo (such as described by Peterson (1951) and Dieminger (1951) for  $F$ -region propagated ground backscatter). At higher frequencies, the slanting portion may flatten out to essentially a constant range (approximately 400 to 500 km at 15 to 20 Mc/s) which may be explained by aspect focusing. That is, the observing frequency is now sufficiently high that refraction in the layer is negligible and the echo is returned from a region where the angle between the line-of-sight and the earth's magnetic field is a minimum. Simultaneous 41 Mc/s radar observations of auroral echoes appear to confirm this latter interpretation.

The refraction required to provide the proper aspect angle relative to the magnetic field must be provided within the  $E$ -region, so it is not surprising that the slant  $E_s$  traces are usually associated with retardation  $E_s$ , which Smith notes "has considerable thickness as evidenced by the observable retardation".

## 5. EQUATORIAL $E_s$

Equatorial  $E_s$  has been observed since the earliest automatic sweep-frequency vertical-incidence sounder was installed at Huancayo, Peru. Sporadic  $E$  is, perhaps, a misnomer for this particular class of echo, inasmuch as it is by no means sporadic in occurrence — appearing regularly on over 95 per cent of the days. However, it certainly falls within the broad definition of "sporadic  $E$ " as proposed by E. K. Smith (1957), which specifically included a "scattering mechanism if such is active."

With the installation of the Stanford fixed-frequency backscatter sounder at Huancayo for the IGY, an anomalous echo appeared almost daily in the east and west directions. This echo was shown (Egan 1959) to be the result of backscattering from field-aligned irregularities in and above the  $E$ -region and which is referred to as equatorial scatter ( $E_qS$ ) by Egan.

Figure 4 is a typical PPI picture of  $E_qS$  echo on a frequency of 18 Mc/s at 1300 LMT. The  $E_qS$  appears fan-shaped to the east and west, begins quite sharply at a range of 200 km and extends out to 400 to 600 km. The scattering mechanism is highly aspect-sensitive, with a maximum normal to the magnetic field. The range variation and the azimuthal variation are primarily determined by the height of the scattering region and the directivity of the antenna.

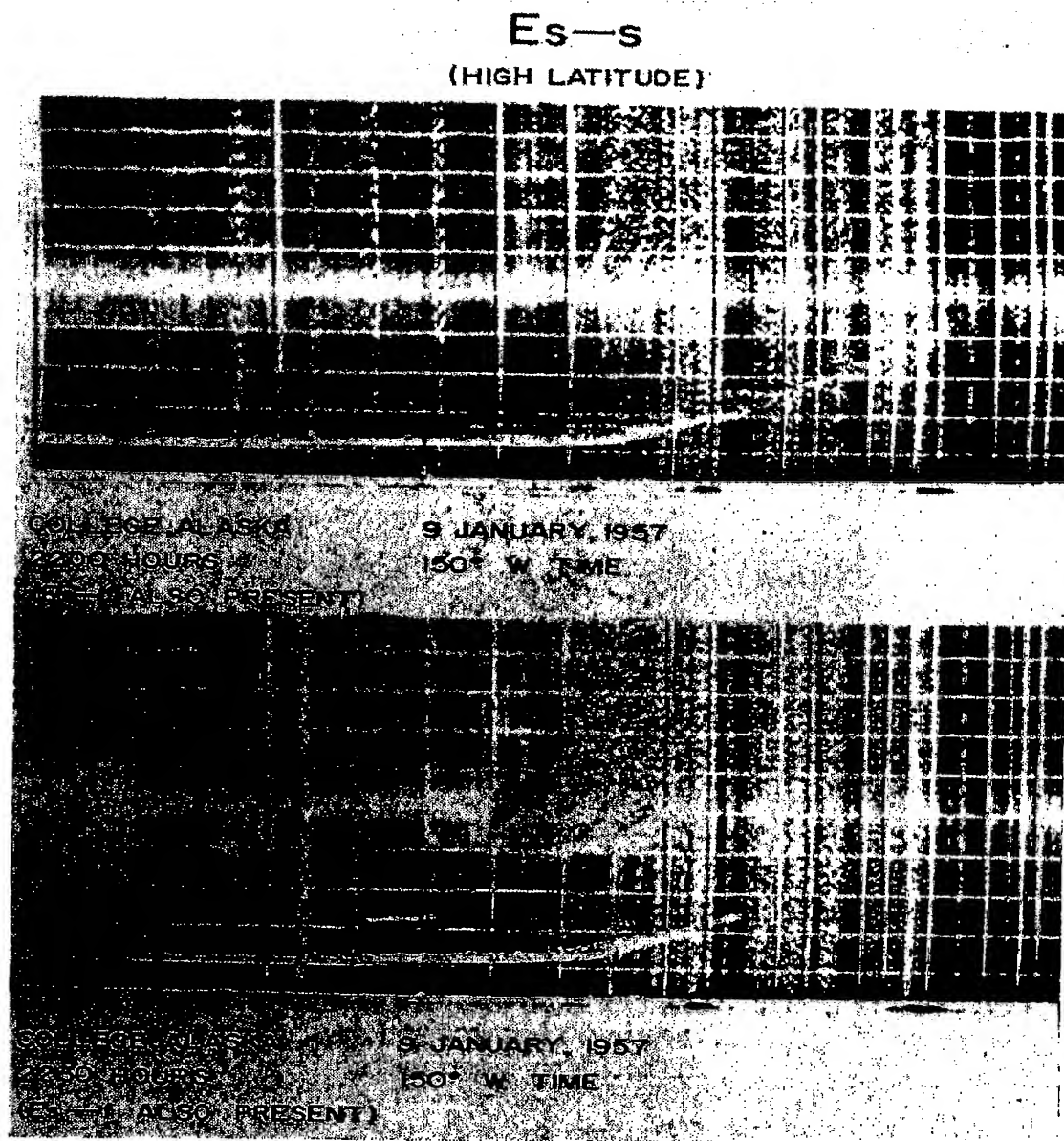


Fig. 3. Ionogram showing high-latitude slant  $E_s$  at College, Alaska.

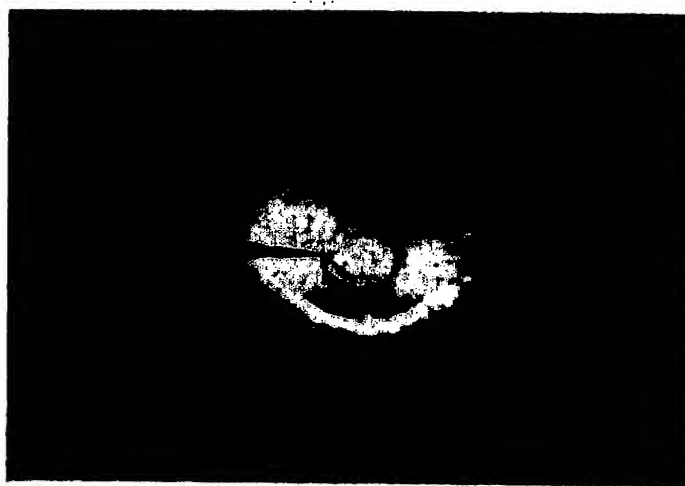


Fig. 4. Backscatter sounder PPI display showing equatorial scatter ( $E_qS$ ) echo in the east and west observed at Huancayo, Peru at 1300 LMT 23 July 1959. Range circles are at 100 km intervals. The wedge of missing echo in the west is due to an incomplete antenna rotation during the picture time interval.

The  $E_qS$  echoes exhibit an interesting diurnal behavior that suggests an east to west movement of the scattering region coincident with the movement of the equatorial electrojet. The echoes appear first in the east in the morning and disappear to the west in the evening but always aligned closely along the dip equator. The scattering region is quite transparent, as can be seen in Fig. 5, where the  $F$ -region propagated ground backscatter



Fig. 5. Long-range (compressed scale) PPI picture taken simultaneously with the PPI of Fig. 4. The  $E_qS$  echo is merged with the transmitted pulse at the center. The first-hop  $F$ -region propagated ground-backscatter echo is seen at all azimuths and is not affected by the presence of the  $E$ -region irregularities. Range marks are at 1000 km intervals.

is not affected, and also is evidenced by the fact that ground backscatter has never been observed as a result of propagation by these irregularities. The echoes also exhibit a high fading rate characteristic of a scattering process, rather than layer reflection.

Matsushita (1953) has shown that vertical drift forces are acting on the ionized region at the magnetic equator. The presence of irregularities is now known to exist, and Martyn (1959ab) has shown that any such irregularities on the under side of a vertically rising region are unstable. That is, they increase in magnitude with time. On the other hand, irregularities on the upper side are smoothed out. Conversely, when the region is moving vertically downward the conditions for stability are reversed—irregularities on the upper side are increased and those on the lower side are smoothed out. The upward drift force is due to the eastward flowing currents of the solar magnetic variation. Matsushita (1957) suggested that the  $E_s-q$  may be caused by this upward drift force and, consequently, that the occasional early disappearance of sporadic  $E$  is the result of a partial cancellation of the eastward current by a westward current due to the lunar magnetic variation. Recently, Knecht (1959) added further support

to this hypothesis, by showing a similar relation for the time of appearance of  $E_s-q$  at Huancayo. Interestingly, this upward drift force reaches a maximum near noon (the peak of the electrojet current), which corresponds to the time of maximum intensity of both  $E_s-q$  and  $E_qS$  echoes.

During the night the region is moving downward, smoothing out lower side irregularities and enhancing those on the upper side. As was pointed out by Martyn (1959ab), however, the gas pressure is lower on the upper side and the irregularities will be smoothed out relatively quickly by diffusion. This agrees well with the observations of  $E_s-q$ , which is seen very infrequently at night (Thomas and Smith 1959), and  $E_qS$ , which was never observed at night with the relatively low power (5 kW) IGY sounder.

In summary, Egan suggested that the oblique incidence  $E_qS$  echo is the result of irregularities in ionization which are aligned with the magnetic field and are present throughout the region in which the equatorial electrojet is flowing. As a result of the upward vertical drift motion of the ionosphere during the day, the field-aligned irregularities, which are observed directly by the oblique incidence sounder, are further enhanced as a result of the instability of these irregularities on the lower side of the vertically drifting region. The enhancement effect is strongest near the bottom of the region and produces the intense equatorial sporadic  $E$  which is observed on the vertical-incidence sounders.

Recently, Bowles, Cohen, Ochs and Balsley (1960) have questioned the applicability of the usual model of thin ellipsoidal field-aligned irregularities (Booker 1956) and, instead, propose a model in which the irregularities are plane wave fronts with wave normals perpendicular to the magnetic field. They put forth this model to explain the equal Doppler shifts they apparently observed at 30 and 60 degrees from the vertical (with opposite signs in the east and west).

## 6. TEMPERATE LATITUDE $E_s$

Sporadic  $E$  at temperate latitudes is perhaps the most explored but least explained of all the sporadic- $E$  types. At this time backscatter observations do not permit a distinction between the various types of  $E_s$  seen on the vertical-incidence sweep-frequency sounder. The most comprehensive backscatter study of temperate latitude sporadic  $E$  has been done during the IGY. Eight of the Stanford fixed frequency backscatter sounders were located between latitudes of 20 and 50 degrees, including one in the southern hemisphere at Camden, Australia. Three of these stations (Stanford, Boulder and Pullman) were located to permit overlapping surveillance of the  $E$ -region—a situation which has proven exceptionally useful for the study of  $E_s$  motion and also permits direct intercomparison of sporadic  $E$  on a synoptic geographical basis.

The appearance of sporadic  $E$  on the PPI scope of temperate-latitude fixed-frequency backscatter stations may assume any form within the limitations imposed by geometrical antenna pattern and  $E_s$  ionization density considerations. Figure 6 is an example of an intense  $E_s$  patch

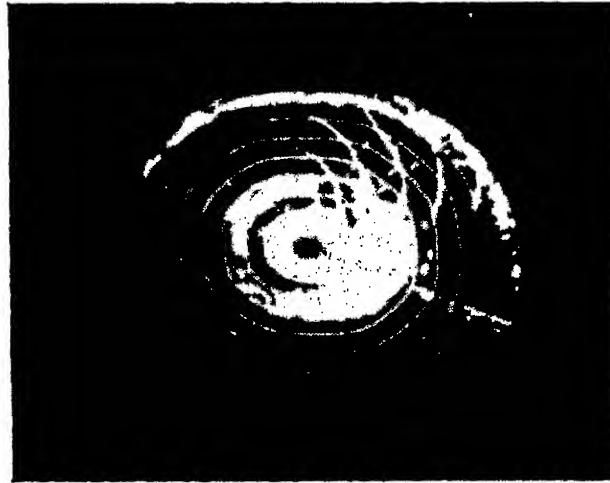


Fig. 6. PPI picture of  $E_s$  observed at Camden, Australia on 30 Mc/s 1300 LMT 28 December 1958. Range marks are at 500 km intervals. One-hop  $F$ -layer propagated ground backscatter is seen in the north at 3500 km.

observed to the southeast at Camden, Australia. An  $E_s$  patch which was observed simultaneously overhead at Stanford on the vertical-incidence sounder is illustrated in Fig. 7. The ionogram of Fig. 8 was taken simultaneously with the backscatter record of Fig. 7.

While a number of important contributions to the knowledge of sporadic  $E$  have been made by sweep-frequency backscatter observations, the total amount of record time of this type of equipment has been relatively

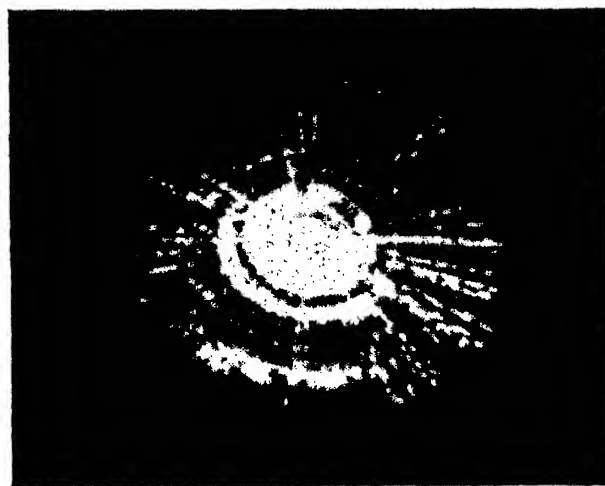


Fig. 7. PPI picture of  $E_s$  observed at Stanford, California, on 18 Mc/s at 2100 LMT 12 June 1959. Range marks are at 500 km intervals. One-hop and two-hop  $F$ -layer propagated backscatter are seen in the south at 2000 and 3500 km respectively.



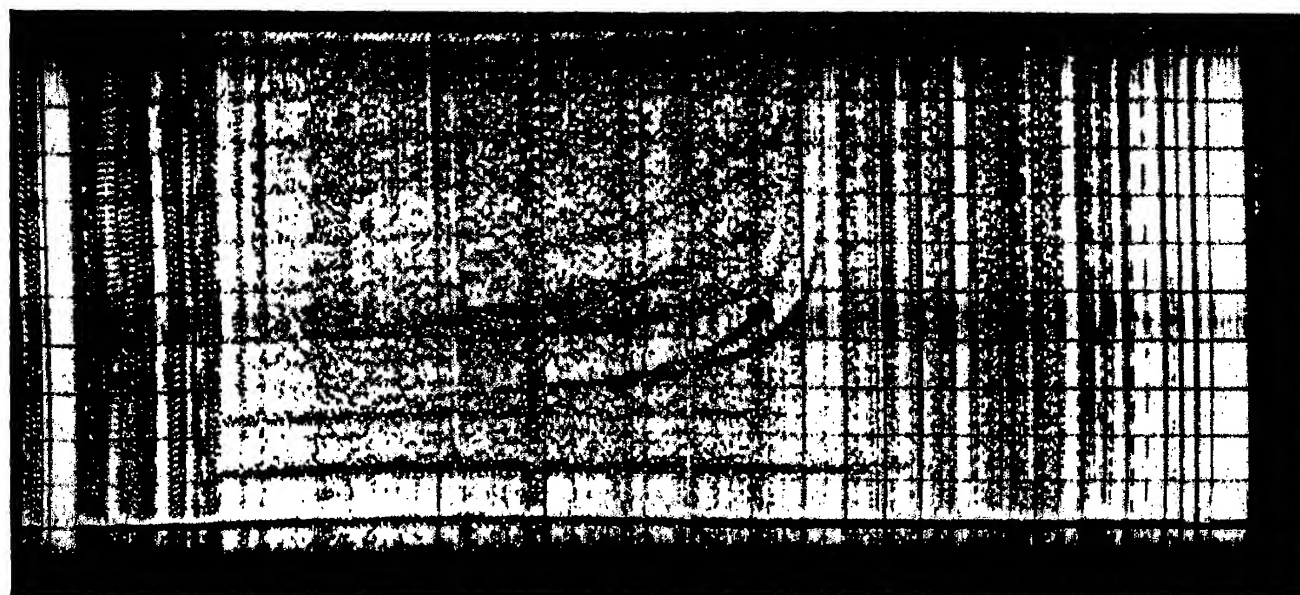


Fig. 8. Ionogram taken at Stanford, California, simultaneously with the PPI of Fig. 4.  $f_oE_s$  is approximately 10.5 Mc/s.

limited by comparison with the tremendous amount of synoptic data available from the IGY fixed-frequency (12, 18 and 30 Mc/s) backscatter sounder network. Consequently, much of the current statistics, both in time and in geographical location, must come from this IGY data.

In addition to the previously discussed limitations on the observation of sporadic  $E$ , an additional factor is very important in the temperate latitudes, where  $F$ -region critical frequencies reach their highest values. During the daytime hours and, in fact, well into the evening hours during the past three years, the  $F$ -layer critical frequency was frequently above the 12 Mc/s backscatter frequency. When this condition occurs, the ranges at which  $E_s$  is normally observed are contaminated by  $F$ -region propagated ground backscatter and sporadic- $E$  patches can usually not be observed. Thus, sporadic- $E$  information obtained on 12 Mc/s is severely limited. To a lesser extent, the 18 Mc/s frequency is similarly affected. Diurnal occurrence statistics cannot be reliably obtained if the  $F$ -layer skip distance is 2000 km or less during the month. To a certain extent, the annual variation of sporadic- $E$  observations will also be influenced by the annual variation in  $f_oF2$ . However, even with these possible limitations, it is encouraging to note that the seasonal and diurnal variations agree with vertical-incidence observations. To illustrate this agreement, the average minutes of the  $E_s$  echo per day, observed at Stanford and Camden, has been plotted for the period October 1957 to December 1958 (Fig. 9). The summer maximum of  $E_s$  occurrence is readily apparent at both stations. In addition, a secondary winter maximum is seen at Stanford which is due almost entirely to  $E_s$  occurring between the local hours of 1800 and 2300. The Far East anomaly may also be seen in the relative  $E_s$  occurrence



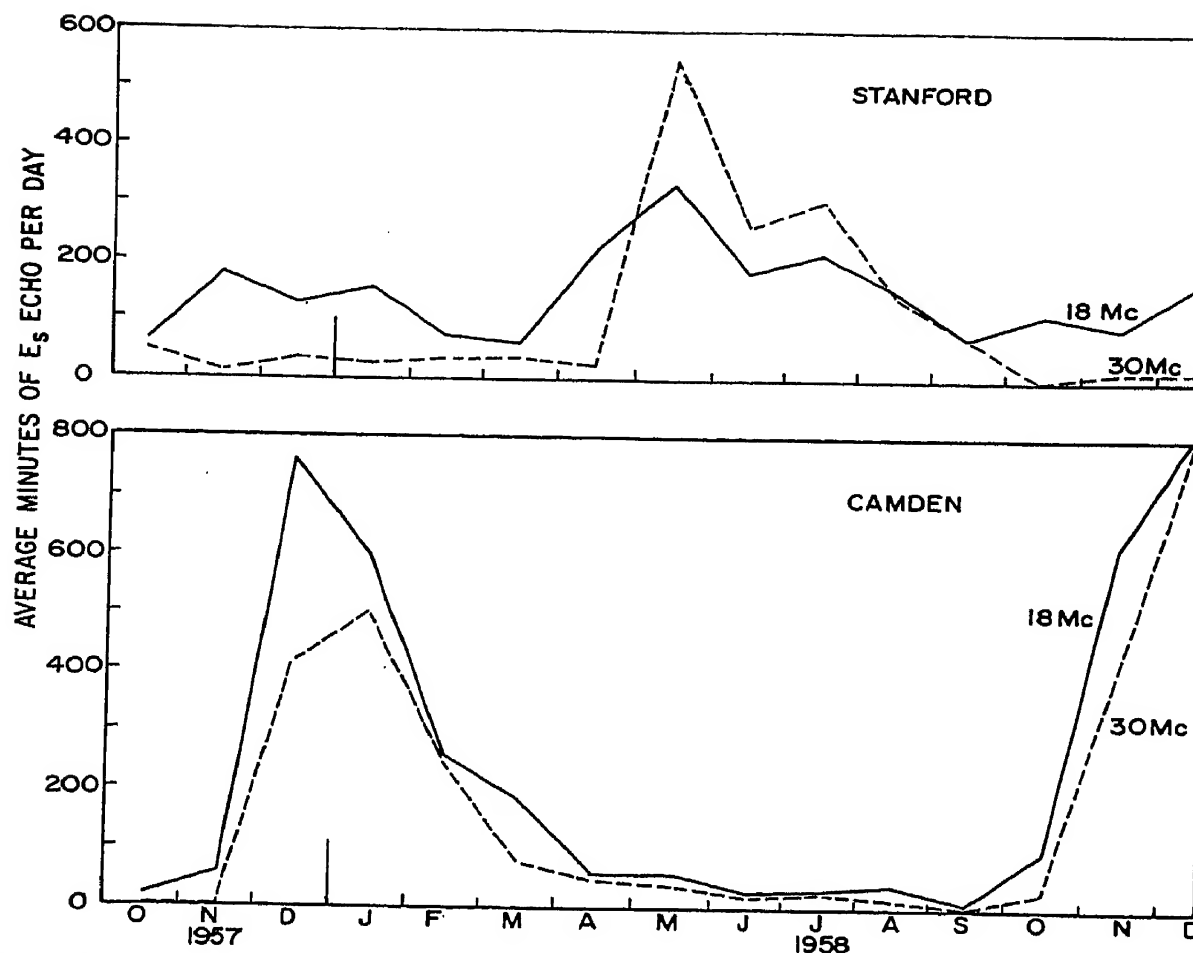


Fig. 9. Average number of minutes of  $E_s$  echo observed per day by months for the period October 1957 to December 1958 at Stanford, California, and Camden, Australia.

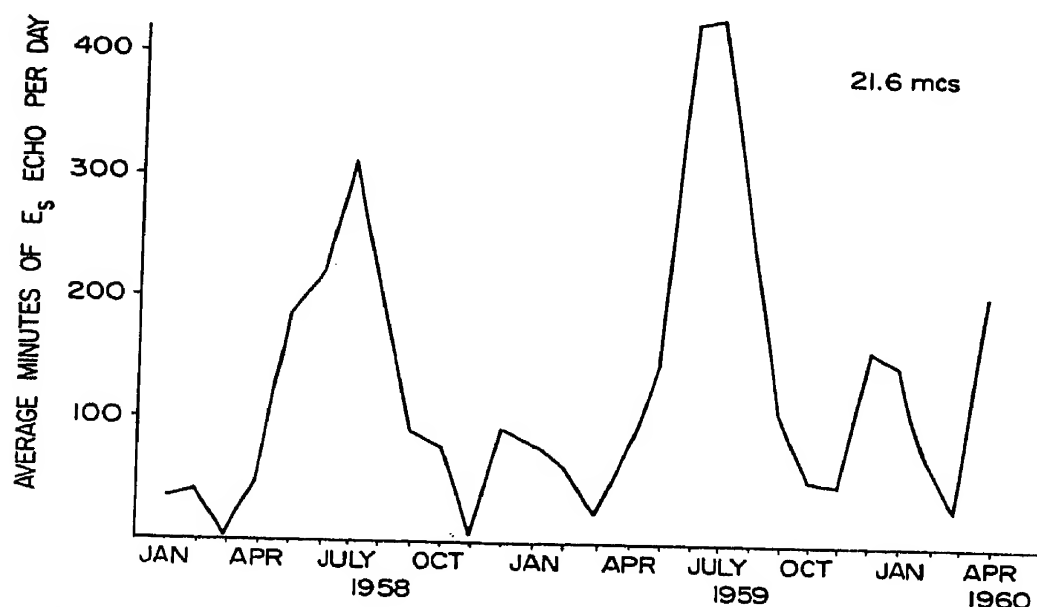


Fig. 10. Summary of backscatter  $E_s$  observations at Puerto Rico from January 1958 to April 1960. Average number of minutes of  $E_s$  echo per day by months observed at 21.6 Mc/s. (Courtesy of Dr. B. Dueño.)

between the Stanford summer maxima and the Camden summer maxima. A comparison between these two stations is especially interesting inasmuch as they are at very nearly the same geographic and geomagnetic latitudes; hence, any latitude effect should not be present, leaving only a hemisphere or longitude effect. In this case a longitude effect is known to exist which will explain the observed differences.

An exceptionally complete set of oblique backscatter records of  $E_s$  observations has been obtained by Dueño (1960) at the University of Puerto Rico on 21.6 and 40.68 Mc/s. The results of his 21 Mc/s observations during a two and one-half year period are summarized in Fig. 10 where the usual summer maximum and secondary winter maximum may be seen. The evening maximum in diurnal occurrence observed at Puerto Rico (Dueño 1961) is quite similar to the evening maximum observed during the winter at Stanford.

Knowing that the backscatter observations coincide with the vertical incidence sweep-frequency soundings, no further analysis of the temporal or geographical variations will be attempted, since statistics are available for vertical soundings (cf. Smith 1957) with more reliability unless the backscatter data are examined in extreme detail.

### *Effect of Earth's Surface Characteristics*

The backscatter sounding program has produced some extremely interesting results insofar as the variation of  $E_s$  occurrence about particular stations is concerned. It has been noted for many years that  $E_s$  activity was far more prevalent to the west of Stanford than to the east. Clark (1957) analyzed the backscatter records from 1953 through 1955 and obtained sporadic- $E$  patch occurrence figures in eight sectors about the station (Fig. 11). The preponderance of  $E_s$  occurrence over water once again raised the question as to whether there is a systematic difference between sporadic  $E$  over land and over water. Or, to extend the question further, perhaps even differences between mountainous regions and plains.

An examination of the Stanford and Camden sporadic- $E$  observations reveals that at both stations  $E_s$  occurs predominantly over water, even though the water lies to the east of Camden and to the west of Stanford. There is no apparent reason to expect this east-west effect to be a result of the northern and southern hemisphere locations of the stations. The over-water effect is so strong, that in the southern hemisphere heavy summer sporadic- $E$  months of December and January, the outline of the east and south coasts of Australia are reproduced in the backscatter data of January 1958 (Fig. 12). A similar effect is also seen in the Stanford data for April 1958 (Fig. 13). It is interesting that although Puerto Rico is essentially surrounded by water there is a marked preference for  $E_s$  to occur in the southeast as seen in Professor Dueño's data at 21 Mc/s (Dueño 1961).

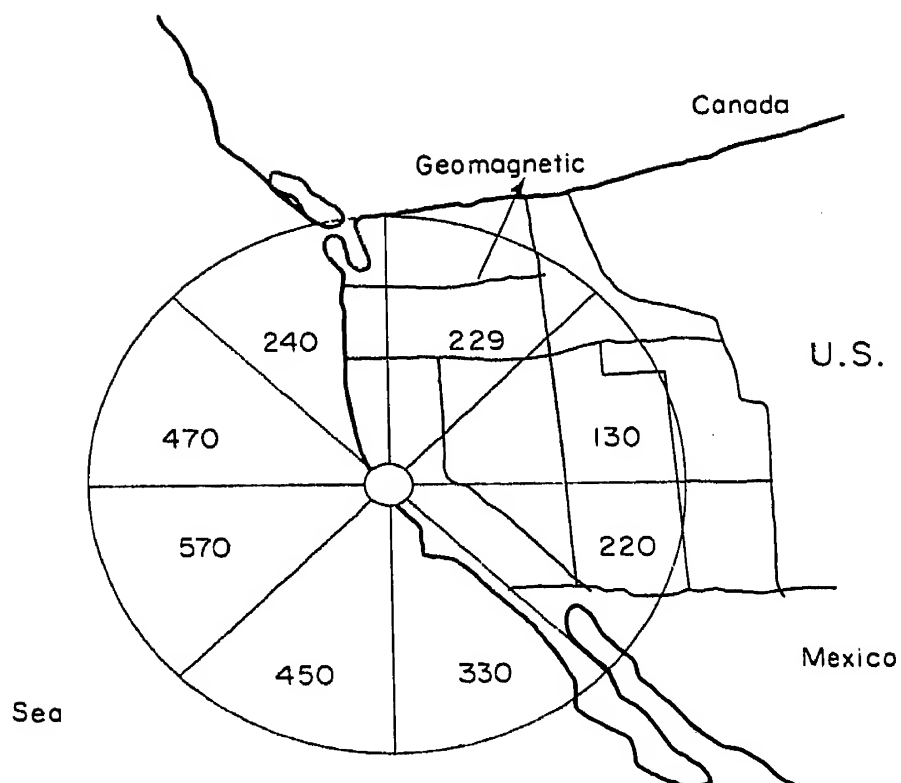


Fig. 11.  $E_s$  patches observed in various directions from Stanford, California, in the years 1953 through 1955 on the 17 Mc/s backscatter sounder.

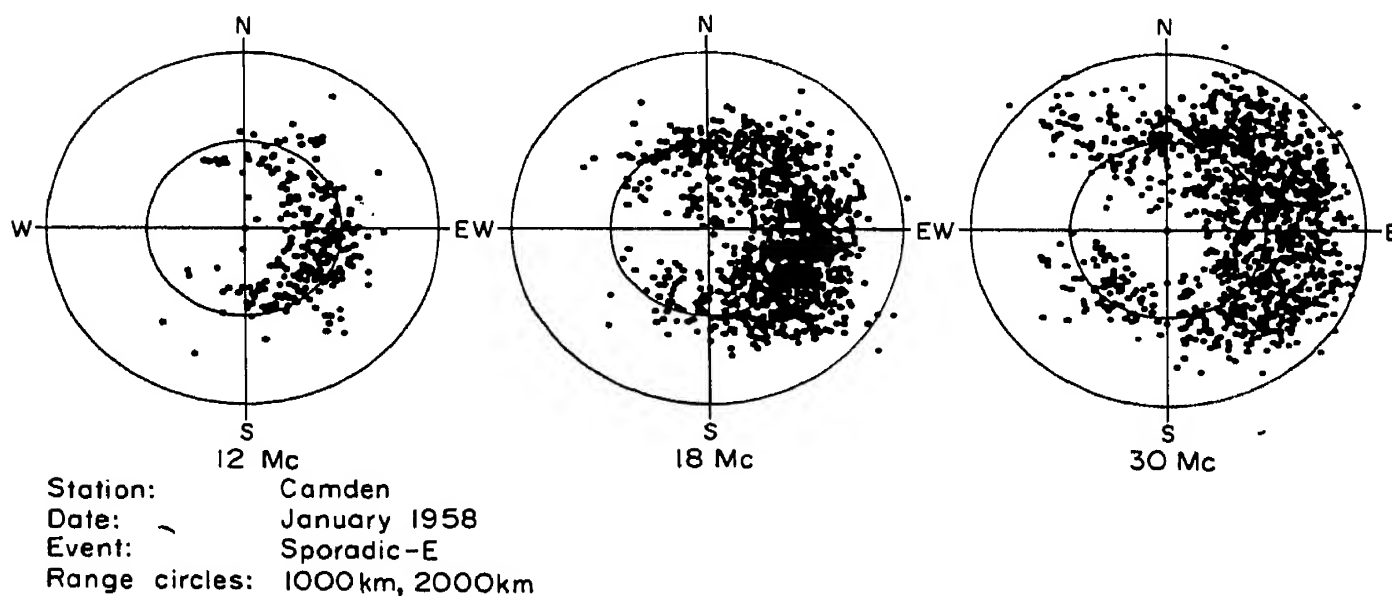


Fig. 12. Polar plot of the apparent centroid of the  $E_s$  patches observed at Camden, Australia, at ten minute intervals during January 1958 on 12, 18 and 30 Mc/s.

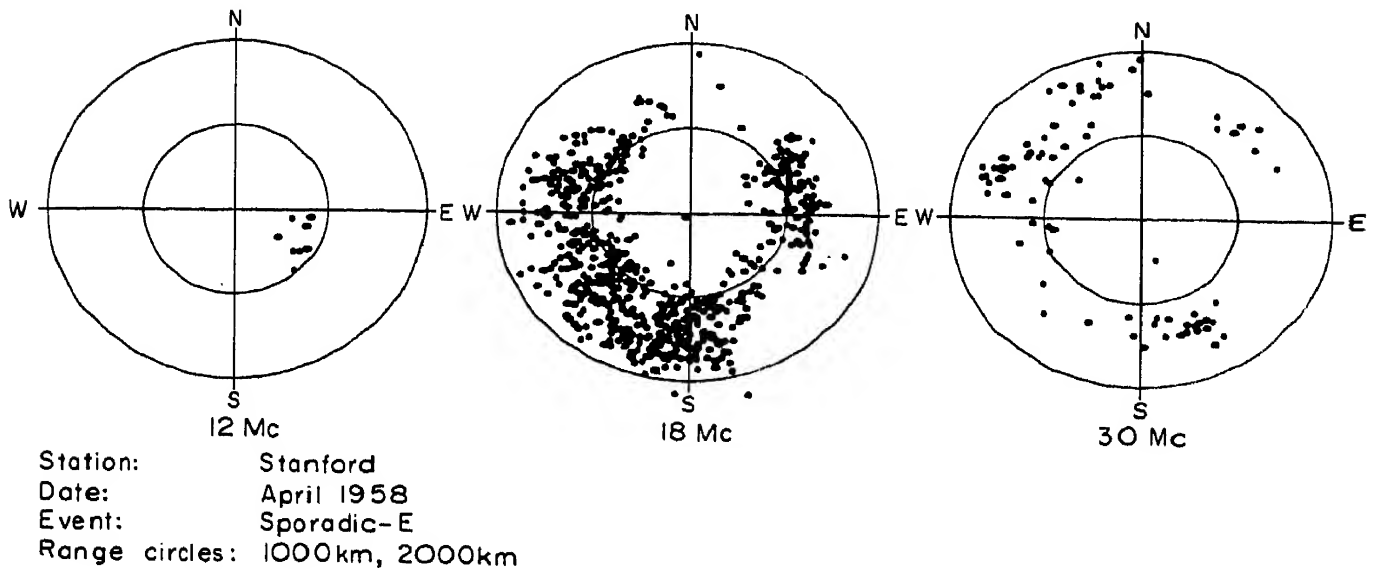


Fig. 13. Polar plot of the apparent centroid of the  $E_s$  patches observed at Stanford, California, at ten minute intervals during April 1958 on 12, 18 and 30 Mc/s.

Analysis of the three station group (Stanford, Boulder and Pullman) has indicated definite groupings of sporadic- $E$  occurrence over mountainous regions, in addition to the preponderance of  $E_s$  occurring over water as observed at coastal stations. In Fig. 14 the data for 18 Mc/s for the month of April 1958 are plotted on a common geographical map. It can be seen that there is a definite preference for sporadic- $E$  occurrence over mountainous regions as compared with other less-mountainous regions. This effect cannot be explained by local site conditions (i.e. antenna screening by mountains or other obstructions).

In the case of both over-water and over-mountain sporadic  $E$ , the question arises as to whether or not variations of the ground backscatter coefficient might be the determining factor rather than actual occurrences of sporadic- $E$  patches. A recent study by the Stanford Research Institute (Nielson, Hagn, Rorden and Clark 1960) has shown that there is less than 10 db difference in backscattered energy between average land and water except for very low angles ( $<10^\circ$ ) where the water backscatter coefficient drops off very rapidly (Fig. 15). Therefore, it appears that the over-water effect is real and a search for possible mechanisms is due. As for the higher occurrence of sporadic  $E$  over mountainous regions, the picture is less clear. It is certainly conceivable that the average ground-backscatter coefficient of mountainous regions is somewhat higher, simply because the angle of incidence is lower on the sides of mountains as compared to flat land. However, such possible mechanisms of sporadic- $E$  formation as the "internal atmospheric gravity waves", proposed by Hines (1960) could be excited by wind systems over the Rocky Mountains. A simple multi-station single-frequency vertical sounder operated for a period of one year should

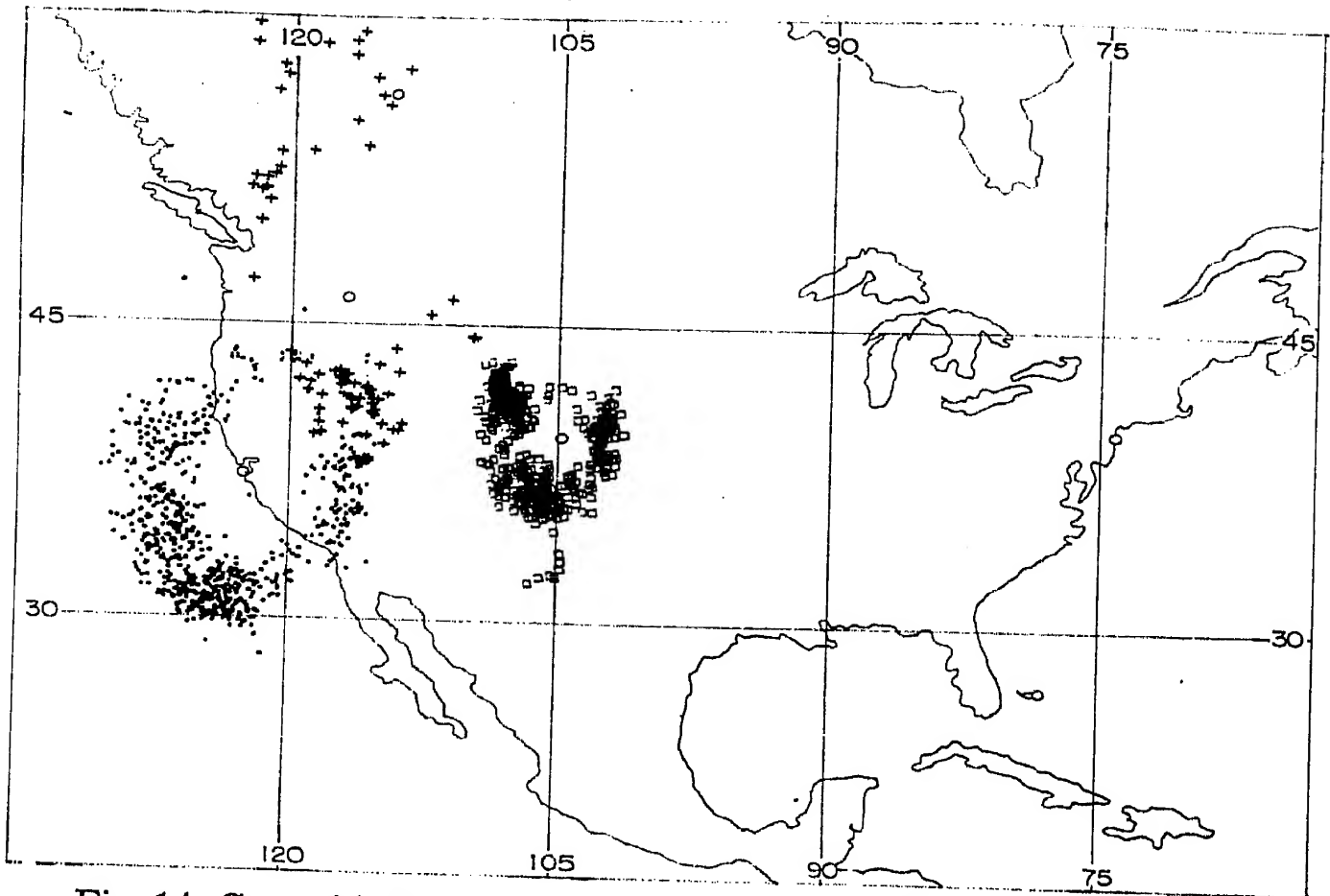


Fig. 14. Centroid of  $E_s$  patches as observed at 10 minute intervals during April 1958 at Pullman, Washington, Boulder, Colorado; and Stanford, California. The symbols are as follows: Points—Stanford; Squares—Boulder; and Crosses—Pullman.

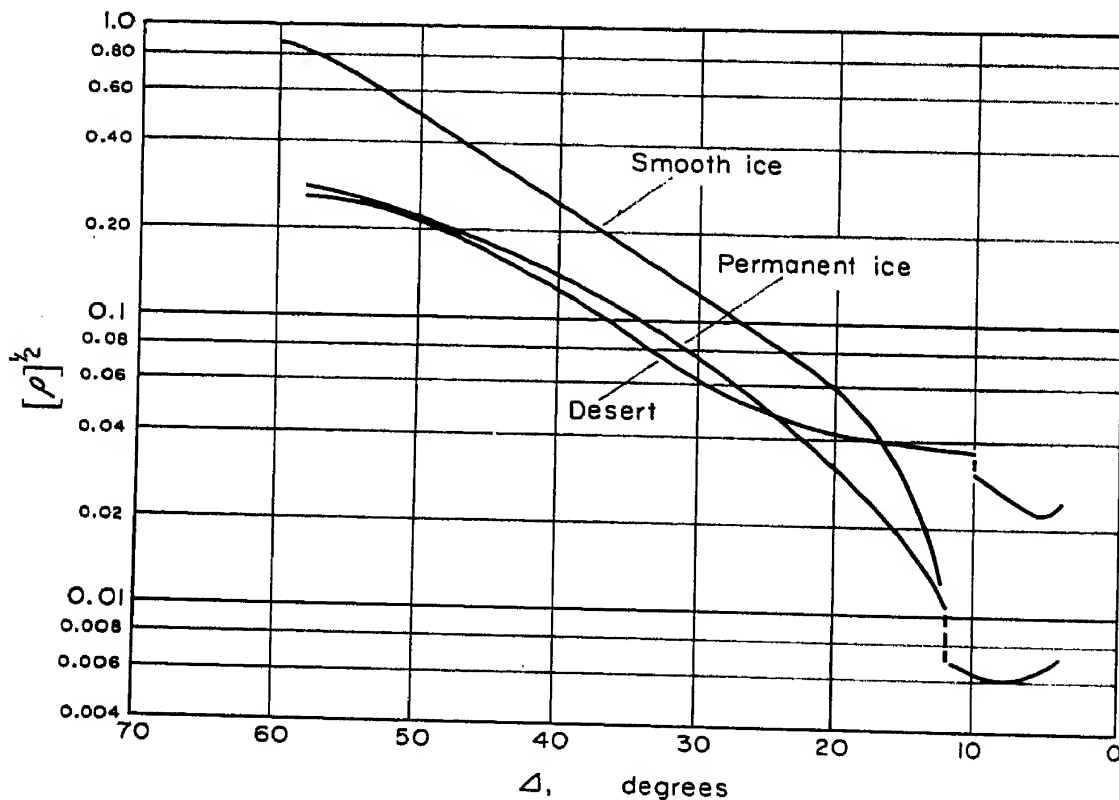


Fig. 15. Measured backscatter coefficient for smooth ice, permanent ice (rough), and desert as a function of angle of incidence. The smooth ice is also representative of smooth ocean.

provide a definite answer to the mountainous region question. Site requirements make such an experiment more difficult in the case of the water-land question.

### 7. DRIFTING $E_s$

While the majority of the  $E_s$  patches which are observed remain nearly stationary, some move in a consistent manner through large distances. At Stanford, in a study of three years of 17.3 Mc/s backscatter records, data on 2700 separate  $E_s$  patches were obtained. Of this total, 264 patches (approximately 10 per cent) were found to move through significant distances. The mean patch-motion speed was 300 km per hour, and the direction of motion was predominately west. In 80 per cent of the cases the direction was within  $\pm 45$  degrees of due west. Figure 16 shows a polar

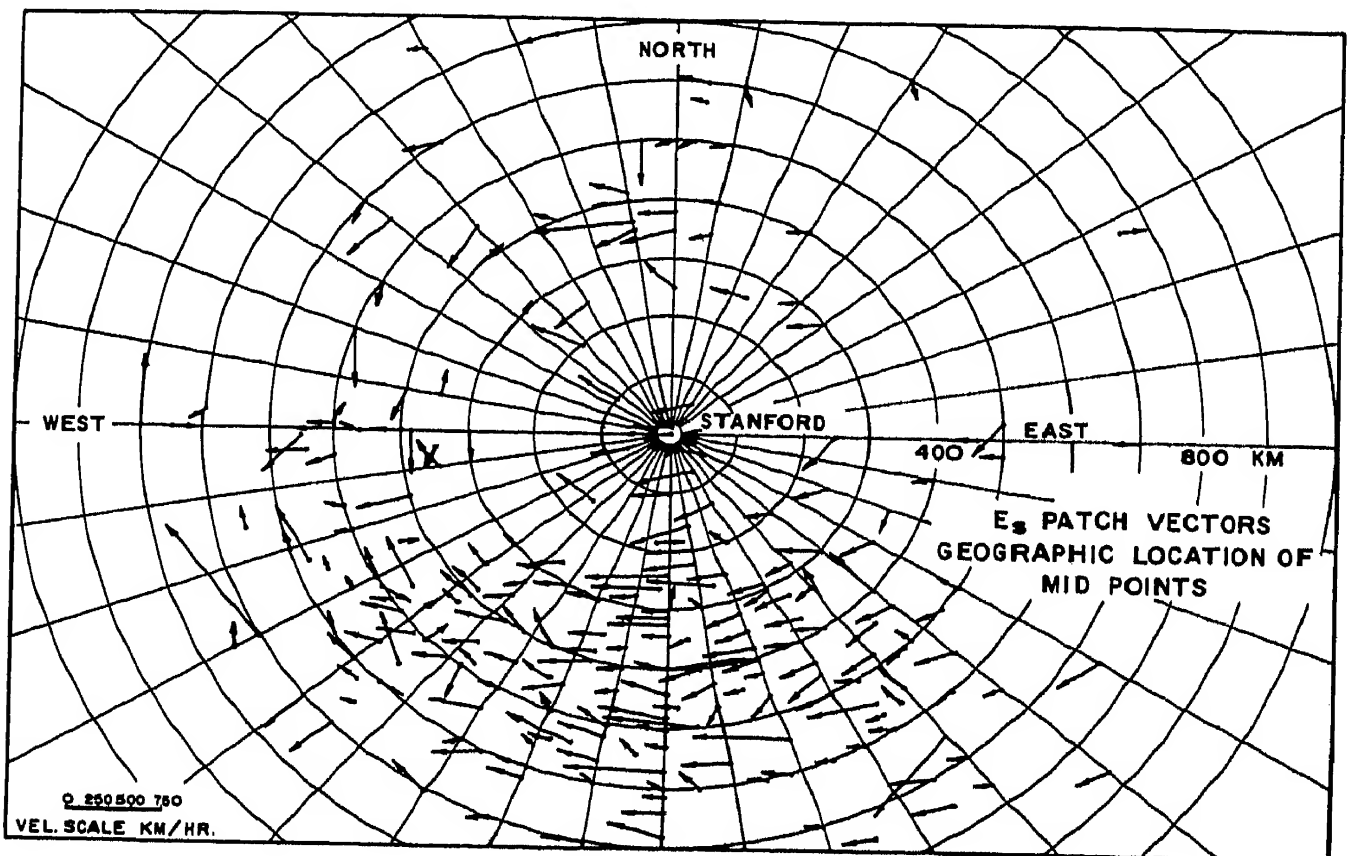


Fig. 16. Velocity vectors of drifting  $E_s$  patches. Vector origin is the mid point of the observed track and the vector length is proportioned to the drift velocity in the direction indicated.

map, centered on Stanford, of the speed and direction of  $E_s$  patch drift observed during this study. The arrows indicate, by their length and direction, the speed and travel direction of the individual patches and the location on the map of the arrow is that of the mid-point of the path traversed by the drifting patches.

The network of IGY backscatter sounders has provided much new data on  $E_s$  patch motion and in particular, the stations at Boulder, Colorado; Stanford, California, and Pullman, Washington provided a regional coverage. Heybourne and Clark (1960) in a report based on these data have investigated the motion of  $E_s$  as viewed from more than one sounder. A number of cases were found in which similar characteristics were clearly apparent at separated stations. Figure 17 shows results of such an obser-

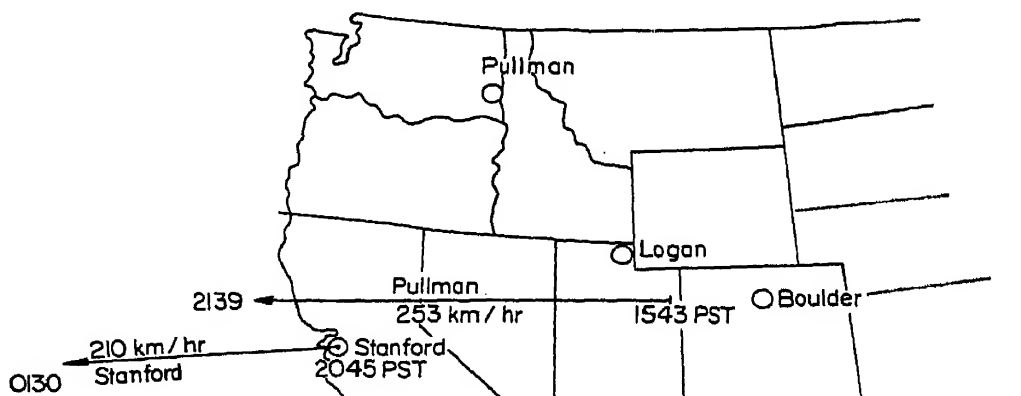


Fig. 17. Map showing drifting  $E_s$  patch tracks as observed at Stanford, California and Pullman, Washington on August 24, 1958. (After Heybourne and Clark)

vation of  $E_s$  patch motion extending through an interval of more than 10 hours and a distance greater than 2000 km.

Preliminary examination of the  $E_s$  data from Camden, Australia appears to show that for this southern hemisphere station, patch motion is predominately westward as it is at Stanford in the northern hemisphere.

#### REFERENCES

- BATES, H. F. (1961) *J. Geophys. Res.* **66**, 447.  
 BOOKER, H. G. (1956) *J. Atmosph. Terr. Phys.* **8**, 204.  
 BOWLES, K. L. and COHEN, R. (1960) *J. Geophys. Res.* **65**, 1853.  
 CLARK, C. (1957) TR No. 24, Radio Prop. Lab., Stanford Univ.  
 DIEMINGER, W. (1951) *Proc. Phys. Soc. Lond.* **64**, 142.  
 DUEÑO, B. (1960) (Private communication).  
 DUEÑO, B. (1962) *Ionospheric Sporadic E*, Pergamon Press, England.  
 EGAN, R. D. (1960) *J. Geophys. Res.* **65**, 2343.  
 HEYBORNE, R. L. and CLARK, C. (1960) SR No. 2, NSFG-6021, Utah State Univ.  
 HINES, C. O. (1960) *Canadian J. Phys.* **38**, 1441.  
 KNECHT, R. W. (1959) *J. Atmosph. Terr. Phys.* **14**, 348.  
 LEADABRAND, R. L. (1955) TR No. 98, Radio Prop. Lab., Stanford Univ.  
 MARTYN, D. F. (1959a) *Proc. Inst. Radio. Engrs.* **47**, 147.  
 MARTYN, D. F. (1959b) *Nature* **183**, 1382.  
 MATSUSHITA, S. (1953) *Rep. Ionosph. Research Japan* **7**, 45.  
 MATSUSHITA, S. (1957) *J. Atmosph. Terr. Phys.* **10**, 163.  
 NIELSON, D., HAGN, G., RORDEN, L. and CLARK, N. (1960) Final Rpt., SRI Proj. 2909, Stanford Res. Inst.

- PETERSON, A. M. (1951) *J. Geophys. Res.* 56, 221.
- PETERSON, A. M., EGAN, R. D. and PRATT, D. S. *Proc. Inst. Radio. Engrs.* 47, 300.
- SILBERSTEIN, R. (1953) *Science* 118, 759.
- SILBERSTEIN, R. (1954) *Trans. Inst. Radio. Engrs.* Ap-2, 56.
- SMITH, E. K. (1957) National Bureau of Standards Cir. 582.
- THOMAS, J. A. and SMITH, E. K. (1959) *J. Atmosph. Terr. Phys.* 13, 295.
- WRIGHT, J. W. and GAUTIER, T. N. (1960) *J. Res. NBS* 64D, 347.



# Sporadic *E* as Observed from Mayaguez, P. R. by Backscatter Sounders\*

B. DUEÑO

Department of Electrical Engineering, University of Puerto Rico, Mayaguez, P.R.

**Abstract**—Sporadic *E* has been studied in the Caribbean-Atlantic area by means of a multichannel backscatter sounder from January 1958 to May 1960. It has been found that  $E_s$  (sporadic *E*) activity increases very rapidly from May to June with the maxima occurring during June and July. During December and part of January there is a minor maximum of activity. More  $E_s$  was observed around 17 30 hours local time and in the due South direction than at any other time and direction. Those  $E_s$  clouds that were found to drift had a mean velocity of the order of 500 km per hour with a prevailing direction to the southeast.

## 1. INTRODUCTION

Sporadic-*E* activity has been recorded at Mayaguez, P. R. (latitude 18°12'25"N) using backscatter techniques, from January 1958 to May 1960. Two channels, one on 21.6 Mc/s and another on 40.68 Mc/s were used during the entire period to record this data. In addition, data was obtained on 49.68 Mc/s from July 1959 to May 1960. Data were obtained continuously and were recorded at one minute intervals on 16 mm film.

## 2. INSTRUMENTATION

The peak pulse power output was approximately one kW on each of the three channels used, namely 21.6 Mc/s, 40.68 Mc/s, and 49.68 Mc/s. The pulse duration was approximately 2 millisec with a pulse repetition frequency of 18.75 p.p.s. The antennas were three-element Yagis mounted on a Bertha mast which rotated 360 degrees alternately in the clockwise and counterclockwise direction.

## 3. METHOD OF OBSERVATION

A range azimuth presentation was used in the scopes for displaying the data in two oscilloscopes, one for each channel. When the 49.68 Mc/s channel was added, its information was displayed on the 40.68 Mc/s scope on every third frame.

One fundamental limitation of the backscatter radar is the amplification of the size of an echo in the azimuthal direction that results from the use

---

\* This research has been sponsored by the AFOSR (ARDC) under contract AF19(638)-172.

of antennas with wide horizontal beam widths. This situation grows worse if the critical frequency of the  $E_s$  layer is high, say of the order of 8 to 9 Mc/s and the frequency of operation is low enough.

By the use of a multiple-channel backscatter radar it is possible to obtain more information about the direction and approximate size of a cloud which appears on a low-frequency channel as an overhead  $E_s$  formation.

Since the average slant distance of the  $E_s$  clouds observed in this experiment is of the order of 1200 km it can be easily shown (Smith 1957, Shearman and Harwood 1960) that  $E_s$  echoes on the 21.6, 40.68 and 49.68 Mc/s channels correspond to  $E_s$  formations with critical frequencies equal to or greater than 4.3, 8 and 10 Mc/s respectively. Thus an  $E_s$  echo that appears in all azimuthal directions on the 21.6 Mc/s channel and in the northeast quadrant on the 49.68 channel at a slant range of 1900 km can be interpreted as an  $E_s$  cloud whose maximum of ionization is to the northeast and whose dimension is possibly greater than 1900 km at the lowest frequency of observation.

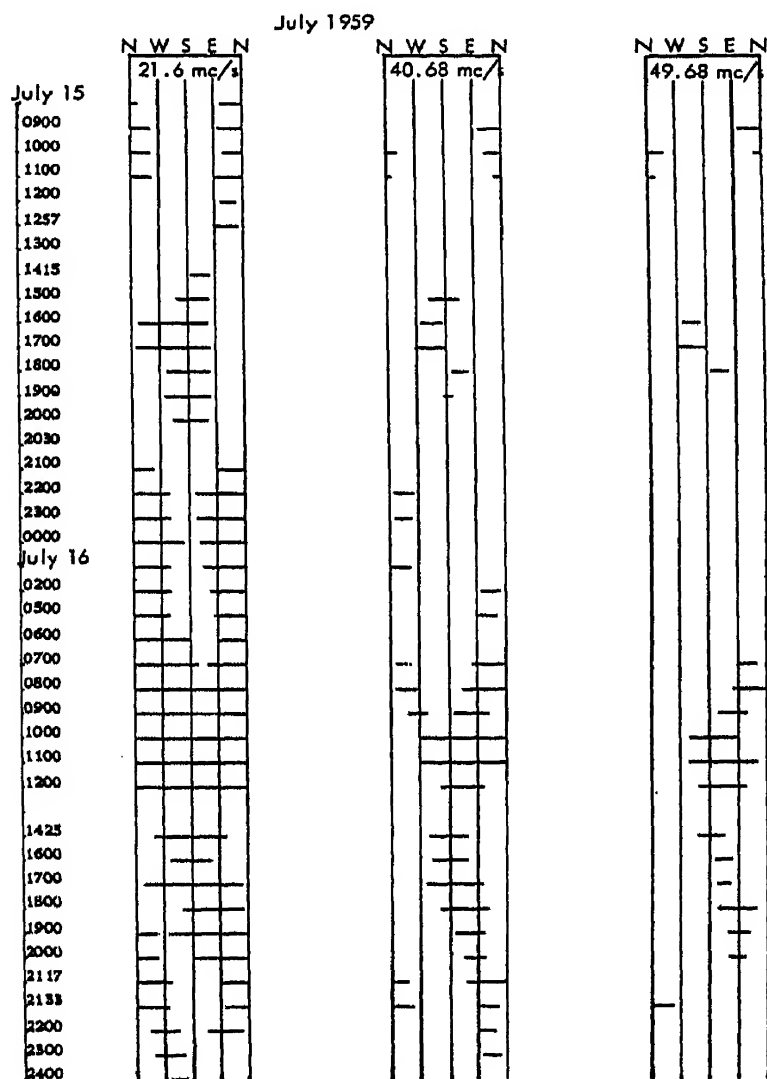


Fig. 1. Sample data for two days of intense  $E_s$  activity.

Figure 1 which illustrates this case, shows data from two days of intense  $E_s$  activity. On the 15th of July 1959 at 08 53 hr an echo is shown in the north-east direction. Simultaneously the 40-68 and 49-68 Mc/s channels show the echo to the northeast at a range of approximately 1500 km implying the  $f_oE_s$  was 10 Mc/s or higher. For that same hour the vertical sounder at Ramey indicated an  $f_oE_s$  of 4 Mc/s so that we may either infer a cloud of  $E_s$  which at P. R. was not very strong but on the contrary very intense at slant range distance of 1500 km or else two separate clouds one intense, and the other weak overhead. On the other hand on the 16 of July 1959 at 08 00 hr the 21-6 Mc/s channel shows an overhead echo in all directions ( $f_oE_s$  from the local vertical sounder was 6-7 Mc/s) while the 49-68 Mc/s channel shows an echo in the NE quadrant at a range of 1900 km. The echo shown on the 40-68 Mc/s channel is intermediate between these two. It seems therefore logical to assume that here we are concerned with only one cloud whose most intense portion was 1900 km to the northeast and whose overall length was greater than 1900 km. Notice that at 09 00 hr the vertical frequency has increased to 12 Mc/s.

Some peculiarities of the motion of  $E_s$  clouds is also brought out by Fig. 1. The 40 Mc/s channel shows a static cloud from 15 58 hr to 16 57 hr on July 15 on the W-S quadrant. However from 16 57 hr to 17 57 hr the cloud moves from the W-S to S-E quadrant which represents a very large velocity of the order of 400 meters per sec.

From 07 00 hr to 20 00 hr on the 16th the 50 Mc/s channel shows motion from NE quadrant at 08 00 to the south at 12 00 and back to the east by 19 00 hr.

Since  $E_s$  echoes are power sensitive, their azimuthal extent decreases as the radio frequency of operation is increased. For this reason the 49-68 Mc/s channel brings out the motion of the  $E_s$  clouds more clearly than the other two channels.

#### 4. SEASONAL AND DIURNAL VARIATIONS OF $E_s$ ACTIVITY

Examination of the  $E_s$  data on the three channels has revealed that the seasonal variation of occurrence is similar to that observed in the continental U.S. by Smith (1957) and by Gerson (1959).

Figure 2 shows the seasonal trend of  $E_s$  obtained in this experiment. The vertical scale represents the monthly sum of occurrences in hours. The upper drawing is the plot for the 21-6 Mc/s channel from January 1958 to April 1960. The lower drawing is the plot for the 40-68 Mc/s channel for the same period of time. The broken line represents the 49-68 Mc/s data.

From this figure it is observed that  $E_s$  activity increases very rapidly from May to June and that the maximum activity occurs during June and

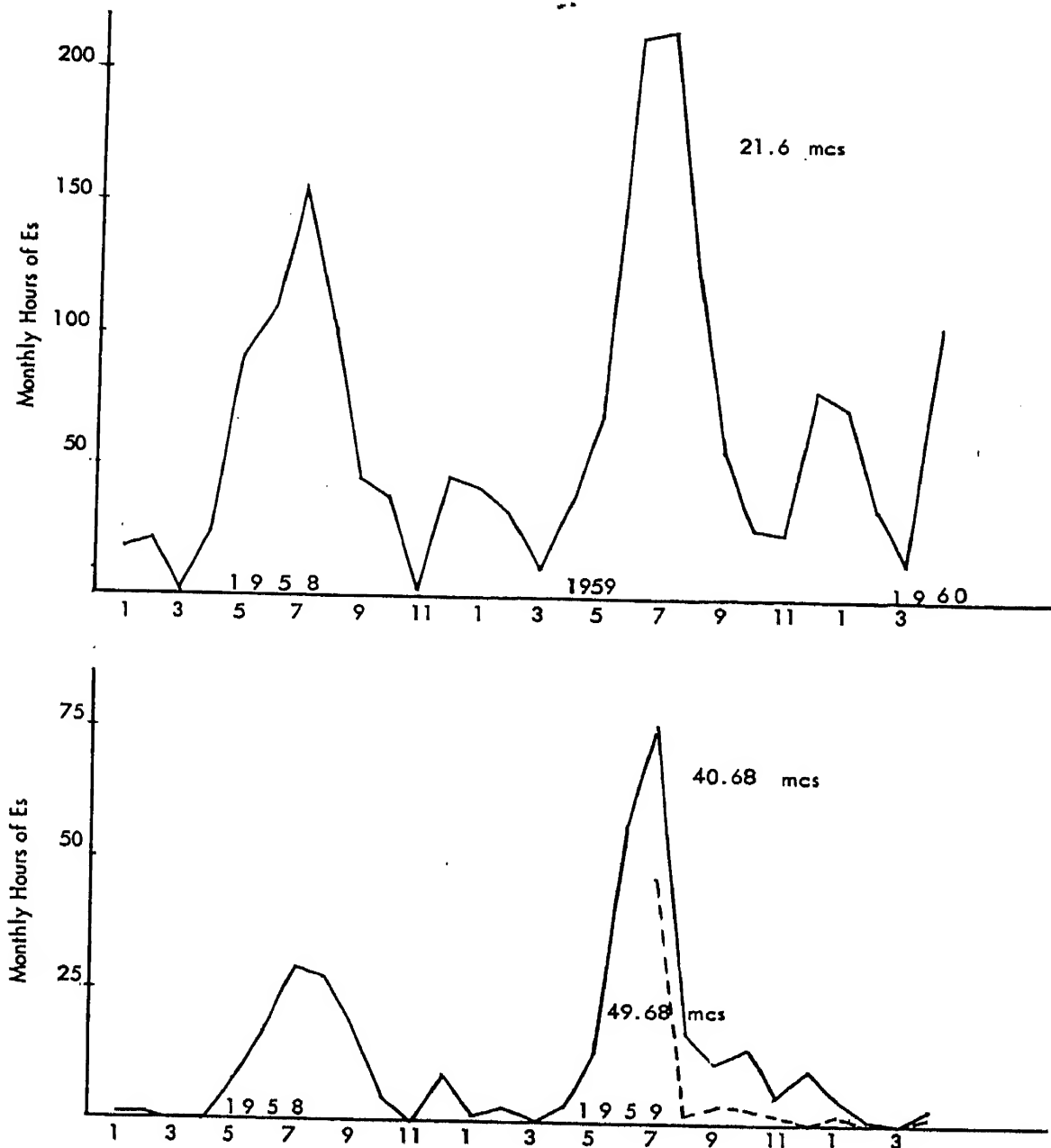


Fig. 2. Distributions of monthly hours of  $E_s$  for the 21.6 Mc/s and 40.68 Mc/s channels. Dotted curve shows 49.68 Mc/s data.

July. There was more  $E_s$  activity recorded during 1959 than during the preceding year. However, the receiving equipment was improved during the 1959 summer resulting in a substantial increase in sensitivity. For this reason the graph cannot be used to determine the ratio of  $E_s$  activity between these two years.

For the period of time studied it appears that November and March are months of minimum  $E_s$  activity, and that during December and part of January there are minor maxima of activity. These winter maxima and the November and March minima are barely perceptible in the graphs by Smith (loc. cit. p. 197).

Figure 2 also shows that 50 Mc/s  $E_s$  activity as observed by backscatter is solely confined to the summer.

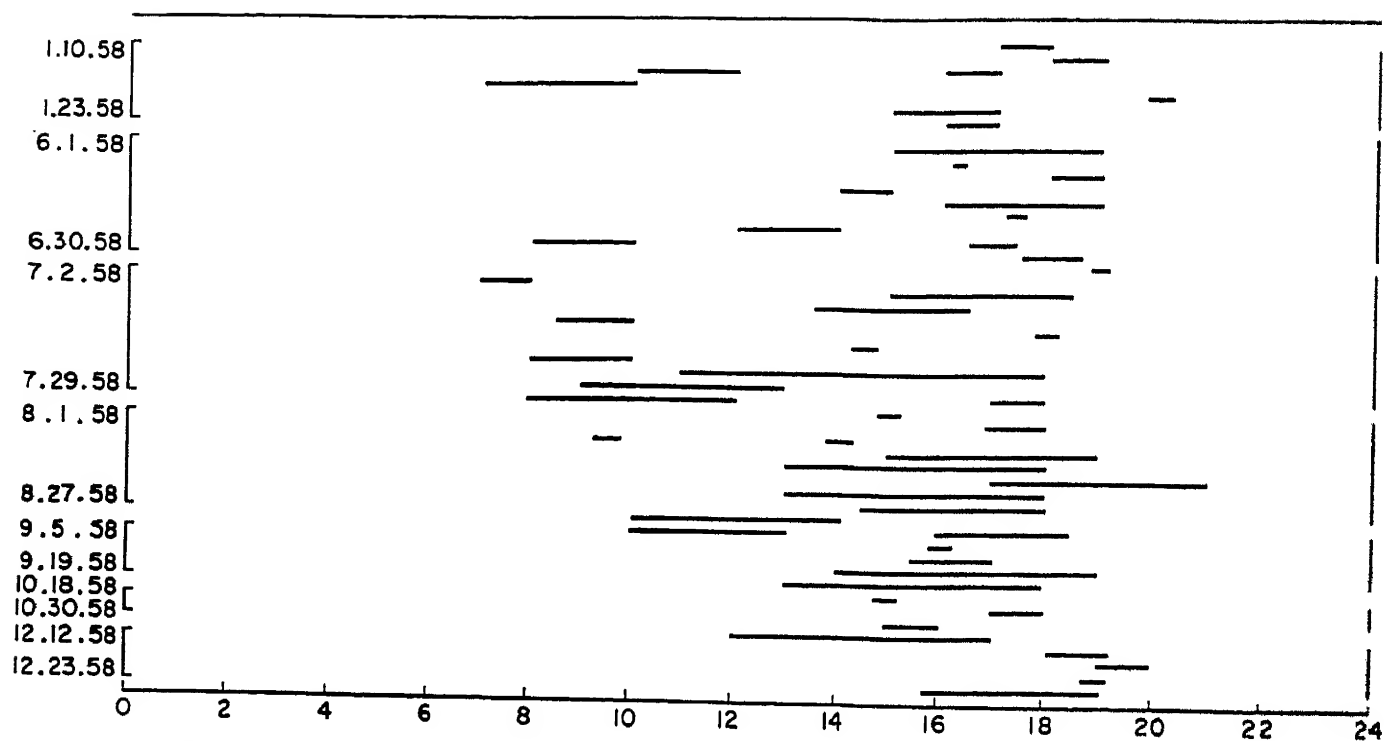


Fig. 3.  $E_s$  occurrences vs time of the day (40-68 Mc/s) for the year 1958.

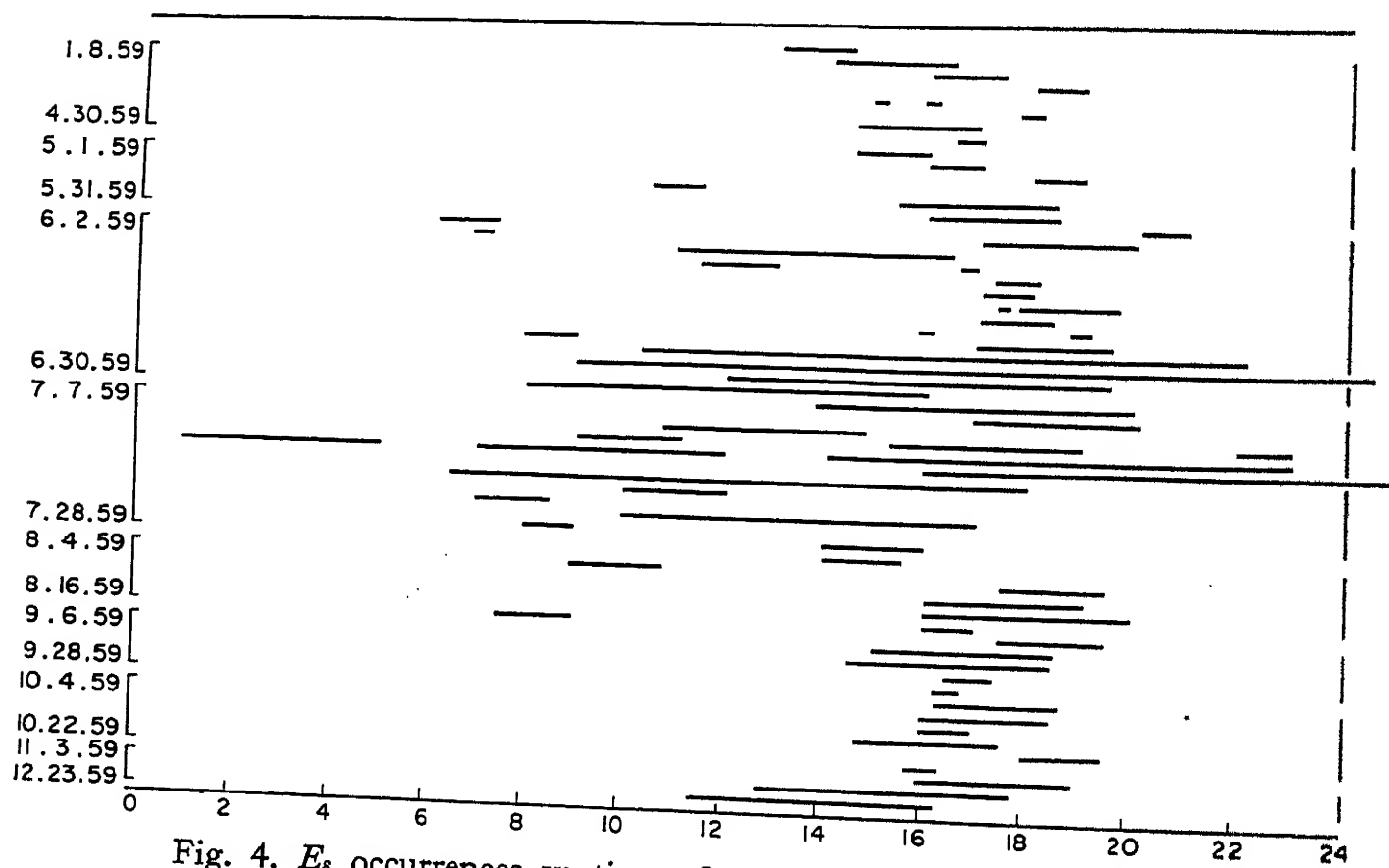


Fig. 4.  $E_s$  occurrences vs time of the day (40-68 Mc/s) for the year 1959.

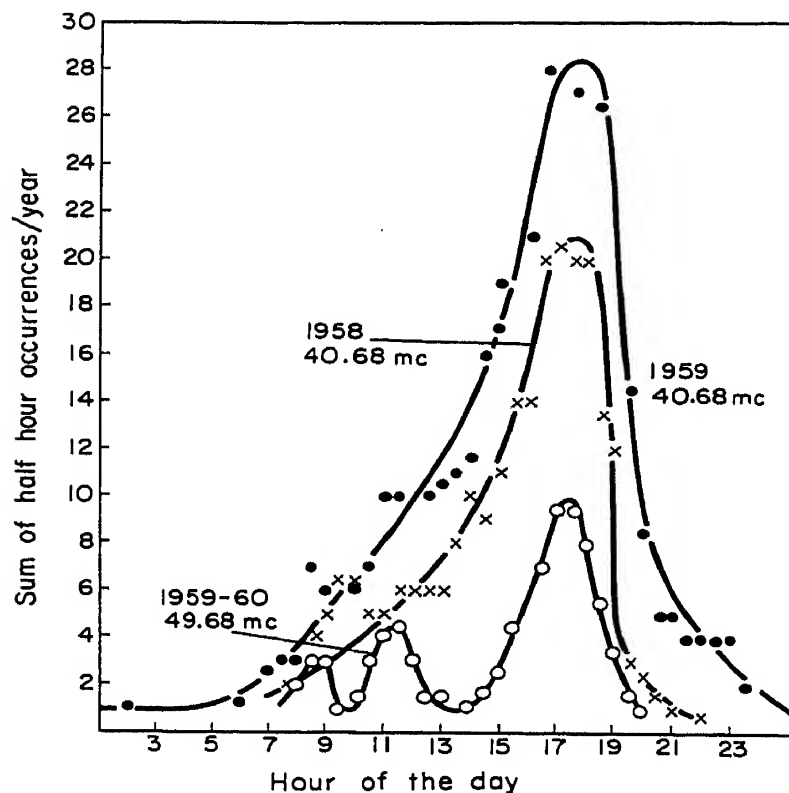


Fig. 5. Diurnal distribution of  $E_s$  occurrences on the 40.68 Mc/s channel for the years 1958 and 1959, and for the 49.68 Mc/s channel.

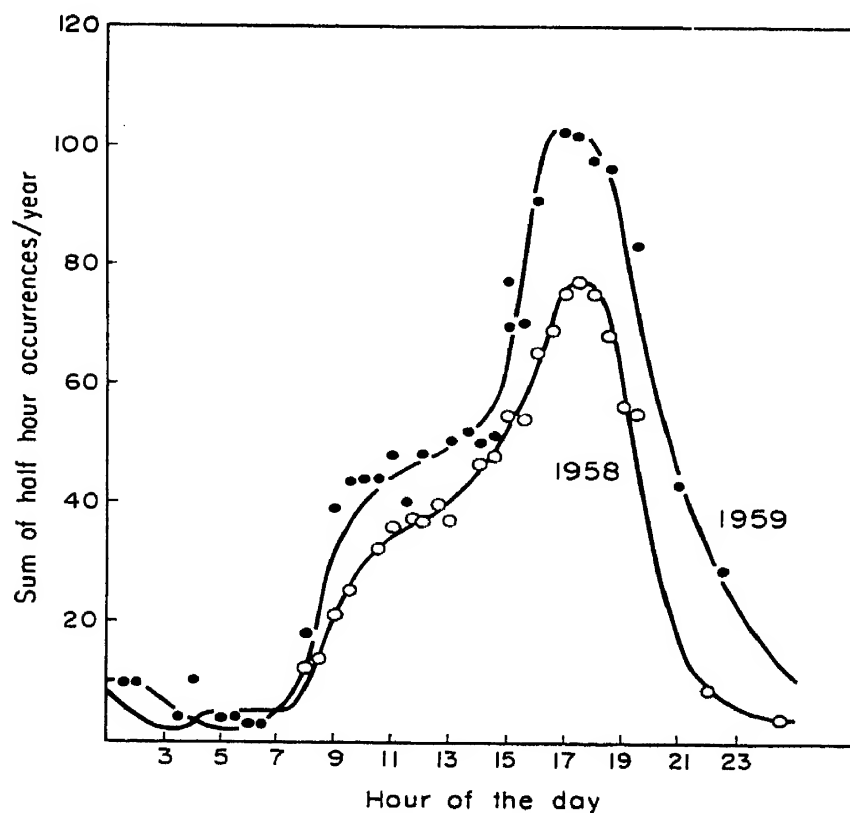


Fig. 6. Diurnal distribution of  $E_s$  occurrences on the 21.6 Mc/s channel for the years 1958 and 1959.

The diurnal variation of  $E_s$  for the 40.68 Mc/s channel for the years 1958 and 1959 are shown in Figs. 3 and 4. Plots similar to these were made for the 21.6 Mc/s and the 49.68 Mc/s channels. By summing the number of occurrences on each half-hour interval in these two figures a more clear representation of the diurnal variation can be obtained. This is shown in Fig. 5 for the 40.68 and 49.68 Mc/s channels and in Fig. 6 for the 21.6 Mc/s channel. From these figures it is obvious that more sporadic  $E$  is observed around 17 30 hr than on any other time during the day. In this respect the 1958 and 1959 data show remarkable agreement even for the 21.6 Mc/s. These figures also show that there is more sporadic  $E$  during the hours before 17 00 than for the hours immediately after 17 00 hr. The 49.68 Mc/s data also shows agreement with these statements. The wiggles displayed by the 49.68 Mc/s curve are obviously due to the limited amount of data available for this channel. Since the graphs shown in Figs. 3 and 4 show little  $E_s$  activity during December and January, Fig. 5 can be taken as representing the true behaviour of  $E_s$  as observed at 40 and 50 Mc/s. On the other hand this is not necessarily true of Fig. 6. The hump at 13 00 hr for the 21.6 Mc/s channel is indicative of a more complicated behaviour. For this channel, Fig. 7 shows the diurnal distribution of

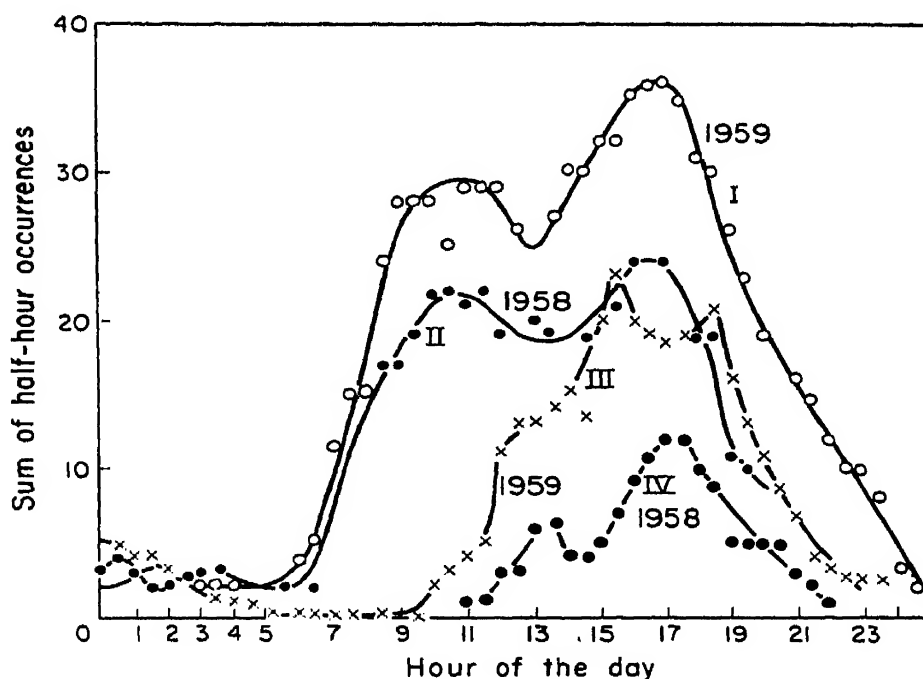


Fig. 7. Diurnal distribution of occurrences for June and July (curves I and II) and for December and January (Curves III and IV). All curves pertain to 21.6 Mc/s data.

occurrences for June and July (curves I and II) and for December and January (curves III and IV). The curves for the winter period (III and IV) show clearly the peak of activity at 17 00 hr which can be interpreted as meaning that the  $f_oE_s$  seldom exceeded a value of 4 Mc/s. On the other hand the curves for the summer period (I and II) appear to be centered

at 13 30 hr but still manage to show a small maxima at 17 00 hr which can be interpreted as meaning that through the daylight hours  $f_oE_s$  most the time exceeded a value of 4 Mc/s so that the 17 00 hr peak, while still being there, would not have been observed had the frequency of operation of the sounder been of the order of 17 Mc/s or lower.

### 5. AZIMUTHAL VARIATION OF SPORADIC $E$

In order to investigate the azimuthal distribution of sporadic  $E$  the azimuthal extent of the echoes were drawn in the quadrants in which they occurred. This was done for both years for all three channels. The plots for 1958 are shown in Figs. 8a and 8b. On this last figure the sum of the occurrences on each thirty degree sector is plotted as a function of azimuth for both channels. The plots for the year 1959 are shown in Fig. 9 for all three channels.

From these figures it is obvious that more  $E_s$  is observed to the south than on any other direction. Since the azimuthal magnification error due to the broad radiation pattern of the antennas used is less pronounced in the higher frequency channels, the curves for 40.68 Mc/s and that for 49.68 Mc/s can be expected to show more detail than those for the 21.6 Mc/s channel. For a given  $f_oE_s$  the extra energy available just at the corner of the radiation beam is needed to produce an echo. On the other hand, the dip in the SE quadrant noticed on the higher frequency curves for both years is not likely to be caused by a property of sporadic  $E$ . It is very probable that this dip is due to a shielding effect of El Cerro Las Mesas, a fairly high hill just to the southeast of the site where this experiment was performed. Due entirely to mechanical considerations the 40.68 Mc/s beam antenna was higher than the one for 21.6 Mc/s, so that the "firing" angle of the latter was greater than that for the former.

Summarizing the information we have thus far: Sporadic  $E$  in the Caribbean-Atlantic area is also a summer-time affair, has a higher probability of occurring around 17 00 hr A.S.T., and is more likely to occur in the south direction.

This preference for the southern direction is not confined to the Caribbean-Atlantic area. Shearman and Harwood (1960) working in England found: "The greatest concentration of echoes is seen to be in the southern semicircle, with no significant bias to west or east." Clark (1957) found at Stanford, California that: "The gross  $E_s$  activity is approximately 40 per cent greater in the south and west than in the north and east."

### 6. MOTION OF $E_s$ PATCHES

In order to study the motion of clouds of sporadic  $E$  the rectangular presentation of range vs. azimuth was transformed into the equivalent plan



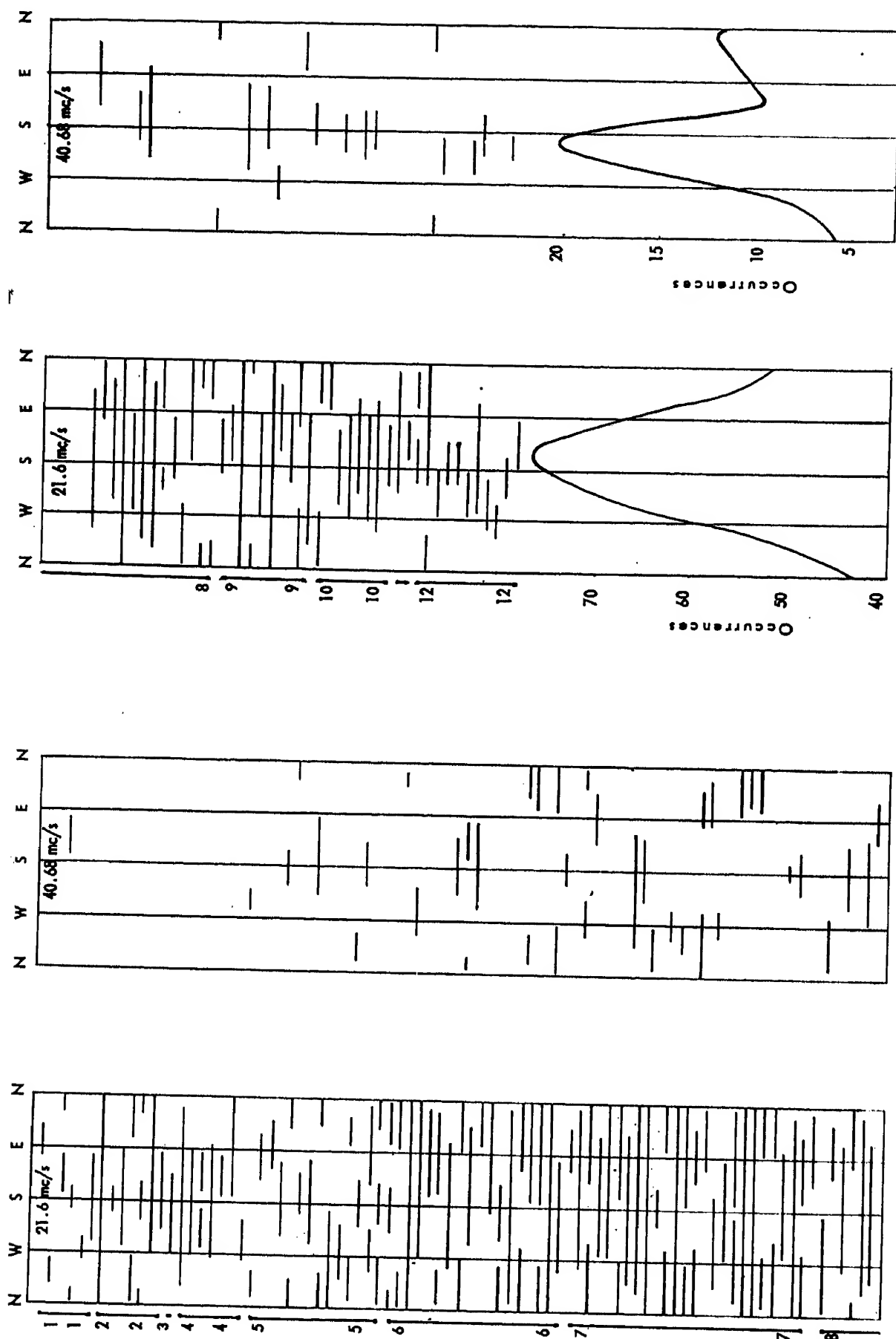


Fig. 8a. Occurrences of  $E_s$  vs azimuth from January to July 1958.

Fig. 8b. Occurrences of  $E_s$  vs azimuth from August to December 1958 and sum of occurrences per thirty degree sector for year 1958.

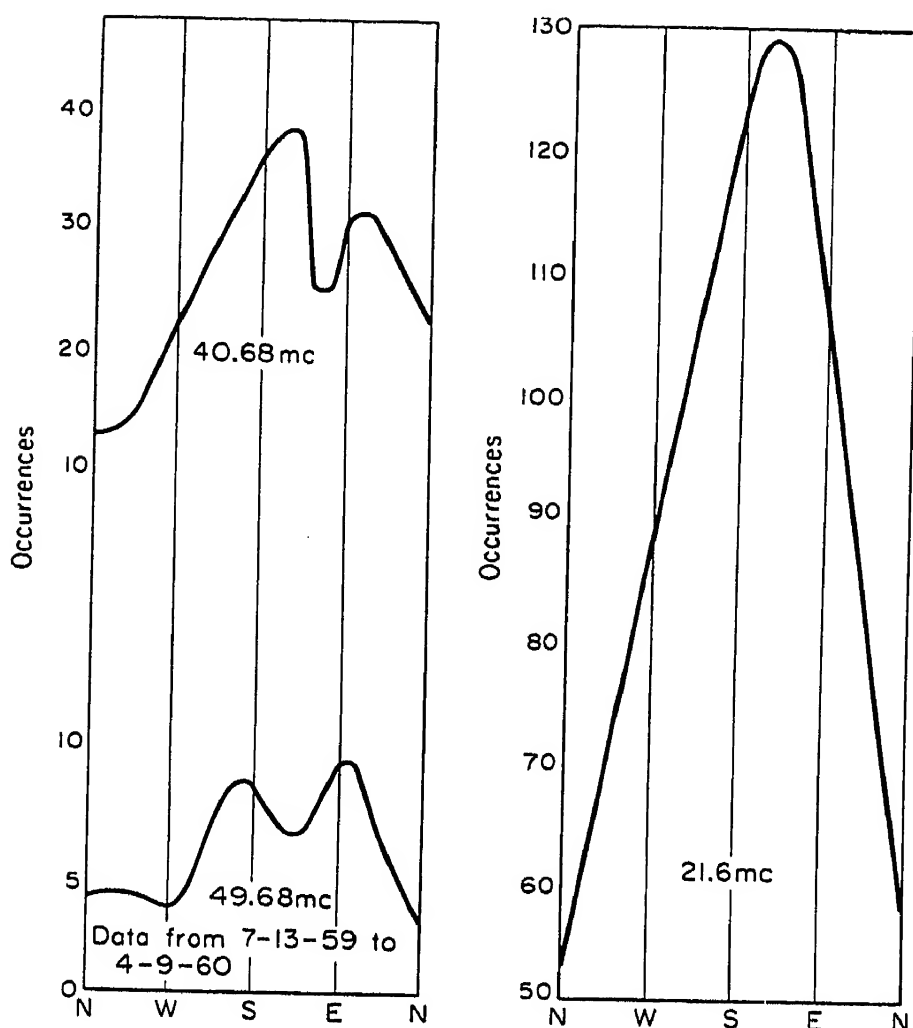


Fig. 9. Occurrences per thirty degree sector for year 1959.

position presentation. This is illustrated in Fig. 10 which shows some sample paths of moving  $E_s$  patches. The complicated path shown in the paper left-hand drawing for July corresponds to the  $E_s$  event on 49.68 Mc/s which is shown in Fig. 1 for July 16, 1959. The inner and outer circle correspond respectively to a range of 1000 and 2000 km. From this figure it will be observed that some of the motions are quite complicated and that there is tendency for some of the  $E_s$  cloud motions to stop when reaching the southerly direction.

Figure 11 shows a polar plot of the measured velocities. Each point is to be interpreted as the end of a vector whose length is equal to the magnitude of the velocity in meters per sec. It will be observed that more of these velocities had direction towards the south-west quadrant than to the other three. This is also shown in the bottom drawing of Fig. 12. The slightly higher number of occurrences on the east-north quadrant over the remaining two others is obviously of no significance.

The upper drawing of Fig. 12 shows the distribution of measured velocities in meters per sec. The average velocity comes out of the order of 150 meters per sec.

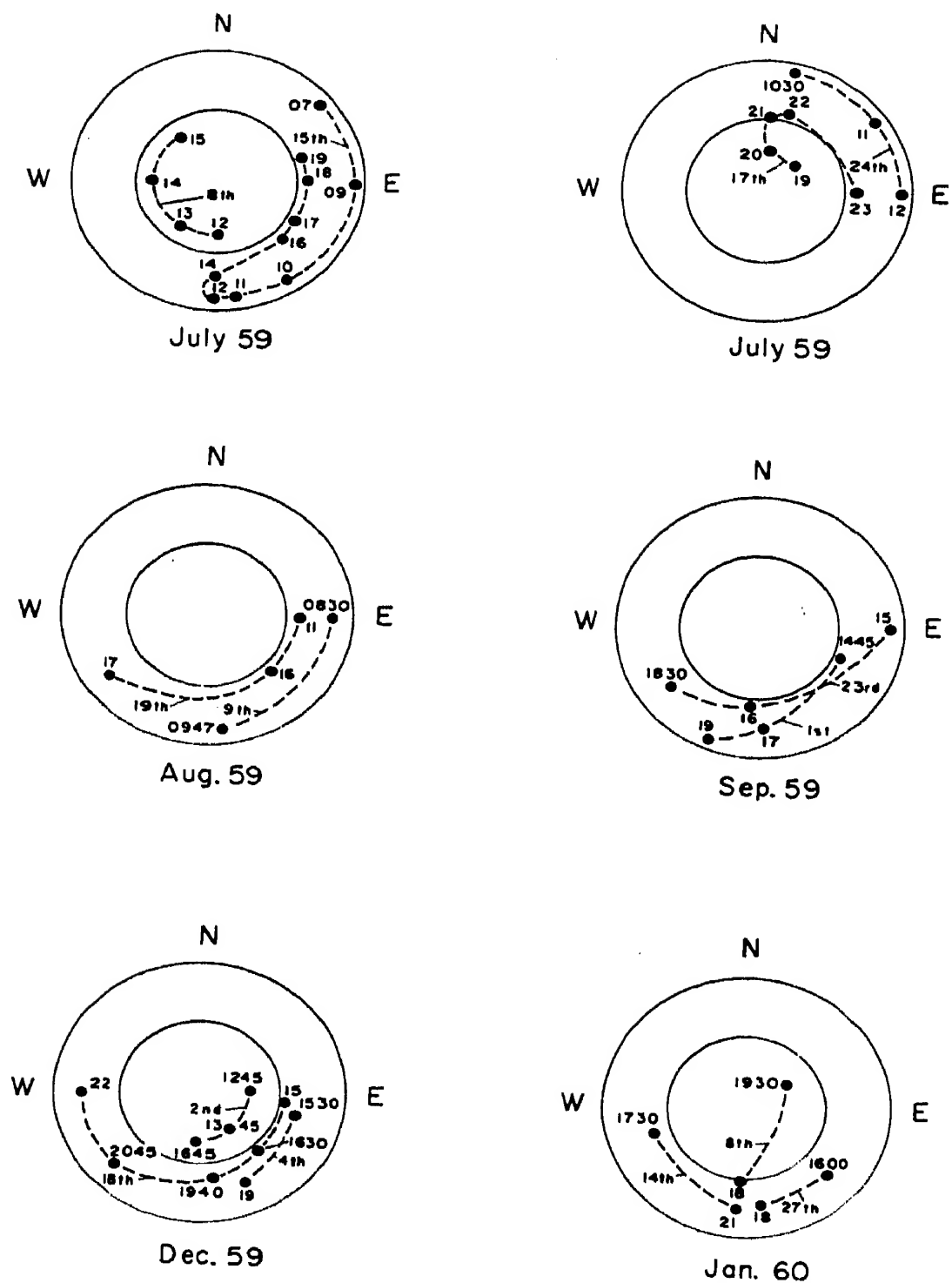


Fig. 10. Sample paths of moving  $E_s$  patches. The inner and outer circles correspond to a range of 1000 and 2000 km.

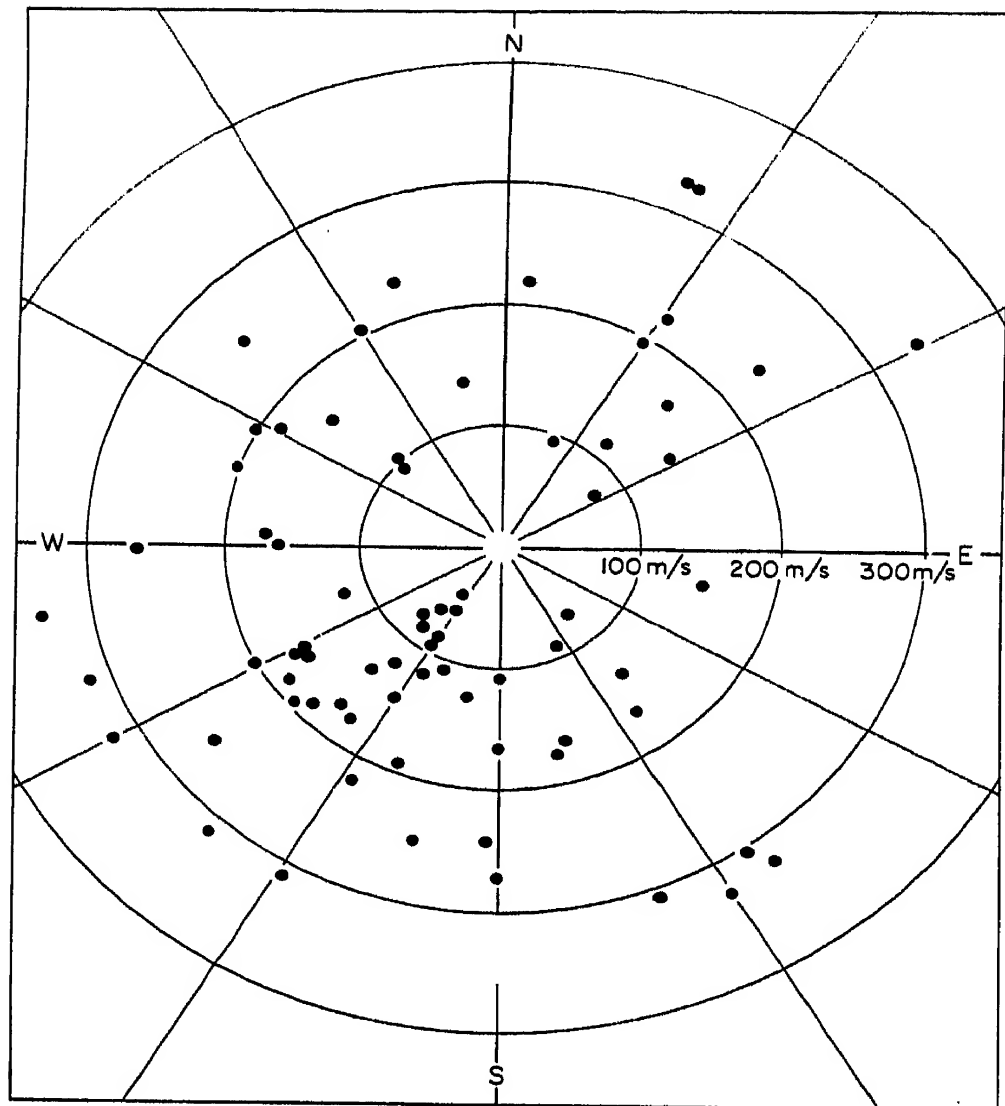


Fig. 11. Polar plot of measured velocities.

This corresponds to a velocity of 540 km per hour and is higher than the value obtained by Shearman and Harwood (1960) (between 200 and 350 km per hour) and the mean value of 303 km per hour obtained by Clark (1957) but in substantial agreement with the values 420 km per hour to 960 km per hour obtained by Davidson (1955).

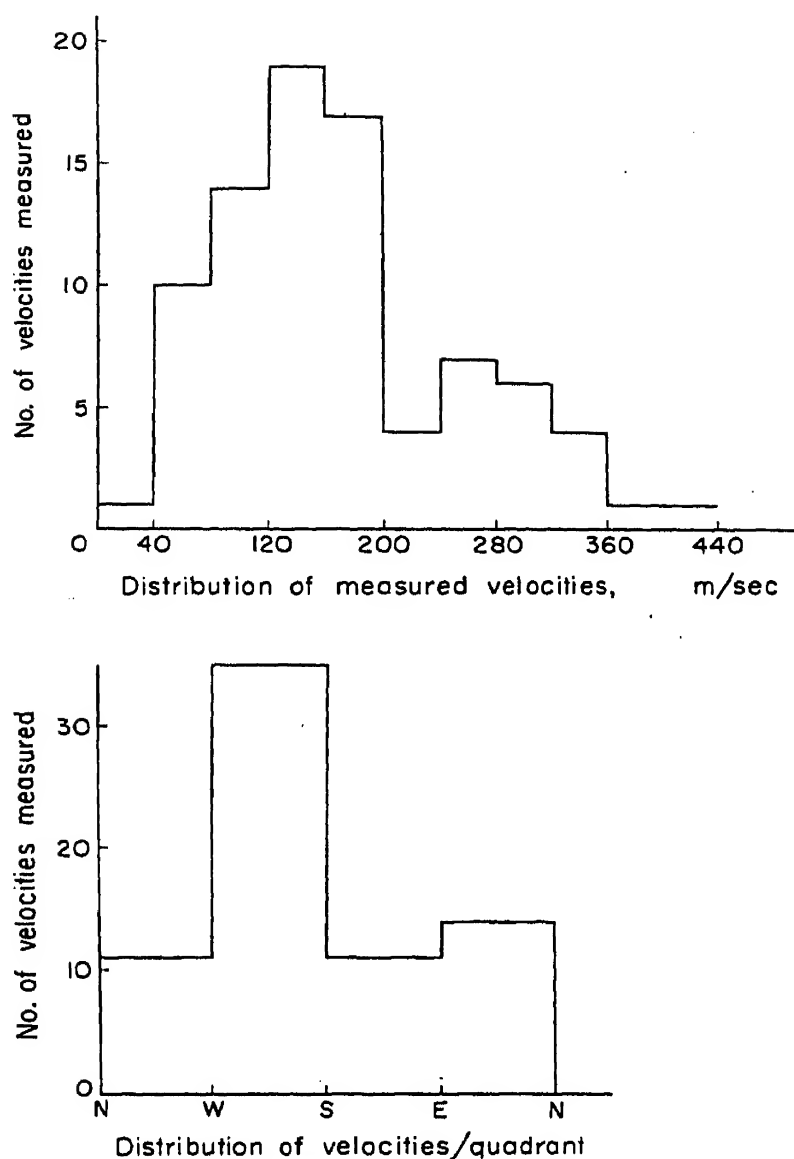


Fig. 12.

## 7. CONCLUSION

The multiple channel backscatter sounder is a powerful method for the study of sporadic  $E$ . In this study it has been found that  $E_s$  in this region shows the well known peak of activity during midsummer and in addition shows a minor maximum of activity during the winter months of December and January.  $E_s$  is more probable to occur at 17 00 hr A.S.T. and in the due south direction. The  $E_s$  clouds, when they drift, have a velocity of the order of 500 km per hour, and their prevailing direction is to the southwest.

## REFERENCES

- CLARK, C. (1957) TR No. 24, Radio Prop. Lab., Stanford Univ.  
 DAVIDSON, D. (1955) TR No. 230, Cruft Lab., Harvard Univ.  
 GERSON, N. C. (1959) *J. Atmosph. Terr. Phys.* **16**, 189.  
 SHEARMAN, E. D. R. and HARWOOD, J. (1960) *J. Atmosph. Terr. Phys.* **18**, 31.  
 SMITH, E. K. (1957) *NBS Cir.* 582, p. 188.

# Report on Recent $E_s$ Work in Brisbane

J. A. THOMAS

Physics Department, University of Queensland, St. Lucia, Brisbane,  
Australia

**Abstract**—A brief summary of Brisbane work during and since the IGY is given. Experimental evidence has been found for the association of  $E_s$  with  $F$ -region irregularities. Very small decreases in the horizontal component of the magnetic field appear to accompany  $E_s$  echoes. Field-aligned columns within the night-time  $E_s$ -region are quite commonly observed and evidence is given which favours the production of an  $E_s$ -layer by vertical ionization redistribution rather than an actual increase of electron content.

## 1. INTRODUCTION

Routine p'f recording has been carried out at Brisbane since 1943 and gradually extended since that time, particularly during the IGY. In addition, several special observing techniques have been in use for varying periods. The compilation of the data is only partially completed and this paper will present only a brief summary of the more recent work.

It should be pointed out that most of the work reported herein has been carried out by various members of the Physics Department, and the name of the worker most actively concerned is given following each section heading.

There are three chief results to report:

- (a) A direct association has been found, on a number of occasions, between rippled ionization contours of the night  $F$ -region and sporadic- $E$  enhancement at points linked magnetically to the  $F$  ripples.
- (b) A small depression in the horizontal component of the earth's magnetic field is found to accompany the detection of  $E_s$  reflections overhead.
- (c) Correlation has been found between aspect-sensitive reflections from field-aligned ionization in the sporadic- $E$  region and the recording of sporadic- $E$  echoes vertically below the region from which the field-aligned echoes have been obtained. These will be dealt with separately and other items of minor interest then outlined.

## 2. ASSOCIATION OF $E_s$ WITH $F$ RIPPLES (BOWMAN)

This work was largely carried out by Bowman and is reported in detail elsewhere (Bowman 1960a, b). Bowman has previously found (using

modified direction-finding techniques) that the varying types of p'f record commonly described as spread- $F$  at middle latitudes occur at times when the ionization contours of the  $F$ -region show a marked degree of rippling or even "wrinkling". Large single frontal ripples, for example, are found to be responsible for resolved range spreading. A cross-section of the true-height ionization contours as a function of time shows a typical kinking of contours of equal ionization, the kink being displaced horizontally with increasing height (Fig. 1). Straight lines joining corresponding points on successive contours have been called "slope lines"; these have a direction which indicates they are projections of the geomagnetic field lines on the perpendicular cross-section of the frontal  $F_2$  disturbance.

When isolated  $E_s$  echoes are recorded they often appear close to the place where the trough or crest slope line of an  $F_2$  irregularity meets the level of the  $E_s$ -layer (Fig. 1). The timing is not always as clear cut as in

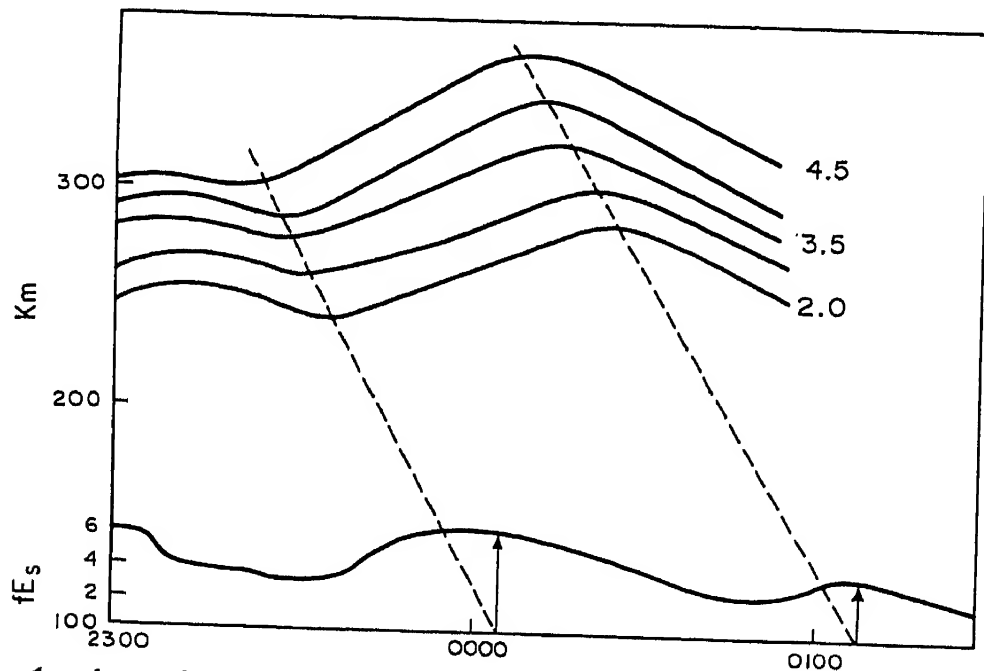


Fig. 1. Association between a double patch of sporadic  $E$  and  $F_2$ -layer irregularities.

the case illustrated, but there is good evidence for the coupling of  $E_s$  and  $F$  along the magnetic field lines. The frontal nature of  $F_2$  irregularities and this magnetic coupling implies frontal  $E_s$  configurations. This is borne out in a number of cases.

Spread  $E_s$  echoes (Thomas 1956) have been resolved and found to correspond to echoes coming from a variety of echoing fronts, sometimes indeed from somewhat different azimuths. Detailed analysis of a few such cases shows evidence for the reproduction in the  $E_s$ -layer of ripple patterns present in the  $F$ -region, though on a reduced vertical scale (Fig. 2). The overall motion of such complete structures appears to be close to the direction of magnetic north, i.e., towards the equator. The size and move-

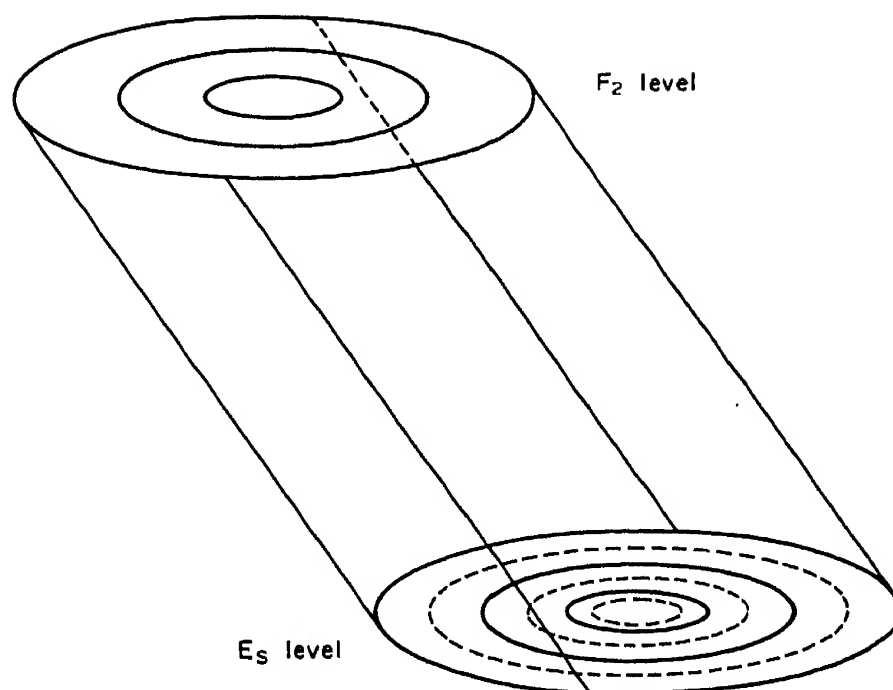


Fig. 2. Proposed relationship between  $F_2$ -layer irregularities and sporadic- $E$  occurrence.

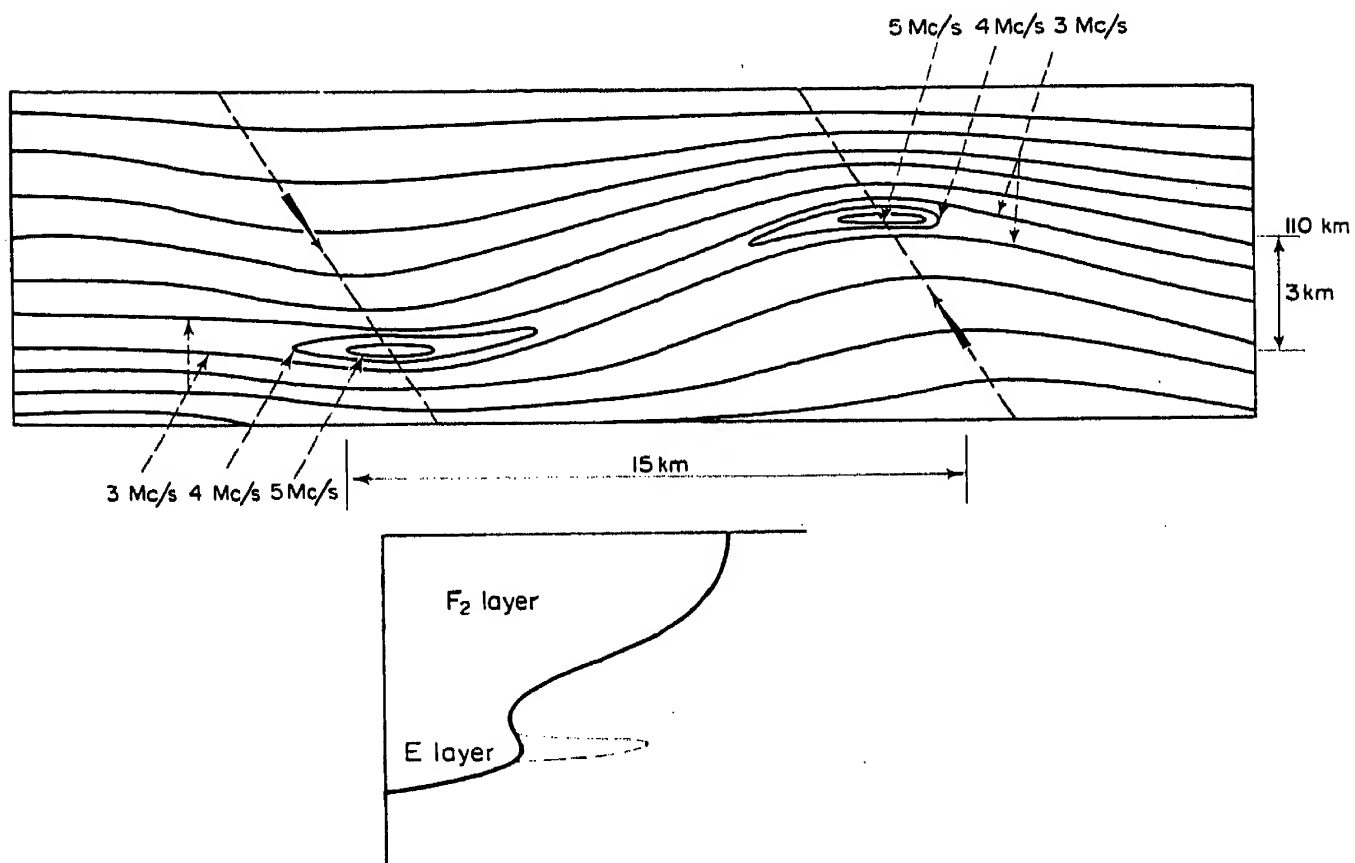


Fig. 3. Proposed distribution of ionization to explain the cloud-like nature and the ripple nature of sporadic- $E$  occurrence.



ment of these  $E$ -region disturbances is in agreement with size and movement of airglow cells (Roach, Tandberg-Hanssen and Megill 1958).

Proposed  $E_s$  ionization contours are given in Fig. 3, where we have a solution to the apparent contrast between the rippled structure and the patchiness necessary to explain blanketing effects. Forces (of the same nature as those causing  $F_2$  ripples) are visualized tending to move ionization along lines of force acting towards the ground at one part of the disturbances, and in the opposite direction at another. Further, if such movements tended to cause a bank-up of ionization near the  $E_s$  level, this would give ionization contours at the higher frequencies (e.g., 4 and 5 Mc/s in Fig. 3) which appear as "clouds", and ionization contours at other frequencies (e.g., 3 Mc/s in Fig. 3) which appear as ripples.

### 3. MAGNETIC CORRELATION (WILKIE)

Hojo and Yonezawa (1953) reported that the geomagnetic declination shows a small deflection in the direction amplifying the diurnal-variation a few hours after the appearance of an intense  $E_s$ -layer. The ionospheric and geomagnetic data used for their analysis were recorded at sites 90 km apart. At Brisbane, with both an ionosonde and a horizontal-component magnetometer operating at the same site, investigations have been carried out to determine any relation between sporadic  $E$  and the variation of the horizontal component of the earth's field.

Preliminary examination of the records showed that on occasions there appeared to be a small reduction in the horizontal component during the time when an  $E_s$  cloud was observed to pass overhead. To check this observation the field was plotted for 5 hours on either side of the time of central passage of the  $E_s$  cloud. Any cases where an individual patch lasted more than 10 hours were neglected and the duration of the  $E_s$  cloud, its critical frequency, height, and type, have not yet been taken into account. Since the  $Sq$  variation of the earth's field is not constant from day to day, and in addition, reverses its sense depending on whether the dynamo current system is North or South of Brisbane, it was necessary to eliminate the period from approximately 07 00 to 13 00 hr from the investigation. The field was plotted for every isolated cloud not occurring either during the period of the main  $Sq$  variation, or during a magnetic storm, and the average for each month was found over a period of 15 months. In almost every month it was found that the field was depressed, at or near the time of central passage of the  $E_s$  cloud. Individual monthly graphs are fairly ragged but an average of all monthly graphs (Fig. 4) shows a smooth symmetrical decrease in the field of maximum amplitude 7 gammas. The average duration of the  $E_s$  clouds over all the months analysed was between 3 and 4 hours, which agrees well with the duration

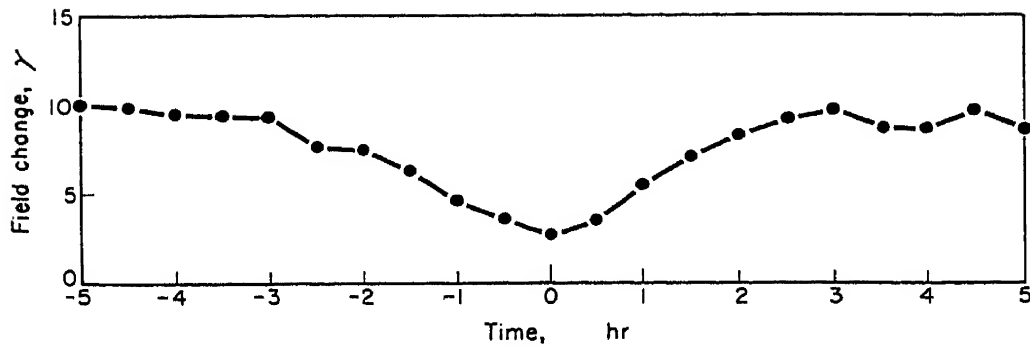


Fig. 4. Average variation of  $H$ -component of the magnetic field associated with the passage of  $E_s$  clouds.

of the average decrease in the field shown in Fig. 4. Correlation in individual cases was not high and one of the best examples is shown in Fig. 5.

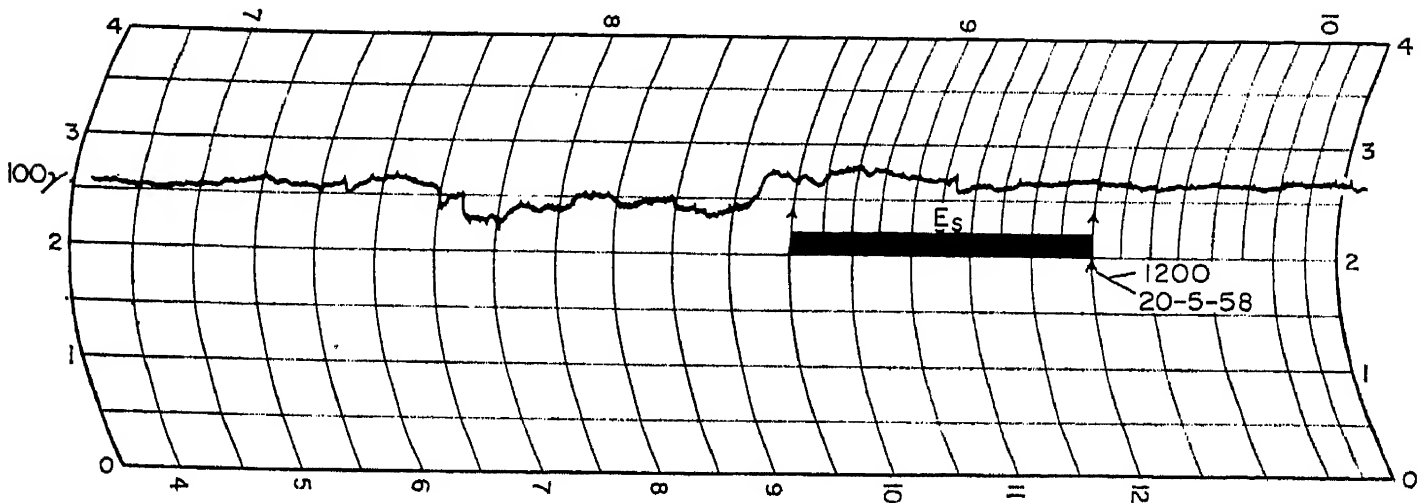


Fig. 5. An example showing the step-like depression in the value of  $H$  prior to the passage of an  $E_s$  cloud. This depression is in fact unusually large, being about six times the average value.

A further test was made by examining the horizontal component for a period of an hour centred on the time of initial occurrence of an  $E_s$  cloud and the time of final observation of the cloud. Over a period of 9 months, this analysis showed that the average decrease over this one hour period associated with the initiation of an  $E_s$  echo was 3 gammas, and a similar rise was associated with the disappearance of the  $E_s$  echoes.

In view of the surprisingly large value of this depression, an analysis was made of the times of occurrence of central passage of the clouds used in the above correlation analysis. These are, in fact, grouped in two periods with a maximum of occurrence at 17 00 hr and at 01 00 hr. Readings of the horizontal component taken at 13, 17, 21, 01, and 05 hr independently of whether sporadic- $E$  echoes occur or not, are shown in Fig. 6. It will be noted that there is a depression of about 7 gammas at 17 00 hr and a smaller depression from the general trend at 01 00 hr. The actual number of occurrences of recorded  $E_s$  echoes (whether they were used in isolated cloud analysis or not) shows a very similar trend in an inverse sense; this

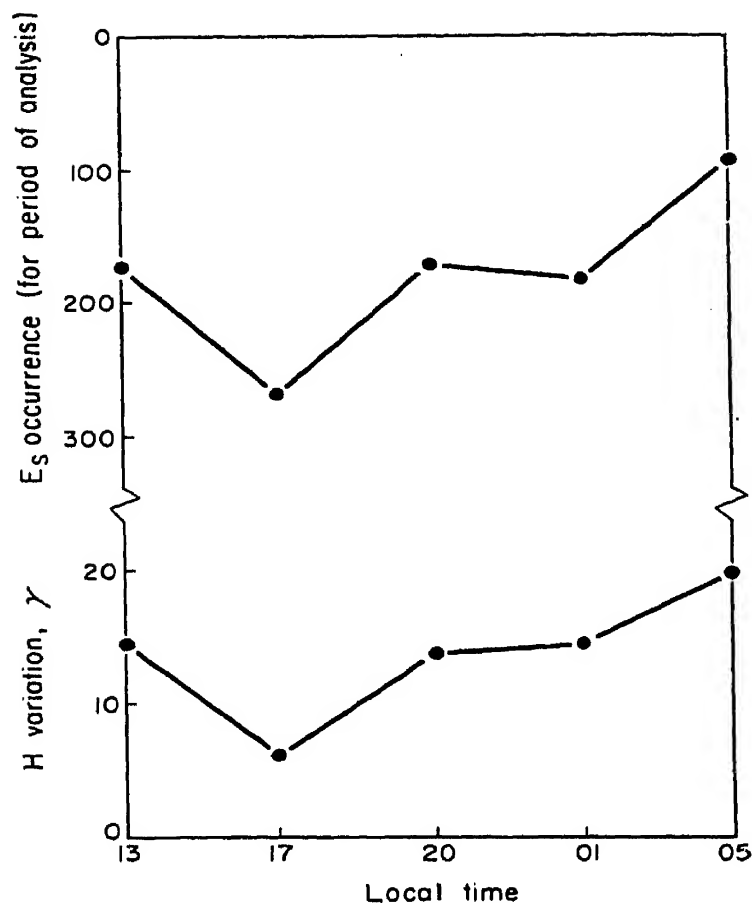


Fig. 6. Four-hourly plots of all  $H$  values (independent of  $E_s$  occurrence) and  $E_s$  echo occurrence figures.

is also plotted in Fig. 6. The implication is that there may be a common cause for both the production of the sporadic  $E$  and the reduction in the horizontal component.

A further test was made using an even number of  $E_s$  clouds for each hour of the day, thus avoiding the effects outlined in the previous paragraph. The result shown in Fig. 7 indicates a smaller depression of 3–4

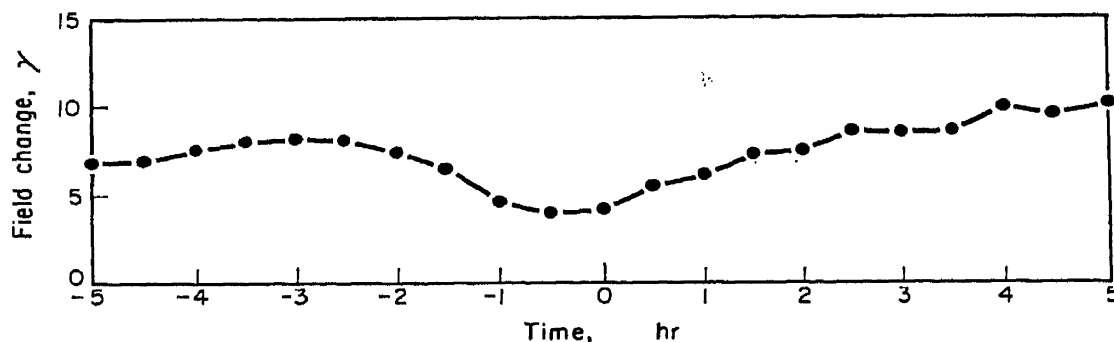


Fig. 7.  $H$  variation associated with  $E_s$  cloud passage, with observations spread evenly throughout the day.

gammas and it therefore appears that this reduction in  $H$  is genuinely associated with the passage of a typical  $E_s$  patch overhead, although further work is obviously necessary before any dogmatic statement can be made.

#### 4. FIELD-ALIGNED IONIZATION (GOODWIN)

Backscatter sounding equipment has been in operation at Brisbane since September, 1959. Recently, improvements to the aerial system have been made, as discussed by Thomas and McNicol (1960). With this improved aerial beam of only 8 degrees total width, high angular resolution is possible, and attempts are being made to correlate field-aligned echoes from sporadic  $E$  with sporadic- $E$  echoes observed at Casino, which is located almost vertically underneath the meridian-section field-aligned echoing point for the  $E$ -region. To date there are few data available, but what there is has shown quite good correlation between the observation of oblique field-aligned echoes and normal-incidence night-time sporadic- $E$  echoes; some information is also obtained on the shape and size of patches. The recording programme and analysis is continuing.

#### 5. PHASE-PATH TECHNIQUES (THOMAS)

For some years phase-path techniques have been used at Brisbane to aid the analysis of various forms of irregular behaviour of the ionosphere (McNicol and Thomas 1960). The technique is particularly useful in analysing complex sporadic- $E$  echoes, enabling the determination of several different types of overlapping sporadic- $E$  echoes. It is useful in the analysis of movements of sporadic- $E$  patches and in the determination of changes in ionization content when sporadic- $E$  patches move overhead. The technique here is to observe the  $F$ -region phase-path, and note any changes in this phase-path which occur when sporadic- $E$  clouds come between the transmitter and the  $F$ -region. Difficulty arises because of the changes in the  $F$ -region which occur independently of the sporadic- $E$  movements, but one would expect that if the sporadic- $E$  patch carries with it any appreciable amount of ionization, the  $F$ -region phase-path should decrease when the  $E_s$  patch intervenes. Accurate counts have been made of the  $F$ -region phase-path fringes over extended periods on either side of isolated  $E_s$  patches, but no consistent result has been found for the change in the  $F$ -region phase-path. It thus appears very probable that the sporadic- $E$  echoes observed on these occasions did not appreciably alter the total amount of ionization below the  $F$ -region but rather merely redistributed it in such a way that  $E_s$  echoes were observed.

Robinson (1960) has suggested one possible way in which such a redistribution might occur in practice. Whitehead (1961) has produced a theory which basically involves vertical redistribution of ionization rather than horizontal transport.

#### 6. AIRGLOW CORRELATION (DANZIGER)

An airglow photometer has been operated at Brisbane for several months of 1960 and measurements have been taken of the green line  $5577\text{\AA}$ .

Analysis of these records shows generally a poor correlation with critical frequency of  $E_s$ , but on occasion a good correlation with the occurrence of spread echoes of sporadic  $E$ . This correlation has been strengthened by the fact that the airglow intensity on these occasions correlates quite well with the quantity  $(fE_s - f_bE_s)$ . The suggestion is put forward that on these occasions the sporadic- $E$  region may well be more turbulent than on other occasions and that this turbulence is associated with the higher air-glow intensity.

## 7. CLOSED SPACED p'f

Equipment is being built at the moment for setting up a chain of closely spaced p'f sounders for the observation of the growth and decay of  $E_s$  patches. The spacing involved between observation points will be of the order of tens of km and it is hoped to have 8 such observation points in close proximity.

*Acknowledgment*—The work reported above is supported by the Radio Research Board C.S.I.R.O., the University of Queensland and part by the Air Research and Development Command under contract AF64(500)-9. This support is gratefully acknowledged.

## REFERENCES

- BOWMAN, G. G. (1960a) *Planet. Space Sci.* 2, 133.  
BOWMAN, G. G. (1960b) *Planet. Space Sci.* 2, 195.  
HOJO, H. and YONEZAWA, T. (1953) *Rep. Iono. Res. Japan* 7, 61.  
MCNICOL, R. W. E. and THOMAS, J. A. (1960) *Aust. J. Phys.* 13, 120.  
ROACH, F. E., TANDBERG-HANSEN, E. and MEGILL, L. R. (1958) *J. Atmosph. Terr. Phys.* 13, 113.  
ROBINSON, B. J. (1960) *J. Atmosph. Terr. Phys.* 19, 160.  
THOMAS, J. A. (1956) *Aust. J. Phys.* 9, 228.  
THOMAS, J. A. and MCNICOL, R. W. E. (1960) *Nature* 187, 398.  
WHITEHEAD, J. D. (1961) *J. Atmosph. Terr. Phys.* 20, 49.

# Recent Sporadic-*E* Experimental Work in the United States

J. F. DEGREGORIO, J. W. FINNEY, K. KILDAHL and E. K. SMITH

Boulder Laboratories, National Bureau of Standards, Boulder, Colorado, U.S.A.

**Abstract**—This paper reports on experimental work carried out by the Central Radio Propagation Laboratory of the National Bureau of Standards during the past three years utilizing the transmitting site at Long Branch, Illinois; the mid-point site at Shickley, Nebraska, and Colorado receiving sites of the National Bureau of Standards. Inconsistencies in the published literature concerning the relationship of sporadic *E* observed at vertical incidence with that recorded on v.h.f. oblique-incidence circuits are found to be largely explained if the different types of sporadic *E* are considered separately and the effect of antenna gain in the v.h.f. circuits is properly evaluated. Fading and direction of arrival are found to give substantial support to a theory of the existence of intense ionization centers for the type of sporadic *E* which provides TV-DX. Evidence of a moving "front" of sporadic *E* some 200 km in depth is derived from a multiple reflection point experiment.

## 1. INTRODUCTION

The work reported in the paper represents a survey of recent findings of the Central Radio Propagation Laboratory sporadic-*E* group of the National Bureau of Standards' Boulder Laboratories. The work of this group is only a fraction of the total work on sporadic *E* at the Boulder Laboratories, as can be seen from the several contributions in this volume by other workers at NBS.

The basic experimental facilities utilized in this program are portrayed in Fig. 1. Long Branch, Illinois, is the major h.f. and v.h.f. transmitting station of CRPL, and Table Mesa (12 miles north of Boulder) is the major receiving facility. The sporadic-*E* program has operated three circuits (30 Mc/s, 50 Mc/s and 74 Mc/s) using 5-element Yagi antennas located at such heights that the direct and ground-reflected rays are received in phase for reflections at 110 km heights at the path midpoint. An NBS Model C-2 ionosonde is located 10 miles west of the geographic midpoint. (This westward deviation from the exact midpoint is intentional.) There is a 4000 foot difference in elevation between transmitting and receiving antennas, so that, for horizontally stratified layers, the reflection point will be closer to the higher terminal (Boulder).

The experimental work described here was performed in the period 1958 through 1960. Terminology and calibration procedures are the same

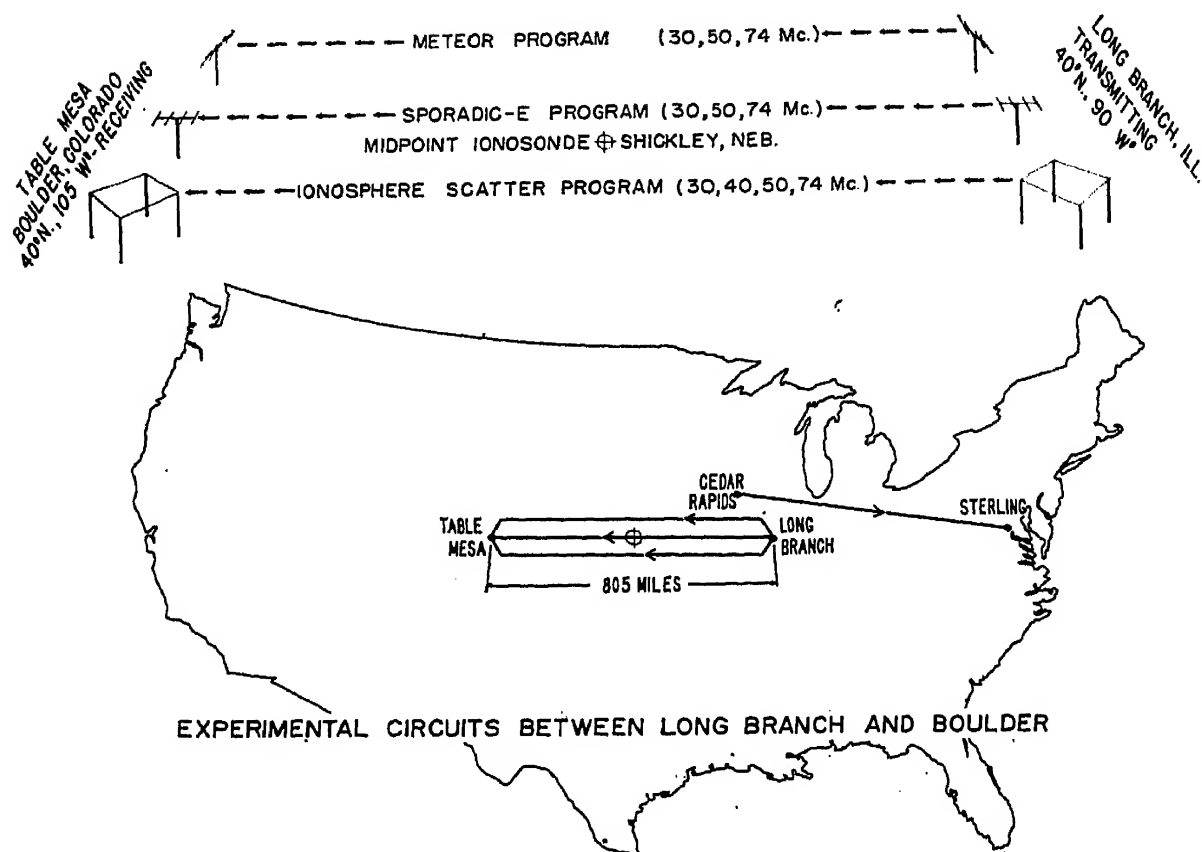


Fig. 1. Experimental circuits between Long Branch and Boulder.

as those developed for the ionosphere scatter program (Bailey, Bateman and Kirby 1955). The results in this paper may be directly compared to those in other publications of the sporadic- $E$  group (Smith 1957, Davis, Smith and Ellyett 1959, Smith 1958, Smith and Finney 1960). Due to the high concentration of sporadic- $E$  events around the summer solstice at these latitudes the specialized experiments have all been carried out during the summer months. However, field intensity on the 50 Mc/s frequency has been monitored throughout the year to determine seasonal variation. The specialized experiments referred to above are as follows:

- (a) The correlation of  $E_s$  field intensities observed over v.h.f. oblique-incidence circuits with distribution of  $f_oE_s$  at an ionosonde located at the midpoint (described in part 2).
- (b) Fading rate at vertical and oblique incidence (described in part 3).
- (c) A multiple-midpoint oblique-incidence experiment designed to give simultaneous patch size and velocity information (described in part 4).

## 2. OBSERVATIONS OF $E_s$ AT OBLIQUE INCIDENCE AND WITH A MIDPOINT IONOSONDE

Considerable data exist in the literature on diurnal and seasonal variation of sporadic  $E$  in the United States (e.g. Davis, Smith and Ellyett 1959), and, as our data are in substantial agreement with the published work, this

information will not be presented explicitly in this paper. Rather, attention will be directed toward the comparison of the statistical distributions of signal level at the three oblique-incidence frequencies (30, 50 and 74 Mc/s) with that of the vertical-incidence "critical frequency",  $f_oE_s$  as observed at the midpoint ionosonde in Shickley, Nebraska. Such a comparison is of technological interest because vertical-incidence data are available from a worldwide network of ionosondes and one would like to use data from this network to predict the effect of  $E_s$  on v.h.f. communications circuits. The approach used in this paper is first to lump all types of  $E_s$  together in considering the relationship of oblique to vertical observations and then to treat the different types separately.

Comparisons of vertical with oblique-incidence data have been reported before (Kono, Uesugi, Hirai and Abe 1954, Davis, Smith and Ellyett 1959), but in these cases the vertical-incidence data came from the nearest available ionosonde (in the second reference it was 400 miles from the midpoint). In the present case the ionosonde was placed to suit the requirements of the experiment.

The five element horizontal Yagis used for both transmitting and receiving in this present program have plane-wave gains of 9 db relative to a dipole and horizontal beamwidths to half-power points of approximately  $60^\circ$ . It has already been reported (Smith 1958) that  $E_s$  reflection coefficients derived from a circuit employing  $6^\circ$  rhombics at both ends are 10 to 15 db lower than those derived from a circuit with Yagis at the same heights provided a reasonably long series of observations is considered. This fact is attributed to off-midpoint contributions to the received signal which are discriminated against by the narrow beam antennas.

The percentage of time the sporadic-*E* power reflection coefficient  $r$  exceeds any value of interest can be derived from Fig. 2. The mean

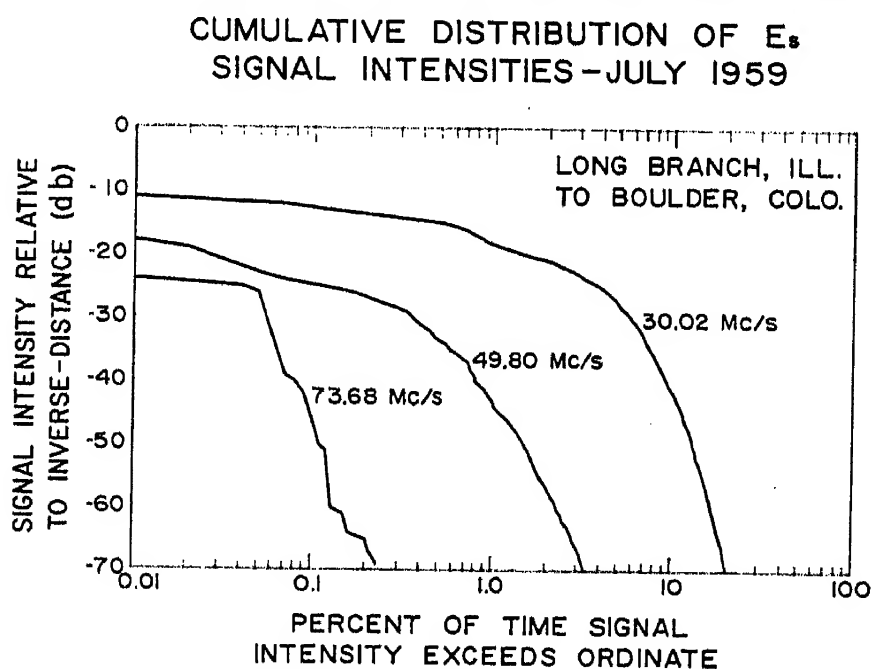


Fig. 2. Cumulative distribution of  $E_s$  signal intensities—July 1959.



statistical values of the frequency exponent  $n$  are in agreement with earlier values (Davis, Smith and Ellyett 1959). These values may be obtained from Fig. 2 from the relations

$$\log_{10} r_1 - \log_{10} r_2 = n \log_{10} \left( \frac{f_2}{f_1} \right)$$

where the subscripts on the reflection coefficients refer to the frequencies  $f_1, f_2$ . A good discussion of the implications of this parameter for equatorial  $E_s$  at vertical incidence is given in a companion paper in this volume (Skinner and Wright 1961).

A comparison was presented in a previous study (Smith 1957) of data for the summer of 1952 of v.h.f. field intensities and  $fE_s$  derived from a Japanese paper (Kono, Uesugi, Hirai and Abe 1954). In this study it was found that when oblique measurements were related to vertical-incidence ones by the secant law (Wright and Gautier 1960) then probabilities of  $fE_s$  occurrence corresponded to probabilities of occurrence of oblique-incidence signal intensities of 0 to  $-20$  db relative to free space. In a subsequent paper (Davis, Smith and Ellyett 1959) this same comparison was made for sporadic  $E$  on the Cedar Rapids to Sterling path and  $fE_s$  observed at Washington, D.C. for the period May 1955 to February 1956. Here it developed that  $fE_s$  in Washington corresponded approximately to  $-70$  db relative to inverse-distance ( $-58$  db relative to free-space), a very serious difference. A similar comparison for the Long Branch to Boulder circuits equipped with Yagi antennas and the midpoint sounder is seen in Fig. 3 for July 1959. For most of the frequency range it is seen that the  $f_oE_s$  distribution corresponds to the occurrence of oblique-incidence  $E_s$  (at the equivalent frequency) for intensity levels between  $-30$  and  $-40$  db relative to inverse distance (reflection coefficients of  $-30$  to  $-40$  db). This result is probably typical of the summer months for this path for a year of high  $E_s$ . It is in reasonable agreement with the Japanese result (Kono, Uesugi, Hirai and Abe 1954), which was also for summer months, but appears to contradict the other U.S. comparison (Davis, Smith and Ellyett 1959).

Several possible answers to the apparent contradiction between these two and the earlier U.S. determinations have been considered. The distribution of  $f_oE_s$  for the Washington, D.C. ionosonde was compared to that for the Shickley midpoint station (two stations with similar geographic and geomagnetic latitudes) for the same period and it was found that the two were almost identical. Therefore, the possibility that the Shickley ionosonde was not operating properly could be dismissed. The earlier U.S. measurements were made with  $25\lambda$  rhombics, the latter with 5-element Yagi antennas. A comparison of these two types of antennas in operation simultaneously over the Long Branch to Boulder path indicated that, whereas the gain of the Yagi (9 db) appears completely realized during  $E_s$

COMPARISON OF OBLIQUE-  
INCIDENCE SIGNAL INTENSITIES  
WITH DISTRIBUTION OF  $f_o E_s$   
AT THE MIDPOINT-JULY 1959

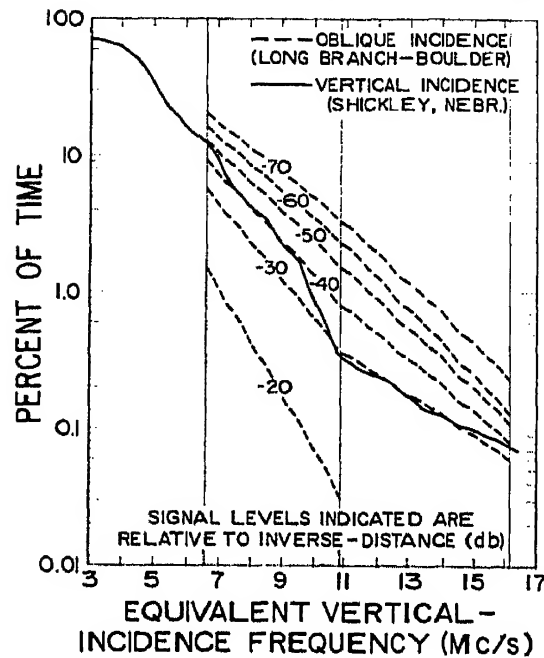


Fig. 3. Comparison of oblique-incidence signal intensities with distribution of  $f_o E_s$  at the midpoint—July 1959.

propagation periods, that of the rhombics was not. This discrepancy can account for 10 to 15 db of the differential. Most important, probably, is the fact that the correspondence varies seasonally. While close to the earlier comparison (Davis, Smith and Ellyett 1959) during off-season months it swings to the situation presented in Fig. 3 at the height of the  $E_s$  season. An additional minor difference is due to the use of  $fE_s$  in the former case and  $f_o E_s$  in the latter.

Although the arguments presented above can explain the discrepancy between the two sets of data they serve to complicate the problem of predicting the distributions of sporadic- $E$  transmission losses on v.h.f. communications circuits from vertical-incidence data. It is seen that not only do high-gain antennas not appear to realize their plane-wave gains during periods of  $E_s$  transmission, but also the correspondence of oblique field intensity and  $f_o E_s$  appears to vary with time.

One possible means of interpreting the seasonal variation in the correspondence of oblique and vertical  $E_s$  data would be to consider the correspondence separately for the different  $E_s$  types. That is, if certain types of  $E_s$  produce more intense reflections at oblique incidence than others, and if these more intense types are more prevalent in the summer relative to the other  $E_s$  types, then the seasonal anomaly would be explained. It is also important to investigate the efficiency of the different types of  $E_s$  in propagating v.h.f. oblique-incidence signals from the standpoint of the

possible structures of the types and in order to ascertain how real are the distinctions between the types.

The results of our attempt to separate out propagation by the different  $E_s$  types for the Long Branch to Boulder path are shown in Fig. 4 for the

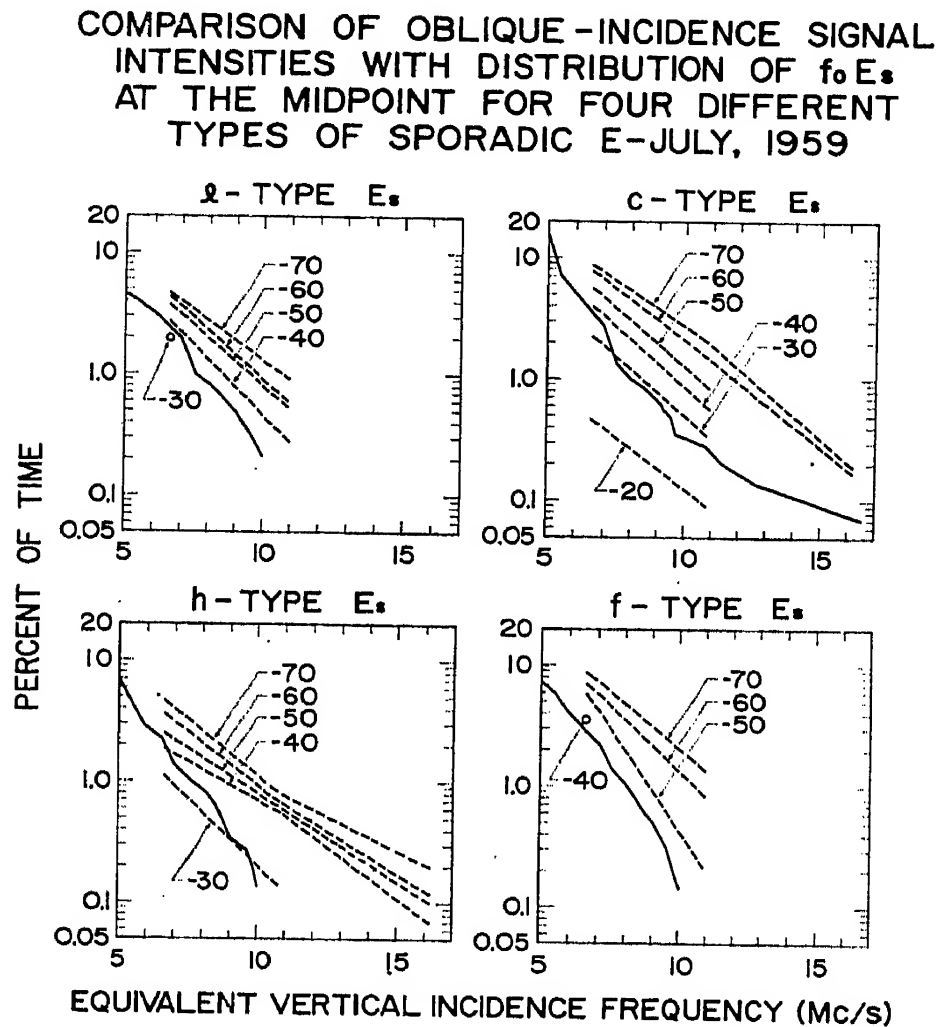


Fig. 4. Comparison of oblique-incidence signal intensities with distribution of  $f_o E_s$  at the midpoint for four different types of sporadic  $E$ —July 1959.

month of July 1959. Only four types occurred in sufficient frequency for statistical treatment. These are  $l$  (low),  $c$  (cusp),  $h$  (high) and  $f$  (flat) types (for definitions and characteristics of the types, see Thomas and Smith 1959). The four plots in Fig. 4 are the same kind as Fig. 3, but are constructed separately for the periods during which the midpoint sounder showed that particular type was active. The reflection height for the oblique paths has been assumed to be 110 km (e.g. Smith 1957) in the determination of the equivalent vertical frequency when plotting the oblique circuit data on Figs. 3 and 4. The observed virtual heights (nearest 2 km) during July 1959 at Shickley were:

$l$  type (115 cases) : 111 km  $\pm$  7 km  
 $c$  type (469 cases) : 111 km  $\pm$  4 km  
 $h$  type (193 cases) : 119 km  $\pm$  7 km  
 $f$  type (219 cases) : 111 km  $\pm$  6 km

The value listed is the median virtual height. Fifty per cent of the cases were recorded at heights within the ranges shown. Also recorded were 28 cases of  $q$ -type (equatorial) and 18 cases of  $r$ -type (retardation)  $E_s$ .

If the equivalent vertical-incidence frequencies of 8 and 10 Mc/s are arbitrarily selected the following comparison can be made from Fig. 4:

$E_s$ Type	Oblique Signal Intensity Corresponding to $f_o E_s$		
	8 Mc/s	10 Mc/s	
$l$	35 db	35 db	below I.D.
$c$	29 db	27 db	below I.D.
$h$	35 db	28 db	below I.D.
$f$	45 db	45 db	below I.D.

Types  $h$  and  $c$  can be seen to provide the most intense oblique reflections for the given values of  $f_o E_s$  while  $f$ -type  $E_s$  provides distinctly weaker reflections. As  $f$ -type is the night-time category this difference can probably be attributed to the effect of daytime absorption which will tend to decrease the  $f_o E_s$  values for the  $l$ ,  $c$  and  $h$  types relative to the oblique values.

The seasonal distribution of these four types for the year 1958 is shown in Fig. 5.  $c$ -type is seen to dominate the summer peak (May–August) and

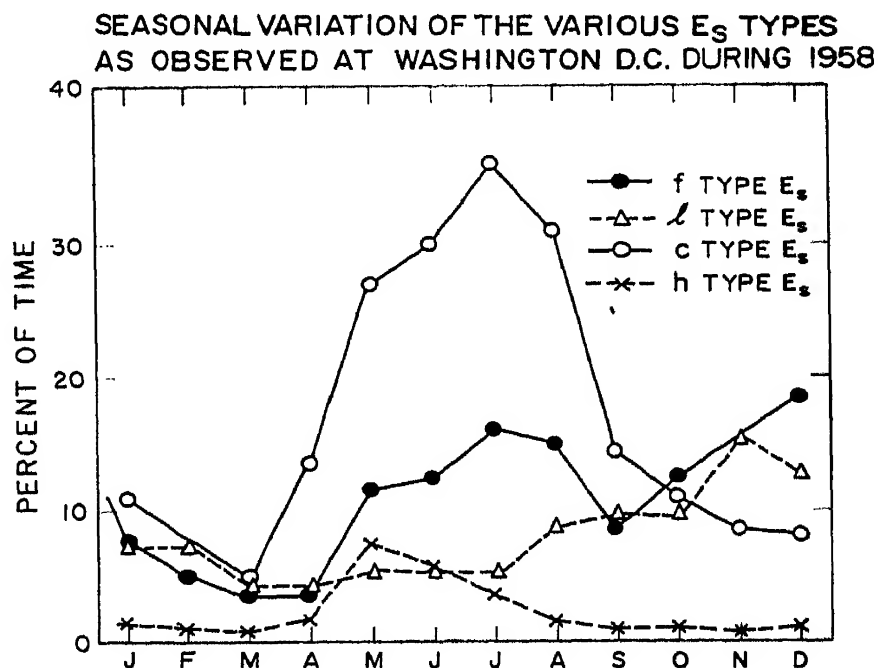


Fig. 5. Seasonal variation of the various  $E_s$  types as observed at Washington, D.C. during 1958.

*h*-type is also a distinctly summer phenomenon. In contrast the *f*- and *l*-types peak during the November–December period and both override *c*- and *h*-types during most of the remainder of the year. It would be expected from these data that a purely summer equivalence between vertical and oblique data (e.g. Fig. 3) would show about 10 db higher reflection coefficients than the corresponding presentation for the whole year. This assumes, of course, that a given type will produce the same vertical to oblique relationships and hold throughout the year (an assumption which has not as yet been tested).

### 3. FADING RATE

Fading rate during  $E_s$  propagation has been recorded simultaneously on fast-speed tape for the three v.h.f. Yagi circuits and, at the midpoint station, fading rate is determined by counting the median crossings. The general conclusions are:

- (a) For the three v.h.f. circuits fading rates vary typically between 0.05 and 0.5 c/s.
- (b) Statistically the fading rate for the midpoint station agreed with that observed over the corresponding oblique frequency.
- (c) Statistically the fading rate increases approximately linearly with frequency for the three v.h.f. circuits.
- (d) The instantaneous correlation of fading at the midpoint station with that of the oblique circuit at the corresponding frequency is poor (typically  $r \sim 0.0$ ).
- (e) If the fading rate (as recorded simultaneously at 30, 50 and 74 Mc/s) is compared for an interval of the order of one minute for the three v.h.f. circuits, the fading rate may be observed to generally increase, but also sometimes decrease, with frequency.

The lack of instantaneous correspondence between the fading rates for the midpoint station and the corresponding oblique frequency can be attributed to the fact that the  $E_s$  reflection for the two cases does not involve identical Fresnel zones. Even for a perfectly horizontal  $E_s$  layer the vertical incidence Fresnel zones are circles and the oblique-incidence ones are ellipses. If the  $E_s$  region is tilted or wavy, then the centers of the two systems of Fresnel zones will not be the same either. Angle of arrival measurements made at Boulder on the 50 Mc/s circuit during  $E_s$  indicate that the signals can arrive from as much as  $20^\circ$  off the great-circle path during weak sporadic  $E$  (normally the beginning and ending of a sporadic- $E$  opening).

The fact that the fading rate may either increase or decrease with frequency over the three v.h.f. circuits seems very significant from the standpoint of the structure of sporadic  $E$ . Scaled antennas mounted the same

number of wavelengths above the ground were used on all three frequencies and the geographical separation between antennas at each terminal was reduced to a minimum. Thus the antenna polar diagrams are independent of frequency, and the same common volumes in the ionosphere were intercepted by the transmitting and receiving antennas for each circuit. The peculiar frequency dependence must therefore be attributed to the structure of the sporadic-*E* region. An example where fading rate decreases with frequency is shown in Fig. 6.

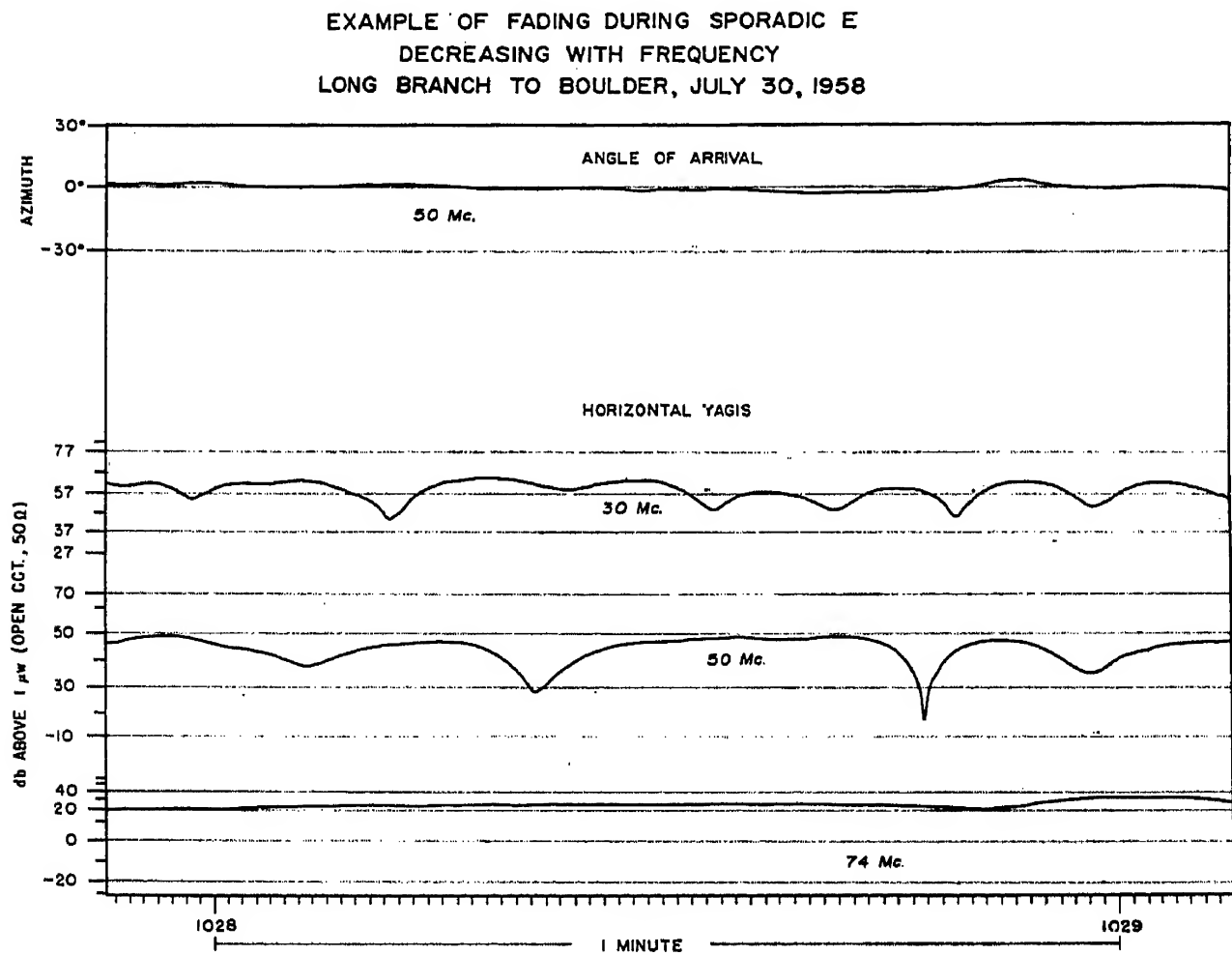


Fig. 6. Example of fading during sporadic *E* decreasing with frequency, Long Branch to Boulder, July 30, 1958.

#### 4. MULTIPLE PATH STUDY

An experiment making use of a network of oblique-incidence circuits arranged as in Fig. 7 to provide three closely spaced (50 km) and two outlying reflection points (200 km from central reflection point) was carried out in the summer of 1960. The equivalent vertical-incidence frequencies were all within the range 10.5 Mc/s to 12.3 Mc/s as shown on p. 140.

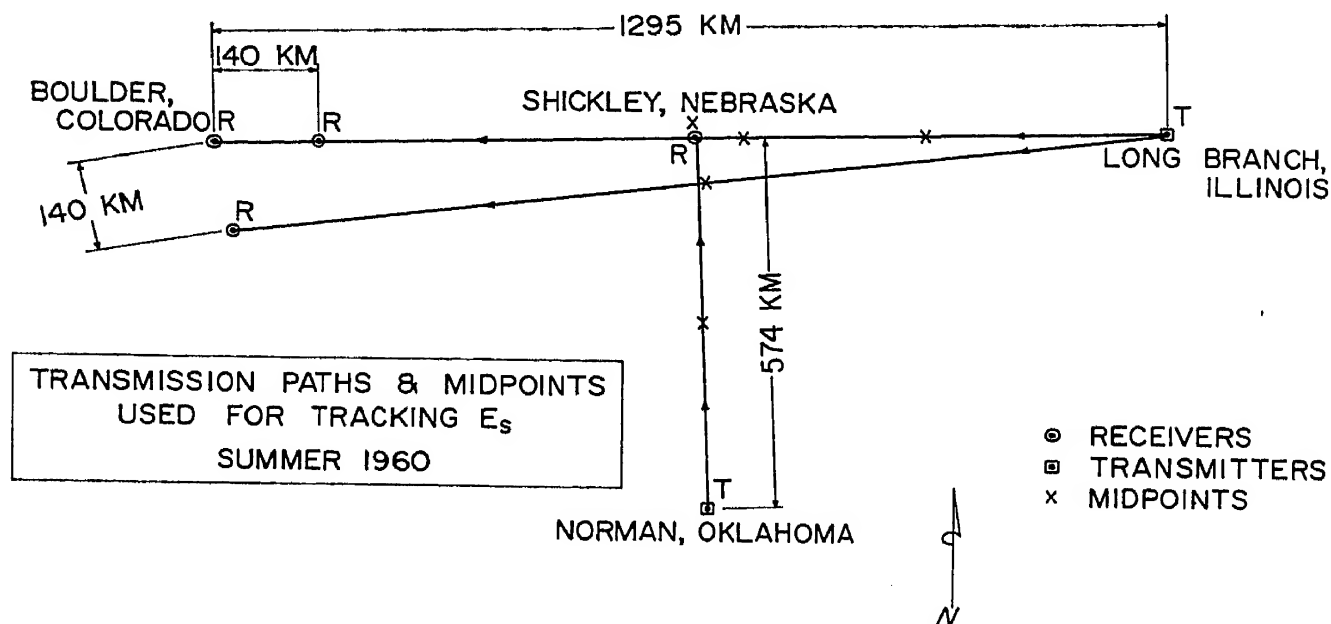


Fig. 7. Arrangement of sites used in the multi-station  $E_s$  experiment.

Path	Distance (km)	Sec	Frequency (Mc/s)	Equivalent V.I. Frequency (Mc/s)
(a) Long Branch-Boulder	1290	4.57	49.800	10.9
(b) Long Branch-Shickley	645	2.85	30.010	10.5
(c) Long Branch-Brush	1200	4.40	49.800	11.3
(d) Norman-Shickley	570	2.44	30.015	12.3
(e) Long Branch-Cheyenne MT.	1300	4.60	49.80	10.8

An example of an isolated  $E_s$  event occurred on July 28, 1960 and is shown in Fig. 8. This particular  $E_s$  patch has a west-to-east phase velocity component of approximately 1400 km/hr and a south-to-north phase velocity of 350 km/hr. The resultant velocity of the patch is then computed to be 330 km/hr in the direction  $14^\circ$  East of North. The actual time durations noted at the reflection points are all comparable and approximately 35 minutes. The "patch" of  $E_s$  therefore appears in this instance as a "front" about 200 km in depth and shows almost no variation in this thickness along a 1000 km width of the front intercepted by the observing points and the Boulder ionosonde. A simulated picture of the  $E_s$  ionization at 1030 MST is shown in Fig. 9.

## 5. CONCLUSIONS

Experimental evidence is presented to show that summer values of  $f_oE_s$  recorded on a C-2 ionosonde correspond approximately to reflection coefficients of  $-30$  to  $-40$  db for oblique paths of 1300 km in length.

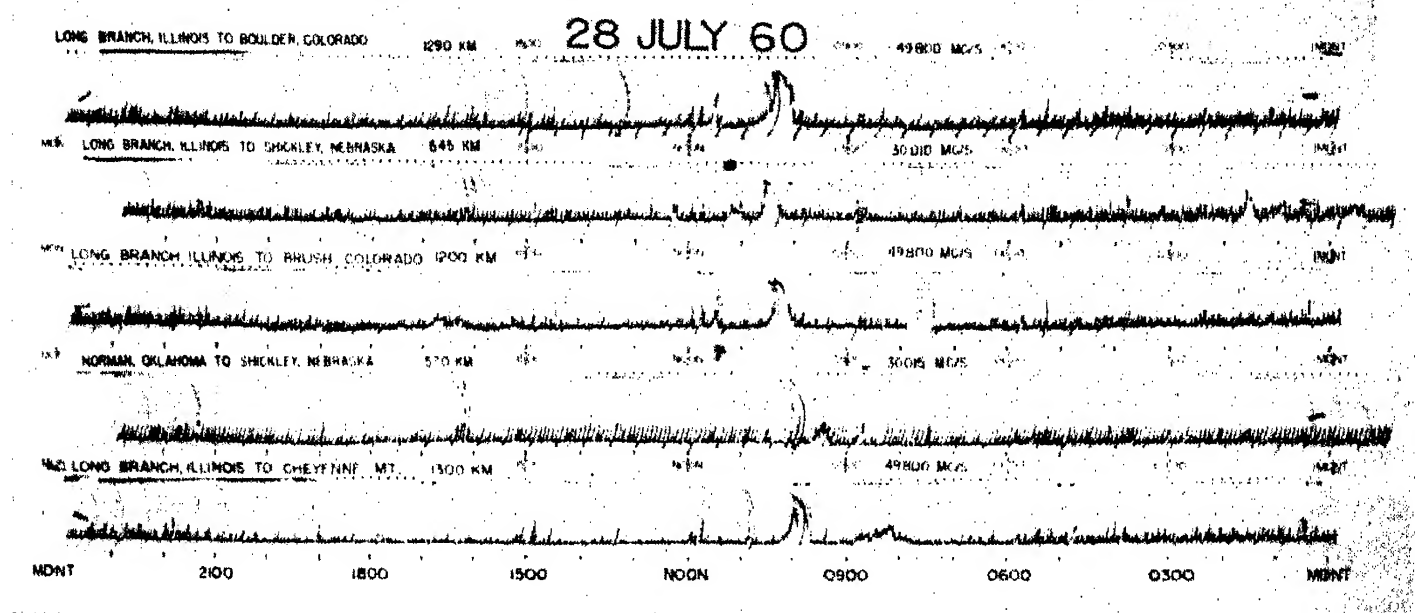
EXAMPLE OF RECORDS OBTAINED DURING THE  
MULTIPLE-STATION E<sub>s</sub> EXPERIMENT.

Fig. 8. Records obtained at the various receiving sites on July 28, 1960.

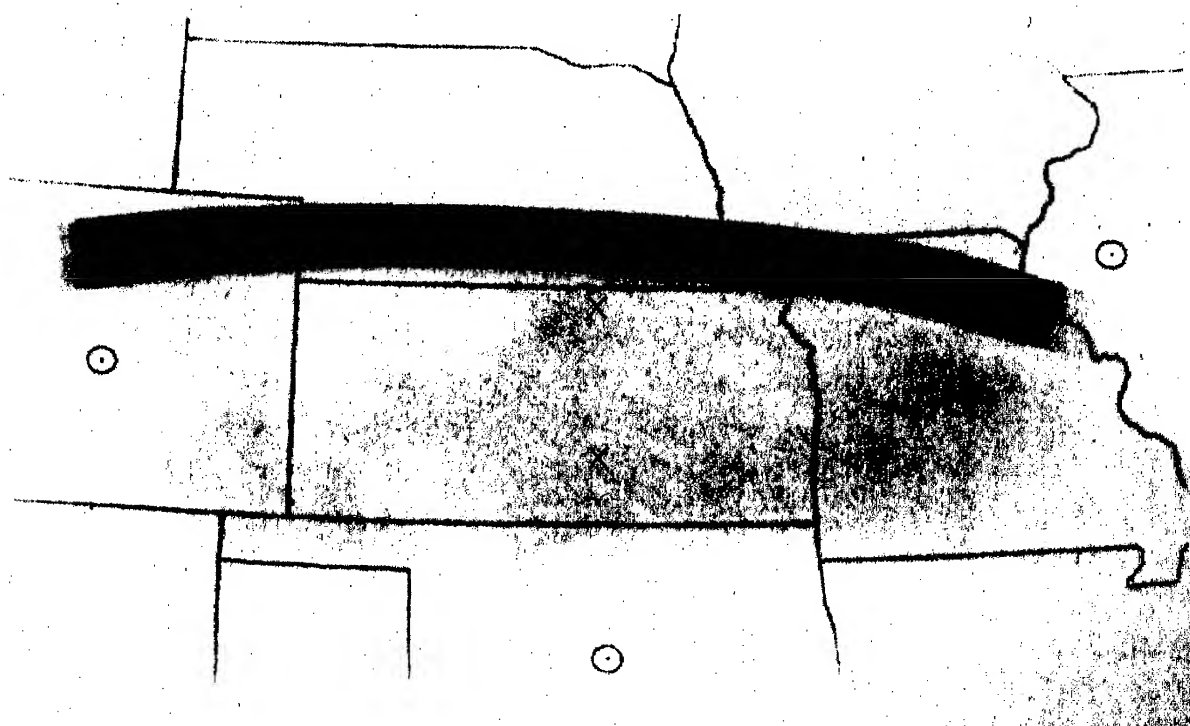
ARTIST'S CONCEPTION OF THE E<sub>s</sub> CLOUD AT 10.30 MST  
JULY 28, 1960

Fig. 9. Artist's conception of the cloud at 10 30 MST, July 28, 1960.



This equivalence is shown to be somewhat dependent on the "type" of sporadic  $E$ .

Fading rate during  $E_s$  propagation is observed at times to decrease with frequency suggesting that the  $E_s$  layer at times consists of blobs whose plasma frequency is approximately equal to  $f_oE_s$ .

Observations utilizing a network of oblique-incidence circuits indicate that  $E_s$  patches can have the appearance of a cloud front with width of 500 to 1000 km and depth at 200 km.

## REFERENCES

- BAILEY, D. K., BATEMAN, R. and KIRBY, R. C. (1955) *Proc. Inst. Radio. Engrs.* **43**, 1181.
- DAVIS, R. M., SMITH, E. K. and ELLYETT, C. (1959) *Proc. Inst. Radio. Engrs.* **47**, 762.
- KONO, T. UESUGI, Y., HIRAI, M. and ABE, G. (1954) *J. Rad. Res. Labs.* **1**, 1.
- SKINNER, N. J. and WRIGHT, R. W. H. (1961) *Ionospheric Sporadic E*, Pergamon Press.
- SMITH, E. K. (1957) *NBS Circular* 582.
- SMITH, E. K. (1958) *AGARDograph* **34**, 129.
- SMITH, E. K. and FINNEY, J. W. (1960) *J. Geophys. Res.* **65**, 885.
- THOMAS, J. A. and SMITH, E. K. (1915) *J. Atmosph. Terr. Phys.* **13**, 295.
- WRIGHT, J. W. and GAUTIER, T. N. (1960) *NBS J. Res.* **64D**, 347.

# Sporadic-*E* Propagation with 3 $\mu$ sec Pulses

G. R. OCHS, R. J. CARPENTER and E. K. SMITH

National Bureau of Standards, Boulder, Colorado, U.S.A.

**Abstract**—Pulse broadening of 3  $\mu$ sec pulses transmitted at 41 Mc/s via  $E_s$  over the 1300 km Long Branch to Boulder path are examined and interpreted.

Some interesting sporadic-*E* records were obtained as a by-product of a meteor echo experiment carried out over the Long Branch, Ill. to Boulder, Colo. path in June, 1959 (Carpenter and Ochs 1962). The experiment consisted of transmitting short pulses (3  $\mu$ sec to half-power point when recorded on the Boulder receiver) at 40.92 Mc/s from Long Branch using a transmitter with 800 kW peak power. The transmitting antenna was a horizontal corner reflector (gain approximately 10 db over a dipole) and the receiving antenna was a five element Yagi. Both antennas were mounted at a height of 52 feet. The data were recorded from the A-scan on motion picture film (16 mm, 24 frames/second). Several instances of sporadic-*E* propagation were then spliced together to make a 10 minute/motion picture film for visual presentation. This paper presents some excerpts from the film. The occurrence time for each instance of  $E_s$  is not available (other than the fact that all of the data were taken in June, 1959).

Signal intensities from  $E_s$  were often very high: much greater than most meteoric reflections. When an  $E_s$  enhancement was first observed it often consisted of modes which differed in delay by 20  $\mu$ sec or more. Later in an  $E_s$  enhancement signals were often strongly received. At these times they were very "clean" and no multipath could be detected.

In Figs. 1, 2 and 3 are seen three series of records taken at 1/2 second intervals. The ordinate scale is linear in amplitude. Time moves from right-to-left in the abscissa scale and the time markers are every 10  $\mu$ sec. Almost no pulse-broadening is discernible in the records of Fig. 1 indicating that any significant multipath components occur certainly less than 1  $\mu$ sec from the principle component (and probably considerably less). This type of record occurred quite frequently. Figures 2 and 3 show cases where multipath components are discernible but still at quite modest delays relative to the principal component (i.e. not more than 3  $\mu$ sec).

In order to derive some physical significance from these delays let us consider an ellipse of revolution (see Fig. 4) defined by locating the two terminals of the circuit at the foci ( $A$ ,  $B$ ) and the assumed reflection point

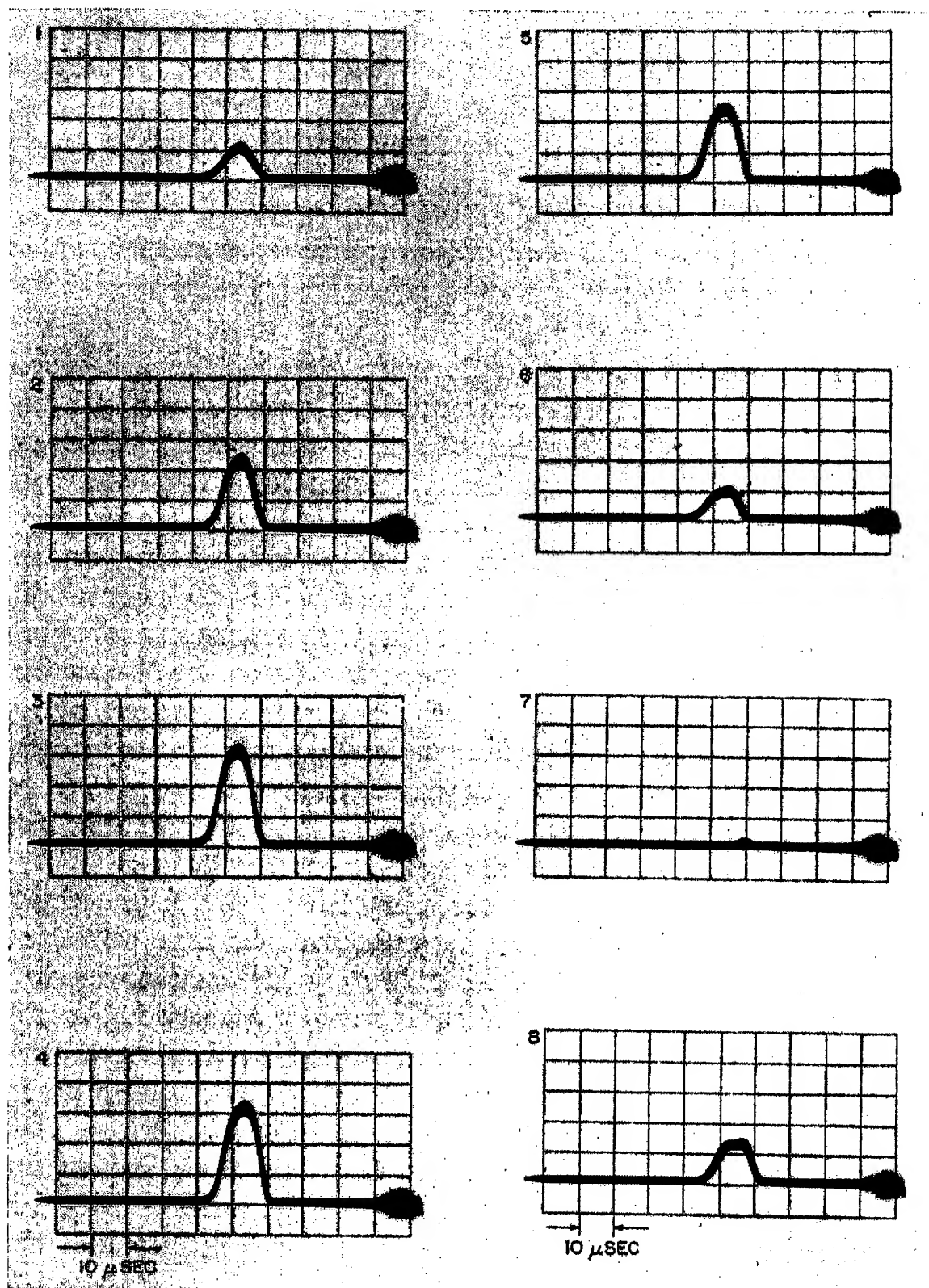
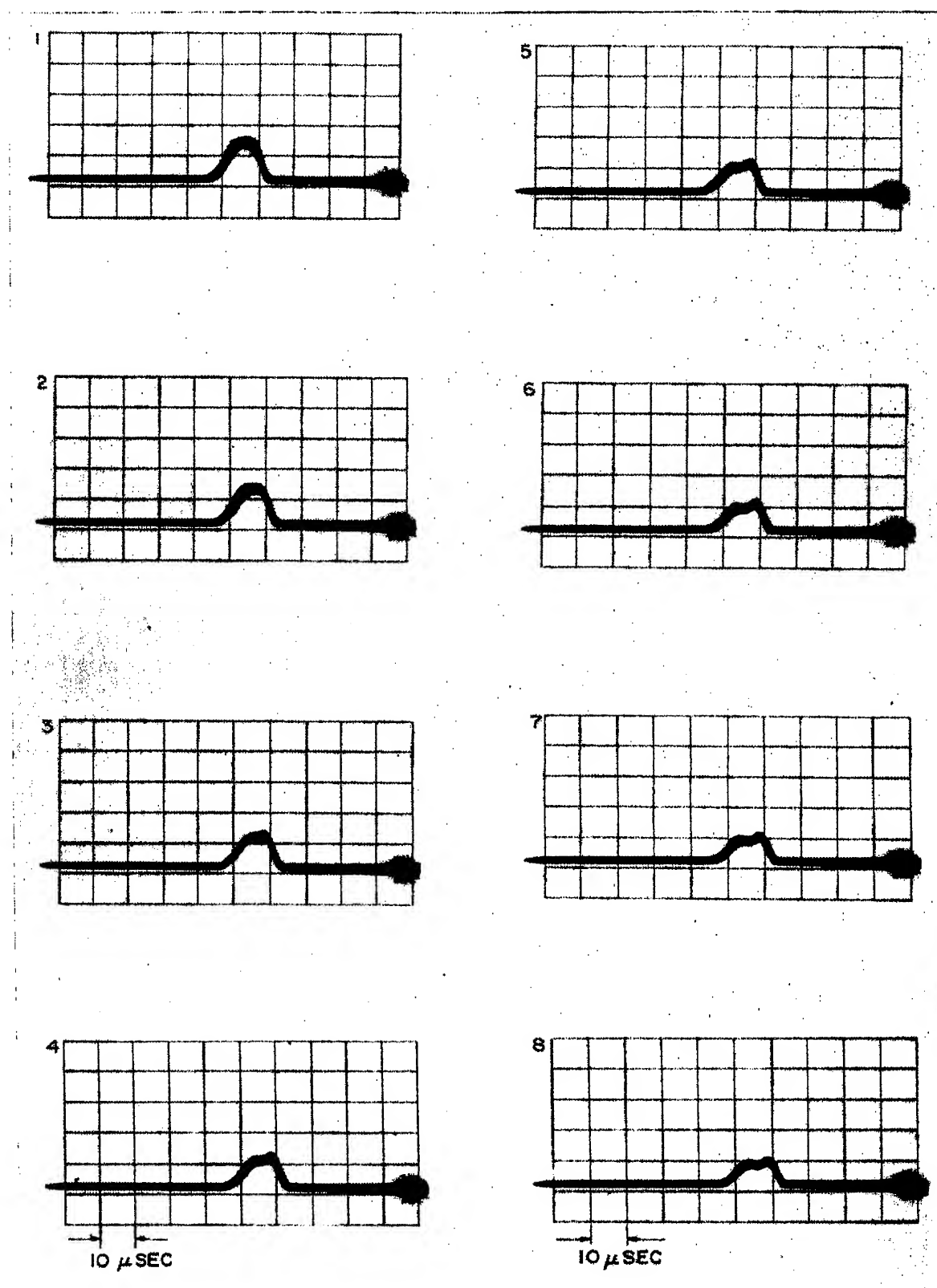


Fig. 1. Reception via sporadic *E* of 3  $\mu$ sec pulses at Boulder. Pictures are taken at 1/2 sec intervals of 40.92 Mc/s transmission from Long Branch. Time moves from right-to-left.



Figs. 2. Reception via sporadic *E* of 3  $\mu$ sec pulses at Boulder. Pictures are taken at 1/2 sec intervals of 40.92 Mc/s transmission from Long Branch. Time moves from right-to-left.

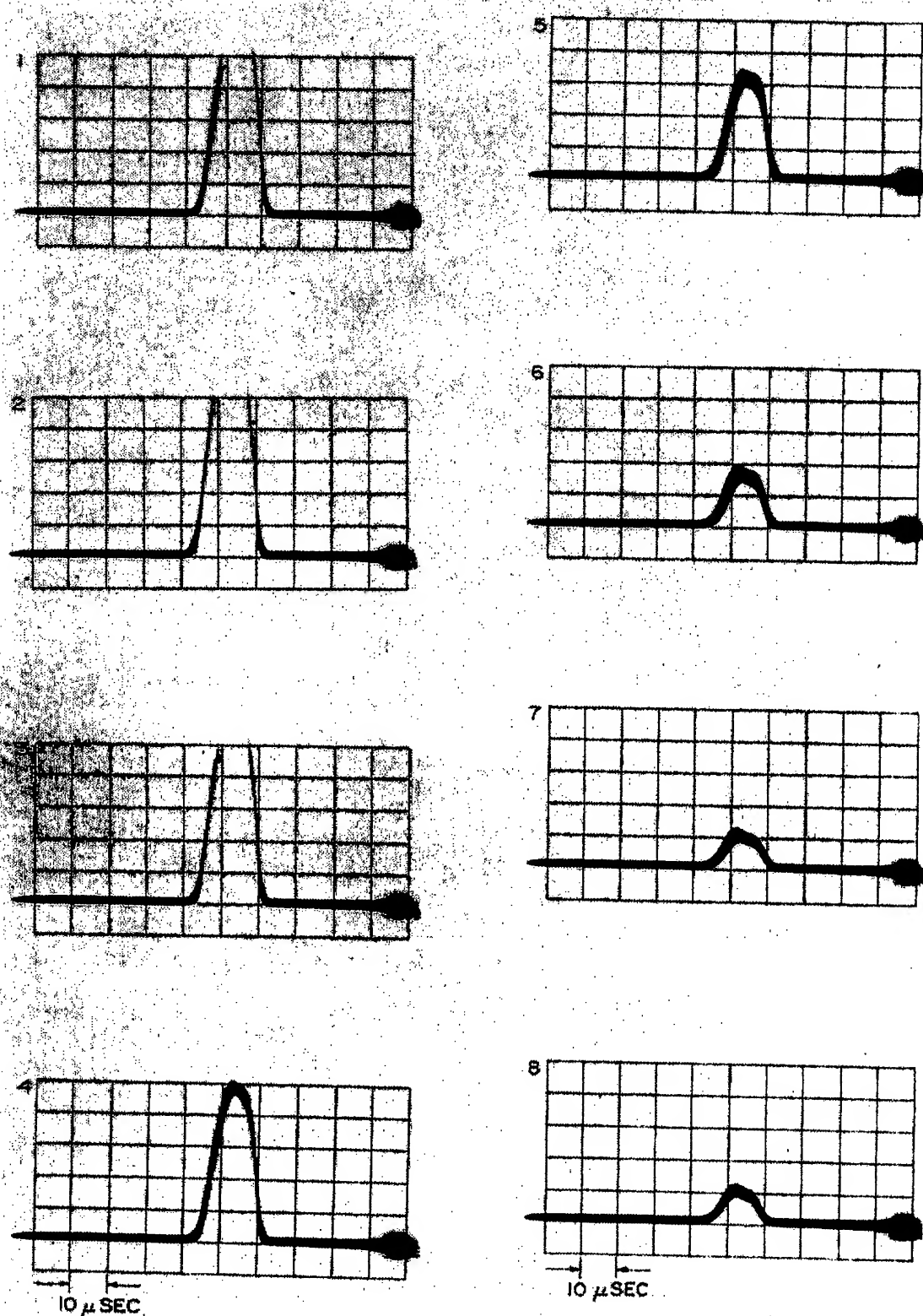


Fig. 3. Reception via sporadic  $E$  of  $3 \mu\text{sec}$  pulses at Boulder. Pictures are taken at  $1/2 \text{ sec}$  intervals of  $40.92 \text{ Mc/s}$  transmission from Long Branch. Time moves from right-to-left.

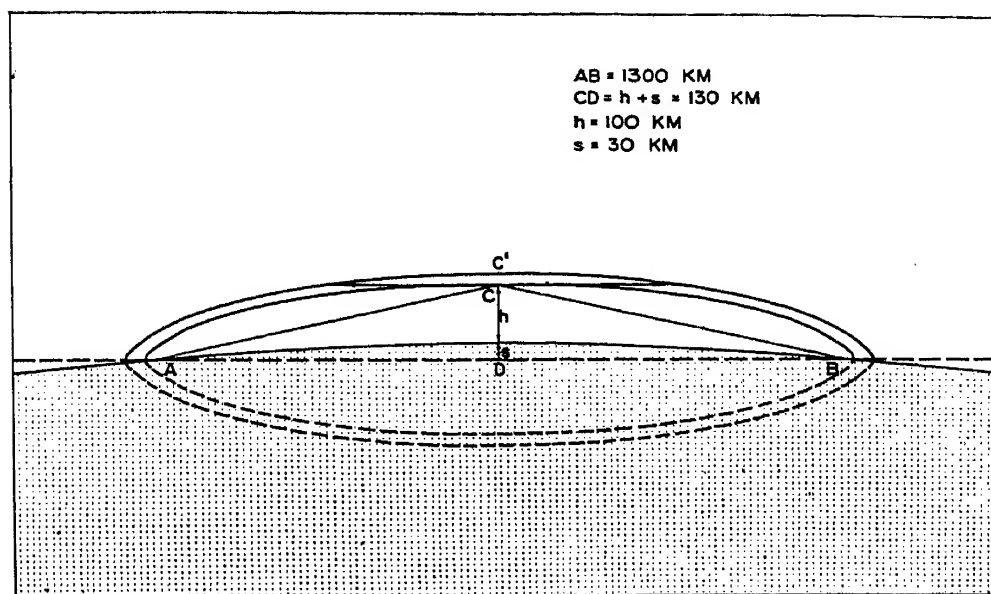


Fig. 4. Geometry of the vertical cross-section of the model.

( $C$ , 100 km above the midpoint of the path) on its surface. Transmitted signals reflected from any point on this surface would arrive at the receiver at the same instant,  $t$ . Let us now consider a slightly longer delay time,  $t + \Delta t$ , such as would occur if the assumed reflection height were increased to  $h + \Delta h$ . We have now defined a second ellipse of revolution again with foci at the terminals ( $A$ ,  $B$ ) but with reflection now taking place at  $C'$ . Let us further assume that sporadic *E* occurs in flat, horizontal strata. A reflection from a height  $h + \Delta h$  will then have the same delay as one from the intersection of a horizontal plane at a height  $h$ , the surface of the ellipsoid passing through  $h + \Delta h$ . This distance is arrived at by solving for the intersection of an ellipse of revolution and a horizontal plane which is parallel to its major axis.

Let  $\Delta d$  represent the increase in total path length

$\Delta h$  the corresponding increase in height alone

$\Delta x$  the corresponding horizontal distance along the path

and  $\Delta y$  the corresponding horizontal distance normal to the path.

Typical values of these parameters are as follows:

$\Delta t$	$\Delta d$	$\Delta h$	$\Delta x$	$\Delta y$
$1/3 \mu\text{sec}$	100 m	255 m	41.4 km	8.1 km
1 $\mu\text{sec}$	300 m	763 m	71.5 km	14.1 km
3 $\mu\text{sec}$	900 m	2.275 km	122.5 km	24.0 km

It can be seen from the above table that there is much greater sensitivity to changes in height than to horizontal deviations. The records in Fig. 1 demonstrate that the range in reflection heights is limited to less than 500 m. In the horizontal plane however there may be components arriving from 10 km away in a direction normal to the midpoint and perhaps 50 km from the midpoint in the plane of propagation.

To the best of our knowledge these records are the first published indications of how little the pulse broadening can be for  $E_s$  propagation over oblique-incidence circuits at v.h.f. The same information has, in fact, been indirectly available for some time through observations of TV-DX. It is not uncommon to observe good TV pictures\* which have been propagated by sporadic  $E$  which must therefore have a horizontal definition of close to 300 lines. This indicates an ability to discriminate between components of the order of  $0.2 \mu\text{sec}$  apart. This is further evidence that at times sporadic  $E$  can take the form of a very thin, quite specular, reflector.

The meteor experiment was carried out by R. J. Carpenter and G. R. Ochs first under the supervision of K. L. Bowles and later R. C. Kirby. The film from which these examples were drawn was presented at the 1960 URSI Spring meeting in Washington, D.C. by Carpenter and Ochs. Special thanks are due to John L. Green and his group at the NBS Long Branch Transmitting Station.

#### REFERENCE

CARPENTER, R. J. and OCHS, G. R. (1962) *NBS J. Res.* **66D**, 249.

---

\* Unfortunately it has not been possible to locate a published example of a TV test pattern propagated by sporadic  $E$ , but one of us (E.K.S.) has seen unpublished photographs of such cases.

# CHAPTER II

## Part B





# Definitions of Frequency Parameters of $E_s$ -Layers and their Accuracy

KARL RAWER

Ionosphären Institut, Breisach/Rh.

**Abstract**—In the case of a semi-transparent layer three frequency parameters are defined in a precise manner; two of them are normally used to describe the ionization of an  $E_s$ -layer. For practical application it is extremely important that the traces of both magneto-ionic components can be distinguished. This can be done in almost every case if the physical information given by the ionogram is considered in detail. A logical system of selection rules is established and explained with ionograms.

## 1. GENERAL CONSIDERATIONS

For thick layers where retardation of the sounding pulse is important critical frequencies of both magneto-ionic components can easily be read. Normally only one frequency parameter is read, viz. that of the so-called ordinary ray,  $f_o^*$ . To read  $f_o$  the observer uses the retardation cusp occurring on the reflected trace ( $f < f_o$ ) as well as on the transmitted trace ( $f > f_o$ ). Deviative absorption often cuts the trace in the vicinity of  $f_o$ ; the true value is then easily found by interpolation between the traces on both sides. In the case of the most strongly ionized layer, normally  $F_2$ , an extrapolation must be made on the ionogram to that frequency which is asymptotic to the high frequency end of the trace. This may introduce some inaccuracy, but in most cases the procedure can be made quite accurate.

With respect to the  $E_s$ -layers the situation is completely different. As a consequence of the extremely small thickness of these layers retardation effects are extremely small; with most ionosondes they cannot be seen on a normal record. Conditions are even more complicated by the fact that  $E_s$ -layers rather often have a cloudy structure, so that they are semitransparent in a more or less large frequency range. As a consequence of lacking retardation the two magneto-ionic traces are often confused and it is difficult to distinguish between them. In the reduction of an  $E_s$ -trace

---

\* Strictly speaking the corresponding ray is characterized by two different features: (1) Its polarization—upgoing and downgoing—is “ionic”, i.e. at the lower border of the ionosphere its sense of rotation is the same as that of the Larmor spiraling movement of positive ions. (2) The ray is reflected at the level where  $X = f_N^2/f^2 = 1$ . In Rawer-Suchy's nomenclature this ray is given by the abbreviation i o i.

two problems arise: (1) to distinguish between both magneto-ionic components, (2) to determine a characteristic frequency in the case of a semi-transparent layer, the reflection coefficient of which is decreasing with increasing frequency.

## 2. SYSTEMATIC DEFINITIONS

These questions are the reason why it has been so difficult to find a general definition of a "critical frequency" characterizing the electron density at the center of an ionized layer. The approach first proposed by our group (Bibl, Busch, Rawer and Suchy 1959) was found when dealing with the  $E_s$ -problem. It seemed to us that the reflection and transmission coefficients of a layer can be used to determine a reasonable characteristic frequency. This, of course, means that the amplitude of the different echoes is a most valuable piece of information which should not be suppressed. Unfortunately most ionosondes of the past do not take account of it as they intend a "black or white" reproduction. The more information exists with respect to the echo traces the easier different features can be distinguished—especially the magneto-ionic components.

Our approach introduces effectively two different sorts of definitions. Physical definitions are bound to the physical nature of the problem, they have a well-defined physical meaning. Unfortunately it is often impossible to obtain them by direct reading of the record. Practical definitions depend on technical details of the recorder, they have no direct physical meaning but they can be read from the record in a rather simple manner.

We first introduced two *practical definitions* which had already been used sometimes but with a less precise definition. We defined the *top frequency*,  $f_t$ , of a layer as the highest frequency for which the layer is reflecting, i.e. for which an echo can be obtained from it, the *blanketing frequency*,  $f_b$ , of a layer as the lowest frequency for which the layer is somewhat transparent, i.e. for which an echo from a higher, more ionized layer can be obtained.

For an  $E_s$  layer by these definitions the limits of the frequency range of practical transparency are determined and  $f_t > f_b$ . For a thick layer without absorption both definitions must give the same value, and this is the traditional critical frequency,  $f_c$ . In the case of a thick, absorbing layer one has  $f_t < f_b$  (the difference normally being small) and the critical frequency lies in between.

Now we come to a *physical definition* of the "critical frequency". It is found as a weighted median between top frequency,  $f_t$ , and blanketing frequency,  $f_b$ . The weight is given by comparison of reflection and transmission coefficient. We defined as *critical frequency* that frequency for which the layer is equally reflecting and transparent, i.e. where reflection and transmission coefficients are equal.

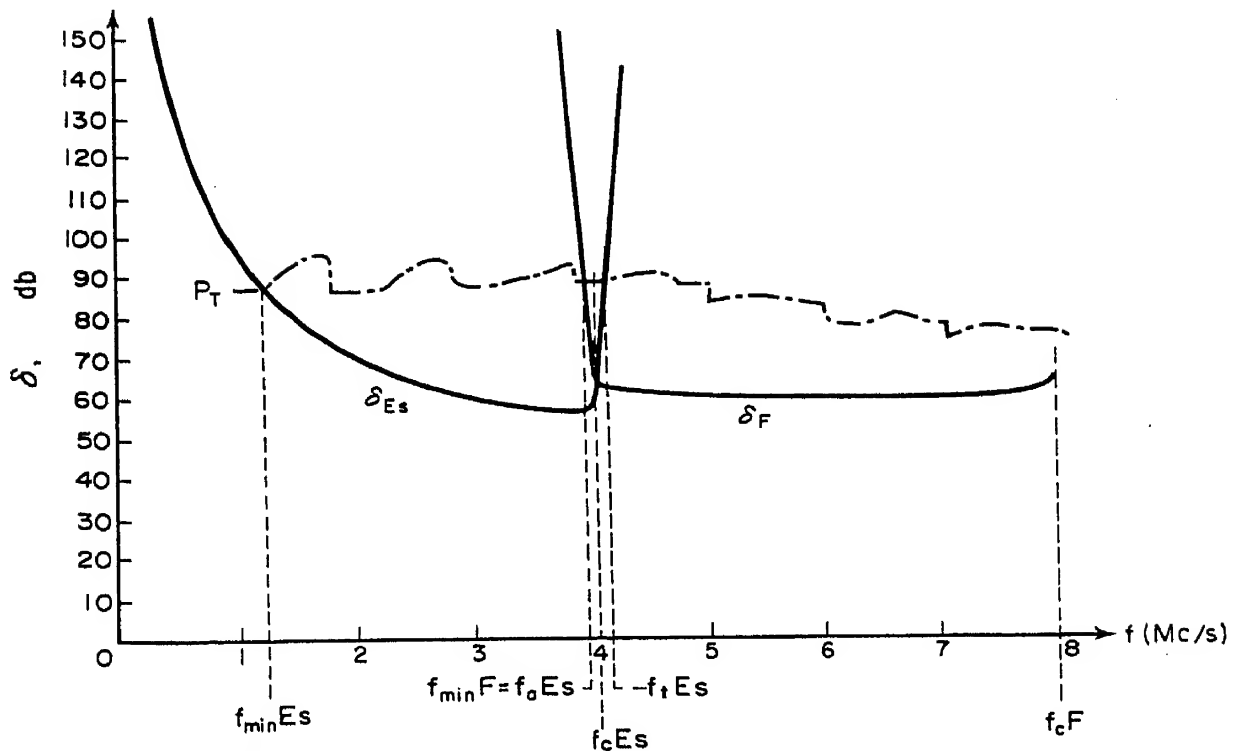


Fig. 1. Reflection and transmission coefficient (db) as functions of the frequency.

The conditions can best be seen from Fig. 1 where (for a thin layer) the frequency variation of both coefficients is given.  $f_t$  as well as  $f_b$  depends on the sensitivity of the equipment and its frequency variation (dotted line in Fig. 1)  $f_c$  by definition is independent on the equipment, but it could only be observed by intercomparison of amplitudes. An effort has been made many years ago (Rawer 1949) to use such a definition in a special experiment. The definition had been generalized for different ratios of the reflection and transmission coefficient. This gives the means to describe the frequency variation of transparency in the interesting range and so a detailed physical description of  $E_s$ -layers could be obtained.

By this and similar investigations some important features of the  $E_s$ -layers could be determined. It appeared (Rawer 1955) that if both magneto-ionic components were treated separately in a large number of cases the temperate latitude  $E_s$ -layer is not seriously transparent. In such cases Briggs (1951) with a special technique could demonstrate that the very small transparency range was present which is required by wave theory in the case of a thin layer. He was even able to find the layer thickness from his observations, and his numerical results (a few km) have meanwhile recently been justified by rocket observations.

But there are other cases where in a certain frequency range the  $E_s$ -layer is effectively transparent due to its cloudiness. These cases occur more often in the equatorial and in the auroral zones, but even in temperate latitudes they constitute about half of all  $E_s$  cases.

3. APPLICATION TO  $E_s$ -LAYERS

This shows that one frequency parameter is not sufficient to give a satisfying description; as first seen by Appleton and Naismith (1940). We should at least have two in order to locate in some way the range of transparency. This could be done on two different ways, viz., using physical or practical definitions. The first ones would be much more adequate as they are independent from the equipment. Unfortunately they could only be used in a routine way if amplitudes were correctly recorded in an unambiguous way. In that case one should introduce at least three values of the ratio of reflection to transmission, for example  $-20$ ,  $0$  and  $+20$  db. (Our old system (Rawer 1949) used five readings, approximately  $-40$ ,  $-20$ ,  $0$ ,  $+20$ ,  $+40$  db). The middle value,  $0$  db corresponds to our definition of the critical frequency,  $f_c$ .

As most existing ionosondes do not reproduce the amplitudes in an unambiguous way only the practical definitions  $f_t E_s$  and  $f_b E_s$  can be used in a general routine program of all ionospheric stations. This means that the results depend in some way on the local ionosonde and its properties.

Of course this is not very promising and one could think that such results were almost useless. However, a detailed investigation showed that for most occasions this is not true. It is evident that a large influence is only to be obtained if the characteristic frequencies are largely variable with sensitivity. For a good ionosonde the sensitivity is only slowly variable with frequency and then we may formulate the condition in a more physical way. Difficulties with  $f_t$  or  $f_b$  must arise if the reflection or transmission coefficient of the layer varies rather slowly with frequency. Now it has been shown (Rawer 1955) that in the range from very small values to about  $-20$  db the frequency variation of the transmission coefficient is mostly so rapid that  $f_b E_s$  does not depend very seriously on the sensitivity. As to  $f_t E_s$ , the situation is similar to those cases where no or nearly no partial reflection occurs. This is about half of all cases in temperate latitudes. For the remaining cases the influence of the equipment cannot be neglected (see Fig. 2). Especially the equatorial " $q$ -type"  $E_s$  shows a very slow change of the reflection coefficient with frequency; therefore the definition of  $f_t E_s$  is rather poor in equatorial regions.\* In these regions amplitude observations would be of great interest.

If the sensitivity of the ionosonde is very high very faint echoes, as can be obtained by scatter or meteoric ionization, may be recorded. In that case the physical meaning of  $f_t E_s$  can be completely changed. The thin ionization phenomenon which is  $E_s$  can no more be studied with such

---

\* It has become usual to write  $f E_s$  instead of  $f_t E_s$  and for the ordinary component  $f_o E_s$  instead of  $f_{to} E_s$ . It must be held in mind, however, that this is not a critical frequency as in the case of thick layers.

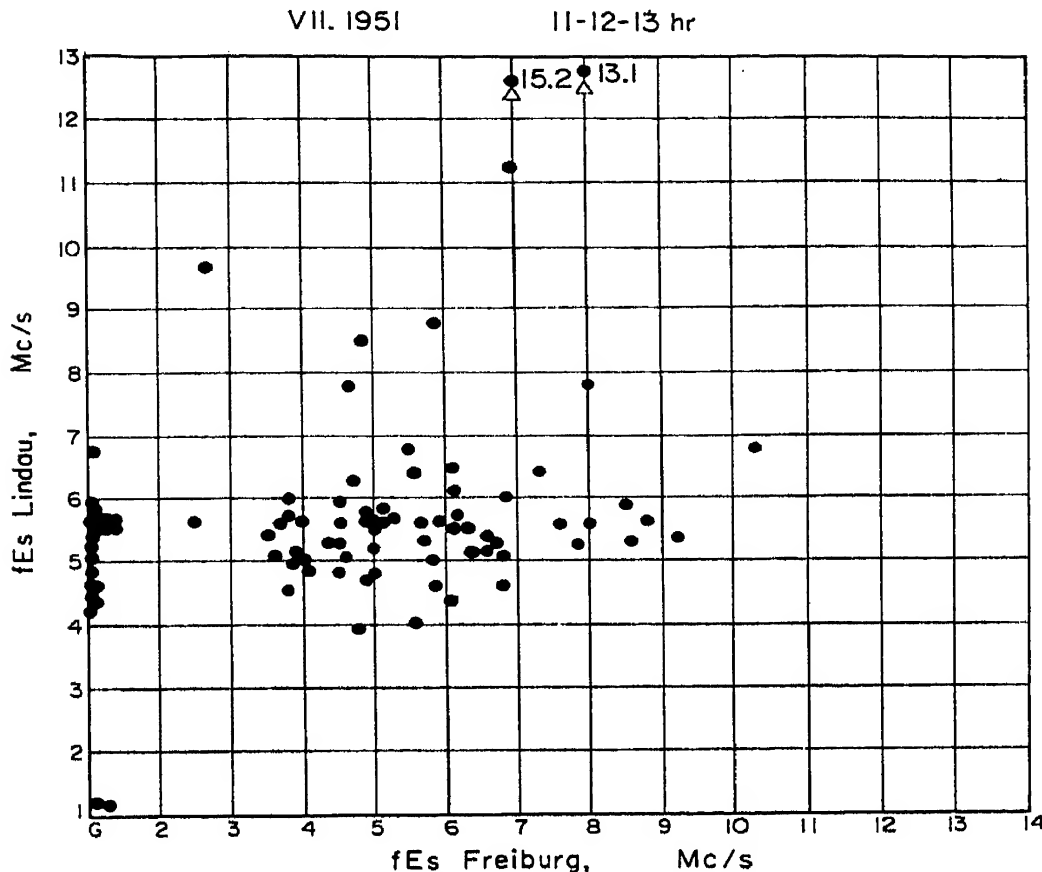


Fig. 2. Correlogram of simultaneously observed  $fE_s$  values from two stations distant by 430 km (Lindau has the more powerful transmitter).

data. It is therefore not recommended to use a very high power ionosonde with the usual reduction schedule for  $E_s$  characteristics. More homogeneous data are collected with the usual medium power ionosondes. This is a consequence of using practical definitions; with amplitude observations high power ionosondes could give very interesting results—but on the basis of physical definitions.

By the fact that  $f_t E_s$  results often depend on the equipment it is rather difficult to make intercomparisons between different stations. Only if it has been established by trial that the sensitivity is comparable can one proceed to establish latitude or similar variations. But as relative intercomparison can always be made, cross correlations obtained with the results of different stations are meaningful (Rawer 1955, Rawer 1958). This enables some intercomparison work to be done in a correct form.

Time variations on a given station can be established if the sensitivity of the equipment was sufficiently constant during the period. It is of great interest to know whether the solar cycle has some influence and where the secular variations come from. Therefore it should be important to have long, homogeneous series of observations avoiding major changes of the sensitivity versus frequency curve of the sounding equipment. Unfortunately such series can not yet be found for more than a few years. This is one of the worst limitations we had to accept when the decision in

favour of practical definitions was made. It would be a great help for future work if sensitivity curves of the equipment were regularly published by the stations.

With the indicated limitations  $f_i E_s$  and  $f_b E_s$  have proved to be useful parameters.

#### 4. DISTINCTION OF THE MAGNETO-IONIC COMPONENTS

In the preceding text we supposed that the observed  $E_s$  trace had a clear physical signification. This is only true if the propagation and reflection mechanism is well defined. As for every other trace on the ionogram this should be clear before reduction is begun. Unfortunately, for a long period this rather trivial point has been neglected when dealing with  $E_s$ -layers. There can be no doubt that the introduction of this distinction first proposed by the author and finally adopted by the World Wide Soundings Committee has been necessary for two reasons: For geophysical applications it is important to have significant numerical values over all the day. For radio propagation applications one must be justified in using the same distance function for all basic data.

In the introduction we have mentioned that it is sometimes difficult to distinguish the magneto-ionic components by inspection of the ionogram, ignoring the polarization of the echoes. It is therefore necessary to use every available information which can be collected from the ionogram. These are: small differences in virtual height and, again, the amplitude of the echoes. Combining these with some general reasoning on absorption and its frequency variation the following instructions have been established.

#### 5. DETAILED INSTRUCTIONS FOR DISTINGUISHING BETWEEN THE MAGNETO-IONIC COMPONENTS

(a) For normal thick reflecting layers, differences in the vertical height of reflection of the two magneto-ionic components generally enable the two traces to be identified easily. The daytime "c" and "h" types of  $E_s$  give traces which can often be identified by the changes in height of the trace due to retardation in the normal  $E$ -layer, Fig. 3. However, for most types of trace the two components are superposed at essentially the same height, and other criteria are necessary.

(b) When absorption is present, a clear distinction is often possible because the absorption of the  $x$ -component is normally greater than that of the  $o$ -component at the same frequency. The  $x$ -component is also greatly weakened at frequencies near the gyrofrequency even when the normal absorption is very small. The different attenuation of the traces can often be used to identify the component, see for example Fig. 3.

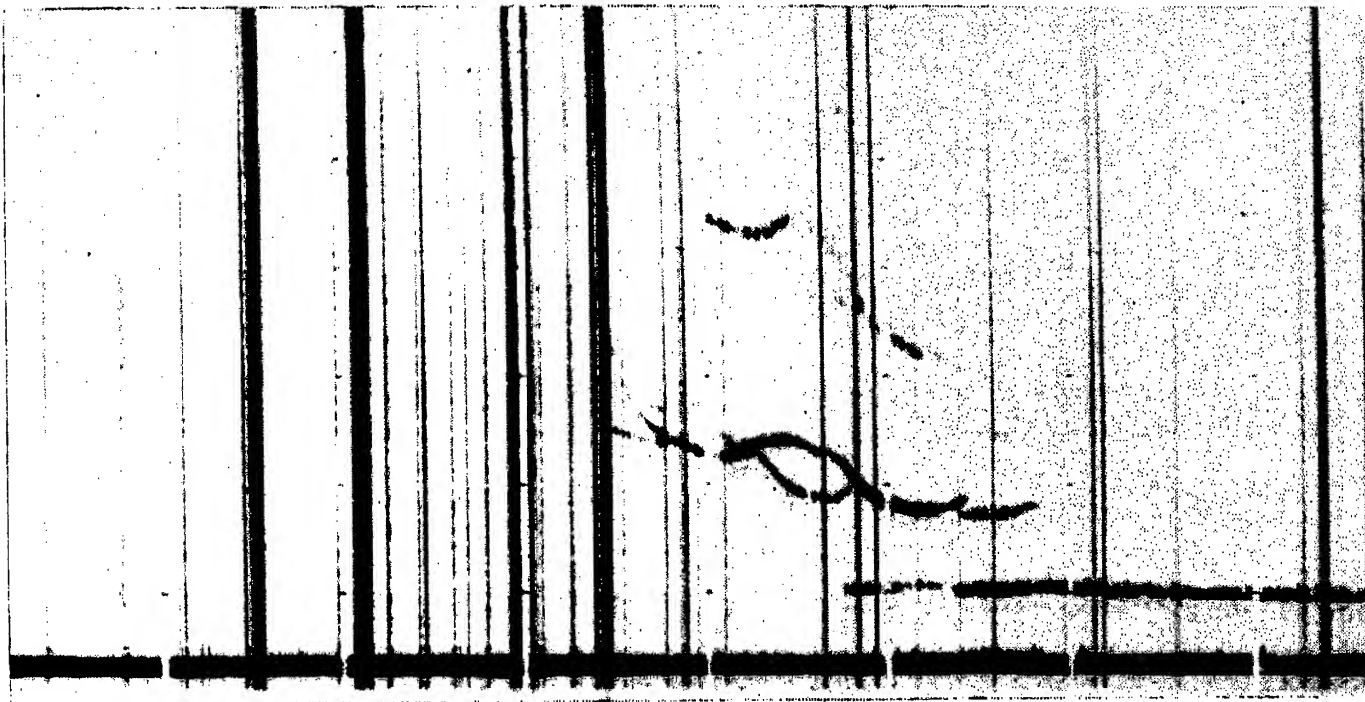


Fig. 3. Ionogram (frequency from right to left, logarithmic scale from 1.25 to 20 Mc/s)\*. Clearly distinct o- and  $\alpha$ -traces of  $E_s$ . F-region o- and  $\alpha$ -traces also distinct. [The right-hand trace near 200 km is  $2 E_s(o)$ .]

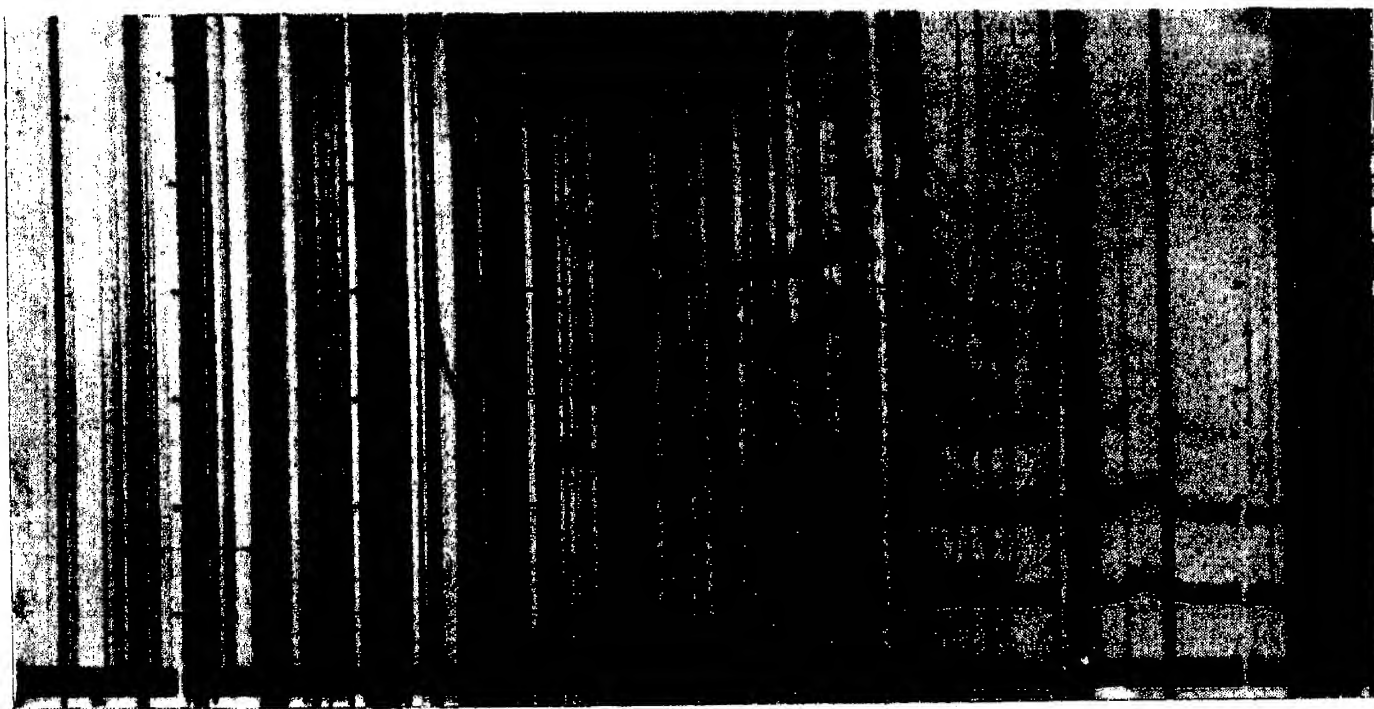


Fig. 4. Ionogram to rule (d) (I). F-traces not well distinct in height at the low frequency end but clearly different in amplitude (here  $\alpha$ -trace stronger).  $f_{\min} F_x$  in center of band 4 (at 4.2 Mc/s).

\* Band switching frequencies (right to left): 1.76, 2.5, 3.52, 5.0, 7.0, 10.0, 14.1 Mc/s.



(c) Systematic inspection of the ionogram can very often determine which component is present at the high frequency end of the trace even in cases where both traces are superposed and show no obvious distinguishing features. The first method depends in essence on comparing the top frequency of the  $E_s$  trace,  $f_t E_s$ , with the minimum frequency of the  $x$ -component trace for the ionogram as a whole,  $f_{\min}(x)$ . This is necessarily above the gyrofrequency\* (Rawer and Suchy 1962). If  $E_s$  traces occur at frequencies above  $f_{\min}(x)$ , the extraordinary component must be present. Hence the top frequency,  $f_t E_s$ , must correspond to the extraordinary component. If the  $E_s$  trace stops at frequencies below  $f_{\min}(x)$  the extraordinary component cannot be present.

Thus

$$\begin{aligned} \text{if } f_t E_s > f_{\min}(x) \quad & f_t E_s = f_x E_s \\ \text{if } f_t E_s < f_{\min}(x) \quad & f_t E_s = f_o E_s. \end{aligned}$$

The rule can only break down if there is a sudden change in the variation of the sensitivity of the ionosonde with frequency. This should not occur with properly maintained modern equipment but is easily recognized when present. Clearly it is not necessary to measure  $f_{\min}(x)$ , it is sufficient to know that  $f_{\min}(x)$  is greater or smaller than  $f_t E_s$ .

(d) The high frequency end of the record should be inspected first. In most cases there is no difficulty in recognizing the two components in the  $F$  traces, and the low frequency end of the  $F$ -region  $x$ -trace is easily found. This is called  $f_{\min} F_x$  and provides a useful practical criterion. Three cases can arise in practice.

(I)  $f_t E_s > f_{\min} F_x$  (Fig. 4)

The  $E_s$  trace must contain an  $x$  component and hence  $f_t E_s = f_x E_s$ .

(II)  $f_t E_s \simeq f_{\min} F_x$  (Fig. 5).

When the top frequency is within less than half the gyrofrequency,  $f_{H/2}$  of  $f_t E_s$ , the top frequency cannot be  $f_o E_s$  without an  $x$ -trace appearing at higher frequencies. Therefore  $f_t E_s = f_x E_s$ .

This is seen by indirect argumentation: Suppose the  $E_s$  trace visible until  $f_{\min} F_x$  is an ordinary trace ( $\delta < \frac{1}{2} f_H$ ). Then the corresponding  $x$ -trace should stop at  $f_{\min} F_x - \delta + \frac{1}{2} f_H$ , and this is higher than  $f_{\min} F_x$ , so that this trace cannot be absorbed and should be visible on the ionogram. As, in the case we consider, this is not true the hypothesis used at the beginning of this consideration must be wrong, so that  $f_t E_s = f_x E_s$ .

(III)  $f_t E_s < f_{\min} F_x$

---

\* This component is reflected at the level where the condition  $X = 1 - Y$  holds. In Rawer-Suchy's terminology it is called " $e \ x \ e$ " (electronic polarization up and down,  $x$ -condition of reflection).

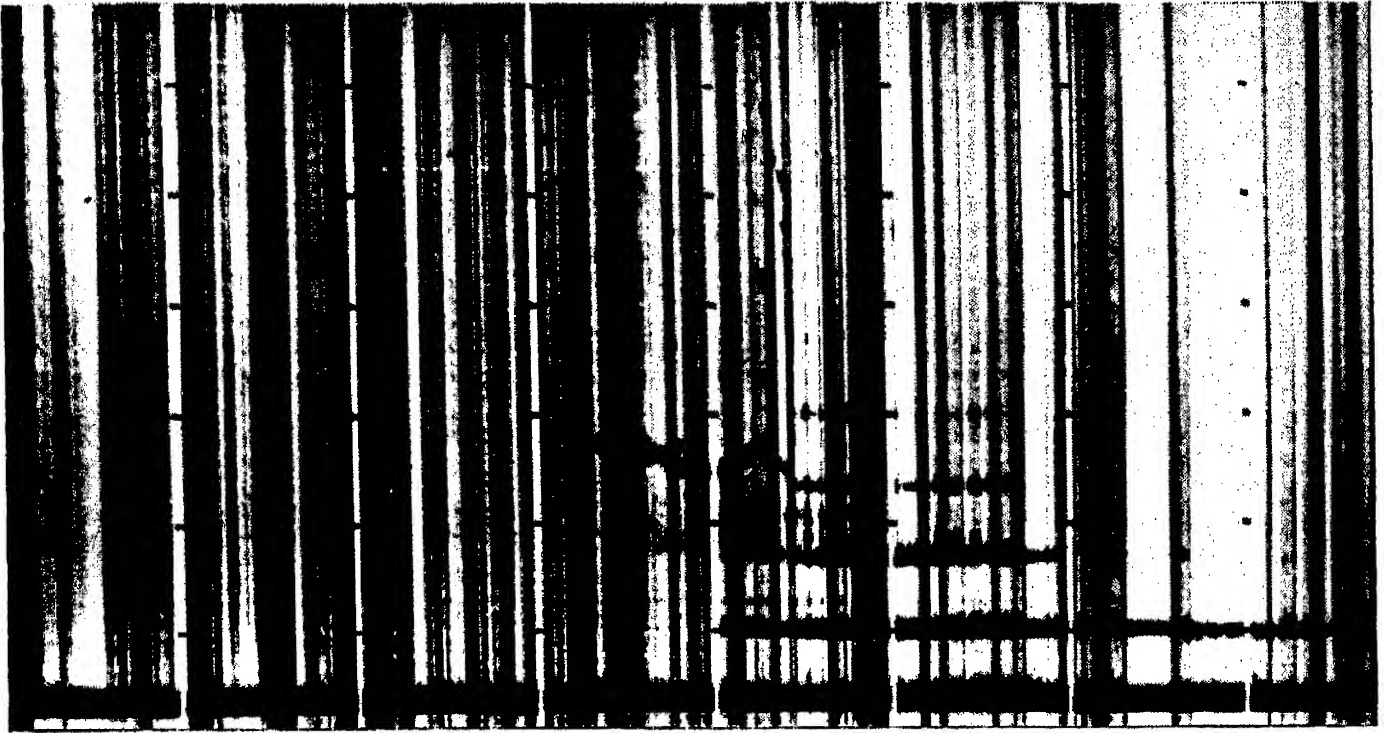


Fig. 5. Ionogram to rule (d) (II).  $F$ -traces well distinct.  $f_{\min}F_x = f_t E_s$  at central bandswitching (5 Mc/s).

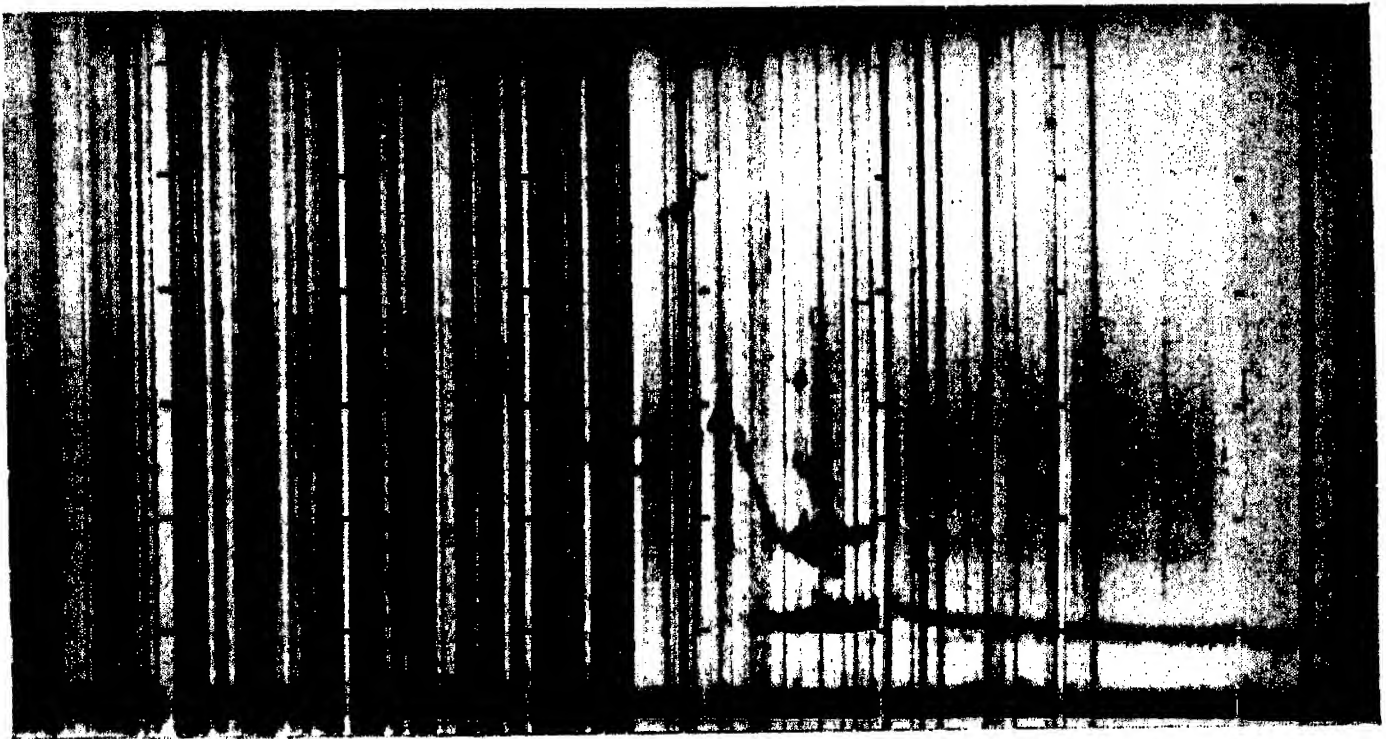


Fig. 6. Ionogram to rule (d) (III)(a).  $F$ -traces well distinct. Large gap between  $f_{\min}F_x$  (5.3 Mc/s) and  $f_t E_s$  (4.5 Mc/s).

Two subcases are possible:

- (a) No  $E$ -region trace (neither  $E$  nor  $E_s$ ) appears within half the gyro-frequency below  $f_{\min}F_x$  (Fig. 6). This shows that, for the ionogram as a whole, the  $x$ -trace stops at  $f_{\min}F_x$ , so that  $f_{\min}F_x = f_{\min}(x)$ . Hence the observed  $E_s$ -trace cannot be an  $x$ -trace and  $f_tE_s = f_oE_s$ .
- (b) Within half the gyrofrequency below  $f_{\min}F_x$  exists a trace obtained from a thick layer of the  $E$ -region ( $E$  or  $E_2$ ). This must be an  $x$ -trace.

It cannot be an ordinary trace from the argument given above which in this case would imply that thick layer echoes of two different regions existed simultaneously and for the same component at the same frequency. This would be a case of partial reflection which is impossible with thick layers.

In this case the low frequency end of this trace,  $f_{\min}E_x$ , is to be found.

With respect to this value the same reasoning as given above is repeated. This gives again three cases the first of which is reproduced in Fig. 7. It is important that  $x$ -traces of  $E$  (Figs. 8 and 9) are not confounded with  $E_s$ -traces.

These rules can fail if the equipment limitation mentioned in "c" above is present.

- (e) There remain the cases where  $f_{\min}F_x$  cannot be determined.

- (I) If this is due to total blanketing, Fig. 10, under conditions we would normally expect to see the  $F$  traces, we should presume that the missing  $F$ -layer  $x$ -trace is replaced by an  $E_s$ -layer  $x$ -trace and therefore

$$f_tE_s = f_xE_s.$$

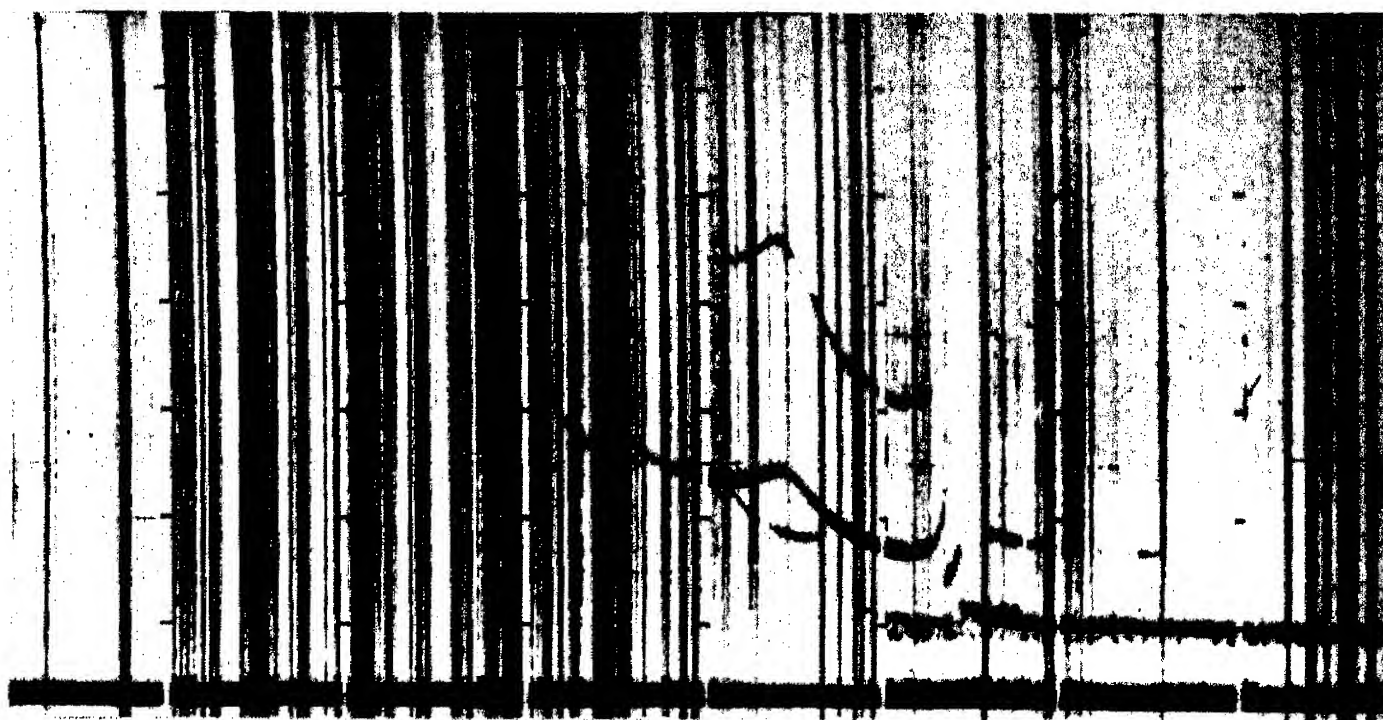


Fig. 7. Ionogram with "low" type  $E_s$ .  $f_tE_s$  at the end of band 3 (at 3.5 Mc/s), clearly higher than  $f_{\min}E_x$  which is in the center of this band (at 3.1 Mc/s).



Fig. 8. Ionogram with visible  $x$ -trace of  $E_o f_{\min} E_x$  at beginning of band 4 (3.5 Mc/s). No  $E_s$ -trace visible.



Fig. 9. Ionogram with faint  $x$ -trace of  $E. f_{\min} E_x$  in the center of band 3 (at 3.0 Mc/s). "Low"  $E_s$  with  $f_t E_s = f_o E_s$  well below that frequency in band 2 (at 2.2 Mc/s).



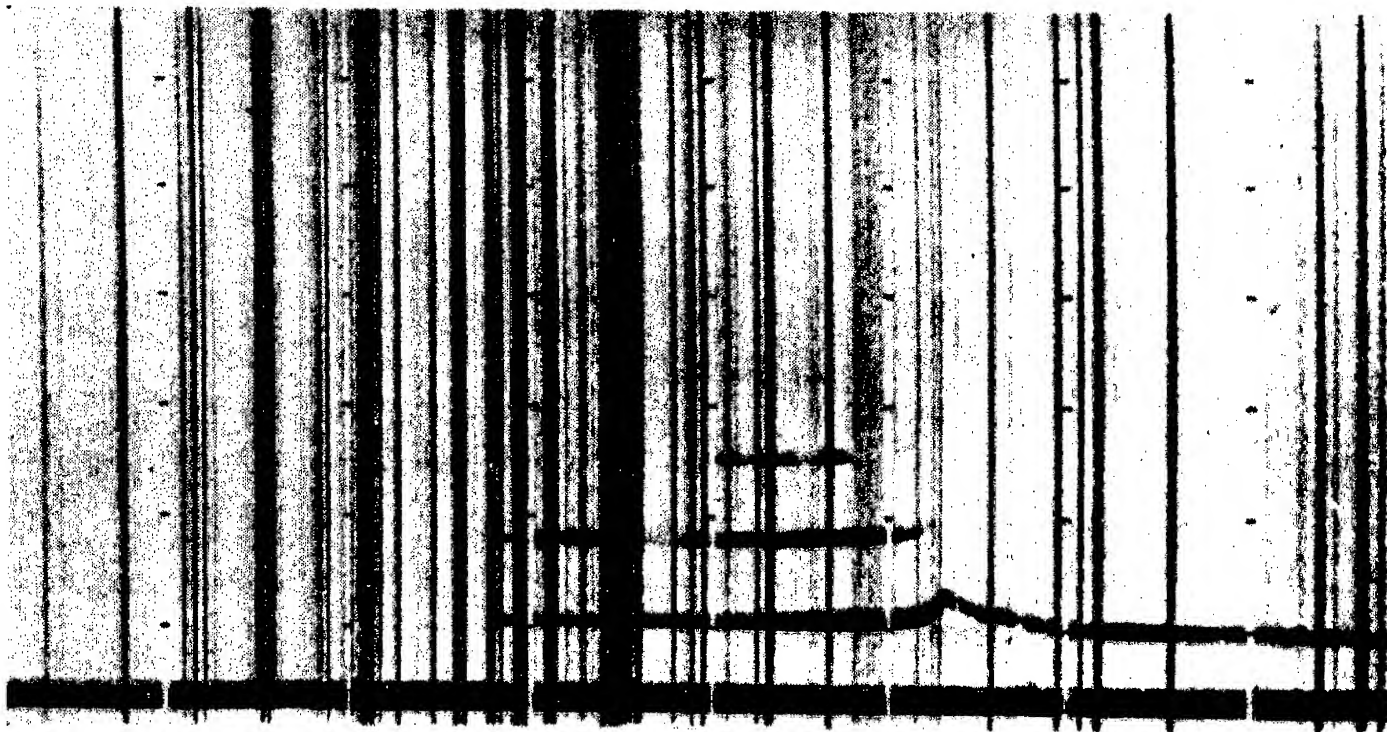


Fig. 10. Ionogram with total blanketing illustrating rule (e) (I). No  $F$ -trace visible.

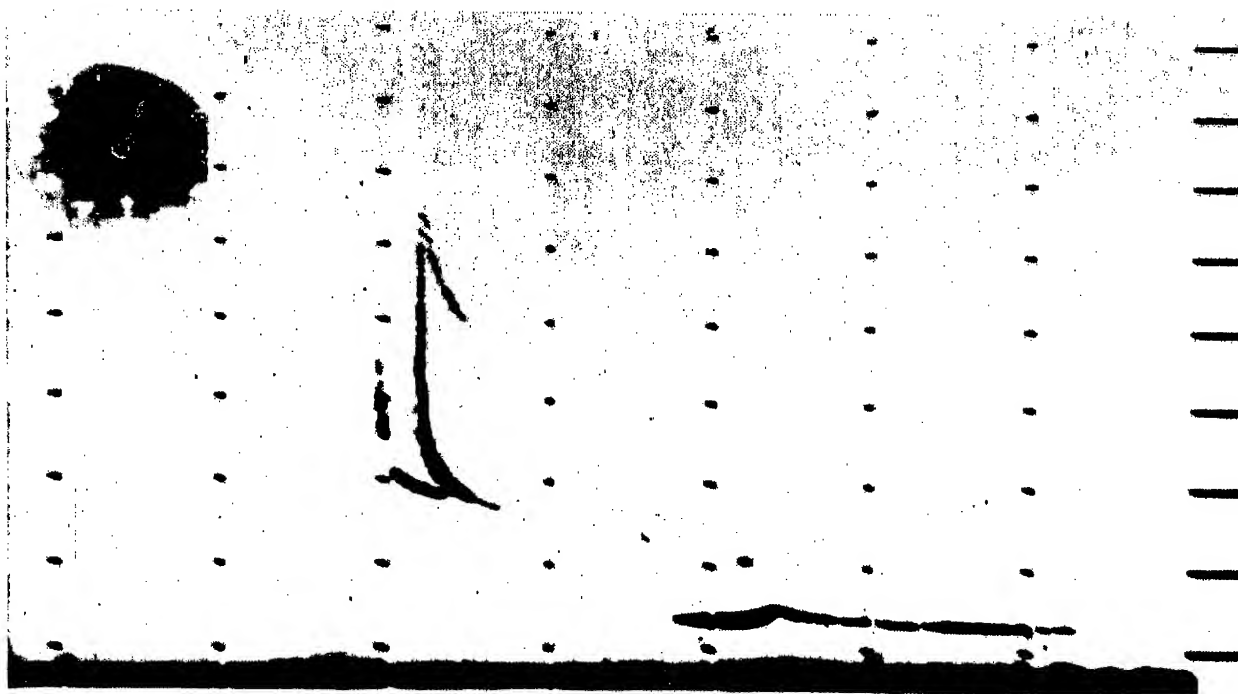


Fig. 11. Uncommon ionogram showing large gap between  $E$ - and  $F$ -traces probably due to blanketing of an oblique sounding ray in the case of a strongly tilted  $F$ -region.

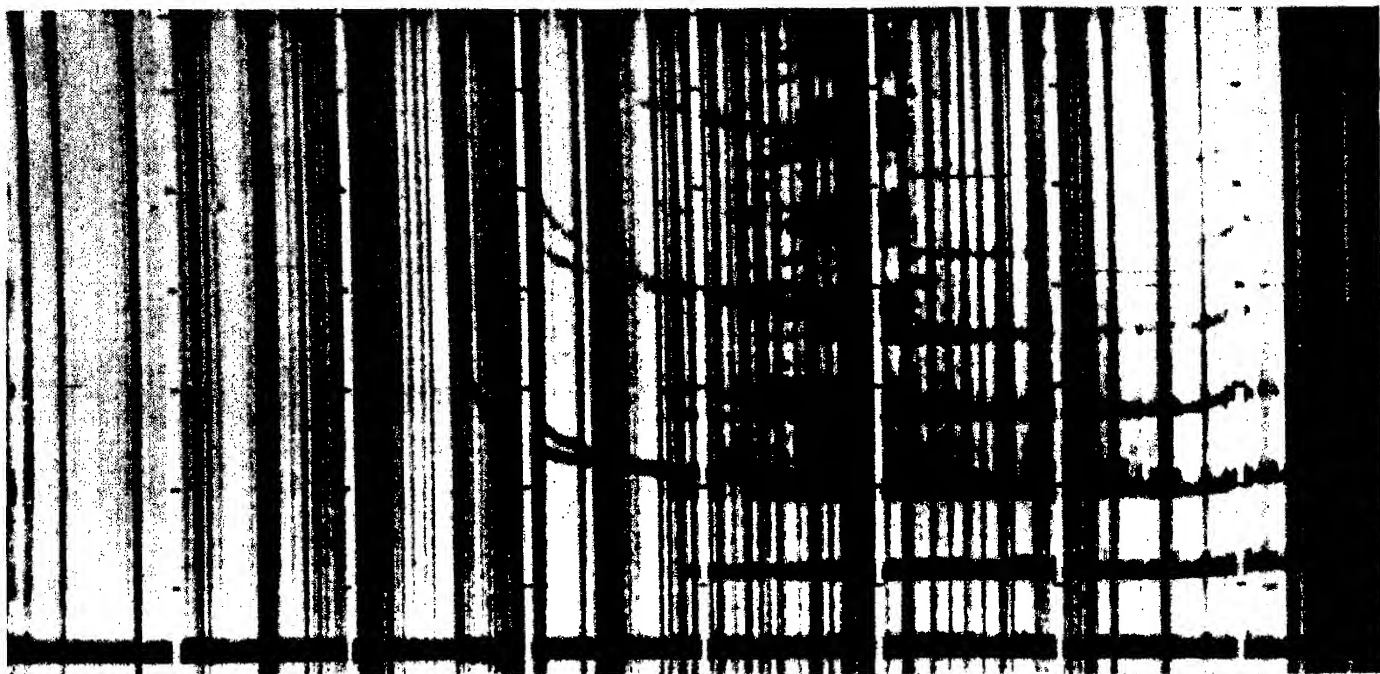


Fig. 12. Ionogram where  $f_{\min} F_x$  is difficult to identify.

Sometimes, but rarely, ionograms are obtained which apparently differ from the cases discussed above. These differences are most commonly due to layer tilts causing oblique sounding. For example see Fig. 11.

- (II) The remaining case where  $f_{\min} F_x$  cannot be determined although an  $F_x$ -trace is present is the only difficult one. These conditions may, for example, be found when both components are superposed (Fig. 12) or scatter is present (Fig. 13).

(f) Only in these difficult cases is it necessary to see whether the  $\alpha$ -trace of  $E_s$  can directly be identified. The most important arguments are retardation or absorption effects (see above, a and b).

(g) Experience obtained at many stations shows that a guess can be made even in these cases where a decision on the basis of the rules given above seems nearly impossible:

- (I) In the absence of absorption it can always be supposed that  $f_t E_s = f_x E_s$ . This is the normal night case (Figs. 12 and 14).
- (II) If absorption is present and  $f_t E_s$  is not considerably higher than  $f_o E$  the guess should be that the  $\alpha$  component of the  $E_s$  trace is absorbed and  $f_t E_s = f_o E_s$ . But under these conditions the identification is nearly always possible with the preceding rules so that uncertain cases are extremely rare.
- (III) If absorption is present and  $f_t E_s$  is considerably higher than  $f_o E$  the guess is that the  $\alpha$ -trace is present and hence  $f_t E_s = f_x E_s$  (Fig. 15).
- (IV) If at night absorption is present but no night  $E$  visible a guess may be made in an appropriate form using  $f_{\min}$ .

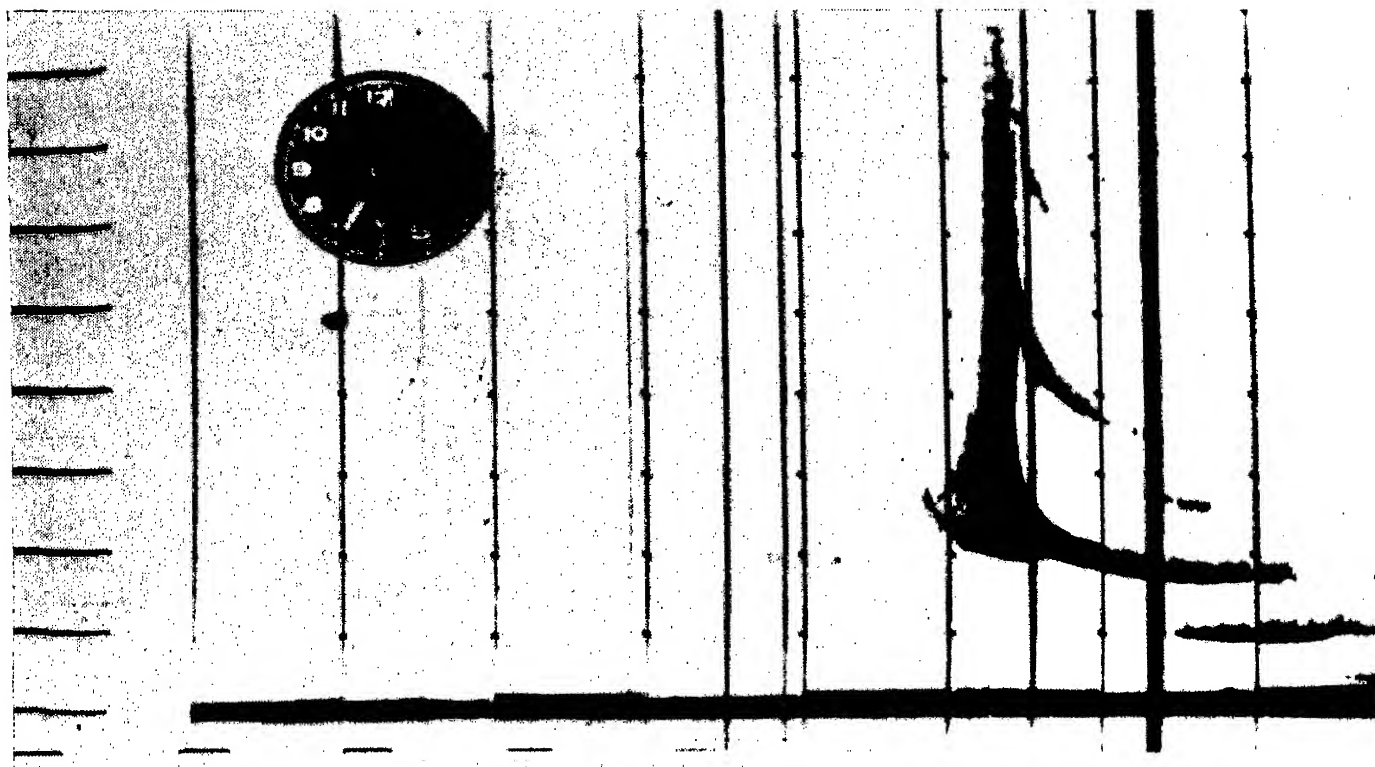


Fig. 13. Ionogram with spread echoes,  $f_{\min}F_x$  difficult to identify.

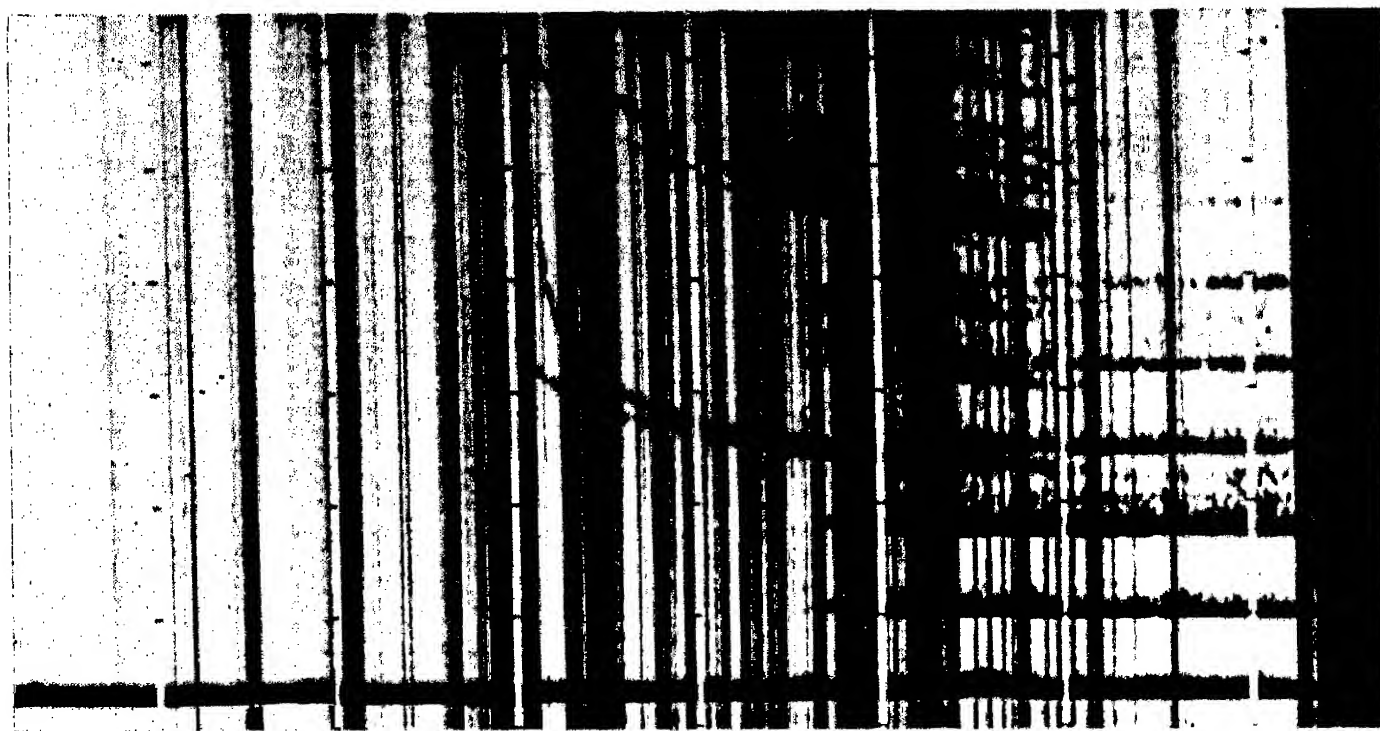


Fig. 14. Ionogram where  $f_{\min}F_x$  is difficult to identify. However  $f_iE_s$  must equal  $f_xE_s$  as absorption is very small: night conditions, rule (g) (I).

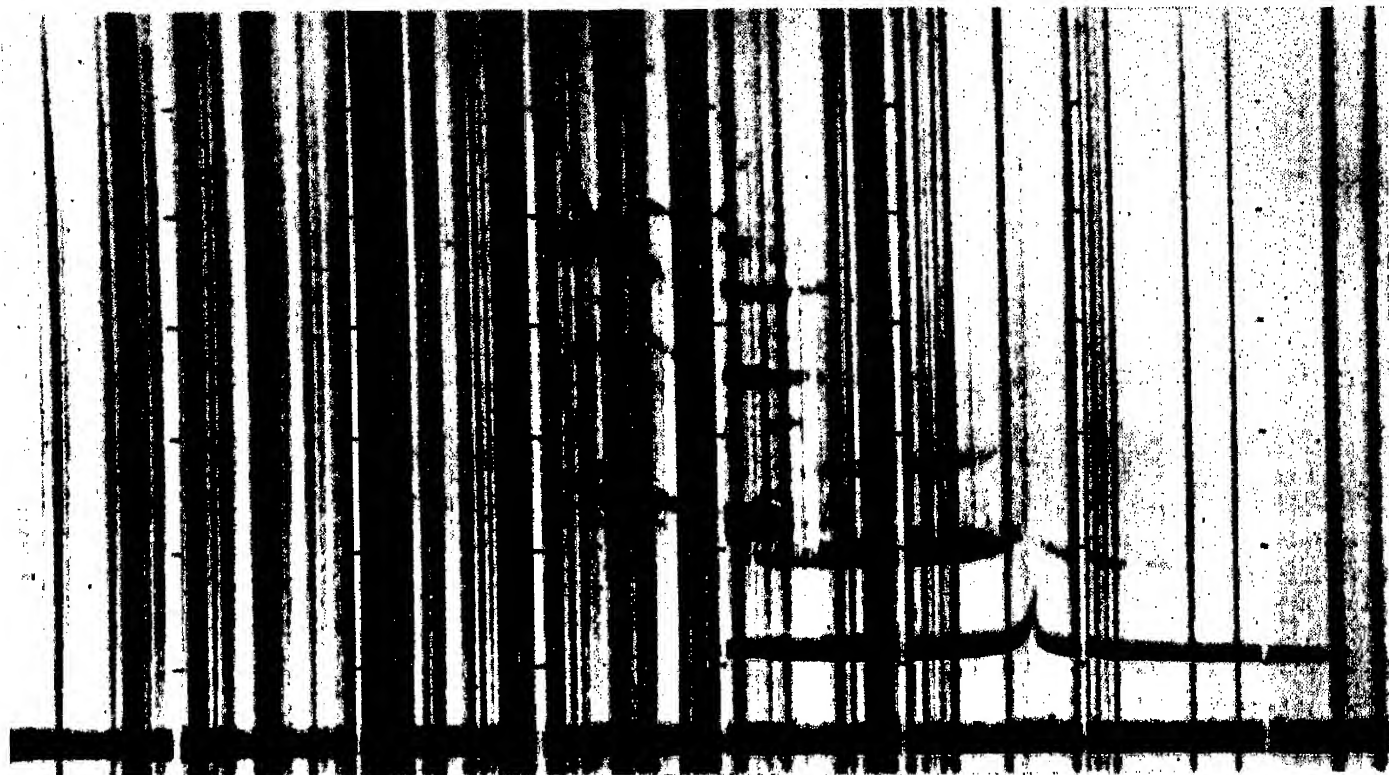


Fig. 15. Ionogram with rather high value of  $f_t E_s$  (5.2 Mc/s) equal to  $f_x E_s$  after rule (g) (III). [In this particular case the cusp of the  $\alpha$ -trace appears at the beginning of band 4, so that rule (a) could be used.]

### CONCLUSION

Summarizing these considerations it can be stated that in almost every really doubtful case the guess can be made that  $f_t E_s = f_x E_s$ .

It seems that by applying these instructions (Piggott and Rawer 1961) during the last year the efficiency of practical  $E_s$  frequency parameters has been considerably improved.

### REFERENCES

- APPLETON, E. V. and NAISMITH, R. (1940) *Proc. Phys. Soc.* **52**, 402.  
 BIBL, K., BUSCH, R., RAWER, K. and SUCHY, K. (1959) *J. Atmosph. Terr. Phys.* **6**, 69.  
 BRIGGS, B. H. (1951) *J. Atmosph. Terr. Phys.* **1**, 345.  
 PIGGOTT, W. R. and RAWER, K. (1961) *URSI Handbook of Ionogram Interpretation and Reduction*, Amsterdam.  
 RAWER, K. (1949) *Nature* **163**, 528.  
 RAWER, K. (1955) *Geofisica Pura e Appli.* **32**, 170.  
 RAWER, K. (1958) *Agardograph*, No. 34, p. 67.  
 RAWER, K. and SUCHY, K. (1962) *Encyclopedia of Physics*, Vol. 49 (in press).



# The Occurrence of Sporadic $E$ during the IGY

H. I. LEIGHTON, A. H. SHAPLEY and E. K. SMITH

Central Radio Propagation Laboratory, National Bureau of Standards, Boulder,  
Colorado, U.S.A.

**Abstract**—This paper presents maps of total  $E_s$  occurrence and considers the temporal variations of the  $E_s$  types observed on ionograms along a meridian chain of stations.

## I. INTRODUCTION

The statistics of  $E_s$  have been treated extensively by Smith (1957) and others for ionosonde data accumulated before the IGY. It is instructive to re-examine some aspects of the subject with IGY data both because the number of vertical-sounding stations reached an all-time peak during the IGY and because the international coordination for the IGY under URSI auspices tended to provide a more nearly homogeneous set of data from the world network of stations. Further, there was initiated for the IGY the first attempt on a world-wide basis to sort  $E_s$  phenomena into more or less distinctive types, according to the appearance of the echo traces on the ionograms.

This note deals with world map patterns of  $E_s$  occurrence and with some diurnal and seasonal occurrence statistics of the separate types of  $E_s$  at selected stations. The work is based upon tabular data provided by stations to the IGY World Data Centers.

## 2. GEOGRAPHICAL OCCURRENCE OF TOTAL SPORADIC $E$

The maps of Figs. 1–6 have been prepared in essentially the same manner as those presented earlier by Smith (1957). The year 1958 has been divided into six time periods: day (06–18 LT) and night (18–06 LT) for the June solstice (May, June, July and August), the December solstice (November, December, January and February), and the equinox months (March, April, and September, October).

In a few instances where data were not available for 1958, data for the corresponding period of 1957 have been substituted. The area between  $\pm 10^\circ$  in dip on the daytime maps has been hatched in order to exclude the equatorial “ $q$ -type” sporadic  $E$  since the occurrence of  $q$ -type  $E_s$  (see Knecht and McDuffie) peaks in too narrow a geographical area to be properly represented on maps drawn to this scale.

JUNE SOLSTICE DAYTIME  
MAY, JUNE, JULY, AUGUST; 0600-1800 LT  
 $fE_s > 5$  Mc 1958

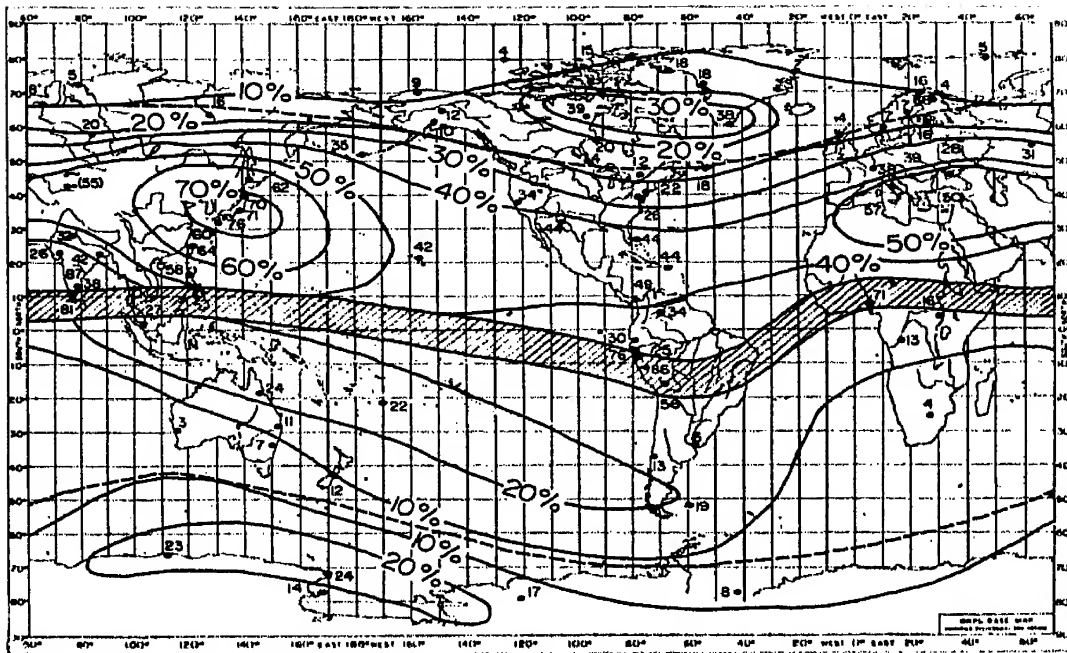


Fig. 1. Map showing per cent of time that  $fE_s$  exceeded 5 Mc/s during daytime hours of the June solstice, 1958.

JUNE SOLSTICE - NIGHTTIME  
MAY, JUNE, JULY, AUGUST; 1800-0600 LOCAL TIME  
 $fE_s > 5$  Mc 1958

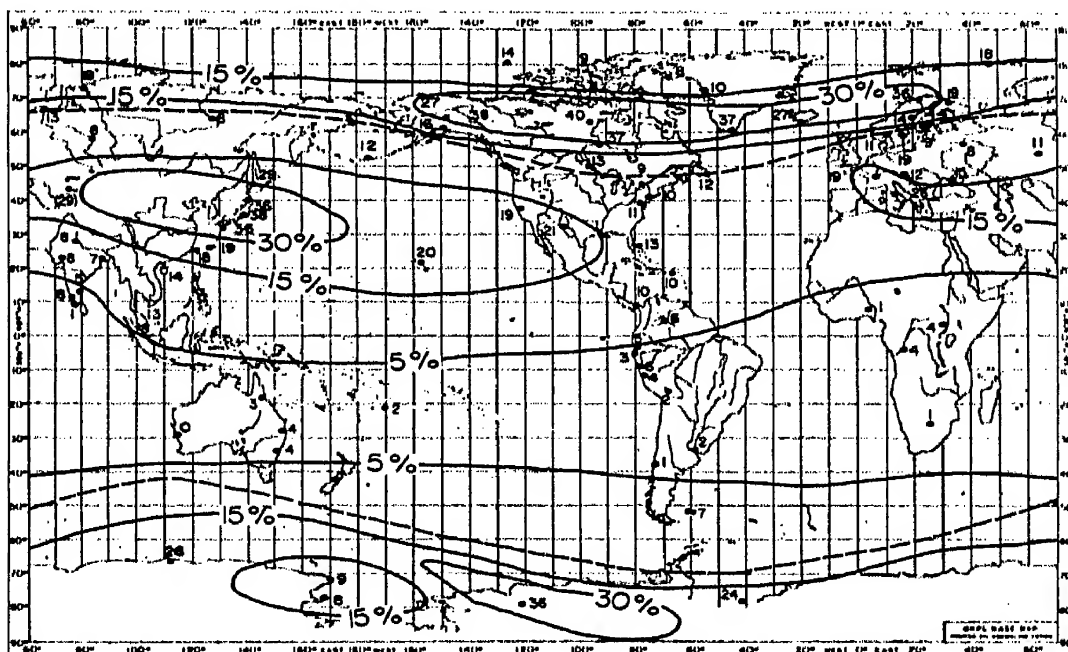


Fig. 2. Map showing per cent of time that  $fE_s$  exceeded 5 Mc/s during night-time hours of the June solstice, 1958.

EQUINOX - DAYTIME  
MARCH, APRIL, SEPT., OCTOBER; 0600-1800 LT  
 $fE_s > 5$  MC 1958

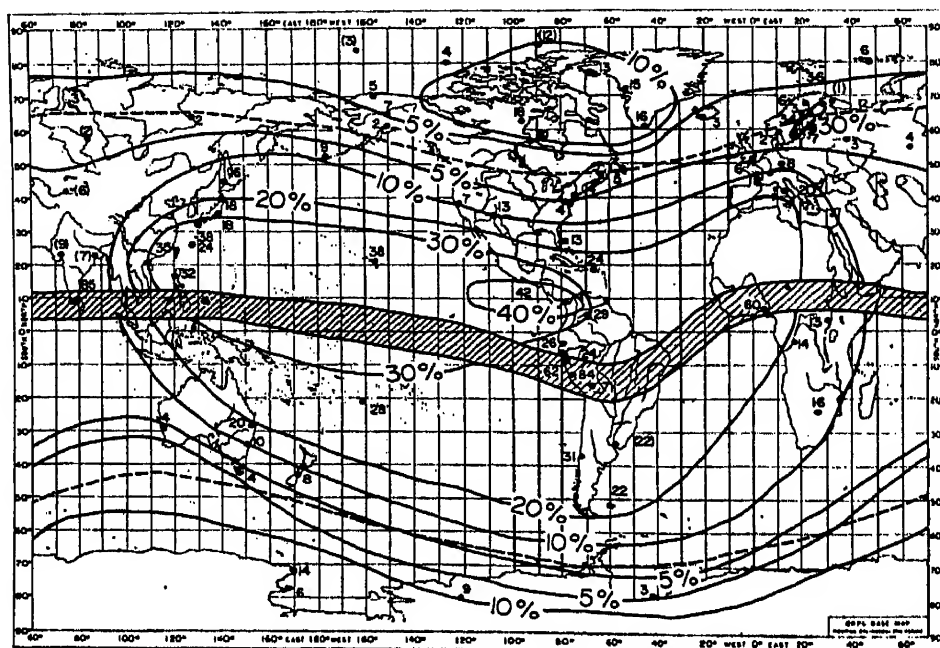


Fig. 3. Map showing per cent of time that  $fE_s$  exceeded 5 Mc/s during daytime hours of the equinoctial months, 1958.

EQUINOX NIGHTTIME  
MARCH, APRIL, SEPTEMBER, OCTOBER; 1800-0600 LT  
 $fE_s > 5$  MC 1958

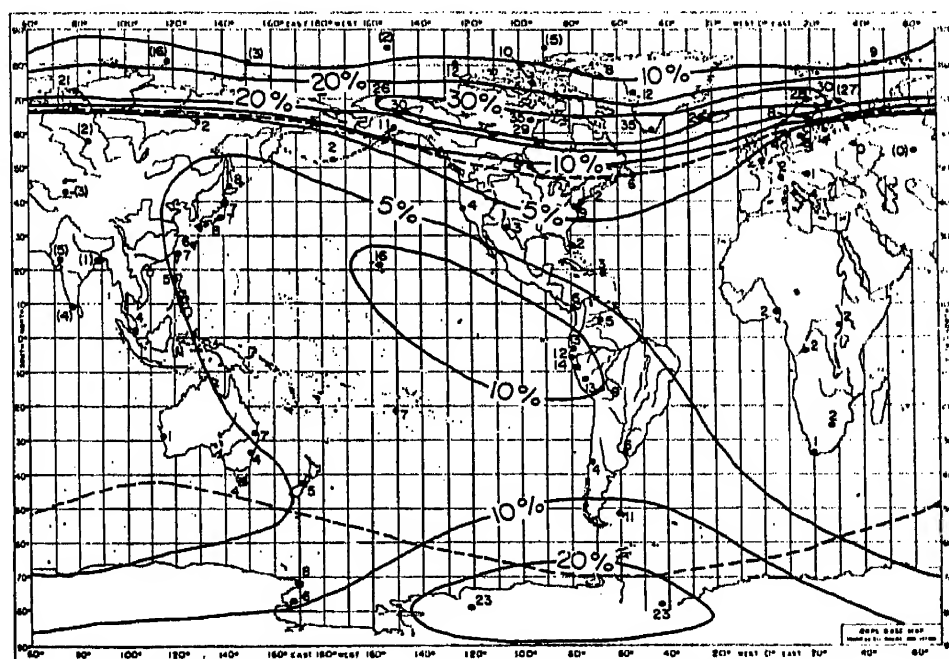


Fig. 4. Map showing per cent of time that  $fE_s$  exceeded 5 Mc/s during night-time hours of the equinoctial months, 1958.

DECEMBER SOLSTICE, DAYTIME  
 NOV., DEC., JAN., FEB.; 0600–1800 LT  
 $fE_s > 5$  Mc 1958

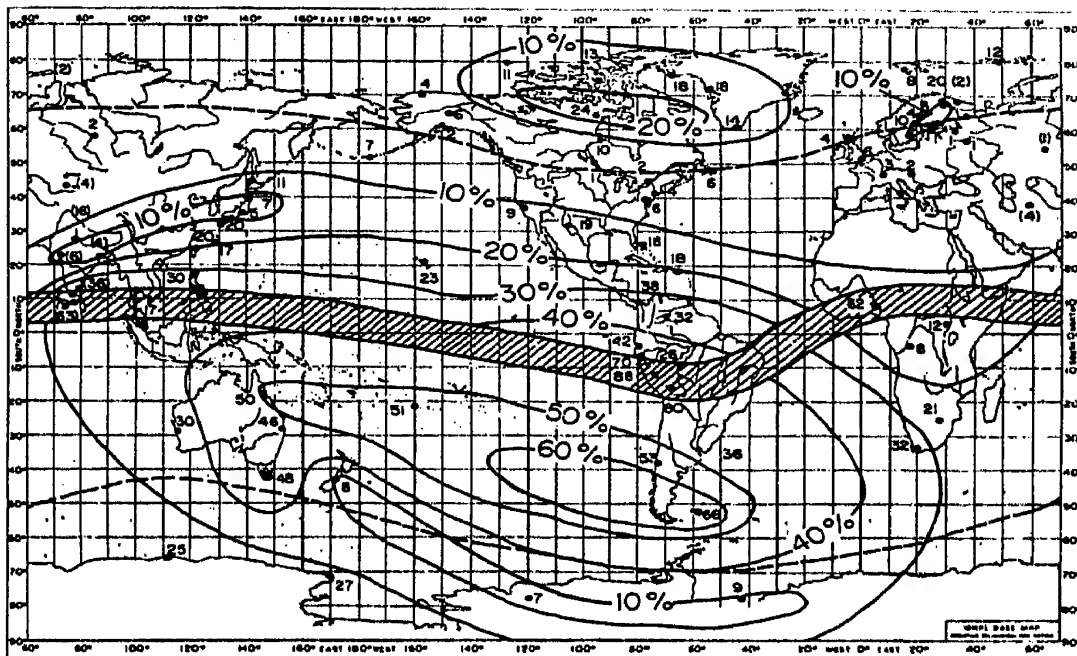


Fig. 5. Map showing per cent of time that  $fE_s$  exceeded 5 Mc/s during daytime hours of the December solstice, 1958.

DECEMBER SOLSTICE NIGHTTIME  
 NOV., DEC., JAN., FEB.; 1800–0600 LT  
 $fE_s > 5$  Mc 1958

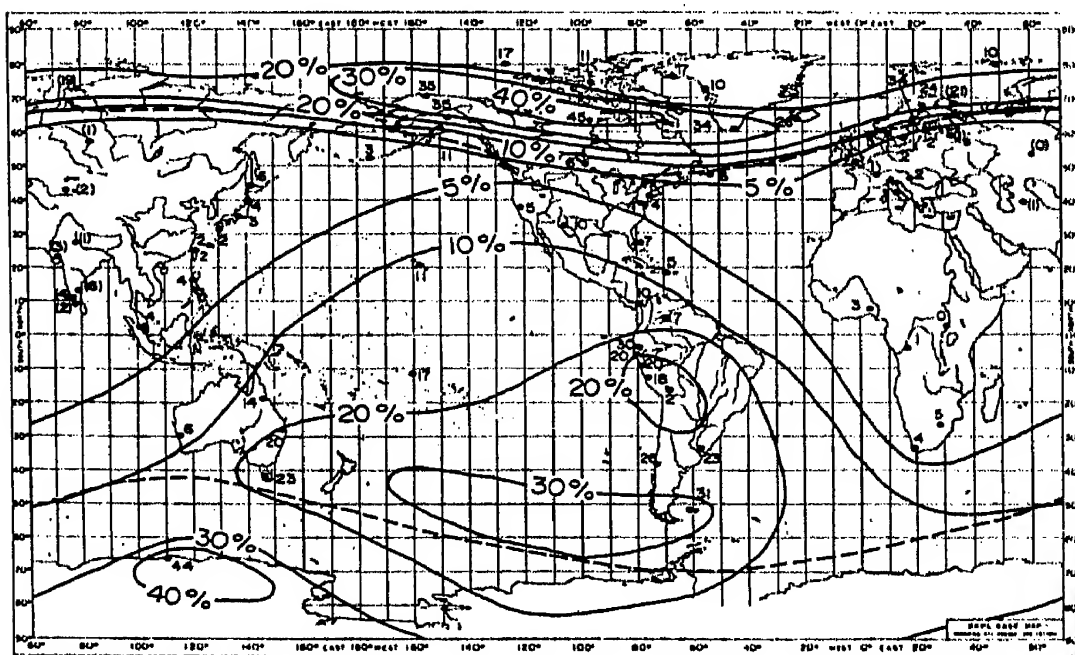


Fig. 6. Map showing per cent of time that  $fE_s$  exceeded 5 Mc/s during night-time hours of the December solstice, 1958.

The values shown beside each station in these figures represent the per cent of the time period during which  $fE_s$  (the top frequency of sporadic  $E$  on an ionogram) exceed 5 Mc/s. The data were scaled from the CRPL-F series charts of  $E_s$  occurrence.

Of particular interest in these charts are the geographical areas where data have become available (in useful quantities) for the first time. One such area is Siberia. There now appears good confirmation that, as one moves around the line of maximum auroral occurrence, a maximum in night-time  $E_s$  occurrence is found over Canada and a minimum over Siberia. This effect is shown in the polar plots of sporadic  $E$  drawn by Smith (1957) but, since there were at that time no data available from Siberia, it could only be surmised that there was no corresponding peak over Siberia. A plausible explanation of this peak in the occurrence of sporadic  $E$  (and certain other arctic phenomena such as polar blackouts) has recently been given by Bellchambers and Piggott (1960) in terms of the concentration of auroral zone effects on the Canadian side of the auroral zone of the earth which also contains the magnetic pole.

Another point of interest is the greater detail now available on the Far Eastern maximum in  $E_s$  occurrence. Additional detail can be seen by comparing the two June solstice maps of this paper with the ones by Smith in Chapter I of this volume. A tongue is now seen to extend from the Far Eastern maximum peak all the way to the Mediterranean. This is what one would expect if, as suggested by Smith and Finney (1960), this peak occurs in local summer in those areas where the geographic latitude is higher than the magnetic latitude. Expressed slightly differently this local summer longitudinal peak is expected to occur in the Northern Hemisphere in those areas above, where the magnetic equator is farthest north relative to the geographic equator, (i.e. from the Far East to Europe). In the Southern Hemisphere the peak would be expected to occur to the south of the most southerly excursion of the magnetic equator (i.e. South America). These relationships can be pretty well seen in Figs. 1, 3 and 5 where the magnetic equator is located in the center of the hatched area. In conformance with this consideration and the suggestion that sporadic  $E$  in temperate latitudes appears to be connected by the horizontal component of the earth's magnetic field,  $H$ , (Heisler and Whitehead 1960, Smith 1957, see Appendix III), one would expect the Far Eastern June solstice maximum should appear in the Southern Hemisphere in South America and Australia during the December solstice. This is seen to occur with a peak canted distinctly toward South America in Fig. 5. The horizontal component of the earth's magnetic field is shown for comparison in Fig. 7. As Southern South America is not an area of high horizontal intensity, whereas Northern Australia is, it appears that both factors probably influence in this  $E_s$  peak.

As before (Smith 1957), the consistently low value of sporadic  $E$  in South Africa corresponds to the low value of  $H$  in that area.

### HORIZONTAL INTENSITY OF THE EARTH'S MAGNETIC FORCE

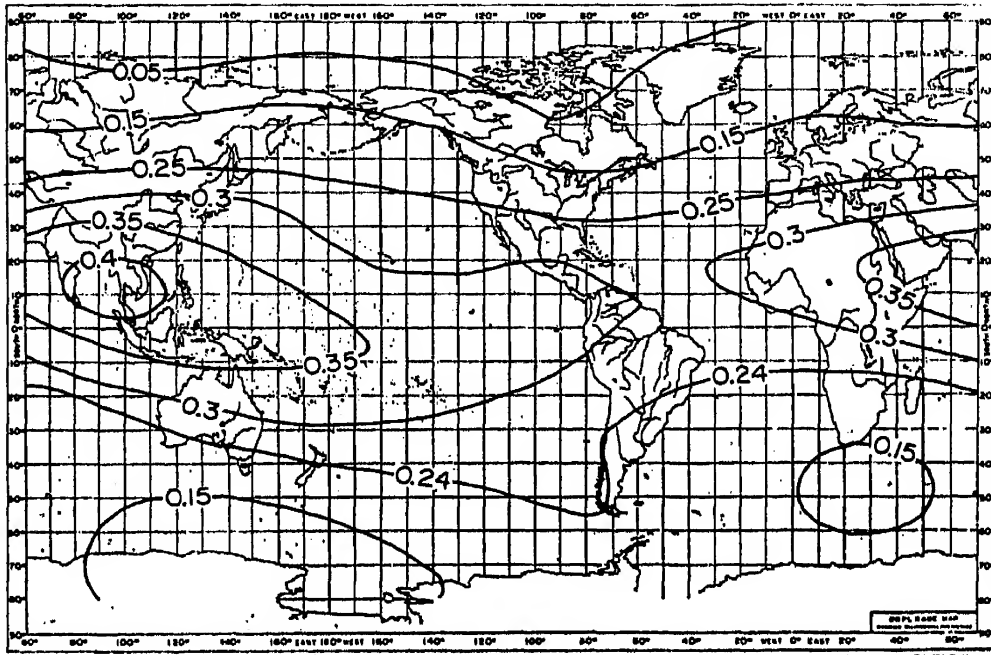


Fig. 7. Map showing the horizontal intensity of the earth's magnetic force expressed in oersteds.

### 3. VARIATION WITH SUNSPOT CYCLE

A simple comparison for  $fE_s > 5$  Mc/s has been made for stations with data available both in 1958 (high sunspot number, high magnetic activity) and in 1954 (low sunspot number, low magnetic activity). A count was made for each time period of the number of stations where  $fE_s > 5$  Mc/s was more abundant in 1958 than in 1954. For each season in the daytime slightly more stations showed more  $E_s$  in 1958 than 1954 (mild positive sunspot correlation). On the other hand, at night for each season slightly more stations recorded more  $E_s$  in 1954 than 1958 (mild negative sunspot correlation). This result may be taken as one more piece of evidence that sporadic  $E$  by and large shows little dependence on sunspot cycle.

### 4. TYPES OF $E_s$

Before 1956 the only  $E_s$  parameters tabulated by the world network of vertical-sounding stations were the top frequency ( $fE_s$ ) and the minimum virtual height ( $h'E_s$ ). More detailed studies were undertaken as research projects, usually employing data for a limited area without opportunity to

test these with the world body of data (i.e. no worldwide consistency). Beginning with 1956,  $E_s$  echo traces from stations in high latitudes were classified according to the recommendations of the report of the URSI High Latitude Committee. Beginning in 1957,  $E_s$  types were recommended for all stations according to a modified scheme advanced by the URSI World-wide Soundings Committee (WWSC). (See Wright, Knecht, and Davies 1957).

In most pre-IGY statistical studies of  $E_s$  and the analyses discussed above, all  $E_s$  types have been lumped together. It is instructive to examine some statistics of individual types both to explore whether the IGY typing scheme is physically meaningful and perhaps to give additional meaning to the lumped statistics.

The classification depends on the appearance of the  $E_s$  echo trace on the ionogram. For the IGY work, eight types were recognized; typical examples are given in Figs. 8 to 10. The types and where they are expected to occur are:

- $h$ —(high), daytime only, (common in temperate latitudes)
- $c$ —(cusp), daytime only, (common in temperate latitudes)
- $l$ —(low), daytime only, (common in temperate latitudes)
- $f$ —(flat), night-time only
- $a$ —(auroral), (common at auroral latitudes)
- $r$ —(retardation), (common at auroral latitudes)
- $q$ —(equatorial), (common at low latitudes)
- $s$ —(slant), always seen in association with another type, (occurs both at low and auroral latitudes)

Figures 11 and 12 show the diurnal and seasonal occurrences, respectively, of each  $E_s$  type at ten stations near the 75th West Meridian from Thule (geographic latitude 77°N) to the South Pole. The data refer only to the hourly ionograms. An allowance has been made for lack of opportunity to observe  $E_s$  echoes because of equipment difficulties (letter symbol  $C$ ) and blackout (letter symbol  $B$ ). When two or more types appear on the same ionogram, each occurrence enters into the statistics.

Some interesting features of these figures are:

- (a)  $f$ -type at Thule, Ellsworth and the South Pole occurs mostly in winter (this being night-time in these areas).
- (b)  $l$ -type proves to be largely a morning and evening type as one approaches the equator.
- (c)  $h$ -type is essentially confined to the lower latitudes of the temperate zones.
- (d)  $a$ - and  $r$ -types are localized to the auroral zone.
- (e) The mid-latitude summer maximum in total sporadic  $E$  is primarily due to  $c$ -type  $E_s$ .



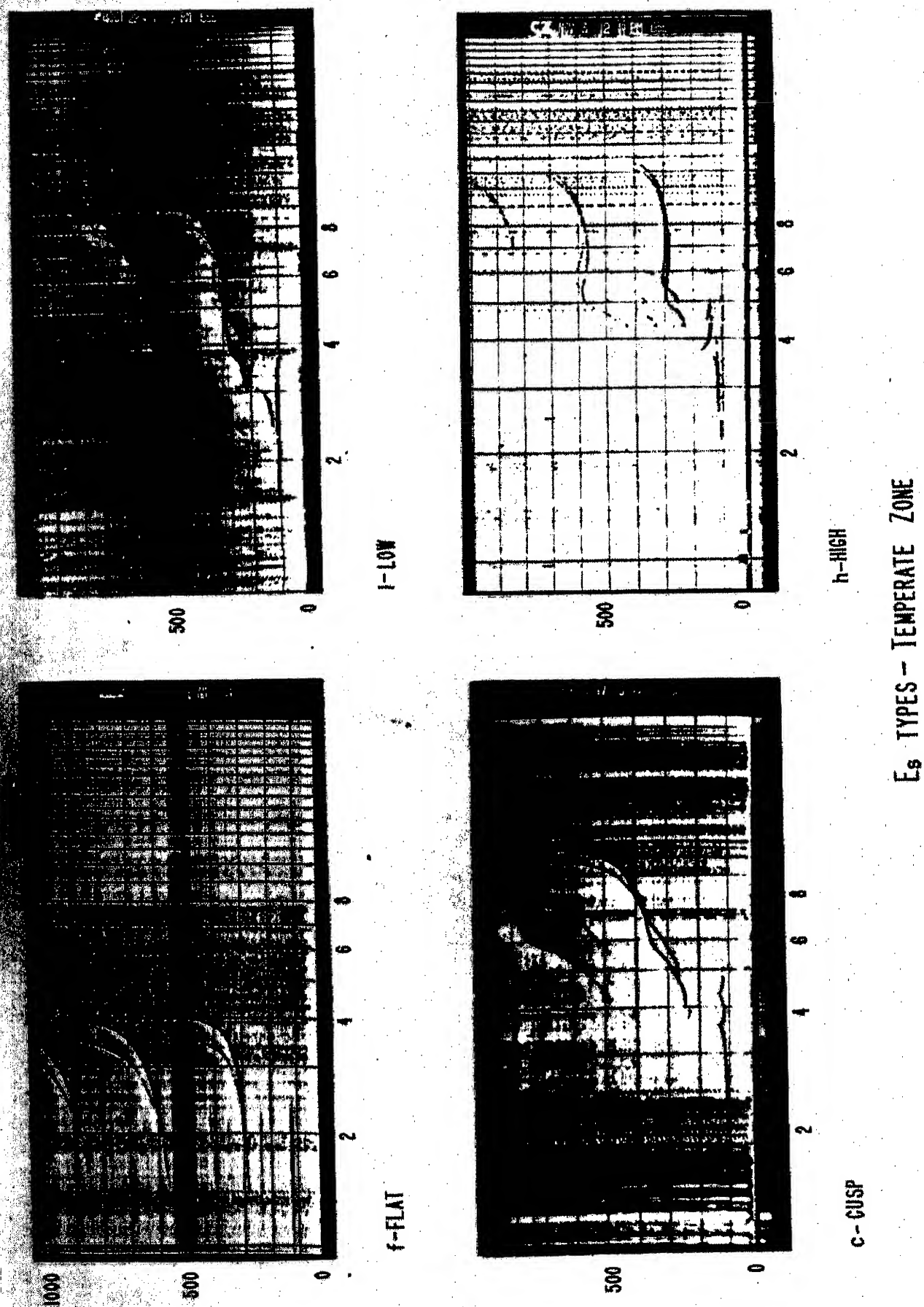


Fig. 8. Sample ionograms showing *E<sub>s</sub>* types which commonly occur in the temperate zone.



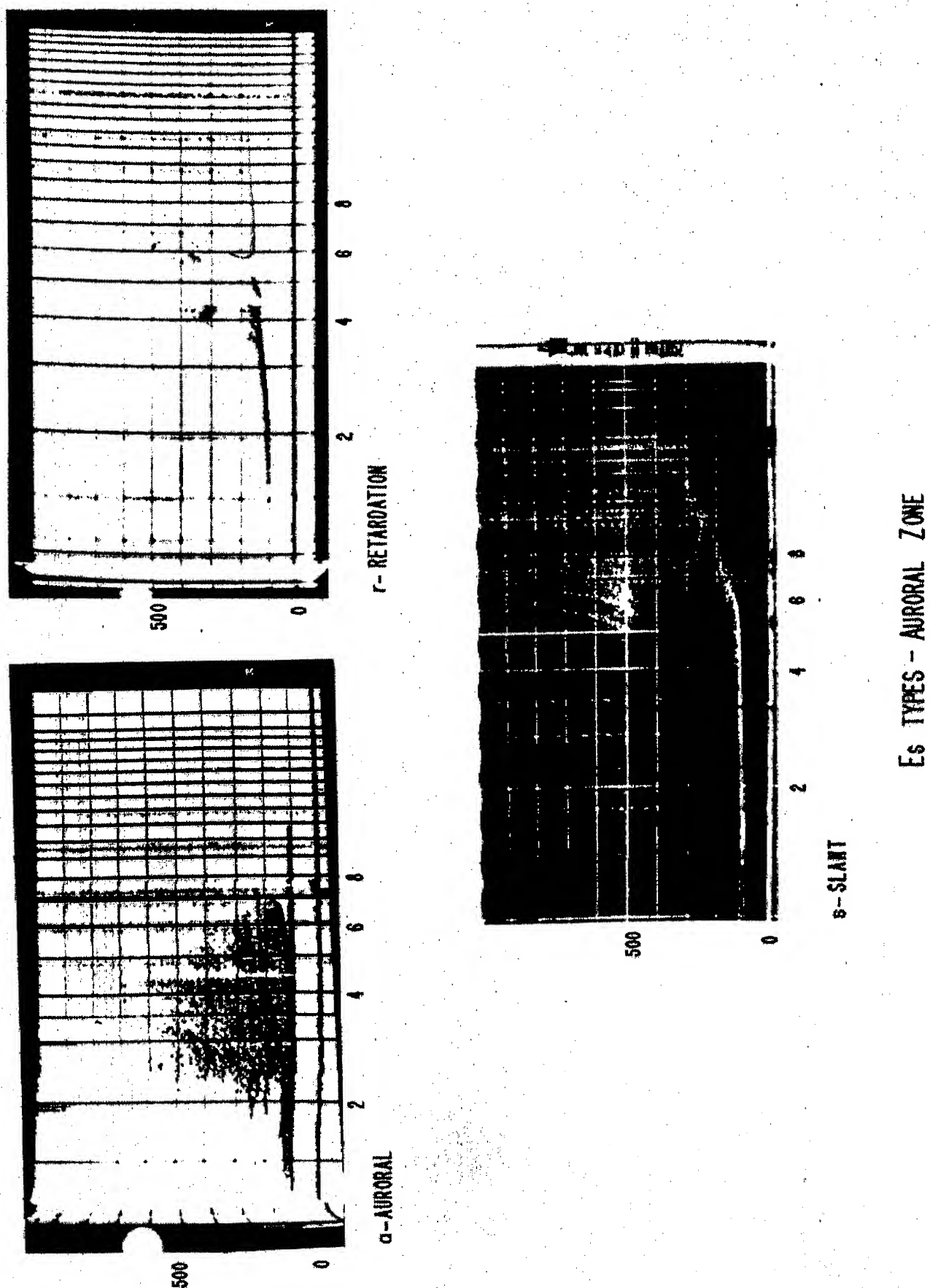
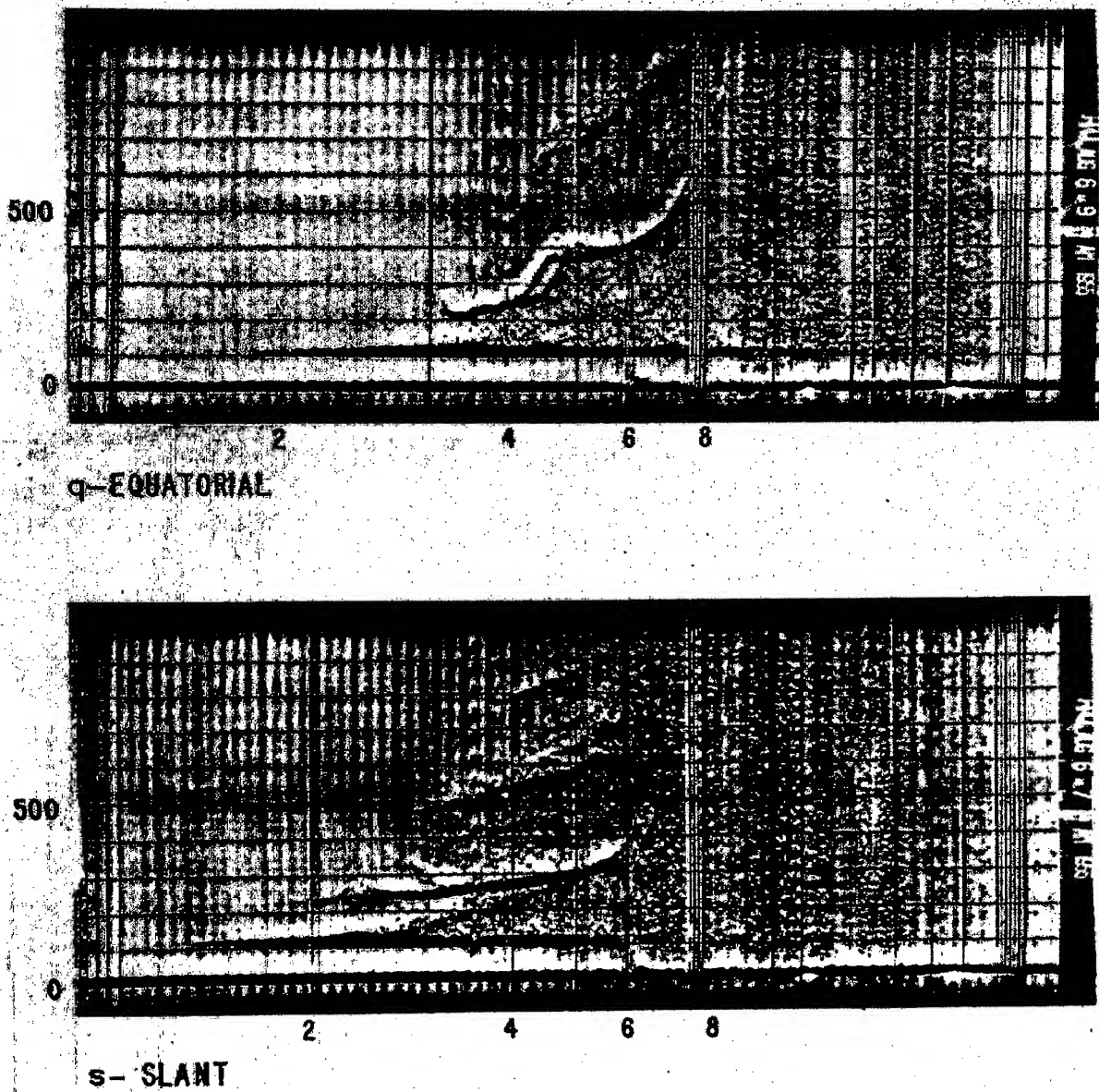


Fig. 9. Sample ionograms showing  $E_s$  types which commonly occur in the auroral zone.



### *E*<sub>s</sub> TYPES - EQUATORIAL ZONE

Fig. 10. Sample ionograms showing *E*<sub>s</sub> types which commonly occur in the equatorial zone.

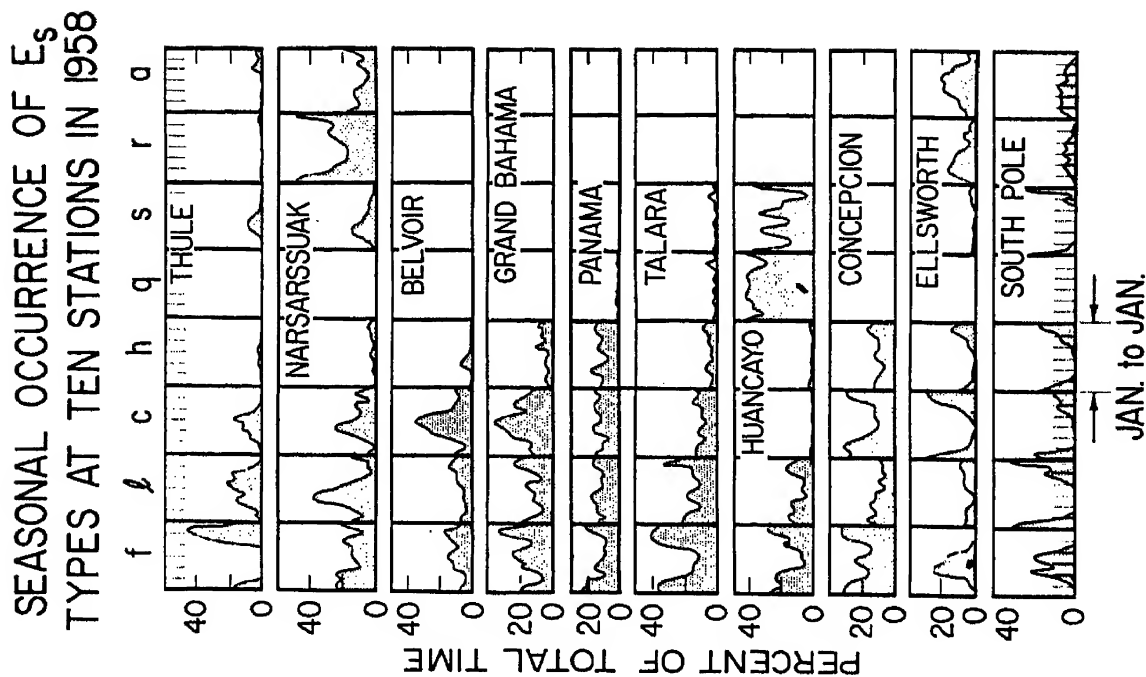


Fig. 12. Seasonal occurrence of  $E_s$  types at ten stations near the 75th meridian during 1958.

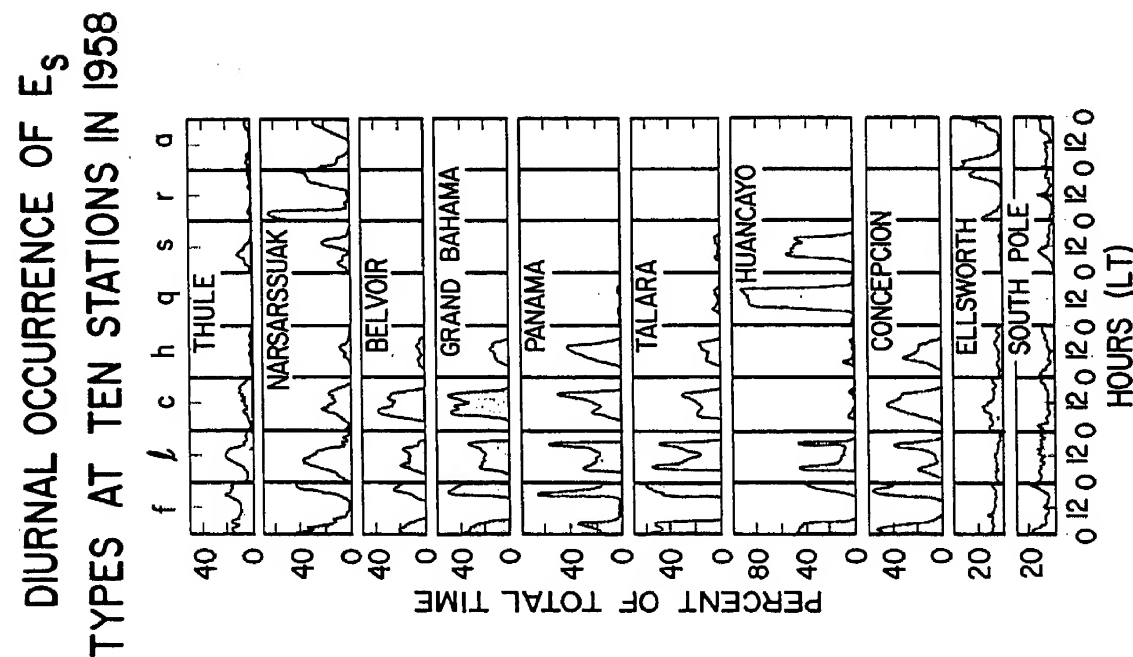


Fig. 11. Diurnal occurrence of  $E_s$  types at ten stations near the 75th meridian during 1958.

- (f) *q*-type is restricted to the immediate vicinity of the magnetic equator and is a daytime, all year phenomenon.
- (g) *s*-type occurs at the magnetic equator (similar times as *q*-type) and in the auroral zone and polar cap.

Any typing scheme has its drawbacks and the one developed by the WWSC should not be considered to be the last word. An example of one of these drawbacks can be seen in Fig. 11 for Panama or Talara where it is clear that the occurrence patterns for *f*- and *l*-types are complementary and if added together provide a much more sensible curve.

*Acknowledgment*—The analysis reported here was carried out under Grant Y/22.7/328 from the National Science Foundation to the National Bureau of Standards.

## REFERENCES

- BELLCHAMBERS, W. H. and PIGGOTT, W. R. (1960) *Proc. Roy. Soc.* **A256**, 200.  
HEISLER, L. H. and WHITEHEAD, J. D. (1960) *Nature* **187**, 676.  
KNECHT, R. W. and McDUFFIE, R. (1961) (this volume).  
SMITH, E. K. (1957) *NBS Circular* 582, U. S. Government Printing Office.  
SMITH, E. K. and FINNEY, J. W. (1960) *J. Geophys. Res.* **13**, 295.  
WRIGHT, J. W., KNECHT, R. W. and DAVIES, K. (1957) *Annals of the IGY* **3**, pt. I, Chap. V, Pergamon Press, London.

# A Note on the Heights of the Different IGY Types of $E_s$

SANFORD C. GLADDEN

Central Radio Propagation Laboratory, National Bureau of Standards, Boulder, Colorado, U.S.A.

**Abstract**—Using 200 station-months of data, the dependence of  $h'E_s$  on season and geographic location was studied. The minimum virtual height of  $E_s$  was found to be generally greater for the  $f$ -type  $E_s$  than for the  $l$ -type  $E_s$ . Some dependence of  $h'E_s$  (for the  $f$ -type and  $c$ -type) on geographic latitude was noted, with lower heights at lower latitudes. No dependence of  $h'E_s$  on sunspot number was found. For any study of  $h'E_s$ , the investigation should be on the basis of  $E_s$  types, rather than on a composite value of  $h'E_s$ .

A survey of existing information on sporadic- $E$  phenomena has been prepared by Thomas and Smith (1959). In this paper, the authors stressed the importance of studying the phenomena by  $E_s$  types rather than combining all  $E_s$  occurrences into one representative quantity. The present author heartily concurs with this point of view.

Since the type of  $E_s$  has only recently begun to appear on punched cards at CRPL along with values of the minimum virtual height of  $E_s$  ( $h'E_s$ ), it has been necessary to transcribe manually the type of  $E_s$  with the accompanying value of  $h'E_s$ . Consequently, although the present study covers some 200 station-months of  $E_s$  data, it is felt that considerably more data should have been included to make the conclusions more reliable.

The stations included in this study comprise 27 stations either operated by the National Bureau of Standards or closely associated with it, and using the same or similar types of ionosondes. In addition, 14 other stations not under the supervision of NBS have been included. While the use of data obtained from stations not under NBS supervision may introduce some heterogeneity in the data, it was felt that their use would give a more rounded picture.

The stations used include both northern and southern hemisphere locations, from about 77°N geographic latitude to 90°S geographic latitude.

One of the problems encountered in the use of these mixed data is that of non-homogeneous values of  $h'E_s$ . At those stations operating under NBS procedures,  $h'E_s$  is presently scaled to the nearest 1 km. At certain other stations,  $h'E_s$  is scaled only to the nearest 5 km. Scaled results of all stations generally conform to the designation of  $E_s$  types according to the classification of the URSI World-Wide Ionospheric Soundings Committee.

The study has been mainly limited to data for the year 1958. For each month of this year, median values of  $h'E_s$  for several types of  $E_s$  were determined for four stations: Huancayo, Washington, St. Johns, and Thule. These data are shown in Fig. 1. From this study it was determined that

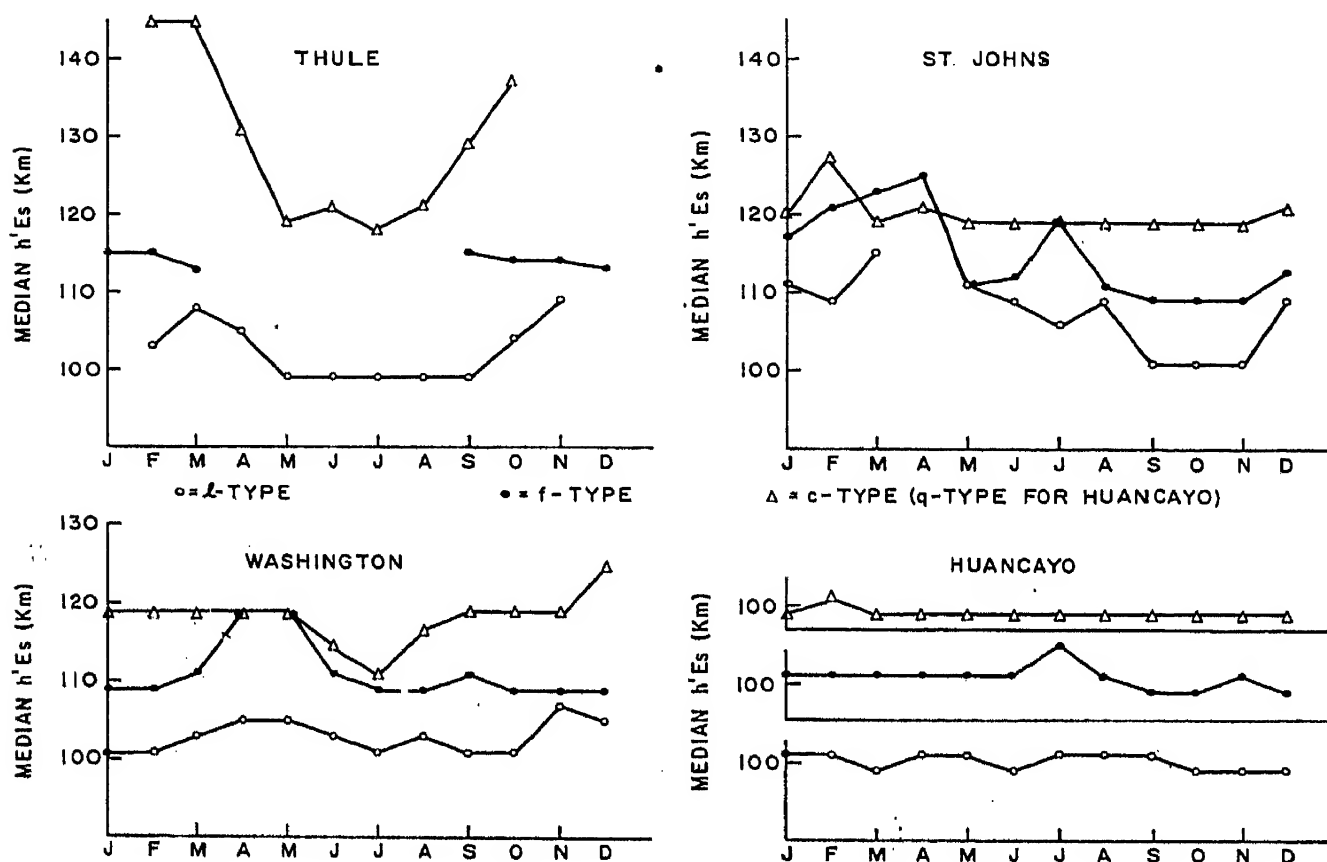


Fig. 1. Monthly median  $h'E_s$  for 1958.

$h'E_s$  for the horizontal type of night-time  $E_s$  ( $f$ -type) was generally greater than that for the day-time horizontal type ( $l$ -type). At Huancayo, there was no appreciable difference in the value of  $h'E_s$  for  $f$ -type,  $l$ -type, and  $q$ -type  $E_s$ .

Three months of 1958—summer, equinoctial, and winter—were examined for northern and southern hemisphere stations. These data are shown in Fig. 2. For the  $f$ -type and  $c$ -type  $E_s$ , there appears to be some dependence of median values of  $h'E_s$  on geographic latitude, with lower heights at lower latitudes. Some dependence upon magnetic dip angle was noted with an apparent minimum value of  $h'E_s$  at about  $40^\circ$  dip angle.

There did not appear to be any dependence of  $h'E_s$  for the  $l$ -type  $E_s$  on geographic latitude or dip angle. Insufficient data were available for other types of  $E_s$  to make even tentative conclusions.

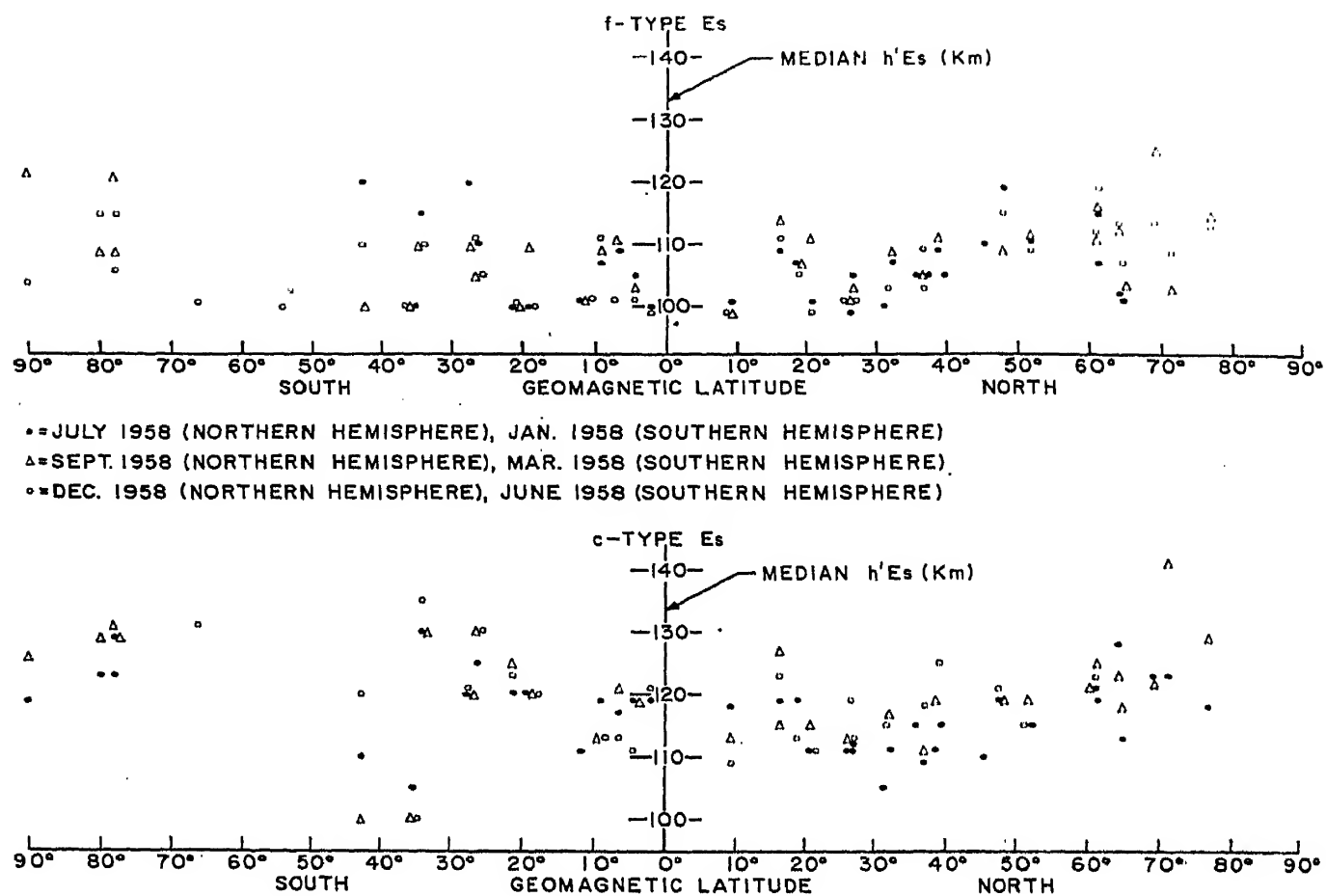


FIG. 2. Dependence of  $h'E_s$  on station location.

Using 8 stations between 9°N geographic latitude and 51°N, median values of  $h'E_s$  for  $c$ -type  $E_s$  were averaged for the periods 08 00–09 00 LST, 12 00–13 00 LST, and 15 00–16 00 LST. The results are shown in Table 1.

Table 1—Average values of  $h'E_s$  ( $c$ -type  $E_s$ ) for 8 stations (9° N–51° N)

	08 00–09 00 LST	12 00–13 00 LST	15 00–16 00 LST
July 1958	116	110	115
September 1958	114	113	117
December 1958	118	116	117

The only definite result appears to be that for the period 12 00–13 00 LST there is a progressive increase in the mean value of  $h'E_s$  from summer to winter.

From a study of data from Huancayo, Washington, and St. Johns for the years 1957, 1958 and 1959, there did not appear to be any dependence

of  $h'E_s$  on sunspot number, although these data apply only to a small part of a sunspot cycle.

Attempts were made to correlate  $h'E_s$  with magnetic character figures, using  $h'E_s$  data from Maui and Washington, and magnetic data from nearby magnetic observatories. Though the results were not conclusive, there appears to be some evidence that  $h'E_s$  on magnetically disturbed days is greater than on quiet days.

## REFERENCE

THOMAS, J. A. and SMITH, E. K. (1959) *J. Atmosph. Terr. Phys.* **13**, 295.



# Variations in Frequency of Occurrence of Sporadic $E$ , 1949–1959

W. B. CHADWICK

Central Radio Propagation Laboratory National Bureau of Standards  
Colorado, U.S.A.

**Abstract**—The question of the dependence of sporadic  $E$  on the sunspot number has been largely unresolved, with many investigators obtaining conflicting results. In this chapter results are given covering daily-hourly values of  $fE_s$  for eleven years at three ionosphere-sounding stations, College, Washington and Huancayo, Peru, chosen as representative of the three main sporadic- $E$  zones. The stations have experienced a minimum of equipment changes and changes of location during this period. Scaling procedures were monitored over the eleven years by a quality-control group at the National Bureau of Standards. The period 1949–1959 was the highest yearly average sunspot number for over 200 years.

Correlation coefficients for yearly count of  $fE_s > 5$  Mc/s vs. yearly sunspot number were found to be: College,  $-0.68$  (daytime only,  $-0.68$ ); Huancayo,  $-0.52$  (night only,  $-0.52$ ); Huancayo,  $-0.42$  (night only). Various hourly and monthly correlations were obtained. Of the 150 coefficients listed in the paper, 144 are negative.

An incidental outcome is the confirming of diurnal and seasonal trends in the auroral, north temperate and equatorial zones, making use of more data than hitherto available.

## 1. INTRODUCTION

Many studies have been made (Wells 1946, Phillips 1947, McGipps 1951, Smith 1951, Matsushita 1953, Peterson 1954, Davis 1955, Besprozvannaya and Lovcova 1956, Smith 1957) in an attempt to determine whether sporadic  $E$  is more prevalent at the low or high part of the cycle of solar activity. In general the results have been inconclusive. For instance, Phillips (1947) reported a negative correlation with sunspot number, at Washington, whereas Wells (1946) found no consistent relationship between sunspot number and sporadic  $E$  at Watheroo, Australia, from 1930 to 1944. Matsushita (1953) obtained at Huancayo a positive correlation of  $0.60$  between monthly median daytime  $fE_s$  and sunspot number for the period August 1944–July 1952. Other reports (\*, †) have noted discrepancies in longtime trends of sporadic  $E$  between Washington and Huancayo. However, the recent record-breaking maximum has given an opportunity for a re-examination of the problem.

---

\* Report IRPL-F12, O.T.S., U.S. Dept. of Commerce, Wash., 1949.

† Report IRPL-R35, O.T.S., U.S. Dept. of Commerce, Wash., 1949.

to compare frequency of occurrence of sporadic  $E$  at widely different levels of sunspot number. Furthermore, it has been possible to choose three representative ionosphere stations, in existence for an extended period of time, and presumably somewhat stable in manner of operation over an eleven year period. It was desired also to choose ionosphere sounding stations under the technical control of one organization. Change of equipment characteristics such as relative power emission and sensitivity of reception throughout the frequency range, as well as changes in interpretation of ionograms, would thus presumably be held to a minimum. (\*) The three stations selected were Fairbanks (College), representative of a location where the auroral type of sporadic  $E$  is prevalent, Washington, a station in the temperate sporadic- $E$  zone, and Huancayo, where equatorial-type  $E_s$  is common in the day hours. Thus all three main sporadic- $E$  zones (Smith 1957, 72–93) are represented. Respective geomagnetic latitudes are  $64^\circ\text{N}$ ,  $50^\circ\text{N}$ , and  $1^\circ\text{S}$ .

The parameter chosen for study was the count of  $fE_s > 5$  Mc/s. By so doing, it was hoped to avoid contamination of the sporadic- $E$  count with scaled values which were really  $fE$  rather than  $fE_s$ , as well as to minimize any possible effect of  $D$ -region absorption (Appleton and Piggott 1954).

## 2. UNIFORMITY OF DATA

The equipment was changed at all three stations during the period covered by this report. Therefore, it was felt desirable to go back prior to 1952 for as few years as possible, and still have an eleven-year period somewhat representative of a particular solar cycle.

### 2.1. *Equipment Changes*, 1949–1959 (Gladden 1959)

- Fairbanks: To March 1951, DTM automatic multifrequency ionosonde  
Since March 1951, CRPL Model C-3
- Washington: To July 1950, CRPL Model C-2  
Since June 1950, CRPL Model C-3  
Both C-2 and C-3 used in June 1950
- Huancayo: To December 1951, DTM automatic multifrequency ionosonde  
Since December 1951, CRPL Model C-3

### 2.2. *Change of Location*

- Washington: To September 1949, Sterling, Virginia ( $39.0^\circ\text{N}$ ,  $77.5^\circ\text{W}$ )  
Since September 1949, Ft. Belvoir, Virginia ( $38.7^\circ\text{N}$ ,  $77.1^\circ\text{W}$ )

---

\* Report IRPL-R34, O.T.S., U.S. Dept. of Commerce, Wash., 1946.

There was no indication in the detailed data of any break in the type of scaled results because of the above, except possibly for Huancayo. Because of the necessity for normalization of certain Huancayo data (see next paragraph) it is believed that the Huancayo data are not so uniform in quality as those for the other two stations.

### 2.3. *Normalization of Data*

Because of an unusual amount of outage attributable to equipment failure, the count for the following months at Huancayo was normalized by multiplying by a factor of proportionality, or, for certain hours, was changed to more nearly correspond to average conditions:

September 1949, May 1950, June 1950, August 1951, September 1951, November 1951, February 1959, April 1959.

The count for the month of March 1959 was entirely empirically supplied, making use of diurnal and seasonal trends in adjacent months and for other years. The large correlation coefficient for March (Table 3) is thus suspect. However, omitting the month entirely and using only 10 years of March data reduced the coefficient only by  $-0.02$  to  $-0.79$ .

### 2.4. *Change of Scaling Practice*

Up until the year 1957, values of  $fE_s$  were recorded\*; in 1957, 1958, 1959, values of  $f_oE_s$  were scaled†. (At Huancayo,  $f_oE_s$  was scaled for the first 4 months of 1949 as well). It was considered better to obtain values of correlation coefficients for unweighted and weighted counts of  $fE_s$  and  $f_oE_s > 5$  Mc/s, rather than to attempt the formidable and extremely time-consuming task of deciding whether each individual value displayed on the original records really was  $f_oE_s$  or  $fE_s$  for the period during which  $f_oE_s$  was scaled. In fact, a large number of values on the tabulation sheets were qualified by  $M‡$ .

## 3. CONVENTIONS USED IN OBTAINING CORRELATION COEFFICIENTS

In obtaining coefficients such as in Tables 1 and 2, the count for the period when  $f_oE_s$  was scaled, was obtained for  $f_oE_s > 4.2$  Mc/s at Fairbanks and Washington, and for  $f_oE_s > 4.6$  Mc/s at Huancayo. The count

---

\*  $fE_s$ : Highest frequency on which echoes of the sporadic type are observed from the lower part of the  $E$ -layer. (CCIR, Sixth Meeting, Geneva 1951.)

†  $f_oE_s$ : The ordinary wave top frequency corresponding to the highest frequency at which mainly continuous trace is observed. (First Report of the Special Committee on World-Wide Ionospheric Soundings (URSI/AGI), September 1956.)

‡ Measurement questionable because the ordinary and extraordinary components are not distinguishable. (Second Report of the Special Committee on World-Wide Ionospheric Soundings (URSI/AGI), May 1957.)

Table 1—Yearly count of  $fE_s > 5$  Mc/s vs. yearly sunspot number, 1949–1959

Station	Correlation Coefficient
Fairbanks (College), Alaska	−0.68
Washington (Sterling, Va.; Ft. Belvoir, Va.)	−0.52
Huancayo, Peru	−0.42

Table 2—Yearly count, selected hours, vs. yearly sunspot number

Station	Hours	Correlation Coefficient
Fairbanks	07 00–20 00, 150°W	−0.63
Washington	19 00–06 00, 75°W	−0.52
Huancayo	19 00–05 00, 75°W	−0.66

was also obtained for  $f_oE_s > 5$  Mc/s at the respective locations. Three sets of coefficients were obtained, (1) using the count for  $f_oE_s > 4.2$  (or 4.6) Mc/s, (2) assigning the count for  $f_oE_s > 4.2$  the weight 3, the count for  $f_oE_s > 5$  Mc/s the weight 1, and (3) using an unweighted average. The coefficients became larger in absolute value (in the negative direction) in proceeding from (1) to (3). The coefficients shown in Tables 1 and 2 are those obtained from process (2).

For Tables 3, 4 and 5, two sets of coefficients were obtained, using process (1) and process (3). The coefficients shown are those obtained from process (3).

In addition, for Tables 3 and 4, comparison was made using smoothed 12-month running average sunspot numbers as well, for both process (1) and process (3). There was little difference in results from the values shown in Tables 3 and 4, and no conclusions of this paper would be changed as a result of the use of average numbers.

#### 4. ESTIMATION OF SUNSPOT NUMBERS FOR THE LATTER HALF OF 1959

At the time of writing this paper, Zurich provisional numbers were available for July and August 1959. The following estimated numbers were used for September through December 1959:

145, 139, 135, 130.

Table 3—Monthly count vs. monthly sunspot number

Station	Jan.	Feb.	Mar.	Correlation Coefficients					Aug.	Sept.	Oct.	Nov.	Dec.
				Apr.	May	June	July						
Fairbanks	-0.56	-0.60	-0.86	-0.58	-0.71	-0.71	-0.59	-0.32	-0.51	-0.41	-0.28	-0.46	
Washington	+0.37	-0.35	-0.19	-0.48	-0.43	-0.41	-0.79	-0.04	-0.59	-0.60	-0.51	-0.50	
Huancayo	July	Aug.	Sept.	Oct.	Nov.	Dec.	Jan.	Feb.	Mar.	April	May	June	
	-0.11	-0.00	-0.47	-0.06	-0.17	-0.44	-0.25	-0.65	-0.81	-0.55	-0.42	-0.19	

Table 4—Monthly count, selected hours\* vs. monthly sunspot number

Station	Jan.	Feb.	Mar.	Correlation Coefficients					Aug.	Sept.	Oct.	Nov.	Dec.
				April	May	June	July						
Fairbanks	-0.60	-0.52	-0.67	-0.61	-0.65	-0.66	-0.46	-0.17	-0.37	-0.26	-0.42	-0.59	
Washington	+0.41	-0.44	-0.39	-0.42	-0.51	-0.35	-0.62	-0.44	-0.28	-0.51	-0.43	-0.40	
Huancayo	July	Aug.	Sept.	Oct.	Nov.	Dec.	Jan.	Feb.	Mar.	April	May	June	
	-0.45	-0.43	-0.62	-0.08	-0.50	-0.70	-0.29	-0.69	-0.49	-0.32	-0.68	-0.53	

\* Fairbanks 07 00-20 00, 150°W time; Washington, 19 00-06 00, 75°W time; Huancayo, 19 00-05 00, 75°W time.

Table 5—Yearly count, by hours, vs. yearly sunspot number

Hour	Station		
	Fairbanks	Washington	Huancayo
	Correlation Coefficients		
00	−0.78	−0.36	−0.30
01	−0.75	−0.50	−0.29
02	−0.74	−0.43	−0.27
03	−0.73	−0.35	−0.39
04	−0.72	−0.44	−0.42
05	−0.59	−0.50	−0.70
06	−0.57	−0.44	−0.63
07	−0.46	−0.57	−0.51
08	−0.61	−0.78	−0.51
09	−0.60	−0.52	−0.50
10	−0.54	−0.24	−0.48
11	−0.56	−0.60	−0.48
12	−0.57	−0.40	−0.44
13	−0.55	−0.38	−0.23
14	−0.56	−0.41	−0.13
15	−0.48	−0.41	+0.11
16	−0.65	−0.46	+0.22
17	−0.67	−0.88	+0.39
18	−0.76	−0.72	+0.07
19	−0.84	−0.69	−0.91
20	−0.88	−0.78	−0.90
21	−0.77	−0.53	−0.92
22	−0.79	−0.07	−0.83
23	−0.83	−0.51	−0.44

The Zurich provisional numbers, when available, turned out to be 146, 140, 136 and 132 respectively.

### 5. DIURNAL, SEASONAL, AND YEARLY VARIATIONS OF COUNT

Figure 1 shows the total count and percentage of  $fE_s > 5$  Mc/s for each year for each station. Also plotted is the yearly Zurich sunspot number.

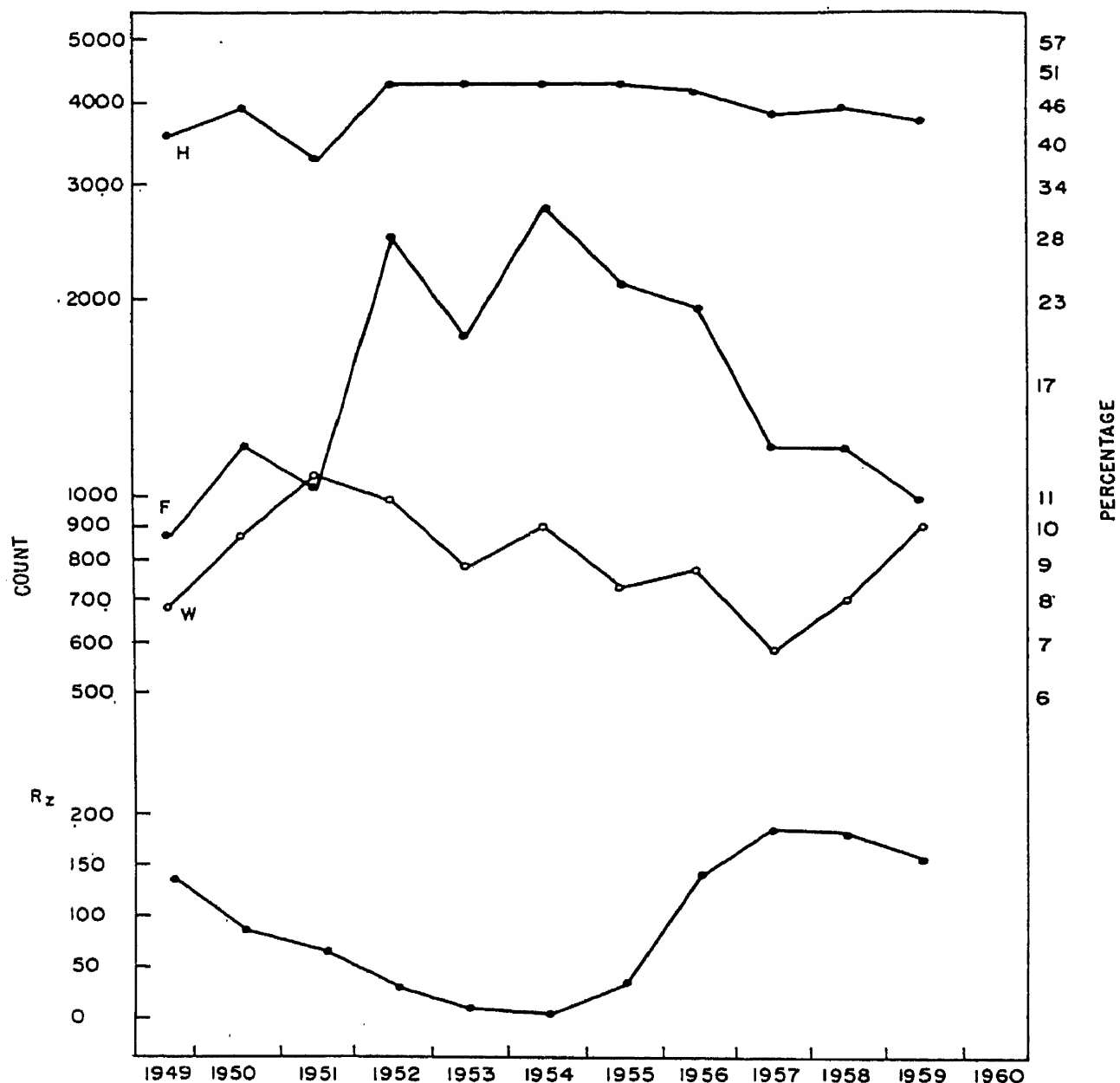


Fig. 1. Yearly Count and Percentage of  $fE_s > 5$  Mc/s vs Yearly Sunspot Number, 1949-1959.

In Figs. 2 and 3, which show the diurnal variation in count and percentage for the period of each of the three stations, the shaded portions represent hours of minimum count. For Washington and Fairbanks, they are hours for which the count is less than half the maximum count for

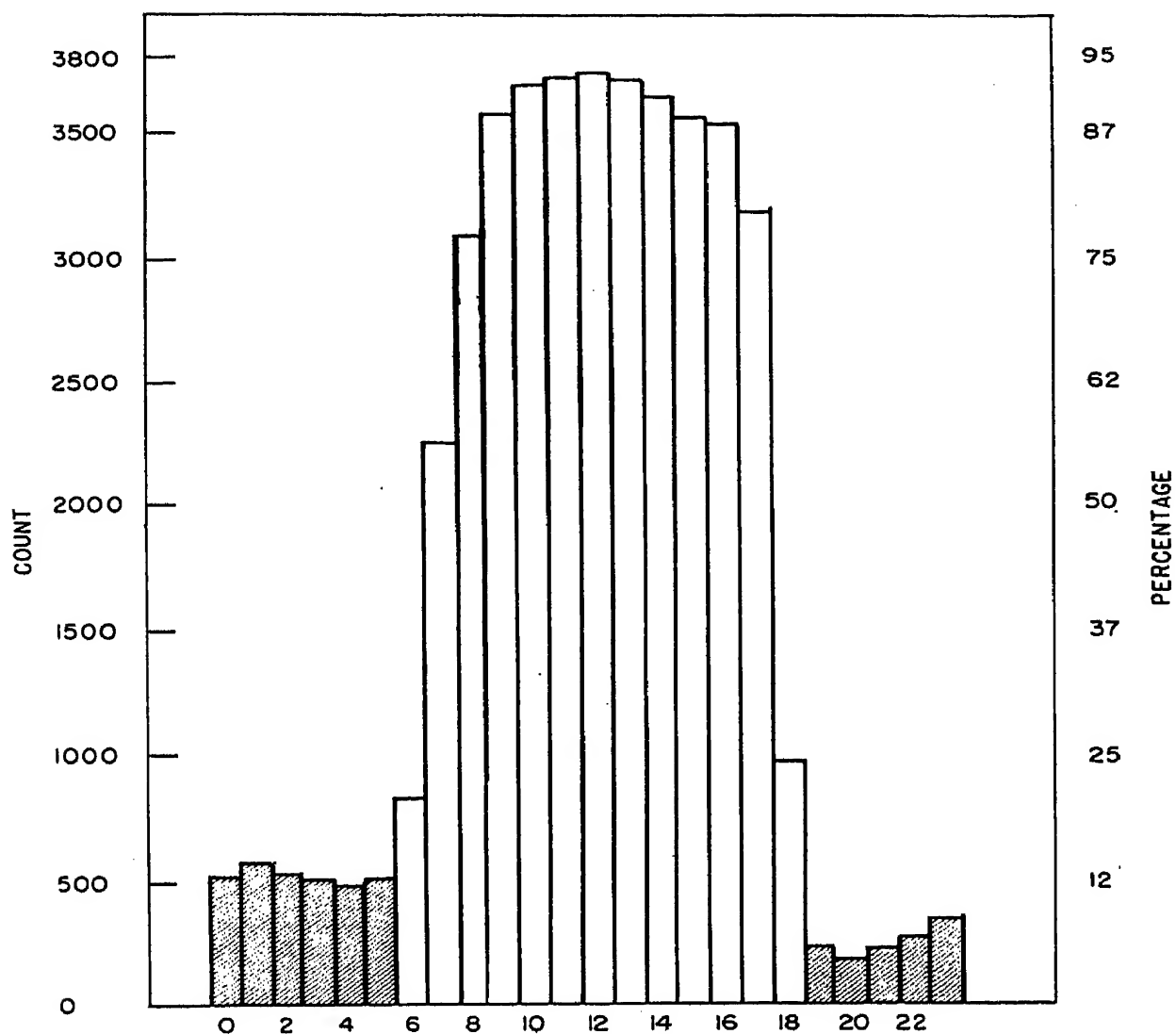


Fig. 2. Diurnal Variation, Count and Percentage of  $fE_s > 5$  Mc/s, Huancayo, 1949–1959.

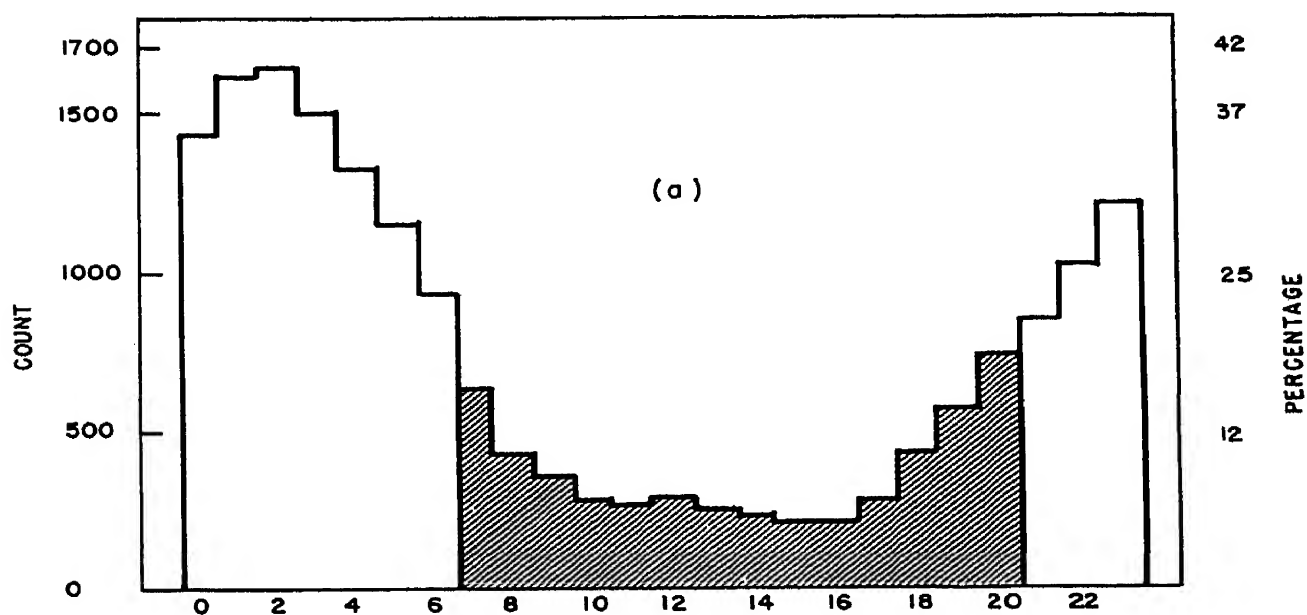


Fig. 3(a). Diurnal Variation, Count and Percentage of  $fE_s > 5$  Mc/s, Fairbanks, 1949–1959.



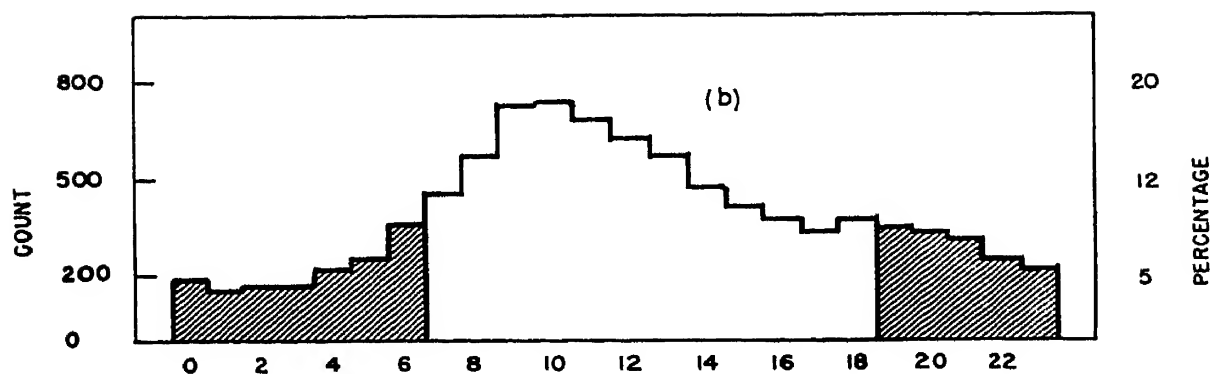


Fig. 3(b). Diurnal Variation, Count and Percentage of  $fE_s > 5$  Mc/s, Washington 1949-1959.

any hour; for Huancayo, one-fifth is used. They do not necessarily correspond to day or night hours.

Figures 4 and 5 show percentages by months, both for all hours and for hours of minimum count.

#### 6. DIURNAL, SEASONAL AND YEARLY CORRELATION COEFFICIENTS

They are presented, both for all hours and for hours selected as above, in Tables 1-5.

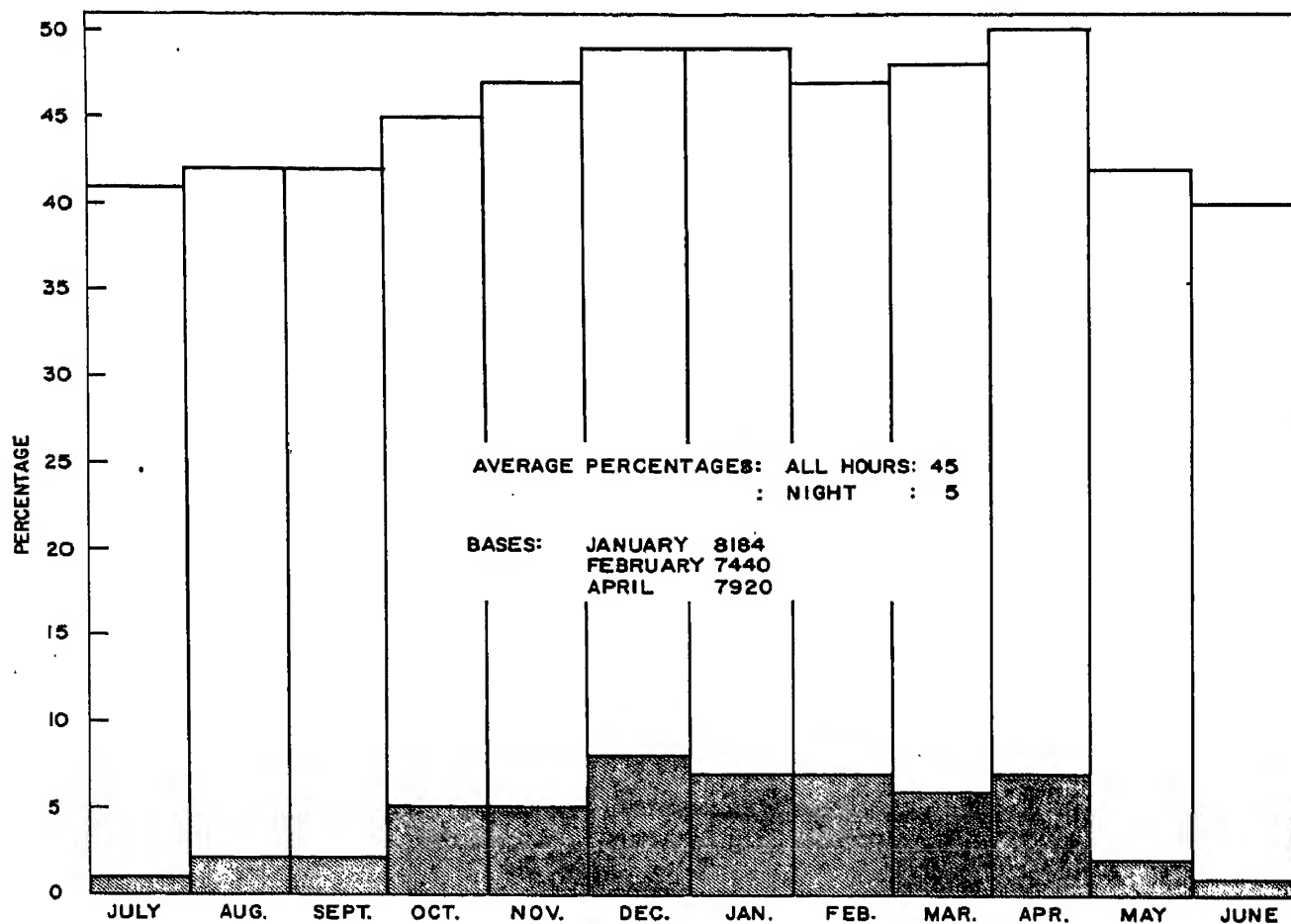


Fig. 4. Monthly Percentages of  $fE_s > 5$  Mc/s, for All Hours, and for Hours of Minimum Count (shaded) 1900-0500, Huancayo, 1949-1959.

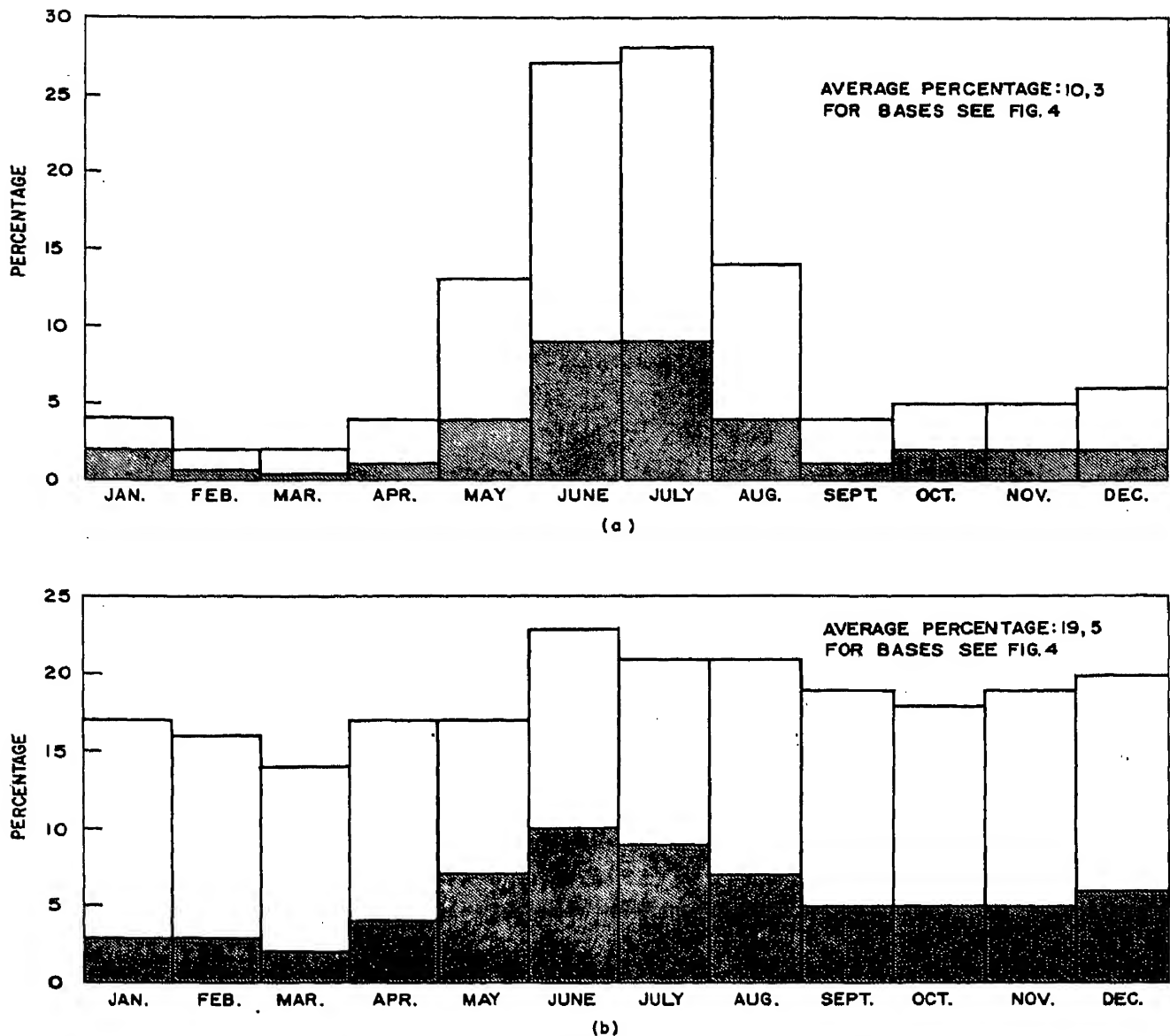


Fig. 5. Monthly Percentages of  $fE_s > 5$  Mc/s, for All Hours, and for Hours of Minimum Count (shaded) (a) 19 00–06 00, Washington, (b) 07 00–20 00, Fairbanks, 1949–1959.

## 7. DISCUSSION OF RESULTS: CONCLUSIONS

In obtaining correlation coefficients between eleven pairs of variables, if there is no auto-correlation a coefficient of  $\pm 0.602$  is significant at the 95 per cent level, and one of  $\pm 0.735$  at the 99 per cent level. While there may be some auto-correlation in these series, it is believed to be slight, so that certain general statements may be made. The coefficients found undoubtedly fail to represent the exact relationship between the variables, in view of the above discussion of the quality and uniformity of the data, and the necessity for adopting certain conventions.

(a) From Fig. 1 and Table 1, it is clear that there is a negative correlation between occurrence of  $fE_s > 5$  Mc/s and sunspot number, for these three stations, and for the period 1949–1959. The correlation coefficient for Fairbanks may possibly be significant at the 95 per cent level.

(b) The diurnal variations, as was expected, followed the pattern previously observed many times for the three main sporadic- $E$  zones—auroral, temperate and equatorial (Smith 1957, 72–93).

(c) The unshaded portions of Figs. 4 and 5 represent a nearly constant count in the cases of Huancayo and Fairbanks (equatorial and auroral types of  $fE_s$ ), but the seasonal variation is clearly shown for Washington. In this connection, it is of interest to compare the coefficients in Tables 1 and 2. The correlation coefficient for the hours of minimum occurrence of  $fE_s$  as defined above at Fairbanks remains possibly significant, at Washington there is no change, while at Huancayo it becomes significant, another indication of the well-known fact that equatorial-type sporadic  $E$  is a daytime phenomenon. Tables 3 and 4 give the comparison month-by-month.

(d) It is of interest to apply the critical levels of 0.602 and 0.735 to the tables of coefficients. However, there is great uncertainty involved as to the accuracy of results. In Table 5 we find the largest coefficients in absolute value arranged in a pattern for Fairbanks (18 00–02 00) and Huancayo (19 00–22 00). For Washington, we have high coefficients at 17 00 and 20 00, and the ones at 18 00 and 19 00 are also worth remarking. Finally, there is a minor pattern of high coefficients at 08 00 (Fairbanks and Washington) and at 05 00–06 00 (Huancayo). It is interesting that the hours of 19 00–22 00 at Huancayo represent the period when the equatorial hump in the ionosphere is present as shown by true-height studies (Wright 1959). Note that there is an abrupt change between the coefficient for 18 00 (+0.07) and for 19 00 (–0.91). Why there should be this definite pattern of coefficients for these stations is hard to explain.

(e) In Table 3 (all hours) the highest coefficients are for the month of March at Fairbanks and at \*Huancayo. If smoothed 12-month running average instead of monthly numbers are used, the respective coefficients are –0.87 and –0.80. At Washington the highest is for July, the corresponding coefficient using running averages being –0.83. No explanation is offered. In Table 4 (selected hours) there is no coefficient significant at the 99 per cent level.

(f) There is a high positive correlation (+0.77) between the total yearly amount of  $fE_s > 5$  Mc/s at Fairbanks and at Huancayo. This is probably due to the large number of occurrences of high values of the auroral type at the former and of equatorial type at the latter station.

(g) The ratio of total occurrence of  $f_oE_s > 5$  Mc/s to  $(f_oE_s \text{ plus } f_h/2) > 5$  Mc/s is essentially constant for 1957, 1958, 1959, at each of these three stations.

---

\* See Section 2.3.

For Fairbanks, the average ratio is: 0.58 range 0.05  
 Washington, the average ratio is: 0.47 range 0.06  
 Huancayo, the average ratio is: 0.92 range 0.05

This means, for instance, that at Washington for these three years about 53 per cent of the values of  $f_oE_s > 4.2$  were between 4.3 and 5.0 Mc/s inclusive. This result indicates that over this range of  $f_oE_s$  the value of “ $b$ ” remained nearly constant in the expression

$$\log_{10}\left(\frac{P_1}{P_2}\right) = b(f_1 - f_2) \quad (\text{Smith 1957, 142}).$$

## REFERENCES

- APPLETON, E. V. and PIGGOTT, W. R. (1954) *J. Atmosph. Terr. Phys.* 5, 141.  
 BESPROZVANNAYA, A. S. and LOVCOVA, V. A. (1956) *Tr. Arctic Res. Inst., Leningrad* 15.  
 DAVIDSON, DAVID (1955) *Tech. Report No. 230*, Cruft Laboratory, Harvard University, Cambridge.  
 GLADDEN, S. C. (1959) *N.B.S. Tech. Note No. 28*, Wash. 91, 93, 105.  
 MATSUSHITA, S. (1953) *J. Geomag. Geoelect., Kyoto* 5, 118.  
 MCNICOL, R. W. E. and GIPPS, G. de V. (1951) *J. Geophys. Res.* 56, 17.  
 PETERSON, A. M. (1954) *URSI-IRE Spring Meeting*, Wash.  
 PHILLIPS, M. L. (1947) *Trans. A.G.U.* 28, 71.  
 SMITH, E. K. (1951) *Tech. Report No 7*, Ionosphere Project, School of Elect. Eng., Cornell University, Ithaca.  
 SMITH, E. K. (1957) *N.B.S. Circular* 582, 101–105.  
 WELLS, H. W. (1946) *Proc. Inst. of Radio Engrs.* 34, 950.  
 WRIGHT, J. W. (1959) *J. Geophys. Res.* 64, 1631.

# Lunar Tidal Variations of Sporadic $E$

S. MATSUSHITA

High Altitude Observatory, University of Colorado, Boulder, Colorado, U.S.A.

**Abstract**—Large and obvious lunar variations of the sporadic  $E$  ( $E_s$ ) occur in spite of a very small lunar effect in the  $E$ -layer. All previous works of the  $E_s$  lunar tidal variations by various researchers and newly obtained results of these variations are described here and compared with the lunar tides in other ionospheric layers and with radio observations of lunar tidal winds in the  $E$ -layer.

Behavior of the  $E_s$  lunar tidal variations is different in middle latitudes (the zone in which  $|B_z| \geq$  about 0.3 gauss, where  $B_z$  is the vertical component of the earth's main magnetic field), low latitudes (about  $0.04 \leq |B_z| <$  about 0.3 gauss), and particularly the magnetic equatorial zone ( $|B_z| <$  about 0.04 gauss). These different behaviors of the  $E_s$  lunar tidal variation is explained theoretically, taking into consideration vertical upward drift motions of charged particles due to the lunar geomagnetic current system and a lunar equatorial electrojet.

## 1. INTRODUCTION

Periodic oscillations of ionospheric parameters, such as height and electron density, plotted with respect to lunar time, have been called the ionospheric lunar tide, which name has come from the analogous oscillation of the ocean and the surface atmosphere. The main period of this ionospheric lunar tidal oscillation is, of course, 12 lunar hours or the semi-diurnal oscillation.

Two main methods have been employed for the analysis of the lunar tide. The first method is described in detail in Chapter 8 of Geomagnetism by Chapman and Bartels (1940). Residual hourly departures from the monthly mean values of ionospheric data in solar time are arranged in lunar time reckoned from lower transit, counting 25 solar hours to a lunar day, and an average variation with respect to lunar time during one lunar month is obtained. After repeating this process and removing a non-cyclic variation, an average variation with respect to lunar time during each season or several lunar months or years is expanded in a harmonic series; the second harmonic indicates the semi-diurnal lunar variation. Its phase,  $t_2$ , indicating a lunar time at which the maximum variation occurs, and its amplitude,  $P_2$ , which is one-half of the total variation, are used for the presentation of the results. The weight of each determination is roughly proportional to  $\sqrt{n}$ , where  $n$  is the number of months' data examined.

The second method is due to Chapman and Miller (1940), and its practical application in detail is described by Tschu (1949) and corrected

by Chapman (1952). In this method the ionospheric data are divided into 12 lunar age groups. The 12 sets of average values, or sequences, of the data in each lunar age group show an ionospheric variation with the lunar age; an overall average value, or sequence, obtained from all these 12 sets may indicate an ionospheric lunar variation after the expansion in a harmonic series. In both methods we need, of course, a careful study of probable errors involved in the analysis. For this purpose, harmonic dials and probable error circles or ellipses are often provided in a similar way as is discussed in Chapter 19 of Geomagnetism.

It should be emphasized here that in the ionospheric atmosphere neutral particles are much more numerous than charged particles and that the latter do not always follow the former's group motion due to the gravitational pull of the moon because of the effect of electric and the earth's magnetic fields. The lunar tidal variation in the ionosphere calculated by the above mentioned methods using ionospheric data obtained by radio waves indicates lunar variations of only charged particles and does not directly indicate that of neutral particles. Thus, for the explanation of lunar tides of the  $E_s$ , drift motions of charged particles due to both electric and magnetic fields should be taken into consideration in addition to lunar tidal motions of neutral particles estimated from geomagnetic variations.

## 2. OBSERVATIONS OF THE $E_s$ LUNAR VARIATIONS

Observed data of the  $E_s$  by vertical-incidence ionosondes are not always very accurate and meaningful, because they are influenced by sensitivities of different ionosondes and also by the absorption of radio waves in the lower ionosphere. Moreover, the "critical frequency",  $f_oE_s$ , cannot always indicate the maximum electron density and is sometimes ambiguous, such as in the equatorial  $E_s$  ( $E_s-q$ ). However, both  $f_oE_s$  and  $h'E_s$  are not meaningless parameters of the  $E_s$  if they are treated carefully. In fact, careful statistical studies of these data give rather reliable results of large lunar variations of the  $E_s$ .

Matsushita (1952, 1953a) first found that the  $E_s$  in middle latitudes and the magnetic equatorial zone shows obvious lunar variations and suggested that this phenomenon may throw some light on the estimation of the  $E_s$  structure. He established that occurrence frequencies of large value of  $f_oE_s$  and of weak or nonexistent  $E_s$  clearly depend on lunar time (see Figs. 1 and 2), and also that values of  $f_oE_s$  and even  $h'E_s$  indicate semi-diurnal lunar variations.

Figure 1 shows average occurrence frequencies of  $f_oE_s$  larger than 10 Mc/s observed at Kokubunji, Tokyo, in summer according to lunar time. Occurrence frequencies of  $G$ - and  $E$ -letter symbols in the  $f_oE_s$  data obtained at Kokubunji, Brisbane and Huancayo are shown in Fig. 2 as a

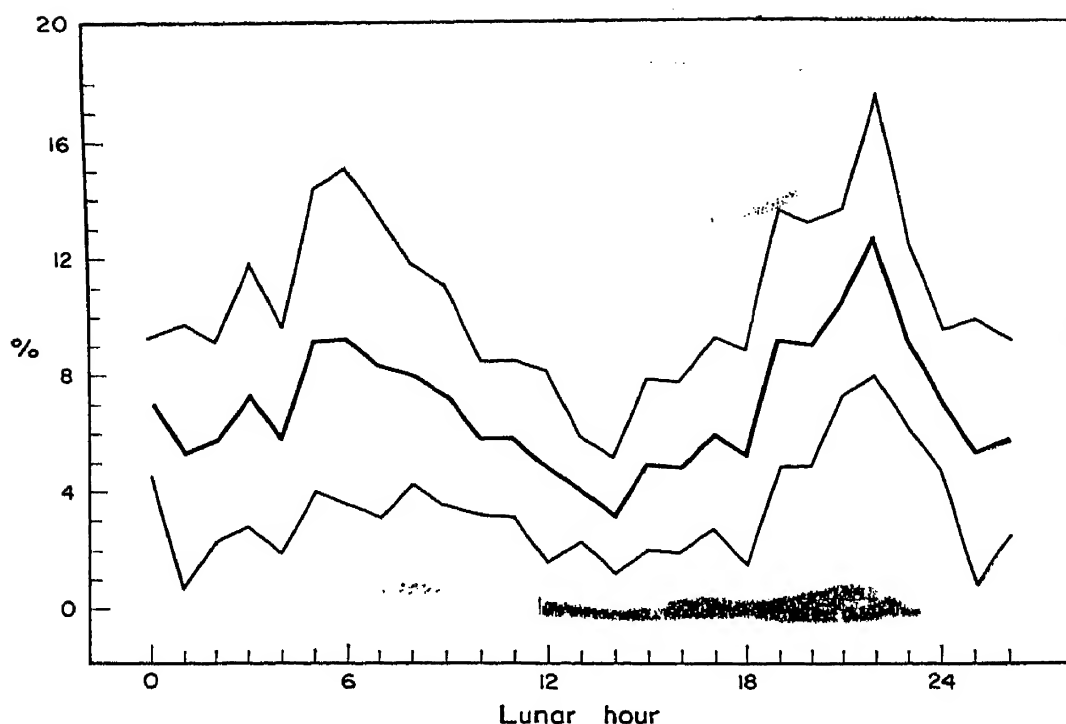


Fig. 1. The thick line is average occurrence frequencies in each lunar time of the  $f_o E_s$  hourly values larger than 10 Mc/s observed at Kokubunji for the summer months of 1949–1951. Almost all errors are contained in the band between the two thin lines.

function of lunar time. The  $G$ -symbol is used in the daytime, the  $E$ -symbol at night, and both indicate absence of  $E_s$  or small  $f_o E_s$  less than the minimum used radio frequency of ionosonde. The  $G$ -symbol also may mean that the  $E_s$  is blanketed by the normal  $E$ -layer. Then Fig. 2 indicates that low values of  $f_o E_s$  or nonexistent  $E_s$  often occur at about 02 00 and about 14 00 hr lunar time, at which times high values of  $f_o E_s$  occur less frequently, as seen in Fig. 1. Also, the lunar time at which high values of  $f_o E_s$  often occur is the time at which low values of  $f_o E_s$  occur less frequently. Thus the phenomenon indicated in Fig. 1 is consistent with that in Fig. 2. Accordingly, we can verify that the  $E_s$  has a semi-diurnal lunar tide even from occurrence frequencies.

Average lunar variations of  $f_o E_s$  obtained at Slough, Washington, Kokubunji, Brisbane and Huancayo are shown in Fig. 3, and harmonic dials are presented in Fig. 4. The lunar variation of  $f_o E_s$  in the magnetic equatorial zone was also obtained by Wright and Skinner (1959) for Ibadan, and Fig. 5 is the harmonic dial of their results; a seasonal variation can be seen. They also obtained a semi-diurnal lunar variation of the apparent partial reflection coefficient of  $E_s$  at solar noon. This parameter is free from the objections to  $f_o E_s$  data, since the effect of absorption is largely eliminated by comparing the amplitude of the  $E_s$  and the  $F2$  reflected echoes, and the equipment sensitivity is monitored daily. The phase of lunar tide of this parameter agrees quite well with that of  $f_o E_s$ . This suggests that  $f_o E_s$  is a reliable indicator of lunar tidal variations of the  $E_s$ .

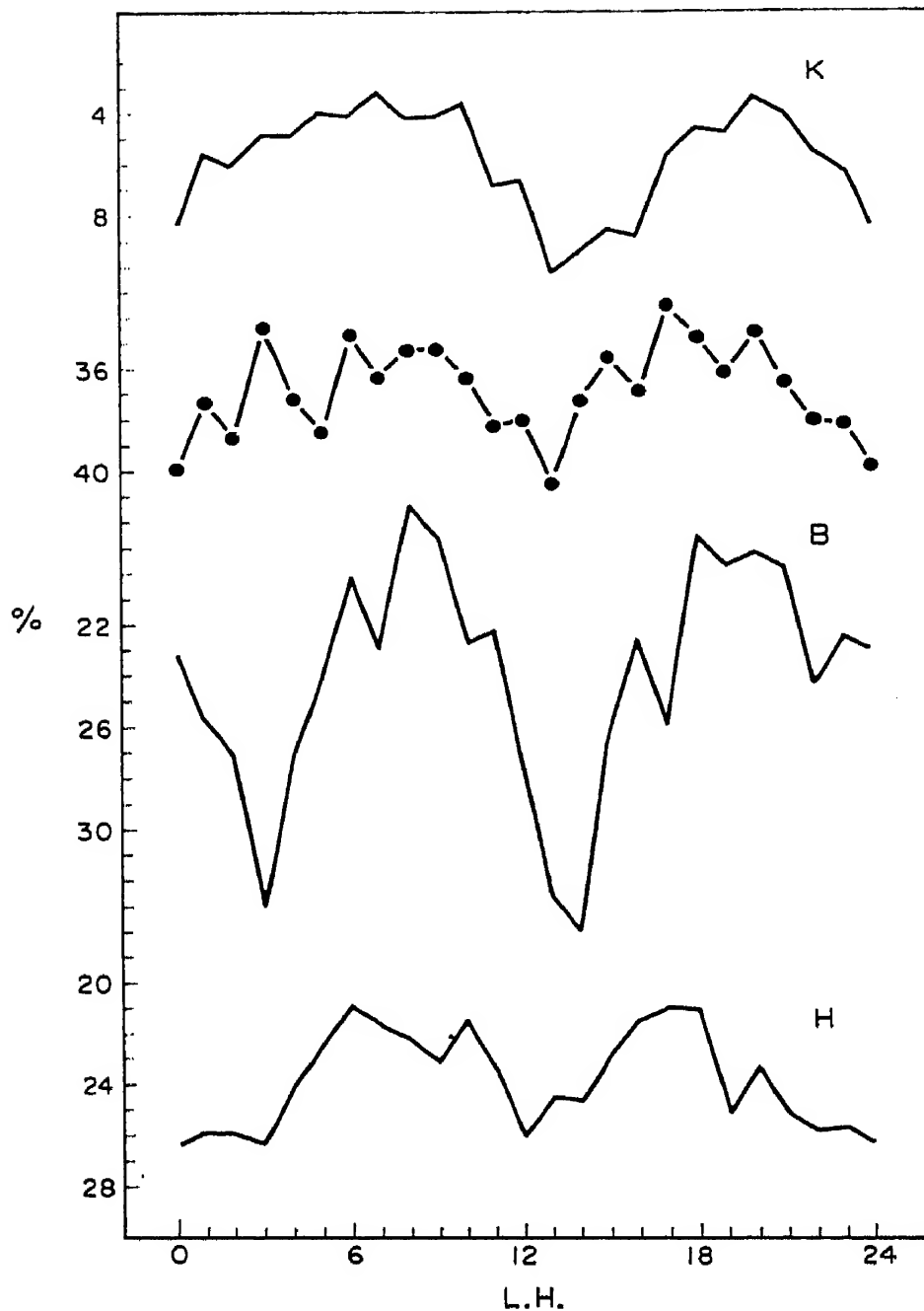


Fig. 2. Average occurrence frequencies in each lunar time of the G- and E-symbols in the  $E_s$  data (which indicate very low values of  $f_oE_s$  or nonexistence of  $E_s$ ) at Kokubunji (the full and chain lines represent summer and winter months of 1949–1951, respectively), Brisbane (summer months of 1950–1952), and Huancayo (all months of 1951). The ordinate graduates downward.



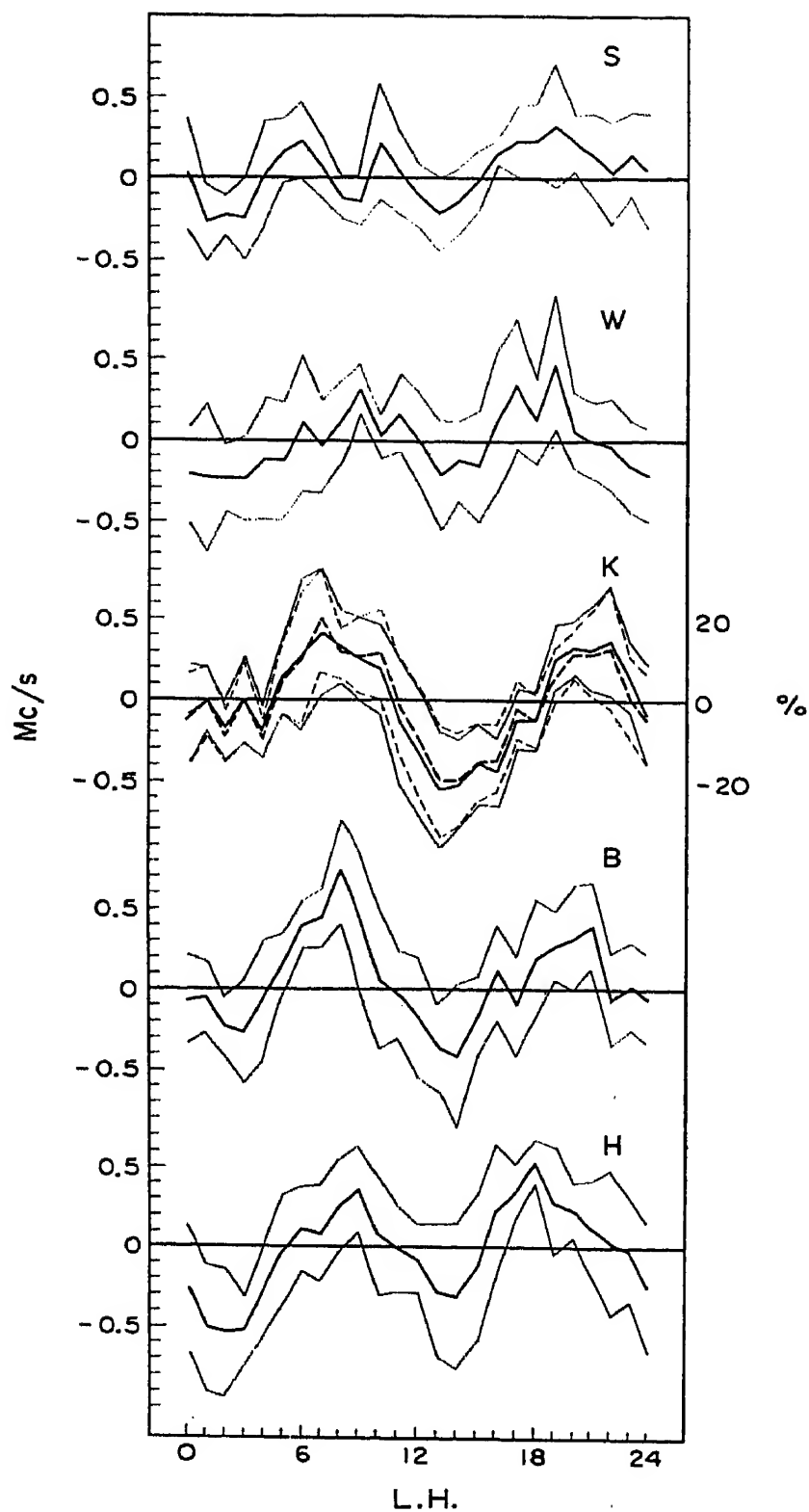


Fig. 3. Thick lines are average lunar variations of  $f_o E_s$  at Slough (1950–1951), Washington (1949–1951), Kokubunji (1949–1951), and Brisbane (1950–1952), for summer months, and at Huancayo for southern solstitial months of 1951. The thick broken line is for  $(200 \Delta f_o E_s / \text{Median } f_o E_s)$  in per cent at Kokubunji. Almost all errors are contained in each band between the two thin lines.

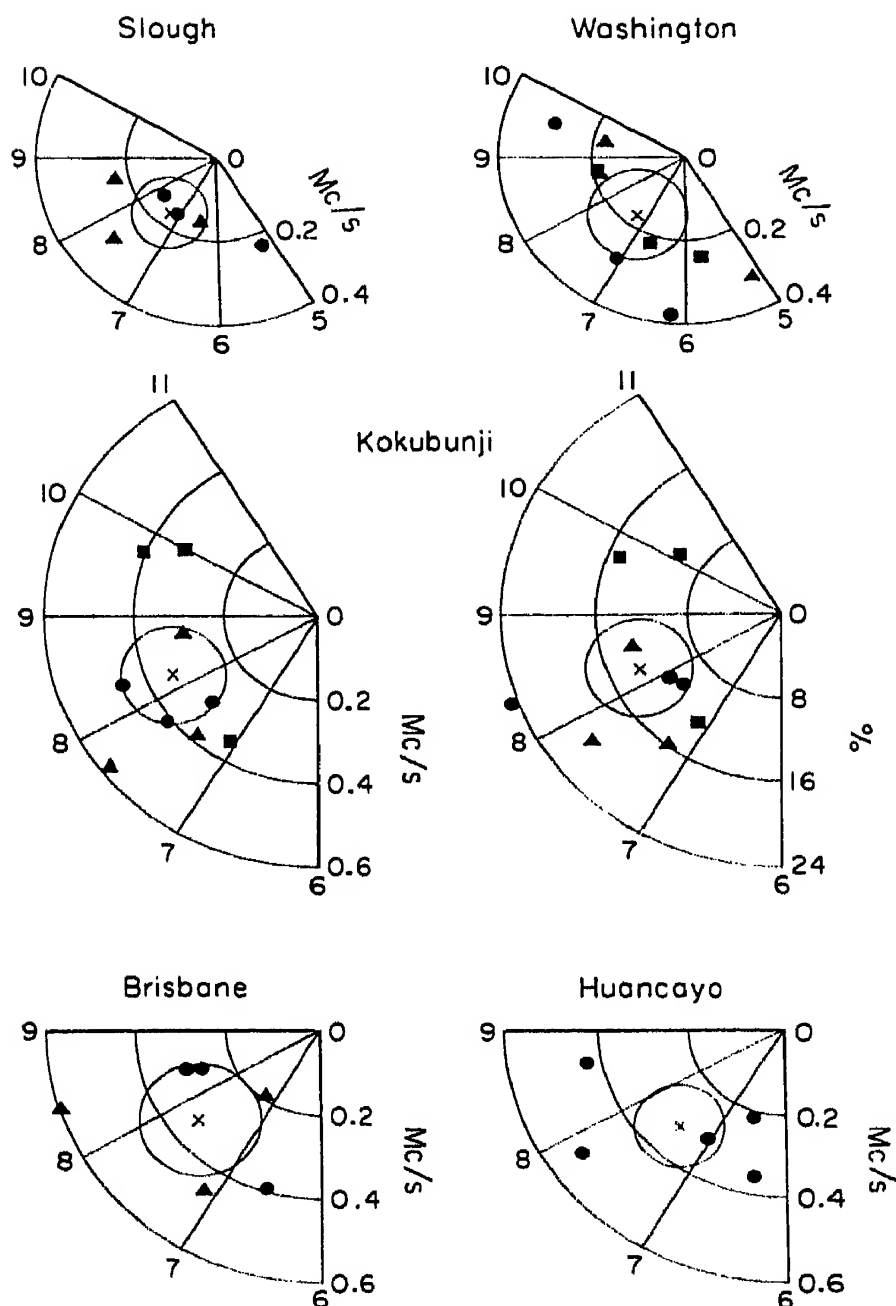


Fig. 4. Harmonic dials and probable error circles of semi-diurnal lunar variations of  $f_o E_s$  for Slough, Washington, Kokubunji (left) and Brisbane, in summer, and for Huancayo in southern solstitial months of 1951. The dial in the right middle is for  $(200 \Delta f_o E_s / \text{Median } f_o E_s)$  obtained at Kokubunji. Squares, triangles, and dots in dials, except for Brisbane, indicate results obtained from the data of 1949, 1950, and 1951, respectively; crosses are mean values. Triangles and dots in the dial for Brisbane show results from the data of summer months 1950–51 and 1951–52, respectively.

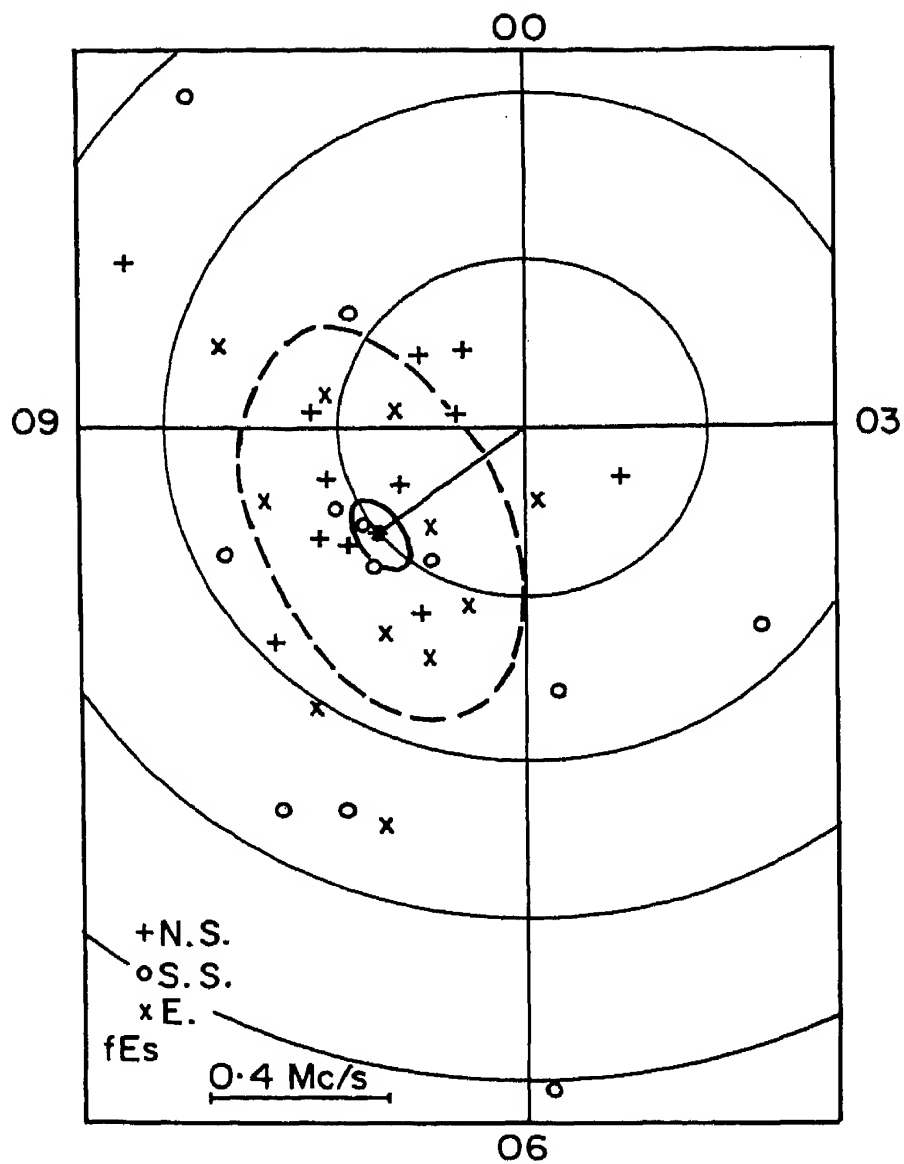


Fig. 5. Harmonic dial of semi-diurnal lunar variations of  $f_oE_s$  obtained at Ibadan by Wright and Skinner (1959). Each point represents one month's data.

As can be seen in Fig. 6, the lunar times at which the  $G$ - and  $E$ -symbols in the  $E_s$  data obtained at Panama Canal (geographic  $9.4^\circ\text{N}$ ,  $79.9^\circ\text{W}$ ) often occur are different from those in middle latitudes and the magnetic equatorial zone. This indicates that the maximum of the semi-diurnal lunar variation of  $f_o E_s$  at the former station in summer during the IGY occurs about three hours earlier than in the latter zones. Then we may roughly conclude that the phase of semi-diurnal lunar variation of  $f_o E_s$  in middle latitudes is similar to that in the magnetic equatorial zone but is different from that in low latitudes.

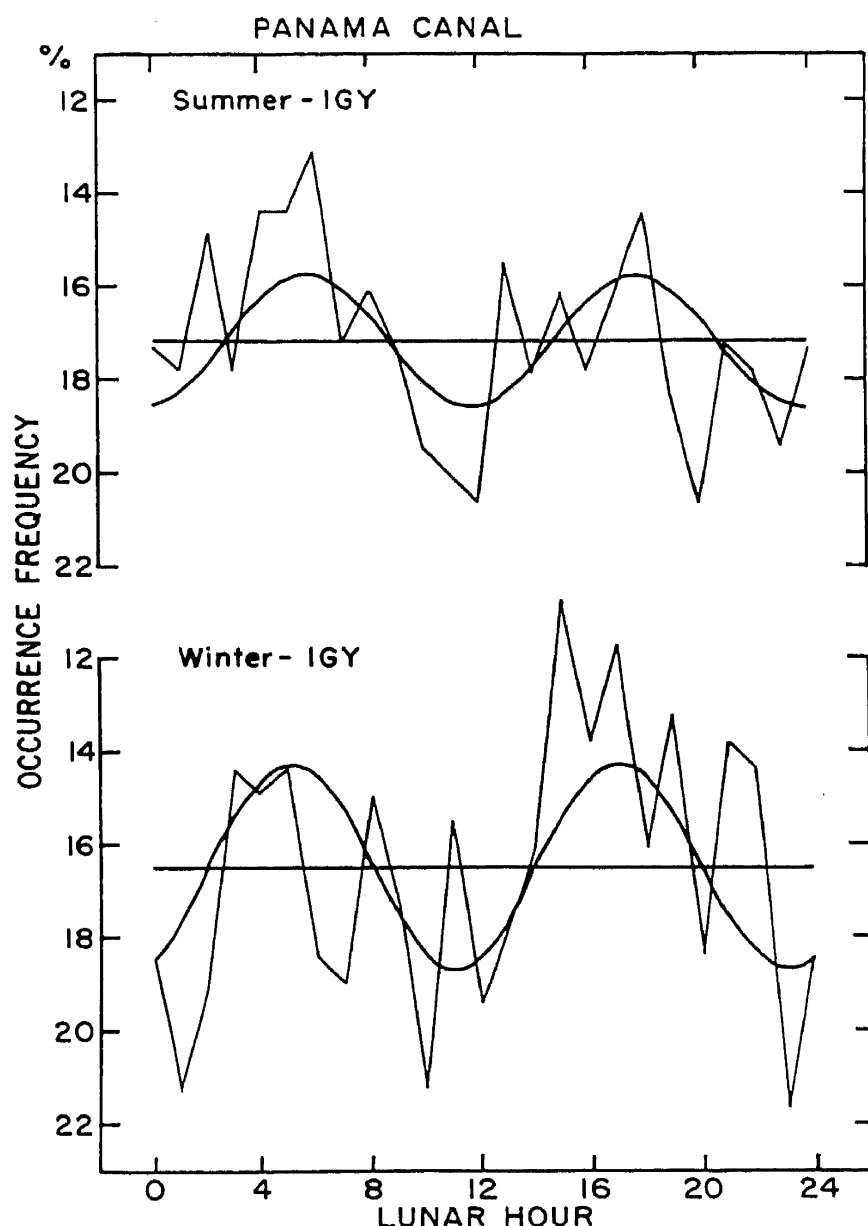


Fig. 6. Average occurrence frequencies in each lunar time of the  $G$ - and  $E$ -symbols in the  $E_s$  data (which indicate very low values of  $f_o E_s$  or absence of  $E_s$ ) at Panama Canal in summer months (top) and winter months (bottom) during the IGY. The smooth curves are the second harmonic of the lunar daily variation of the occurrence frequency. The ordinate graduates downward. A phase shift is noticed between this and Fig. 2.

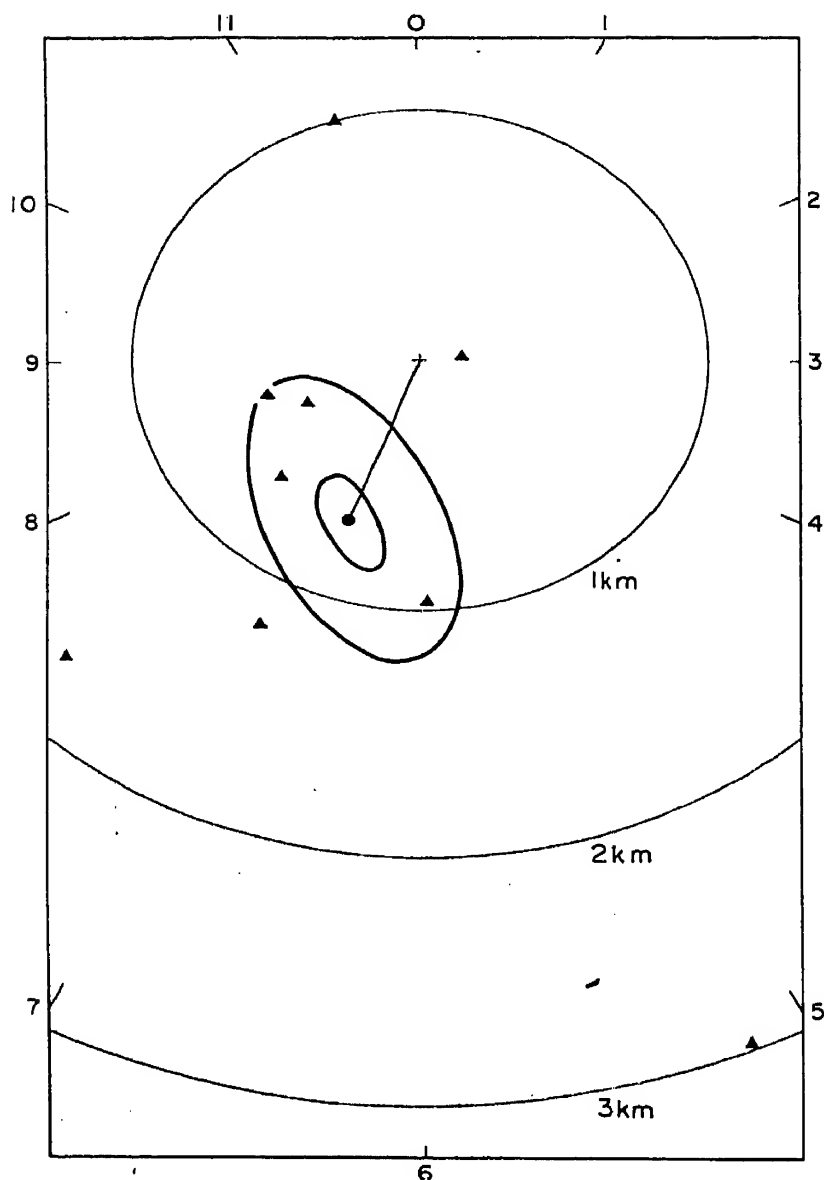


Fig. 7. Harmonic dial of semi-diurnal lunar variations of  $h'E_s$  obtained at Brisbane by Thomas and Svenson (1955). ▲ Individual months, ● mean.

Matsushita (1953a) obtained lunar tidal variations of  $h'E_s$  for five widely spread stations using routinely published data, and Wright and Skinner (1959) obtained lunar  $h'E_s$  variations for Ibadan using daytime data which were carefully scaled on routine ionograms. Thomas and Svenson (1955) examined the lunar tide of  $h'E_s$  for Brisbane using special night-time measurements (see Fig. 7), and Swarm and Helliwell (1956) studied it for Stanford using a special technique of height observation. Gazzard (1958) made a similar analysis of Brisbane  $h'E2_s$  data for 1952–1953 and obtained 1.5 km and 1.5 hr for amplitude and phase.  $E2_s$  is a sporadic  $E$  which appears at about 140 km in Australia, but it is not internationally accepted. The  $E2_s$  result cannot be compared with other results of the  $E_s$ .

All studies of semi-diurnal lunar variations of  $f_oE_s$  and  $h'E_s$  are compiled in Table 1. In middle latitudes and the magnetic equatorial zone the maximum of the  $f_oE_s$  semi-diurnal lunar variation occurs at 07 00–08 00 hr and has an amplitude of 0.2–0.4 Mc/s. The maximum of  $h'E_s$  lunar tide occurs at 06 00–07 00 hr in both middle latitudes and the magnetic equatorial zone, but the amplitude in the latter zone is much smaller than that in middle latitudes. Then we may conclude that the behavior of the lunar tidal variation of the  $E_s$  is slightly different in the three zones, middle latitudes, low latitudes and the magnetic equatorial zone.

In order to compare the semi-diurnal lunar variation of the  $E_s$  with that in the  $E$ -layer, Table 2 is provided, in which all previous results of the variation in the  $E$ -layer are compiled. Since the maximum electron number density,  $N_m$ , can be obtained by

$$N_m = 1.24 \times 10^4 f_o^2, \text{ here } f_o \text{ is in Mc/s,}$$

$(200 \Delta f_o / \text{Mean } f_o)$  in Table 2 approximately indicates  $(\Delta N_m / \text{Mean } N_m)$  in per cent, where  $\Delta$  indicates the difference from the mean value. There can be seen a six-hour phase lag of  $h'E$  between Slough and Canberra, which was an important fact in Martyn's theory (1948) of ionospheric lunar tide. However, these early observations of the  $E$ -layer unfortunately include both the  $E$  and the  $E_s$  in the data. Since the  $E_s$  has a remarkable lunar tidal variation, it should be carefully excluded from the  $E$  data, in order to study only the  $E$  lunar tide. The study at Ottawa in Table 2 took this fact into consideration but showed an uncertain result, as is indicated in the table. Thus the real existence of a lunar variation of the  $E$ -layer cannot yet be taken as established, although Harnischmacher (1955) mentions that there remains a small lunar influence in the  $E$ -layer when the effect of season, solar activity and solar local time are removed. It is very interesting that the  $E_s$  has large and obvious lunar variations in spite of a very small lunar effect in the  $E$ -layer. Matsushita (1962) thoroughly reviewed lunar tides in all ionospheric layers and concluded that except for  $E_s$  only the  $F2$ -layer has obvious lunar variations. The amplitude of lunar variation of  $f_oE_s$  is larger than that of  $f_oF2$ , although the amplitude of the  $h'E_s$  lunar variation is smaller than that of the  $F2$  height variation.

Observed results of lunar tidal winds in the  $E$ -region by radio fading methods are all collected in Table 3. There is one more report by Harnischmacher and Rawer (1958), who observed the direction of the  $E$ -region motion at Freiburg in the fall of 1956 and 1957 with the fading method and established that daily variations of the direction of the motion vary with the lunar age. These observed results are discussed in the next section from the view of lunar tidal winds directly responsible for geomagnetic lunar variations and indirectly for the  $E_s$  lunar variations.

Table 1—Semi-diurnal lunar variations of the  $E_s$ 

Station	$f_o E_s$			$h' E_s$			Studied by
	$P_2$	$t_2$	$n$	$P_2$	$t_2$	$n$	
Slough 51.5°N 0.6°W	Mc/s 0.17	hr 7.2	8 May-Aug. '50-'51	km	hr		MATSUSHITA, 1953a
Washington 39.0°N 77.5°W	0.17	7.2	12 May-Aug. '49-'51	0.46	5.8	13 '49-'50	MATSUSHITA, 1953a
Stanford 37.4°N 122.2°W				0.59	6.4	6	SWARM & HELLIWELL, 1956
Kokubunji 35.7°N 139.5°E	0.35*	8.2	12 May-Aug. '49-'51				MATSUSHITA, 1952, 1953a
Ibadan 7.4°N 3.9°E	0.41	7.5	36 7-17 G.M.T. Nov. '53- Oct. '56	0.22	7.0	12 8-16 G.M.T.	WRIGHT & SKINNER, 1959
Huancayo 12.1°S 75.3°W	0.33	7.5	6 Nov.-Feb. '50-'51	0.19	1.3?	13 '51-'52	MATSUSHITA, 1953a
Brisbane 27.5°S 152.9°E	0.34	7.7	8 May-Aug. '50-'52	0.70	5.7	13 '51-'52	MATSUSHITA, 1953a
				0.69	6.7	12 night Dec. '52- Nov. '53	THOMAS & SVENSON, 1955

\*  $P_2$  for  $(200 \Delta f_o E_s / \text{Mean } f_o E_s)$  is 13.3 per cent

Table 2—Semi-diurnal lunar variations of the *E*-layer

Station	200 $\Delta f_o E$ / Mean $f_o E$			$f_o E$			$h' E$			Studied by
	$P_2$	$t_2$	$n$	$P_2$	$t_2$	$n$	$P_2$	$t_2$	$n$	
	%	hr		Mc/s	hr		km	hr		
Slough 51.5°N 0.6°W							0.93	11.25	12	APPLETON & WEEKES, 1938, 1939
Freiburg 48.1°N 7.6°E							0.07	8.5	'49-'59	ROUGERIE, 1961
Ottawa 45.4°N 75.7°W							1.46	5.7	1952	LITTLEWOOD & CHAPMAN, 1953
							0.40	9.5	May-Aug. 1954	DATARS, 1954
							0.50	0.5- 5.9	12 Sept. '54- Sept. '55	JELLY, 1956
							0.36- 0.59	1.1- 10.7	Apr.-Sept. 1956	HOGG, 1956
Ashkhabad 37.9°N 58.4°E				0.013	3.9	~90				BENKOVA & ZAGULYAEVA, 1960
Brisbane 27.5°S 152.9°E							0.5	4.5	June '43- Dec. '47	MARTYN, 1950
Canberra 35.3°S 149.2°E	0.26	3.8	120 '37- '46	0.13	4.8	48 '41- '44	0.19	5.1	48 '41-'44	MARTYN, 1948



Table 3—Semi-diurnal lunar winds observed in the *E*-region

Station	Northward	Eastward	Data Period	Studied by
Cambridge 52.2°N 0.1°E	$\frac{P_2}{m/s}$ 14	$\frac{P_2}{m/s}$ 16	day, '49-'51	PHILLIPS (reported by Briggs & Spencer, 1954)
	$\frac{t_2}{hr}$ 2.9	$\frac{t_2}{hr}$ 5.7		
	Not detectable (<10 m/s)		day, '49-'51	PHILLIPS, 1952
	Not detectable (<10 m/s)		day, June '52	SPENCER, 1954
Montreal 45.4°N 73.8°W	14?	12?	day, Sept. '52	SPENCER, 1954
	24	21	mainly day, '50-'51	CHAPMAN, 1953
Washington 39.0°N 77.5°W	Not detectable (<10 m/s)		day, '51-'52	GREENSTONE (reported by Briggs & Spencer, 1954)

3. THEORY OF THE  $E_s$  LUNAR VARIATIONS

All components of the geomagnetic variation field indicate a semi-diurnal lunar variation. The only reasonable explanation of this phenomenon is a dynamo theory. A coupling effect of the vertical component of the earth's main magnetic field,  $B_z$ , and a horizontal wind system at about 100 km altitude in the ionosphere, due to the lunar tidal force in that region, causes an electric current system in this electrically conductive region; this electric current system may be the cause of the lunar magnetic variation. Based on geomagnetic data obtained at five stations, Pavlovsk, Pola, Zikawei,

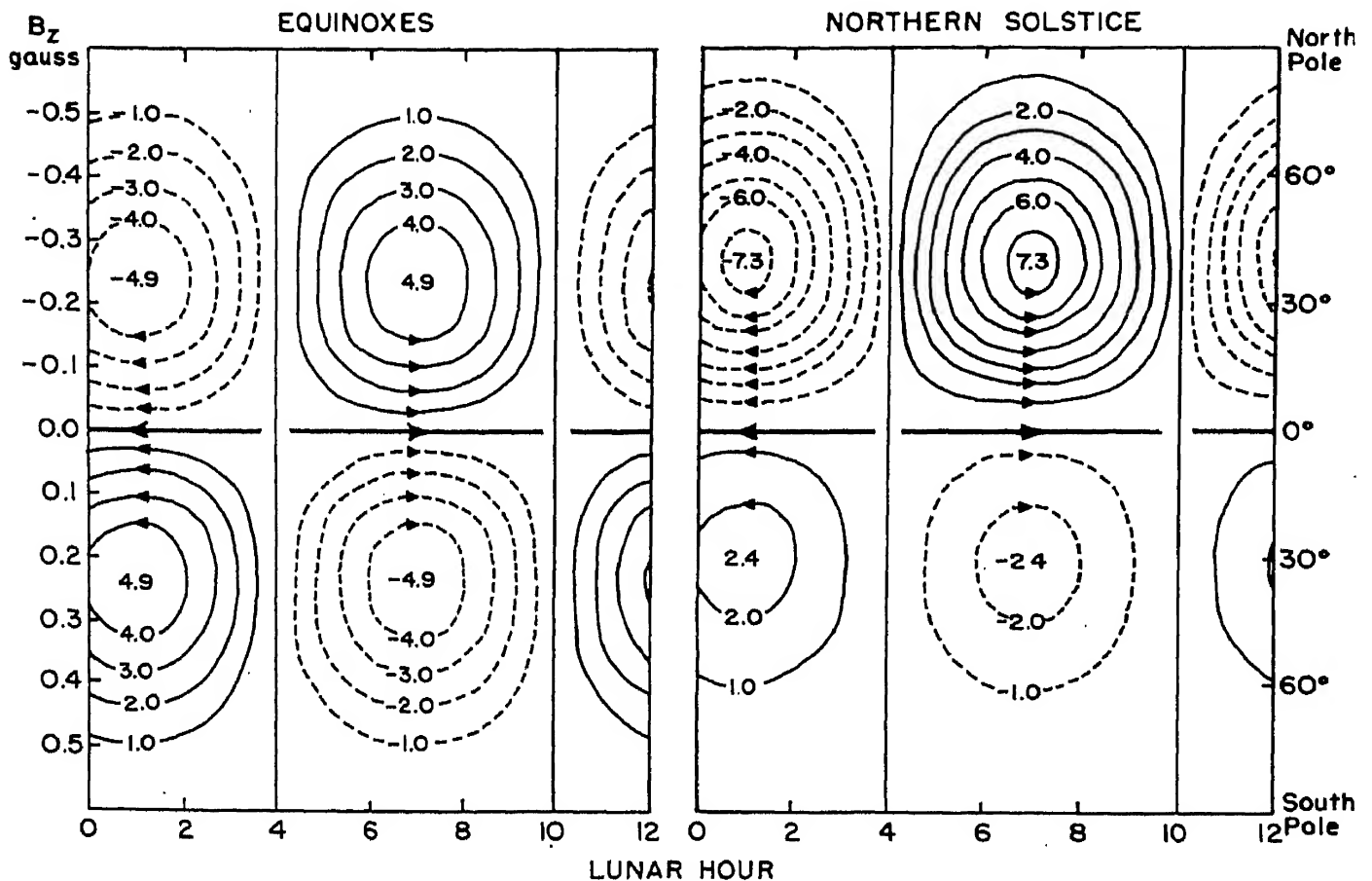


Fig. 8. Speculated lunar electric currents and lunar equatorial electrojet in the ionosphere at about 100 km altitude. These are mean for a lunation in equinoxes (left) and in northern summer (right). The current-lines are drawn at intervals of 1000 amperes.

Manila, 1897–1930, and Batavia 1888–1890, Chapman and Bartels (1940) obtained a current system. However, this current system was not always satisfactory in comparison with actual lunar variations derived from each component of geomagnetic data. Using recently obtained results of lunar geomagnetic analysis and recently developed theories and values of the anisotropic electrical conductivities in the ionosphere, Matsushita (1962) suggested a new current system which is responsible for the semi-diurnal lunar geomagnetic variation (see Fig. 8). The following five points must be emphasized in regard to this current system:

(1) The meridian on which the center or focus of the oval current systems is located will be higher in summer than in winter.

(2) In order to eliminate longitudinal inequalities, the best ordinate of the current system will be  $B_z$ , in the same way as was suggested by Matsushita (1960) for the solar quiet daily current system,  $Sq$ .

(3) The intensity of the lunar current in summer will be about three times larger than that in winter, based on an analysis of lunar geomagnetic variations.

(4) It is doubtful that the current system in the summer hemisphere flows over even  $30^\circ$  latitude in the winter hemisphere, such as is indicated by Chapman and Bartels. The boundary between current systems in the summer hemisphere and in the winter hemisphere usually seems to be the magnetic equator, in the same manner as in equinoxes.

(5) During solar daylight hours, a lunar equatorial electrojet seems to flow in a narrow zone centered on the magnetic equator. This is an analogy with the equatorial electrojet in the solar geomagnetic variation due to high Cowling electric conductivity during solar daytime.

As an approximation of the current system shown in Fig. 8, except the magnetic equatorial zone, we may indicate a current function  $R$  by

$$R = a \times 10^{-6} \cos(2\lambda + 150^\circ) P_3^2 \text{ e.m.u.},$$

where  $a$  is the distance between the earth's center and the layer in which the lunar current flows,  $P_3^2$  is the Schmidt's normalized spherical function and  $\lambda$  is the lunar local time reckoned in angular measure. An estimation of the distribution of gas density and of other physical behavior with height based on rocket observations leads to

$$\Sigma_1 = 6.9 \times 10^{-9} \text{ e.m.u. and } \Sigma_2 = 1.5 \times 10^{-8} \text{ e.m.u.},$$

where  $\Sigma_1$  and  $\Sigma_2$  are total Pedersen and total Hall conductivities, respectively (Matsushita 1953b). Except for the magnetic equatorial zone, then, we can calculate the electric field  $E$  at different locations as is shown in Fig. 9, and also, we can obtain the southward and eastward components of the lunar tidal wind velocity,  $V_x$  and  $V_y$ , as follows:

$$V_x = 1.7 \sin \theta \cos \theta \sin(2\lambda + 60^\circ) \text{ m/sec},$$

and

$$V_y = 1.7 \sin \theta \sin(2\lambda + 150^\circ) \text{ m/sec},$$

where  $\theta$  is the colatitude (for its detail, see Matsushita (1962)). This is smaller than the value of the lunar wind observed by radio waves shown in Table 3 but is at least 100 times larger than the surface lunar tidal wind (Bartels 1928, Chapman 1951) and has a remarkable phase lag.

In the magnetic equatorial zone we have no dynamo electric field because  $B_z = 0$ , accordingly, we need not pay much attention to the lunar tidal wind. Let the subscripts  $x$  and  $y$  indicate the southward and eastward

components and  $I$  be the total electric current. Since  $I_x \sim 0$  in this zone,  $E_x \sim 0$ . Then the only electric field with which we are concerned is  $E_y$ , and

$$E_y \sim I_y/\Sigma_3 \sim \Delta X/2\pi\Sigma_3,$$

where  $\Delta X$  is the northward component of the lunar geomagnetic variation due to the external field, and  $\Sigma_3$  is the total Cowling conductivity. Taking  $\Delta X/2\pi \sim 0.5 \times 10^{-5} \sin(2\lambda + 240^\circ)$  e.m.u. based on results of  $\Delta X$  obtained at Huancayo and Ibadan and  $\Sigma_3 \sim 10^{-7}$  e.m.u. gives

$$E_y \sim 0.5 \times 10^2 \sin(2\lambda + 240^\circ) \text{ e.m.u.},$$

which is adopted for the equator in Fig. 9.

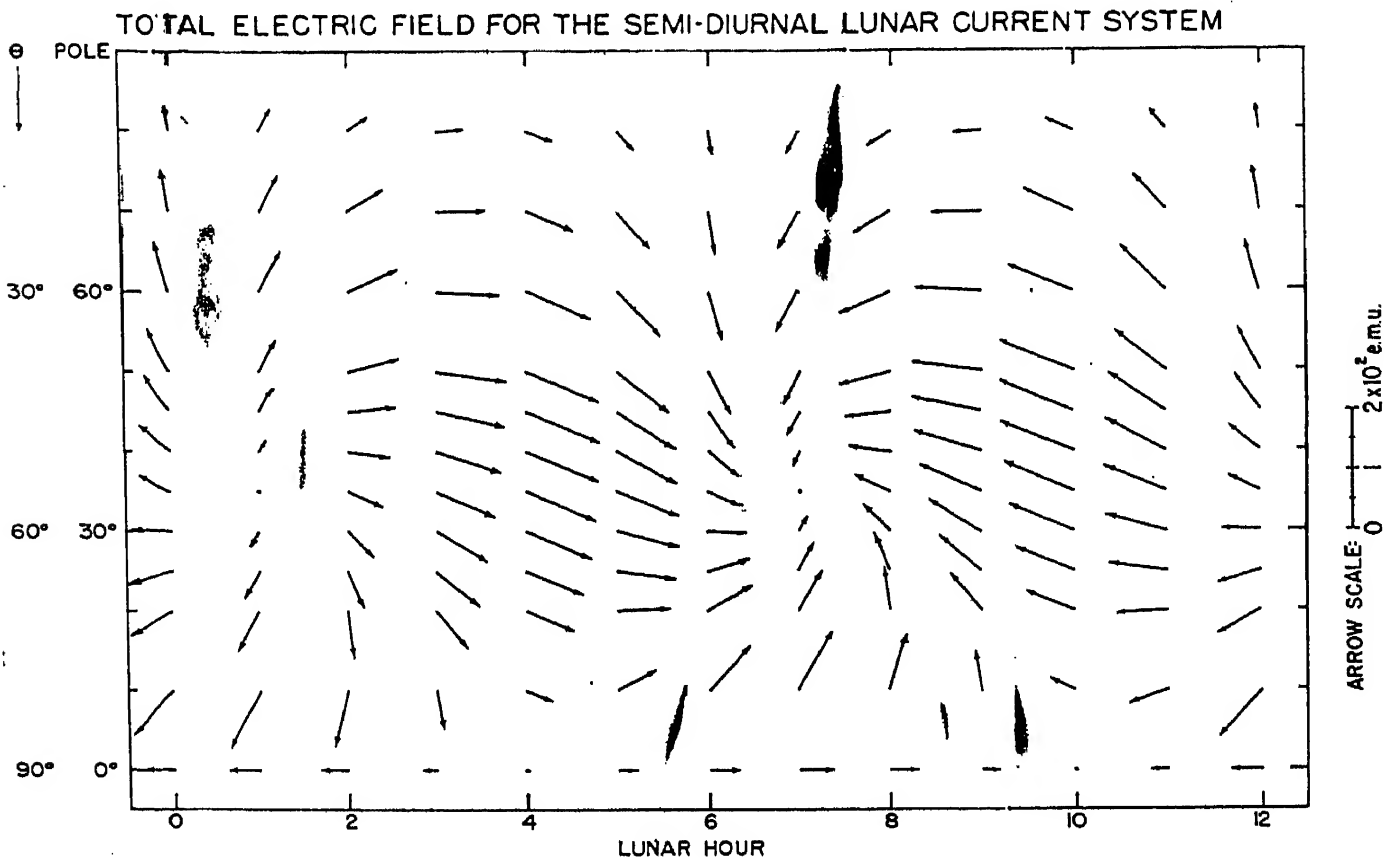


Fig. 9. Distribution of the total electric field for the lunar current system (equinoxes) in the northern hemisphere. The ordinate can also be shown by  $B_z$  as is indicated in Fig. 8.

These electric fields are an important factor in vertical drift motions of charged particles, since the vertical upward drift speed of electrons and ions,  $W$ , in the  $E$ -region can be represented by the following equations:

In the zone away from the magnetic equator

$$W = -\cot \phi (e/m_i) \{v_i/(\nu_i^2 + \omega_i^2)\} E_x + (q_i + q_e p_i/p_e) E_y, \quad (3.1)$$

and in the magnetic equatorial zone

$$\begin{aligned} W &= (q_r + e_r p_r \sigma_1/\sigma_2) E_y \\ &= \{(q_r + e_r p_r \sigma_1/\sigma_2)/\Sigma_3\} I_y. \quad (r = i \text{ and } e) \end{aligned} \quad (3.2)$$

Here the subscripts  $i$  and  $e$  indicate ions and electrons;  $m_r$ ,  $e_r$ ,  $\nu_r$ , and  $\omega_r$  are the mass, charge (in e.m.u.), collisional frequency with neutral particles, and gyrofrequency of a particle of the  $r^{\text{th}}$  kind of gas (i.e., ions and electrons);  $\phi$  is the magnetic dip angle;  $\sigma_1$  and  $\sigma_2$  are the Pedersen and Hall conductivities;  $B$  is the earth's main magnetic field; and

$$\begin{aligned} p_r &= (1/m_r \nu_r) \{ \nu_r^2 \cos^2 \phi / (\nu_r^2 + \omega_r^2) + \sin^2 \phi \}, \\ q_r &= (1/B) \{ \omega_r^2 / (\nu_r^2 + \omega_r^2) \} \cos \phi. \end{aligned}$$

At altitudes lower than about 120 km the second term of the right side of equation (3.1) is much smaller than the first term. Thus we have

$$W = -\cot \phi (e/m_i) \{ \nu_i / (\nu_i^2 + \omega_i^2) \} E_x. \quad (3.3)$$

Equation (3.3) can also show vertical drift speeds caused by other current systems, such as the  $Sq$  current, when  $E_x$  is obtained from these other currents. The value of  $W$  caused by the  $Sq$  current is generally much larger than that caused by the lunar dynamo current, because  $E_x$  of the former current is larger than that in the latter current. However, even this large  $W$  caused by the  $Sq$  current affects little of the electron density in the  $E$ -layer, which is almost in Chapman distribution. Then it is quite natural that we cannot establish the lunar variation in the  $E$ -layer due to the small lunar  $W$ . On the other hand large lunar variations of the  $E_s$  indicate that the way of formation of the  $E_s$ , whatever it is, should be very easily affected by the lunar  $W$ . One possible estimation which satisfies this condition is that the  $E_s$  away from the magnetic equator is thin ionized layers or clouds formed by vertical drift motions of charged particles, which have a sharp upward decreasing gradient. Equation (3.3) can also be used for this vertical motion, and  $W$ , hence  $E_x$ , should have a sharp upward decreasing gradient: vertical wind shears may produce such  $E_x$  (Matsushita 1962). Thus a suggestion that vertical wind shears are the major cause of the  $E_s$  in temperate latitudes can be made for the explanation of the  $E_s$  lunar tides, while the same conclusion from other data has been reached by Whitehead (1961). Details are discussed in other articles of this book by Whitehead and by Matsushita.

Let the drift speed responsible for the formation of the  $E_s$  in temperate latitudes be indicated by  $W_{E_s}$ , and another vertical drift speed caused by the lunar dynamo current system be indicated by  $W_L$ , both of which can be calculated by equation (3.3) using different values of  $E_x$ . Here  $W_{E_s}$  sharply decreases with height, but  $W_L$  does not change much with altitude. Let it be assumed that  $W_{E_s}$  distributes uniformly with lunar time. Since  $W_L$  is different at different lunar time, a superposed value of  $W_{E_s}$  and  $W_L$  changes with lunar time and indicates the lunar variation of  $h'E_s$ . In the lunar dynamo current, the maximum of  $E_x$ , hence that of  $W_L$ , occurs at about 06 00 hr lunar time in the zone  $\theta \leq 45^\circ$  and  $\theta \geq 135^\circ$  (or  $|B_z| > \text{about}$

0.3 gauss) as in seen in Fig. 9. Then the lunar variation of  $h'E_s$  reaches the maximum at this time due to the effect of  $W_{E_s} + W_L$ , and one or two hours later the lunar variation of  $f_oE_s$  may reach the maximum. In the same way, due to the effect of  $W_{E_s} - W_L$ , the lunar variation of  $h'E_s$  reaches the minimum at about 00 00 hr lunar time, and that of  $f_oE_s$  reaches the minimum at 01 00–02 00 hr. It is also understandable from this effect that large or small values of  $f_oE_s$  often occur at the time of the maximum or minimum of the lunar variation of  $f_oE_s$ , as is seen in Figs. 1, 2 and 3 and Table 1.

The maximum speed of  $W_L$  can be estimated as 2 to 4 per cent of the maximum\* of  $W_{E_s}$ . Then it is not difficult to explain the approximately 0.2 Mc/s amplitude of  $f_oE_s$  semi-diurnal lunar variation and several hundred meter amplitude of  $h'E_s$  lunar variation by this additional drift speed,  $W_L$ . For example, if  $W_L = 0.02 \times 3$  m/sec, the increased height of the  $E_s$  by  $W_L$  during three hours is 648 m, which is a proper value as is indicated in Table 1.

In low latitudes the maximum of  $E_x$ , hence the maximum of  $W_L$ , occurs earlier than that in middle latitudes as seen in Fig. 9. This will be the reason why the phase of lunar variation obtained at Panama Canal is different from the phase in middle latitudes.

In a narrow zone centered on the magnetic equator, one type of  $E_s$ , called equatorial  $E_s$  ( $E_{s-q}$ ), is predominant during daylight hours and has a correlation with the intensity of the solar equatorial electrojet (Matsushita 1951, also see the other article by the author in this book). As equation (3.2) can be applied to not only lunar but also solar equatorial electrojets, the vertical drift speeds,  $W_{s-q}$ , caused by the solar electrojet is proportional to the eastward intensity of the solar jet,  $I_y(S)$ . Then the correlation between the  $E_{s-q}$  and the jet-intensity,  $I_y(S)$ , may indicate that the  $E_{s-q}$  is correlated with  $W_{s-q}$ . Since the  $E_{s-q}$  itself seems to be irregularities or disturbances involved in the solar electrojet (see Bowles and Cohen's article in this book), it can be assumed that these irregularities, namely the  $E_{s-q}$ , are caused by  $W_{s-q}$ .

The  $E_{s-q}$  often disappears around noon or early afternoon solar local time, if these times lie between 00 00 and 03 00 or between 12 00 and 15 00 hr lunar time as shown in Fig. 10 (Matsushita 1955, 1957). This is confirmed by Egan (1960), and is consistent with a result obtained at Huancayo in Fig. 2, which indicates that low values of  $f_oE_s$  or absence of  $E_s$  occurs most frequently at 00 00–03 00 and 12 00–15 00 hr lunar time. An explanation of the  $E_{s-q}$  disappearance is as follows:

The lunar electric current systems responsible for the lunar geomagnetic variation is superposed on the solar electric current system. The manner

---

\* 3 to 5 m/sec. See Matsushita (1962).

of superposition of these two currents depends on the lunar age. At new and full moon, for example, a westward lunar electrojet flows in the magnetic equatorial zone at 00 00–03 00 and 12 00–15 00 hr lunar time. Then the vertical upward drift speed of charged particles,  $W_{S-q}$ , due to the eastward solar electrojet,  $I_y(S)$ , is weakened by the downward drift speed,  $-(W_{L-q})$ , due to the westward lunar electrojet,  $-I_y(L)$ , at these lunar times. Thus the  $E_s-q$  due to  $W_{S-q}$  disappears by the weakening of the upward motion, namely by the effect of  $(W_{S-q}) - (W_{L-q})$  caused by  $I_y(S) - I_y(L)$ .

This explanation was supported by Knecht (1959), who studied the variability of the time of first appearance of the  $E_s-q$  in the morning solar time. If the explanation is correct, during new and full moon the contribution of the lunar electric current is such that it adds to the eastward flowing solar electric current during the solar early morning hours 06 00–10 00 hr (i.e.,  $(W_{S-q}) + (W_{L-q})$ ); whereas during the first and third quarters the lunar contribution weakens the eastward flowing current during the solar early morning hours (i.e.,  $(W_{S-q}) - (W_{L-q})$ ). Then the  $E_s-q$  should appear earlier during the new and full moon and later at the first and third quarters, which was exactly the dependence obtained by him.

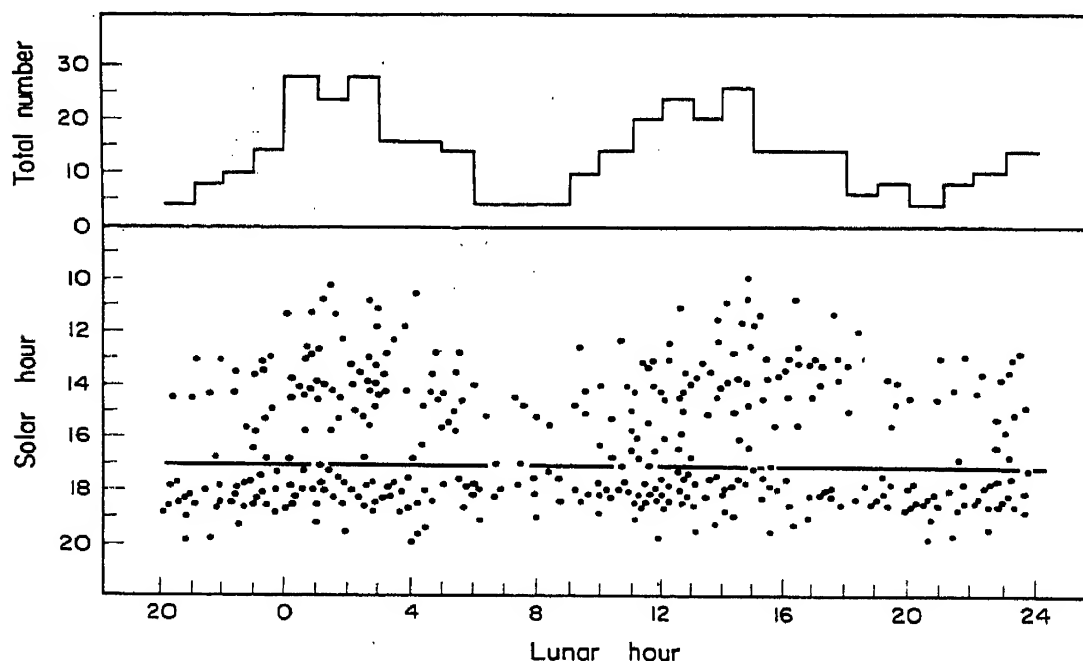


Fig. 10. Dots on lower graph indicate solar and lunar times of sudden disappearances of the equatorial  $E_s$ . Upper histogram indicates total number by lunar hour of such disappearances, which take place before 17 00 hr solar time.

It is also understandable that the phase of lunar variation of  $f_oE_s$  at Ibadan and Huancayo in Table 1 is 7.5 hr. because of the effect of  $(W_{S-q}) + (W_{L-q})$ . The amplitude of the  $f_oE_s$  lunar variation at these stations is a few per cent of  $f_oE_s$  during solar daytime;  $W_{L-q}$  is also a few per cent of  $W_{S-q}$ . It will also be due to  $(W_{S-q}) + (W_{L-q})$  that the phase

of  $h'E_s$  lunar variation at Ibadan is 7 hr. The reason that the amplitude of lunar variation of the  $E_s$  height at magnetic equatorial stations is smaller than that in middle latitudes is the different mechanisms of lunar variation of the  $E_s$  between the two zones.

Different behavior of the  $E_s$  lunar tidal variation in middle and low latitudes and the magnetic equatorial zone based on observations is thus explained, taking into consideration vertical upward drift motions of charged particles due to the lunar geomagnetic current system and a lunar equatorial electrojet, both of which are newly introduced.

In conclusion, the author wishes to thank the Boulder Laboratories of the National Bureau of Standards for extending him their facilities under his appointment as a guest worker. The work reported here was supported by the National Academy of Sciences under grant NSF-09427.

#### REFERENCES

- APPLETON, E. V. and WEEKES, K. (1938) *Nature* **142**, 71.  
 APPLETON, E. V. and WEEKES, K. (1939) *Proc. Roy. Soc. A* **171**, 171.  
 BARTELS, J. (1928) *Handbuch der Experimentalphysik*, Leipzig, Band 25, Teil 1, 163.  
 BENKOVA, N. P. and ZAGULYAEVA, V. A. (1960) I.A.G.A.-I.U.G.G. Helsinki Meeting.  
 BRIGGS, B. H. and SPENCER, M. (1954) *Rep. Prog. Phys.* **17**, 245.  
 CHAPMAN, J. H. (1953) *Canadian J. Phys.* **31**, 120.  
 CHAPMAN, S. (1952) *Aust. J. Sci. Res. A* **5**, 218.  
 CHAPMAN, S. and BARTELS, J. (1940) *Geomagnetism*, Clarendon Press, Oxford.  
 CHAPMAN, S. and MILLER, J. C. P. (1940) *Mon. Not. Roy. Ast. Soc. Geophys. Suppl.* **4**, 649.  
 DATARS, W. R. (1954) Radio Physics Lab. Project Report 3-1-2, Defence Research Telecommunications Establishment, Canada.  
 EGAN, R. D. (1960) *J. Geophys. Res.* **65**, 2343.  
 GAZZARD, A. D. (1958) *Aust. J. Phys.* **11**, 272.  
 HARNISCHMACHER, E. (1955) *C. R. Acad. Sci.* **240**, 553.  
 HARNISCHMACHER, E. and RAWER, K. (1958) *Geofisica Pura e Applicata* **39**, 216.  
 HOGG, D. E. (1956) Radio Physics Lab. Project Report 3-1-5, Defence Research Telecommunications Establishment, Canada.  
 JELLY, D. H. (1956) Radio Physics Lab. Project Report 3-1-4, Defence Research Telecommunications Establishment, Canada.  
 KNECHT, R. W. (1959) *J. Atmosph. Terr. Phys.* **14**, 348.  
 LITTLEWOOD, C. A. and CHAPMAN, J. H. (1953) Radio Physics Lab. Project Report 3-1-1, Defence Research Telecommunications Establishment, Canada.  
 MARTYN, D. F. (1948) *Proc. Roy. Soc. A* **194**, 429.  
 MARTYN, D. F. (1950) U.R.S.I. Special Report No. 2, Brussels.  
 MATSUSHITA, S. (1951) *J. Geomag. Geoelect.* **3**, 44.  
 MATSUSHITA, S. (1952) *J. Geomag. Geoelect.* **4**, 39.  
 MATSUSHITA, S. (1953a) *Rep. Ionosph. Research Japan* **7**, 45.  
 MATSUSHITA, S. (1953b) *J. Geomag. Geoelect.* **5**, 109.  
 MATSUSHITA, S. (1955) *J. Geomag. Geoelect.* **7**, 91.  
 MATSUSHITA, S. (1957) *J. Atmosph. Terr. Phys.* **10**, 163.  
 MATSUSHITA, S. (1960) *J. Geophys. Res.* **65**, 3835.  
 MATSUSHITA, S. (1962) *Handbuch der Physik* (in press).  
 PHILLIPS, G. J. (1952) *J. Atmosph. Terr. Phys.* **2**, 141.



ROUGERIE, P. (1961) *Ann. de Géophys.* 17, 145.

SWARM, H. M. and HELLIWELL, R. A. (1956) U.S.A. U.R.S.I.-I.R.E. Fall 1956 Meeting.

THOMAS, J. A. and SVENSON, A. C. (1955) *Aust. J. Phys.* 8, 554.

TSCHU, K. K. (1949) *Aust. J. Sci. Res. A* 2, 1.

WHITEHEAD, J. D. (1961) *J. Atmosph. Terr. Phys.* 20, 49.

WRIGHT, R. W. and SKINNER, N. J. (1959) *J. Atmosph. Terr. Phys.* 13, 217.

# On the Width of the Equatorial $E_s$ Belt

R. W. KNECHT and R. E. McDUFFIE

National Bureau of Standards, Boulder, Colorado, U.S.A.

**Abstract**—This short paper reports an analysis of two years observations of equatorial sporadic  $E$  taken at a chain of vertical soundings stations in the vicinity of the magnetic equator in Peru. The results suggest that equatorial  $E_s$  occurs in a belt having a width of about 700 kilometers which agrees very well with the width for the equatorial electrojet as deduced from geomagnetic observations.

One of the least sporadic kinds of sporadic  $E$  observed at vertical incidence is the so-called equatorial or Huancayo type, now internationally designated  $E_s-q$ .  $E_s-q$  occurs regularly during the daylight hours in a narrow belt close to the magnetic equator. Usually it is readily distinguishable from the other types of  $E_s$  seen on ionograms by several characteristics:

- (a) It is always largely transparent to probing radio waves; that is, it never blankets reflections from higher layers.
- (b) It usually shows a well-defined lower edge lying between 100-110 km with scattered and diffuse echoes above the principal echo.
- (c) In well-developed cases, the diffuse echoes are contained below a sharp upper boundary that starts at about  $f_oE$  and increases in height with increasing frequency.
- (d) Multiple echoes are not observed.

These features can be seen in Fig. 1, an ionogram taken at Huancayo, Peru at 08 00 on the 10th of December 1959, illustrating a typical occurrence of  $E_s-q$ .

$E_s-q$  has been shown to be related to the equatorial electrojet (Matsushita 1951). Recently a lunar dependence has been discovered in both the times of early afternoon disappearance of  $E_s-q$  (Matsushita 1957) and of first appearance in the morning (Knecht 1959). Since lunar effects are prominent in equatorial geomagnetic variations and, hence, presumably in the electrojet as well, the association between  $E_s-q$  and the electrojet is further strengthened by this discovery. In view of this association, determining the width of the equatorial belt in which  $E_s-q$  occurs then becomes important as a means of estimating the width of the electrojet current system.

During the International Geophysical Year, a chain of close-spaced ionospheric vertical sounding stations was operated in the vicinity of the magnetic equator in Peru and Bolivia. Participating in this cooperative

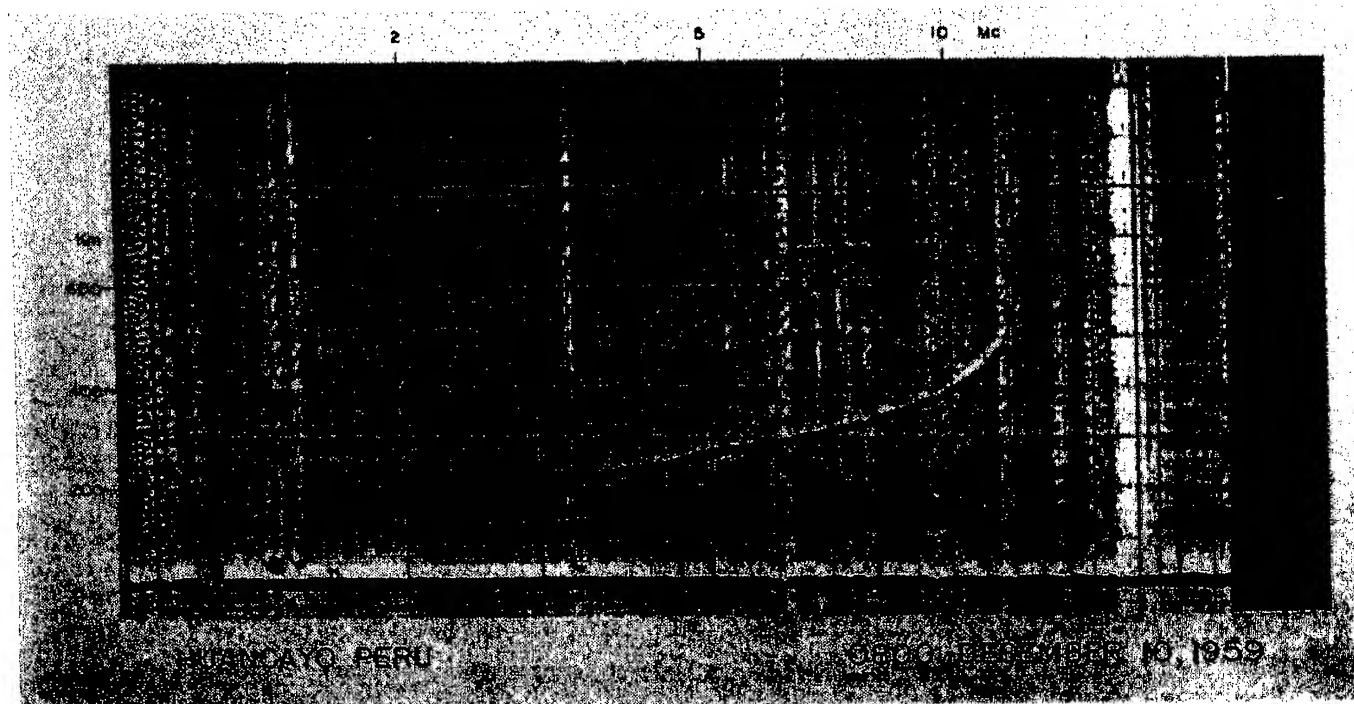


Fig. 1. Equatorial sporadic  $E$  ( $E_s$ - $q$ ) as observed at Huancayo, Peru—  
0800 December 10, 1959.

undertaking were the National Bureau of Standards, the Instituto Geofísico de Huancayo, and the University of San Andrés, La Paz, Bolivia. Certain particulars of the seven stations whose data have been used in this analysis are given in Table 1.

Table 1.

	Geographic		Geomagnetic	Dip*	Months of Data Used
	Latitude	Longitude	Latitude		
Talara	S4·6°	W81·3°	N6·6°	13°	24
Chiclayo	S6·8	W79·8	N4·4	9	18
Chimbote	S9·1	W78·6	N2·2	6½	23
Huancayo	S12·0	W75·3	S0·6	2	23
Juliaca	S15·5	W70·2	S4·5	-2½	3
La Paz	S16·5	W68·0	S5·0	-5	15
Ilo	S17·4	W71·2	S6·5	-7	4

The months July 1957 through June 1959 were used in this study. However, only the data from Talara, Chimbote and Huancayo were essentially complete for the 24-month period. This was because the ionosondes at

\* based on "Carta Geomagnética del Perú—época 1955.0, published by the Instituto Geofísico de Huancayo, Peru.

Chiclayo and La Paz were moved to Ilo and Juliaca and operated at these locations during the early months of 1959 in order to get better geographical coverage to the south of the dip equator.

Figure 2 shows the percentage occurrence of  $E_s$ - $q$  during the daylight hours (06 00–18 00 LST) as indicated on the hourly tabulations prepared

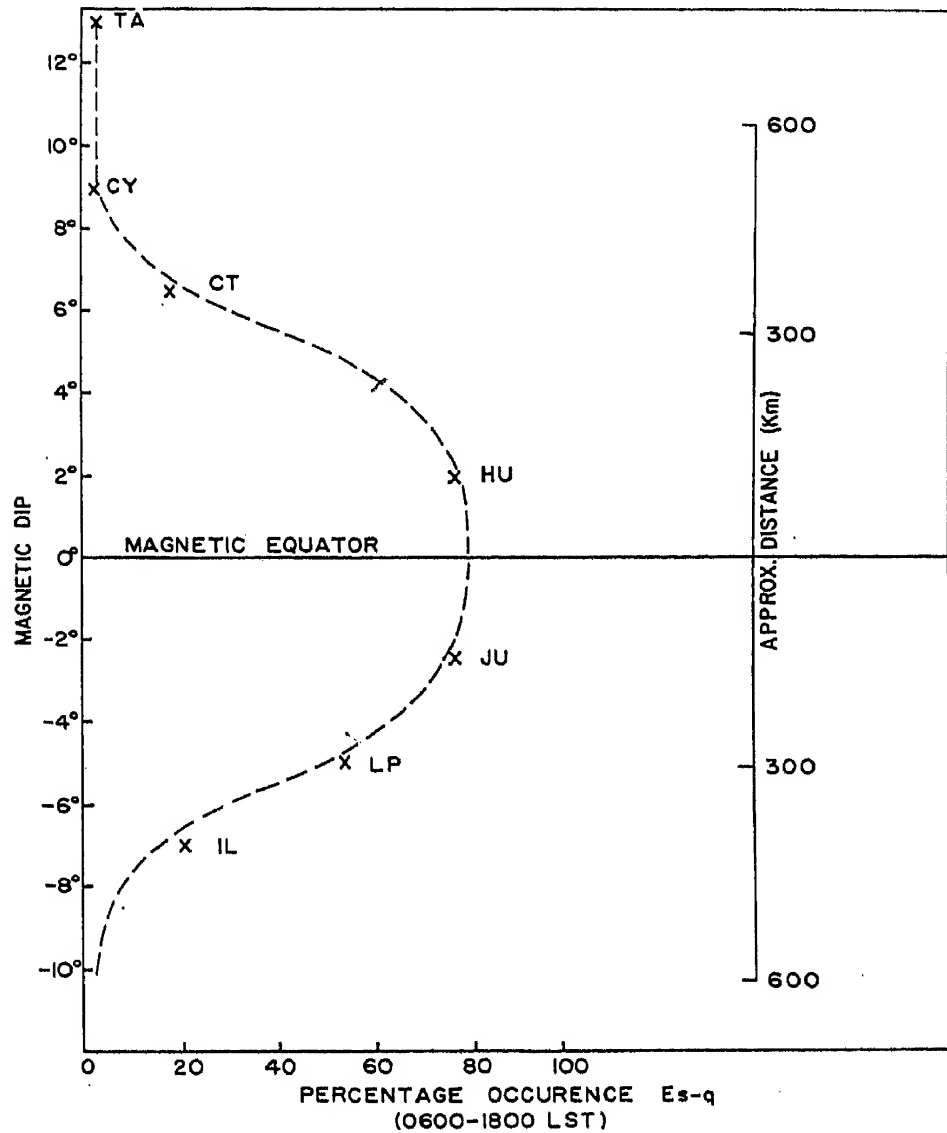


Fig. 2. Percentage occurrence of  $E_s$ - $q$  along the chain of vertical soundings stations. (Note that the right-hand scale refers to distance perpendicular to dip isoclines and not to station separation.)

by each of the stations along the chain. The points plotted are average values determined from all of the data being considered. It can be seen that at Huancayo and Juliaca  $E_s$ - $q$  was observed on 77 per cent of the hourly ionograms between 06 00 and 18 00, at La Paz 54 per cent, at Ilo 22 per cent, at Chimbote 18 per cent, and at Chiclayo and Talara only 3 per cent and 4 per cent, respectively. A smooth curve symmetric with respect to the dip equator can readily be passed through the observed points. It would appear, therefore, that the  $E_s$ - $q$  belt, at least at the longitudes in

question, during the period studied, has a "half-power" width of about  $11^\circ$  in dip (from  $5\frac{1}{2}^\circ\text{N}$  to  $5\frac{1}{2}^\circ\text{S}$ ) or, referring to the right-hand scale of the figure showing distance between the dip isoclines in this area of South America, about 700 km. This is a somewhat narrower belt than has been proposed by earlier workers using data necessarily obtained at more widely-spaced locations (Matsushita 1951, Smith 1957). Forbush, in an independent study of geomagnetic variations during the same period at a number of the same locations used in the  $E_s$ - $q$  analysis, assuming a uniform current density, has deduced an electrojet width of 660 km (Forbush 1960).

In the course of this study of the occurrence of  $E_s$  at low latitudes, another effect was noted. Not only does the occurrence of  $E_s$ - $q$  reach a peak in a narrow zone near the dip equator, but the occurrence of the temperate latitude variety of blanketing  $E_s$  is sharply reduced there; this reduction, to almost zero, occurring in an even narrower zone. For example, the occurrence of blanketing by  $E_s$  to frequencies greater than 5 Mc/s was at least 15 times less prevalent at the two locations within  $2\frac{1}{2}^\circ$  of the dip equator than at the stations having dips of  $5^\circ$  or more. This observation tentatively suggests that the formation of temperate latitude  $E_s$  is strongly inhibited at locations where the magnetic field is within, say,  $2^\circ$  to  $4^\circ$  of being horizontal.

#### REFERENCES

- MATSUSHITA, S. (1951) *J. Geomag. Geoelect.* 3, 44.  
MATSUSHITA, S. (1957) *J. Atmosph. Terr. Phys.* 10, 163.  
KNECHT, R. W. (1959) *J. Atmosph. Terr. Phys.* 14, 348.  
SMITH, E. K. (1957) National Bureau of Standards. Circular 582, 39.  
FORBUSH, S. (1960) Private Communication.

# The Night-*E* Layer

G. A. M. KING

Geophysical Observatory, D.S.I.R., New Zealand

**Abstract**—The properties of the night-*E* layer are detailed under the headings “Geographical and Temporal Occurrence”, “Relation with the Aurora”, “Relation with Magnetic Activity”, and “The Ionization Profile”. The association with the aurora is very direct, and there is also a suggested association with the *F*-region; both are important for auroral theory.

## 1. INTRODUCTION

In addition to the normal *E*-layer, generated by solar photon radiation, there is observed a thick layer in the *E*-region which is especially common at auroral latitudes. Canadian workers (Meek and Davies 1946) named this layer “night-*E*”, and the name has been adopted internationally (*Annals of the IGY* Vol. III Pt. I). A description and some excellent illustrations of night-*E* are given by Hanson, Hagg and Fowle (1953).

We shall make a clear distinction between night-*E* and the *E*-layer at night which shows continuity with the daytime *E*-layer over sunrise and sunset (Watts and Brown 1954). The critical frequency of this latter layer, the ‘normal *E*-layer at night’, lies between 0.7 and 0.8 Mc/s at sunspot maximum and between 0.5 and 0.6 Mc/s at sunspot minimum in temperate latitudes, (W. S. Hough private communication). Only for a layer with critical frequencies significantly above these values will the name “night-*E*” be used.

Another distinction which will be carefully preserved is that between night-*E* and sporadic *E* of type *r*. The latter behaves like a “thin layer”, producing neither retardation in nor blanketing of the *F*-region; almost certainly, type *r* *E*<sub>s</sub> is due to echoes received obliquely from “clouds” of ionization. On the other hand, night-*E* is definitely a thick layer overhead, for there are no *F*-region echoes below  $f_oE$  (night-*E*) and there is retardation on *F* above  $f_oE$ . This is a rather fine point of ionogram interpretation which often causes difficulty in routine readings.

An attempt will be made here to deduce the properties of the night-*E* layer using the literature but interpreting and supplementing it by examination of ionograms from various stations.

## 2. GEOGRAPHICAL AND TEMPORAL OCCURRENCE

The night-*E* layer can be found at any latitude except perhaps in the equatorial belt, but the higher values of critical frequency are confined to

auroral latitudes. Thus, at a low latitude station like Rarotonga (geomagnetic latitude  $21^{\circ}\text{S}$ ) a critical frequency of  $1.5\text{ Mc/s}$  will be exceeded only a few times a year, while in the auroral zone  $1.5\text{ Mc/s}$  occurs every day and  $4\text{ Mc/s}$  is common. This difference between high and other latitudes is made to appear more pronounced by the conditions of routine ionospheric recording; in temperate latitudes broadcast interference usually obscures everything below  $1.6\text{ Mc/s}$ , excluding observation of practically all occurrences of night- $E$ ; at high latitudes the interference is less, so that all occurrences above  $1\text{ Mc/s}$  can be observed.

Unfortunately, routine tabulations of ionospheric data are not suitable for studying the occurrence even at high latitudes, and present knowledge of the geographical distribution is meagre.

The temporal behaviour has been studied at Kiruna (geomagnetic latitude  $65^{\circ}\text{N}$ ) by Lindquist (1951a)—his  $NI$  layer can reasonably be identified with night- $E$ . It seems that at this station, near the maximum of the auroral zone, the layer is most likely to occur near local midnight, but the occurrence is high during all dark hours. For comparison, Fig. 1 presents a

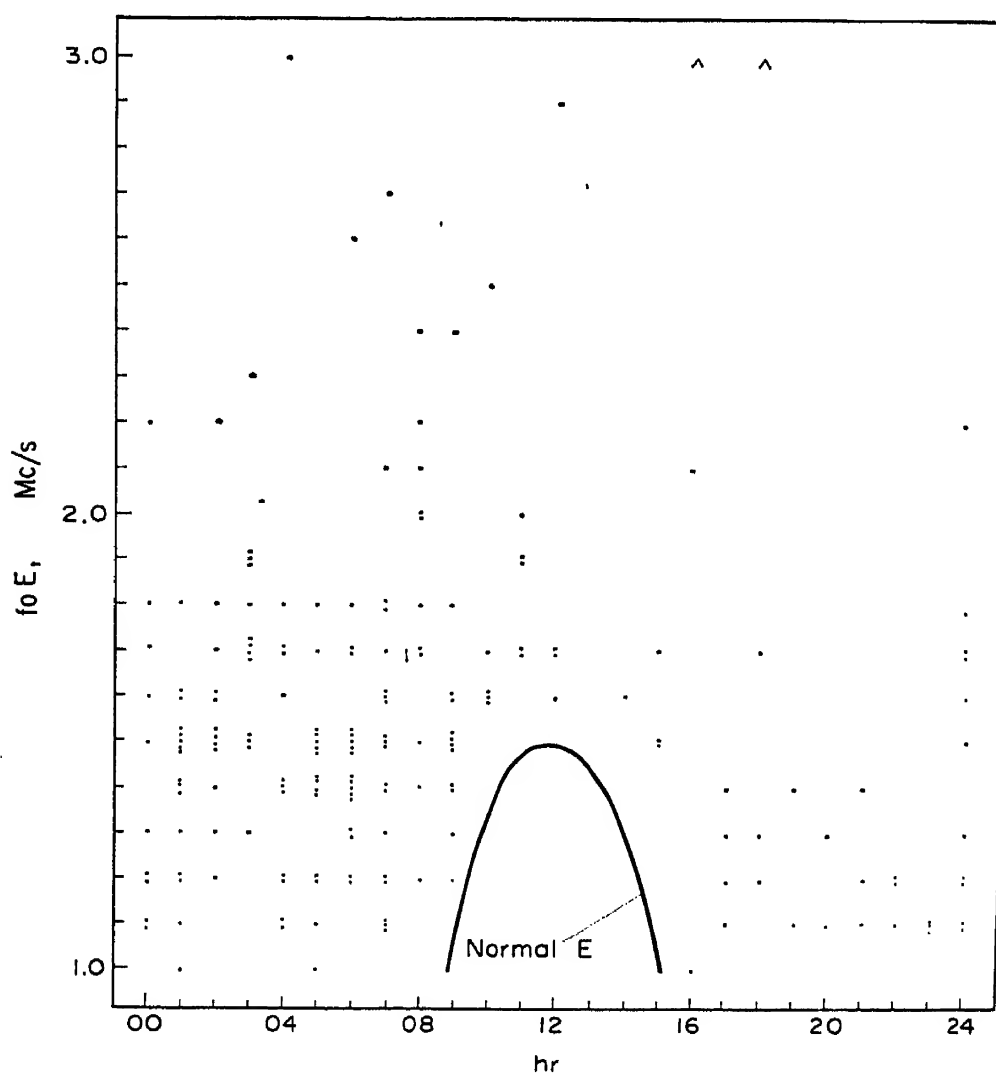


Fig. 1. Scatter diagram of  $f_oE$  (night- $E$ ) at Hallett, June, 1958.

scatter diagram of  $f_oE$  (night-*E*) during a midwinter month at Hallett (geomagnetic latitude 75°S), a station inside the southern auroral zone; here the greatest occurrence is at 06 00 hr. Later, when the relation between night-*E* and the aurora is discussed, it will appear that we should regard this kind of data with reserve. A point of interest is the appearance of night-*E* during daylight hours, when its presence raises the values of  $f_oE$  above those expected for the normal *E*-layer.

Lindquist also considered the seasonal variation at Kiruna, finding maxima in March and November. There is need for a wider study of the seasonal pattern for stations at various latitudes.

### 3. RELATION WITH THE AURORA

The connection between night-*E* and aurorae was summed up by Hanson, Hagg and Fowle thus: "Night-*E* is certainly an exclusively auroral-zone phenomenon. During magnetic and ionospheric storms, the aurora may be seen well south and north of its normal location, and then night-*E* may be seen within this extended zone. However, there does not seem to be a direct hour-to-hour correlation with aurora or other ionospheric phenomena". Lindquist (1951a, b) on the other hand presented examples in which the aurora was directly associated either with the *NI* layer (night-*E*) or with auroral blackout, at the same time pointing out that *NI* appears before and after almost every blackout. The statistics which he presented, however, were only mildly suggestive of a connection between the two phenomena.

It is worthwhile to enquire into the reasons why statistical methods fail, and for this purpose we shall look closely at the data for Hallett, June 1958. The lower solid line in Fig. 2 gives the percentage occurrence of night-*E*

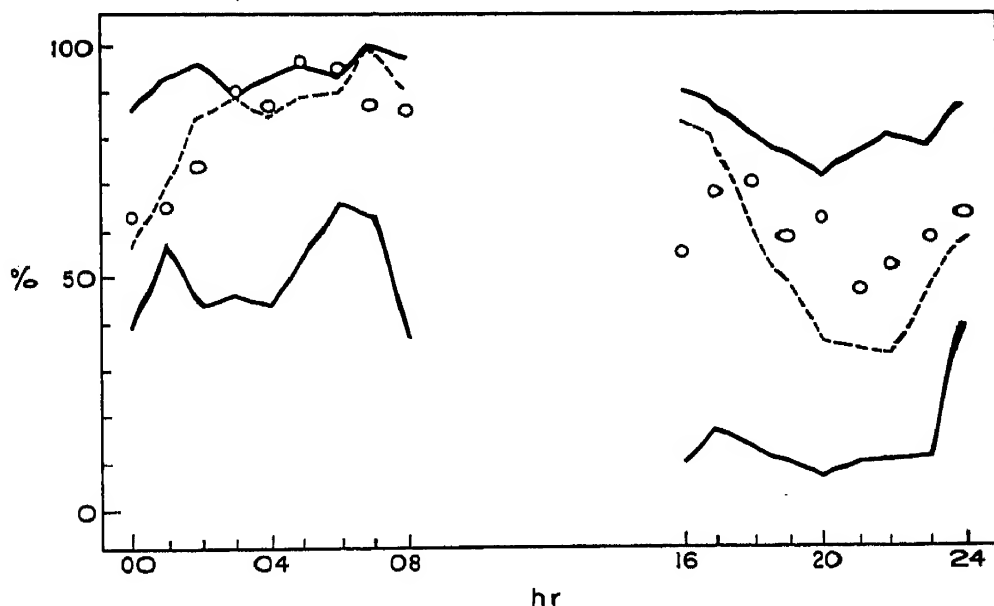


Fig. 2. Frequency of occurrence of night-*E* at Hallett, June, 1958.  
See text.



at each hour of darkness, using the numerical values already given in the scatter diagram, Fig. 1. Now, there are many reasons for not always entering a numerical value when the layer is present—reasons explained in standard reading terminology by the symbols,  $F$ ,  $N$ ,  $L$ ,  $A$ ,  $B$ ,  $S$  or  $E$ —and it is only when there is neither a value nor a symbol that we can assume that the layer is absent. For example, among the thirty observations at 17 00 hr there were five numerical values, but only for four of the remaining observations could it be said that there was no night- $E$ ; thus the greatest possible occurrence at this hour would be twenty-six. The upper solid line in Fig. 2 gives this greatest possible occurrence at each hour. The dotted line gives the greatest possible occurrence of values exceeding 1 Mc/s; i.e., the symbol  $E$  has not been counted. Obviously, the statistics based on numerical values only are almost worthless.

The reasons for poor auroral statistics are the incidences of twilight, moonlight, and cloud. Because of these factors, it is necessary to take auroral data for the whole observing season to get meaningful values; therefore, the auroral and ionospheric data are not strictly comparable. The occurrence of aurora anywhere in the sky during the 1958 observing season is plotted on Fig. 2 as open circles (data from Hatherton and Midwinter 1960). In this example, the auroral and night- $E$  statistics are not inconsistent with the hypothesis that the two phenomena are directly related.

To establish a direct connection, it is necessary to examine a sufficiently large number of individual cases when the interpretation of both ionospheric and auroral records is unambiguous. In a preliminary study of this kind, using data for May, 1958, at Hallett, K.J. Salmon and the writer found an excellent correspondence between overhead aurora and night- $E$ ; also, aurora low in the sky was accompanied by night- $E$  at lower frequencies and greater virtual heights (unpublished study).

It should be noted at this stage that type  $A$  aurora is not expected to correlate with phenomena in the  $E$ -region of the ionosphere, as it consists principally of the red OI emissions which come from  $F$ -region heights. However, the green OI line (5577 Å) and the negative bands of ionized molecular nitrogen are associated with aurora at  $E$ -region heights and the possibility suggests itself of a quantitative connection between night- $E$  and the luminosity in one of these emissions.

This possibility has been examined by Omholt (1955) working at Tromsø (geomagnetic latitude 67°N). He compared the zenithal auroral luminosity in the 4278 Å band of  $N_2^+$  with the critical frequency of an ionospheric layer which, from his careful description, we can identify with night- $E$ . He found that the luminosity varied as the fourth power of the critical frequency, in agreement with a theory based on the recombination of electrons in constant proportion to the number of excited  $N_2^+$  ions.

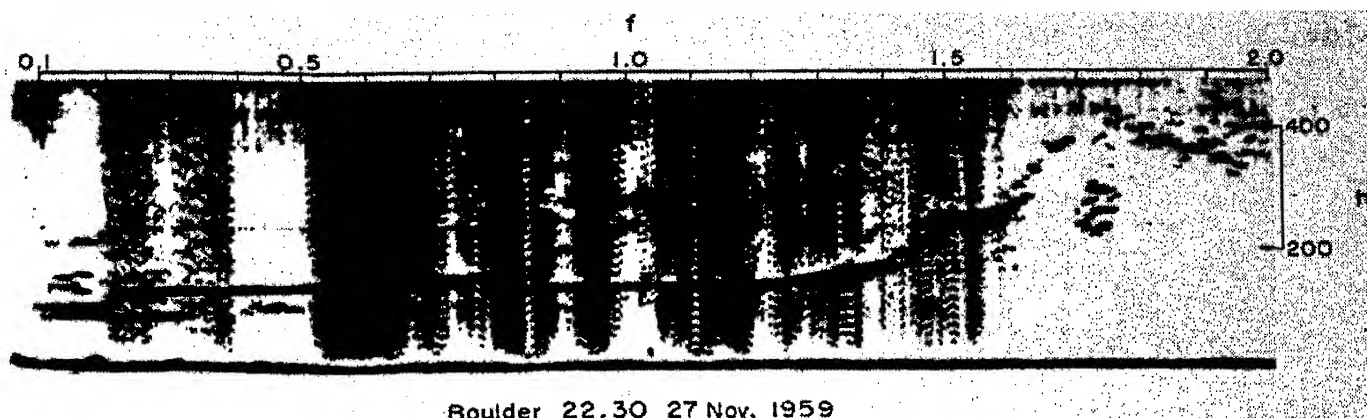


Fig. 3. Low frequency ionogram at Boulder; 22 30, 27 November, 1959.

The occurrence of aurorae in middle latitudes allows us to establish the spatial relation between night-*E* and the aurora. Figure 3 shows a low frequency ionogram, covering the frequency range 0.05 to 2.0 Mc/s, taken at Boulder (geomagnetic latitude 49°N) on 27 November, 1959, when an aurora was visible in the northern sky. The critical frequency of the night-*E* layer is 1.7 Mc/s, and the visible aurora was *at least* 200 km from the station. It appears, then, that the ionization in the *E*-region can extend a considerable distance on the equatorward side of the visible aurora; of course, the occurrence of night-*E* at low latitudes establishes the same point. This conclusion is not at variance with Omholt's findings, as the luminosity expected from a critical frequency of 1.7 Mc/s, using his dependence on  $(f_oE)^4$ , is below the visual threshold.

#### 4. RELATION WITH MAGNETIC ACTIVITY

It is commonly accepted that auroral and magnetic activity go together. Therefore, we should expect to find a connection between night-*E* and magnetic activity. In fact, from observations at very high latitudes we get a fairly clear picture of the relations between all three phenomena.

Figure 4 illustrates two typical patterns of behaviour at Hallett. The first, from 07 15 to 08 00 U.T. (in the evening) shows a sequence of ionograms including a brief period of auroral blackout which is preceded and followed by night-*E*; the all sky camera photographs show the passage overhead of active aurora, and the magnetic record had a large bay with a range in *H* of 700  $\gamma$ . The second sequence does not have a blackout period but at 1855 has night-*E* almost to 7 Mc/s near the time that a bright system of auroral bands passed overhead; accompanying magnetic activity is slight (range in *H*, 80  $\gamma$ ). Clearly the difference between these patterns depends on the height of the ionization associated with the aurora (ignoring here the possibility of low level ionization from X-rays). In the first case,

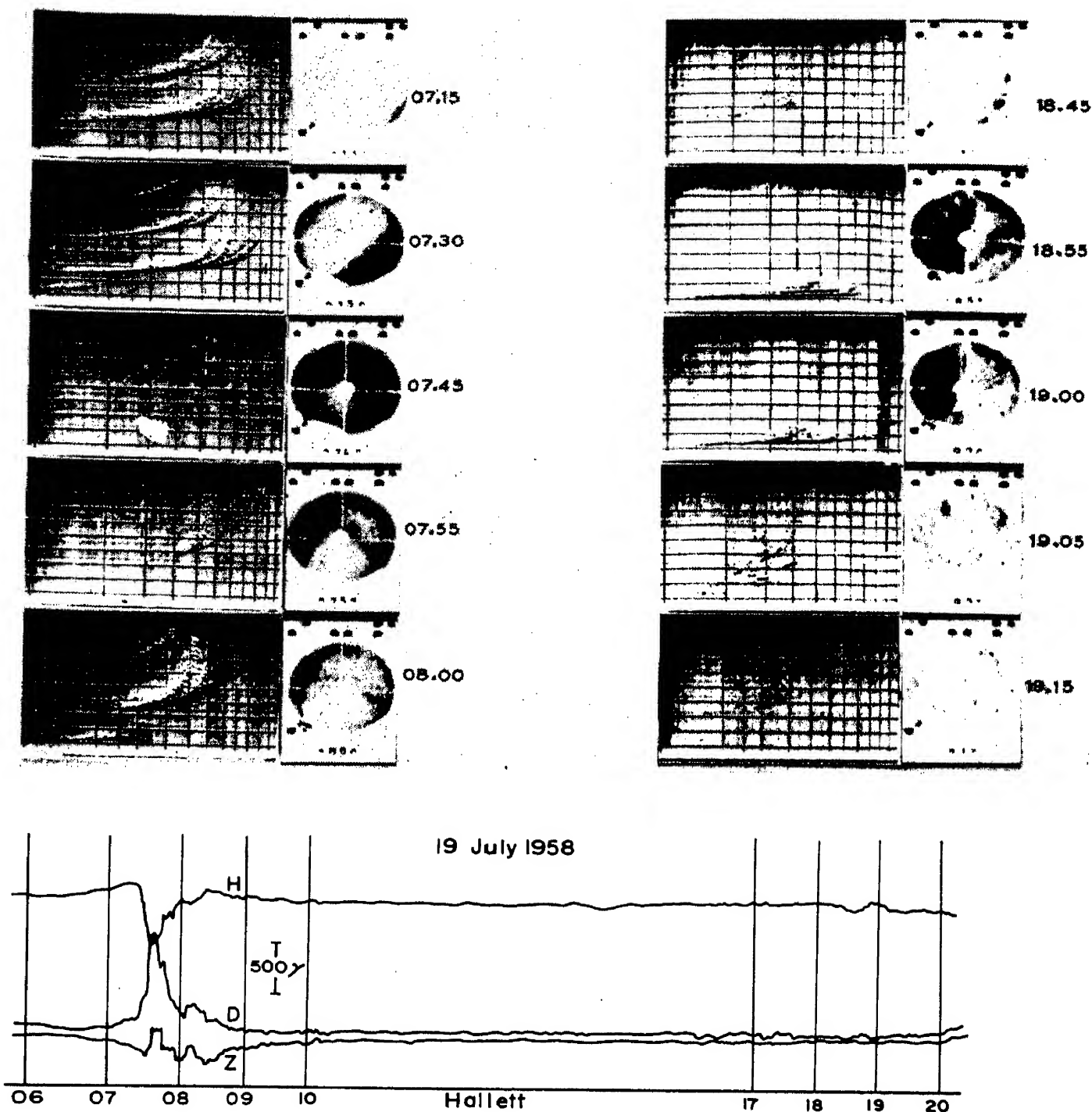


Fig. 4. Ionospheric, auroral, and magnetic records for two types of activity on 19 July, 1958, at Hallett. Times are U.T.

the ionization extends down to levels where it causes ionospheric absorption and also where charge separation is enough to produce a large magnetic effect (Bless, Gartlein, Kimball and Sprague 1959). In the second case, the ionization is higher, so there is little ionospheric absorption and also charge separation is smaller, so that the magnetic effect is small.

For the middle latitude example, we shall look again at the event of 27–28 November, 1959. Figure 5 shows the horizontal magnetic records

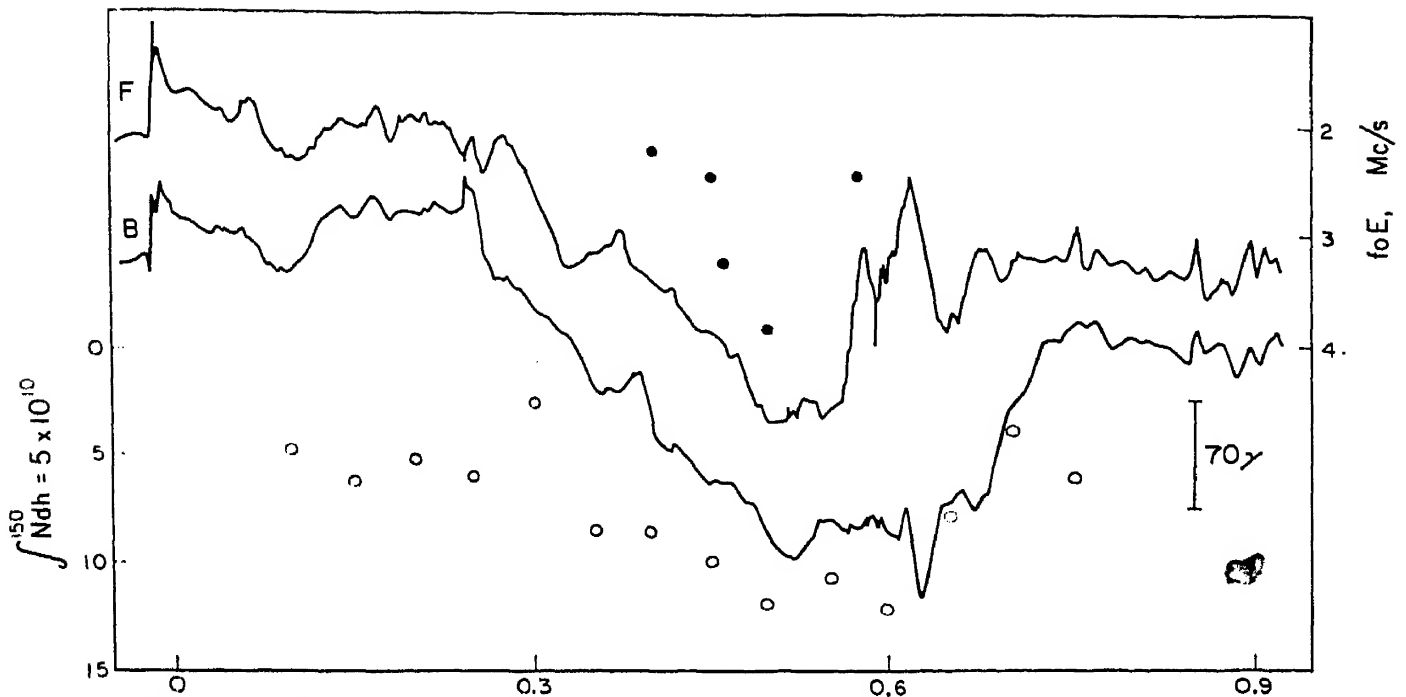


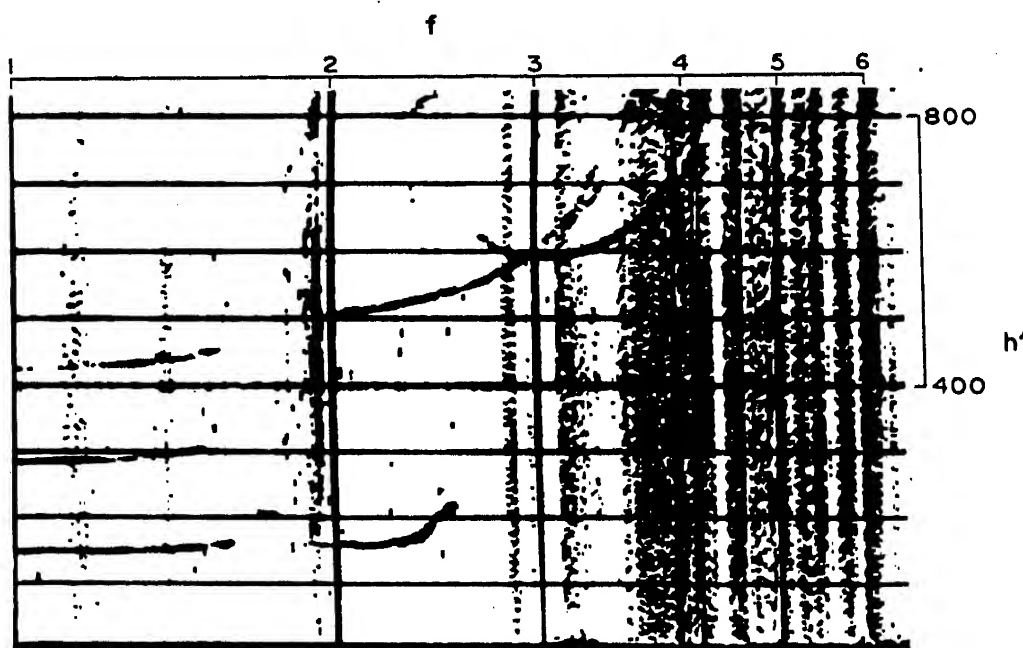
Fig. 5. The horizontal magnetic records at Fredericksburg and Boulder,  $f_oE$  (night-*E*) at Fort Monmouth, and  $\int_{Ndh}^{150}$  at Boulder on 28 November, 1959. Times are U.T.

from Fredericksburg (upper trace) and Boulder (lower trace). These stations are on the same geomagnetic latitude, but Fredericksburg is approximately one hour fifty minutes in time to the East of Boulder. There is a striking similarity between the records except over the period 05 30 to 07 30 U.T.; the difference is brought about by the fact that recovery from the negative phase occurred at both stations near local midnight. Ionospheric records from Fort Belvoir, the station nearest to Fredericksburg, were unsuitable for studying night-*E* because of broadcast interference, but records were available from Fort Monmouth, two degrees north of Fredericksburg and a little to the east. At Fort Monmouth, the auroral activity was overhead, and  $f_oE$  (night-*E*) reached nearly 4 Mc/s; the few values of  $f_oE$  that could be read through the sporadic *E* are plotted as dots on Fig. 5 (the scale is inverted for easier comparison with the magnetic records). It can be seen that  $f_oE$  decreased at about the time that magnetic recovery occurred at Fredericksburg. Excellent low-frequency ionograms were available at Boulder (Fig. 3 is the record at 05 30 U.T.), and they have been analysed between 00 00 hr and 07 30 hr U.T. to give  $N(h)$  profiles; the open circles in Fig. 5 give the total electron content of the *E*-region up to 150 km (inverted scale). The shape of the negative magnetic phase is approximately reproduced by the electron content curve, and again local magnetic recovery occurs at the same time as the decrease in night-*E*. It is interesting to note that the positive phase of the magnetic storm from 00 00 to 03 00 hr U.T. is also associated with increased *E*-region content.

This example suggests that the storm variations in the magnetic field are due to currents which flow mainly in the local ionosphere—for the first five hours of the storm the current system covered a zone of longitude that included both magnetic stations, and it decayed progressively from east to west, ending at the longitude of each station near local midnight. The behaviour of the night- $E$  layer is similar, suggesting that there is a close connection between night- $E$  and the ionization responsible for the changing magnetic field; of course, the connection certainly is not simple, and probably depends on the variation of collision frequencies with height, the pattern of atmospheric motions in the  $D$  and  $E$ -regions, and the electron density profile.

### 5. THE IONIZATION PROFILE

Using the normal methods of  $N(h)$  analysis, we can derive the ionization profile when night- $E$  is present. For example, Fig. 6 is an ionogram taken



Adak 00.35 31 Mar. 1960

Fig. 6. Ionogram at Adak: 00 35, 31 March, 1960.

at Adak on 31 March, 1960, at 00 35; the corresponding “real height” profile is given by the solid line in Fig. 7. There are two important assumptions made in deriving this profile:

- (1) That ionization below  $h'E$  can be neglected.
- (2) That the electron distribution is monotonic up to the maximum of the  $F$ -region.

With regard to the first,  $h'E$  is determined in this case by inability to record below 1 Mc/s; it is likely that the minimum virtual height, 145 km,

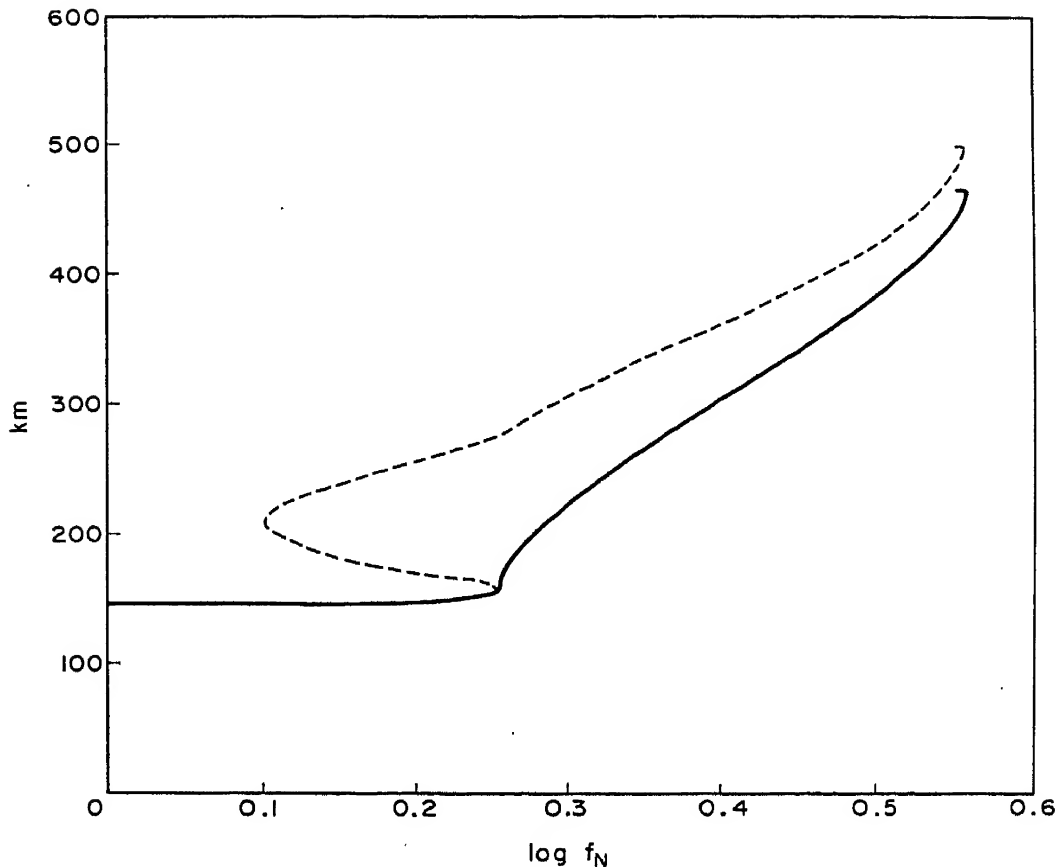


Fig. 7. Electron density profiles ( $h$  versus  $\log f_N$ ) corresponding to Fig. 6. The solid line gives the monotonic profile; the dotted line includes a valley.

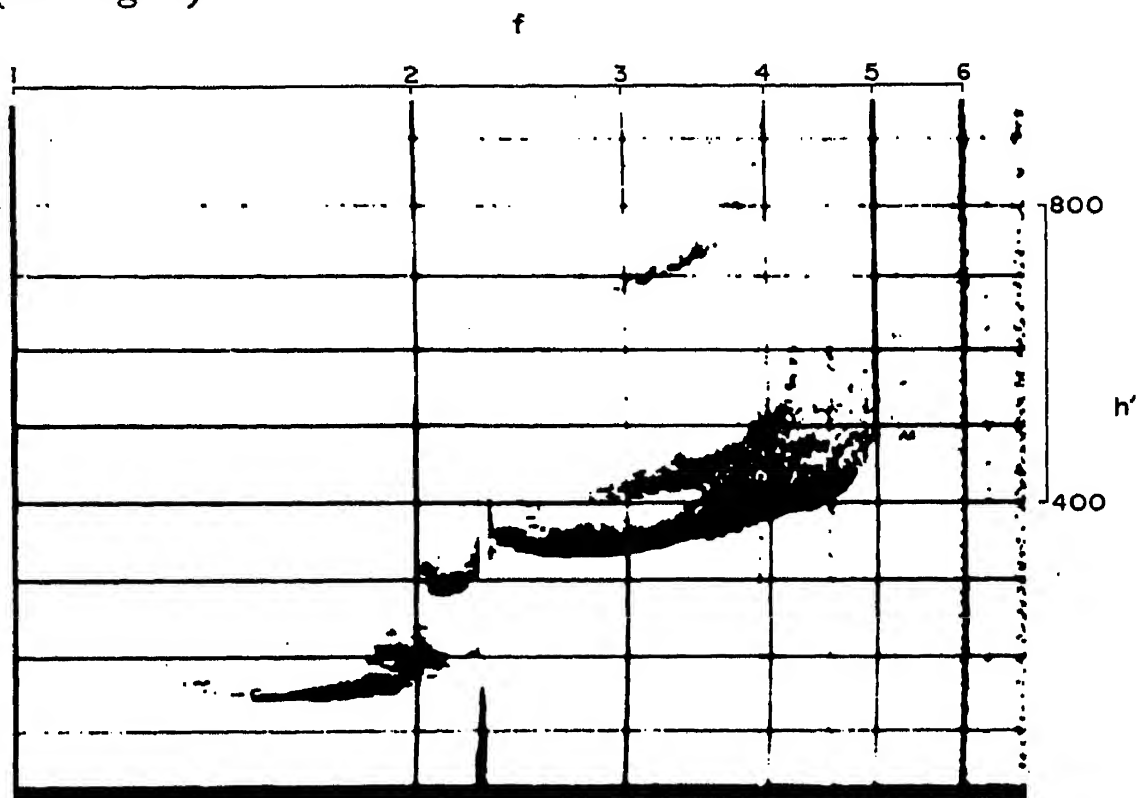
on this record is well above the bottom of the ionized regions. Profiles deduced for a night-*E* layer should not be taken too literally, unless  $f_oE$  is at least three times the minimum observed frequency.

The assumption of a monotonic electron distribution is the only one which yields a unique ionization profile, and there is an infinite set of distributions with “valleys” between night-*E* and *F* all corresponding to the original virtual-height curve; one of this set is shown by the dotted line in Fig. 7. In theory, use of the **X** trace from the *F*-region can limit the set of valley distributions to those which give a reasonably correct *F*-region profile, but practical difficulties, especially the fact that the ionosphere is probably not horizontally stratified, usually prevent this refinement.

There are five facts that give some information about the valley between night-*E* and *F*:

- (a) Although the virtual-height curve most often tends to infinity at  $f_oE$ , there are times when it is clearly finite; in such cases, there can be no valley between *E* and *F*.
- (b) When observing conditions are suitable, we can see the **Z** trace of the *F*-region after conversion in *E*; this signifies that the valley is not deep.

- (c) When the active aurora is a long way from the zenith, the  $E$ -layer is high and definitely continuous with  $F$ ; at times, it is difficult to know whether the layer should be called  $E$  or a stratification of  $F$ , especially when its minimum virtual height exceeds 200 km, but careful examination shows that these "high  $E$ " layers develop into the more usual night- $E$  based near 100 km.
- (d) Some examples of night- $E$  are associated with a stratification of  $F$  (see Fig. 8).



Pt. Barrow 20.45 02 Dec. 1958

Fig. 8. Ionogram at Point Barrow; 2045, 02 December, 1958.

- (e) Limited analyses of both  $O$  and  $X$  traces indicate that the valley is probably full and that the distribution approximates a monotonic function.

It seems likely, then, that the night- $E$  layer is thick, extending up to the  $F$ -region, and there is a possibility that the ionization of the layer is associated with the  $F$ -region ionization.

Before leaving the  $N(h)$  profile, it is as well to mention the effect of the night- $E$  layer on the study of  $F$ -region storms; Theissen (1947), Mason (1958) and Haubert (1959) have mentioned its appearance during night-time storms at middle latitudes. Now, one of the commonest means of studying storms in the  $F$ -region is by the variation in virtual height, which at night is considered to approximate to the real height of the region. That this is quite wrong during disturbed conditions is apparent from Figs. 6 and 7—the minimum virtual height,  $h'F$ , is 503 km, while the real height



at 2 Mc/s is only 222 km, if we accept the monotonic distribution, or 306 km, if we put in a very generous valley between *E* and *F*; thus, most of the apparent change in  $h'F$  from normal conditions is due to a change in the *E*-region ionization. While this may seem to be an extreme case, we must remember that few stations in middle latitudes can record satisfactorily below 1.6 Mc/s, and errors exceeding a hundred kilometres will be common.

## 6. DISCUSSION

In the previous sections, we have examined some properties of the night-*E* layer. The most significant property is the quantitative connection with the aurora, and it is desirable that more experiments like that of Omholt's be done to remove any doubts about the connection. A very powerful tool then becomes available for studying the aurora—one that does not suffer from the observational difficulties of optical methods (although it has difficulties of its own). Optical observations focus attention on localized volumes of high activity, such as arcs and rays, while observations of night-*E* direct attention to activity spread over much larger volumes. This difference in emphasis gives us a wider field for testing theories of the aurora; for example, a satisfactory theory must account for the presence and detailed shape of night-*E* on the low-latitude side of visual aurora—faint optical activity has been noted at the lower latitudes, but has never been prominent enough to demand explanation, while on the ionograms the night-*E* is conspicuous.

The study of night-*E* also promises to yield a quantitative relation between the aurora and magnetic activity, amplifying the qualitative relations that have been found (Meek 1953, 1954, Heppner 1954, Bless, Gartlein, Kimball and Sprague 1959). However, as the magnetic effects are probably associated with the electron distribution near 100 km, the normal ionograms are not adequate to this problem; there is need for records of the highest quality extending down to 300 kc/s. The way in which the magnetic field changes are brought about is not clear, so there is need also for theoretical development. Unfortunately, during many periods of activity this study is hampered by ionospheric absorption.

The possibility was suggested earlier that the ionization in the night-*E* layer is associated with the *F*-region; if this were established it would be of paramount importance in auroral theory. Now, at low latitudes there is little doubt that the formation of night-*E* depends on travelling disturbances in the *F*-region at night (see Fig. 9). We must ask, then, if this is also the case at other latitudes (Fig. 8 is a high latitude record) or whether there are really two types of night-*E*, one associated with travelling disturbances and the other with the aurora. The writer inclines to the view that all night-*E* is connected with the *F*-region.





Rarotonga 03.14 01 July 1960

Fig. 9. Ionogram at Rarotonga; 03 14, 01 July, 1960.

At the beginning, we distinguished between night- $E$  and the normal  $E$ -layer at night, using a somewhat arbitrary frequency criterion. The existence of the normal  $E$ -layer at night is not wholly expected, as, if the rate of electron recombination obtaining at sunset were to continue into the night,  $f_oE$  would be much less than the observed values. Three ways of maintaining the normal  $E$  present themselves:

1. The recombination rate is less at night because of a dual machinery (Mitra 1954).
2. There is enough Lyman- $\alpha$  radiation scattered to the night side of the earth to create a layer; certainly, some is scattered (Kupperian, Byram, Chubb and Friedman 1959).
3. Ionization is continually supplied from the  $F$ -region.

If the last alternative were correct (low-frequency ionospheric soundings at the dip equator will decide between it and the other possibilities), we may have been guilty of creating an artificial distinction between night- $E$  and the normal  $E$  at night.

Finally, we note that some statistical studies of night- $E$  can only be done if reliable routine scalings of the layer become available. At present, some stations never report night- $E$ , some record it only if there be no other feature in the  $E$ -region, while others record numerical values but do not otherwise note the presence of the layer; it is rare to find satisfactory tabulations of night- $E$ . Of course, there are many factors which complicate its scaling, but the layer has properties of sufficient importance to warrant the extra effort needed to produce good routine data.

*Acknowledgments*—This work was carried out at the Geophysical Observatory, D.S.I.R., New Zealand (Superintendent, Mr. J. W. Beagley) and at the National Bureau of Standards, U.S.A., in association with the High

Altitude Observatory, University of Colorado; the support of U.S. I.G.Y. Project 50.4 is gratefully acknowledged.

The magnetogram in Fig. 4 was kindly supplied by Magnetic Survey, D.S.I.R., New Zealand (Superintendent, Mr. A. L. Cullington), and those in Fig. 5 are from the Magnetic Data Centre (by courtesy of Dr. S. Matsushita). The ionograms in Figs. 6 and 8 were supplied by Data Centre A (by courtesy of Mr. S. Ostrow), and that in Fig. 3 is due to Mr. W. S. Hough, of the National Bureau of Standards.

#### REFERENCES

- BEYNON, W. J. G. and BROWN, G. M. (1957) *Annals of the IGY* Vol. III, Pt. I. (Pergamon Press, London).
- BLESS, R. C., GARTLEIN, C. W., KIMBALL, D. S. and SPRAGUE, G. (1959) *J. Geophys. Res.* **64**, 949.
- HANSON, G. H., HAGG, E. L. and FOWLE, D. (1953) *D.R.T.E. Rep.* No. R-2.
- HATHERTON, T. and MIDWINTER, G. G. (1960) *J. Geophys. Res.* **65**, 1401.
- HAUBERT, A. (1959) *J. Atmosph. Terr. Phys.* **15**, 84.
- HEPPNER, J. P. (1954) *J. Geophys. Res.* **59**, 329.
- KUPPERIAN, J. E., BYRAM, E. T., CHUBB, T. A. and FRIEDMAN, H. (1959) *Planet. Space Sci.* **1**, 3.
- LINDQUIST, R. (1951a) *Chalmers Tek. Hogs. Hand.* No. 103.
- LINDQUIST, R. (1951b) *Ark. for Geofysik* **1**, 247.
- MASON, R. F. (1958) *N.Z. J. Geol. Geophys.* **1**, 519.
- MEEK, J. H. (1953) *J. Geophys. Res.* **58**, 445.
- MEEK, J. H. (1954) *J. Geophys. Res.* **59**, 87.
- MEEK, J. H. and DAVIES, F. T. (1946) *Canadian Observers Instruction Book*.
- MITRA, A. P. (1954) *Penn. State Univ. Sci. Rep.* No. 68.
- OMHOLT, A. (1955) *J. Atmosph. Terr. Phys.* **7**, 73.
- THEISSEN, E. (1947) *Die Naturwiss.* **12**, 371.
- WATTS, J. M. and BROWN, J. N. (1954) *J. Geophys. Res.* **59**, 71.



# CHAPTER II

## Part C



# A Theoretical Study of Sporadic- $E$ Structure in the Light of Radio Measurements

KAZUHIKO TAO\*

National Bureau of Standards, Boulder, Colorado, U.S.A.

**Abstract**—The theoretical aspects of the mechanisms of sporadic- $E$  reflections are described from both the standpoint of a thin layer and a scattering model. For the thin-layer model, thin dielectric layers which have various distributions of electron density are considered. It is also pointed out that the scattering theory for which an auto-correlation function of the fluctuation of electron density is given by modified Bessel functions of the fourth through the seventh order is an available model for sporadic- $E$  scatter. Moreover blobs of ionization which have a horizontal scale of the order of 200 m and a vertical scale of about 50 m are considered for sporadic- $E$  scatter. The frequency and distance dependences of the oblique v.h.f. propagation by means of the sporadic- $E$  layer are discussed by comparing the theoretical results with experimental evidence.

## 1. INTRODUCTION

We have seen that there are several types of sporadic- $E$  delineated by their differing diurnal or seasonal occurrence times or latitude variation (Smith 1957). Some types of sporadic- $E$  echoes on ionograms have the appearance of reflections from a thin layer, and other types suggest the scattering mechanism. In this paper, we shall confine our attention to sporadic- $E$  echoes which are frequently observed in middle latitudes.

The theory concerning a thin layer which has a cloud-like form is described in Section 2 and a sporadic- $E$  model is given in Section 3 from the standpoint of scattering theory. Distance and frequency dependences of sporadic- $E$  propagation are stated in Sections 4 and 5 together with a comparison of theoretical with experimental results. In Section 6 a relationship is derived between  $f_oE_s$  and the measured field strength observed over an oblique v.h.f. propagation path during periods of sporadic- $E$  enhancement.

## 2. THIN LAYER MODEL FOR SPORADIC $E$

### 2.1 *Outline of the Model*

Measurement of the electron density within the sporadic- $E$  layer has shown that relatively sharp variations in the gradients of electron density

---

\* On leave from Radio Research Laboratories, Japan.

exist in both the horizontal and vertical directions. Although the theory of reflection from a thin ionized layer has been developed by Hartree (1929), Booker (1938), Rydbeck (1942, 1946) and Rawer (1939), another treatment will be developed in this paper. We shall postulate many thin dielectric layers in the  $E$ -region which have limited extent in the horizontal direction. The basic idea for this model was developed by Friis, Crawford and Hogg (1957), in order to explain the persistent tropospheric field strengths beyond the horizon. We shall apply this concept to the problem of sporadic  $E$ .

According to diffraction theory, if a layer has a reflection coefficient  $\rho$ , the received power is given in the form,

$$P_r = P_t \frac{A_t A_r}{\lambda^2 d^2} \rho^2 \quad (2.1)$$

where  $P_t$  is the transmitting power,  $A_t$  and  $A_r$  are the effective areas of transmitting and receiving antennas.  $d$  is the distance between the transmitter and receiver. This relation is appropriate when the following conditions are satisfied,

$$b > \frac{\sqrt{d\lambda}}{\theta}, \quad a > \sqrt{d\lambda}, \quad (2.2)$$

where  $\theta$  is the grazing angle to the layer and  $a$  and  $b$  are horizontal dimensions as shown in Fig. 1.

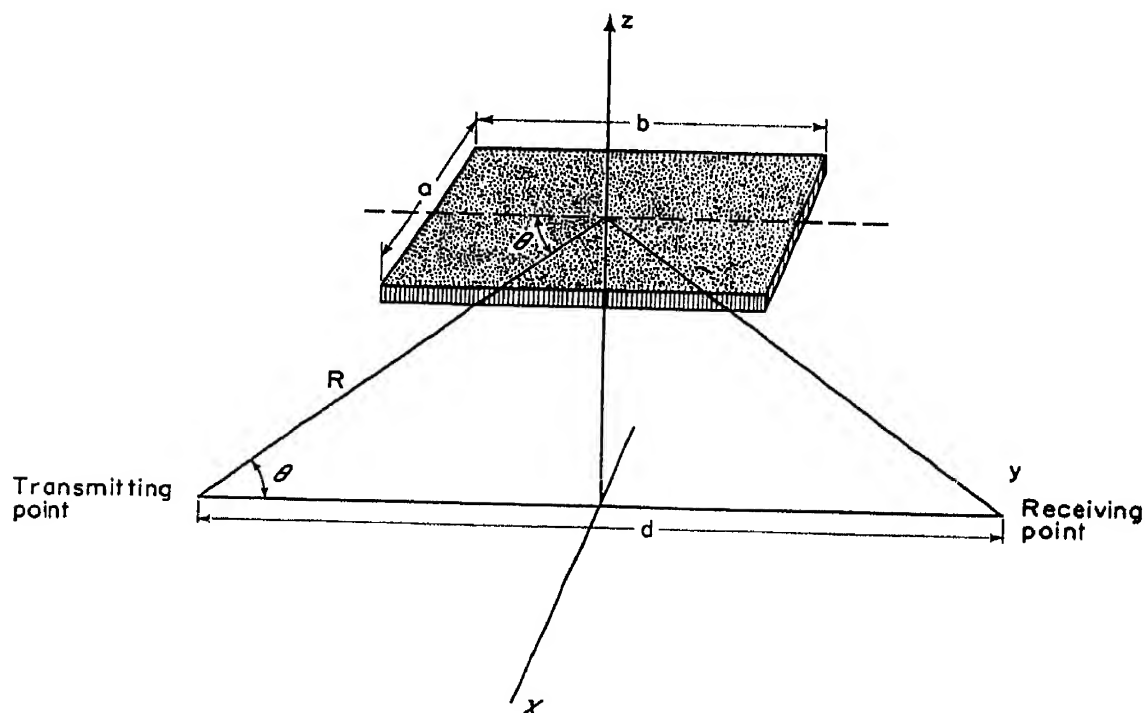


Fig. 1. Geometry of a thin layer model.

## 2.2 Calculation of the Reflection Coefficient

Let us assume that the layer is composed of many thin layers whose dielectric constants differ one from their neighbors by an increment  $\Delta\epsilon$ . Provided that  $1 \gg \theta^2 \gg d\epsilon$ , the reflection coefficient of the boundary between thin layers is given in the simpler form for both polarizations.

$$d\rho = \frac{d\epsilon}{4\theta^2}. \quad (2.3)$$

We shall next assume the vertical distribution of electron density in the sporadic-*E* layer to be in the following form.

$$N = N_{\max} \left\{ 1 - \left( \frac{z}{\Delta h} \right)^{2n} \right\}, \quad n = 1, 2, 3, \dots \quad (2.4)$$

where  $\Delta h$  is a half-thickness of the layer.

This distribution of electron density is shown in Fig. 2 as a parameter of various values of  $n$ . If we put  $n = 1$ , this is a parabolic distribution. In rationalized MKS units, the dielectric constant is given in the following form for the ionosphere, neglecting the effect of collisions and of the earth's magnetic field,

$$\epsilon = 1 - \frac{Ne^2}{m\epsilon_0\omega^2},$$

if we put

$$f_N = \frac{N_{\max}e^2}{4\pi m\epsilon_0},$$

the dielectric constant for the observing frequency  $f$  is in the form,

$$\epsilon = 1 - \frac{f_N^2}{f^2} \left\{ 1 - \left( \frac{z}{\Delta h} \right)^{2n} \right\}. \quad (2.5)$$

The reflected field from any incremental layer is obtained by considering the phase difference

$$dE_r = d\rho E_i \exp \left[ -j \left( \frac{4\pi z}{\lambda} \right) \sin \theta \right] dz. \quad (2.6)$$

Differentiating (2.5) with respect to  $z$  and inserting this into (2.6), we get

$$dE_r = \frac{n f_N^2}{2 f^2} \frac{z^{2n-1}}{(\Delta h)^{2n} \theta^2} E_i \exp \left[ -j \left( \frac{4\pi z}{\lambda} \right) \sin \theta \right] dz. \quad (2.7)$$

The complete reflected field ( $f > f_N$ ) is obtained by integrating the reflections from all increments within the layer

$$E_r = n \frac{f_N^2 E_i}{f^2 (\Delta h)^{2n} \theta^2} \int_0^{\Delta h} \exp \left[ -j \left( \frac{4\pi z}{\lambda} \right) \sin \theta \right] z^{2n-1} dz. \quad (2.8)$$



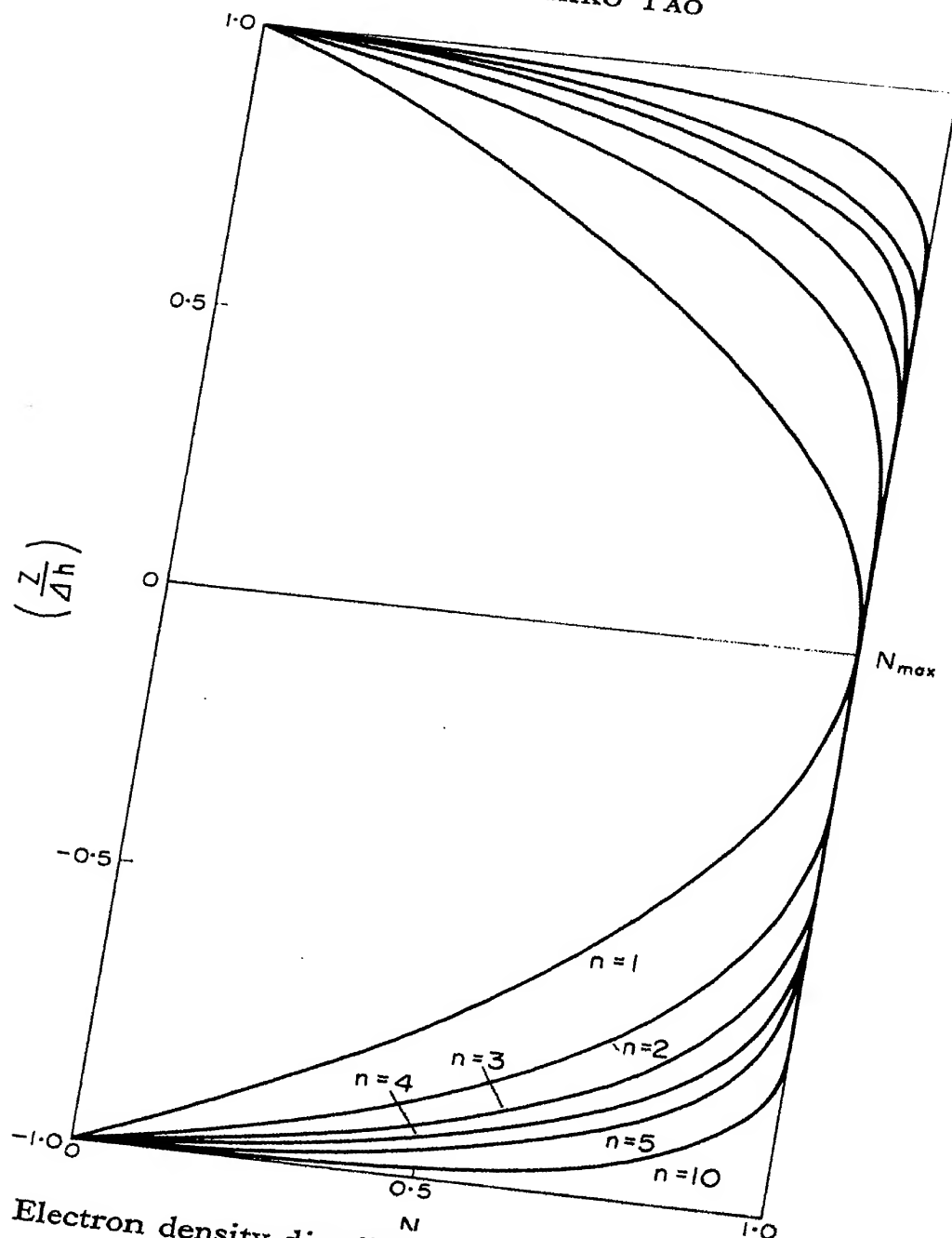


Fig. 2. Electron density distribution in the sporadic-E layer.

After evaluating this integral, we get

$$\begin{aligned}
 E_r = & n \frac{f_N^2 E_i \lambda^{2n}}{f^2 (\Delta h)^{2n} \theta^2 (4\pi \sin \theta)^{2n}} \left[ (2n-1) \sum_{m=1}^n (-1)^{m+1} \frac{(2n-2)!}{(2n-2m)!} \right. \\
 & \times \left( \frac{4\pi \sin \theta \Delta h}{\lambda} \right)^{2n-2m} \cos \left( \frac{4\pi \sin \theta \Delta h}{\lambda} \right) + \sum_{m=1}^n (-1)^{m+1} \frac{(2n-1)!}{(2n-2m+1)!} \\
 & \times \left. \left( \frac{4\pi \sin \theta \Delta h}{\lambda} \right)^{2n-2m+1} \sin \left( \frac{4\pi \sin \theta \Delta h}{\lambda} \right) - (2n-1)! \right]. \quad (2.9)
 \end{aligned}$$

The total reflection coefficient is defined as follows

$$\rho = \frac{E_r}{E_i} \quad (2.10)$$

In order to calculate the received power from the formula (2.1), it is convenient to use the reflection coefficient expressed as a power ratio.

If we put  $L = 4\pi \sin \theta \Delta h / \lambda$  in (2.9) and let  $k = n - m$ ,  $\rho^2$  is expressed in simpler form

$$\rho^2 = \frac{f_N^4 n^2 [(2n-1)!]^2}{f^4 \theta^4 L^{4n}} \left[ (-1)^n \sum_{k=0}^{n-1} \frac{L^{2k}}{2k!} (-1)^k \left( \cos L + \frac{L \sin L}{2k+1} \right) + 1 \right]^2 \quad (2.11)$$

Therefore the received power is obtained by combining formulae (2.1) and (2.11).

### 3. SCATTERING MODEL FOR SPORADIC $E$

#### 3.1 Outline of this Model

Some types of sporadic  $E$ , particularly those which are frequently observed during evening hours in middle latitudes, have many features of scattering phenomena. This scatter would be due to the irregularities of electron density occurring in the lower ionosphere. Recently Booker (1959) has suggested that the phenomenon of sporadic  $E$  can, in some cases, be explained from the standpoint of scattering theory. The phenomenon of sporadic  $E$ , however, generally appears to have a denser concentration of electron density than the normal scattering phenomena. For this reason, it seems inappropriate to use the auto-correlation functions which are used to account for the normal scattering phenomena. Let us at first consider a generalized auto-correlation function of the electron density for the scattering model of sporadic  $E$ . We shall take the following correlation function

$$C_n(\rho) = C(0) \left[ \frac{2^{1-n}}{\Gamma(n)} \right] \rho^n K_n(\rho), \quad \rho = \frac{r}{l} \quad (3.1)$$

where  $K_n(\rho)$  is the modified Bessel function of the second kind of order  $n$  and  $\Gamma$  is the gamma function.  $C(0)$  is the time variance  $\langle (\Delta n)^2 \rangle$  of the refractive index  $n$  of the atmosphere and  $l$  is the scale of turbulence. This correlation function was derived by Muchmore and Gallet (private communication). If we put  $n = \frac{1}{2}$  in the above formula, we can derive an exponential correlation function which was derived by Booker and Gordon (1950). Also the modified Bessel function of the first order is obtained in the case of  $n = 1$ , which is used by Norton and his collaborators (Norton 1956) in order to account for tropospheric scattering. While considering

$n = \frac{1}{2}$  and  $n = 1$ , we shall pay more attention to the higher orders of  $n$  in this correlation function.

When  $n$  is an integer,  $K_n(\rho)$  is defined by the equation

$$K_n(\rho) = \lim_{\epsilon \rightarrow 0} \frac{\pi}{2} \{I_{-n-\epsilon}(\rho) - I_{n+\epsilon}(\rho)\} \cot \pi \epsilon, \quad (3.2)$$

where

$$I_n(\rho) = \sum_{m=0}^{\infty} \frac{\rho^{n+2m}}{2^{n+2m} m! \Gamma(n+m+1)},$$

$$I_{-n}(\rho) = \sum_{m=0}^{\infty} \frac{\rho^{-n+2m}}{2^{-n+2m} m! \Gamma(-n+m+1)},$$

and which gives\*

$$K_n(\rho) = \frac{1}{2} \sum_{m=0}^{n-1} \frac{(-1)^m (n-m-1)!}{m! (\rho/2)^{n-2m}} + (-1)^{n+1} \sum_{m=0}^{\infty} \frac{(\rho/2)^{n+2m}}{m! (n+m)!} \{ \log(\rho/2) - \frac{1}{2} \Psi(m+1) - \frac{1}{2} \Psi(n+m+1) \}, \quad (3.3)$$

where  $\Psi(m+1) = -\gamma + (1 + \frac{1}{2} + \frac{1}{3} + \dots + 1/m)$

$$\gamma = \lim_{m \rightarrow \infty} \{1 + \frac{1}{2} + \frac{1}{3} + \dots + 1/m - \log m\} = 0.5772157 \dots$$

(Euler's constant).

The calculated curves of this correlation function (3.1) for various values of  $n$  are shown in Fig. 3. In addition to these curves, the exponential and the Gaussian models are plotted in this figure. Models of the exponential, the Gaussian and the modified Bessel function of the first order have been used so far in order to explain both the ionospheric and tropospheric scattering cases. Although these correlation functions are proper for the phenomena of normal scattering, they may not be appropriate for the scattering model of sporadic  $E$  which appears to have denser concentrations of electrons. There is also another trouble that the frequency dependence of sporadic- $E$  propagation may be difficult to explain from the correlation functions normally used in scattering theory. As will be seen from the figure, however, a correlation function of the modified Bessel function of higher order seems appropriate for the sporadic- $E$  model.

### 3.2 Scale of the Sporadic- $E$ Irregularities

It is necessary to note that the scale of turbulence which is represented in the correlation function (3.1) does not describe the scale of irregularities of the sporadic  $E$ , but expresses the usual scale of turbulence responsible for the normal scattering phenomena. So we must define the sporadic- $E$  irregularities from the correlation curves which are found in Fig. 3. We

---

\* cf. Watson *Theory of Bessel Function*.

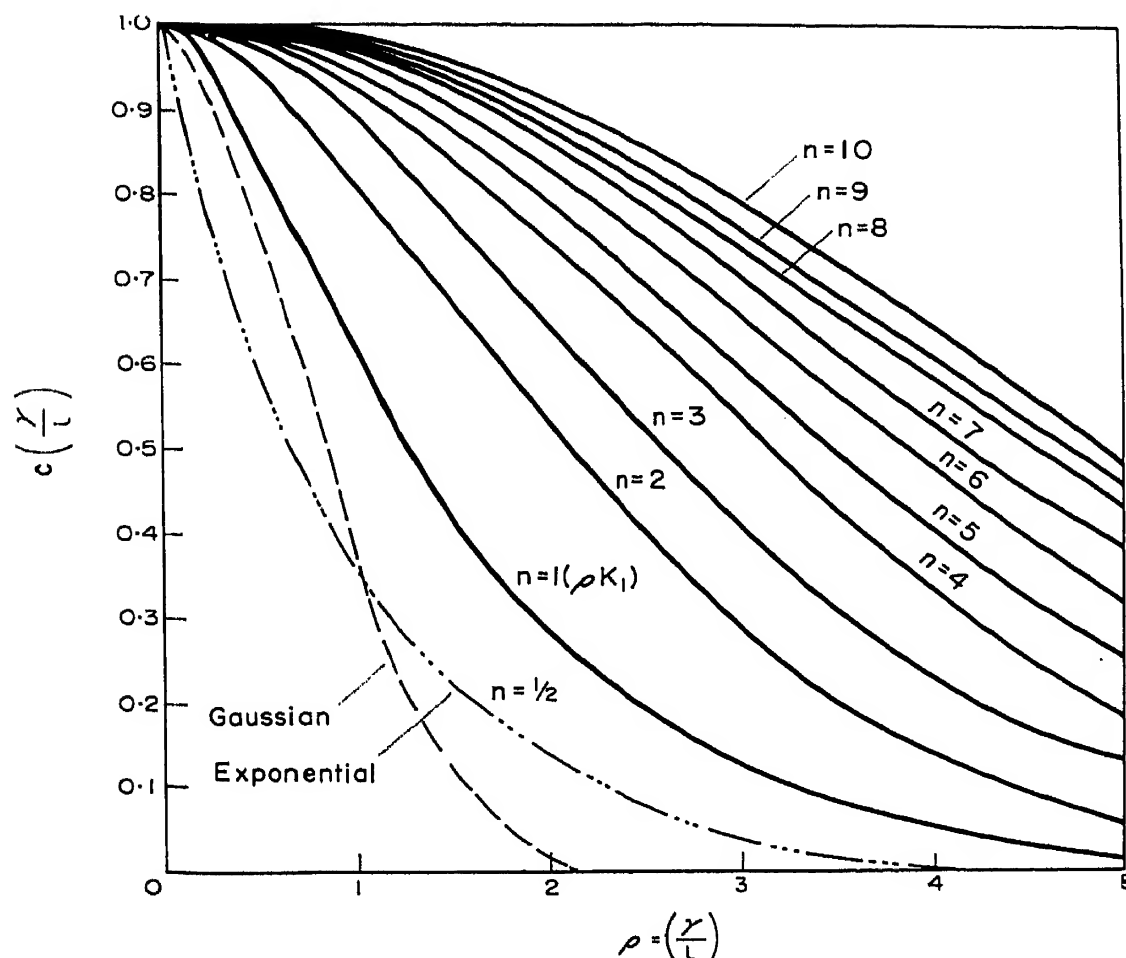


Fig. 3. Autocorrelation function of the modified Bessel function  $[2^{i-n}/\Gamma(n)]\rho^n K_n(\rho)$

shall consider a model wherein a sporadic-*E* cloud which has a large horizontal dimension contains a large number of small irregularities.

Although there exists some confusion concerning the use of the word "scale" to describe the size of irregularities of electron density in the ionosphere, we shall define the "scale" of irregularities to mean the distance in which the correlation is reduced to a specified value, such as 0.5, in accordance with Booker's definition (1958).

From the correlation curves shown in Fig. 3, the scale of the sporadic-*E* irregularities,  $L$ , may be put in the form

$$L = ml, \quad (3.4)$$

where  $l$  is the scale of normal turbulence and  $m$  is an arbitrary multiplication factor. If we take the correlation curve of  $n = 5$  as an example for the scattering model of sporadic *E*, the correlation function decreases to the 0.5 value at a separation of  $r = L = 3.5l$ . Therefore the scale of the sporadic-*E* irregularities has dimensions of  $m$  times (3 ~ 4 times) the scale of the normal turbulence. Numerical estimation of the scale of the sporadic-*E* irregularities  $L$  will be given later.

### 3.3 Scattering Cross-Section

The scattering cross-section is given by

$$\begin{aligned}\sigma(q) &= \frac{k^4 \sin^2 \chi}{16\pi^2 v} \operatorname{Re} \left\{ \frac{16\pi j v l}{q} \int_0^\infty r C_n(\rho) e^{-jq\rho} dr \right\} \\ &= \frac{k^4 \sin^2 \chi l^3}{\pi q} \int_0^\infty \rho C_n(\rho) \sin(q\rho) d\rho,\end{aligned}\quad (3.5)$$

where

$$q = 2kl \sin \frac{\theta}{2} \cong kl\theta, \quad \rho = \frac{r}{l}$$

$\theta$ : scattering angle.

Inserting (3.1) into (3.5) and remembering  $C(0)$  is set equal to

$$\left\langle \left( \frac{\Delta\epsilon}{\epsilon} \right)^2 \right\rangle / 4,$$

the scattering cross-section is obtained in the form (see for example Norton 1956, 1960).

$$\sigma_n = \frac{\left\langle \left( \frac{\Delta\epsilon}{\epsilon} \right)^2 \right\rangle \Gamma(n + \frac{3}{2}) \sin^2 \chi \left\{ 1 + \left[ \frac{\lambda}{4\pi l \sin \theta/2} \right]^2 \right\}^{-(n+3/2)}}{2^{2n+4} \sqrt{\pi} \Gamma(n) k^{2n-1} l^{2n} (\sin \theta/2)^{2n+3}} \quad (3.6)$$

where  $\chi$  is the angle between the direction of scattering and the direction of the incident electric field.

If we put  $n = \frac{1}{2}$  in the above formula,  $\sigma_{1/2}$  is obtained in the form (when the scale of turbulence is large compared with the wave length)

$$\sigma_{1/2} = \frac{\langle (\Delta\epsilon/\epsilon)^2 \rangle \sin^2 \chi}{32\pi l \sin^4 \theta/2} \quad (3.7)$$

which is the Gordon's formula (1955) for the tropospheric scattering case. This was also derived by Booker for the ionospheric scattering case (Bailey 1952).

We have the relation of

$$\left\langle \left( \frac{\Delta\epsilon}{\epsilon} \right)^2 \right\rangle = \left( \frac{\lambda}{\lambda_N} \right)^4 \left( \frac{\Delta N}{N} \right)^2$$

in the ionosphere, so, using the scale of sporadic- $E$  irregularities, formula (3.6) is expressed in the form

$$\sigma_n = \frac{\left( \frac{\Delta N}{N} \right)^2 \left( \frac{\lambda}{\lambda_N} \right)^4 \Gamma(n + \frac{3}{2}) (m)^{2n} \sin^2 \chi \left[ 1 + \left\{ \frac{m\lambda}{4\pi L \sin \theta/2} \right\}^2 \right]^{-(n+3/2)}}{2^{2n+4} \sqrt{\pi} \Gamma(n) (2\pi/\lambda)^{2n-1} L^{2n} (\sin \theta/2)^{2n+3}} \quad (3.8)$$

The received power is obtained from the relation

$$P_r = \frac{P_t b A}{R^2 \sin \theta/2} \sigma_n(\theta, \lambda), \quad (3.9)$$

where  $b$  is the layer thickness and  $A$  is the effective area of the receiving antenna.

### 3.4 Generalized Scattering Cross-Section in the Anisotropic Case

Although the irregularities contributing to the normal scattering phenomenon in the lower ionosphere can be considered isotropic (Booker 1959), the irregularities of sporadic *E* may have an anisotropic structure, such as an ellipsoidal shape, because the scale of the sporadic-*E* irregularities is larger than the scale of the normal turbulence. The scattering theory in an anisotropic turbulence has been developed by several researchers (Booker 1956, Staras 1955, Renau 1961). One may develop the scattering cross-section (3.8) in the case of anisotropic irregularities. The generalized scattering cross-section is given in the form

$$\sigma_n = \frac{\left(\frac{\Delta N}{N}\right)^2 \left(\frac{\lambda}{\lambda_N}\right)^4 \Gamma\left(n + \frac{3}{2}\right) (m)^{2n} \sin^2 \chi L_1 L_2 L_3 \left(1 + \frac{1}{q^2}\right)^{-(n+3/2)}}{2^{2n+4} \sqrt{\pi} \Gamma(n) k^{2n-1} (\sin \theta/2)^{2n+3} [(L_1^2 \sin^2 \gamma + L_2^2 \cos^2 \gamma) \sin^2 \Phi + L_3^2 \cos^2 \Phi]^{n+3/2}} \quad (3.10)$$

where

$$q \cong \frac{2k \sin \theta/2}{m} [(L_1^2 \sin^2 \gamma + L_2^2 \cos^2 \gamma) \sin^2 \Phi + L_3^2 \cos^2 \Phi]^{1/2}$$

and  $L_1$ ,  $L_2$ ,  $L_3$  are different scales of the sporadic-*E* irregularities in directions parallel, normal and vertical to the mean horizontal drift (assumed to lie in the direction of maximum elongation).  $\gamma$  is the angle between the mean drift and the great circle plane. The angle between the plane containing the scattering blob under consideration and the great circle plane is denoted by an angle  $\Phi$ . This generalized scattering cross-section has been also obtained by Norton (1960) for the tropospheric scattering case.

If the sporadic-*E* irregularities exist near the great circle plane, we may put  $\Phi \approx 0$  and in such a case the formula (3.10) becomes

$$\sigma_n = \frac{\left(\frac{\Delta N}{N}\right)^2 \left(\frac{\lambda}{\lambda_N}\right)^4 \Gamma\left(n + \frac{3}{2}\right) (m)^{2n} L_1 L_2 L_3 \left[1 + \left(\frac{m \lambda}{4\pi L_3 \sin \theta/2}\right)^2\right]^{-(n+3/2)}}{2^{2n+4} \sqrt{\pi} \Gamma(n) k^{2n-1} L_3^{2n+3} (\sin \theta/2)^{2n+3}} \quad (3.11)$$

Moreover we can get the scattering cross-section available for the scattering model of sporadic  $E$ , by putting  $n = 5$  into (3.11) and letting  $m = 3.5$  as suggested earlier.

$$\sigma_5 = 1.03 \times 10^2 \frac{\left(\frac{\Delta N}{N}\right)^2 \left(\frac{f_N}{f}\right)^4 L_1 L_2 \left[1 + \left(\frac{3.5\lambda}{4\pi L_3 \sin \theta/2}\right)^2\right]^{-13/2}}{(2\pi L_3/\lambda)^9 L_3^3 (\sin \theta/2)^{13}} \quad (3.12)$$

### 3.5 Relationship between $E_s$ Scattering and Normal Scattering in the Ionosphere

Although it has not yet been clarified as to what kind of mechanisms produce these sporadic- $E$  irregularities, it is interesting to consider that these irregularities may have a close connection with turbulence produced by wind shear prevailing in this region. Gallet (1955) proposed a mechanism of stratification of sporadic  $E$  by considering the mixing process in a turbulent region. Recently Layzer (see his article in this book) has suggested that it may be necessary to consider very strong wind shears such as about 100 m/sec/km in order to maintain turbulent motion in this region and these wind shears may occur in a narrow layer of the order of 1 km in thickness. If we consider such a jet-like high shear layer, this layer may be expected to act as a partial reflector or scattering source due to fluctuations of electron density produced by turbulent mixing. Also, the recent experimental evidence has shown that wind shear as high as 140 m/sec/km exist in the 100 ~ 110 km region while, simultaneously, ionogram records show sporadic  $E$  near the level of maximum shear (Storey 1960).

According to Gallet (1955), the fluctuation of electron density is produced by the transport process.

$$\left(\frac{\Delta N}{N}\right)^2 \cong \frac{1}{3} l_0^2 \left(\frac{\text{grad } N}{N}\right)^2.$$

$l_0$  means the largest scale of turbulence in the layer. As the ambient daytime electron density in the  $E$  region is  $N \cong 10^5 \text{ cm}^{-3}$  and the layer thickness of sporadic  $E$  may be considered to lie in ranges from a few kilometers down to a few hundred meters, the value of  $(\Delta N/N)^2$  in the daytime is the order of unity to  $10^{-1}$ . Since the sharp gradient of the electron density will decrease with disappearance of the sporadic- $E$  clouds, the value of  $(\Delta N/N)^2$  will also decrease to the order of  $10^{-3}$  or  $10^{-4}$  corresponding to normal scattering. As the sporadic- $E$  clouds disappear or move to other places, the high concentration of electron density in this region decays to the normal state and therefore the number of  $n$  ( $n = 5 \sim 6$ ) in the correlation function will tend to small numbers such as  $n = 1$ . In

this case, as the irregularities are considered as isotropic, we can obtain the scattering cross-section from (3.6) by putting  $n = 1$ .

$$\sigma_1 = 1.17 \times 10^{-2} \frac{(\Delta N/N)^2 (f_N/f)^4}{(2\pi l/\lambda) l (\sin \theta/2)^5} \quad (3.13)$$

This formula represents the normal scattering case. Although there is still some ambiguity concerning the scale of turbulence in the ionosphere, we have taken a value of  $l = 15$  m as the average scale of turbulence corresponding to v.h.f. forward scattering ( $f = 50$  Mc/s) (Tao 1958). Booker (1959) has also recently suggested the presence of irregularities of the electron density with scales in ranges from 20 to 60 meters in the lower ionosphere. Several calculated curves of the basic transmission loss for the  $E_s$  scattering and the normal scattering are shown in Fig. 6 by using the formulas (3.12) and (3.13).

#### 4. DISTANCE DEPENDENCE OF SPORADIC-*E* PROPAGATION

An experimental determination of distance dependence is shown in Fig. 4. This experiment was carried out, using the frequency of 49.68 Mc/s, in the summer of 1959 by the Radio Research Laboratories and K.D.D. (Japan's Overseas Radio and Cable System) in Japan in order to examine the distance dependence of the sporadic-*E* propagation with the cooperation of the NBS Central Radio Propagation Laboratory. The more detailed analysis of this experiment has been published in other papers (Tao, Sawaji, Sakurazawa and Yamaoka 1960, Miya, Sasaki and Ishikawa 1961).

The transmitting point was Okuma, Okinawa, and the receiving points were Yonago, Akita and Hakodate in Japan. In addition to the summer (1959) data, we have added the observations at Hiraiso during the summer period of 1958. Distances between the transmitting point and each receiving point are shown in Table 1.

The 10 per cent, 50 per cent and 90 per cent values of the statistical cumulative distribution of the  $E_s$  signals are plotted in Fig. 4. Statistical results of  $f_o E_s$  measured at the ionosonde stations in Japan during the same period are indicated in Table 2.

We shall next examine this distance dependence from the theoretical point of view. The most appropriate theoretical curves for the experimental result are shown in Fig. 5 and Fig. 6 derived from the thin layer theory and the scattering theory described in Sections 2 and 3 respectively. As measurements indicate that the layer thickness of sporadic *E* ranges from a few kilometers down to 50 meters, curves pertinent to these ranges are shown in Fig. 5 and Fig. 6, and seem to fit the observations reasonably well.



Table 1

Rec. Station	Long.	Lat.	Distance	Rec. Antenna	Antenna Gain	Antenna Height Above Ground
Yonago	133°22'E	35°27'N	1100km	2-stack 5-element Yagi	14.3db	18.4m
Hiraiso	140°37'E	36°22'N	1590km	Rhombic	20.0db	15.0m
Akita	140°32'E	39°44'N	1820km	2-stack, 5-element Yagi	14.1db	30.0m
Hakodate	140°43'E	45°24'N	2020km	5-element Yagi	9.1db	6.0m*

\* Approximately 280m above the sea.

Table 2.

Ionosonde Station	$f_oE_s$ (10%)	$f_oE_s$ (50%)	$f_oE_s$ (90%)
Yamagawa	10.5 Mc/s	6.2 Mc/s	3.4 Mc/s
Kokubunji	10.8 Mc/s	6.4 Mc/s	4.0 Mc/s
Akita	12.8 Mc/s	7.2 Mc/s	4.3 Mc/s

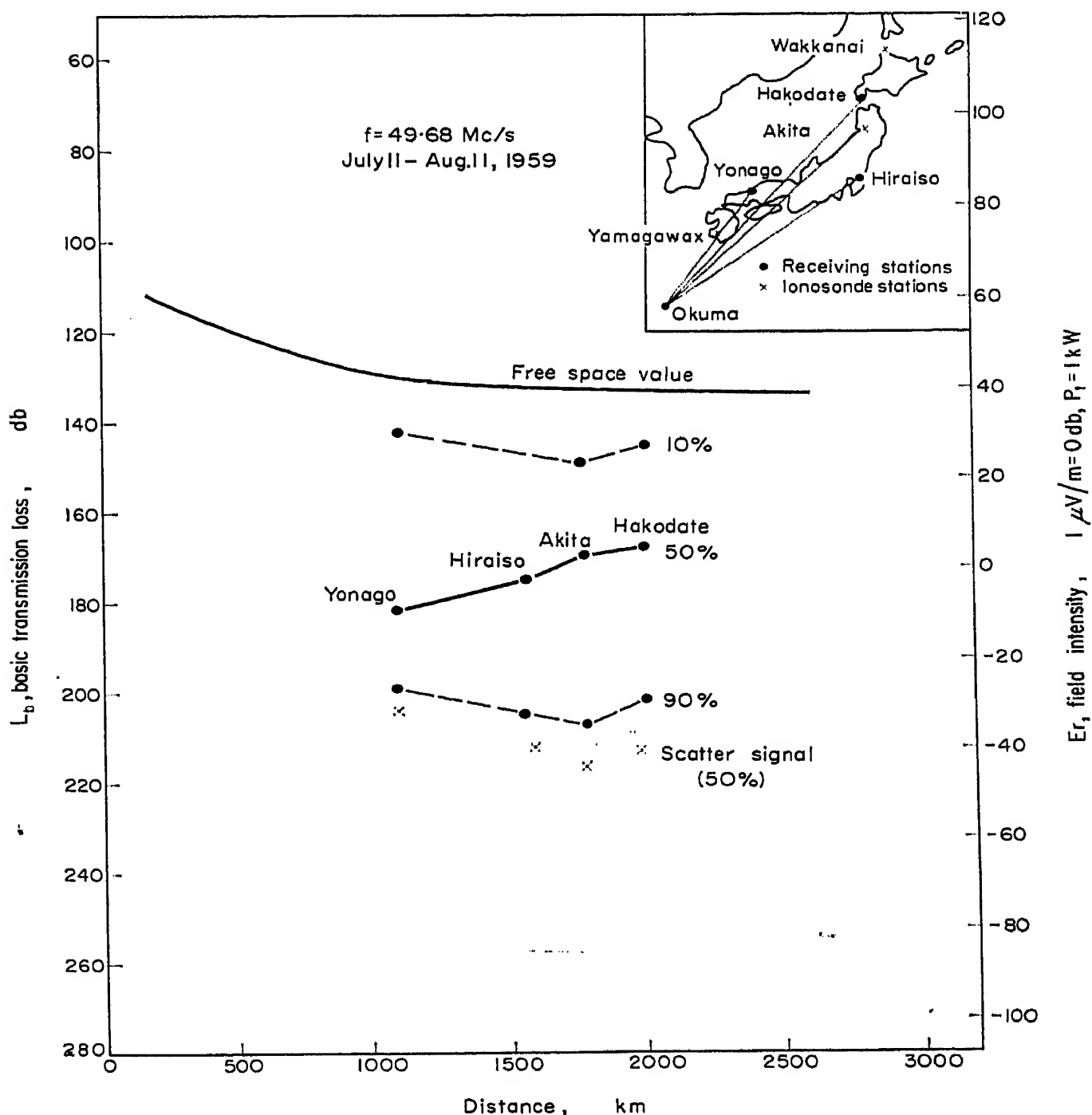


Fig. 4. Experimental results of the distance dependence of sporadic-E propagation

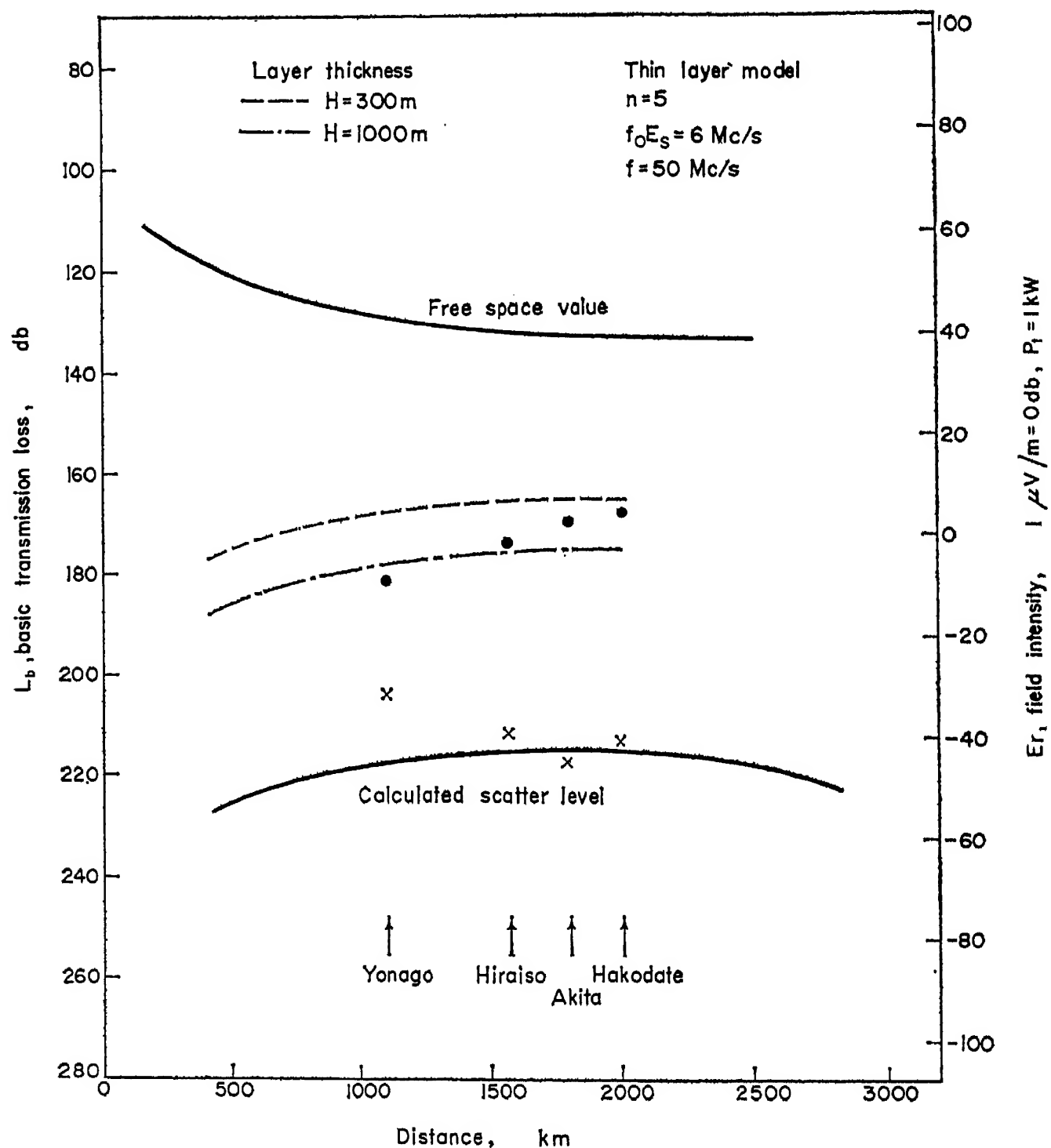


Fig. 5. Distance dependence of sporadic-E propagation (thin layer model).

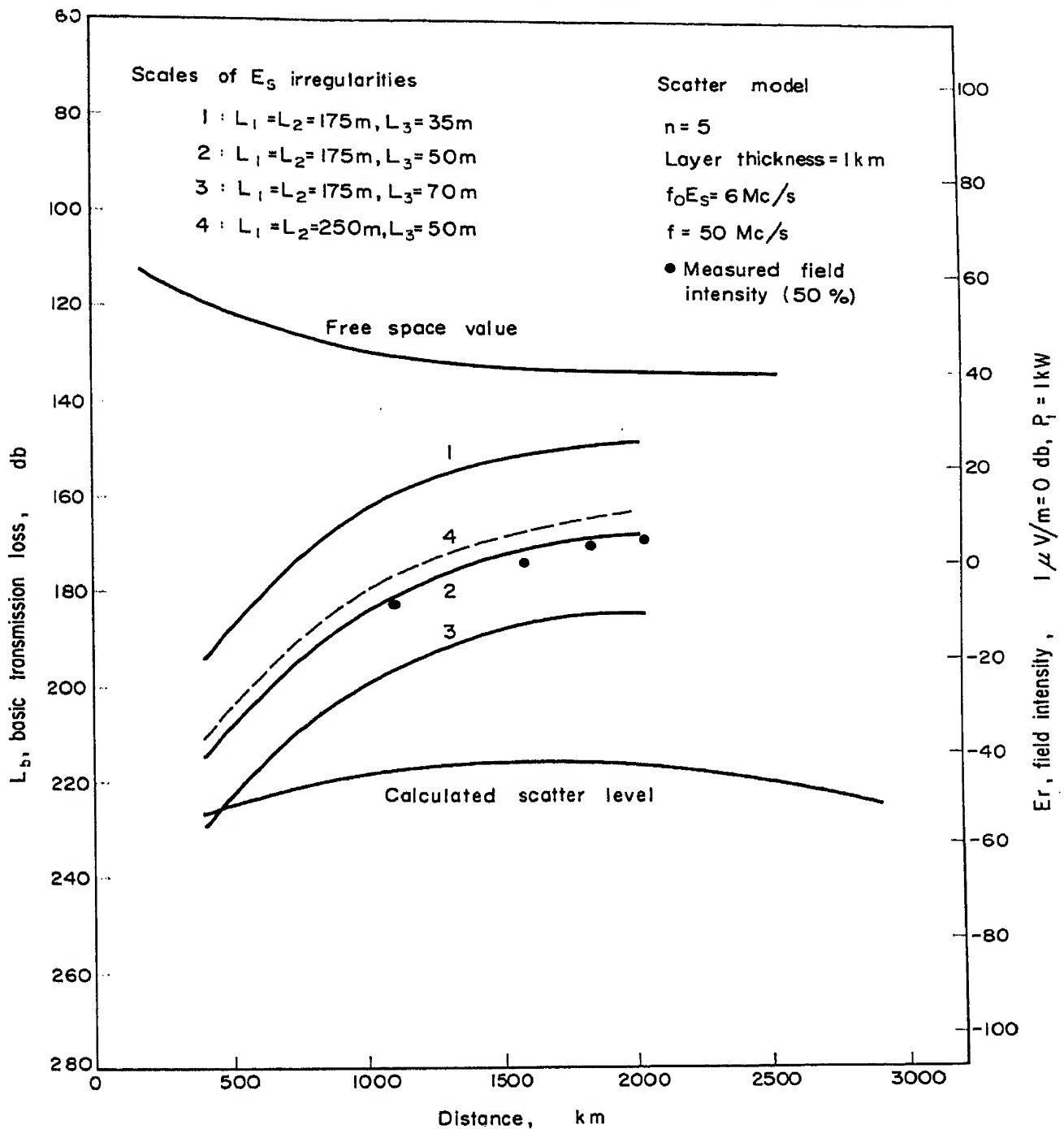


Fig. 6. Distance dependence of sporadic-*E* propagation (scatter model).

### 5. FREQUENCY DEPENDENCE OF SPORADIC-*E* PROPAGATION

It is well known that the scattered power in normal ionospheric scatter propagation is inversely proportional to about the fifth or sixth power of frequency (Booker 1959, Bailey 1955, Bray, Saxton, White and Luscombe 1956, Wheelon 1957). Experiments show, however, that the frequency exponent increases in the case of sporadic *E*. It is reported by Davis, Smith and Ellyett (1959) that the median value of the frequency exponent in sporadic-*E* propagation is 12 during summer time in 1955 and 17 during winter time. This experiment was carried out between Cedar Rapids and

Sterling and signal intensities were recorded simultaneously at 27.775 Mc/s and 49.8 Mc/s. These experimental results are plotted with dotted curves in Fig. 7. In a recent experiment which has been carried out by the Central

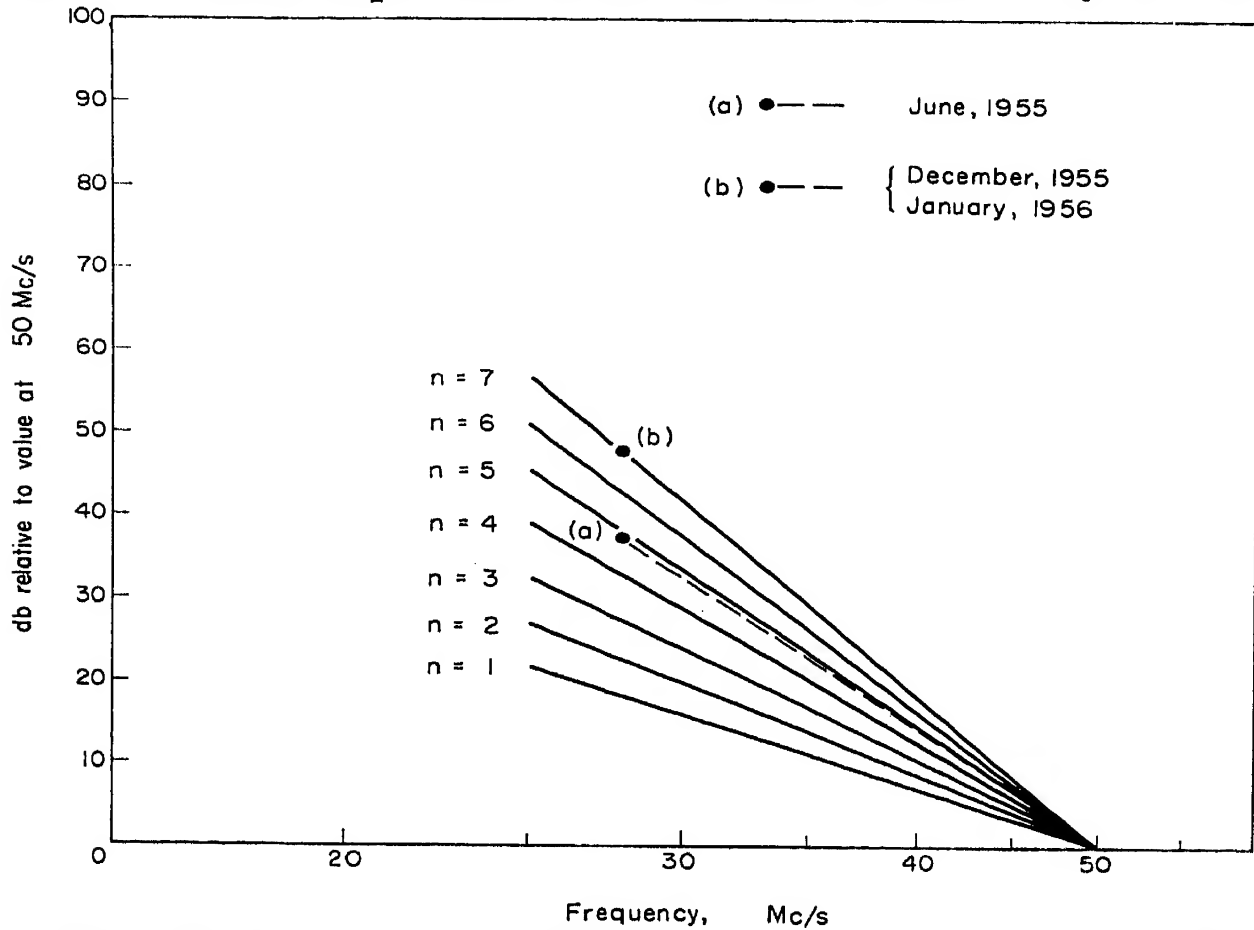


Fig. 7. Experimental results of the frequency dependence of sporadic- $E$  propagation

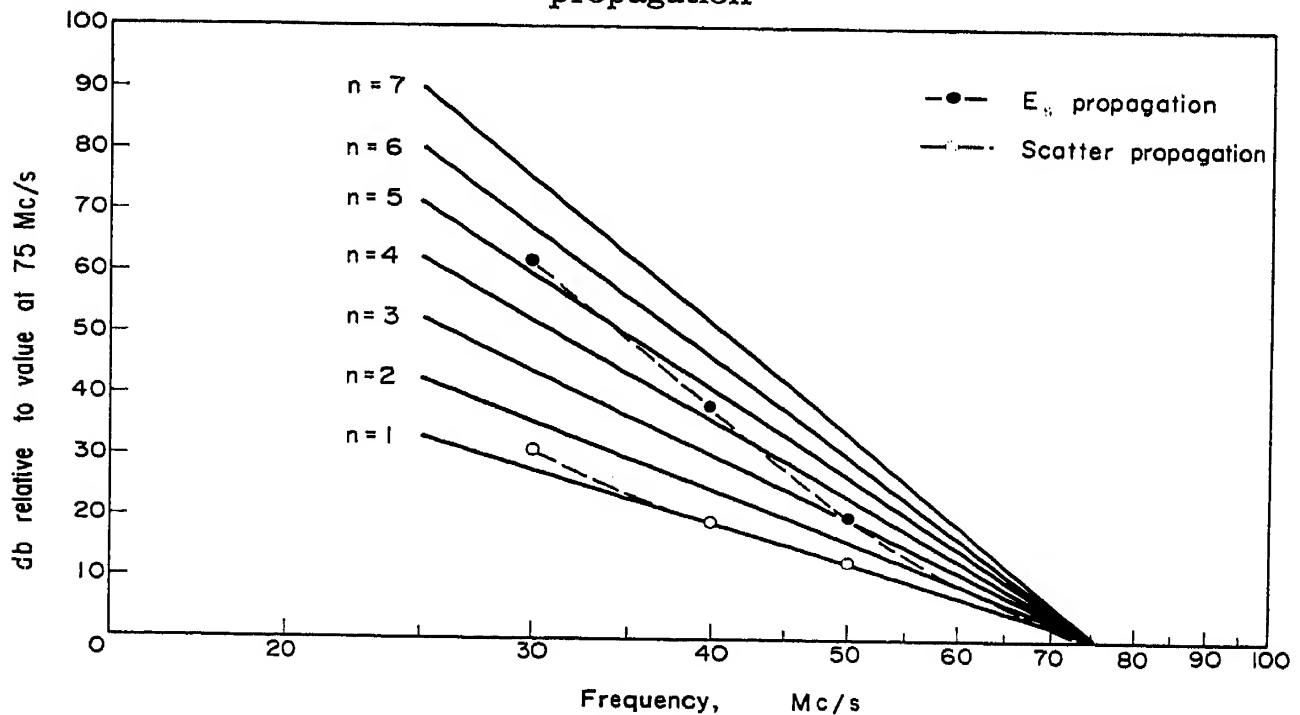


Fig. 8. Experimental results of the frequency dependence of sporadic- $E$  propagation and normal scatter propagation.

Radio Propagation Laboratory in order to examine the frequency dependence of scatter propagation using five different frequencies, that is, approximately 30, 40, 50, 74 and 108 Mc/s, Blair (1959) reported on the frequency dependence of sporadic-*E* propagation besides that of the normal scatter propagation. This experimental evidence is shown with a dashed curve in Fig. 8. An additional dashed curve representing normal scatter propagation is also plotted in the same figure. The curve shows that the signal enhancement due to sporadic *E* diminishes rapidly with frequency when compared with normal scattering.

We shall try to check this frequency dependence from the theoretical point of view. In Fig. 9 are plotted the theoretical curves derived from the

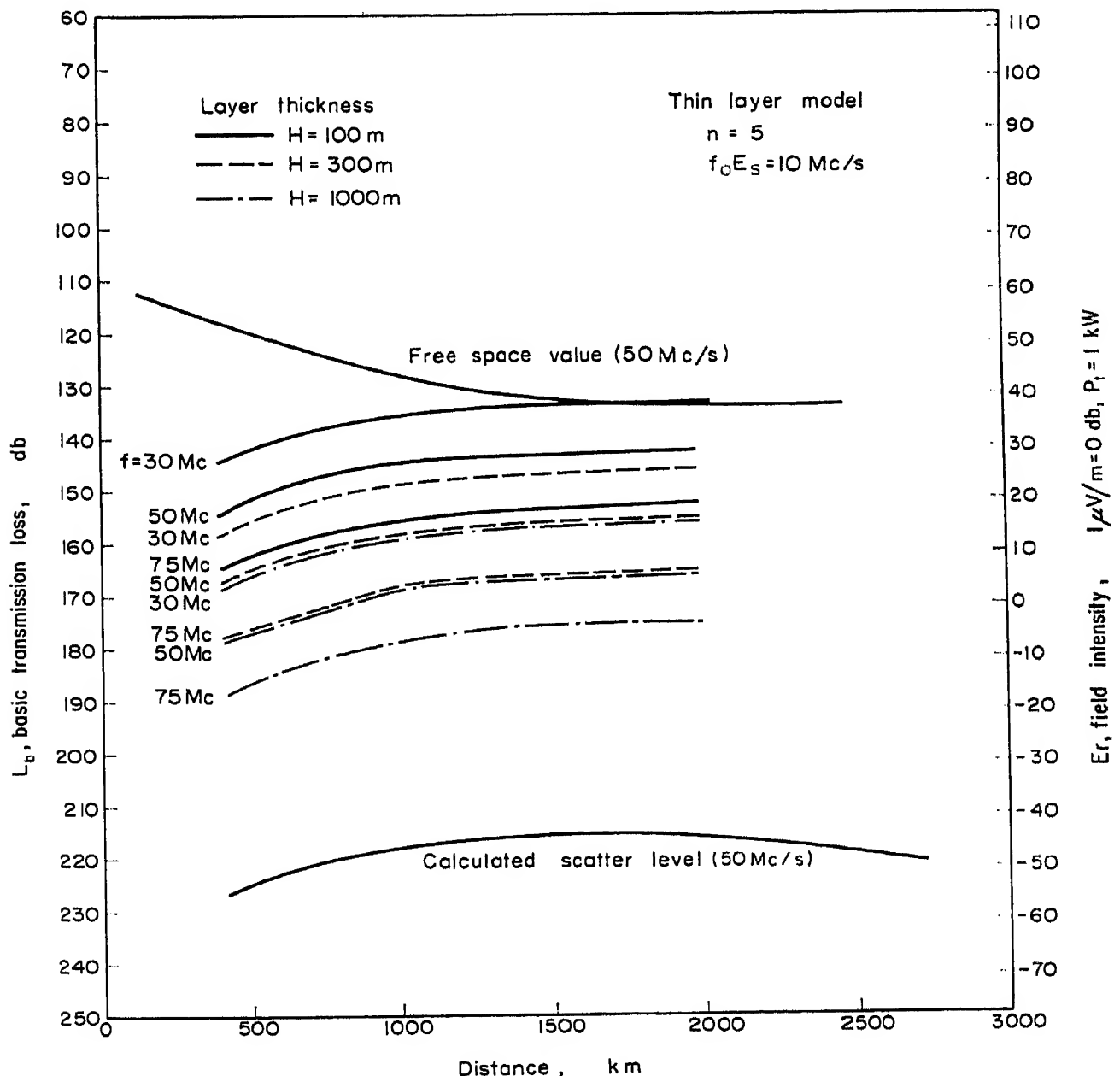


Fig. 9. Frequency and distance dependences of sporadic-*E* propagation by means of the thin layer model.

thin layer theory with frequency (30 Mc/s, 50 Mc/s, 75 Mc/s) as a parameter and several layer thicknesses (100 m, 300 m, 1000 m) with fixed value of the critical frequency of  $E_s$  ( $f_o E_s = 10$  Mc/s) and an exponent of the electron distribution ( $n = 5$ ). The corresponding calculation is given in Fig. 10 by using the scattering model.

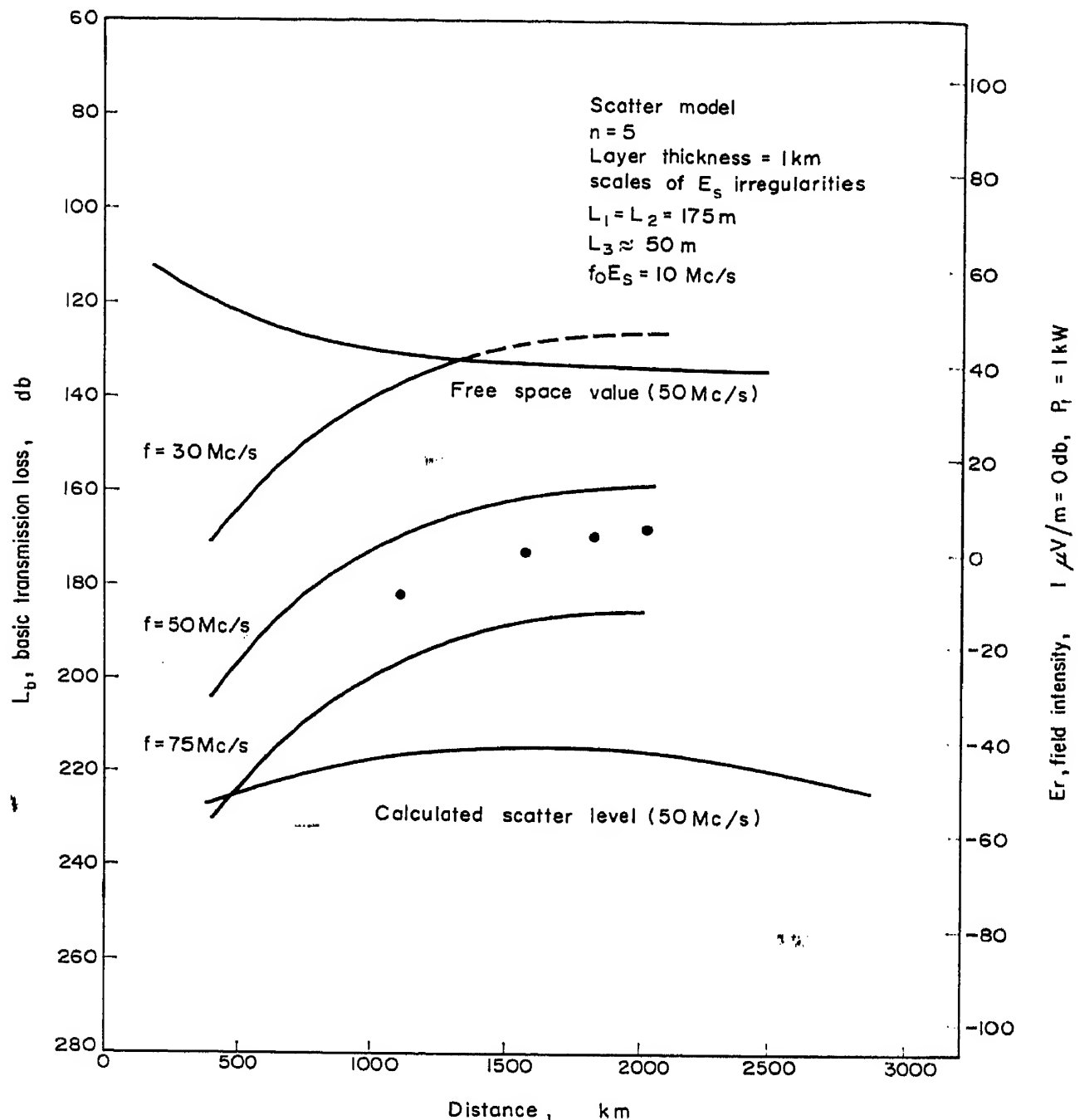


Fig. 10. Distance and frequency dependences of sporadic- $E$  propagation by means of the scatter model.

Concerning the frequency dependence, the thin layer model which is described in this paper does not seem to be a good fit. The scattering model which has an auto-correlation function of the modified Bessel function of a high order seems to be preferable as will be seen from the

formula (3.12) or Figs. 7, 8 and 10. From the scattering theory for sporadic  $E$  (i.e. equations (3.8) and (3.9)), we get

$$P_r \propto \frac{1}{f^{(2n+5)}}$$

If we take a high order value of  $n$  in the correlation function, that is,  $n = 4 \sim n = 7$ , we obtain

$$P_r \propto \frac{1}{f^{13}} \sim \frac{1}{f^{19}}.$$

Therefore we can explain the frequency dependence of sporadic  $E$  by considering an auto-correlation function which has a very slow decrease with  $\rho$  ( $= r/l$ ). In Figs. 7 and 8 are drawn families of curves with various values of  $n$  in the modified Bessel function of  $n$  order. From these figures, the auto-correlations of the modified Bessel function with  $n = 4 \sim n = 7$  seem to be reasonable for the scattering model of sporadic  $E$ . It is also of interest to note that the curve of  $n = 1$  fits the normal ionospheric scatter propagation measurements. Although Norton (1959) has stated in his recent paper that this  $\rho K_1(\rho)$  correlation function has definite advantages over the exponential model for describing the turbulence of refractivity in the troposphere and stratosphere, it also seems to be quite good for the normal turbulence situation in the ionosphere.

## 6. CORRELATION BETWEEN $f_oE_s$ AND FIELD STRENGTH

In this section, we shall briefly consider a correlation between  $f_oE_s$  and the received  $E_s$  field strength. Figure 11 shows some correlograms between these parameters. The normalized  $E_s$  field strengths are the hourly median values observed at Yonago during the period January to December in 1958. As the ionosonde station at Yamagawa is situated almost exactly at the midpoint between Okuma (transmitting point) and Yonago (receiving point), it is appropriate to use values of  $f_oE_s$  observed at Yamagawa to investigate a relationship between the field strength and  $f_oE_s$ . Since the field strength used in this analysis is the hourly median value, the corresponding value of  $f_oE_s$  is interpolated from the measured values at each hour. A more rigorous analysis has been made by Yamaoka (1960) by using the instantaneous value of field strength and the value of  $f_oE_s$  observed every 15 minutes. This is shown in Fig. 12 and data during periods of July and August in 1959 are used. From these figures, it is interesting to note that the field strength increases abruptly in the interval from  $f_oE_s = 8$  Mc/s to  $f_oE_s = 10$  Mc/s. Although the cause of this increase is not yet clear, it may be related to the fact that this interval is near to the



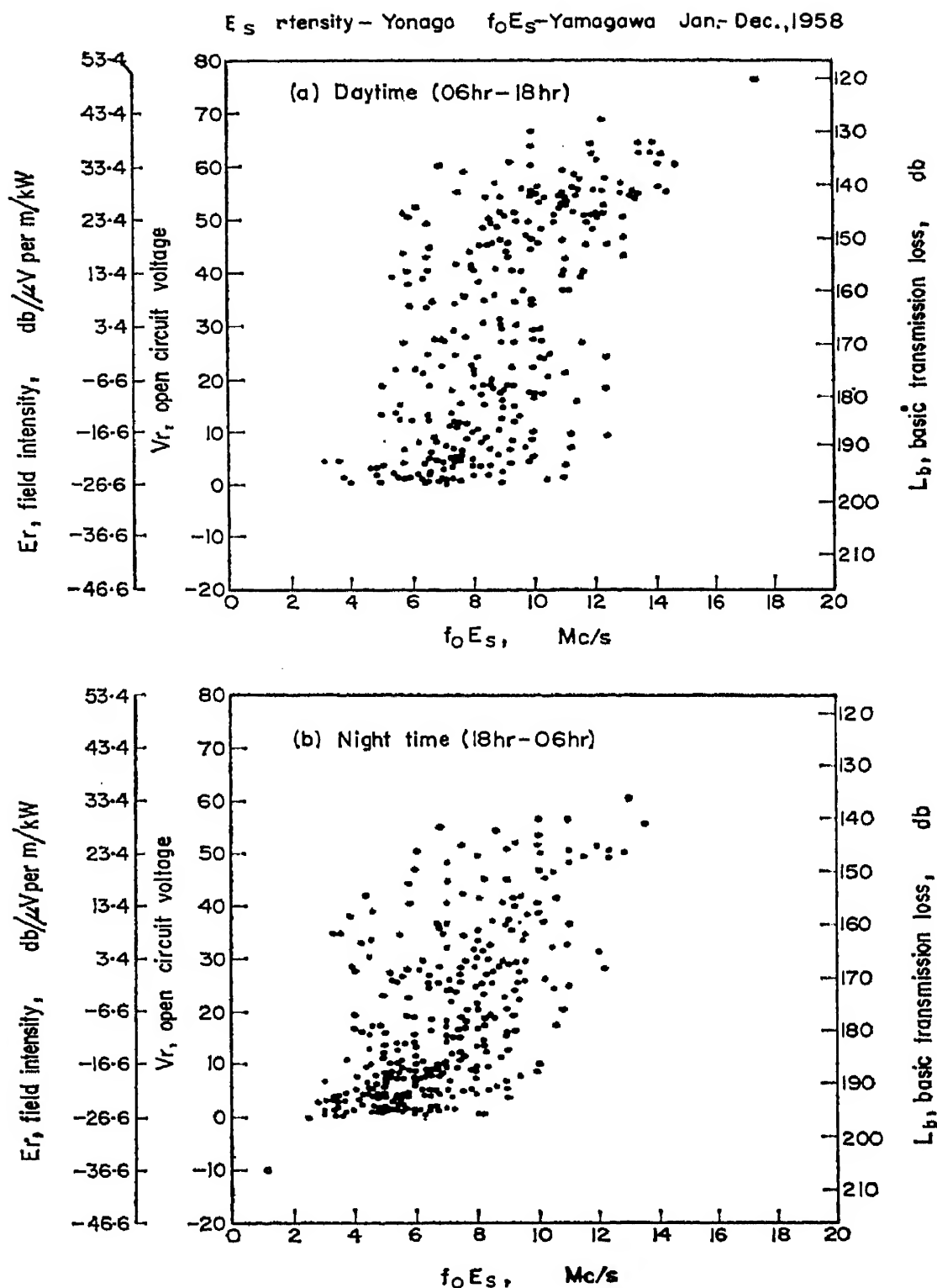


Fig. 11. Correlation between  $f_o E_s$  and field strength of sporadic  $E$ .

plasma frequency for normal reflection in this transmission circuit (i.e. 49.68 Mc/sec  $\theta \sim 12$  Mc). This seems to suggest that there are two modes of sporadic- $E$  propagation, that is, the high field strength corresponding to high values of  $f_o E_s$  seems to be due to the reflection mechanism and the relatively low field strength is due to the scattering mechanism. Theoretical curves calculated from the thin layer and scattering models are compared with some measured field intensities for various values of  $f_o E_s$ . From

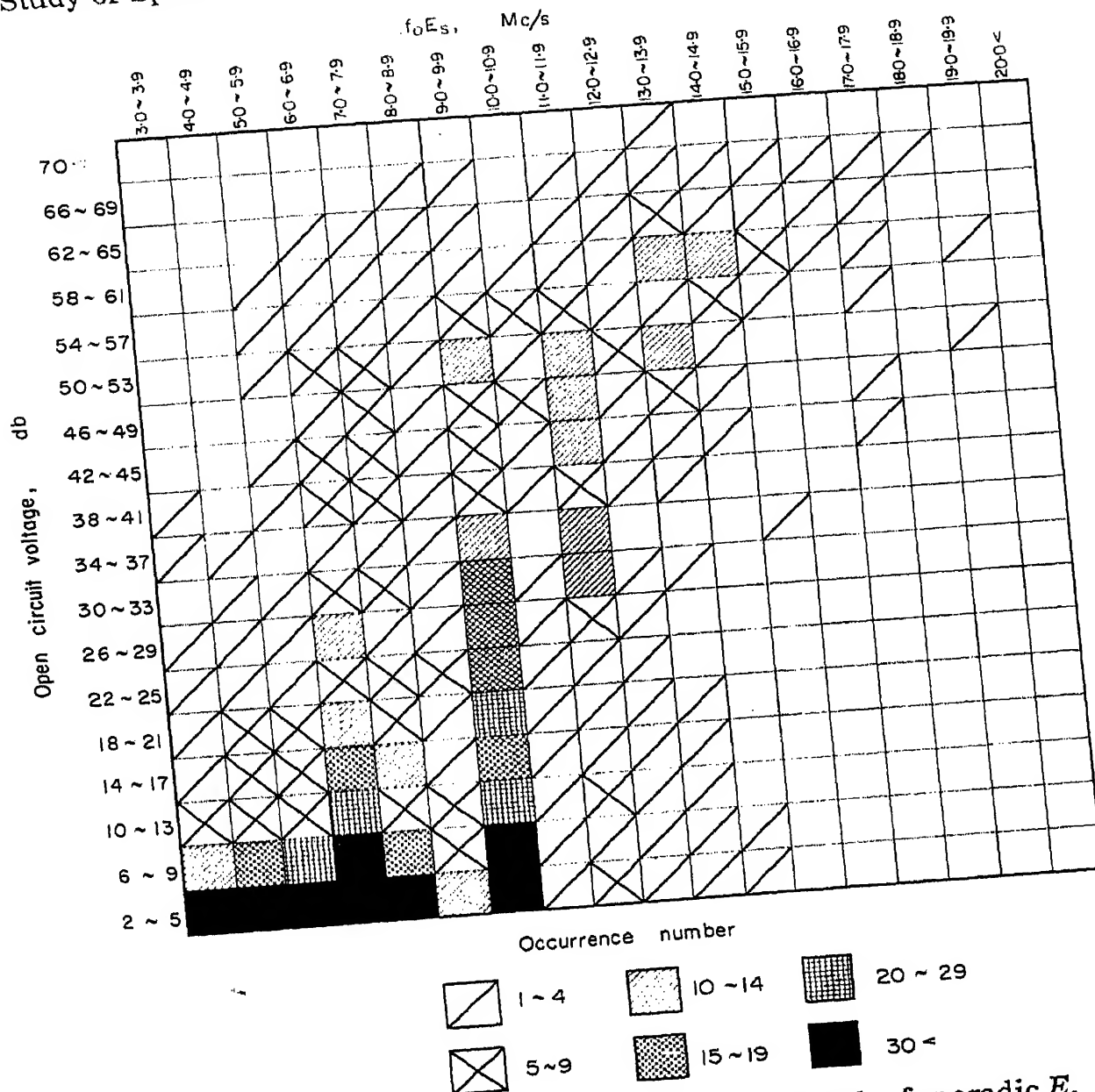


Fig. 12. Correlation between  $f_o E_s$  and the field strength of sporadic *E*.

Fig. 13 it can be seen that a fairly high field intensity of sporadic-*E* enhancement corresponding to a comparatively high plasma frequency may be explained by reflection from a thin ionized layer, whereas a relatively low sporadic-*E* field intensity may be produced by the scattering mechanism.

## 7. CONCLUSIONS

From the above theoretical investigation for the sporadic-*E* model, some conclusions may be drawn.

- (i) High field strength of sporadic-*E* enhancements may be explained by reflection from a thin layer with electron density approaching the

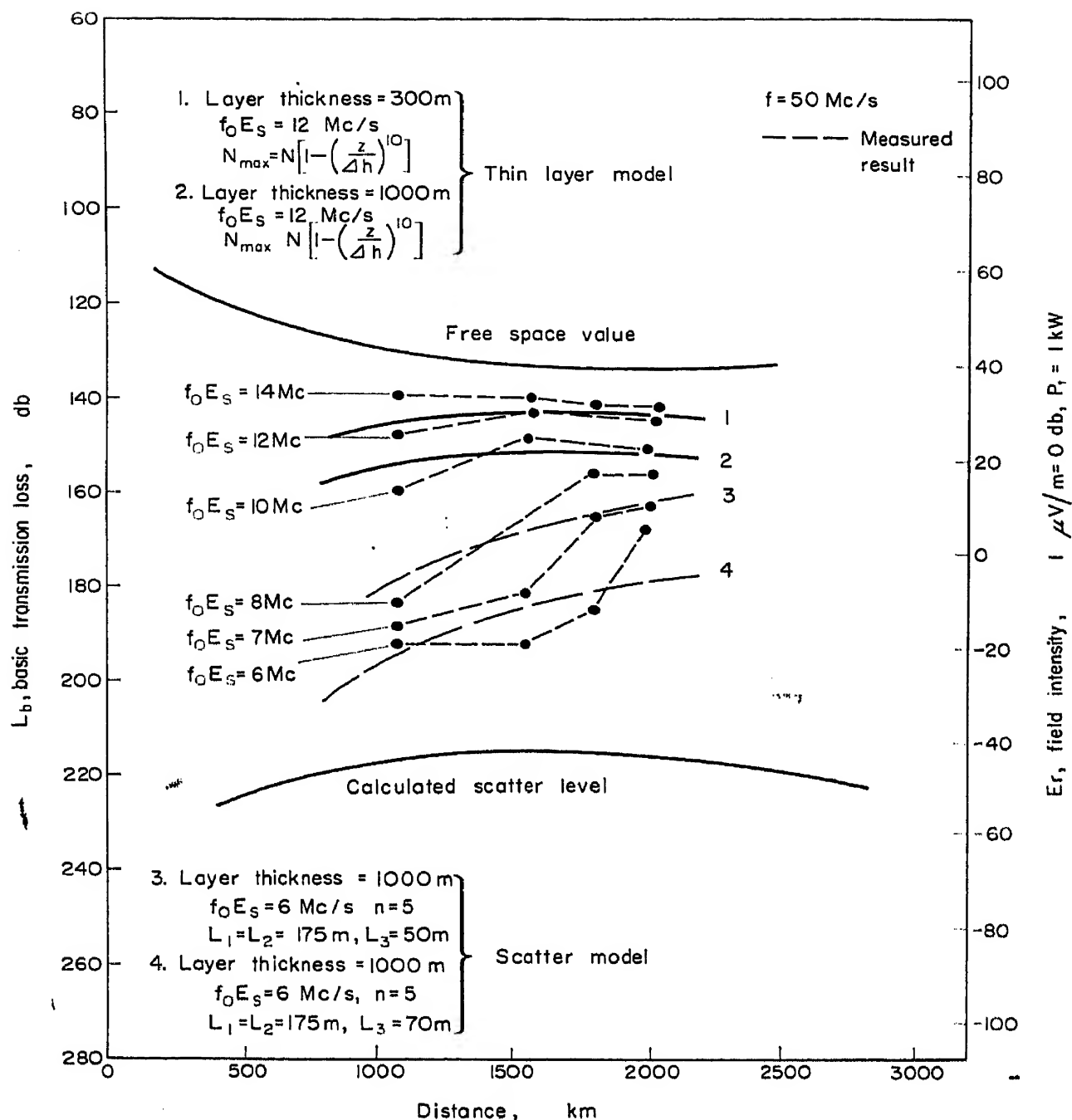


Fig. 13. Theoretical explanation for a relationship between  $f_0 E_s$  and  $E_s$  field intensity.

necessary plasma density (i.e.  $2 \times 10^6 \text{ e/cc}$  for the Okuma-to-Yonago circuit).

(ii) Relatively low field strength of sporadic  $E$  may be explained by the scattering model.

(iii) The scattering model for sporadic  $E$  is expressed through an auto-correlation function of the modified Bessel function of higher order. Each blob of ionization may be considered to have a horizontal scale of the order of 200 m and a vertical scale of 50 m.

(iv) Concerning the frequency dependence of sporadic  $E$ , the thin layer theory developed in this paper does not seem to be appropriate, however, this frequency dependence can be explained by the scattering model.

(v) If we assume a layer thickness of sporadic *E* of 300 m  $\sim$  1000 m, we can explain the distance dependence of the median field strength from both the thin layer and the scattering theories.

*Acknowledgment*—This research has been carried out as a part of the sporadic-*E* project at the Boulder Laboratories. The author wishes to express his sincere thanks to Dr. E. K. Smith for his help and advice given throughout the course of this study. The author is much indebted to Dr. R. M. Gallet, Dr. K. Davies, Mr. V. Agy, Mr. J. Watts, Dr. H. H. Howe, Mr. J. W. Finney and Mr. J. F. DeGregorio at the Boulder Laboratories for their kind suggestions and discussions. His cordial thanks are also due to Messieurs A. Sakurazawa, K. Sawaji and M. Yamaoka at the Radio Research Laboratories in Japan for their effort in arranging necessary data.

#### REFERENCES

- BAILEY, D. K. (1952) *Phys. Rev.* **86**, 41.  
 BAILEY, D. K. (1955) *Proc. Inst. Radio Engrs.* **43**, 1181.  
 BLAIR, J. C. (1959) *NBS Tech. Note* 9.  
 BOOKER, H. G. (quoted by APPLETON NAISMITH and INGRAM) (1938) *Proc. Phys. Soc.* **51**, 81.  
 BOOKER, H. G. (1956) *J. Atmosph. Terr. Phys.* **8**, 204.  
 BOOKER, H. G. (1958) *Proc. Inst. Radio Engrs.* **46**, 298.  
 BOOKER, H. G. (1959) *J. Geophys. Res.* **64**, 2164.  
 BOOKER, H. G. and GORDON, W. E. (1950) *Proc. Inst. Radio Engrs.* **38**, 401.  
 BRAY, W. J., SAXTON, J. A., WHITE, R. W. and LUSCOMBE, G. W. (1956) *Proc. Inst. Radio Engrs.* **103**, 236.  
 DAVIS, R. M. (1959) *Proc. Inst. Radio Engrs.* **47**, 762.  
 FRIIS, H. T., CRAWFORD, A. B. and HOGG, D. C. (1957) *Bell Sys. Tech. J.* **36**, 627.  
 GALLET, R. M. (1955) *Proc. Inst. Radio Engrs.* **43**, 1240.  
 GORDON, W. E. (1955) *Proc. Inst. Radio Engrs.* **43**, 23.  
 HARTREE, D. R. (1929) *Proc. Camb. Phil. Soc.* **25**, 97.  
 MIYA, K., SASAKI, T. and ISHIKAWA, M. (1961) *J. Res. NBS*, **65D**.  
 NORTON, K. A. (1956) *Inst. Radio Engrs.* **CS-4**, 39.  
 NORTON, K. A. (1959) *J. Atmosph. Terr. Phys.* **15**, 206.  
 NORTON, K. A. (1960) *J. Geophys. Res.* **65**, 2029.  
 RAWER, K. (1939) *Ann. d. Physik.* **35**, 385.  
 RENAULT, J. (1961) *J. Res. NBS* **65D** (in press).  
 RYDBECK, O. E. H. (1942) *J. Appl. Phys.* **13**, 577.  
 RYDBECK, O. E. H. (1946) *Trans. Chalmers, Univ. Tech.* **34**.  
 SMITH, E. K. (1957) *NBS Cir.* 582.  
 STARAS, H. (1955) *Proc. Inst. Radio Engrs.* **43**, 1374.  
 STORY, L. R. O. (1960) (Private communication to Dr. E. K. Smith).  
 TAO, K. (1958) *J. Radio Res. Lab.* **5**, 20.  
 TAO, K., SAWAJI, K., SAKURAZAWA, A. and YAMAOKA, M. (1960) *J. Radio Res. Lab.* **7**, 177.  
 WHEELON, A. D. (1957) *J. Geophys. Res.* **62**, 93.  
 YAMAOKA, M. (1960) *J. Radio Res. Lab.* **7**, 599.

# The Turbulence Criterion in Stably Stratified Shear Flow and the Origin of Sporadic *E*

DAVID LAYZER

Harvard College Observatory, Cambridge, Massachusetts, U.S.A.

**Abstract**—This article explores the hypothesis that sporadic *E* and other stratification phenomena are caused by aerodynamic processes which distort the normal electron-density gradient in such a way as to produce partially reflecting layers. Measurements of winds in the upper atmosphere have shown that exceptionally high wind shears, of the order 100 (m/sec)/km, are confined to narrow layers with roughly the same geometrical properties as the layers responsible for discrete radio reflections. Since high wind shears tend to promote and maintain turbulence, the question naturally arises whether these high-shear layers are turbulent, and if so whether turbulence can render such a layer partially reflecting to radio waves of appropriate wavelengths. In order to answer the first question, we give in Section II a detailed discussion of the turbulence criterion in stably stratified shear flow. Previous work on this subject is reviewed and a somewhat simplified derivation of Townsend's criterion is given. A new necessary condition for the maintenance of turbulence is suggested, namely that the lifetime of turbulent eddies be smaller than the characteristic period of gravitational oscillations in the fluid. This condition turns out to be more stringent than the usual energy requirement. The resulting value of the critical Richardson number is  $Ri_c = 1/25$ . If this value is correct, turbulence in the 80–120 km region will be confined to the high-shear layers, if it occurs at all. In Section III we investigate the effect of a narrow turbulent layer on the electron-density profile. As a result of turbulent mixing, the electron-density profile may develop a shelf-like near-discontinuity capable of reflecting radio waves. Finally, the effects of meteor ionization are studied. It is shown that the ionization generated by meteors may be regarded as spatially homogeneous and that the contribution of meteor-generated ionization to the electron-density profile does not change its character in a qualitative way.

## 1. INTRODUCTION

It is well known that the normal ionospheric layers—*D*, *E*, *F*<sub>1</sub> and *F*<sub>2</sub>—result from broad peaks in the profile of electron density versus height. This is clearly shown by the variation of virtual height (*h'*) with frequency (*f*) on ionosonde records. If the electron density increased monotonically with height, *h'* would increase smoothly with *f* and the ionosonde records would not show their characteristic jumps. In recent years rocket flights have produced direct evidence for peaks at approximately the predicted heights.

Chapman's theory of layer formation accounts for these peaks along the following lines. The rate of ionization produced by a beam of radiation traversing an atmosphere of variable density varies directly as the intensity

of the beam and as the density of particles capable of being ionized by the incident radiation. A beam entering the earth's atmosphere from above encounters an ever-increasing particle density, but the beam continually diminishes in intensity as it penetrates deeper. The rate of ionization is therefore a strongly peaked function of path length along the ionizing beam. From this it follows that the contribution to the electron-density profile from a given photo-ionization process also has a definite peak. As several distinct photo-ionization processes, involving distinct wavelength regions and distinct atomic and molecular species, produce free electrons, the resultant electron-density profile should—and, according to rocket measurements, does—have a complicated shape. Chapman's theory predicts that the height of any given peak should vary markedly, according to a particular law, with the zenith angle of the sun, and this prediction has been borne out by experiment.

Ionospheric soundings and other radio experiments have shown that in addition to the normal ionospheric layers there exist numerous other layers of a different kind. These layers occur in the height range 65–130 km. They differ most conspicuously from the normal ionospheric layers in the following respects. (i) They are transient, lasting from a few minutes to at most a few hours. (ii) They are always partially transparent. (iii) They are narrow, with half-thicknesses of the order of 1 km. (This follows from the well-known experimental result that the virtual heights of such layers do not increase appreciably with increasing frequency.) (iv) The heights at which they most frequently occur show no marked dependence on the zenith angle of the sun. Careful statistical studies have failed to reveal either diurnal or seasonal variations in the heights of occurrence, though such variations are very conspicuous in the height of maximum *E*-layer ionization.

The most highly reflecting of the transient layers occur in the *E*-region and are responsible for the phenomenon known as sporadic *E* ( $E_s$ ). Sporadic *E* has been much more extensively studied than the reflections from temporary strata below the *E*-layer. From a theoretical point of view, however, there is as yet no compelling reason to regard sporadic *E* as inherently different from the less conspicuous phenomena that occur at lesser heights. I shall accordingly use the word stratification as a blanket term meaning stratification in the lower ionosphere as well as sporadic *E*. Of course an adequate theory of ionospheric stratification would have to account for the exceptionally high reflectivity of  $E_s$  layers.

As yet very little is known about the nature of the reflecting strata or about how they come into being. The narrowness of the layers and the absence of diurnal and seasonal variations in their preferred heights of occurrence rule out the possibility that they are formed in the same way as the normal ionospheric layers. More generally, these two characteristics

of ionospheric stratification make it seem unlikely that either corpuscular or electromagnetic radiation from the sun plays an important part in producing the temporary strata. One cannot rule out this possibility entirely, but the difficulties it raises are so great that one is inclined to explore other avenues first.

A reflecting stratum could be produced in any of the following three ways: (a) by greatly enhanced ionization in a narrow region; (b) by a near-discontinuity in the electron-density profile, e.g., a ledge or a step; (c) by turbulence, especially in a region where the electron-density gradient is large.

The first mechanism requires that the electron density in the reflecting stratum be considerably higher than in the region immediately below it. Several possible sources of enhanced ionization have been suggested—solar corpuscles, cosmic rays, meteors, and thunderstorms. That some of these agencies occasionally play a part in the production of reflecting strata seems to be well established. In the auroral zone auroral activity and the incidence of sporadic  $E$  show a strong positive correlation. A marked rise in the incidence of sporadic  $E$  has also been found to accompany some meteor showers. The existence of a positive correlation between thunderstorms and the incidence of sporadic  $E$  has not been definitely established, however. From a careful statistical study of geographical and temporal variations in the incidence of sporadic  $E$ , Smith (1957) has concluded that although the sources of enhanced ionization mentioned above may contribute to the phenomenon they cannot be responsible for the major part of it.

If we accept this conclusion we are left with the following alternatives. (i) There exists an as yet undiscovered source of enhanced ionization—presumably (because of the character of the geographical and temporal variations in the incidence of sporadic  $E$ ) a terrestrial one. (ii) Stratification results in some way from the redistribution of existing ionization rather than the production of extra ionization. In the absence of definitive experimental data bearing on this question, let us adopt the second alternative as a working hypothesis. We are then left with mechanisms (b) and (c).

The underlying premise of the theory to be developed in this article is that stratification in the ionosphere results, not from the absorption of ionizing radiation or corpuscles at discrete levels, but from aerodynamic processes. More specifically, I shall try to show that aerodynamic processes can distort the “normal” electron-density gradient—i.e., the gradient that would obtain in an atmosphere free from winds—in such a way as to produce partially-reflecting strata. It is worth noting that any explanation along these lines has a certain amount of experimental evidence in its favor at the outset. Aerodynamic phenomena in the upper atmosphere



exhibit little, if any, dependence on the height or zenith angle of the sun. As we have already noted, this is also true of ionospheric stratification. On the other hand, aerodynamic processes act on the existing electron-density gradient, which undergoes large diurnal and seasonal variations. These variations combine with the diurnal and seasonal variations in the aerodynamic state of the upper atmosphere to produce a complicated pattern of change. Ultimately it may be possible to predict some features of this pattern and to compare them with experiment, but in this article we shall discuss only the basic physical mechanisms.

The fact that meteor showers and enhanced auroral activity tend to be accompanied by increased incidence of sporadic  $E$  also fits into the framework of the proposed explanation. Meteors and auroral particles could supply the raw material—extra ionization—from which aerodynamic processes (as yet unspecified) might fashion reflecting strata.

The aerodynamic phenomena that we shall be concerned with are wind shear and turbulence. These are related as follows. In a stably stratified atmosphere wind shear provides the only source of energy to maintain turbulence. If the wind shear is not sufficiently great a turbulent regime cannot be maintained. At any given level in the atmosphere there is a critical value of the wind shear below which the local rate of dissipation of energy exceeds the rate of production. This does not mean that turbulence cannot exist in a region where the wind shear is less than this critical value, since advection and turbulent diffusion can transport turbulence from regions where it is produced to regions where it is destroyed. However, if a steady turbulent regime obtains, there must evidently be some region where the wind shear exceeds the critical value. Thus a knowledge of the critical value as a function of temperature gradient and other relevant atmospheric parameters is fundamental in any theoretical study of wind shear and turbulence in the upper atmosphere.

The problem can be reduced to that of finding the critical value of a single dimensionless parameter, the Richardson number  $Ri$  (defined in the next section). In 1920 Richardson derived the value unity for  $Ri_c$ . A few years later Prandtl and Taylor showed that this value necessarily follows from the momentum-transfer theory of turbulence.\*

Recently Townsend, following an approach used by Ellison in a related

---

\* Booker recently applied Richardson's criterion to the ionosphere. He concluded that the observed wind shears could maintain turbulence throughout the ionosphere and he interpreted the observed irregular winds as corresponding to the high-energy end of a turbulence spectrum similar to the Kolmogorov spectrum. This conclusion is no longer widely accepted, for two reasons. First, radar observations of meteors appear to be inconsistent with the assumption of a Kolmogorov spectrum. Second, as Hines has shown, the irregular winds have a simple and natural interpretation in terms of atmospheric waves propagating upward. Such waves combine the properties of sound waves and gravity waves.



study, has derived a formula for  $Ri_c$  involving a number of unknown parameters. With reasonable assumptions about the values of these parameters, Townsend's formula gives a value for  $Ri_c$  considerably smaller than 1. ( $Ri_c$  is inversely proportional to the square of the minimum wind shear required to maintain turbulence.) In the next section we shall derive a simpler and more stringent criterion than Townsend's. From the resulting value for  $Ri_c$  one would infer that only exceptionally high wind shears—of the order of  $100/(\text{m/sec})/\text{km}$  at a height of 100 km—could maintain turbulence. Now wind shears of this order of magnitude are occasionally observed, but they appear to be confined to narrow layers. Indeed the available data, which are as yet fragmentary and incomplete, suggest that high-shear regions have roughly the same geometrical properties (thickness, height distribution, and perhaps even lateral dimensions) as the strata responsible for the reflection of radio waves. It is tempting to speculate that these two manifestations of discrete structure are two sides of the same coin. The question then arises: Can a narrow turbulent layer embedded in a nonturbulent medium reflect radio waves in the manner observed?

It is well known that a turbulent region in the ionosphere would scatter radio waves. This kind of scattering has been studied by Villars and Weisskopf, Gallet, and others. It is caused by fluctuations in the electron density arising primarily from mixing of layers with unequal numbers of electrons per unit mass by the vertical component of the turbulent velocity field. A turbulent layer of the kind envisaged here would certainly scatter in accordance with this mechanism. However, it will be shown in Section III that if the layer is sufficiently thin, turbulent mixing can produce an entirely different effect—a near-discontinuity in the mean electron-density profile—which may well be more effective than turbulent scattering in producing the desired reflections.

It should be stressed that the present hypothesis for the origin of stratification in the ionosphere rests on theoretical and experimental foundations that are far from secure. It is essentially a working hypothesis, rather than an attempt to provide a final solution of the problem. This article will have served its main purpose if it stimulates experimental or theoretical investigations that destroy its main contentions.

## 2. THE TURBULENCE CRITERION

We consider the simplest example of a shear flow in a stably stratified atmosphere. Let the mean motion be in the  $x$  direction and the gravitational acceleration in the negative  $z$  direction. We assume that the gradients of mean velocity, mean temperature, and mean density are all vertical. We also assume that if turbulence is present its scale is so small that local

properties of the turbulent velocity field do not depend on derivatives of the velocity gradient, the temperature gradient, or the density. We introduce the abbreviations

$$\omega_s^2 \equiv \left( \frac{dU}{dz} \right)^2, \quad (2.1)$$

$$\omega_g^2 \equiv \frac{g}{T} \left( \frac{\partial T}{\partial z} + \frac{g}{c_p} \right). \quad (2.2)$$

$\omega_s$  is the mean-velocity gradient or wind shear. In (2.2) the quantity in parentheses is the gradient of what meteorologists call "potential temperature"; it is the difference between the actual temperature gradient and the temperature gradient that would prevail in an adiabatic atmosphere. By the definition of a stably stratified atmosphere, the right-hand side of (2.2) is positive. The frequency  $\omega_g$  has the following physical interpretation: A fluid element that undergoes a small displacement from its equilibrium position experiences a restoring force proportional to the displacement which tends to produce a harmonic oscillation of frequency  $\omega_g$ .

The Richardson number is defined as the square of the ratio of  $\omega_g$  and  $\omega_s$ :

$$Ri \equiv \left( \frac{\omega_g}{\omega_s} \right)^2 = \frac{g \left( \frac{\partial T}{\partial z} + \frac{g}{c_p} \right)}{T \left( \frac{dU}{dz} \right)^2}. \quad (2.3)$$

Under the present simplified assumptions the only dimensionless parameters that are relevant to the stability problem are the Richardson number  $Ri$  and the Reynolds number  $Re$ . [For a discussion of this point see Batchelor (1953a) and Townsend (1958).] We assume that the Reynolds number is much larger than its critical value. In these circumstances viscosity has little effect on the part of the turbulence spectrum that contains most of the energy, and the stability of the flow against turbulence hinges entirely on the value of  $Ri$ . It is worth emphasizing that this conclusion rests on very general arguments which have been repeatedly tested and confirmed by laboratory experiments.\*

---

\* Nevertheless, attempts to deduce the critical value of  $Ri$  from meteorological data have not yielded a clear-cut result. Sutton (1955) concludes an account of several empirical determinations of  $Ri_c$  with these words: "Thus at present some support can be found from meteorological data for almost any value of  $Ri_c$  between 0.04 and 1, an unsatisfactory state of affairs which emphasizes the need for further research work on this fundamental aspect of atmospheric turbulence." In addition to the meteorological data there exist certain relevant hydrographic measurements by Jacobsen pertaining to the flow of fresh water over salt water in the Kattegat. From these measurements Taylor (1931) derived values for  $Ri$  ranging from 2.6 to 120. Yet in every case the flow was turbulent. As Townsend (1958) has pointed

Two distinct methods have been used in studies of hydrodynamic stability—the method of small disturbances and the energy method. In the first method one derives from the equations of motion a linearized description of small disturbances of the unperturbed motion and seeks to determine the values of the appropriate dimensionless parameters for which all small disturbances tend to die out. This program leads to exceedingly intricate mathematical problems, but it has been carried out successfully for a number of particular flows (see, e.g., Lin 1955). In the second method one considers the balance between production and dissipation of turbulent energy in the fully developed turbulent flow and seeks to determine the values of the appropriate dimensionless parameters for which such a balance is possible. In order to evaluate the terms in the energy equation one needs to know the turbulent velocity field. To obtain this accurately one would have to solve the equations of motion, with appropriate boundary conditions, for developed turbulent flow, which of course cannot be done. In practice one uses a simple model of the turbulent velocity field. Since the assumed velocity field does not satisfy the equations of motion, the energy method yields only sufficient conditions for stability and necessary conditions for instability. In applications to ordinary stability problems the energy method has, in fact, yielded estimates of the critical Reynolds number  $Re_c$  that are smaller by factors of 50–100 than those given by the method of small disturbances.

The reason for this poor showing is easy to understand. At moderately high Reynolds numbers the production and dissipation of turbulent energy depend upon virtually distinct regions of the turbulence spectrum. The eddies responsible for the production of turbulent energy are also those which contain most of the turbulent energy, while those mainly responsible for the dissipation of turbulent energy contain a negligible proportion of the energy. In order to derive an estimate of the critical Reynolds number by means of the energy method one must make assumptions about the

---

out, however, one must exercise great care in interpreting experimental results relating to irregular motions in a stably stratified medium. When  $Ri < Ri_c$  the irregular motions will have essentially the same properties as in ordinary turbulent flow in the absence of buoyancy forces. When  $Ri > Ri_c$  true turbulence can no longer occur, by the definition of  $Ri_c$ , but another kind of irregular motion can occur. If the Reynolds number is sufficiently high, small disturbances of the mean motion will give rise to gravity waves of frequency  $\omega_g$  given by (2.2). An irregular collection of gravity waves may bear an instantaneous resemblance to a turbulent velocity field but the rates of energy dissipation and of mass, momentum, and energy transport are entirely different in the two kinds of flow. In fact Taylor showed that the effective diffusion coefficient for the vertical transport of salinity deduced from Jacobsen's measurements was much smaller than the value appropriate to a turbulent flow with the observed value of the turbulent viscosity coefficient  $\nu_t = \langle uw \rangle / \omega_s$ , though it was much larger than the molecular value. For a fuller discussion of these matters see Townsend (1958).

relative length and velocity scales of the two kinds of eddies. Since the values derived for  $Re_c$  depend very sensitively on these assumptions, which in the absence of a proper theory are bound to be very crude, it is not surprising that these estimates differ so much from the values given by the method of small disturbances.

The situation is entirely different when buoyancy forces are present and  $Re \gg Re_c$ . The rate at which turbulence does work against gravity in a stably stratified medium depends primarily on properties of the energy-containing eddies, as does the rate at which turbulence extracts energy from the mean flow. Moreover, since the effects of viscosity are of no direct interest, we may also express the turbulent dissipation rate in terms of parameters pertaining to the energy-containing eddies. Thus all the terms in the energy equation depend only on properties of the energy-containing eddies. It is true that, as long as we do not have a detailed description of the turbulence, we cannot evaluate these terms precisely, but the uncertainties affect only ratios of order unity, some of which are known approximately from experiment. The energy method may therefore be expected to yield considerably closer estimates of  $Ri_c$  than of  $Re_c$ .

Let  $\epsilon_s$  denote the rate [measured in (erg/g)/sec] at which the turbulence extracts energy from the mean flow. Let  $\epsilon_g$  denote the rate at which the turbulence does work against gravity and  $\epsilon_t$  the rate at which turbulent energy is dissipated as heat. We assume that the flow is statistically steady. The equation of turbulent energy balance then reduces to:

$$\epsilon_s = \epsilon_g + \epsilon_t, \quad (2.4)$$

since advection and turbulent diffusion do not occur. Let  $u$ ,  $v$ ,  $w$  denote the Cartesian components of the turbulent velocity field and let the brackets  $\langle \rangle$  indicate time averages. Finally, let  $\theta$  denote the difference between the temperature of a fluid element and the appropriate mean temperature  $T(z)$ . The three rates are then given by

$$\epsilon_s = - \langle uw \rangle \frac{dU}{dz} = |\langle uw \rangle| \omega_s, \quad (2.5)$$

$$\epsilon_g = - \frac{g}{T} \langle \theta w \rangle, \quad (2.6)$$

$$\epsilon_t = \frac{1}{2} \langle u^2 + v^2 + w^2 \rangle \omega_t. \quad (2.7)$$

The expressions for  $\epsilon_s$  and  $\epsilon_g$  are average values of the corresponding terms in the turbulent energy equation, and the equation for  $\epsilon_t$  may be regarded as the definition of  $\omega_t$ .

Suppose that a fluid element initially at height  $z$ , whose temperature is the same as the mean temperature  $T(z)$ , undergoes a small displacement  $(\xi, \eta, \zeta)$ . If the element remains at the same pressure as its surroundings

and does not exchange heat with them, then its final temperature will differ from the mean temperature  $T(z + \zeta)$  appropriate to the height  $(z + \zeta)$  by an amount

$$\theta = -\left(\frac{\partial T}{\partial z} + \frac{g}{c_p}\right)\zeta. \quad (2.8)$$

Using this expression for  $\theta$ , we can rewrite (2.6) in the form

$$\epsilon_g = \langle w\zeta \rangle \omega_g^2, \quad (2.9)$$

where  $\omega_g^2$  is given by (2.2).

*Richardson's criterion* (cf. Richardson 1920; Goldstein (ed.) 1938, pp. 229–232). The turbulent viscosity is defined by

$$|\langle uw \rangle| = \nu_t \omega_s. \quad (2.10)$$

According to the mixing-length theory of turbulence,  $\nu_t$  is also given by

$$\nu_t = \langle w\zeta \rangle. \quad (2.11)$$

Using (2.10) and (2.11) we can rewrite (2.5) and (2.9) in the forms

$$\epsilon_s = \nu_t \omega_s^2, \quad \epsilon_g = \nu_t \omega_g^2. \quad (2.12)$$

A necessary, though not a sufficient, condition for the maintenance of turbulence is

$$Rf \equiv \frac{\epsilon_g}{\epsilon_s} < 1. \quad (2.13)$$

The dimensionless number  $Rf$  is known as the flux Richardson number. By (2.12)

$$Rf = Ri^2, \quad (2.14)$$

from which Richardson's criterion  $Ri < 1$  follows at once.

Taylor (1931), in his discussion of the Kattegat data, showed these data to be consistent with (2.13) but not with (2.14).

*Townsend's criterion.* Instead of introducing the hypothesis (2.11) we proceed as follows (cf. Taylor 1922). The displacement  $\zeta(t|\tau)$  suffered by a fluid element in the time interval  $\tau$  is given by

$$\zeta(t|\tau) = \int_0^\tau w(t-p)dp. \quad (2.15)$$

In this equation  $\zeta$  and  $w$  are to be interpreted as random variables. Assuming that the turbulence is statistically stationary, we have

$$\begin{aligned} \langle w(t)\zeta(t|\tau) \rangle &= \left\langle \int_0^\tau w(t)w(t-p)dp \right\rangle = \\ &= \int_0^\tau \langle w(t)w(t-p) \rangle dp = \langle w^2 \rangle \int_0^\tau f(p)dp, \end{aligned} \quad (2.16)$$

where  $f(p)$  is the auto-correlation coefficient of the random function  $w(t)$ . We may identify the characteristic time defined by  $f(p)$  with the reciprocal of the characteristic frequency  $\omega_t$  defined by (2.7):

$$\int_0^\infty f(p) dp = \omega_t^{-1}. \quad (2.17)$$

For simplicity we make the common assumption that the auto-correlation coefficient is exponential in form. From (2.17) and the requirement  $f(0) = 1$  it then follows that

$$f(p) = e^{-p\omega_t} \quad (2.18)$$

so that

$$\int_0^\tau f(p) dp = \omega_t^{-1}(1 - e^{-\tau\omega_t}). \quad (2.19)$$

Finally, we assume that the time intervals  $\tau$  are distributed according to the probability law that governs the intervals between the collisions of a molecule in a perfect gas:

$$P(\tau) = \omega_t e^{-\tau\omega_t}. \quad (2.20)$$

We then have, by (2.16), (2.19), and (2.20),

$$\begin{aligned} \langle w\zeta \rangle &= \int_0^\infty \langle w(t)\zeta(t|\tau) \rangle P(\tau) d\tau = \\ &= \langle w^2 \rangle \int_0^\infty d\tau P(\tau) \int_0^\tau f(p) dp \approx \frac{1}{2} \langle w^2 \rangle. \end{aligned} \quad (2.21)$$

We can now replace (2.9) by

$$\epsilon_g = \frac{1}{2} k_g \langle w^2 \rangle \omega_p^2 \omega_t^{-1}, \quad (2.22)$$

where  $k_g$  is close to 1. We also replace (2.5) and (2.7) by the equations

$$\epsilon_s = \frac{3}{8} k_s \langle w^2 \rangle \omega_s, \quad (2.23)$$

$$\epsilon_t = \frac{3}{2} k_t \langle w^2 \rangle \omega_t. \quad (2.24)$$

In laboratory turbulence the number  $k_t$  has been found to be of order unity (see Batchelor 1953b, p. 106). The coefficient  $\frac{3}{8}$  in (2.23) is close to the experimental value of the shear correlation coefficient as measured near the center of the flow in turbulent wakes and mixing layers (Townsend 1956, pp. 152, 179). However, if the energy-containing eddies are appreciably anisotropic  $k_s$  may be substantially greater than 1. We shall return to this point later.

We can eliminate the turbulent intensity from (2.22), (2.23), (2.24) by working with ratios of the  $\epsilon$ s and  $\omega$ s. We obtain

$$\frac{\epsilon_g}{\epsilon_s} = \frac{5}{4} \frac{k_g}{k_s} \frac{\omega_g^2}{\omega_s \omega_t}, \quad (2.25)$$

$$\frac{\epsilon_t}{\epsilon_s} = 1 - \frac{\epsilon_g}{\epsilon_s} = \frac{15}{4} \frac{k_t}{k_s} \frac{\omega_t}{\omega_s}, \quad (2.26)$$

whence

$$\left(1 - \frac{\epsilon_g}{\epsilon_s}\right) \frac{\epsilon_g}{\epsilon_s} = \frac{75}{16} \frac{k_g k_t}{k_s^2} \left(\frac{\omega_g}{\omega_s}\right)^2, \quad (2.27)$$

or

$$(1 - R_f)R_f = \frac{75}{16} \frac{k_g k_t}{k_s^2} Ri. \quad (2.28)$$

This relation between  $Ri$  and  $R_f$  replaces the relation (2.14), based on the mixing-length theory.

The left-hand side of (2.28) takes on its maximum value (for  $R_f \geq 0$ ) when  $R_f = \frac{1}{2}$ . Hence

$$Ri < Ri_c = \frac{4}{75} \frac{k_s^2}{k_g k_t}. \quad (2.29)$$

To every value of  $Ri < Ri_c$  there correspond two possible values of  $R_f$ —one less than  $\frac{1}{2}$ , the other greater than  $\frac{1}{2}$ . According to (2.25) and (2.26) the first possibility corresponds to flows in which the greater share of the power extracted from the mean flow is dissipated by turbulence and the smaller share is used to overcome the buoyancy forces, while the second possibility corresponds to flows with the reverse distribution of power. On physical grounds it seems unlikely that the second possibility can be realized in any actual flow. (One might argue, for example, that a characteristic feature of turbulent motion is its tendency to maximize the turbulent dissipation rate  $\epsilon_t$ .) But the physically plausible inequality

$$R_f \leq \frac{1}{2} \quad (2.30)$$

does not actually follow from the assumptions thus far introduced.\*

Townsend's argument differs from the preceding one in that it makes explicit use of the equation governing turbulent temperature fluctuations. Townsend's formula for  $Ri_c$  is

$$Ri_c = \frac{1}{12} \frac{k_u^2}{k_\theta^2} \frac{L_\epsilon}{L_\theta}. \quad (2.31)$$

The parameters that appear in this equation are related to those previously defined by:

$$k_u = \frac{2}{3} k_s, \quad 2m k_g k_t = 4k_\theta^2 \frac{L_\theta}{L_\epsilon}, \quad (2.32)$$

---

\* Townsend (1958) has concluded that (2.30) *does* follow from assumptions essentially equivalent to the present ones, but I believe that his argument contains a mathematical slip.

so that (2.31) is equivalent to (2.29). Moreover, the argument leading to (2.21) indicates that  $k_\theta$  (the correlation coefficient of  $\theta$  and  $w$ )  $\approx \frac{1}{2}$ , and we have implicitly assumed that the length scales denoted by  $L_\theta$  and  $L_\varepsilon$  are identical. Thus the correspondence between (2.31) and (2.29) is essentially complete.

*A more stringent criterion.* We have not as yet imposed any restrictions on the velocity field other than the energy equation (2.4), which, as we have seen, does not exclude the physically unrealistic condition  $\epsilon_g > \epsilon_t$ . The following considerations suggest a new necessary condition which, in conjunction with the energy equation, leads to a more stringent condition than (2.30) and to a smaller value of  $Ri_c$  than the one given by (2.29).

Let us consider the motion of a fluid element initially at the mean temperature of its surroundings. If  $w(0) = w_0$ , then at time  $t$ ,  $w(t) = w_0 \cos \omega_g t$  see [the remark about  $\omega_g$  following (2.2)]—provided that the fluid element in question has retained its integrity. The last proviso requires  $t$  to be smaller than  $\omega_t^{-1}$ , the lifetime of a turbulent eddy. It follows that if  $\omega_t \leq \omega_g$  it would be possible to follow a typical element through a major part of a complete gravitational oscillation. But if this were possible the motion would not be truly turbulent, and our derivation of equations (2.22), (2.23), (2.24) would be invalid. We would in fact be dealing with the kind of irregular wave motion discussed at the beginning of this section. We therefore postulate as a second necessary condition for the maintenance of turbulent shear flow

$$\omega_t > \omega_g. \quad (2.33)$$

By (2.22) and (2.24)

$$\left(\frac{\omega_t}{\omega_g}\right)^2 = \frac{1}{3} \frac{\epsilon_t}{\epsilon_g} \frac{k_g}{k_t} = \frac{1}{3} \frac{k_g}{k_t} \left(\frac{1}{Rf} - 1\right), \quad (2.34)$$

whence

$$Rf < \frac{k_g}{k_g + 3k_t} \approx \frac{1}{4}. \quad (2.35)$$

Thus we arrive at an upper limit for  $Rf$  that is only half as great as the one given by Townsend [our (2.30)], which in turn is half as great as the one postulated by Richardson. From (2.28) we now obtain, as a necessary condition for the maintenance of turbulence,

$$Ri < Ri_c = \frac{48}{75} \left(\frac{k_s}{k_g + 3k_t}\right)^2 \approx \frac{1}{25}, \quad (2.36)$$

or

$$\omega_g \lesssim \frac{1}{8} \omega_s. \quad (2.36')$$

Because, according to (2.35), a rather small fraction of the power extracted from the mean flow is used in overcoming the buoyancy forces,



it is reasonable to assume that the structure of the turbulence is not very different from what it would be in the absence of buoyancy forces. There is consequently a good prospect of some day obtaining reasonably accurate values for  $k_g$ ,  $k_s$ , and  $k_t$  from laboratory experiments. At present, however, we can do no better than to set them all equal to 1.

The value 0.04 for  $Ri_c$  given by (2.36) is approximately equal to the lowest value of  $Ri_c$  that has been derived from meteorological observations and to the lower limit 0.05 estimated by Townsend (1958) on the basis of some recent experimental studies. Schlichting (1935) obtained the value  $Ri_c = \frac{1}{25}$  for boundary layer flow by the method of small disturbances. The present result indicates that the value of  $Ri_c$  is not as sensitive to the boundary conditions of the flow as has been previously supposed.

### 3. APPLICATION TO THE UPPER ATMOSPHERE

The most prolific sources of information about winds and turbulence in the region above 80 km are: radio-echo observations of meteor trails (Greenhow and Neufeld 1959 and references cited therein); visual and photographic observations of meteors and noctilucent clouds (Millman 1959 and references cited therein); and photographic observations of sodium trails laid down by rockets (Manring 1959 and references cited therein). Greenhow has derived from the radio-echo observations an accurate and detailed statistical picture of large-scale wind structure in the meteor region (80–100 km). He cites  $0.01 \text{ sec}^{-1}$  [ $10(\text{m/sec})/\text{km}$ ] as a typical value of the wind shear in this region, and  $0.1 \text{ sec}^{-1}$  as an approximate upper limit of the observed wind shears.

Photographic records of sodium trails are the most promising source of information about small-scale motions in the entire region above 80 km. The analysis of such records should soon provide a definitive answer to the question whether the small-scale irregular motions that are known to occur in the region between 80 and 100 km have the properties of hydrodynamic turbulence. At the present time, however, all that can be said is that the existing data do not provide convincing support for the widely-held belief that hydrodynamic turbulence—of any intensity—regularly prevails over a wide range of heights in the ionosphere.

According to the turbulence criterion derived in the preceding section, only wind shears near the upper end of the observed range are capable of maintaining turbulence at a height of 100 km. Greenhow and Neufeld (1959, Fig. 4, p. 2131) have found that fewer than 1 per cent of the wind shears measured over a height difference of 0.4 km exceed  $0.07 \text{ sec}^{-1}$ . The largest gradients are probably confined to layers 1 or 2 km thick; a gradient of order  $0.1 \text{ sec}^{-1}$  extending over a vertical distance of as much as 3 km would give rise to wind speeds of order 300 m/sec—approximately

the speed of sound at the heights under consideration—and such high wind speeds have not been reported.\* On the other hand, there is no reason to suppose that the horizontal dimensions of the high-shear layers are appreciably less than the average horizontal wind-correlation scale of about 150 km.

Long (1959) has pointed out that strong velocity concentrations, or jets, are characteristic of the flow of stably stratified fluids, and has put forward theoretical considerations based on boundary-layer theory to elucidate the general phenomenon of jets.

Let us, then, assume as a working hypothesis that there exist regions in the ionosphere whose horizontal dimensions are of the order of 100 km, whose vertical dimensions are of the order of 1 km, and within which the wind gradient is large enough to maintain turbulence. Let us further assume that the turbulent region is embedded in a nonturbulent medium and has more or less distinct boundaries. (This is an obvious oversimplification, because turbulence will tend to diffuse out of such a region, thus blurring its boundaries. But we are here concerned with only the gross aspects of the phenomenon.)

How will the turbulence affect the electron-density profile in such a layer? The answer depends on the ratio between the recombination time and the mixing time for the layer in question. Since turbulent mixing is essentially a diffusion process the mixing time increases as the square of the thickness ( $d$ ) of the layer. It is given approximately by the formula

$$t_{\text{mixing}} = \frac{d^2}{2\langle w\zeta \rangle} = \frac{d^2\omega_t}{\langle w^2 \rangle}. \quad (3.1)$$

To get an estimate of  $t_{\text{mixing}}$  we set

$$\langle w^2 \rangle^{1/2} = 10 \text{ m/sec}, \quad \omega_t = 0.05 \text{ sec}^{-1}, \quad d = 1 \text{ km}. \quad (3.2)$$

These values give

$$t_{\text{mixing}} = 500 \text{ sec}. \quad (3.3)$$

The recombination time is given by

$$t_{\text{recomb}} = \frac{1}{N_e a} \equiv \tau, \quad (3.4)$$

where  $N_e$  is the electron density and  $a$  is the recombination coefficient. The following table, constructed from data given by Bates (1953 p. 599), gives values of  $N_e$ ,  $a$ ,  $\tau$ , at four heights. A comparison between the table

---

\* Dr. Allan F. Cook has kindly informed me that recent photographs of a meteor train by the Harvard meteor expedition in New Mexico show a narrow high-shear layer in which the wind speed does in fact approach 300m/sec.

Table 1.

$h$ (km)	$N_e$ (cm $^{-3}$ )	$\alpha$ (cm $^3$ sec $^{-1}$ )	$\tau$ (sec)
75	$2.5 \times 10^2$	$1 \times 10^{-6}$	4000
90	$1.5 \times 10^4$	$3 \times 10^{-8}$	2200
110	$1.5 \times 10^5$	$1 \times 10^{-8}$	700
200	$2.5 \times 10^5$	$7 \times 10^{-9}$	600

and (3.3) indicates that the available data are not inconsistent with the hypothesis that  $t_{\text{mixing}} < t_{\text{recomb}}$ .

If this is so, the turbulence will not introduce fluctuations into the electron-density profile. Rather, it will tend to bring about a uniform concentration of electrons throughout the turbulent layer; in the case of complete mixing the number of electrons per unit mass will remain constant through the layer so that  $N_e$  will actually decrease with height within the layer. Figure 1 shows schematically the perturbed electron-density profile in the ideal case of a turbulent layer with sharp boundaries and perfect mixing. In reality the profile will have small-scale irregularities and the transitions between the turbulent layer and the nonturbulent medium above and below it will be more gradual than in the figure.

The jump in electron density at the bottom of the turbulent layer is given approximately by the equation

$$\Delta N_e = \left( \frac{dN_e}{dh} \right) d. \quad (3.5)$$

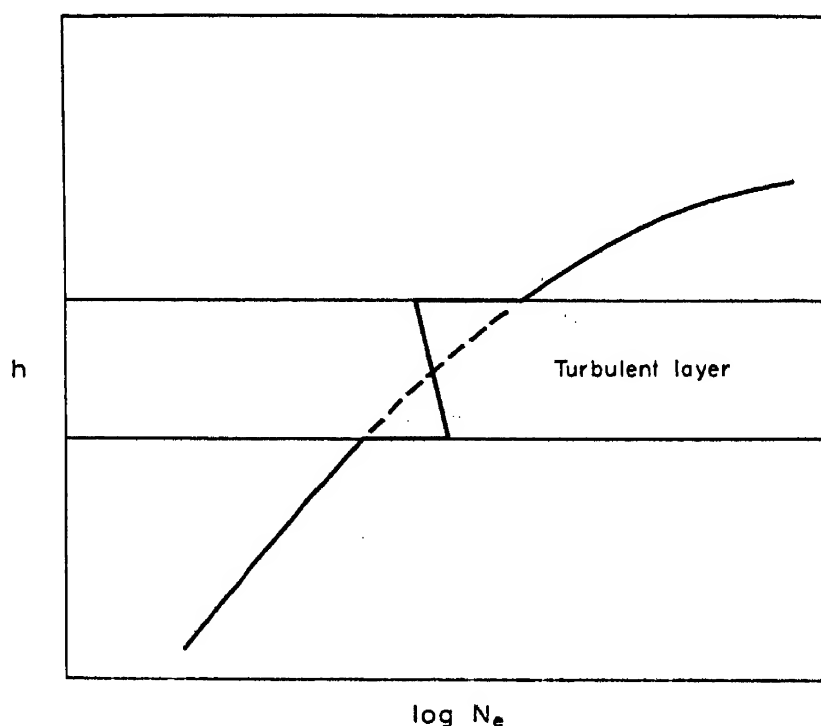


Fig. 1. Electron-density profile in the presence of a turbulent layer (schematic).

In the lower part of the  $E$ -region  $dN_e/dh \approx 10^4 \text{ cm}^{-3} \text{ km}^{-1}$  and  $N_e \approx 10^4 \text{ cm}^{-3}$ , so that  $\Delta N_e/N_e \approx 1$ . The present mechanism obviously cannot, however, produce electron densities appreciably greater than the peak density in the  $E$ -layer. Experimental evidence that such high-density layers exist would be *prima facie* evidence in favor of the view that more than the redistribution of existing ionization by this mechanism is involved in the formulation of these intense reflecting layers.

The present hypothesis suggests three related problems, whose solutions could hardly fail to bring us closer to an understanding of ionospheric stratification: (i) What is the nature of the flow in and around a turbulent horizontal jet embedded in a nonturbulent, stably stratified medium? (ii) What is the nature of the resulting electron-density profile? (iii) What are the reflection properties of such a layer?

The last question is especially intriguing because the wavelengths corresponding to frequencies in the range 0.5–3.0 Mc/s are neither very small compared with the assumed width of the turbulent layer nor very large compared with the probable scale of the turbulence. One would therefore expect reflections from such a layer to exhibit pronounced interference effects (fading) depending in a distinctive way on frequency and angle of incidence.

*Meteor Ionization.* The ionization produced by meteors is initially highly non-uniform, being concentrated in long, thin cylinders. As soon as a trail is formed, however, its cross-section begins to increase, as a result of molecular diffusion. Now, the mean age of the ionization trails which at any given instant are responsible for the major part of the meteor ionization is roughly equal to the recombination time  $\tau$ . Hence the radius  $r$  of a typical trail satisfies the inequality

$$r \gtrsim \sqrt{(4D\tau)}, \quad (3.6)$$

$D$  being the molecular diffusion coefficient. Let  $n$  denote the incident flux of meteors at, say, the 100-km level. At any given instant the average number of trails passing through a surface element of unit area is about  $n\tau$ , if we count only trails that make a substantial contribution to the total meteor ionization. If the trails were uniformly distributed in space and had equal radii, they would begin to overlap when  $r$  became comparable to the radius  $a$  defined by

$$\pi a^2 = \frac{1}{n\tau}. \quad (3.7)$$

Hence the meteor ionization will exhibit substantial departures from uniformity only if  $r \ll a$ , i.e., only if

$$4\pi Dn\tau^2 \ll 1. \quad (3.8)$$

Let  $q$  denote the line density of electrons for some particular class of meteor trails. The space density of electrons produced by these trails is given by

$$\Delta N_e(q) \approx qn(q)\tau. \quad (3.9)$$

If meteor ionization is to have an appreciable effect,  $\Delta N_e$  must be at least as great as the electron density that would prevail in the absence of meteors. Calling this density  $N_e$ , we obtain a second inequality,

$$qn(q)\tau \gtrsim N_e. \quad (3.10)$$

From (3.10) and (3.8) we obtain

$$q \gg 4\pi D\tau N_e \quad (3.11)$$

as a condition that meteor ionization (due to meteors in a given class) shall be quantitatively significant and significantly non-uniform. In the region 90–100 km the right-hand side of (3.11) is of order  $10^{13}$ – $10^{14}$ .

For such meteors reliable statistics are available (Upton and Hawkins 1958). These show that the corresponding values of  $\Delta N_e$  are completely negligible, not only in comparison with typical daytime values of  $N_e$  in the meteor region but also in comparison with the ionization produced by smaller meteors. This conclusion applies also to the ionization produced during meteor showers (Hawkins, private communication). We conclude that the ionization generated by meteors may be regarded as spatially homogeneous.

The length of a typical ionization trail is of the order of 10 km. It follows that the scale of vertical variations in  $\Delta N_e$  is at least of this order of magnitude. Thus the contribution of meteor-generated ionization to the electron-density profile does not change the character of the profile in a qualitative way, so that the preceding discussion does not need to be modified in any essential respect to allow for the effects of meteor ionization.

*Acknowledgments*—I am indebted to Dr. Allan F. Cook, Prof. F. L. Whipple, and Dr. G. S. Hawkins for discussions on the interpretation of the meteor data; to Dr. E. K. Smith for discussions on the interpretation of experiments relating to sporadic  $E$ ; and to Dr. E. Manring for putting at my disposal and discussing with me his unpublished observations of sodium trails.

*Note added in Proof (19 July 1962)*

According to Martyn (*Phil. Trans. Roy. Soc.* 246, 306, 1953; see also Whitehead, *J. Atmosph. Terr. Phys.* 20, 49, 1961), horizontal winds in the ionosphere can give rise to a vertical drift of ionization. In the presence of such a drift a thin turbulent layer of the kind discussed in the preceding paper would act as an ionization trap. A downward drift, for example, would bring ionization into the layer from above,

but there would be no compensating flux of ionization out of the layer at its lower boundary, since turbulent mixing would inhibit drift across the layer. The density of ionization would accordingly build up in the turbulent layer, while just below it the ionization would be depleted. The electron-density profile would thus develop a narrow spike and, immediately below it, a broader, shallower depression; if the drift were upward instead of downward, the spike would lie below the depression. The growth of the spike is ultimately limited by recombination and, to a lesser extent, diffusion. If  $V$  is the vertical drift velocity,  $d$  the width of the turbulent layer, and  $\tau$  the normal recombination time, then the steady-state value of the mean electron density in the spike exceeds the normal electron density at the same height by the factor  $\sqrt{(V\tau/d)}$ , which, for plausible values of the parameters involved, may be considerably greater than 1. A detailed discussion of the present mechanism for producing enhanced ionization in a narrow layer will be published elsewhere.

## REFERENCES

- BATCHELOR, G. K. (1953a) *J. Roy. Met. Soc.* **80**, 339.  
 BATCHELOR, G. K. (1953b) *Homogeneous Turbulence*, Cambridge Univ. Press.  
 BATES, D. R. (1953) *The Physics of the Upper Atmosphere in The Earth as a Planet* (ed. G. P. Kuiper), University of Chicago Press.  
 BOOKER, H. G. (1956) *J. Geophys. Res.* **61**, 673.  
 ELLISON, T. H. (1957) *J. Fluid Mech.* **2**, 456.  
 GALLET, R. M. (1955) *Proc. Inst. Radio Engrs.* **43**, 1240.  
 GOLDSTEIN, S. (ed.) (1938) *Modern Development in Fluid Dynamics*, Oxford Univ. Press.  
 LIN, C. C. (1955) *The Theory of Hydrodynamic Stability*, Cambridge Univ. Press.  
 LONG, R. R. (1959) *J. Geophys. Res.* **64**, 2151.  
 MANRING, E. R., BEDINGER, J. F., PETTIT, N. B. and MOORE, C. B. (1959) *J. Geophys. Res.* **64**, 587.  
 MILLMAN, P. M. (1959) *J. Geophys. Res.* **64**, 2122.  
 RICHARDSON, L. F. (1920) *Proc. Roy. Soc. A* **97**, 354.  
 SCHLICHTING, H. (1935) *Z. Angew. Math. Mech.* **15**, 313.  
 SMITH, E. K. (1957) *NBS Cir.* 582.  
 TAYLOR, G. I. (1922) *Proc. London Math. Soc.* (2) **20**, 196.  
 TAYLOR, G. I. (1931) *Rapports et Proces-Verbaux du Conseil Permanent International pour l'Exploration de la Mer* **76**, 35.  
 THOMAS, J. A. and SMITH, E. K. (1959) *J. Atmosph. Terr. Phys.* **13**, 295.  
 TOWNSEND, A. A. (1956) *The Structure of Turbulent Shear Flow*, Cambridge Univ. Press.  
 TOWNSEND, A. A. (1957) *J. Fluid Mech.* **3**, 361.  
 UPTON, E. and HAWKINS, G. S. (1958) *Ap. J.* **128**, 727.  
 VILLARS, F. and WEISSKOPF, V. F. (1954) *Phys. Rev.* **94**, 232.  
 VILLARS, F. and WEISSKOPF, V. F. (1955) *Proc. Inst. Radio Engrs.* **43**, 1232.

# The Formation of a Sporadic-*E* Layer from a Vertical Gradient in Horizontal Wind

J. D. WHITEHEAD

Radio Research Board Laboratory, Electrical Engineering School,  
University of Sydney, Sydney, Australia.

**Abstract**—A horizontal wind shear leads to vertical movement of ions and electrons, which gives rise to the formation of thin layers of ionization. The probability of the layer appearing depends on the horizontal component of the earth's magnetic field. This is the same as the probability observed for sporadic-*E* critical frequency ( $f_oE_s$ ) to exceed 5 Mc/s in different parts of the world. The hypothesis that all temperate zone sporadic *E* is due to horizontal wind shears is given further support because it shows how sporadic *E* once formed will tend to persist, gives the correct height at which the layer is most likely to form and is satisfactory so far as orders of magnitude of the various quantities are concerned. It also leads to an explanation of the relationship between the *F*-region travelling disturbances and sporadic *E*.

The electron density distribution arising from the vertical movement is discussed, taking into account recombination and diffusion.

The magnetic effects of sporadic-*E* clouds are discussed.

## 1. INTRODUCTION

In a recent communication Heisler and Whitehead (1960a) noted that the fraction of time the critical frequency of the sporadic-*E* layer ( $f_oE_s$ ) exceeded 5 Mc/s depended on the horizontal component of the earth's magnetic field for stations situated in the temperate zone. There was no correlation with total intensity of the magnetic field. The fraction of time increased as the horizontal component increased. It is of interest to inquire which of the various theories suggested to account for sporadic *E* would show this relationship (see Thomas (1958)). Ionization by neutral particles or meteors does not depend on the earth's field at all: ionization by charged particles may be confined to a thin layer by the action of the earth's magnetic field, but it appears that the total intensity of the earth's field is of importance here. Martyn (1953) suggested an instability mechanism for the growth of sporadic-*E* clouds and Dungey (1956, 1959) considered the effect of a wind shear but neither led to the dependance on the horizontal component of the earth's magnetic field.

The purpose of this paper is to show that vertical shear of horizontal wind does lead to this relationship, and to discuss in detail the formation of the sporadic-*E* layer.

The mathematical derivation of the vertical movement of ions and electrons when a horizontal wind shear is present has already been given

by Whitehead (1961), and this paper is confined more to a discussion of the physical reason for the boundary conditions used in the derivation, and the physical meanings of the results given.

## 2. DERIVATION OF THE VERTICAL VELOCITY OF THE IONS

A horizontal movement of the neutral air in the presence of ions and electrons will tend to move the ions and electrons in varying degrees, polarizing the medium and producing electric fields inside the medium. Further, ions and electrons moving in the earth's magnetic field are acted on by forces at right angles to both the velocity and field. The equations of motion are easily written down and may be solved provided suitable boundary conditions are inserted.

Recently measurements of the velocity of neutral air movements have been made in the lower ionosphere by following meteor trails visually and with radar (Millman (1959), Greenhow and Neufeld (1959)). These measurements have shown that:

- (a) the vertical velocity is always small;
- (b) the horizontal velocity is the same over horizontal distances exceeding 100 km;
- (c) the horizontal velocity often reverses in direction over a height range of about 6 km and has a root-mean-square value of about 25 m/sec, giving a vertical shear of about 12 m/sec/km. L. R. O. Storey (private communication) reports values of wind shear of up to 150 m/sec/km, but presumably the vertical scale is much smaller than 6 km in this case.

Although the meteor measurements refer to 80–100 km heights, it seems reasonable to assume that the same general conditions will hold in the 100–120 km height range.

Let us take axes  $x$ ,  $y$  and  $z$ ,  $z$  being vertically upwards and  $x$  being parallel to the horizontal component of the earth's magnetic field. Let  $U_x$ ,  $U_y$ , and  $U_z$  be the components of the velocity of the air movement. It seems reasonable to assume then that  $U_z = 0$  and that  $U_x$  and  $U_y$  are functions of the height  $z$  only. As the horizontal distances involved are about 100 km, we also assume a flat earth and constant direction and magnitude of the earth's magnetic field.

The polarization electric fields will have components  $E_x$ ,  $E_y$ , and  $E_z$ . Because of the uniformity over horizontal distance, we will assume that  $E_x$  and  $E_y$  are constant over the whole region, although  $E_z$  is a function of  $z$ . Two other conditions are assumed:

- (1) There is no vertical current flow.
- (2) The total currents flowing in the horizontal  $x$  and  $y$  directions are zero, although currents in different directions may flow at different



heights. This assumption implies that the current return outside the local wind system is small. This is likely to be so as the length of path for such a current flow is much larger than the path for a current return at a different height within the layer.

An alternative boundary condition suggested by L. R. O. Storey and C. O. Hines (private communications) is that the electric fields are zero. In this case, expression (1) is as given with all the terms in  $\bar{U}$  omitted. Many of the conclusions reached are not affected, except those given in Section 7.

Here are the orders of magnitude of the various quantities involved in the basic equations. At a height of 120 km the electronic collision frequency is about  $2 \times 10^4$  per sec. This is between the value given by Nicolet (1953) of  $10^4$  per sec and those deduced from the values given by Whitehead (1959a, b) for a height of 110 km ( $1.3 \times 10^4$  per sec and  $1.9 \times 10^4$  per sec). The positive ions present are principally those of atomic oxygen having a mass about  $3 \times 10^4$  of the electrons. Their angular gyro-frequency is therefore about  $3 \times 10^2$  per sec. The collision frequency of ions is about  $1/30$  that of electrons or at 120 km about  $7 \times 10^2$  per sec—a little greater than the gyro-frequency. As sporadic  $E$  most often occurs below 120 km (for instance, Becker (1958) gave values of  $h'E_s$ , 75 per cent of which were equal to or less than 120 km) it appears that the ionic collision frequency is a few times the gyro-frequency in the sporadic- $E$  layer.

Not until we descend below the main part of  $E$ -region does the electronic collision frequency become equal to the electronic gyro-frequency. We will assume, therefore, that, in the region we are concerned with here, the electrons gyrate many times between collisions.

The space charges existing within the region are much smaller than the total charge of electrons present. We also neglect the presence of negative ions (Nicolet and Aikin 1960). Therefore, we can assume that there is only one species of ion.

Starting with the basic equations expressing the fact that the acceleration of the charged particles is zero on the average and inserting the boundary conditions assumed for the problem, it is possible to calculate the (equal) vertical velocity of the electrons and ions. The mathematics is given in Whitehead (1961)\*: some care has to be taken in the derivation, because the component of the electric field parallel to the magnetic field is very small compared to that perpendicular to the magnetic field. It cannot be neglected, however, because it has an appreciable effect on the electron motion.

---

\* In the paper referred to, left-handed axes were used in error. Here right-handed axes are used by changing the signs of all the  $y$  velocities.

The expression for the vertical velocity is the following rather complicated expression:

$$V_z = \frac{\nu_i \omega_{Hi} \cos \theta}{(\nu_i^2 + \omega_{Hi}^2)} \times$$

$$\left\{ \left[ \frac{\omega_{Hi}}{\nu_i} (\bar{U}_{yG} - \bar{U}_{yF}) + \sin \theta (\bar{U}_{xG} - \bar{U}_{xF}) \right] \int_{-\infty}^{\infty} G dz \int_{-\infty}^{\infty} F dz \right.$$

$$+ \left[ \frac{\omega_{Hi} \sin \theta}{\nu_i} (U_x - \bar{U}_{xF}) + (U_y - \bar{U}_{yF}) \right] \left[ \int_{-\infty}^{\infty} F dz \right]^2$$

$$+ \left[ \frac{\omega_{Hi} \sin \theta}{\nu_i} (U_x - \bar{U}_{xG}) + (U_y - \bar{U}_{yG}) \right] \left[ \int_{-\infty}^{\infty} G dz \right]^2 \Bigg\}$$

$$\times \frac{1}{\left[ \int_{-\infty}^{\infty} F dz \right]^2 + \left[ \int_{-\infty}^{\infty} G dz \right]^2} \quad (2.1)$$

where  $\nu_i$  = collision frequency of ions

$\omega_{Hi}$  = gyro-frequency of ions

$\theta$  = dip angle

$F = N\nu_i\omega_{Hi}/(\nu_i^2 + \omega_{Hi}^2)$

$G = N\nu_i^2/(\nu_i^2 + \omega_{Hi}^2)$

$N$  = electron density

$$\bar{U}_{xF} = \frac{\int_{-\infty}^{\infty} F U_x dz}{\int_{-\infty}^{\infty} F dz} \text{ etc.}$$

### 3. DISCUSSION OF THE VARIATION OF VERTICAL VELOCITY WITH HEIGHT

We first of all see in this expression for  $V_z$  that  $\bar{U}_{xF}$ , etc., are average values of the horizontal velocity taken over a certain height range. For instance, the averages taken with respect to  $G$  are roughly mean values of velocity from the base of the ionosphere up to the region where  $\nu_i = \omega_{Hi}$ , at about 130 km. The averages taken with respect to  $F(U_{xF}, U_{yF})$  are mean values about the region where  $\nu_i = \omega_{Hi}$ .

In the absence of wind shears (i.e.  $U_x$  and  $U_y$  independent of height) we see that

$$V_z = 0.$$

This arises because the electrical fields built up by polarization just prevent the vertical movement of ions or electrons.

The quantity which is of most interest in the formation of sporadic *E* is shown in Section 4 to be  $dV_z/dz$  at the heights at which  $V_z \sim 0$ . It is

known from the meteor observations that  $U_x$  and  $U_y$  are subject to quite violent fluctuations over a height range of the order of 10 km. Thus terms such as  $U_x - \bar{U}_{xF}$  will generally be larger in magnitude than  $\bar{U}_{xF} - \bar{U}_{xG}$ , and the variation of  $\nu_i$  with  $z$  is unimportant compared with the variations of  $U_x$  and  $U_y$  with  $z$ . Also the two terms

$$\int_{-\infty}^{\infty} F dz \quad \text{and} \quad \int_{-\infty}^{\infty} G dz$$

are of the same order of magnitude, and may be taken to be equal. Under these circumstances

$$\frac{dV_z}{dz} \sim \frac{\omega_{Hi}^2 \cos \theta \sin \theta}{\nu_i^2 + \omega_{Hi}^2} \cdot \frac{dU_x}{dz} + \frac{\nu_i \omega_{Hi} \cos \theta}{\nu_i^2 + \omega_{Hi}^2} \cdot \frac{dU_y}{dz}$$

Furthermore, if we consider the region below 120 km,  $\nu_i > \omega_{Hi}$  and approximately

$$\frac{dV_z}{dz} \sim \frac{\omega_{Hi} \cos \theta}{\nu_i} \cdot \frac{dU_y}{dz} \quad (3.1)$$

Thus we see that in this region, the E-W air movements are more important in producing vertical ion drift than are N-S winds.

Before this equation can be interpreted in terms of the possibility of sporadic-*E* formation we must first look at the effect of the vertical velocity of electrons and ions on the electron density distribution.

#### 4. THE EFFECT OF A VERTICAL VELOCITY OF IONIZATION ON THE ELECTRON DENSITY DISTRIBUTION IN THE IONOSPHERE

Suppose we take as a model ionosphere, one in which the rate of formation of electrons and ions  $q$  per sec per cc does not vary with height, and the electrons and ions disappear by recombination at a rate equal to  $\alpha N^2$  where  $N$  is the electron density and  $\alpha$  a constant. The ambient electron density in the absence of vertical movement of ionization is given by

$$N_o = \sqrt{\frac{q}{\alpha}}$$

We now introduce a vertical velocity of ionization given by

$$V_z = -V_o \sin 2\pi z/\lambda$$

where  $\lambda$  is the vertical "wavelength" of the movement. The rate of increase of electron density is given by

$$\frac{\partial N}{\partial t} = \alpha N_o^2 - \alpha N^2 + \frac{\partial}{\partial z} (NV_o \sin 2\pi z/\lambda) \quad (4.1)$$

Under steady conditions,  $dN/dt = 0$  and

$$0 = 1 - \left(\frac{N}{N_o}\right)^2 + R \frac{\partial}{\partial \gamma} \left(\frac{N \sin \gamma}{N_o}\right) \quad (4.2)$$

where  $\gamma = 2\pi z/\lambda$

and  $R = 2\pi V_o/\lambda \alpha N_o$

A maximum value of  $N$  occurs at  $\gamma = 0, 2\pi$  etc. and is given by

$$\frac{N_{\max}}{N_o} = \frac{R + \sqrt{R^2 + 4}}{2} \sim R \quad \text{if } R \gg 1 \quad (4.3)$$

If we take  $\alpha$  for the *E*-region to be  $10^{-8}$  cm<sup>3</sup>/sec and  $N_o$   $1.5 \times 10^5$ /cm<sup>3</sup> during the day and  $10^4$ /cm<sup>3</sup> at night (Mitra 1952) then  $1/\alpha N_o \sim 700$  secs during the day and  $\sim 10^4$  secs at night.  $2\pi V_o/\lambda$  is the maximum gradient of the vertical movement. If this is  $\frac{1}{4}$  of the vertical shear of horizontal wind, it would be 3 m/sec/km from the meteor results, making  $R = 2.1$  (day) and 30 (night). According to Storey, the wind shear may be up to ten times this, giving a maximum value of  $R \sim 21$  (day) and 300 (night).

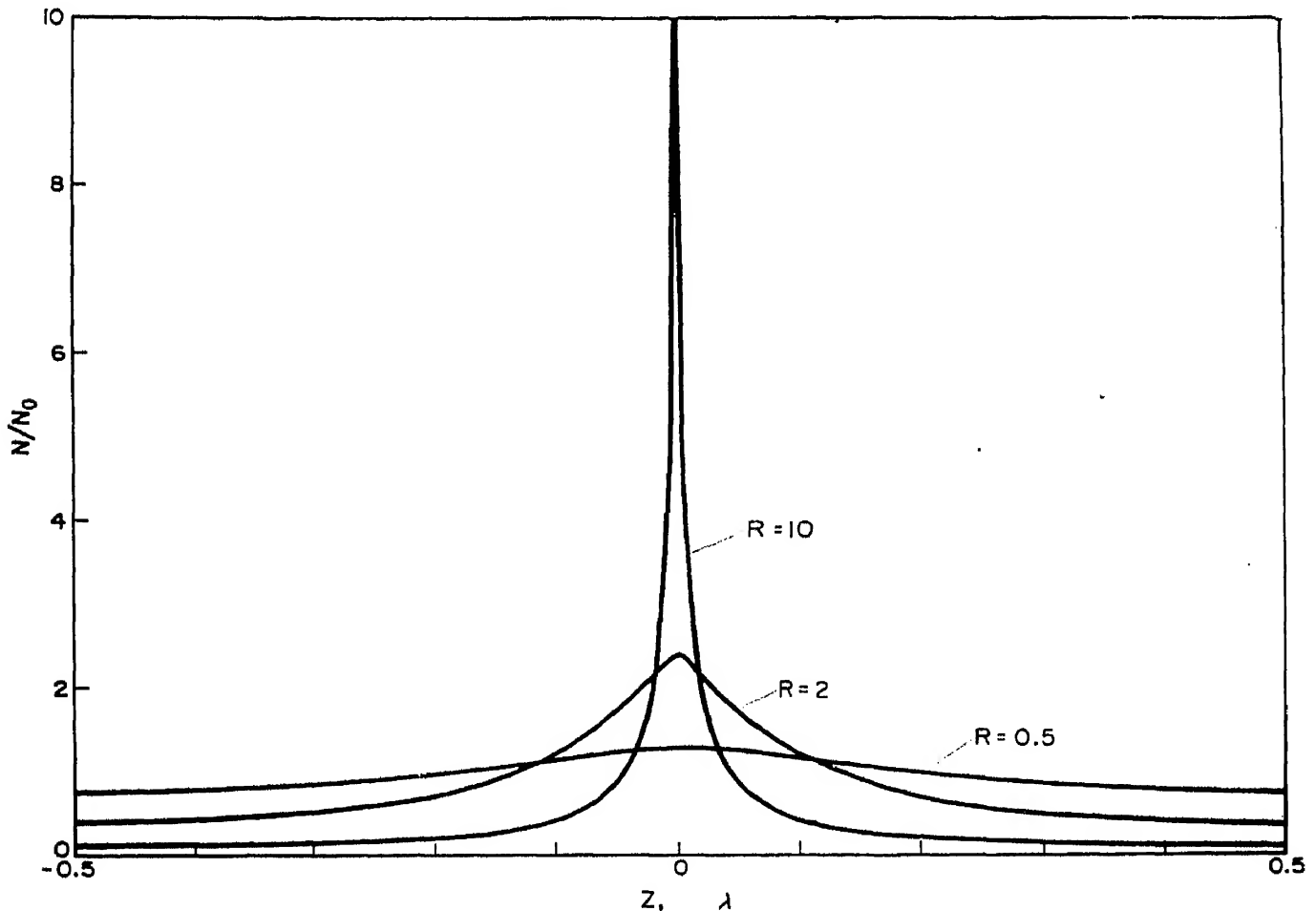


Fig. 1. The electron density distribution for  $R = 0.5, 2$  and  $10$ .

The minimum value of electron density is of less importance to us. It is given by

$$\frac{N_{\min}}{N_0} = \frac{\sqrt{(R^2 + 4)} - R}{2} \sim \frac{1}{R} \quad \text{if } R \gg 1 \quad (4.4)$$

The differential equation (4.2) has been solved to give the complete electron density distribution for various values of  $R$  using the automatic digital computer at Sydney University (SILLIAC). This is plotted as a function of height (in units of one wavelength of vertical movement) in Fig. 1 for  $R = 0.5$ , 2 and 10. The most noticeable feature of the distribution is that the layer bears no resemblance to a parabolic distribution: apart from the extreme tip, it is almost cusp-shaped. This is shown more

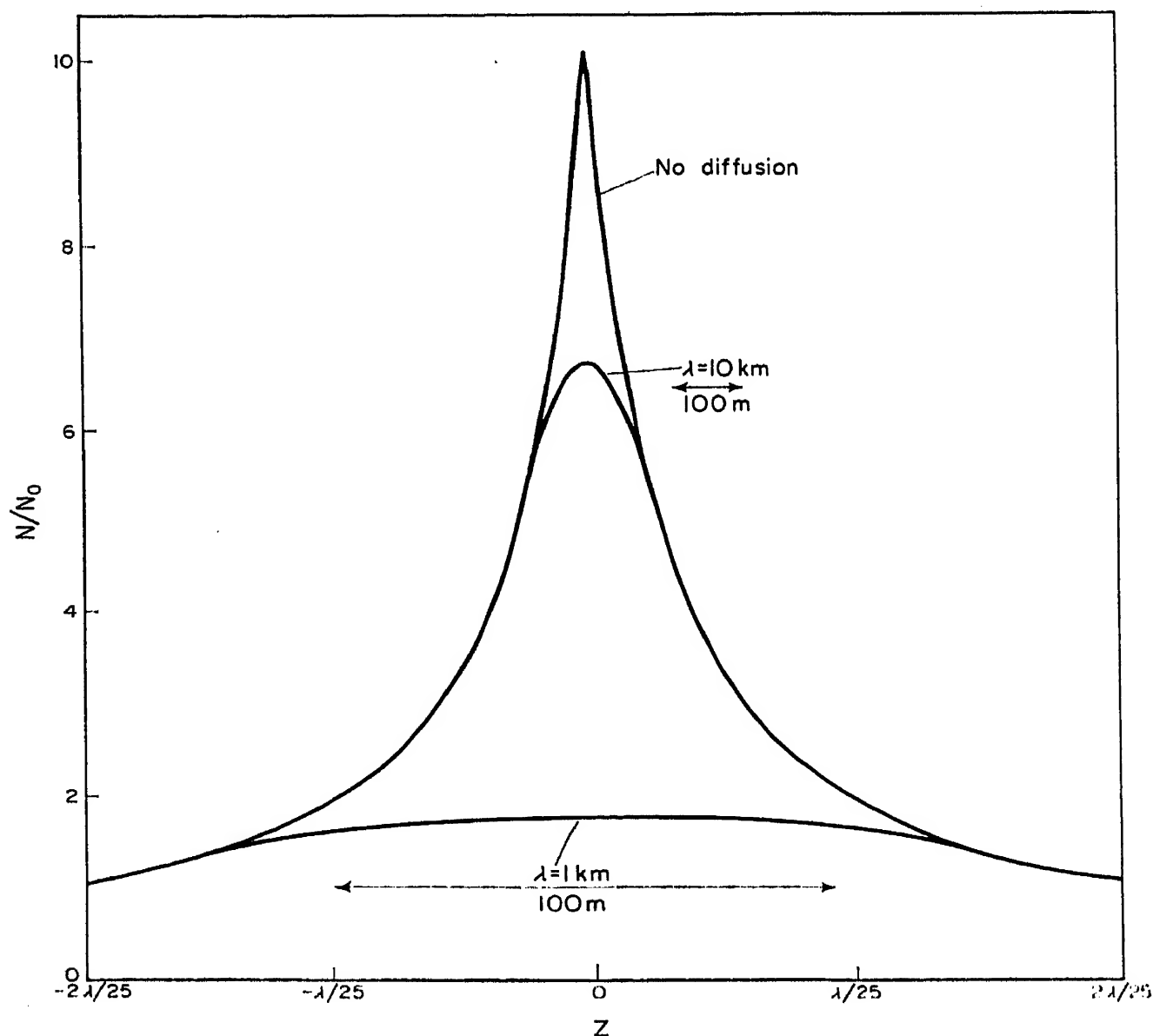


Fig. 2. The electron density distribution near the maximum, neglecting diffusion and taking it into account with  $\lambda = 10$  km and  $\lambda = 1$  km.  $R = 10$ .

clearly in Fig. 2, where the electron density distribution near the maximum is plotted out on an expanded height scale for  $R = 10$ . Such a distribution might explain in part why sporadic *E* is often transparent over a range of frequencies below  $f_oE_s$ . It also shows that one has to be rather careful when talking about the thickness of the sporadic-*E* layer, because this quantity varies rapidly with probing frequency. However, if the thickness is defined as the width of the distribution when the electron density has dropped to half its peak value, it is possible to find how the thickness varies with  $R$ . This is shown in Fig. 3, the scales appropriate to  $\lambda = 10$  km and  $\lambda = 1$  km being shown for comparison. Even for  $\lambda = 10$  km, the thickness falls to  $\sim 200$  m for  $R = 10$ .  $1/\alpha N$  at the peak is about 70 sec (daytime) and if we take the diffusion coefficient  $D$  of ions to be  $\sim 50$  m<sup>2</sup>/sec (the ions having a mean free path  $\sim \frac{1}{2}$  m and mean velocity of  $\sim 300$  m/sec at the usual height of sporadic *E*), diffusion becomes important for a scale length  $L = \sqrt{(50 \times 70)} \text{ m} \sim 60$  m. Diffusion becomes increasingly important for

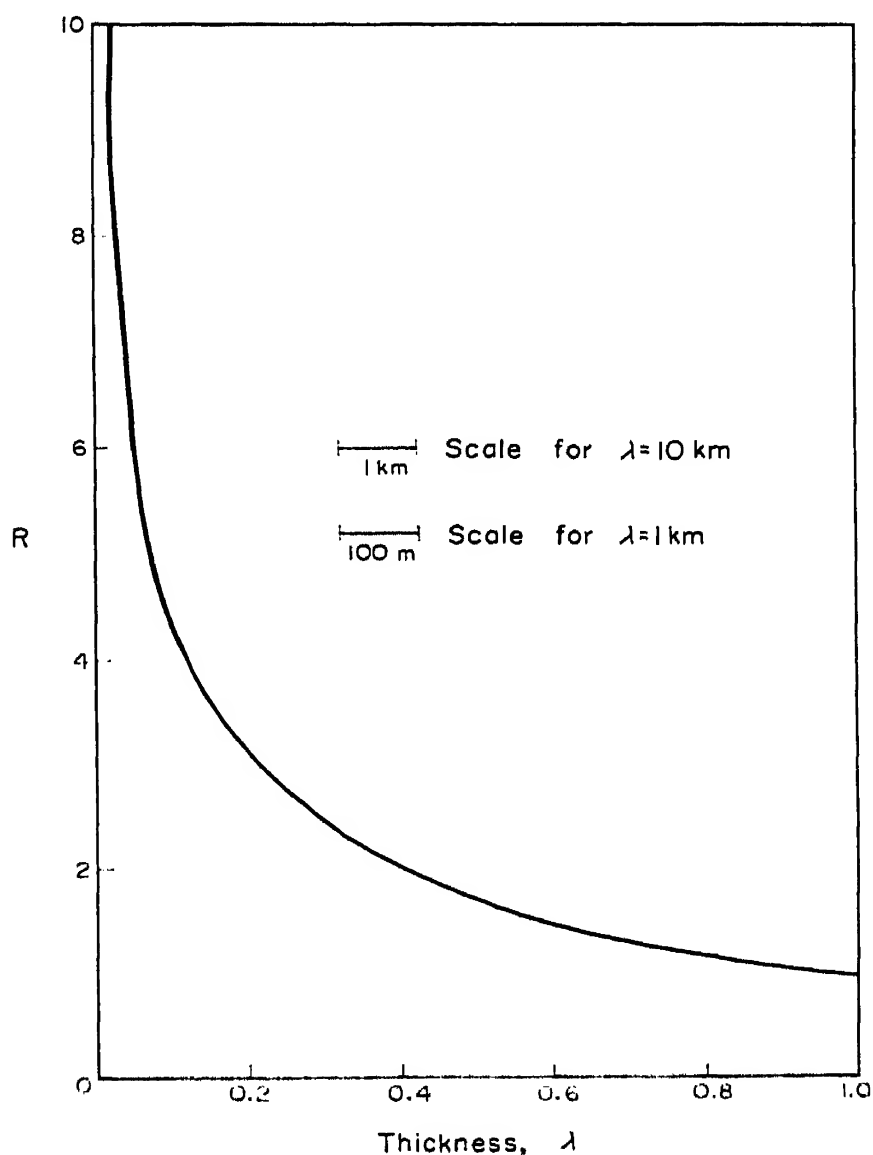


Fig. 3. The thickness of the layer as a function of  $R$ .

large values of  $R$ ; at night, it is the dominating factor in determining  $N_{\max}$ . The effect of diffusion is discussed in more detail in Section 5.

Because of the rapid recombination in the dense sporadic- $E$  layer, the total electron content falls when the layer is formed as shown in Fig. 4. Although this calculation cannot be applied directly to night values of  $R$  (because of the effect of diffusion), yet the effect of the rapid recombination and subsequent fall in electron content should be more noticeable at night

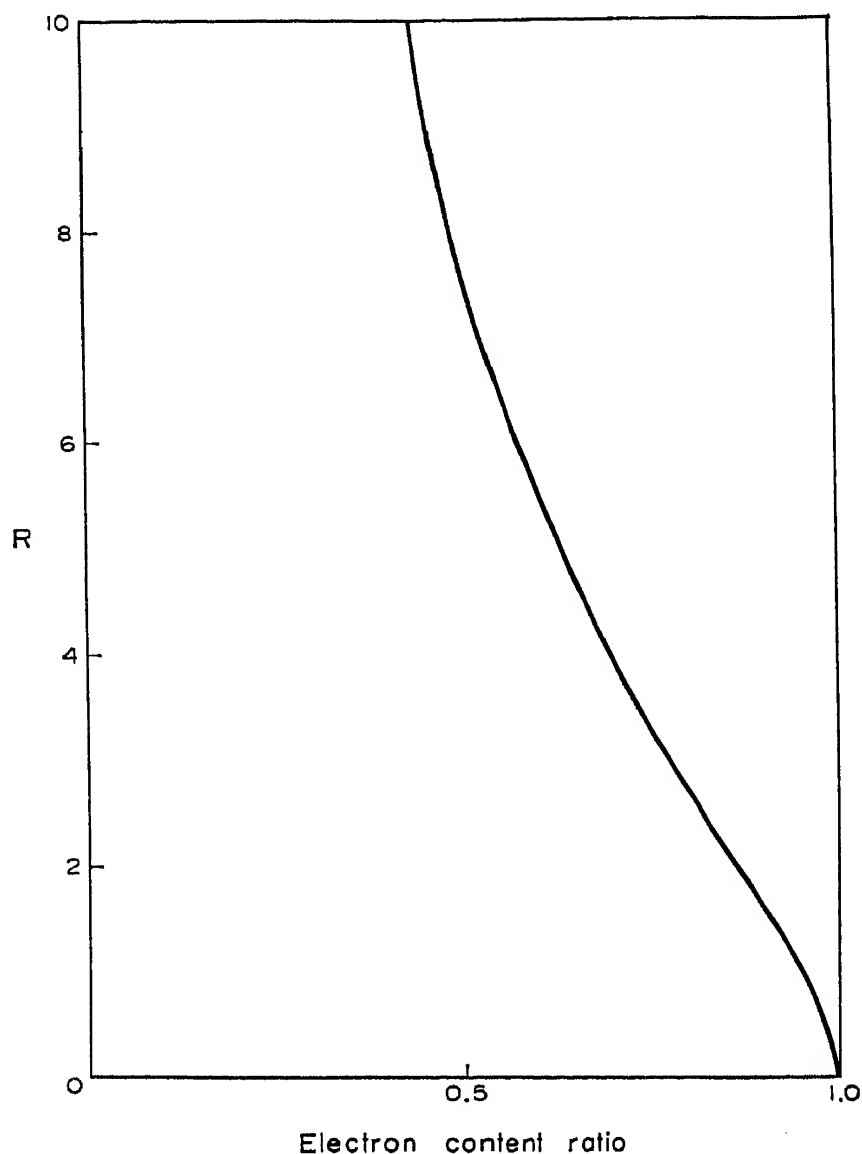


Fig. 4. The electron content as a function of  $R$ .

than during the day. A programme is being prepared in this laboratory to investigate the electron content in the lower ionosphere before and after sporadic- $E$  appearances.

It is of interest to enquire how quickly the peak electron density grows with time after the imposition of the vertical movement. In this discussion,  $N$  denotes the peak electron density at a time  $t$ ,  $N_{\max}$  the final peak electron density from equation (4.3) and  $N_{\min}$  from equation (4.4).

Equation (4.1) may be written

$$\frac{\partial N}{\partial t} = \alpha(N + N_{\min})(N_{\max} - N)$$

which can be integrated to give

$$\frac{N_{\max} - N}{N + N_{\min}} = \frac{N_{\max} - N_0}{N_0 + N_{\min}} \exp(-\alpha(N_{\max} + N_{\min})t)$$

If  $R \gg 1$ , this becomes

$$\frac{RN_0 - N}{N} = (R - 1)\exp(-R\alpha N_0 t) \quad (4.5)$$

Figure 5 shows  $N/N_0$  plotted against  $\alpha N_0 t$  for  $R = 10$  and illustrates the slow initial growth followed by one with a time constant of  $1/R\alpha N_0$ .

If we take a general vertical movement rather than the particular case we have dealt with above, it is possible to find the vertical velocity at the peak electron density.

In equilibrium

$$0 = q - \alpha N^2 - \frac{d(NV)}{dz}$$

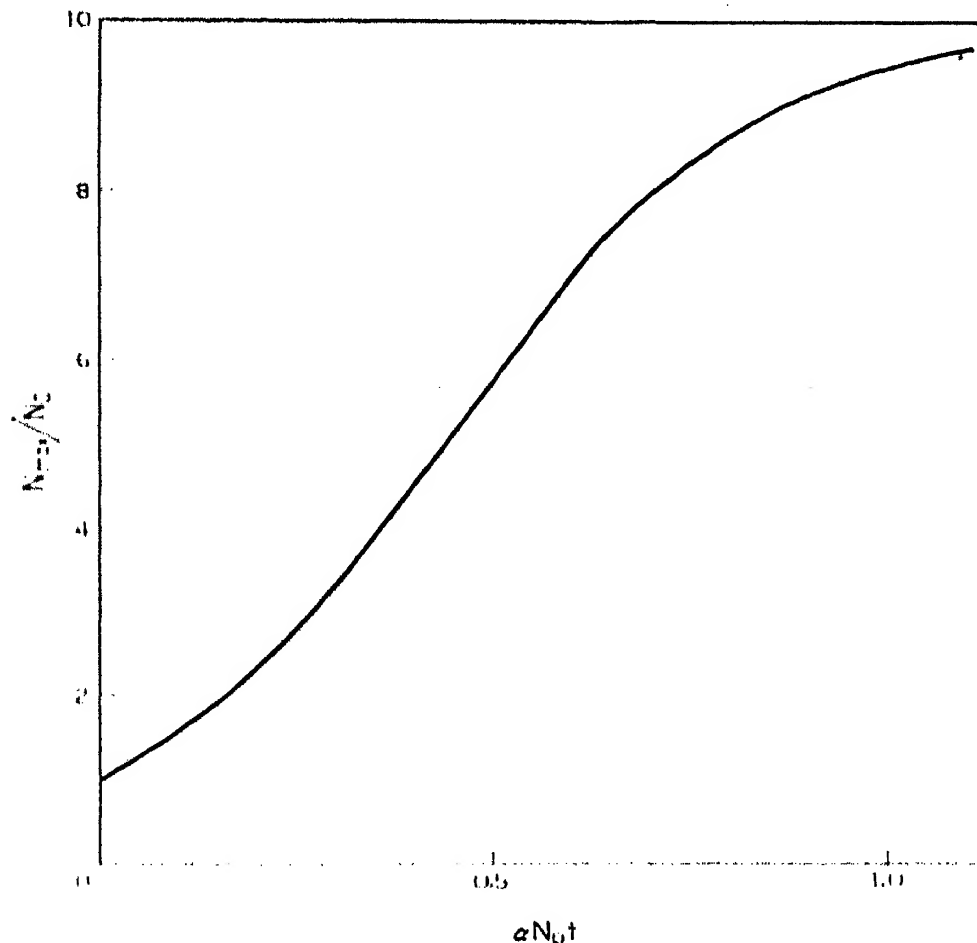


Fig. 5. The growth of a sporadic cloud: the peak electron density against time.



Differentiating with respect to  $z$  and putting  $dN/dz = 0$  we get that at the peak electron density

$$V_z = \frac{N d^2V/dz^2}{d^2N/dz^2}$$

$d^2N/dz^2$  will be large at the peak and therefore  $V_z \sim 0$ . We will assume that the sporadic- $E$  layer forms at the height at which  $V_z$  is exactly zero.

### 5. THE EFFECT OF DIFFUSION ON THE PEAK ELECTRON DENSITY

The effect of diffusion is to introduce an additional term into equation (4.2) to give

$$\begin{aligned} 0 = 1 - (N/N_o)^2 + R d\left(\frac{N \sin \gamma}{N_o}\right)/d\gamma \\ + (2\pi/\lambda)^2 (D/\alpha N_o) d^2(N/N_o)/d\gamma^2 \end{aligned} \quad (5.1)$$

A very approximate solution to this equation has been found graphically by rounding off the peak of the layer with a parabola until the last term in this equation is sufficiently small to give the correct value of  $N_{\max}$ . The resultant electron density distribution taking  $\lambda = 10$  km,  $N_o = 1.5 \times 10^5$  /cm<sup>3</sup> and  $V = 23$  m/s ( $R = 10$ ) is shown in Fig. 2.

This solution will become a poor one for large values of  $R$ , and for night time in particular, a different method must be used. Roughly speaking for  $R \gg 1$  we can say that the layer peak grows at a rate of  $\alpha N_o R$ , recombines at a rate  $\alpha N_{\max}$  and diffuses away at a rate  $D/L^2$  where  $L$  is the thickness of the layer. For large values of  $R$  where diffusion is important, the layer will be approximately parabolic and  $L$  will have a meaning. Because the rate of formation  $\alpha N_o^2$  must equal the average rate of recombination,  $L \sim \lambda N_o^2/N_{\max}^2$ . Then we can write

$$\begin{aligned} \alpha N_o R &\sim \alpha N_{\max} + D/L^2 \\ &= \alpha N_{\max} + DN_{\max}^4/\lambda^2 N_o^4 \end{aligned} \quad (5.2)$$

At night, the recombination term can be neglected and

$$\begin{aligned} \frac{N_{\max}}{N_o} &\sim (\alpha N_o R \lambda^2/D)^{1/4} \\ &= (2\pi V_o \lambda/D)^{1/4} \end{aligned}$$

In Section 6, we show that  $\lambda$  cannot exceed about 20 km, and taking  $V_o \sim 23$  m/sec

$$\frac{N_{\max}}{N_o} \sim 15, \text{ giving } N_{\max} \sim 1.5 \times 10^5/\text{cm}^3$$

This result which is somewhat less than the values of  $N_{\max}$  frequently observed cannot be regarded as unsatisfactory in view of the very rough approximation used.

Equation (5.2) has another interesting feature. Writing

$$R = 2\pi V_o / \lambda \alpha N_o$$

we have

$$2\pi V_o / \lambda = \alpha N_{\max} + DN_{\max}^4 / \lambda^2 N_o^4.$$

Differentiating with respect to  $\lambda$  and keeping  $V_o$ ,  $N_o$ ,  $\alpha$  and  $D$  constant, we get

$$-\frac{2\pi V_o}{\lambda^2} = \alpha \frac{\partial N_{\max}}{\partial \lambda} + \frac{DN_{\max}^3}{\lambda^2 N_o^4} \cdot \frac{\partial N_{\max}}{\partial \lambda} - \frac{2DN_{\max}^4}{\lambda^2 N_o^4}.$$

To find the peak value of  $N_{\max}$  for varying  $\lambda$  we put  $\partial N_{\max} / \partial \lambda = 0$  and find that

$$\frac{DN_{\max}^4}{\lambda^2 N_o^4} = \frac{\pi V_o}{\lambda} = \frac{\alpha N_o R}{2}.$$

Substituting in (5.2), we have

$$\alpha N_o R = \alpha N_{\max} + \frac{\alpha N_o R}{2}$$

or

$$\frac{N_{\max}}{N_o} = \frac{R}{2}.$$

The interesting thing is that this peak value (which is half that found neglecting diffusion) occurs for

$$\begin{aligned} \lambda &= \frac{D}{\pi V_o} \left( \frac{N_{\max}}{N_o} \right)^4 \text{ from above} \\ &= \frac{D}{\pi V_o} \frac{\pi^4 V_o^4}{\lambda^4 \alpha^4 N_o^4} \end{aligned}$$

whence

$$\lambda = \left( \frac{\pi^3 D V_o^3}{\alpha^4 N_o^4} \right)^{1/5}$$

Taking  $V_o = 10$  m/sec, this equation gives  $\lambda = 5$  km during the day, and  $\lambda = 30$  km at night, as large as the permissible value. However, the day-time value of  $\lambda$  appears to have some significance, for instance Briggs (1958) found two sporadic-*E* layers separated by 5 km and Pfister (1958)

found stratification in  $E$ -region electron densities with a spacing of about 6 km, increasing with height, as would be expected from the increase in  $D$ .

## 6. THE FORMATION OF SPORADIC $E$

The probability of formation of sporadic  $E$  increases as the following quantities increase:

- (a)  $N_o$ , which decreases rapidly below the maximum of  $E$ -region.
- (b)  $dU_y/dz$  and  $dU_x/dz$ , the wind shears which decrease with increasing height, perhaps as quickly as  $\nu_i$ .
- (c)  $1/D$  which also decreases with height.
- (d)  $\frac{\nu_i \omega_{Hi} \cos \theta}{\nu_i^2 + \omega_{Hi}^2}$  which has a peak value at  $\nu_i = \omega_{Hi}$  and decreases more slowly than  $1/\nu_i$  below this height.

It becomes obvious that sporadic  $E$  will tend to form at a definite height, and that this height will be below  $\nu_i = \omega_{Hi}$  but above the level where  $N_o$  falls so quickly, i.e. just below the maximum of  $E$ -region, at its normally observed height. At this height,  $dV_z/dz$  is given by equation (3.1). To assist in the formation of a layer,  $dV_z/dz$  must be negative, and therefore *the westward component of the neutral air wind must be decreasing with height.*

Equation (3.1) can also be used to give the world-wide distribution of sporadic  $E$ . Fixing  $V_o$  and allowing  $\lambda$  to vary to give the largest value of  $N_{\max}$  we see that

$$N_{\max} \propto N_o^{4/5} \nu_i^{-1} \omega_{Hi} \cos \theta.$$

Taking  $\nu_i$  to be the collision frequency at the maximum of  $E$ -region  $\nu_i \propto \cos \chi$ , and  $N_o \propto (\cos \chi)^{1/2}$  where  $\chi$  = zenith angle of the sun. Thus

$$N_o^{4/5} \nu_i^{-1} \propto (\cos \chi)^{-0.6}.$$

The temperate zone extends north and south to a latitude of about  $60^\circ$  (Smith 1958) and sporadic  $E$  occurs most frequently at summer midday. At this time, throughout the temperate zone

$$\begin{aligned} \chi &< 60^\circ - 23^\circ \\ &= 37^\circ \end{aligned}$$

so that  $\cos \chi$  varies from 0.8 to 1, and  $(\cos \chi)^{-0.6}$  varies from 1.12 to 1. On the other hand, the term  $\omega_{Hi} \cos \theta$  is proportional to the horizontal component of the earth's magnetic field which varies by a factor of almost 3 over the temperate zone. Thus we expect the maximum electron density to be dependent mainly on the horizontal component of the earth's magnetic field. This is precisely the relationship found by Heisler and Whitehead (1960a) for the percentage of time  $f_oE_s > 5$  Mc/s, and appears to provide very strong evidence in favour of this means of sporadic- $E$  production.

So far we have only considered the gradient of  $V_z$  required to produce sporadic  $E$ , and the height at which it is most likely to appear. It is possible to estimate the maximum vertical scale structure of the wind from the following consideration. Sporadic  $E$  appears low down in  $E$ -region at such a height that  $U_y = \bar{U}_y$  where the average is taken over a range of heights from about the level where  $\nu_i = \omega_{Hi}$  down to just below where the layer itself is and is weighted fairly evenly over this range. This condition leads to the gradient of  $V_z$  at the sporadic- $E$  level falling off more rapidly than  $V_o/\lambda$ , so that because the range of integration is about 10 km, the gradient becomes only 1/5 for  $\lambda = 30$  km as for  $\lambda = 10$  km if  $V_o$  is kept constant. Thus the effective vertical wave-length will not greatly exceed 30 km. This limitation is most important at night, and shows that the peak electron density will then be determined principally by diffusion. In fact the limitation at night is stronger than deduced above, because the height of the bottom of  $E$  layer moves upwards and thus reduces the height range of the integration to less than the 10 km assumed.

## 7. THE PERSISTENCE OF A SPORADIC- $E$ LAYER

### *The Need for a Persistence Mechanism*

It might be thought that a sporadic- $E$  layer would persist for just as long as the wind system. However, small changes in the winds result in the layer being formed at a different height, and the original layer decaying. For instance, if the wind system has a quasi-period of 1 hr and  $\lambda = 5$  km, the height at which  $V_z = 0$  changes at the rate of  $\sim 2$  m/sec. If the layer is 100 m thick (determined by diffusion) it will only have  $\sim 50$  seconds to form as against  $\sim 200$  seconds required (taking  $R \sim 8$ ) from equation (4.5). The peak electron density would be much less than that for a constant wind.

### *The Way in which a Layer once Formed tends to Persist*

Suppose a dense layer has been formed at a height a little below  $E$ -region maximum and the winds are suddenly changed. Looking back at equation (2.1), it will be seen that because most of the electrons are near the maximum (for  $R = 10$ , over 50 per cent of all the electrons are within  $\lambda/10$  of the peak),  $\int_{-\infty}^{\infty} F dz$  becomes small and  $\int_{-\infty}^{\infty} G dz \gg \int_{-\infty}^{\infty} F dz$ . Moreover  $\bar{U}_{yG}$  becomes very close to the value of  $U_y$  at the peak value of  $G$ , i.e. at the peak of the layer. Thus  $U_y - \bar{U}_{yG}$  will remain small at the peak of the layer, in spite of the wind change, and so layer formation at *the same height* continues.

What happens is that the sporadic- $E$  layer forms a region of high conductivity and the electric fields are almost entirely the result of winds in the layer itself.

## 8. THE EFFECT OF A SPORADIC-*E* CLOUD ON THE EARTH'S MAGNETIC FIELD

Initially the boundary conditions were fixed so that no net horizontal current flows. Infinite equal but opposite current sheets produce no magnetic effect outside the sheets. However, this situation is modified by current leakage allowing some net horizontal current, and by the current sheets themselves having only an extent of about 100 km. The result is that the currents which arise because of the horizontal winds do indeed cause a change in the earth's magnetic field.

It turns out that during the formation of a sporadic-*E* cloud, the horizontal component of the earth's magnetic field should decrease by a few  $1/10 \gamma$  and should incline to the West a few seconds of an arc. In a private communication, J. A. Thomas reported that a decrease in horizontal component of  $\sim 7\gamma$  has been observed, much larger than that predicted by the theory.

## 9. THE ASSOCIATION BETWEEN SPORADIC-*E* AND *F*-REGION TRAVELLING DISTURBANCES

There have been reports of an association between sporadic-*E* and *F*-region travelling disturbances (Heisler and Whitehead (1960b), Bowman (1960)). The explanation appears to be that the electric fields produced in *E*-region by the same horizontal winds giving rise to sporadic *E* are transferred along the magnetic field lines (which are almost equipotentials) and cause movements of ions to form a ripple in the *F*-region isoionic contours. The details will not be discussed here, but it appears that the association would not be expected to be a very close one and that both E-W and N-S winds play a part.

## 10. CONCLUSIONS

The mechanism for the formation of a sporadic-*E* layer from a vertical gradient in horizontal winds appears to explain many of the features observed, in particular the global distribution of sporadic *E*, its height of occurrence, the observations of stratification and its association with *F*-region travelling disturbances. Detailed observations of the horizontal winds are required, perhaps following the method used by Blamont (1959). It would also be valuable to have more detailed knowledge of changes in the earth's magnetic field associated with sporadic *E* and the actual current flows measured by rocket magnetometers passing through a sporadic-*E* cloud. Much more detail is also required of the shape, thickness and fine structure of the electron density distribution, and of the electron content.

The persistence mechanism may explain the long lifetime of meteoric  $E_s$  (Naismith 1954) and also suggests how a dense blob of ionization, artificial or natural, may grow to form an  $E_s$  cloud.

*Acknowledgments*—This work has been carried out as part of the investigations of this laboratory sponsored by the Radio Research Board of the Commonwealth Scientific and Industrial Research Organization. The author wishes to thank Dr. G. H. Munro and Mr. L. H. Heisler for helpful discussion and Miss R. C. Nathan for assistance with the calculations.

#### REFERENCES

- BECKER, W. (1958) AGARDograph 34, Sporadic-*E* Ionization p. 59 (N.A.T.O. Advisory Group for Aeronautical Research and Development).  
BLAMONT, J.-E. (1959) *Comptes Rendus* **249**, 1248.  
BOWMAN, G. G. (1960) *Planet. Space. Sci.* **2**, 195.  
BRIGGS, B. H. (1958) AGARDograph 34, Sporadic-*E* Ionization p. 151 (N.A.T.O. Advisory Group for Aeronautical Research and Development).  
DUNGEY, J. W. (1956) *J. Atmosph. Terr. Phys.* **8**, 39.  
DUNGEY, J. W. (1959) *J. Geophys. Res.* **64**, 2188.  
GREENHOW, J. S. and NEUFELD, E. L. (1959) *J. Geophys. Res.* **64**, 2129.  
HEISLER, L. H. and WHITEHEAD, J. D. (1960a) *Nature* **187**, 676.  
HEISLER, L. H. and WHITEHEAD, J. D. (1960b) *J. Geophys. Res.* **65**, 2767.  
MARTYN, D. F. (1953) *Phil. Trans. of Roy. Soc. A* **246**, 306.  
MILLMAN, P. M. (1959) *J. Geophys. Res.* **64**, 2122.  
MITRA, S. K. (1952) *The Upper Atmosphere* p. 290, The Asiatic Society, Calcutta.  
NICOLET, M. (1953) *J. Atmosph. Terr. Phys.* **3**, 200.  
NICOLET, M. and AIKIN, A. C. (1960) *J. Geophys. Res.* **65**, 1469.  
PFISTER, W. (1958) AGARDograph 34, Sporadic-*E* Ionization p. 183 (N.A.T.O. Advisory Group for Aeronautical Research and Development).  
SMITH, E. K. JR. (1958) AGARDograph 34, Sporadic-*E* Ionization p. 1 (N.A.T.O. Advisory Group for Aeronautical Research and Development).  
THOMAS, J. A. (1958) AGARDograph 34, Sporadic-*E* Ionization p. 23 (N.A.T.O. Advisory Group for Aeronautical Research and Development).  
WHITEHEAD, J. D. (1959a) *J. Atmosph. Terr. Phys.* **16**, 99.  
WHITEHEAD, J. D. (1959b) *J. Atmosph. Terr. Phys.* **16**, 283.  
WHITEHEAD, J. D. (1961) *J. Atmosph. Terr. Phys.* **20**, 49.

# Structure of $E_s$ at Temperate Latitudes

K. RAWER

Ionosphären-Institut im Fernmeldetechn. Zentralamt der Deutschen Bundespost,  
Breisach/Rh., Germany

**Abstract**—A description of the behaviour of  $E_s$  is first given by appropriate statistical means i.e. with auto- and cross-correlation functions and by the fluctuation range. The different effects appearing in monthly median values of top and blanketing frequencies are described. Some results concerning the electron density profile of  $E_s$  layers can be deduced from routine and special observations. Different methods and results are given in order to describe one of the most unique features of  $E_s$ , viz. its variable transparency properties. A suitable model of the electron density distribution in three coordinates can be given. By comparison of the observations with different theories it is concluded that different from the other ionospheric layers  $E_s$  has a "meteorological" behaviour; vertical exchange trapped by some discontinuity, eventually wind shears, seems to be the most probable explanation.

## INTRODUCTION

It has been known for a long time that the frequency-characteristics of the  $E_s$ -layer are highly variable in time and space. The modern technique of direct recording of characteristics (Nakata, Kan and Uyeda 1953, Bibl 1960a) provides a powerful tool to follow rapid variations of both the top and blanketing frequency of  $E_s$  layers. Typical examples are given in Figs. 1 and 2.

Each of these figures shows three records, each as a function of the hour. The lowest record is that which is of most interest here; it gives  $f_t E$ , the top frequency of the  $E$ -region. The variable white traces on this record indicate the frequency range where echoes had been obtained from the corresponding height range. Except for the time between 01 00 and 03 00 hr the lower limit of this range is given by the mf broadcasting band. The upper limit can be identical with  $f_o E$  or  $f_x E$  or  $f_o E_s$  or  $f_x E_s$ . In Fig. 1. we have winter night conditions so that echoes from the  $E$ -layer appear only after 07 00 hr. All other echoes are from  $E_s$ . As a result of gyro absorption (p. 156, my other contribution) there is a discontinuity near 2.6 Mc/s; at frequencies below that limit the gyro absorption was too strong for the  $x$ -component to appear. So upper range limits seen below this value correspond to  $f_o E_s$ , limits above generally to  $f_x E_s$ . Figure 2 has been obtained in summer. During daytime  $f_o E$  is quite visible as a small dark band passing rather regularly through the echo range (see 10 00–17 00 hr). This is the effect of selective absorption near  $f_o E$ . Only when blanketing is rather strong does this band disappear as can be seen between 05 00 and 07 00 hr. In daytime the lower limit for the visibility of the  $x$ -component is well above  $f_o E$ , at noon at about 5 Mc/s. Both magneto-ionic components can be seen separately between 03 00 and 04 00 hr for example.

The record in the middle gives virtual heights,  $h'$  (inscribed from top to bottom).  $E$ - and  $E_s$ -traces can be seen near 110 km, the double echo near 220.  $F$ -echoes are found at about this level in daytime but at more than 260 km at night. Appearance

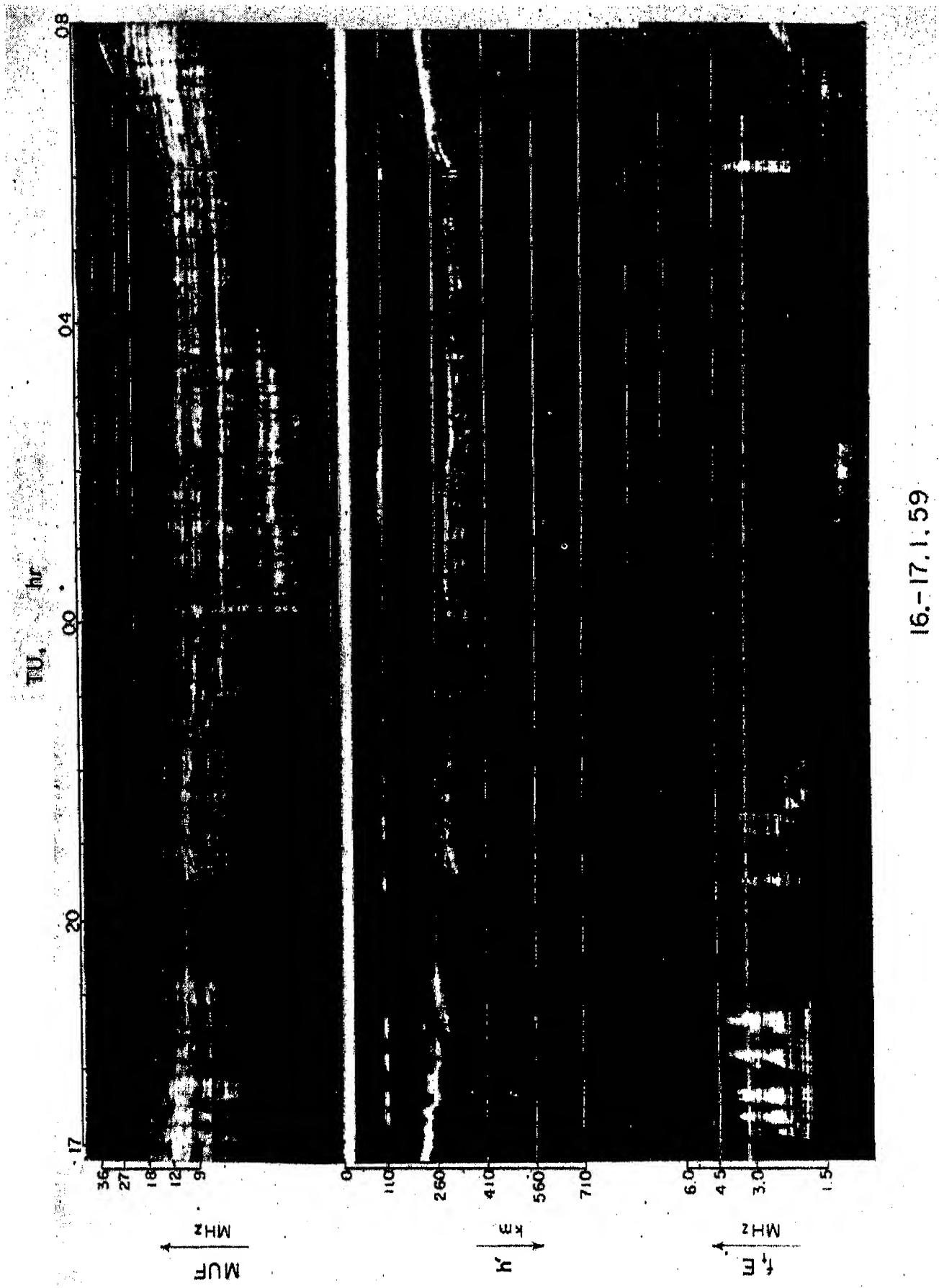
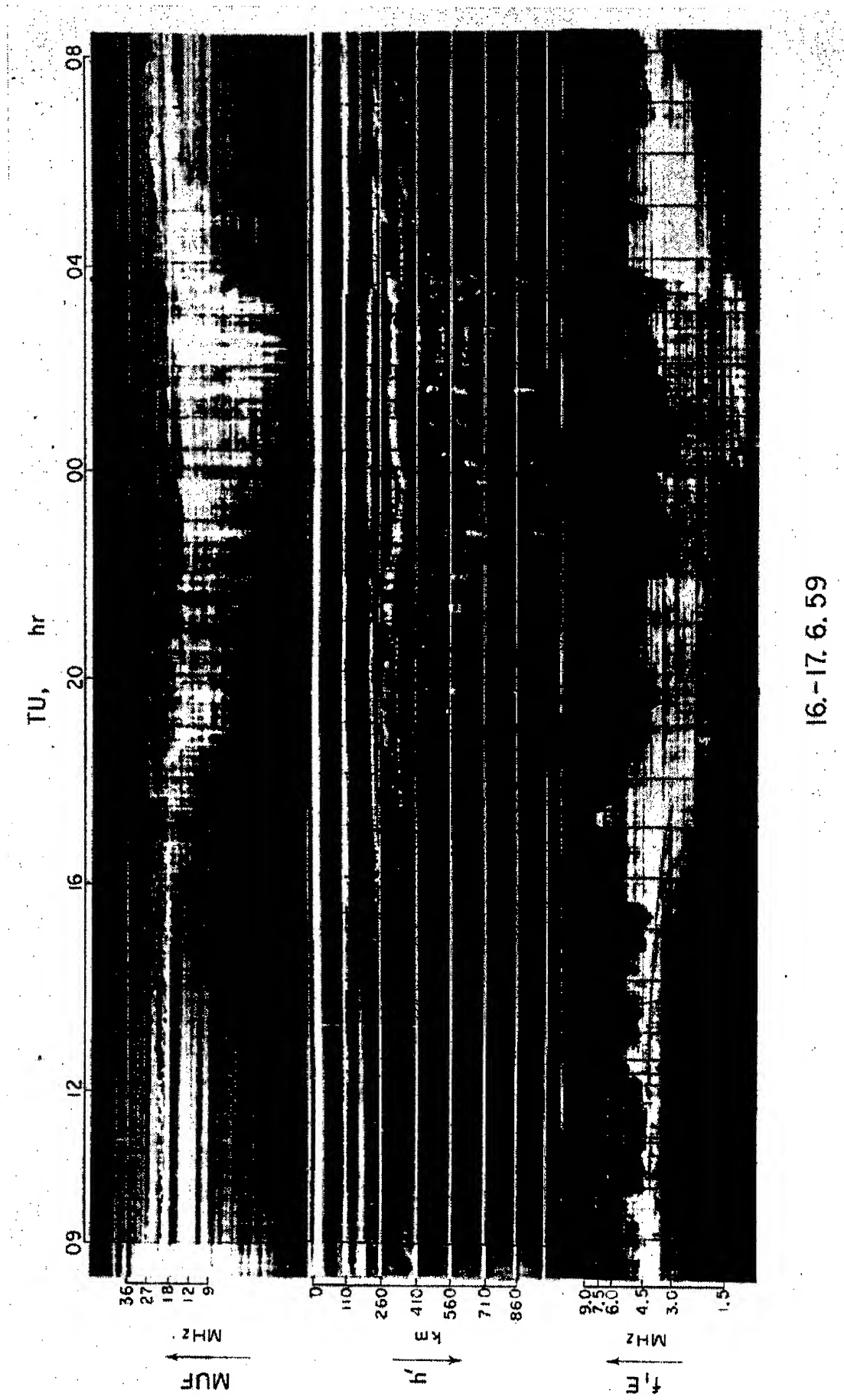


Fig. 1. Record of characteristics  $MUF$ ,  $h'$  and  $f_oF_2$  of  $E_s$  (16/17-1-59).





16.-17. 6. 59

Fig. 2. Record of characteristics  $MUF$ ,  $h'$  and  $f_1E$  with longlasting  $E_s$  (16/17-6-59).  
(MHz = Mc/s)

and disappearance of  $E_s$  is readily seen in this record, the double echo shows that the  $E_s$ -cloud was overheads. Blanketing can also be seen as in these cases the  $F$ -trace is interrupted, at least at lower  $F$ -heights. This can be seen on Fig. 1. several times between 17 00 and 19 00 hr, also between 20 00 and 22 00 hr and after 06 00 hr, on Fig. 2. at 17 00 and 04 00–05 00 hr.

The uppermost record gives the “ $MUF\ 3000$ ”. The white bands in this record are the usable frequency range after the N. Smith transformation. Its lower limit in most cases is given by blanketing by normal  $E$ , but when blanketing by  $E_s$  occurs it can also be seen on these records. So the four “flashes” of  $E_s$  between 17 00 and 18 30 hr on the lower record of Fig. 1 can also be seen as blanketing flashes on the uppermost record. It is similar with 20 30, 21 10, 06 00 hr on Fig. 1, also with 17 00–18 00 and 04 00–05 00 hr on Fig. 2.

We learn from these records that important variations of  $fE_s$  can occur, the duration of a “flash” being often quite short, a few minutes only (Fig. 1). On the other hand one has also cases where the variation of the  $E_s$ -data is rather slow; important  $E_s$ -ionization can be present for hours (Fig. 2). It is not quite the same with blanketing;  $f_bE_s$  has a preference for short flashes, cases of long-lasting heavy blanketing are not quite so frequent.

In the presence of such rapid fluctuations it is difficult to determine a representative value of ionization or blanketing. It is evident that if readings are taken only once an hour these are not all representative for the hour. In this respect  $E_s$  parameters differ from most other conventional characteristics. With quarter-hourly readings the situation is only slightly better. It must be clearly stated that “spot readings” if not used for instantaneous comparison are only valuable as a mass, the statistical behaviour of which is the only useful information. Some average, e.g. a time integral over the  $f_oE_s$  or  $f_bE_s$  curve respectively, would be a more representative parameter. (Bibl 1960b) has recently tried to approximate this idea by a suitable reduction of such records; his “dynamic measure of  $E_s$ ” is a representative value for the hour obtained by multiplication of the median value by the number of “flashes” per hour.

## 1. STATISTICAL PROPERTIES

The conventional characteristics,  $f_oE_s$  and  $f_bE_s$ , are interchanged in the form of hourly tabulations. Considering the rapid variations in time and space we should first look for the statistical behaviour of these data. When treating this problem two difficulties have been encountered which are of a general nature.

1.01. As we explain in detail in our other contribution the conventional frequency characteristics  $f_oE_s$  and  $f_bE_s$  are not independent of the sensitivity of the ionosonde and, in particular, its variation with the frequency. Therefore in most cases it is not useful when the measured values are directly intercompared. However, the *relative variations* of these parameters are significant. (This is true if the frequency variation of sensitivity

is not extremely anomalous.) Therefore correlation methods can be used successfully; this is true for the variations in time and space, especially if results from different stations are to be compared afterwards (Rawer 1955).

1.02. The other difficulty comes from the fact that classical *correlation methods* can only be applied when all entries are numerical ones. Unfortunately ours occasionally disappear. So non-numerical correlation methods had to be applied. Instead of the rather laborious methods of size classification (Fisher 1925) a very simple counting method has been introduced by the author (Rawer 1951). In its present form (Lovera 1953, Rawer 1959) the resulting "correlation number" is equivalent to the "classical correlation coefficient" in the case of Gaussian distribution of both variables.

1.03. These difficulties being resolved we can proceed to a *statistical analysis* either by auto-correlation or by cross-correlation between stations. Unfortunately the fluctuations are so large that an isolated determination of a correlation value is not significant. This can for example be seen by looking at Figs. 1 and 2. Therefore we have determined correlation numbers for many individual sets of data; the median value of these can be considered as being significant. The final result of our correlation study will be the median auto-correlation or correlation function, i.e. the median value of the correlation number  $R$  as a function of time difference or local distance. It must, of course, be admitted that significant differences may exist for example between day and night or between north-south and east-west direction. Unfortunately the material we could investigate until now is not yet large enough to look for all possible differentiations.

### 1.1 *Auto-correlation*

1.10. A reasonable set of *homogeneous data* is obtained if the observations of two fixed hours which differ by  $\Delta t$  are intercompared for all days of a month. As we use a correlation method only the relative variations are important so that it does not matter if the median values of both hours are different. Unfortunately hourly readings are not enough to give the most interesting part of the auto-correlation function. Therefore our results are especially based on the observations of Lindau (Germany), a station which reduced quarter-hourly values during the IGY. For smaller time difference it is very difficult to get results from routine stations. If an auto-correlator was at hand one could of course use the curves of  $f_o E_s$  visible on records like Fig. 1.

1.11. The *results* of all determinations we have made with numerical values from routine scaling are shown in Figs. 3 and 4. First of all it can be seen that the dispersion of individual series of observations is very large. Only the medians of many determinations give a monotonic curve. The median curve for the top frequency  $f_o E_s$  (some older results obtained with  $f E_s$  are also given), Fig. 3, is nearly linear if a logarithmic time scale is used.

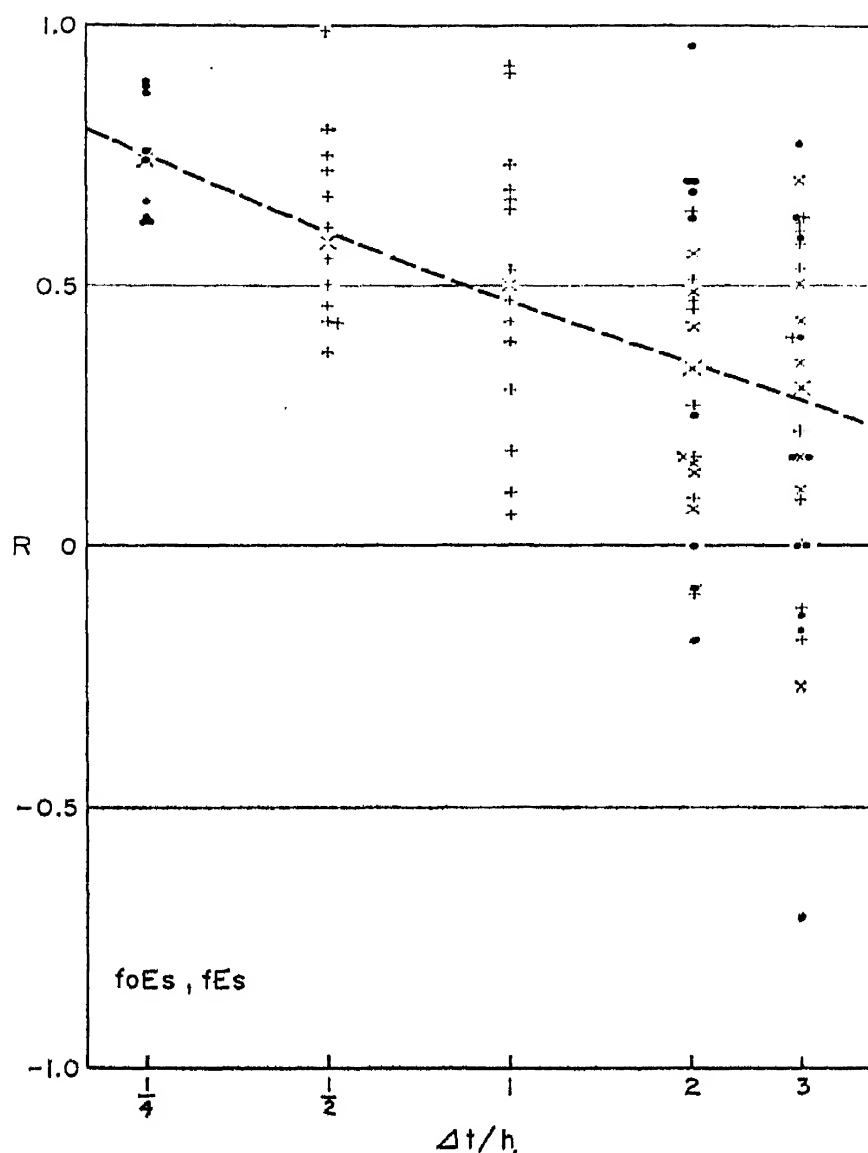


Fig. 3. Auto-correlation function for  $f_o E_s$  or  $f E_s$ .

In the most interesting range it can approximately be described in the following form:

$$\text{correlation number } R = 0.47 - 0.45 \log (\Delta t / 1 \text{ hr})$$

This formula is only valid in the limited range  $15 \text{ min} < \Delta t < 5 \text{ hr}$ .

1.12. It is also interesting to look for the *dispersion* of the data and we may try to give the deciles in a similar form for the same range:

$$\text{Lower decile: } R_{\min} = 0.53 - 0.73 \log (\Delta t / 20 \text{ min})$$

$$\text{Upper decile: } R_{\max} = 0.5 - 0.25 \log (\Delta t / 10 \text{ hr})$$

1.13. Roughly Fig. 3 can be described by saying that the *auto-correlation* of  $f_o E_s$  falls to 0.5 at about  $t = 1 \text{ hr}$ ; this is also that range where no (individual) negative  $R$ -values are found. Even if the median  $R$ -value is

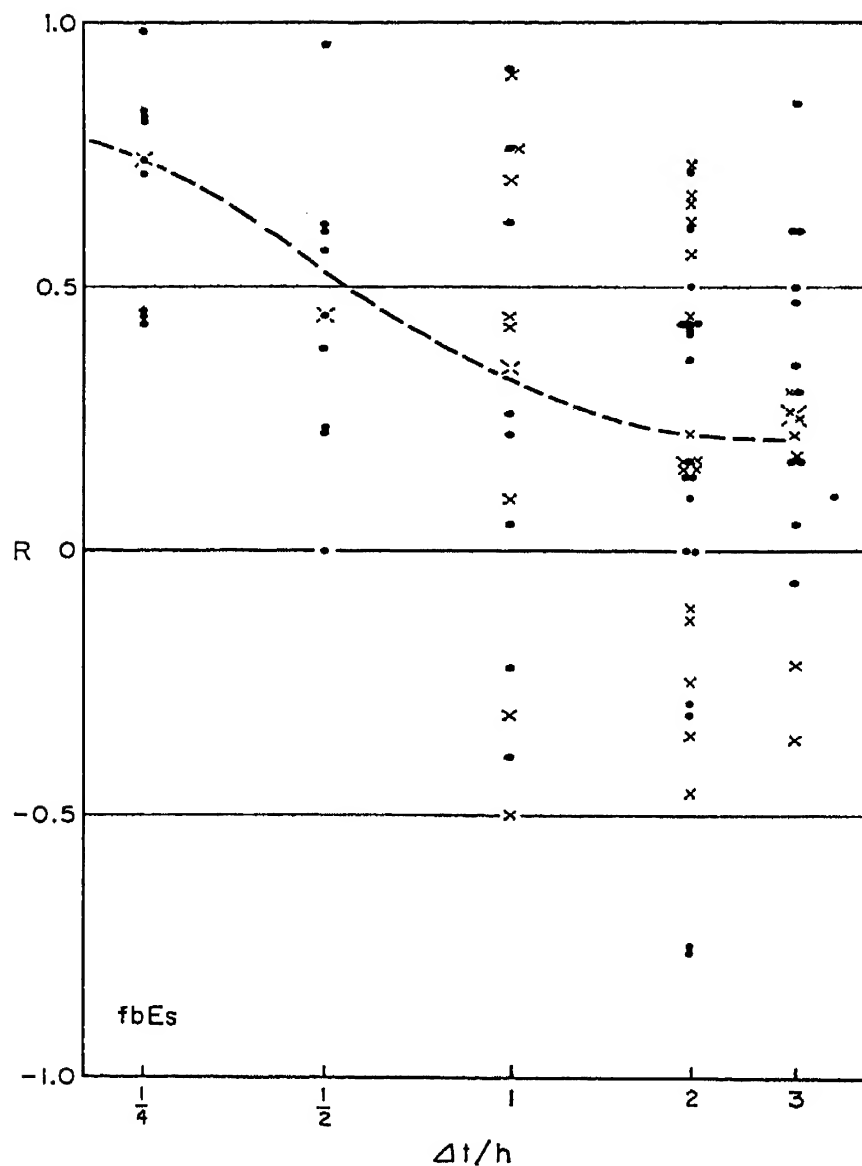


Fig. 4. Auto-correlation function for  $f_b E_s$ .

always positive, some individual correlation number may be negative for  $\Delta t \geq 1$  hr. For  $f_b E_s$  the time constant is shorter, of the order of  $\frac{1}{2}$  hr. (Fig. 4).

It is not likely that significant differences exist in this respect between different temperate latitude stations, but it seems rather certain that the conditions are different in the equatorial belt, i.e. in that zone where the "q type"  $E_s$  occurs regularly during daylight hours.

## 1.2 Cross-correlation

1.21. Now we come to cross-correlations between distant stations. The first work on these lines was done fifteen years ago in a European network of stations (Höchtel and Rawer 1949) with all observations of individual days. In that case a *systematic error* was introduced by the median diurnal variation of the parameter; this influence tends to give a positive correlation

value even if the occurrence of  $E_s$  is locally completely independent. However, the dispersion of the results is so large for individual days that for distances greater than 500 km one occasionally has negative correlation numbers. The error can be avoided if a daily characteristic is used instead of an instantaneous one. The highest  $fE_s$  value of each day has first been used by us, then the total number of readings where  $fE_s$  was greater than a fixed-frequency value. Also in that case, with several sets of observations we found enough dispersion. The average result was that the correlation function dropped rapidly between 300 and 600 km, zero correlation was practically attained when the distance was larger than 1500 km. This is shown by Fig. 5. (Traditional correlation coefficients  $r$  have been used in that figure, whilst the other results are expressed by correlation numbers (Rawer 1959).)

1.22. Later on we avoided the effect of diurnal variation by working with restricted time periods every day. According to the monthly median curve these hours had been chosen in a way that the median diurnal variation was neglectable. The difficulty with this work was that *short distance* pairs of stations working under similar technical conditions are rather rare. In particular for distances less than 500 km only a small number of pairs were available at all so that stations with rather different equipment had to be used. These pairs are: Freiburg-Schwarzenburg (140 km),

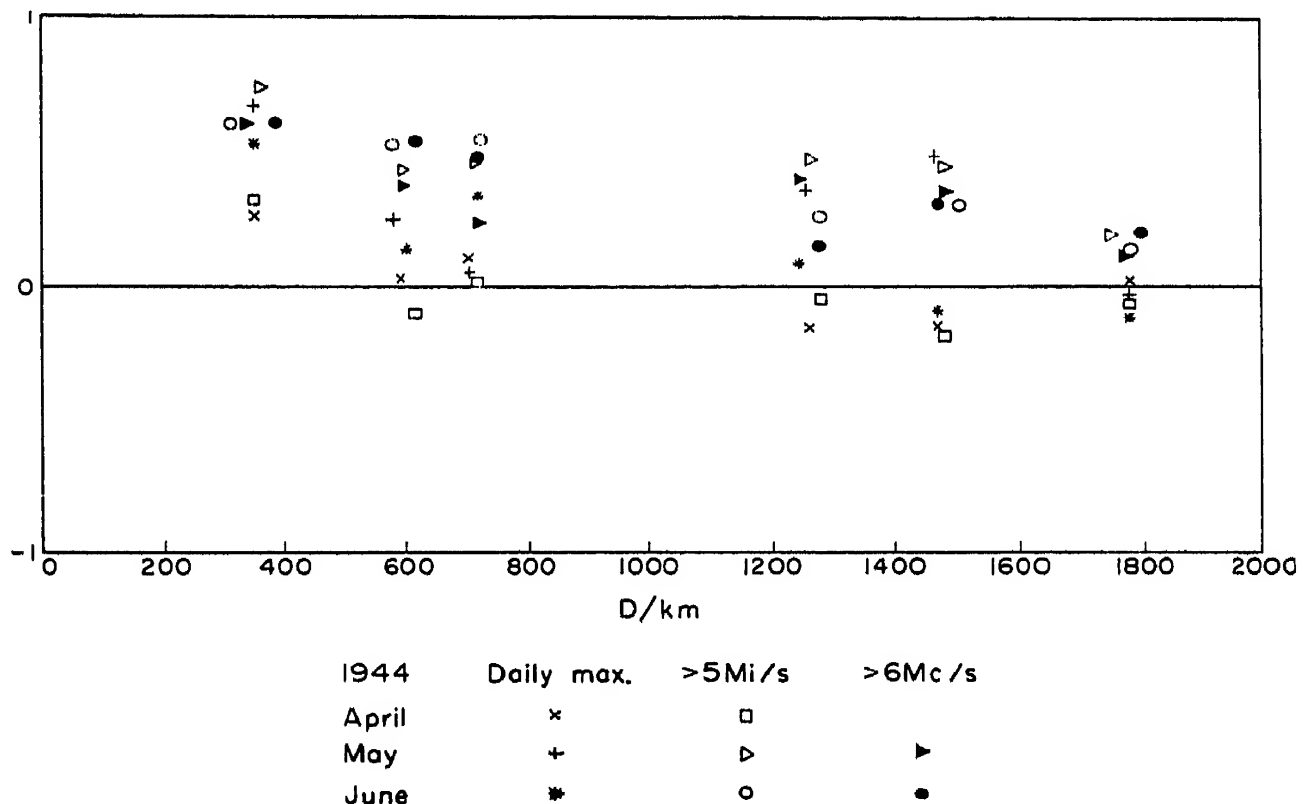


Fig. 5. Monthly values of cross-correlation of  $fE_s$  from either daily maximum value ( $\times + *$ ) or number of hourly observations greater than 5 or 6 Mc/s ( $\square \triangleright \circ$  and filled symbols) for April, May and June 1944.

Freiburg–Lindau (430 km). For medium distance we have mainly used Australian stations: Canberra–Brisbane (960 km), Canberra–Hobart (870 km).

1.23. All results obtained in this way have been plotted on Fig. 6 for  $f_oE_s$  (resp.  $fE_s$  for older measurements) and on Fig. 7 for the blanketing frequency  $f_bE_s$ . Here, again the dispersion is large in spite of the fact that every set has been obtained with at least 60 pairs of observations.

However, the medians given in Fig. 6 are quite continuous for  $f_oE_s$ .

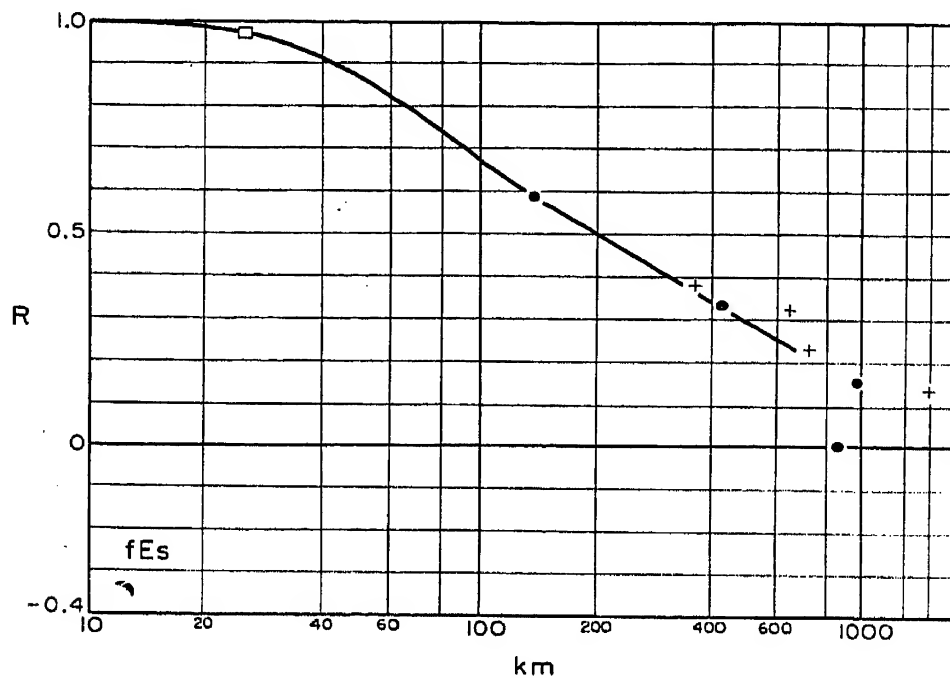


Fig. 6. Cross-correlation function for  $f_oE_s$  or  $fE_s$ .

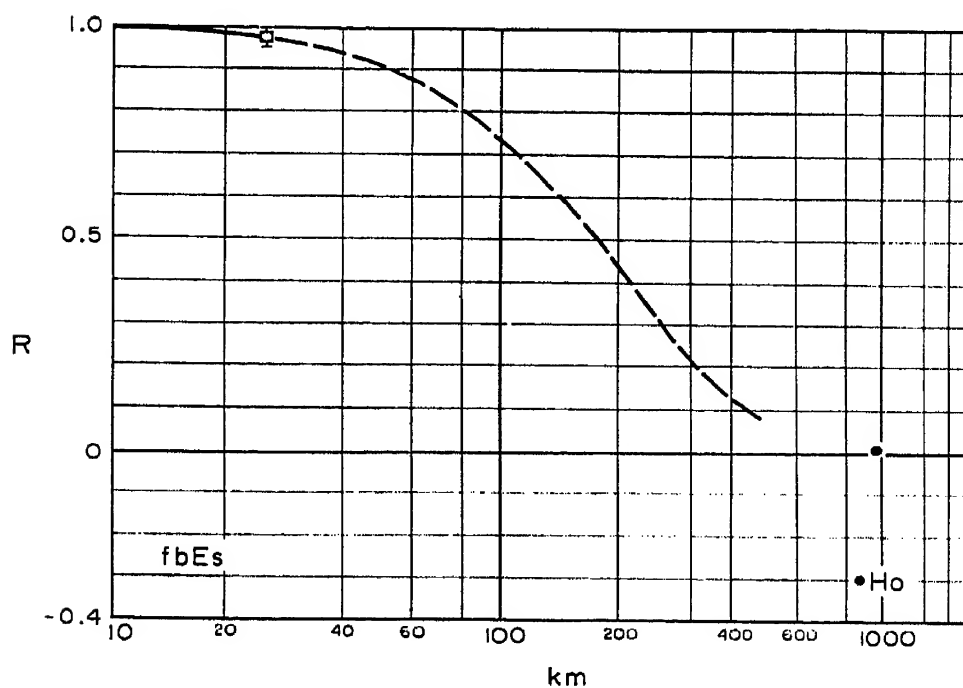


Fig. 7. Cross-correlation function for  $f_bE_s$ .

The data for  $f_b E_s$  are not very many, but it seems that the decrease is more rapid than with  $f_o E_s$ . Remembering that  $f_o E_s$  and  $f_b E_s$  roughly describe maximum and minimum electron density we may summarize the results in the following form: The *correlation range* is somewhat larger for the maximum than for the minimum electron density; it is of the order of 200 km for the first and 100 km for the second parameter. (We define the range by a correlation number of 0.5.) It must be emphasized here that a high degree of correlation found between two phenomena does not yet mean that there is no difference at all between both. For this reason the diameters found with the correlation analysis are only an upper limit for the patch dimensions.

1.24. The world-wide network of ionospheric routine stations is concentrated on the three longitudes  $10^\circ\text{E}$ ,  $130^\circ\text{E}$  and  $90^\circ\text{W}$ . As the medium latitude difference in each chain is of the order of more than  $5^\circ$  the network is not dense enough for this sort of investigations. Distances of 100 km and smaller ones are needed. We made a *special experiment* using one sender on a fixed frequency (4.2 Mc/s) and two spaced receiver,  $A$ ,  $B$ , at a distance of 50 km; one was at vertical and the other one at oblique incidence, so that the reflexion points were separated by 25 km. A correlation number could be determined by distinguishing four cases according to the presence of an  $E_s$  echo: at  $A$  and  $B$ ,  $A$  and not  $B$ ,  $B$  and not  $A$ , neither. The total number of hours where these cases have been observed are: 265.5, 41.1, 41.2, 524. This corresponds to a correlation number of 0.976 for 25 km. This value can be considered as an upper limit for the correlation number of  $f_o E_s$ . It is as near to the correct value as appearance and disappearance of the echo follows the fluctuations of  $f_o E_s$ ; the agreement was rather good in the conditions of our experiment.

“Faute de mieux” we have introduced these results also into Figs. 6 and 7.

### 1.3 *Fluctuation Range*

1.30. With Figs. 3, 4, 6 and 7 we have learned something about the statistics of  $E_s$  ionization. But this is not yet enough to give a satisfying description of the statistical behaviour of  $E_s$ . The definition of correlation coefficients or numbers is independent of the absolute *importance of fluctuations*. We have also made cross-correlations with  $f_o E$ , the critical frequency of the normal  $E$ -layer; the correlation-radius was found to be not larger than 500 km. However, for a given hour the fluctuations of  $f_o E$  are extremely small, so that the ionization is truly homogeneous. From a low correlation value alone one cannot conclude that the individual values are very variable. A conclusion affords some numerical information on the fluctuation range.

1.31. For some ionospheric characteristics this range is very small. For



$f_oE_s$  the *decile range* it is about  $\pm 6$  per cent. The first statement is now that this range is extremely high for  $f_oE_s$ , of the order of  $\pm 100$  per cent. For  $f_bE_s$  it is considerably smaller,  $\pm 50$  per cent in the worst cases. In Fig. 8 we

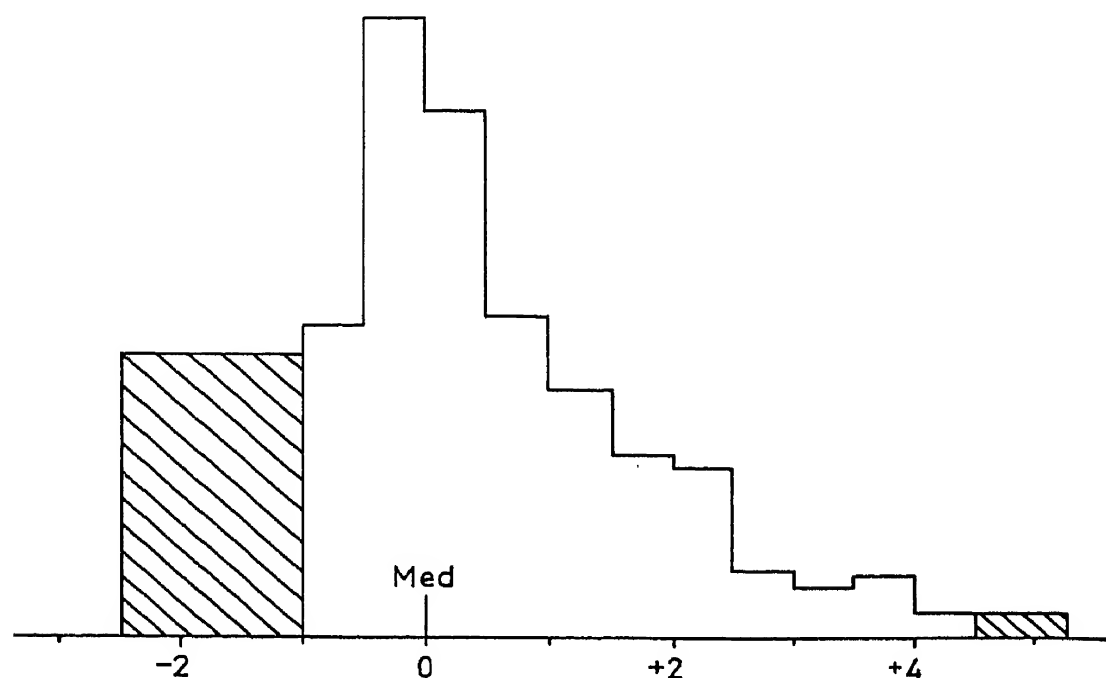
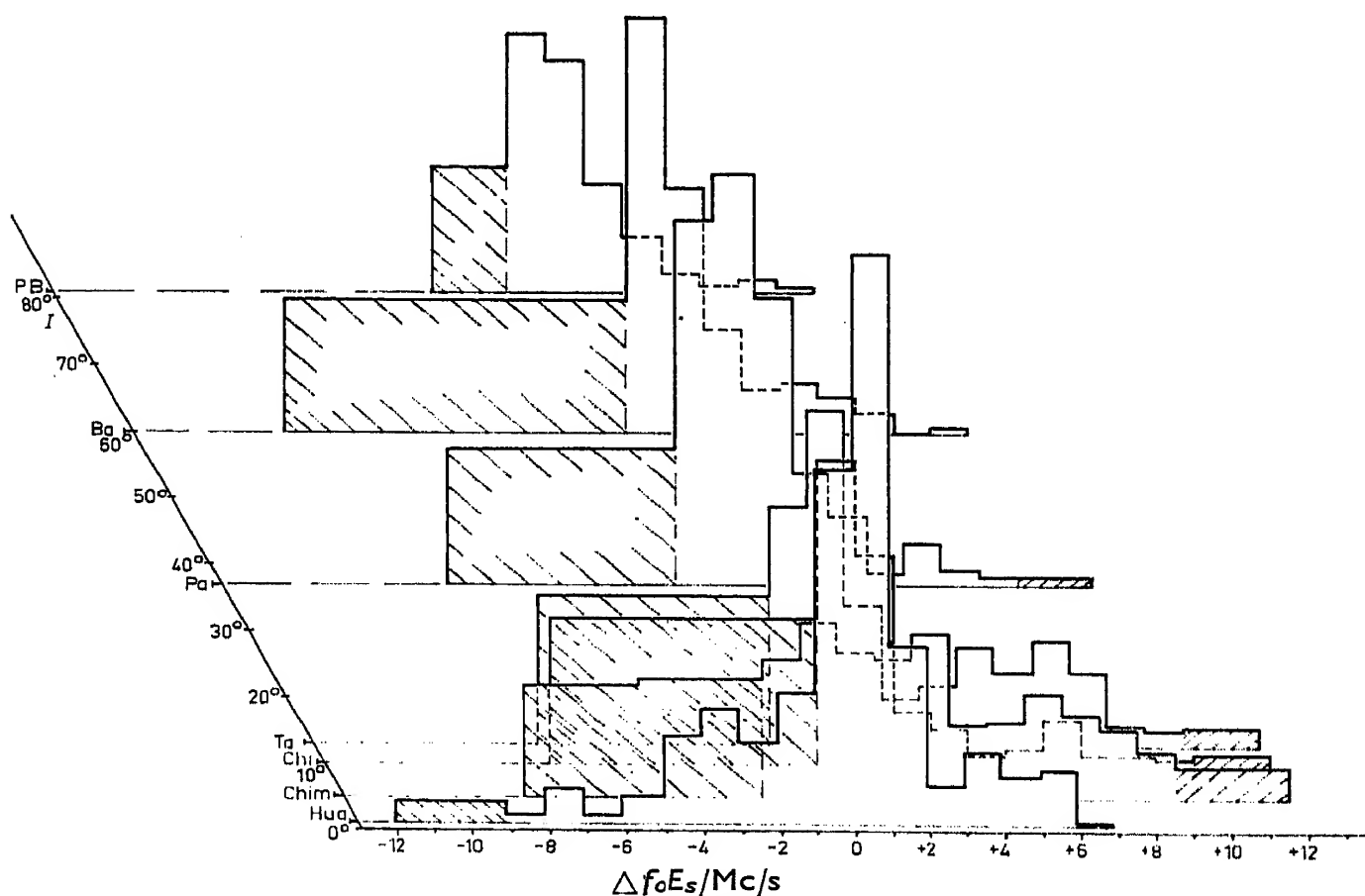
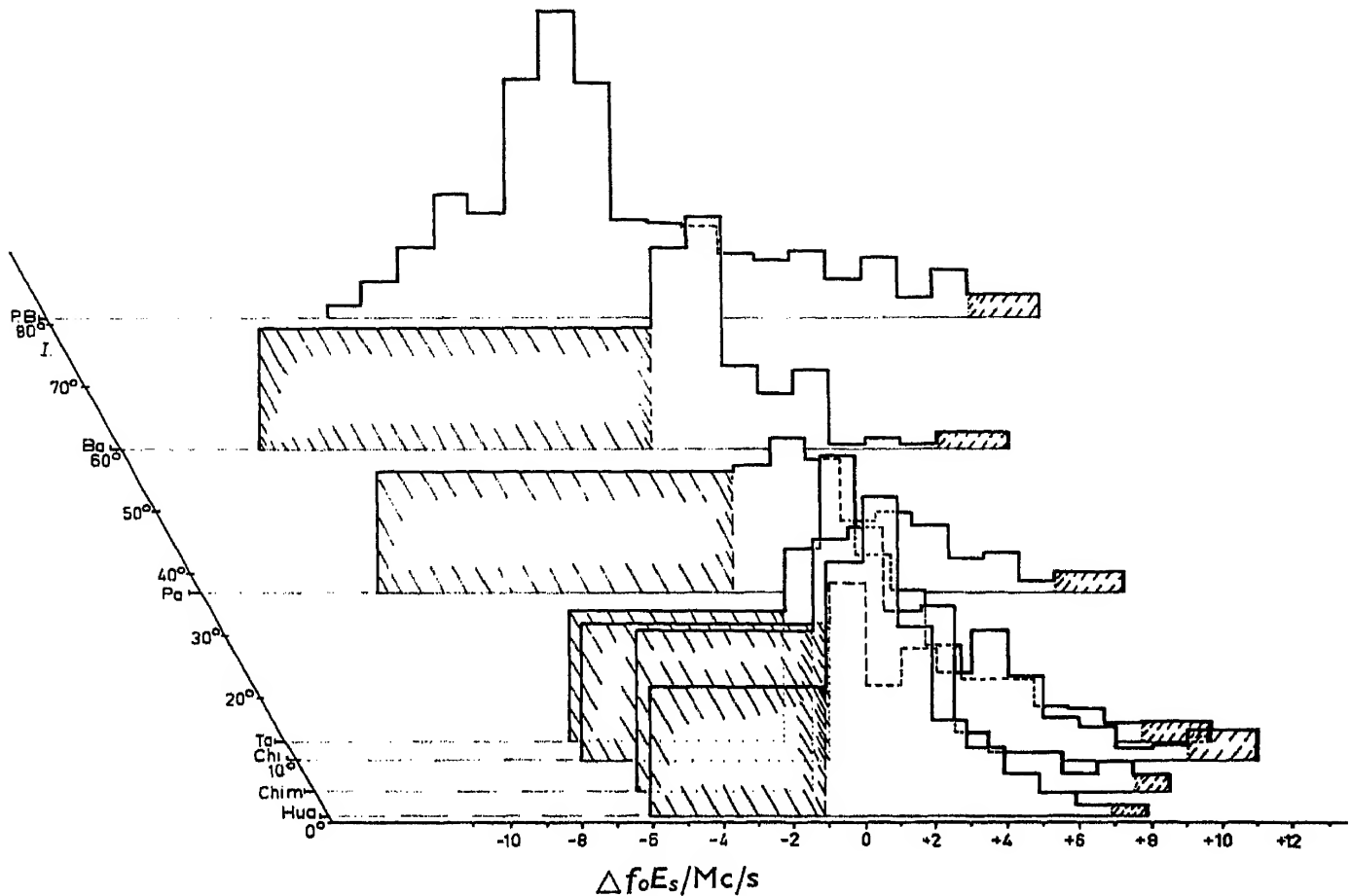


Fig. 8. Statistical distribution functions of  
(a)  $f_oE_s$ , (Mc/s) summer noon values Freiburg (1948-51)



(b)  $f_oE_s$ , (American stations, January 1958) day.



(c)  $f_o E_s$ , (American stations, January 1958) night.  
(hatched fields: left side: below  $f_o E$  (a, b) or lower recorder limit;  
right side: higher values.)

give some distribution functions for the difference of individual values against the monthly median. Figure 8a is for summer noon conditions at a temperate latitude station, it covers more than 1300  $fE_s$  readings obtained during a total of 16 months. An important fraction are those cases where no  $E_s$  was observed ( $fE_s = - - G$ ). This is the large block at the left side, it contains more than one quarter of all values. The distribution is asymmetric, viz. expanded towards high values.\* This asymmetry would appear even more clearly if we had plotted maximum electron densities (which correspond to  $f_o E_s$  (Bibl 1960 b)). This is a remarkable feature of the statistics of  $E_s$  ionization.

1.32. The distribution given in Fig. 8a shows an increased probability about 2 Mc/s above the median. Inspection of mass plots of stations at different latitudes shows a typical phenomenon which must be described here. Even at medium latitude for some summer month in day time the mass plots split up into two distinct groups, one slightly above  $f_o E$  and the other one at higher values. This occurs rather regularly at low latitudes.

\* This cannot be explained with the mixture of  $f_x E_s$  and  $f_o E_s$  which contains an  $E_s$  mass plot because the corresponding frequency shift of 0.6 Mc/s is too small.

Figure 8b gives some distribution curves (obtained from the day observations of only one month) for stations of different latitudes. A double cusp curve appears at Talara (inclination  $+13^\circ$ ); the dispersion range is much larger than at other stations. As we approach the dip equator the lower values tend to disappear (Chimbote). During daylight hours  $E_s$  appears regularly with a high ionization. It must be retained that the rather small maximum at Huancayo corresponds to the upper cusp of the transition region whilst the maximum concentration at higher latitudes corresponds to the lower one which is situated near  $f_oE$ . All this proves that the statistics of  $E_s$  ionization are very far from a Gaussian distribution.

1.33. With this result it is evident that a description by fixed probability ratios can be very misleading. As *quartiles* are used successfully for other characteristics we may see whether they can be useful here. This is certainly not so for the lower quartile, as at temperate latitude it falls most often into the "G-cases" where no  $E_s$  is observable. The upper quartile may be more useful except from some apparent discontinuities which must appear in the transition region where the distribution has two cusps. In Figure 9 we give a map of the ratio upper quartile over median value

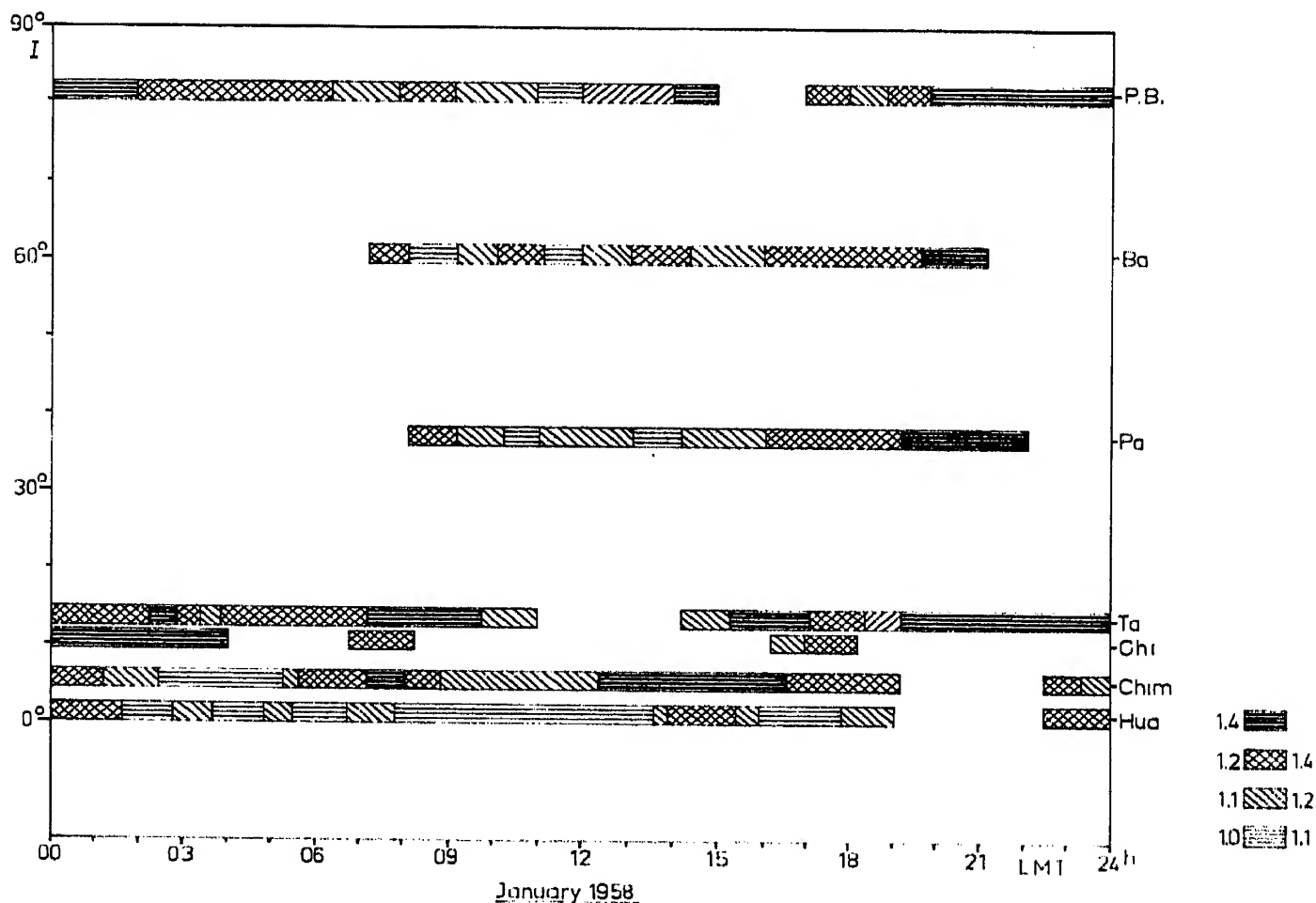


Fig. 9. Ratio of upper quartile over median  $f_oE_s$  (American stations, January 1958). Ordinate magnetic dip  $I$ . (Blank space: no precise information).

for a winter month in the American continent down to the dip equator. For temperate latitude winter, the ratio is roughly of the order of 1.2 during the day but considerably higher in the night, about 1.5. (Values are missing in the late night when the median was inferior to the lower frequency limit.) Large values occur at Talara, day and night, also at Chimbote for most hours. At Huancayo the concentration is on the upper cusp only, and therefore here the lowest values of the ratio are found, most inferior to 1.1. For illustration we may mention that for  $f_oF2$  the ratio is of the order of 1.15. So  $f_oE_s$  has the largest fluctuation of the current ionospheric parameters.

#### 1.4 Summary on statistical behaviour

Auto- and cross-correlation function on one side, fluctuation range on the other are sufficient to give a usable description of the statistical behaviour of a parameter. So, we are now able to summarize this chapter.

1.41.  $f_oE_s$  which is a measure of the *maximum plasma frequency* of an  $E_s$  layer (see Section 5) undergoes very important and rather irregular fluctuations. As on the other hand the correlation range can be quite narrow in time and space (down to 10 min and 50 km) the phenomenon is sometimes localized to a small area and/or duration. In the median, however, the ranges are about 1 hour and 200 km. These values give an upper limit of the size of " $E_s$  patches", more precisely they give the rough structure of the phenomenon. It must be emphasized that this rough description does not take account of the certainly existing fine structure; we shall see in Section 5 that fine structure only can explain the observed transparency of the layer, i.e. the difference between  $f_oE_s$  and  $f_bE_s$ .

1.42.  $f_bE_s$ , which is a measure of the *minimum plasma frequency* of an  $E_s$  layer (see Section 5) undergoes smaller but also quite irregular fluctuations. As the correlation range is smaller than for  $f_oE_s$ , we may conclude that the *relative* changes in time and space are nearly of the same order as for  $f_oE_s$ . The statistical distribution of  $f_bE_s$  is also asymmetric, extended towards higher values; in the average aberrant high values are more different from the median than are aberrant low values, but the first ones have a shorter lifetime.

## 2. MONTHLY MEDIAN RESULTS

With these large fluctuations the question arises whether the monthly medians of our parameters have enough physical meaning to be studied in detail. It is not too difficult to find special cases where this appears to be questionable, but there is a large domain where the median has at least in some way a representative character. For example  $f_bE_s$  with its smaller fluctuation range shows a marked difference between daytime when blanketing is frequent and important and night-time when it is rather rare.

Also  $f_oE_s$  nearly everywhere shows a clear statistical difference between day and night and has some quite marked periods of increased occurrence. On the other side our basic information is limited by the fact that with a total of 30 observations every month and hour and with the large fluctuations the smaller variations of the median are not significant. Therefore we should not pay too much attention to detail features of the monthly median curves.

## 2.1 The Top Frequency $f_oE_s$

2.11. What are the main features of the median curve  $f_oE_s$ ? Let us look at Fig. 10 where one year's set for a temperate latitude station is reproduced. The first impression is that a great *regularity* appears in these curves. They look not too much different from similar curves of  $f_oF2$ . At night, a continuous decrease of  $f_oE_s$  can be seen which is even more regular than the behaviour of  $f_oF2$  at many stations. Of course, this is only a statistical result indicating that the probability of  $E_s$  ionization decreases during the night. (For an individual night it could well occur that no  $E_s$  is observed before midnight whilst an important ionization is seen during one of the last night hours.) Also in daytime there is a certain regularity with a first maximum near noon and, eventually, a second maximum in the early evening.

2.12 The *seasonal effect* is very marked. The number of occurrences as well as the median  $f_oE_s$  values are much lower in winter than in summer and this is true for day and night. In temperate latitudes  $E_s$  is, essentially, a summer phenomenon. Summer should be interpreted here in the meteorological sense, i.e. the high temperature period at the ground which is about May through September for the northern hemisphere. (This is slightly delayed against the period of maximum solar height.) The summer preference must be remembered as one of the most regular features of  $E_s$  at temperate latitudes. It is also true for the southern hemisphere as can be seen from Fig. 11. Only near the equator is the phenomenon less clear. This can be seen from Fig. 12 where the old parameter,  $\overline{fE_s}$ , has been plotted against month and hour, for several years.

The summer preference appears even more clearly in the statistics of high  $E_s$  ionization. In Fig. 13 we have plotted the number of cases where  $f_oE_s$  was greater than 6.5 Mc/s which is a rather large ionization value for temperate latitudes\*. The season of maximum appearance at temperate latitudes is very clearly summer; in the northern belt this is even valid for Dakar (latitude 15°N, inclination +17°) but in the southern belt Tsumeb

---

\* This count corresponds roughly to older statistics with  $fE_s > 7$  Mc/s as in these cases the  $x$ -component of the  $E_s$  trace is always present.

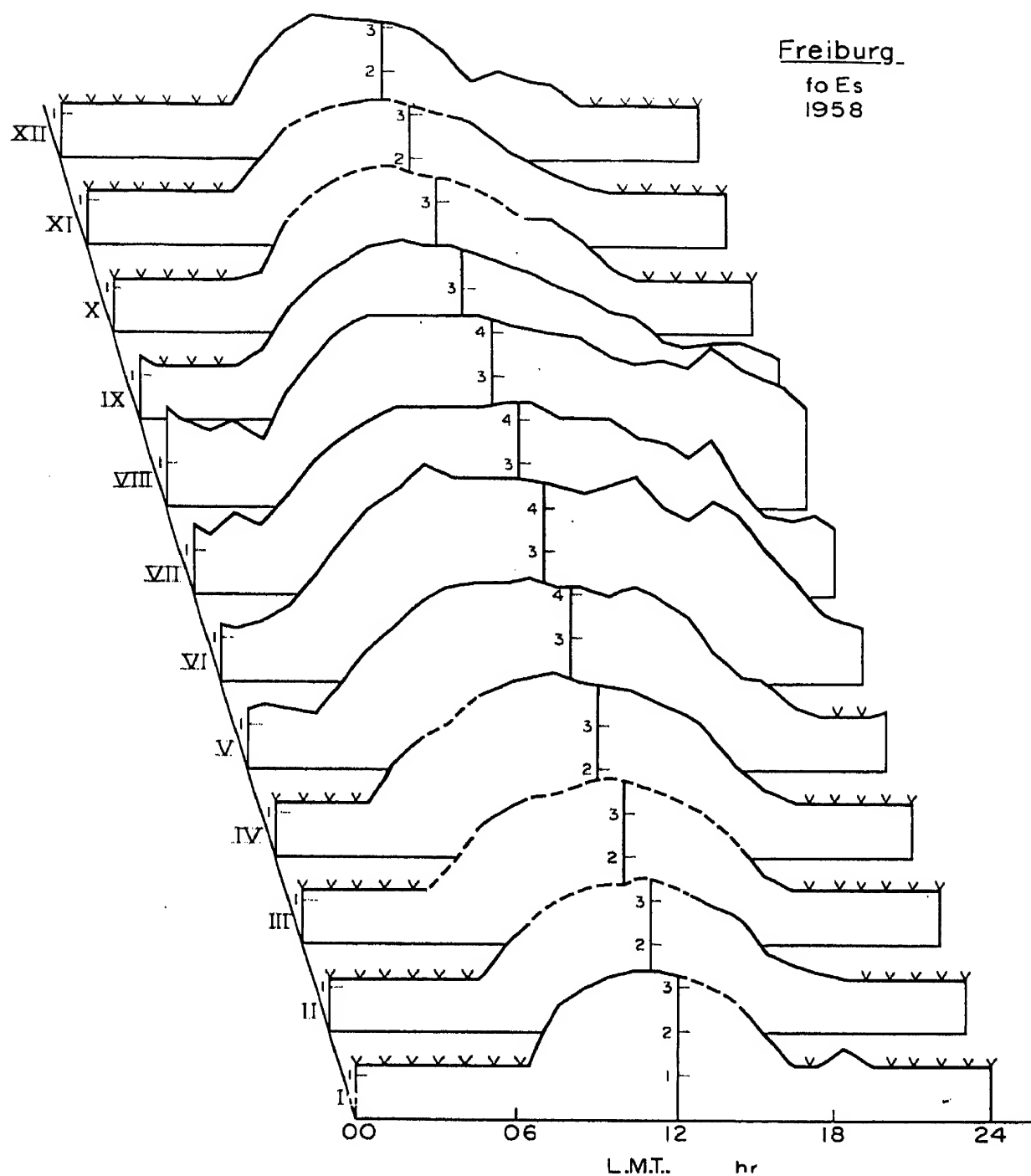


Fig. 10. Median  $f_oE_s$  Freiburg 1958 (broken lines: below  $f_oE$ ; arrows: below lower limit of recorder).

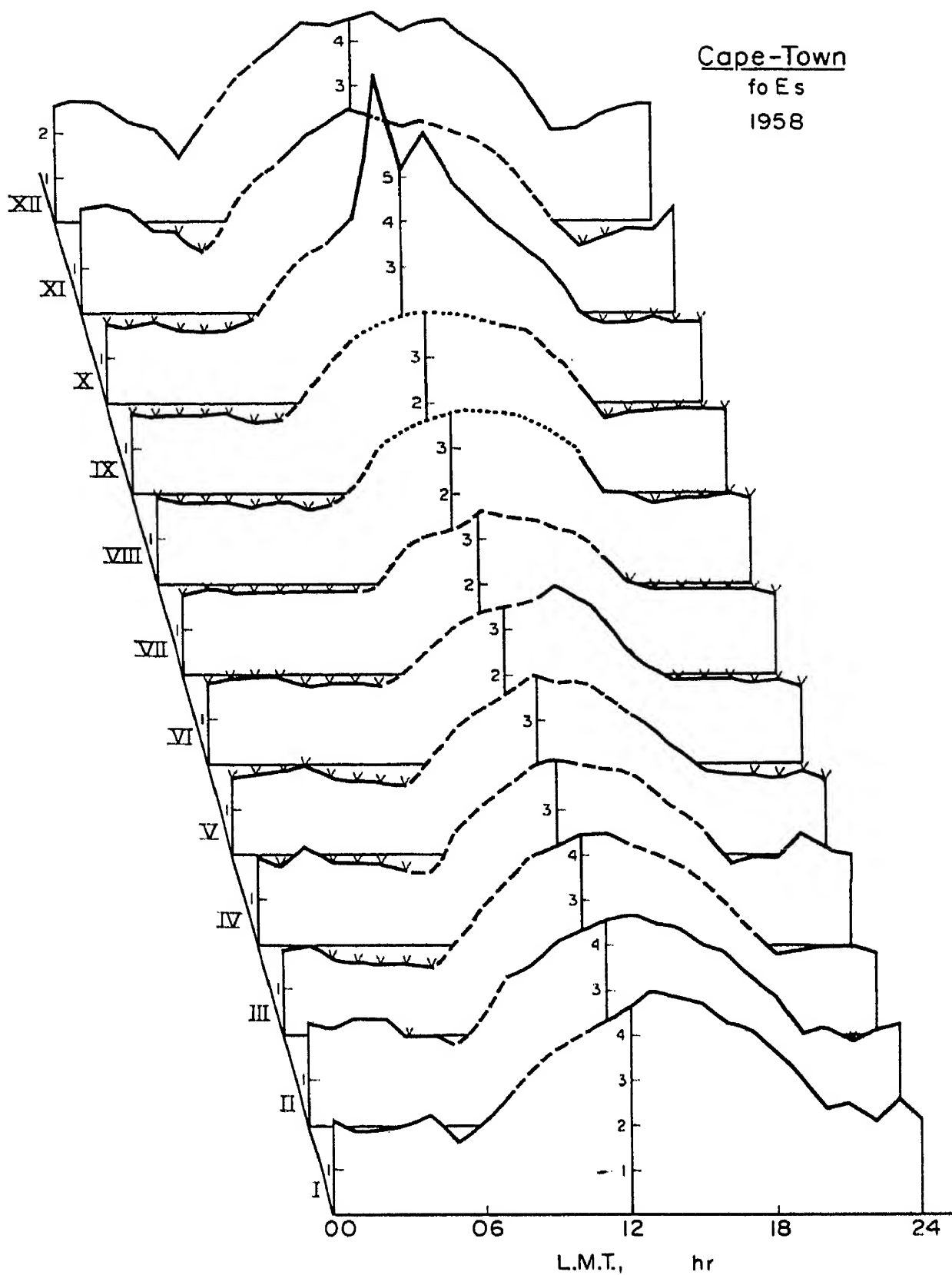


Fig. 11. Median  $f_oE_s$  Capetown 1958 (see 10; dotted lines: no observations).

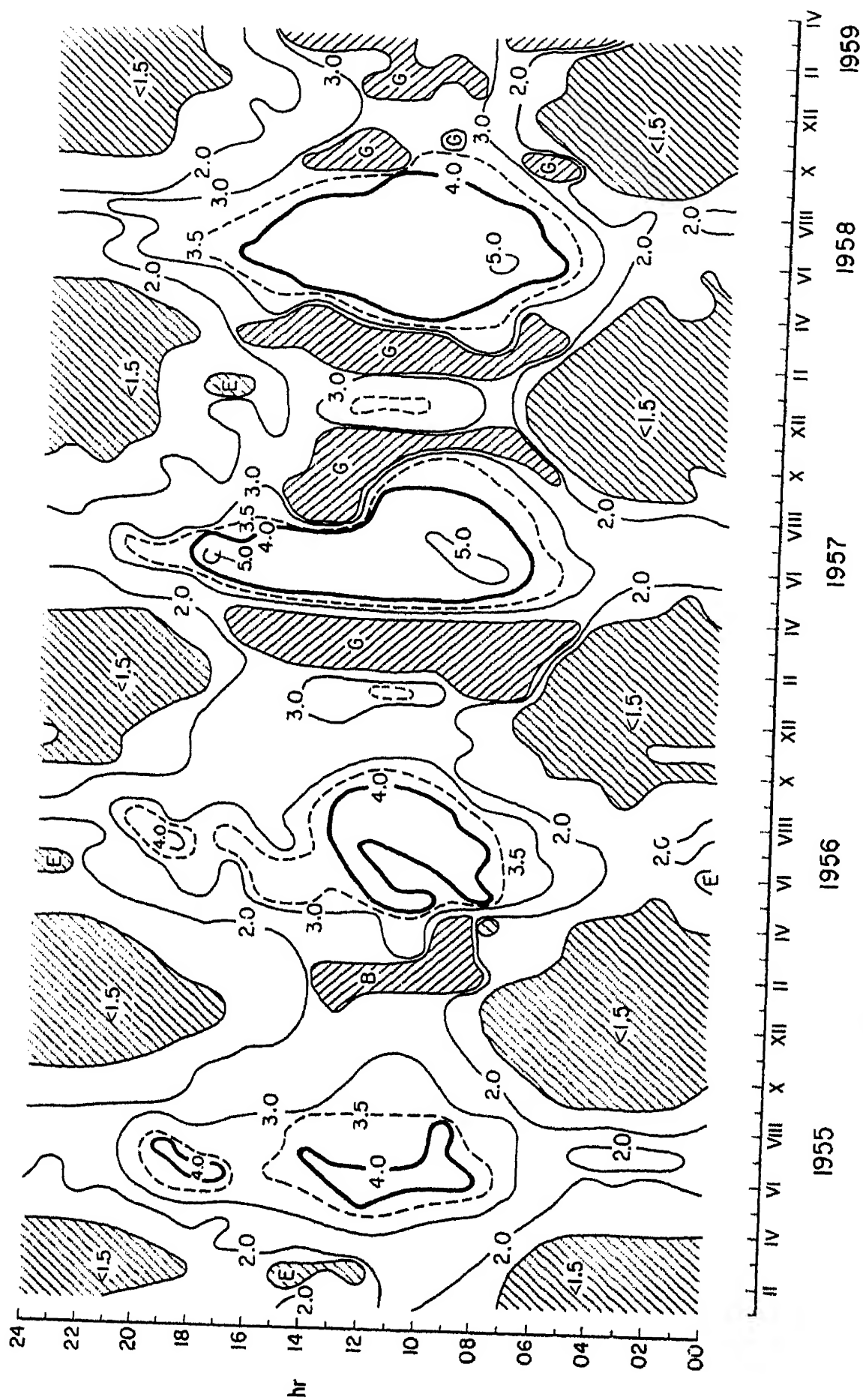


Fig. 12. Seasonal and diurnal variation of median  $fE_s$ .  
(a) Freiburg (48.1°N, 7.8°E),



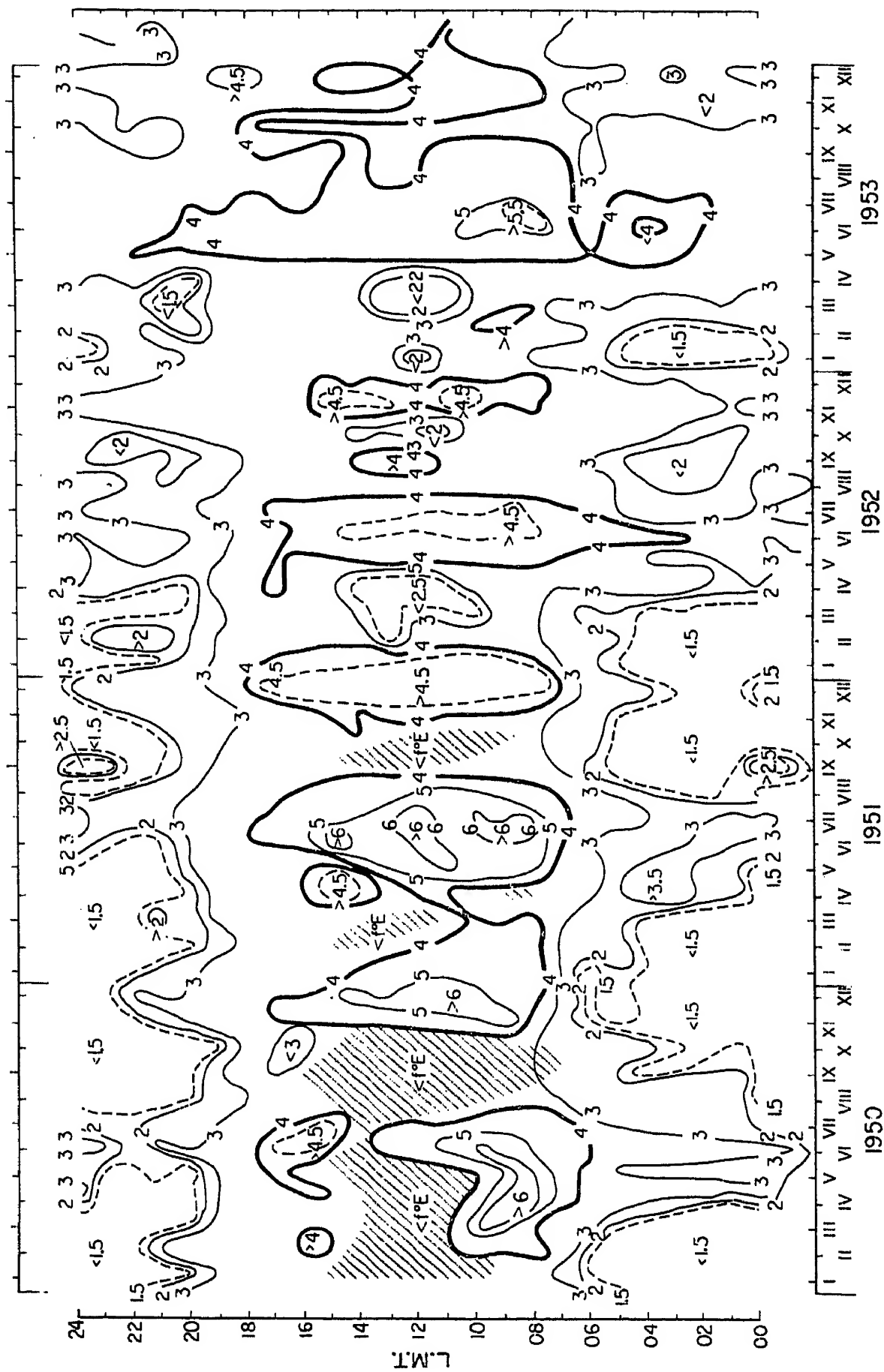


Fig. 12. (*cont'd*)  
(b) Dakar (14.6°N, 17.3°W).

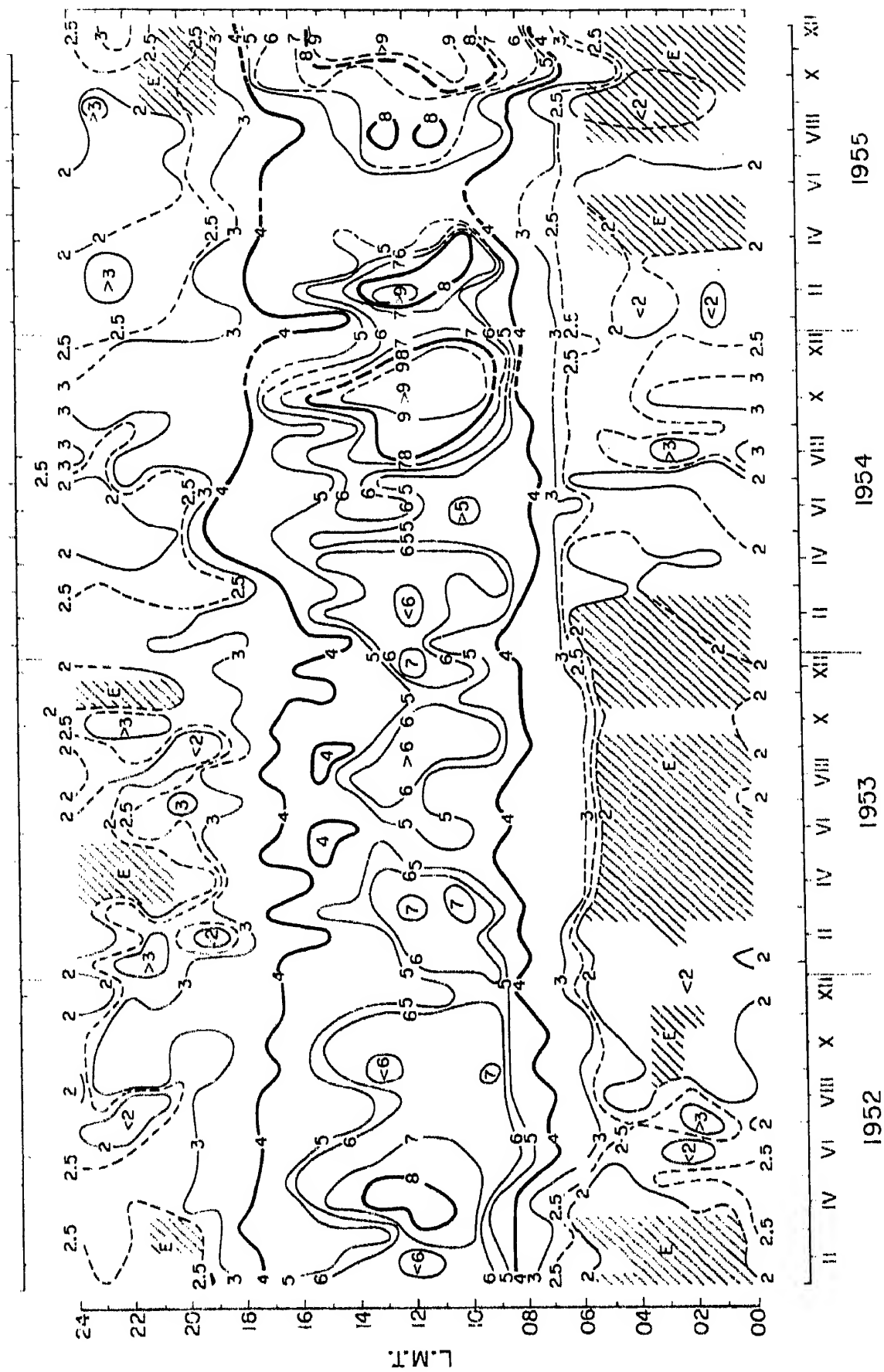


Fig. 12. (*cont'd*)  
(c) Djibouti (11.5°N, 43.1°E)

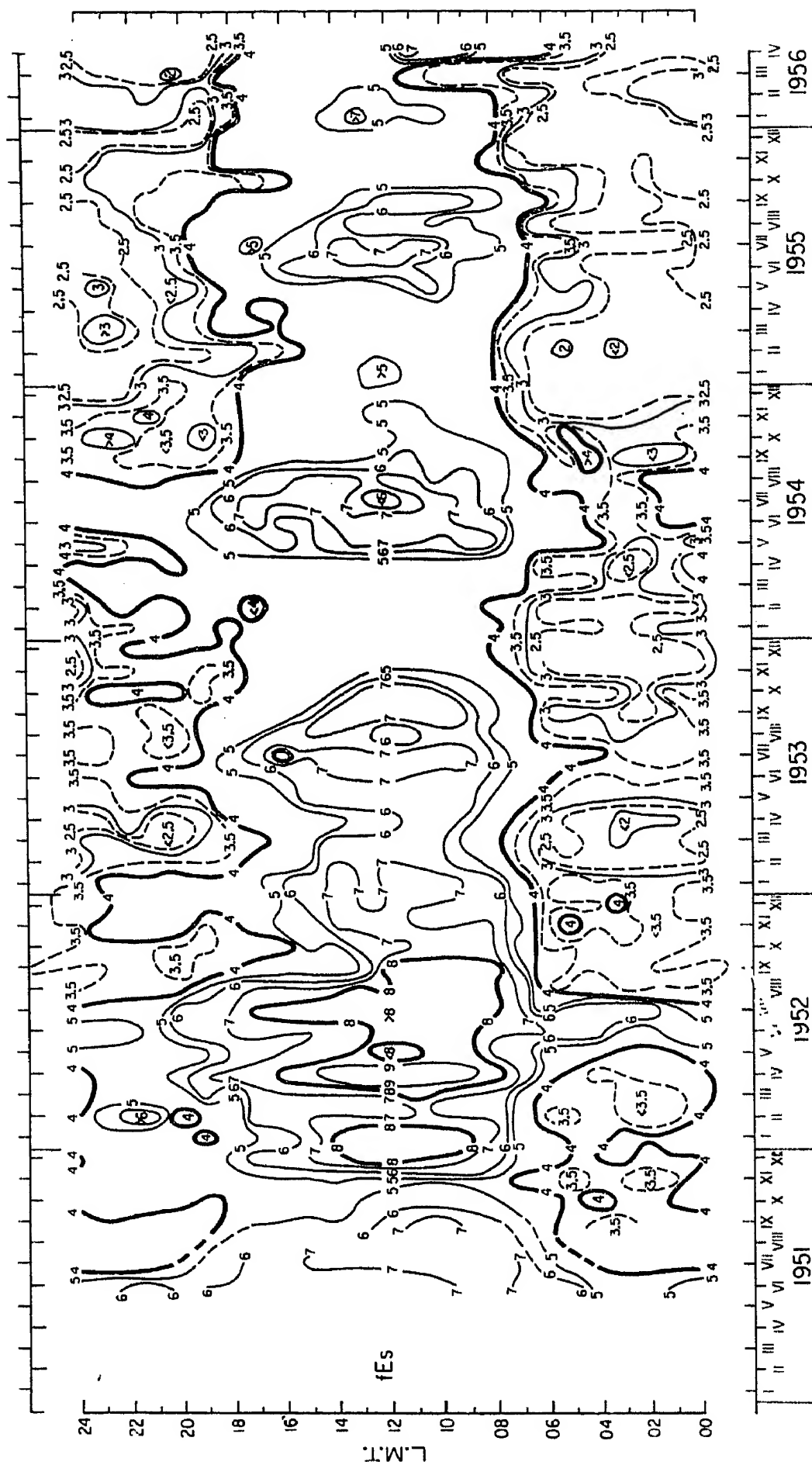


Fig. 12. (*cont'd*)  
(d) Nha-Trang (12.2 N, 109.2 E).

( $19^\circ\text{S}$ ,  $-54^\circ$ ) shows two maxima, one in summer and one in winter. On the other side in South Africa the total number of high values is very small and centered on local summer. As a general rule for temperate latitudes we may state that high values are very rare during seasons other than summer.

2.13. *Near the dip equator* the absolute number of high values increases enormously (in Fig. 13 a reduced root scale has been used). At Djibouti

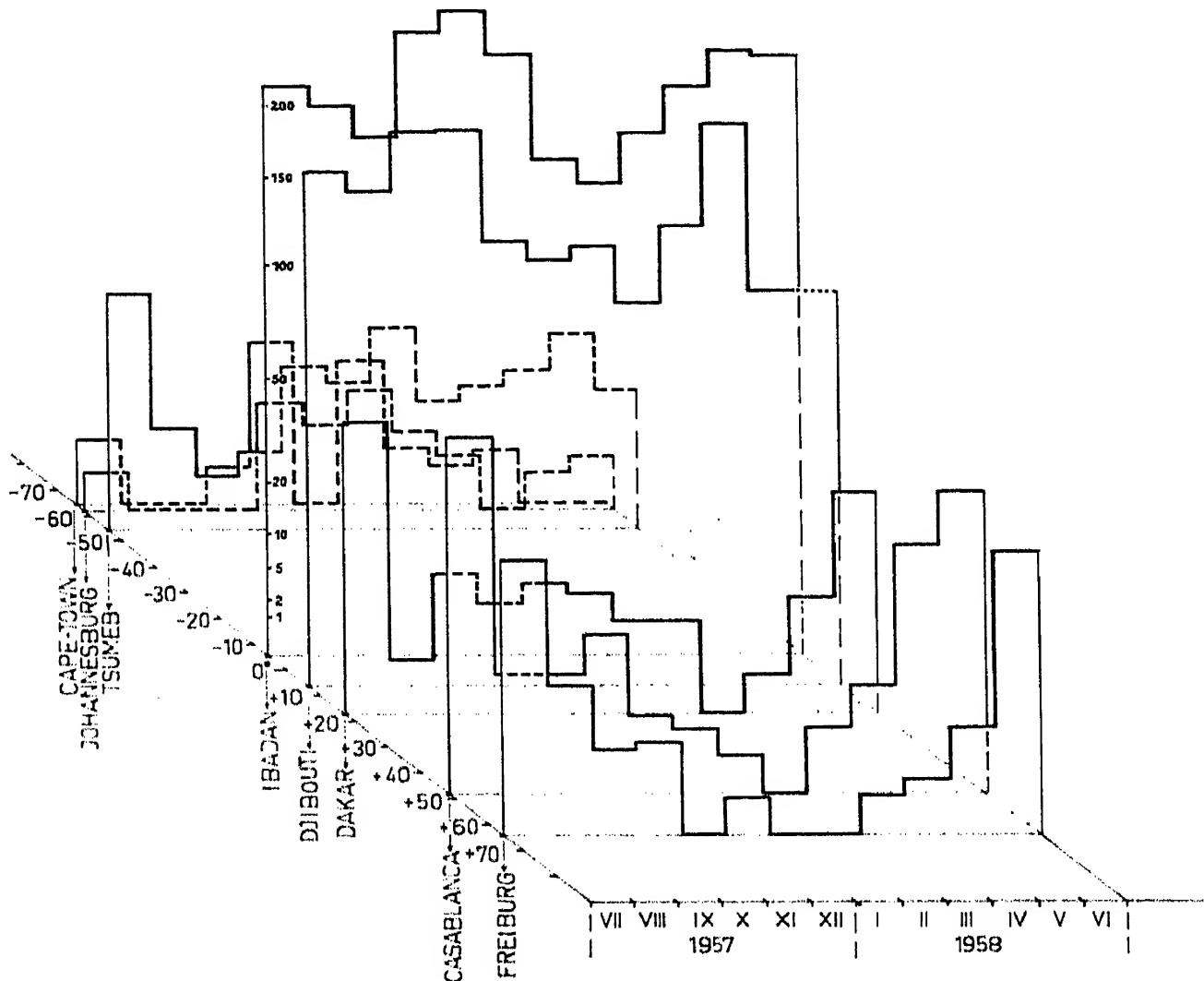


Fig. 13. Probability of high  $f_oE_s$  values ( $>6.5$  Mc/s), seasonal variation in Europe and Africa (counts per month in a square root scale).

( $12^\circ\text{N}$ ,  $+6^\circ$ ) as well as at Ibadan ( $7^\circ\text{N}$ ,  $-6^\circ$ ) the seasonal effect is only small, two shallow maxima appear with one month's delay after the equinoxes. The total number of observations of high  $E_s$  ionization is many times that observed at temperate latitudes; nearly all these are daytime observations. The highest values are found at Ibadan; Djibouti which is at the same absolute dip value has less. Also Tsumeb gives rather large numbers. This seems to show that the dip equator effect is not a unique function of the dip. The conditions are discussed in detail in S. Matsushita's contribution.

2.14. As Fig. 12 covers several years, by intercomparison we can learn something about the “*secular*” variation. Looking at all figures the most striking features are (1) that the correlation between different stations is not good, (2) that no clear trend with the solar cycle can be seen. As a proof for the first statement we may look at Figs. 12c and d, two stations at nearly the same latitude and inclination. Highest concentration occurs at Nha-Trang in 1952, at Djibouti in 1954/55. As to the second statement looking at Freiburg (Fig. 12a) or Nha-Trang (Fig. 12d) one should state a positive correlation with solar activity (the sunspot minimum was in 1954), but a negative one at Djibouti (Fig. 12c) and none at all at Dakar (Fig. 12b).

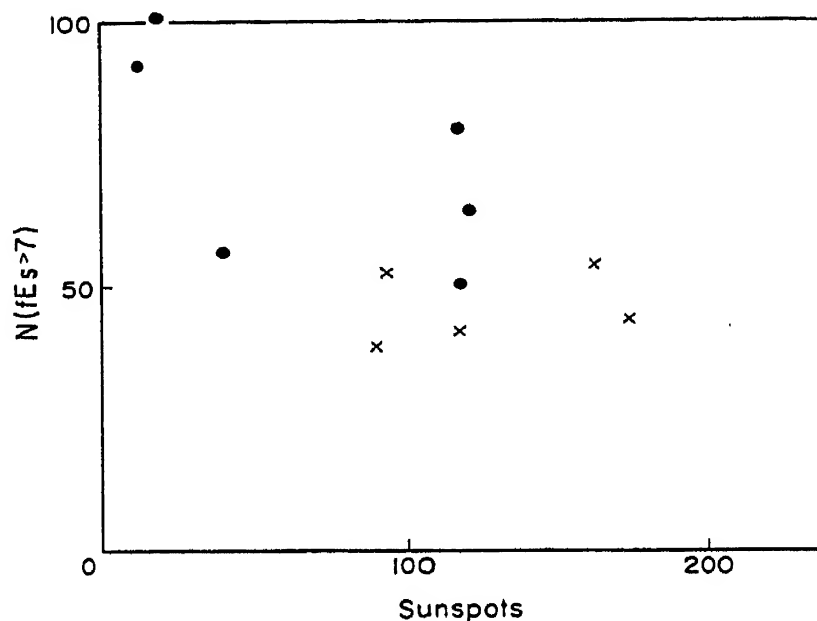


Fig. 14. Correlogram between probability of high  $fE_s$  ( $>7$  Mc/s) and (gliding) mean sunspot number. (Every point correspond to a summer term; dots Brisbane 1943–49, crosses Freiburg 1947–51).

For any other ionospheric layer one has found a quite regular correlation with the sunspot number. No similar general relation seems to be valid for  $E_s$  at temperate and low latitudes. (The situation is different in the auroral zones because the auroral  $E_s$  ionization is correlated with the number of auroral disturbances, hence, in some way with the sunspot number.) This is a very important result because it excludes the eventuality that  $E_s$  ionization could be due to a solar wave radiation similar to that which causes the other layers.

2.15. Instead of considering median values we may now look for the occurrence of high  $E_s$  ionization. A correlogram between the total number of observations above fixed values and the sunspot number is given in Fig. 14 for two temperate latitude stations, one in the northern and one in the southern hemisphere. Each point corresponds to one summer. The diagram indicates no correlation.

One difficulty of all such series is that for most stations the sensitivity is not constant over years, as the equipment has been changed and replaced several times during a solar cycle. It seems, however, that with modern equipment this only introduces a minor error, just for counts of high values.

From the old literature we may cite three rather long series of observations made at 52°N (Appleton and Naismith 1940), 48°N (Brand and Zenneck 1944, Rawer 1955) and 28°S (McNichol and De V. Gipps 1951); unfortunately different definitions have been used. From these series we come to the following conclusions: At Slough (52°N) a positive correlation was found for the number of intense  $E_s$  cases in summer, but it vanishes when yearly numbers are used; no correlation was found with rather small  $E_s$  ionization. At Brisbane (28°S) (McNichol and De V. Gipps 1951) a negative correlation was reported for high  $E_s$  ionization—and a positive one for small ionization.

With the observations made at Kochel and later at Freiburg we have established a long series of counts. In Fig. 15 we have built up a graph indicating the number of high values from 1940 to 1959 at 48°N. Apart from the summer preference which is clearly visible on the noon values (Fig. 15a) we have a maximum in 1949/50 and another, smaller one in 1958/59. Minima occurred in 1942/43 and 1953/55. There are some phase differences, but the average correlation with the sunspot number seems to be positive. Unfortunately the midnight values of the same period (Fig. 15b) show a rather different pattern.

There can be no doubt that important fluctuations between different years exist. This can be seen from all series covering many years. We cannot exclude a component related to the sun's activity but first evidence is that the major fluctuations are not world-wide. The conditions could be similar to those in climatology where also important differences exist between different years, the changes being often quite independent in different parts of the world. We may see in Section 5 that this analogy eventually has some significance.

2.16. A small *lunar effect* on the top frequency has been found at different places (Matsushita 1953, Rawer 1955). At Freiburg with the noon observations of 16 summer months we mainly found a lunar 24 hr modulation of nearly 0.3 Mc/s, the positive phase being at about 17 00 hr lunar time. This is interesting as the 24 hr lunar oscillation should normally be less important than the 12 hr oscillation which is directly excited by gravitational forces. Details are discussed in a contribution by S. Matsushita.

## 2.2 The Blanketing Frequency $f_b E_s$

We should now consider the second routine parameter, viz. the blanketing frequency. Whilst  $f_o E_s$  characterizes the top ionization which is only seldom reached,  $f_b E_s$  describes that part of the  $E_s$  phenomenon

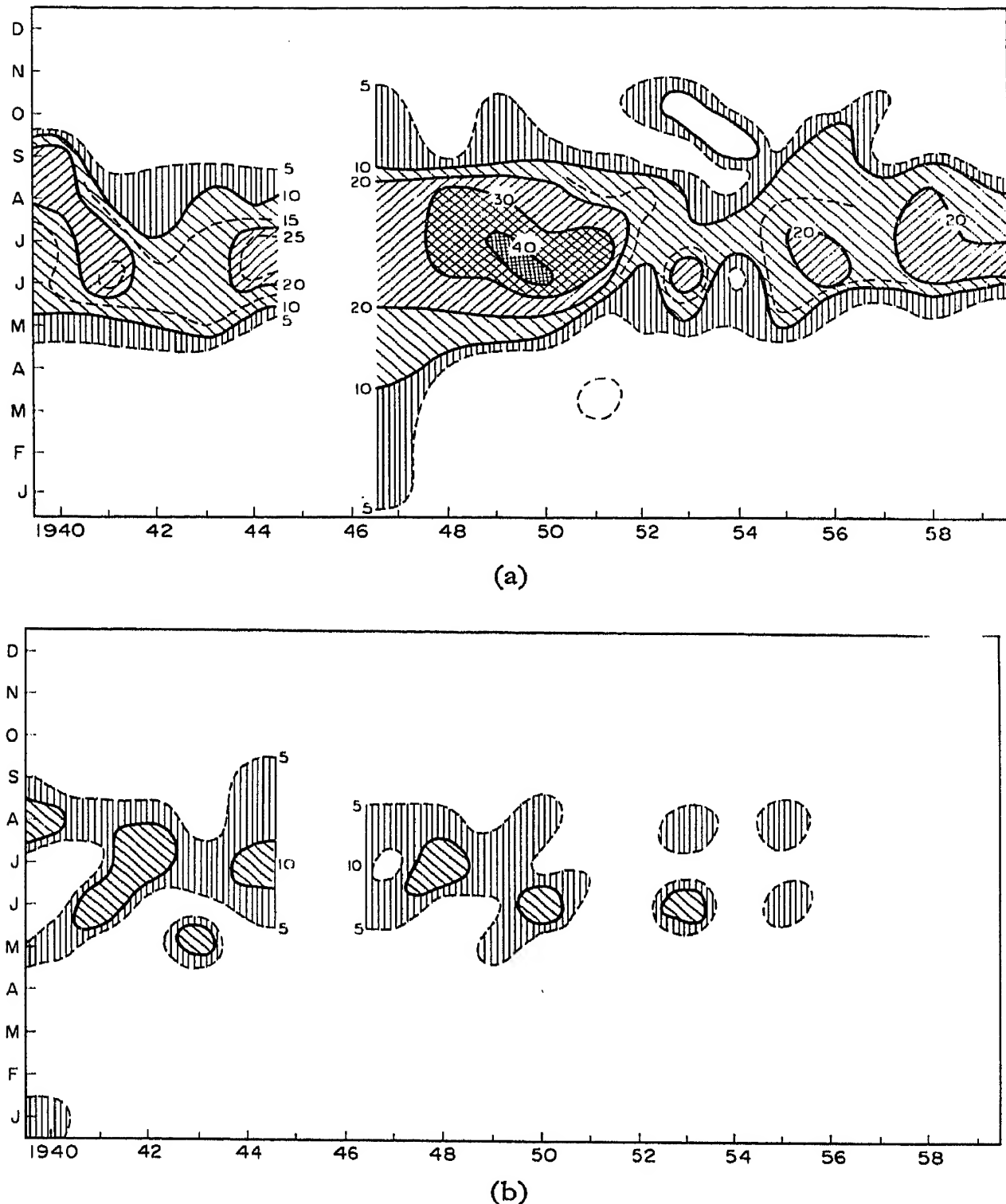


Fig. 15. Long term variation (Freiburg) of probability of rather important  $E_s$  ( $fE_s > 6$ ,  $f_oE_s > 5.4$  Mc/s).  
(a) noon, (b) midnight values. (Ordinate: month).

which is more or less widespread. So, if a high value of  $f_bE_s$  is observed this means that much more ionization exists in the area of the station than if the same numerical value was obtained with  $f_oE_s$ . Therefore it is evident that  $f_bE_s$  at no instant can be greater than  $f_oE_s$  and that it should also be less variable than the top frequency.

2.21. Summarizing the observations at temperate latitudes we may say that there is a large number of cases where the layer is opaque, i.e.  $f_b E_s$  is nearly equal to  $f_o E_s$ , and there is another large number of cases where no blanketing can be seen on the record, i.e.  $f_b E_s$  is inferior to the lower limit of the recorder. (Roughly speaking this lower limit normally corresponds to an electron density value of the order of  $10^{10} \text{ m}^{-3}$  whilst the highest observed values come to nearly  $10^{12} \text{ m}^{-3}$ .) So important *variations of blanketing conditions* exist.

2.22. Figure 16 shows one year's set of *monthly median* curves of  $f_b E_s$  for a northern temperate latitude station. Monthly median values  $\overline{f_b E_s}$  are

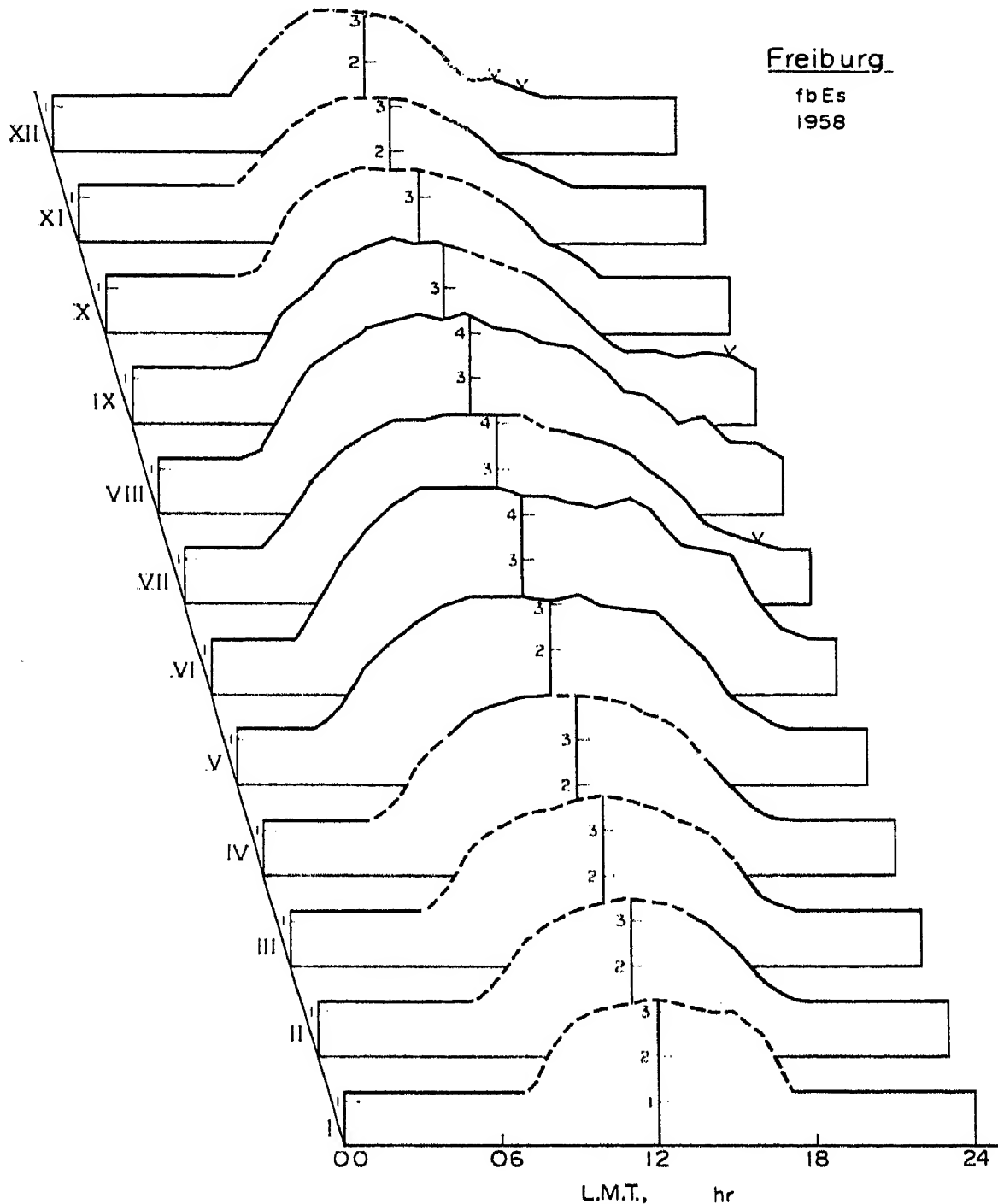


Fig. 16. Median  $f_b E_s$  Freiburg 1958 (see 10.).



found to show a rather regular behaviour. In the summer months where  $E_s$  is frequent, blanketing also is frequent, and the median value  $f_b E_s$  is generally slightly above that of  $f_o E$ , the critical frequency of the normal  $E$ -layer. For the other months, where  $E_s$  is less frequent we have many cases where the median value  $\overline{f_b E_s}$  is below  $\overline{f_o E}$ ; in these cases no true value can be given as the normal ionization hides the homogeneous  $E_s$  ionization which at any case is small. In these cases we have interrupted curves. Winter curves are often interrupted whilst a diurnal maximum clearly appears in summer. It can be seen by intercomparison of Figs. 10 and 16 that the ionization density corresponding to  $f_b E_s$  is much less than the top electron density as measured by  $f_o E_s$ .

2.23. The *seasonal behaviour* can be studied by looking at Fig. 17. We should remember three features from these figures: (a) The diurnal and seasonal behaviour is most regular, it is more similar to the graphs of  $\overline{f_o E}$  than to those of  $\overline{f_b E_s}$ . (b) The absolute value  $\overline{f_b E_s}$  is considerably less than that of  $\overline{f_o E_s}$ . (c) The magnetic equator has some effect on the  $\overline{f_b E_s}$  plot but it is small (Rawer 1953). We do not have the "G-case" ( $\overline{f_o E} > \overline{f_b E_s}$ ) at Djibouti whilst for example at Johannesburg it is quite frequent.

2.24. As to the *long term variations* it is difficult to obtain a clear picture from the median as during the day  $\overline{f_b E_s}$  is quite near to  $\overline{f_o E}$ , or even below in the "G-case". Now, as  $\overline{f_o E}$  depends clearly on the solar activity an apparently similar behaviour must be found for  $\overline{f_b E_s}$ . Also, if the extra  $E_s$  ionization is nearly independent of the solar cycle—as it looks likely—the effective ionization value will nevertheless depend on the basic ionization existing in the  $E$ -layer, at least in those cases where the extra ionization is not very important.

Therefore, in order to see whether the extra ionization itself depends on the solar cycle, we must look at the highest  $f_b E_s$  values. Fig. 18 is a correlogram between counts of high  $f_b E_s$  ( $> 5$  Mc/s) against the sunspot number, each point corresponding to one summer period (similarly as in Fig. 14). No clear correlation is visible.

### 3. PROFILE OF THE $E_s$ -LAYER

#### 3.1 The Virtual Height $h' E_s$

The minimum virtual height of  $E_s$  has more physical significance than that of a thick layer.  $h' E_s$  should be nearly equal to the true height of the  $E_s$ -layer as this layer is so thin that no appreciable retardation occurs. Difficulties could only arise in those cases where  $f_o E_s$  is only slightly greater than  $f_o E$  and retardation in  $E$  plays a rôle. If the conventions are correctly followed  $h' E_s$  is read only when the end of the trace appears to

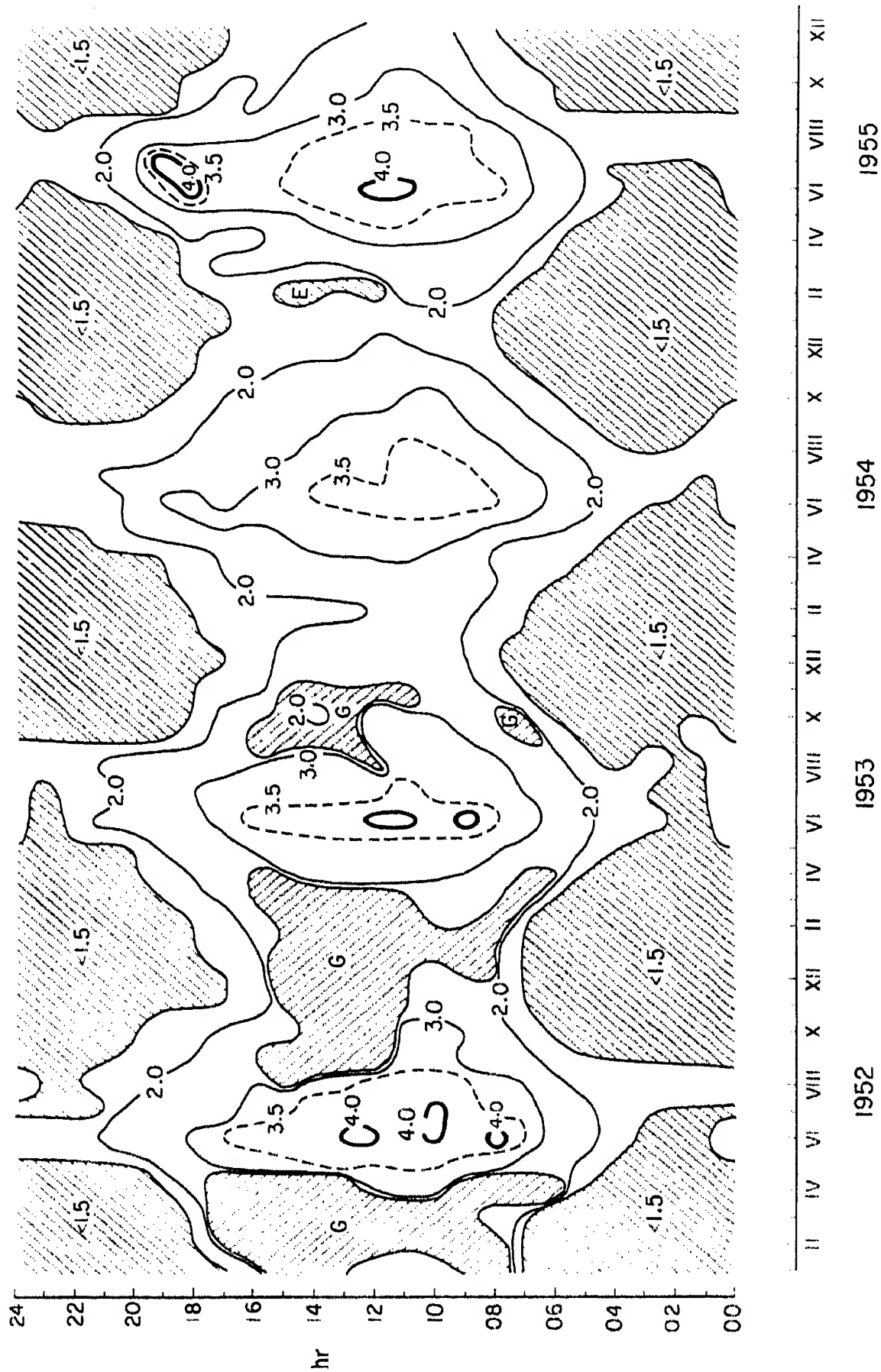


Fig. 17. Seasonal and diurnal variation of median  $f_b E_s$ .  
(a) Freiburg 1952-55.

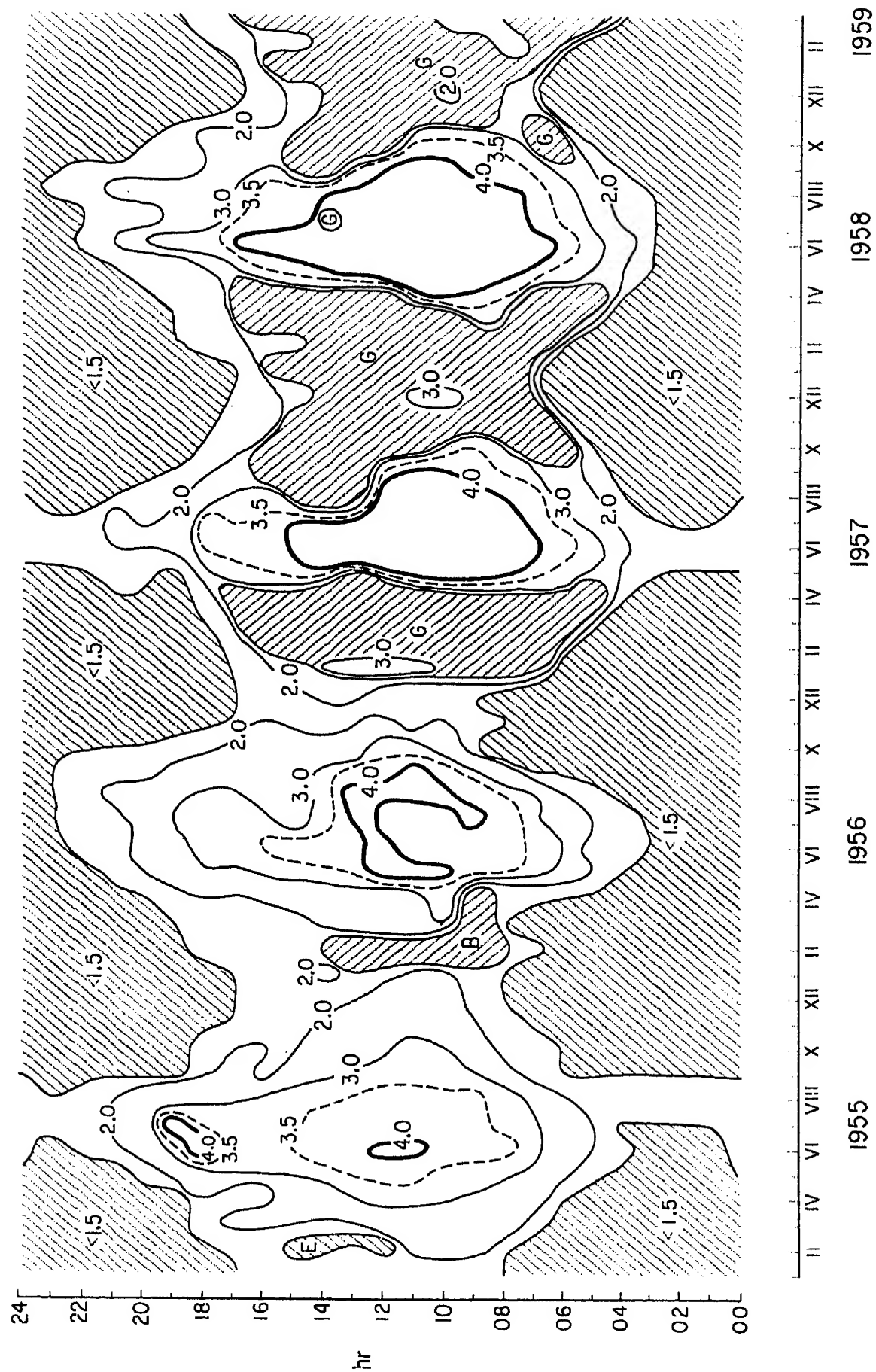


Fig. 17 (*cont'd*)  
(b) 1955-59.

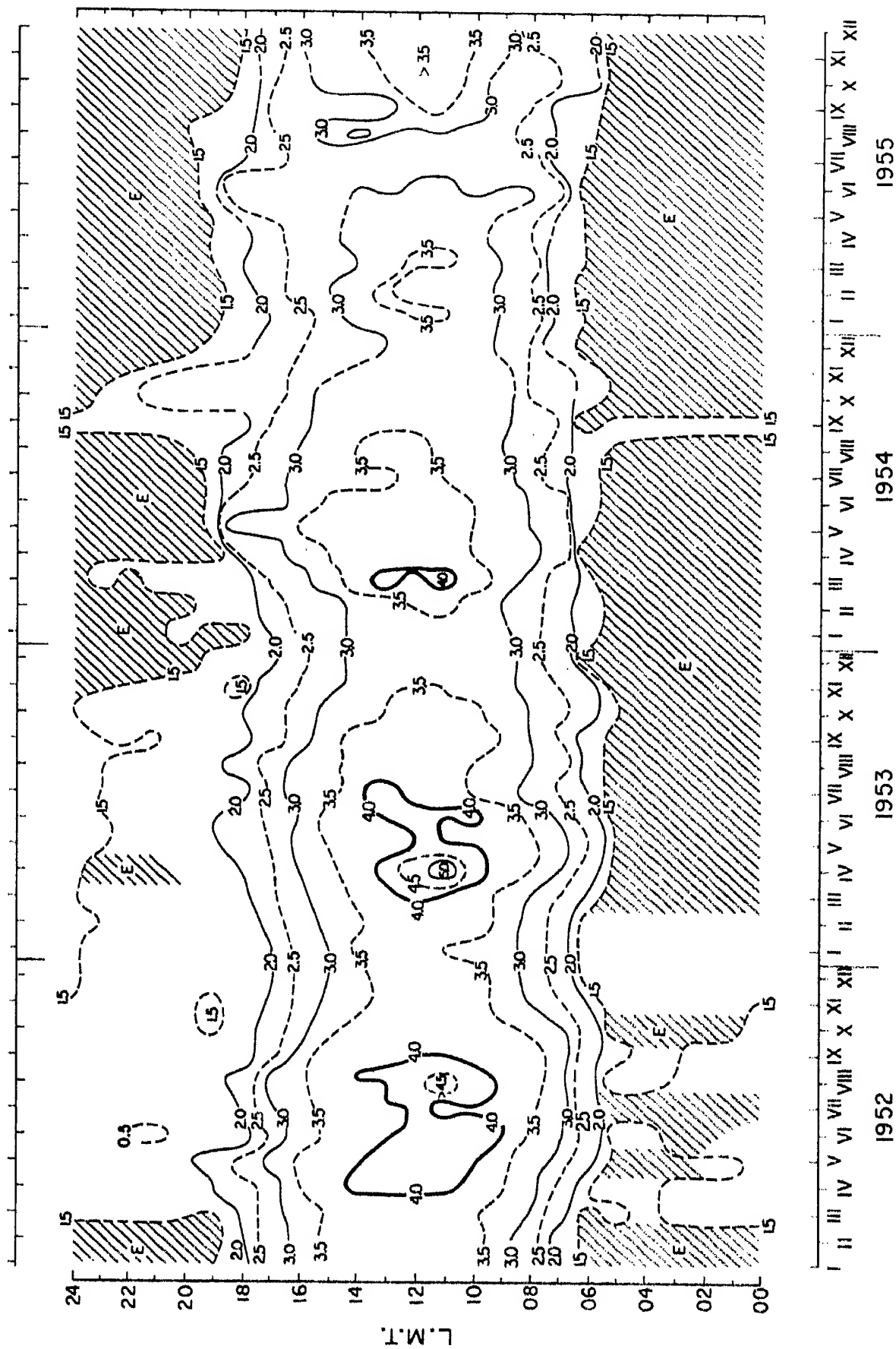


Fig. 17 (*cont'd*)  
(c) Djibouti 1952-55.

be horizontal; in that case the difference between virtual and true height should be small. The results on  $h'E_s$  are discussed in S. C. Gladden's contribution.

For our final discussion we need one special feature which has recently been found by Bibl on direct records of characteristics (Bibl 1959).

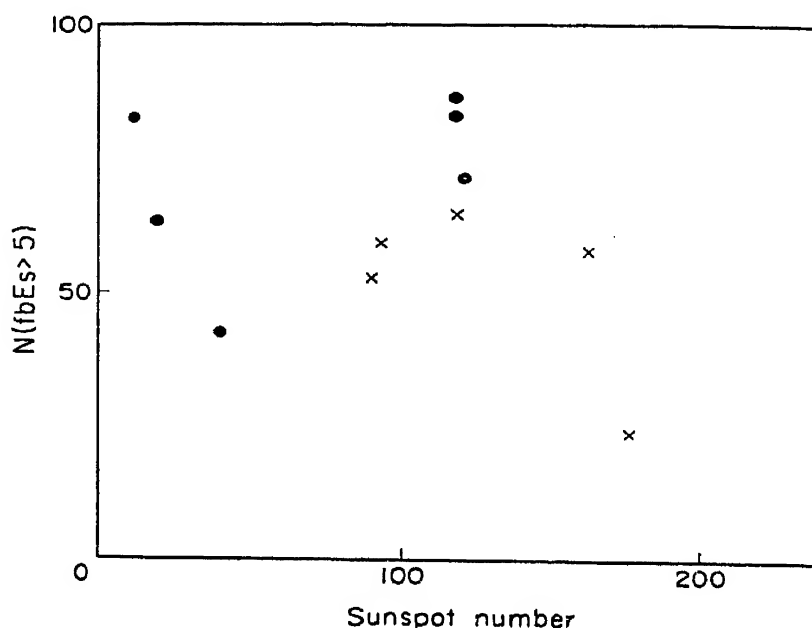


Fig. 18. Correlogram between probability of high  $f_b E_s$  ( $> 5$  Mc/s) and (gliding) mean sunspot number (see Fig. 14).

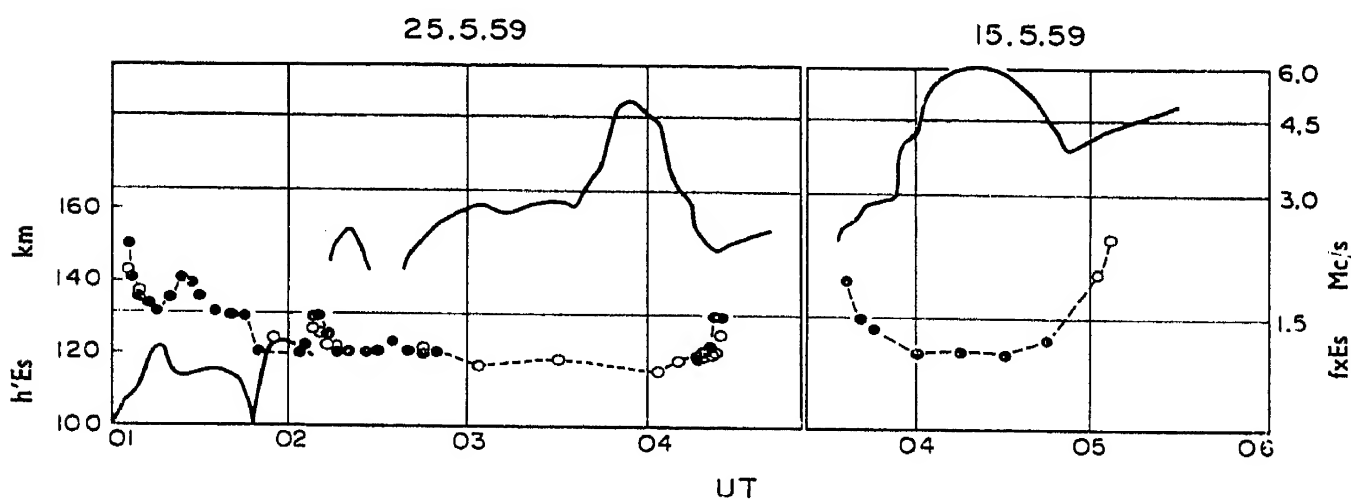


Fig. 19. Simultaneous variation of  $f_x E_s$  (thick curve) and  $h' E_s$  (points and thin curves).

Figure 19 shows simultaneous variations of  $f_x E_s$  and  $h' E_s$ ; the largest ionization values correspond to the minimum height values. This is only one example for Bibl's general statement that the  $E_s$  ionization has a tendency to increase with decreasing height and vice versa.

### 3.2 The Thickness

Recent rocket observations have shown that  $E_s$  is a very thin layer, only a few km thick; these are reported in C. Seddon's contribution.

3.20. The same conclusion, though with less accuracy, can also be deduced from the ionograms. No *retardation* cusp can be seen normally on an  $E_s$  trace so that the thickness cannot be determined as for other layers. (Some rare "cusps" which have been found have the form of a hook, the thickness value found from the form of these traces is smaller than something like 5 km).

3.21. Another way can be used when an  $M$ -echo is present. This is reflected at the upper boundary of  $E_s$ . By comparison with the  $E_s$ -echo which is reflected at the lower boundary the thickness  $\Delta$  can be found from

$$\Delta = 2 h'(F) - h'(M) - h'(E_s)$$

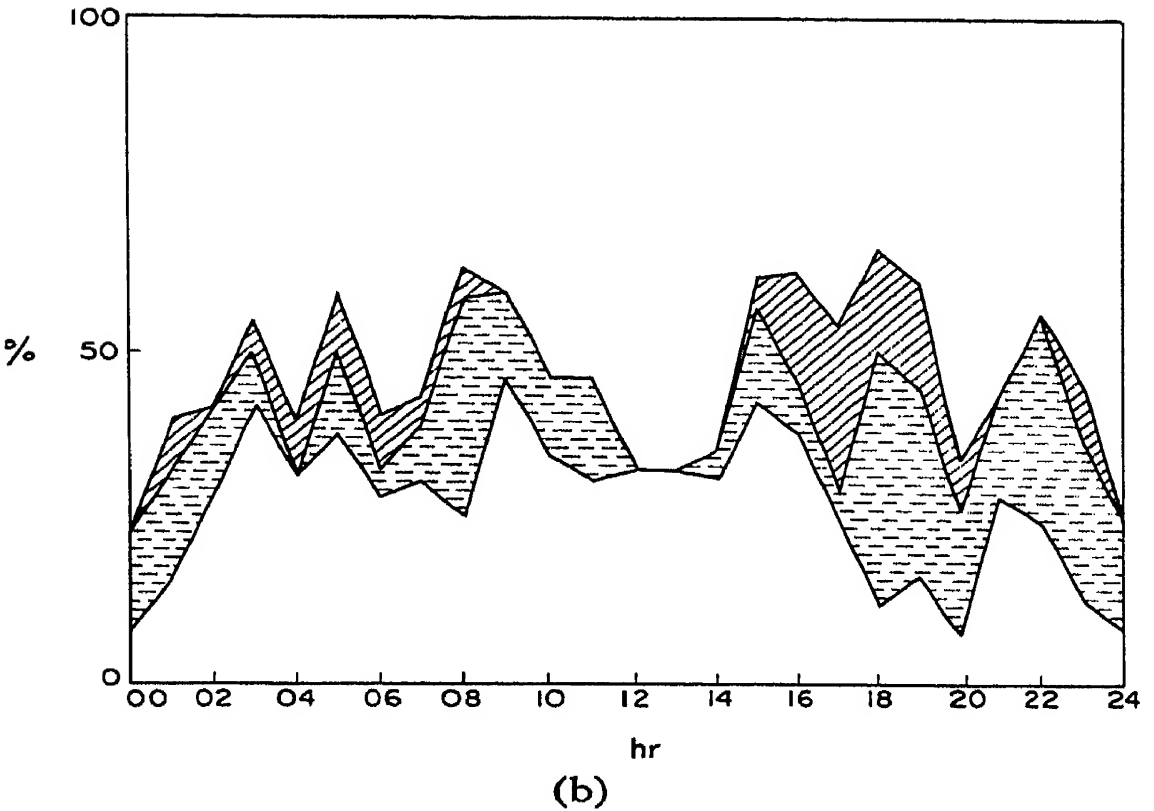
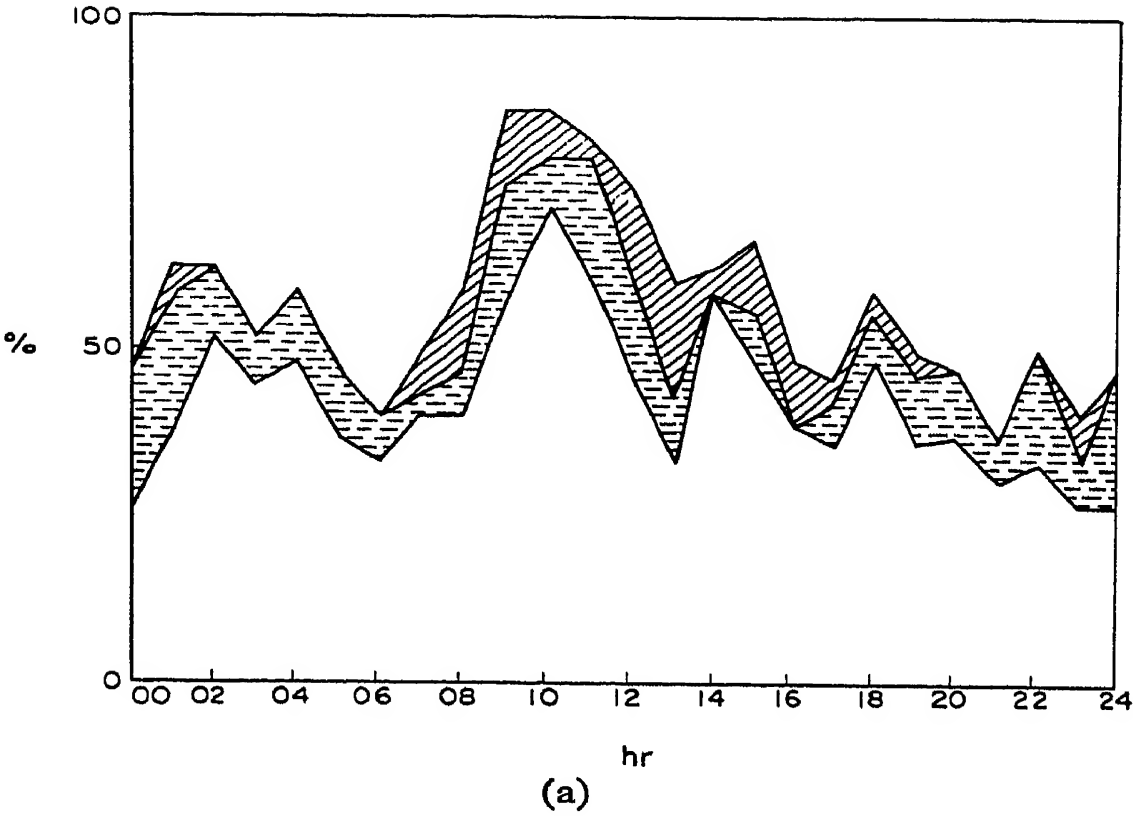
The  $h'$  readings must, of course, be made at the same sounding frequency; the method fails when the ray path of the  $M$ -echo is not mainly vertical. With an accuracy of about  $\pm 2$  km one finds values of a few km (Rawer 1955).

3.22. Similar results have been obtained by Briggs (1951) with accurate measurements of the *partial reflection* near the critical frequency of "completely opaque"  $E_s$ -layers; the result is interpreted in terms of wave optics using results calculated by the author with a suitable layer model (Rawer 1939). The average of a few such determinations was 5.5 km.

### 3.3 Sharpness of Echoes

3.31. Most temperate latitude  $E_s$  echoes are quite sharp, indicating that the reflection surface is well defined and rather smooth over several Fresnel zones. In particular absorption investigations have shown that opaque  $E_s$  layers normally give a well defined echo with a higher *reflection coefficient* than that of normal thick layers (Bibl, Paul and Rawer 1959), the same studies have shown that with these opaque  $E_s$  layers one only rarely has the long term "focusing fading" which is so frequent with normal layers. The majority of transparent  $E_s$  layers also give quite sharp echoes, at least at temperate latitudes.

3.32. By inspection of individual ionograms we have tried to give a *classification* of echoes in three classes (Rawer 1955). Some statistical results of this analysis for March 1952 are shown in Fig. 20a to d. At temperate latitude (Fig. 20a) about 70 per cent of all  $E_s$ -echoes are sharp, truly diffuse echoes are seen in no more than 10 per cent (less than it would be with  $F$ -echoes). As we approach the equator the relative importance of diffusion increases (Fig. 20b). At the dip equator (Fig. 20c) we have much diffusion, in particular in daytime when the  $q$ -type  $E_s$  occurs. Also at the southern side of the dip equator (Fig. 20d) diffusion



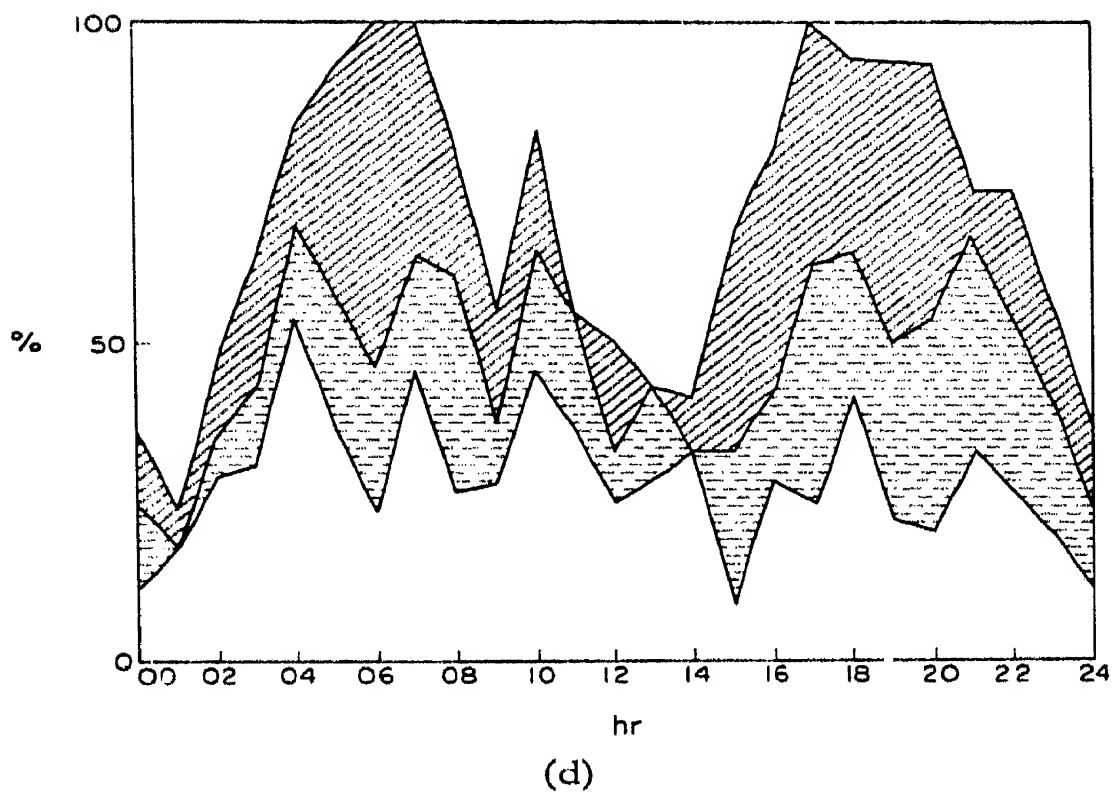
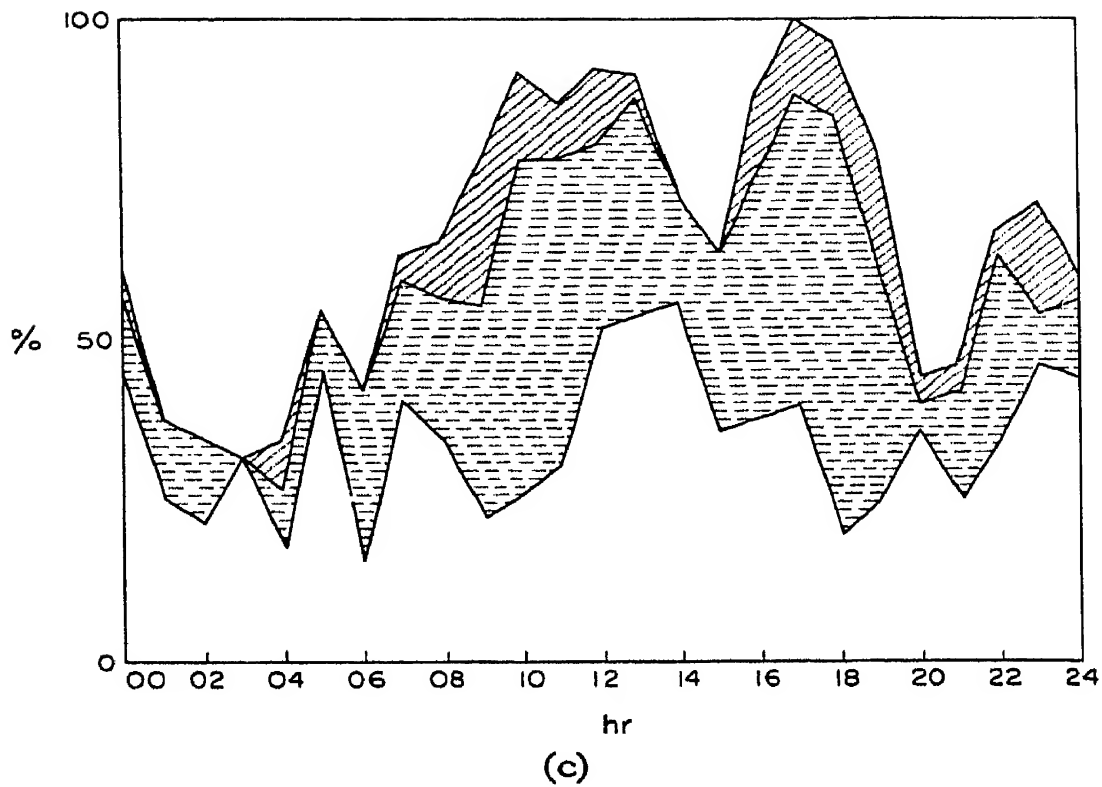


Fig. 20. Classification according to echo sharpness (March 1952).  
 (a) Freiburg, (b) Dakar, (c) Djibouti, (d) Lwiro (2.2 S, 28.8 E),  
 (lower blank: sharp; broken hatched: slightly diffuse; hatched:  
 diffuse).



is very frequent with a maximum in the morning and another one in the evening. In this special example we find the maximum diffusion at Lwiro (Fig. 20d) and not at Djibouti which is near to the dip equator.

3.33. If we had some information on the *direction of arrival* of  $E_s$ -echoes we could come to conclusions regarding the roughness of the reflecting surface. Also if oblique-incidence echoes were frequent we would have an easy explanation for the difference between  $f_oE_s$  and  $f_bE_s$ , as, in that case, one would expect  $f_oE_s$  to correspond to the oblique soundings. With this idea a test experiment using antennae commutation was designed (Bibl, Harnischmacher and Rawer 1955); a large number of unpublished observations with this method clearly showed that  $E_s$ -echoes are practically always vertical, i.e. inside a cone of  $\pm 10$  per cent from the vertical. This result obtained at Freiburg certainly cannot be expected to be valid in the equatorial belt. It is also not true in the auroral zones but certainly valid for temperate latitudes.

Thus, seen as a radio phenomenon, temperate latitude  $E_s$ -echoes are better defined than the echoes coming from most normal layers.

#### 4. TRANSPARENCY CHARACTERISTICS

Transparency has always been considered as being a special characteristic of  $E_s$ -layers. If care is taken in distinguishing the magneto-ionic components one can show that at temperate latitudes non-transparent  $E_s$ -layers exist rather often (Rawer 1955). Nevertheless in the majority of cases  $f_oE_s$  is greater than  $f_bE_s$  and this means transparency. It seems to us that just this property of the layers should be more precisely investigated.

##### 4.1 *Classification by Transparency*

By inspection of individual ionograms each of these has been classified according to five classes of transparency (Rawer 1955), ranging from complete blanketing ( $f_bE_s = f_oE_s$ ) to complete transparency (in the frequency range which could be observed). Distinction of magneto-ionic components was done according to the rules given in the author's first contribution. Figure 21, for example, shows results of March 1952 for four stations; the classes are (from bottom to top): Completely opaque—mainly opaque—difficult to decide—mainly transparent—completely transparent. The monthly contributions of the classes are given in percentages so that the upper curve shows the total occurrence of  $E_s$  during that month. The equipment at the four stations was identical.

In northern temperate latitudes (Fig. 21a) March is a month of rather infrequent  $E_s$ , nevertheless a total of more than 50 per cent is obtained. Complete blanketing covers about half of all daytime cases, it is less frequent at night. The next important class is the completely transparent layers, the

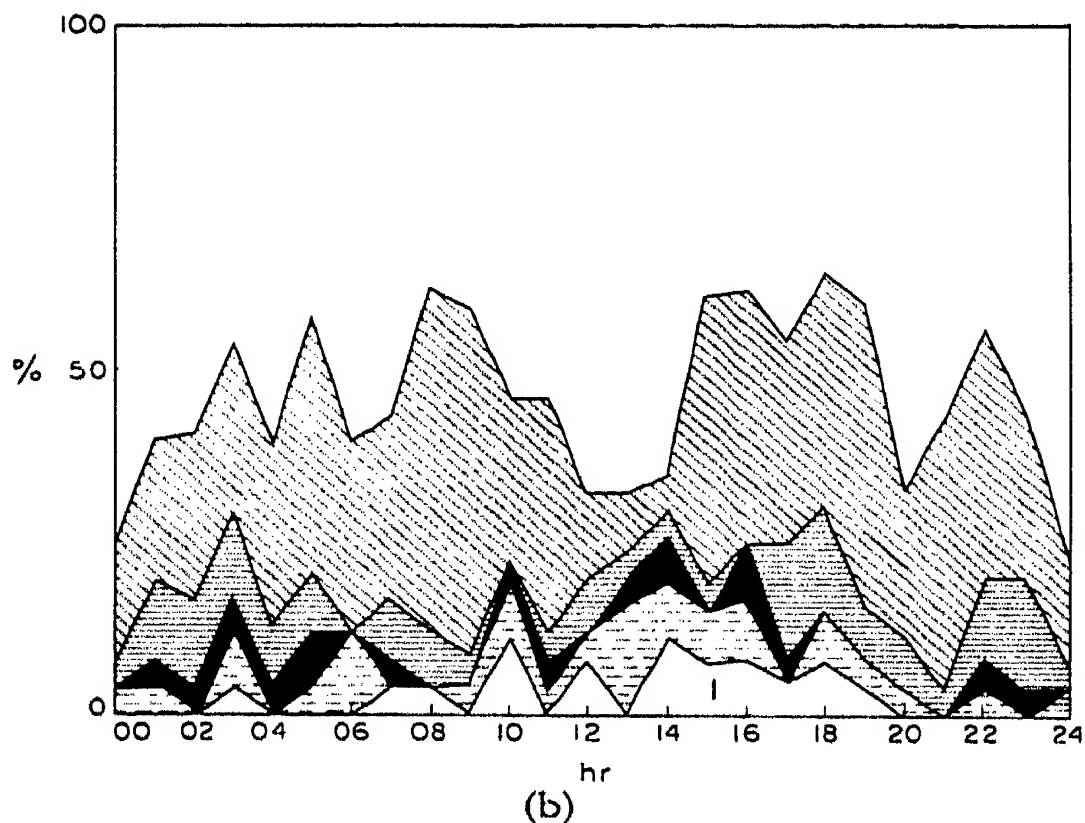
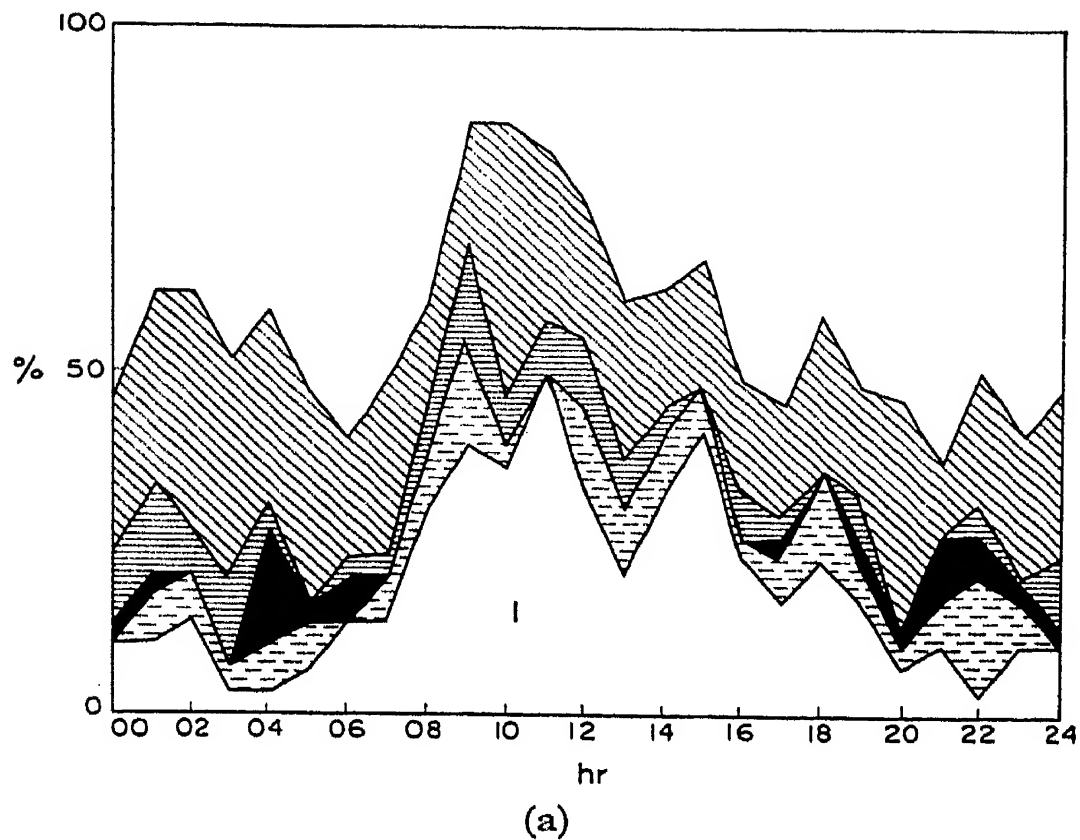
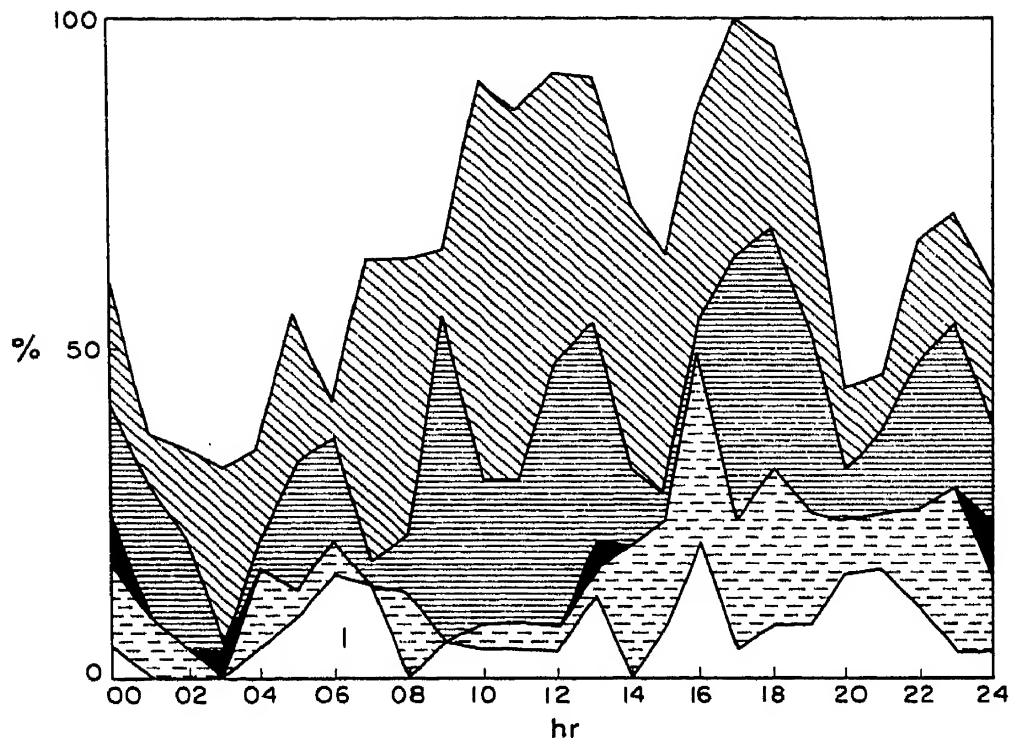
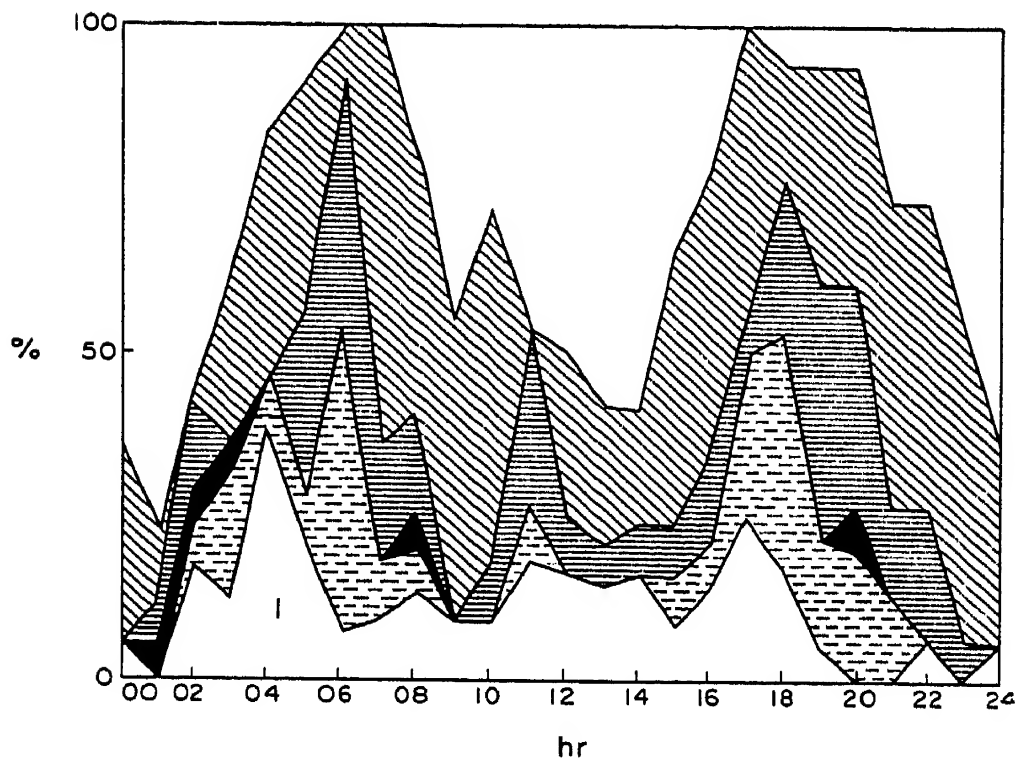


Fig. 21. Classification according to transparency, month and station see Fig. 20. (Transparency varies from total opacity to complete transparency from bottom (1) to top hatched field.)



(c)



(d)

Fig. 21. Classification according to transparency, month and station see Fig. 20. (Transparency varies from total opacity to complete transparency from bottom (1) to top hatched field.)

intermediate classes being rather rare. At a lower latitude (Fig. 21b, c) the transparent cases are more important than the other ones; no day preference is seen at Dakar, but at Djibouti which is near to the equator one has  $E_s$  about 90 per cent of the time in the middle of the day, nearly all of them being highly transparent. A low latitude station south of the magnetic equator (Fig. 21d) shows two maxima of occurrence, in the morning and in the evening\*, the contribution of blanketing layers being increased as compared with the dip equator. The conclusion is that blanketing is more frequent at temperate latitudes, the dip equator layer ("q-type") being highly transparent.

#### 4.2 The "Blanketing Power"

4.20. For the last several years the magneto-ionic components have been distinguished in the reduction of  $E_s$ . Therefore a rather precise indication of blanketing conditions can now be obtained from the routine observations by intercomparison of  $f_oE_s$  and  $f_bE_s$ . The difference ( $f_oE_s - f_bE_s$ ) can be called the "transparency range"; however, we prefer a relative measure and have chosen the ratio  $f_bE_s/f_oE_s$ ; by definition it is called "blanketing power". It vanishes for a completely transparent layer ( $f_bE_s = 0$ ) whilst it becomes "1" for a completely opaque layer ( $f_bE_s = f_oE_s$ ). No numerical value is obtained when no  $E_s$ -trace was present, a limiting value only when blanketing is not observable.

4.21. The "blanketing power" was determined day by day for 15 stations, most of them are in the Western hemisphere†. The *dispersion* of these values is large.

A typical example of one month's mass-plot of blanketing power for a medium latitude station is given in Fig. 22. The median value is very high in daytime and considerably lower at night. A large number of daytime values are practically "one"; transparency is not a necessary characteristic of  $E_s$ -layers.

4.22. From such mass-plots medians and quartile values have been determined. Some of these results are presented as a function of magnetic dip in *world maps*. As an example we give in Fig. 23 the medians for June and in Fig. 24 for December 1958. From these maps three latitude ranges are clearly visible:

- (a) A very large range of medium latitude between about  $20^\circ$  and  $80^\circ$  of magnetic dip. In this range the difference between the stations are rather small. High day values and lower night values are characteristic for this region.

\* This may partially be due to an effect of blanketing by normal  $E$  and of absorption; the chance to observe  $E_s$ -layers with rather small ionization is smaller near noon.

† This special work was supported by "Deutsche Forschungsgemeinschaft" (Ra 68/11).

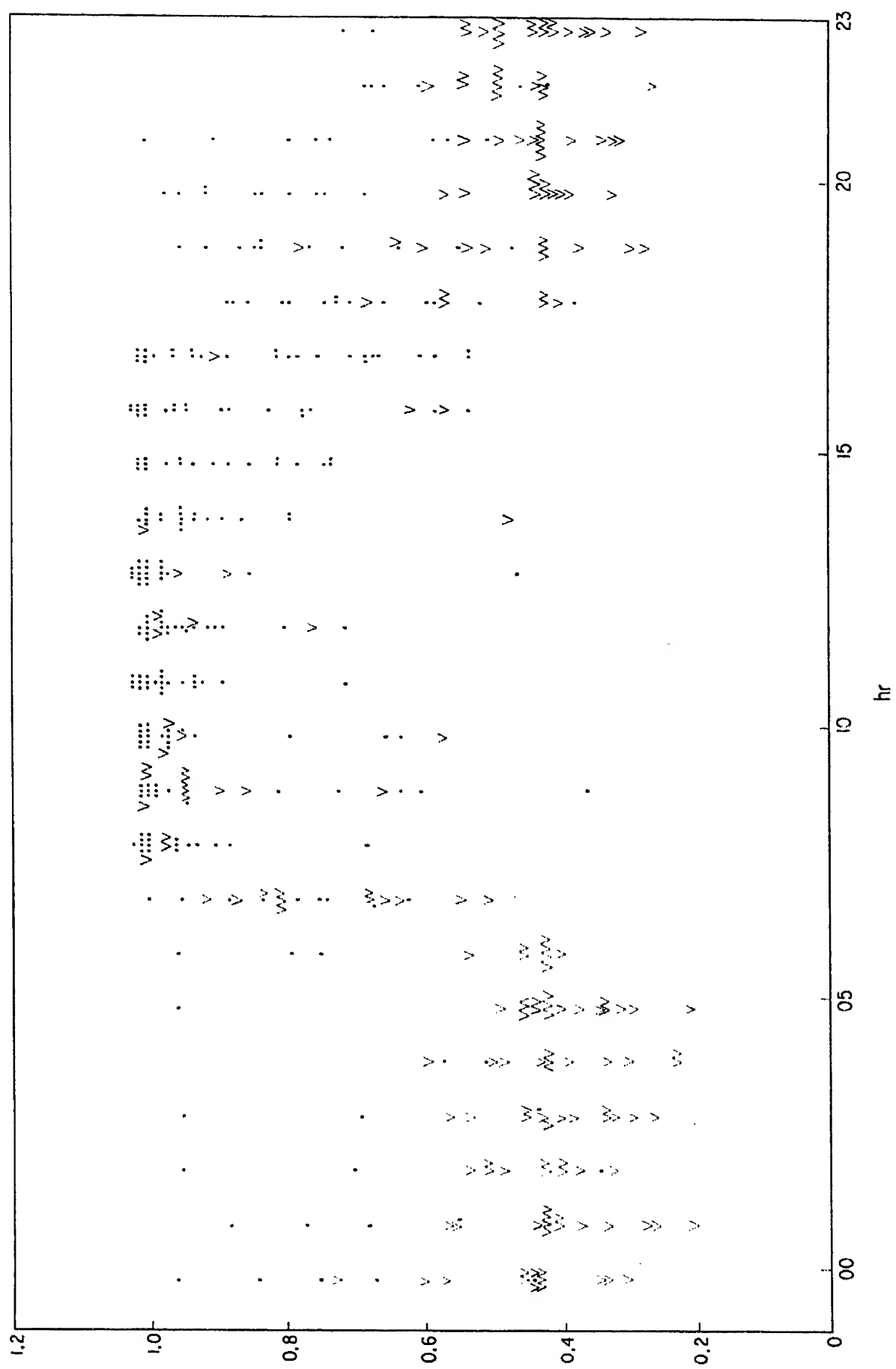


Fig. 22. Massplot of "blanketing power" (Grand Bahama 26.6 N, 78.2 W, December 1958).

- (b) Near the magnetic equator we have lower daytime values whilst night values are about the same as in medium latitudes. This means that the typical “equatorial  $E_s$ ” which is a daytime phenomenon is highly transparent.

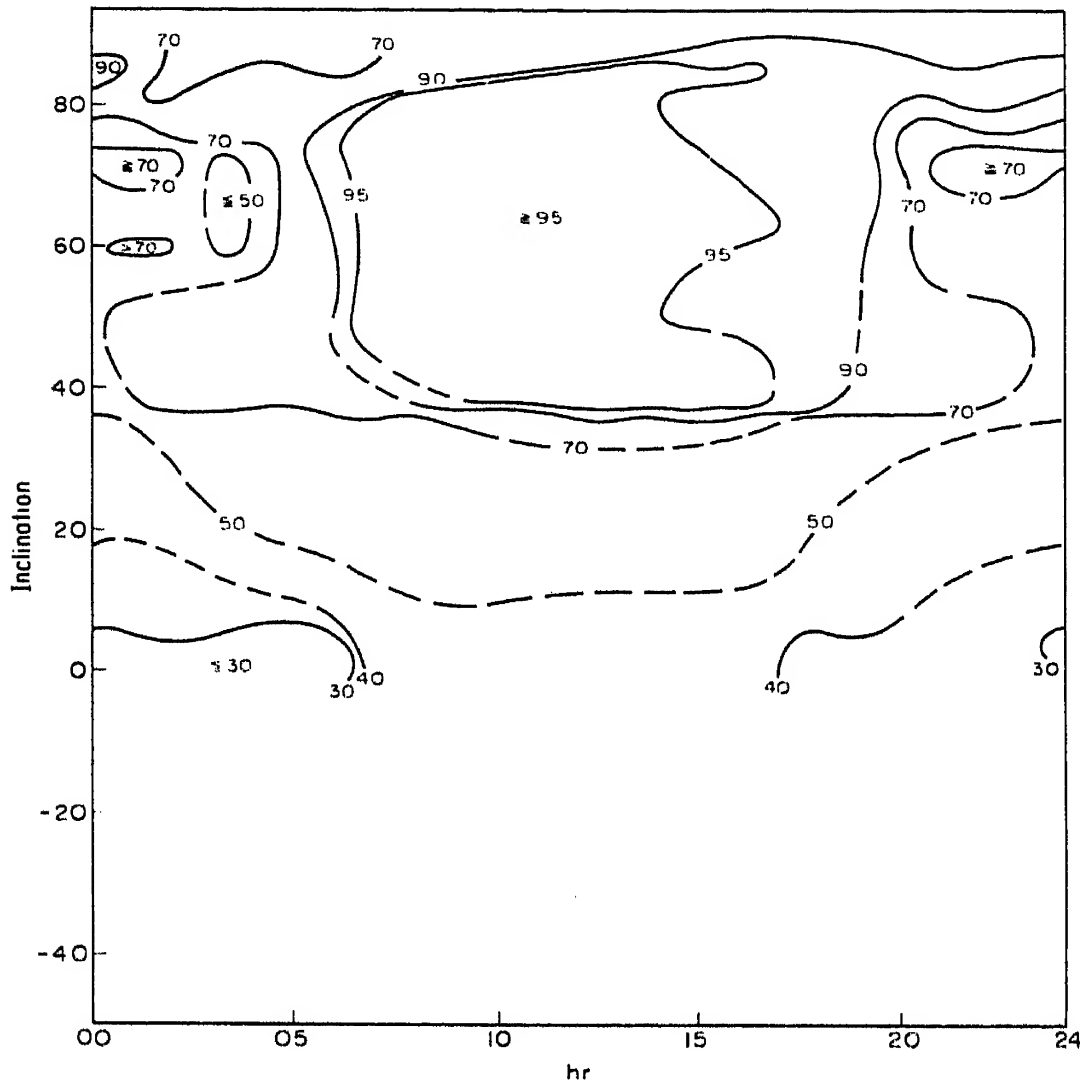


Fig. 23. “Blanketing Power”, median map (America, June 1958).

- (c) In the auroral zone the polar types of  $E_s$  become important and we find here a second, night-time maximum. This corresponds to the statistics of polar  $E_s$  types.

4.23. Our statistical results prove that the *distinction of magneto-ionic components* for the  $E_s$ -traces is an important step forward. It enables us now to give precisions with respect to the world-wide behaviour of the  $E_s$ -layer which could not have been obtained before.

### 4.3 Reflection Function

4.30. The routine parameters  $f_oE_s$  and  $f_bE_s$  cannot give a complete description of all essential properties of a transparent layer. Therefore we have

proposed to measure the reflection coefficient as a function of frequency as a special experiment. As this is rather difficult with an absolute method, another way has been indicated which is independent on variations of transmitted power and receiver sensitivity (Rawer 1949); this is the *comparison* of the *amplitudes* of  $E_s$ - and  $F$ -echoes on a suitable ionogram. The following method was used for the experiments which have been

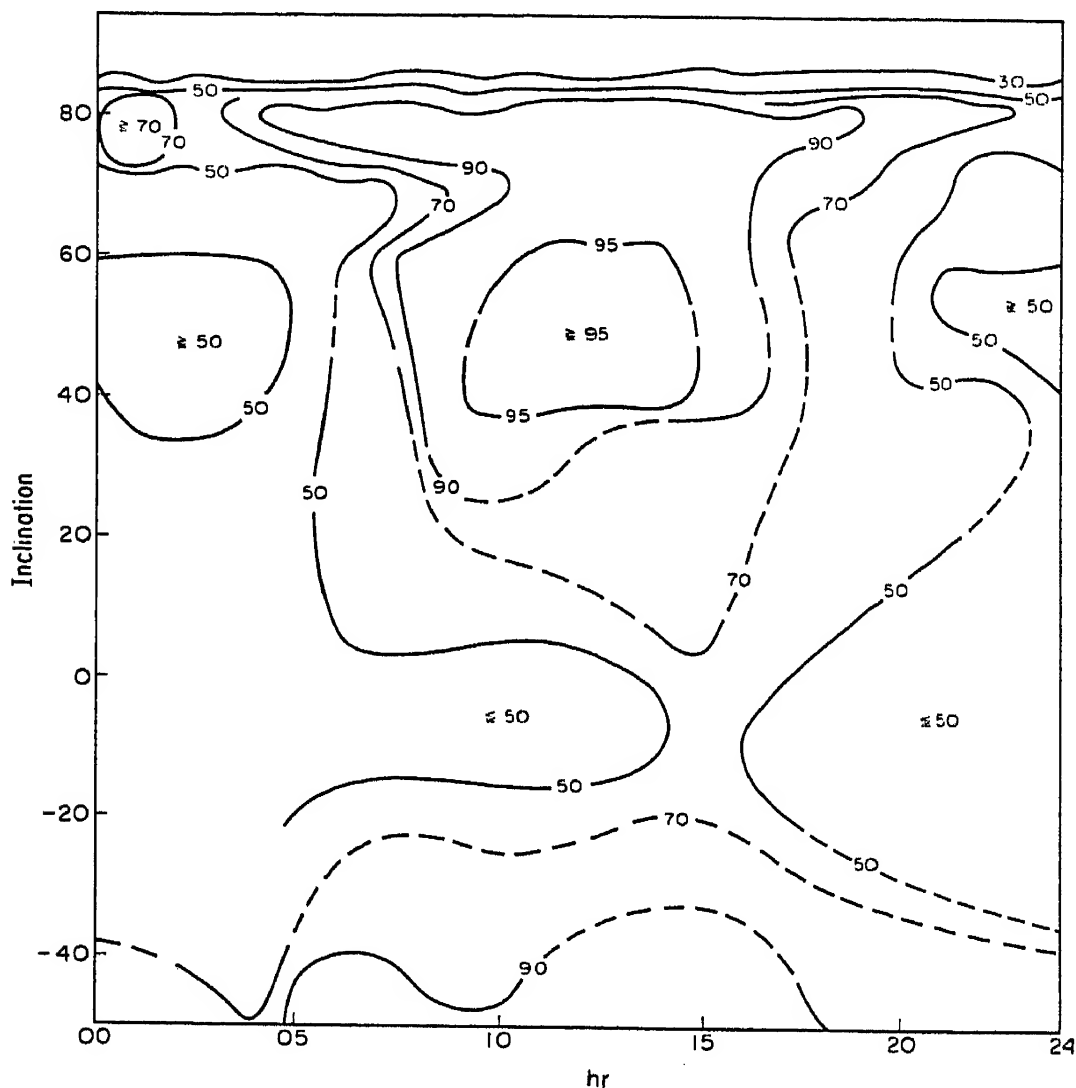


Fig. 24. "Blanketing Power", median map (America, December 1958)

made for some years at Freiburg. The receiver had a logarithmic sensitivity curve so that fixed amplitude ratios could easily be read by an observer looking at the echo pattern on the c.r. tube of the ionosonde. Five amplitude ratios were selected, viz. 100, 10, 1, 0.1 and 0.01, i.e. 40, 20, 0, -20 and -40 db; the corresponding frequencies  $f_1 \dots f_5$  were noted by the observer. In doubtful cases the highest frequency was written down which gave the desired amplitude ratio.  $f_3$  is very nearly the "critical frequency" according to our conventions.

4.31. It was found that the conventional characteristic  $f_b E_s$  was nearly equal to  $f_1$  whilst the identification of  $f_4, f_5$  was only possible after *distinction*

of both *magneto-ionic components*. The rules explained in the first contribution of the author have been applied in a suitable form; they are mainly based on the fact that the absorption is different for the two components. With these rules and the recorded ionogram the observed values  $f_3$ ,  $f_4$  and  $f_5$  could be identified as due to the  $o$ - or  $x$ -component. A set of reduced values was then constructed by subtracting  $\frac{1}{2}f_H$  from those readings which were identified as  $x$ -components. Besides in many cases the components could be clearly separated by differential absorption.

4.32. Some statistical results of these observations are presented in Fig. 25 where the differences  $(f_5 - f_1)$ ,  $(f_4 - f_1)$  and  $(f_3 - f_1)$  have been plotted; the results are given for all hours, and for day hours and night hours separately.  $(f_5 - f_1)$  is the total *range of transparency* between  $-40$  and  $+40$  db,  $(f_4 - f_1)$  the range corresponding to  $-20$  and  $+40$  db. Routine readings of  $f_oE_s$  are between  $f_5$  and  $f_4$ , rather often near  $f_4$ .  $(f_3 - f_1)$  is the range where blanketing is important; in most cases this range is much smaller than those involving  $f_4$  or  $f_5$ . This means that the transparency curve is asymmetric, the range of high transparency being larger. On the other hand we have many cases where the layer was completely blanketing; (the small numbers at the bottom give the number of observations where the difference was zero). In this respect a typical difference appears at night between the summer period of maximum occurrence (Fig. 25a) and the other months (Fig. 25b). In the last case total blanketing is extremely rare at night. No big differences are visible during the day except for the total number of cases; it is interesting to note that without serious changes in its form the distribution has only half the dispersion in March that it had in June. In nearly half of all cases no serious transparency was present ( $f_5 - f_1 \leq 0.2$  Mc/s).

4.33. For certain theoretical applications it is more interesting to know the *ratios* of our frequencies than their difference. Examples of such statistics have been published (Rawer 1955, Rawer 1958). We can summarize this investigation by the following table showing that—for the ratios only—no serious differences exist between different months;  $(f_5/f_3)^2$  corresponds to the ratio of electron densities of top and median ionization. In nearly half of all cases the top density was only 10 per cent higher than the median one. Cases with a ratio greater than 2 are very rare; they are more frequent in summer.

Table 1—Distribution of  $(f_5/f_3)^2$ , Freiburg 1952

	$1 < \dots \leq 1.1$	$1.1 < \dots \leq 2$	$2 < \dots \leq 3$	$3 < \dots$	
March	51	43	5	1	%
June	45	42	7	6	

It seems as if the ratio was larger in summer than in winter nights.



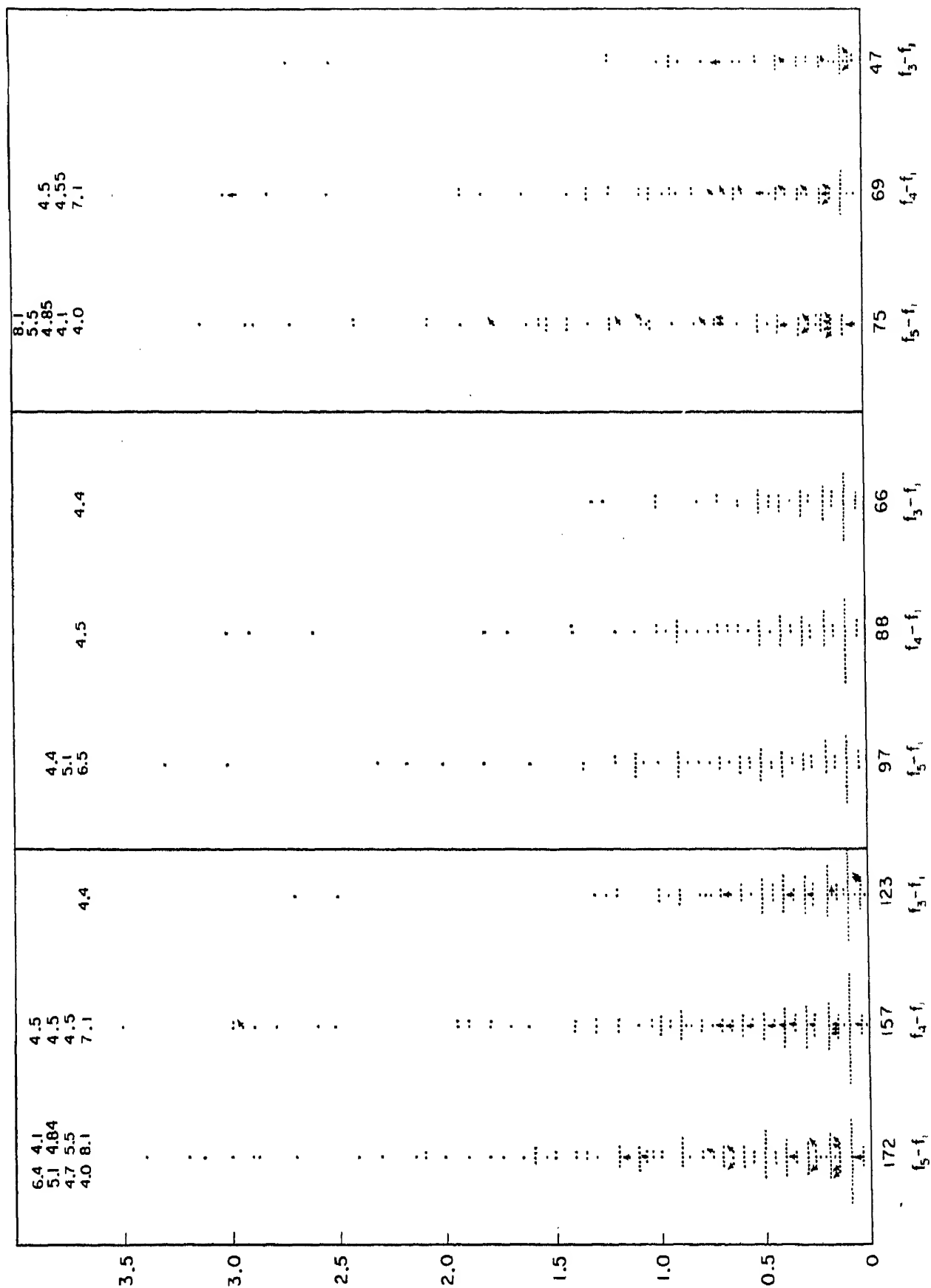


Fig. 25. Statistical results of systematic observations of the reflection function, Freiburg 1952. (a) June,

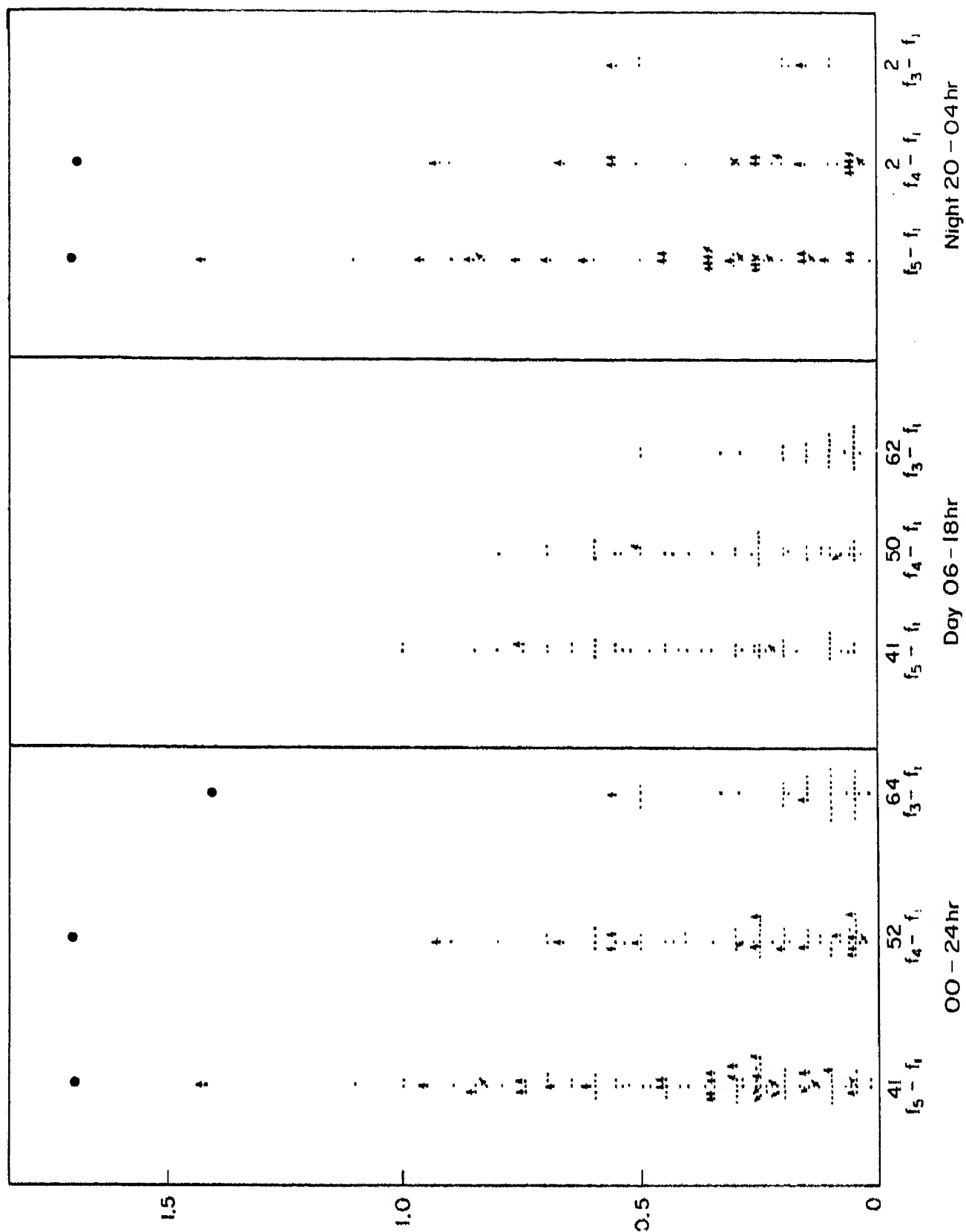


Fig. 25 (cont'd)  
(b) March.

4.34. The “critical frequency”  $f_3$  separates two *subranges*. It appears that the medians of  $f_5/f_3$  (the upper variation ratio) normally are much greater than those of  $f_3/f_1$  (the lower variation ratio). This indicates again the asymmetry of the transparency curve. As a general rule one can say that the upper variation ratio is considerably farther from “1” than the lower one. This means that if transparency exists at all there is only a small frequency range where an  $E_s$ -layer is slightly transparent but a rather large one where it is quite transparent and gives a faint echo.

## 5. THEORETICAL CONCLUSIONS

### 5.1 *Possible Models of Layer Structure*

5.10. For thick layers the *interpretation* of a virtual height versus frequency record is reasonably unambiguous in the sense that the corresponding layer should be horizontally stratified with a continuous electron density profile depending on the height only. This is not so for  $E_s$  at least not in those cases where true transparency is observed somewhere in the frequency range. We discuss briefly some of the models which have been proposed.

5.11. A *thin, homogeneous layer* easily explains those cases where no transparency occurs. We have seen that at temperate latitudes this applies to about  $\frac{1}{3}$  of all cases. The thickness of the layer (3.2) only varies between one and a few km, upper and lower boundary being well defined. Partial wave reflexion on such a layer exists (Briggs 1951) but it covers only a very small frequency range (Rawer 1939), so it can be neglected in the interpretation of ionograms. Therefore this model cannot be applied in cases where the layer is substantially transparent.

5.12. Transparency can be explained when the *layer has “holes”*, i.e. patches with smaller electron density than has the rest of the layer. The simplest model of this sort as indicated in Fig. 26 (line (a), left side) admits only two values of electron density. Consequently the reflection coefficient admits only three values, viz. one when the frequency  $f$  is below the minimum plasma frequency ( $f_b E_s$ ), zero when it is above the maximum plasma frequency ( $f_o E_s$ ) and an intermediate value (given by the geometry) when it is in between (Fig. 26a, right side).

The horizontal structure can be large in terms of wavelength but it must not be too large as compared with the Fresnel zones, otherwise the layer must be nearly always either blanketing or transparent. With patches of about 1 km diffraction should still be important and oblique radiation should be observed—and this would be in disagreement with the temperate latitude observations (3.33). With larger patches (5 km or more) transparency could still be explained and lateral diffraction would be small enough. From the cross-correlation function (1.24) we can only determine

the size of the  $E_s$ -fields, but not the microstructure which is decisive for transparency. Apart from transparency  $M$ -echoes can also be explained with the present model which is quite satisfying to explain the observations on a fixed frequency. However, the observed reflection function is continuous (4.32) and not discontinuous as Fig. 26a. So the observed variations with frequency are not explained by the present model.

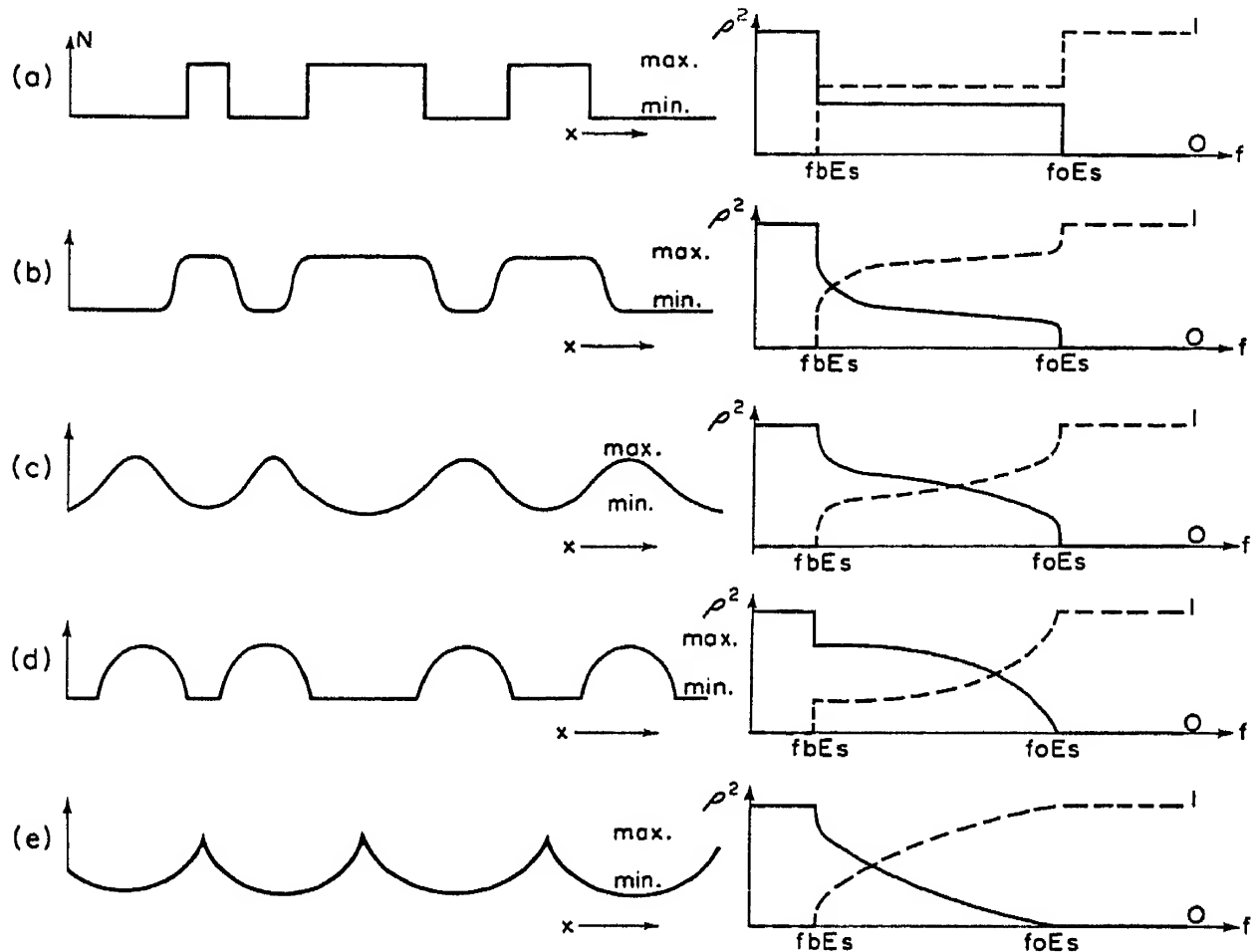


Fig. 26. Models for electron density distribution in the horizontal plane (left side) and corresponding reflection and transmission curves (full and broken curves on the right side).

5.13. It is not too difficult to change the last model, so that the reflection function becomes continuous. Different forms of *clouds with continuous gradations* in electron density are shown in Figs. 26b–e, together with the corresponding reflection functions. These are thin layers with a basic ionization corresponding to the blanketing frequency, containing stronger ionized “clouds”, the nucleus of which has an ionization corresponding to the top frequency. The asymmetry as observed by the reflection functions (4.34) can best be explained with contours like Fig. 26d or e.

This is a rather general model. It covers 5.11 (homogeneous ionization) and 5.12 (discontinuous “contours”) as special limiting cases.

5.14. Another, different model has often been quoted as explaining the

characteristic features of  $E_s$ . This is the *scattering layer*, i.e. a layer which can be compared in some way to a fog bank. It is discussed in K. Tao's contribution. We feel that with this model one encounters serious difficulties to explain some of the characteristic features of temperate latitude  $E_s$ , in particular—strong blanketing (2.24),—many cases of complete blanketing (4.1; 4.21; 4.33),—sharp echoes (3.32), without “ripples” (3.31),—vertical incidence of the echoes (3.33).

5.15. As a *summary* we may say that the temperate latitude observations of  $E_s$  can be explained by rather flat ionization “clouds” in thin layers (5.13) degenerating in about 30 per cent of all cases into a homogeneous layer (5.11). The observed reflection functions indicate that in transparent layers the “cloud contours” correspond most often to something like Fig. 26e. The very last end of the observed high frequency tail of the reflection function (4.32) could be due to diffraction effects.

## 5.2 *The Energy Balance*

With this result we admit that  $E_s$  phenomena must be explained by an increased ionization in a very thin, flat layer. We have excluded the possibility that some special character of existing ionization, for example scatter phenomena, might be at the origin of the observed echoes. Increased ionization means either a rearrangement of existing ionization or a special ionization process. Before we discuss some possible explanations, we should have an idea of the numerical importance of such processes.

5.21. The energy for establishing an ionized layer is measured by the number of ionization processes which are needed in the equilibrium state. This depends essentially on the inverse process. The effective recombination process in the  $E$ -region corresponds to a coefficient of about  $2 \times 10^{-14} \text{ m}^3\text{s}^{-1}$ . Supposing a homogeneous layer Table 2, for some values of the plasma frequency, gives first the probability of occurring at certain top frequencies (at Freiburg), then the corresponding electron density  $N$  and the time during which by recombination this value falls to 10 per cent when the ionization source is suddenly stopped. Finally for a rather thick layer (3 km) the number  $P$  of ionization processes is indicated which is needed at the equilibrium state. The last line shows the power needed for these ionization processes with a rather large cloud of  $100 \times 100 \text{ km}^2$  (supposing 12 eV per ionization).

The conclusion is that little power is needed to explain the extra  $E_s$  ionization. Our estimate is certainly too high as the basic values used in Table 2 are large and the mean ionization is certainly nearer to  $f_b E_s$  than to  $f_o E_s$ .

## 5.3 *Possible Origin of the Ionization*

5.30. Many hypotheses have been forwarded in order to explain the extra

Table 2  
Energy needed for a  $100 \times 100 \text{ km}^2 E_s$  layer

$f_N/\text{Mc/s}$	10	7	5	3	2	1
Probability $f_e E_s > f_N$	1	8	25	80	90?	?? %
$N(\text{m}^{-3})$	$1.24.10^{12}$	$6.08.10^{11}$	$3.10.10^{11}$	$1.12.10^{11}$	$4.96.10^{10}$	$1.24.10^{10}$
decrease time	6 min	12 min	24 min	1.1 hr	2.5 hr	10 hr
$P(\text{m}^{-2}\text{s}^{-1})$	$9.2.10^{13}$	$2.2.10^{13}$	$5.8.10^{12}$	$7.5.10^{11}$	$1.5.10^{11}$	$9.3.10^9$
power(kW)	1700	418	110	14	2.85	0.17

ionization which appears in so irregular a way. We have demonstrated the following characteristic features of temperate latitudes  $E_s$  which should be explained by a satisfying hypothesis:

- (a) basic ionization as described by  $f_b E_s$ :
  - 1—rather irregular appearance (1.11)
  - 2—regular median behaviour (2.23)
  - 3—small dip-equator effect (2.23)
  - 4—no outstanding dependence on solar activity
- (b) top ionization as described by  $f_o E_s$ :
  - 1—very irregular appearance (1.11 ... 1.13)
  - 2—absolute values sometimes equal, sometimes large compared with the ambient ionization (2.22, 2.23)
  - 3—preference of daytime, decrease of probability during night hours (2.11)
  - 4—summer preference (2.12)
  - 5—very important positive effect at the dip equator (2.13)
  - 6—no direct correlation with solar activity (2.14)
  - 7—long term fluctuations similar to those in climatology (2.15)
- (c) height:
  - 1—rather constant range
  - 2—systematic decrease with increasing ionization (3.1)
- (d) thickness:
  - 1—between one and a few km (3.2)
- (e) structure:
  - 1—reflecting level rather flat (3.32; 3.33)
  - 2—30 per cent completely blanketing (4.1; 4.32)
  - 3—70 per cent transparent up to complete transparency (4.22; 4.33)

5.31. Solar radiation being excluded by the appearance at night it is quite clear from the irregularity with which  $E_s$  appears in time (1.1) and space (1.2) as well as from its small thickness (3.2) that this layer cannot be due to any form of ionization by UV or X-ray *wave radiation of extra-terrestrial origin* anyhow.

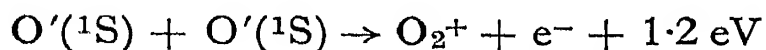
5.32. *Extra-terrestrial corpuscular radiation* can explain the auroral forms but not temperate and low latitude  $E_s$  which is discontinuous with the auroral layers. Against this hypothesis are b3, b4 and, in particular, b5. There can not be any doubt that at least some terrestrial “disposition” plays an important rôle.

5.33. *Meteors* give quite another type of ionization structure which has been observed with high power sounders (Naismith 1956). The correlation with  $E_s$  is bad (Pineo 1950), also the diurnal variations are quite different.  $E_s$  and forward-scatter seem to be clearly distinct phenomena, relations found between this type of propagation and meteoric ionization columns cannot be generalized for our problem.

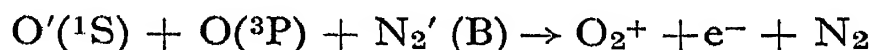
5.34. If we turn now to possible terrestrial sources the *thunderstorm* theory has a historical priority at least at low latitudes. Whilst b4 would well agree it is quite clear that b5 cannot be understood on this basis. A recent, very serious investigation in India (Kotadia 1958) has shown that no correlation with  $E_s$  exists.

5.35. *Shock waves* forming out of sound waves coming from the lower atmosphere seem to play an important rôle in the solar atmosphere. In the terrestrial atmosphere absorption seems to be too high, so that the waves disappear before they reach the critical level. It seems improbable that ionization could be formed in this way.

5.36. Ionization by *collisions with excited molecules* or atoms has been proposed in different forms: Molecular recombination of two metastable oxygen atoms (Rawer 1940, Jouaust 1952, Gauzit 1943) according to

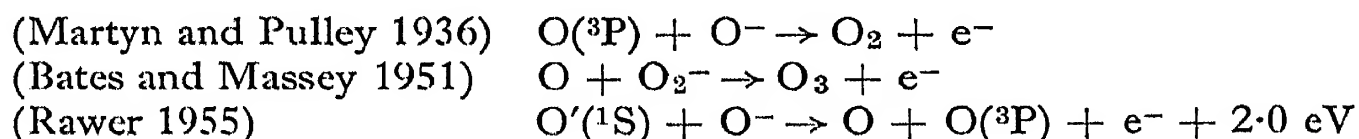


or in a triple collision with one excited O-atom only and an excited  $\text{N}_2$  molecule (Rawer 1940, Jouaust 1952):



The total number of metastable atoms is high but the probability of these collisions is only high enough if some concentration process is active (Rawer 1955). This introduces a meteorological aspect into our problem, which could fit with b1, b2, b4, b6, b7. If on the other side equatorial  $E_s$  is continuous with the temperate latitude form it seems difficult to account for b5.

5.37. *Charge transfer processes* make it possible to profit from the negative ion stock which is probably rather important at night but less in daytime. Possible reactions are



The probability situation is similar to that in 5.36, also the meteorological aspect comes in. It seems difficult to account for b5 as magnetic control cannot work for ions at a level where the collision number largely exceeds the ion gyrofrequency.

5.38. *Rearrangement* of existing *ionization* is thought by Martyn (1950) to be most efficient. As, generally speaking, the electron density gradient points upwards an ionized air mass moving downwards should simultaneously be compressed and so the plasma density be increased; this could explain the formation of ionized clouds. This is a meteorological process which fits well with b1, b2, b4, b6, b7. Also magnetic control is possible for electrons so that b5 can also be understood. A sort of "trapping"



of the plasma clouds seems to be needed with this theory, some meteorological discontinuity could do that. It is well known that one form of  $E_s$  develops from above, the so called "sequential  $E_s$ " (McNichol and De V. Gipp 1951). Now as recently shown by Bibl (1959) the more frequent "continuous height" form also seems to get higher concentration by moving downwards. These observations seem to be in favour of the present theory. It is especially important in this respect that Bibl also shows that the plasma density decreases when the height is increasing again.

As to possible "traps" there are recent rocket observations indicating that  $E_s$  occurs at heights where important winds shears occur most often. As known from other atmospheric phenomena these could well act as traps. 5.39. Quite recently Bibl (1960) gave new evidence that  $E_s$  formation depends in some way on an instability existing at the bottom of the  $F$ -region. Studying one year's continuous observations of characteristics he established three hourly ionospheric character figures indicating

—the fluctuations of  $MUF(3000)F_2$ : Fig. U,

—the fluctuation of  $h'F$ : Fig. H

—the number of occurrence and intensity of  $E_s$  "pulses": Fig. E.

These figures were intercompared by the method of partial correlation, the magnetic character being simultaneously considered (local character:  $K$ , planetary character:  $P$ ). As a first intercomparison Bibl looked for the days of maximum disturbance out of 10, 15, or 20 days. The mean partial correlations he found are given in Table 3.

Table 3—Partial correlation values

Characters intercompared/invariable			maximum fluctuation
U E	/	H K	-0.03
H E	/	U K	0.62
K E	/	U H	-0.51
H K		U E	0.64

The large value of [H E] shows that days with important fluctuations of  $h'F$  are also days with important  $E_s$  whilst the  $MUF$  fluctuations do not interfere with  $E_s$  as shown by [U E]  $\approx 0$ .

Another interesting feature is the negative correlation [K E] showing that  $E_s$  is less frequent for these rather (rare) days of magnetic disturbance where the  $F$ -region was not influenced. As most of these days are found to have large  $h'F$  fluctuations (see [H K]) by the positive [H E] correlation both effects cancel so that the total correlation {H E} is practically zero.

## 5.4 Conclusions

Quite different from the normal thick layers due to cosmical radiation influences  $E_s$  seems to be a "meteorological" phenomenon, the only one well known in the ionosphere except for winds. Therefore the behaviour of this layer is completely different from the normal layers. As to the energy it is probable that existing molecular excitation or ionization (5.36 ... 5.38) is concentrated in a small height range by vertical exchange, trapped by some discontinuity, which is eventually formed by strong wind shears. Rearrangement of ionization seems to be a rather probable process.

*Acknowledgment*—Mrs. B. Brake has prepared the major part of the statistical data used in the present paper.

## REFERENCES

- APPLETON, E. V. and NAISMITH, R. (1940) *Proc. Phys. Soc.* **52**, 402.  
 BATES, D. R. and MASSEY, H. S. W. (1951) *J. Atmosph. Terr. Phys.* **2**, 1.  
 BIBL, K. (1959) *Ann. de Geophys.* **16**, 148.  
 BIBL, K. (1960a) *Archiv Elektr. Übertragung*, **14**, 341.  
 BIBL, K. (1960b) *J. Geophys. Res.* **65**, 2333.  
 BIBL, K., HARNISCHMACHER, E. and RAWER, K. (1955) *Phys. of Ionosph., Phys. Soc.*, p. 113.  
 BIBL, K., PAUL, A. and RAWER, K. (1959) *J. Atmosph. Terr. Phys.* **16**, 324.  
 BRAND, J. O. and ZENNECK, J. (1944) *Schriften Deutsch. Akad. Luftfahrt*, **8**, No. 1.  
 BRIGGS, B. (1951) *J. Atmosph. Terr. Phys.* **1**, 343.  
 FISHER, R. A. (1925) *Statistical Methods for Research Workers*, Edinburgh.  
 GAUZIT, J. (1943) *Cahiers de Physique*.  
 HÖCHTL, F. and RAWER, K. (1949) *Ann. de Géophys.* **5**, 150.  
 JOUAUST, R. (1952) *C. R. Paris* **214**, 441.  
 KOTADIA, K. M. (1958) *Studies in the Physics of the Ionosph. at Low Latitudes*, Thesis, Ahmedabad, India.  
 LOVERA, G. (1953) *Geofisica Pura e Applicata* **24**, 1.  
 MARTYN, D. F. (1950) *Rep. Proc. 11 Meet. URSI*, **44**.  
 MARTYN, D. F. and PULLEY, O. O. (1936) *Proc. Roy. Soc. A* **154**, 755.  
 MATSUSHITA, S. (1953) *Rep. Ionosph. Res. Japan* **7**, 45.  
 McNICOL, R. W. E. and DE V. GIPPS, G. (1951) *J. Geophys. Res.* **56**, 17.  
 NAISMITH, R. (1956) *Nuovo Cimento, Suppl. al Vol. IV, Ser. X, No. 4*, 1413.  
 NAKATA, Y., KAN, M. and UYEDA, H. (1953) *Rep. Ionosph. Res. Japan* **7**, 129.  
 PINEO, V. C. (1950) *Science*, **112**, 50.  
 RAWER, K. (1939) *Ann. d. Physik.* **35**, 385.  
 RAWER, K. (1940) *Naturwiss.* **28**, 577.  
 RAWER, K. (1942) *Ann. d. Physik* **42**, 294.  
 RAWER, K. (1949) *Nature* **163**, 528.  
 RAWER, K. (1951) *J. Atmosph. Terr. Phys.* **2**, 38.  
 RAWER, K. (1953) *C.R. Paris* **237**, 1102.  
 RAWER, K. (1955) *Geofisica Pura e Applicata* **32**, 170.  
 RAWER, K. (1958) *AGARDograph* **34**, 67.  
 RAWER, K. (1959) *Geofisica Pura e Applicata* **43**, 218.

# Interrelations of Sporadic $E$ and Ionospheric Currents

S. MATSUSHITA

High Altitude Observatory, Boulder, Colorado, U.S.A.

**Abstract**—Several different electric current systems in the ionosphere at about 100 km altitude have been postulated from studies of quiet and disturbed variations of the geomagnetic field. Almost all of these ionospheric current systems are related to different types of sporadic  $E$  ( $E_s$ ), although the mechanism involved in the relationship is not the same in each case.

It is suggested that equatorial  $E_s$  is a kind of irregularity in the equatorial electrojet due to vertical drifts.  $E_s$  occurring in temperate latitudes is postulated to be mainly a thin patchy layer which is due to vertical drift motions of charged particles caused by wind shears; however, occasionally a thick cloud is formed by descending ionization from the upper ionosphere. In both cases  $E_s$  is affected by the solar daily quiet ionospheric current. In high latitudes predominant types of  $E_s$ , such as slant, retardation and auroral types, together with the disturbed ionospheric currents, are due to charged particles penetrating into the lower ionosphere from outside the earth's atmosphere, as can be clearly seen during geomagnetic bays. This interrelation also occurs occasionally at the time of geomagnetic sudden commencements. Retardation type of  $E_s$  and so-called night- $E$  are thick patchy layers, and auroral  $E_s$  is formed by field-aligned clouds, all of which are caused mainly by electron impact. These interrelations of  $E_s$  and ionospheric currents are discussed in the present article and an estimation of structures and causes responsible for the different types of  $E_s$  is presented.

## 1. INTRODUCTION

A major portion of the geomagnetic variation observed at the earth's surface is believed to result from several different electric currents in the ionosphere (named "ionospheric currents" in the present article), although some of the remaining variations are caused by changes of the magnetic field which originate outside of the earth's atmosphere and also are influenced by electric currents induced in the earth's interior. These different ionospheric currents are all supposed to flow at approximately the same altitude, about 100 km, at which height the effective electric conductivity is a maximum. Observations by rocket magnetometers verify the existence of the ionospheric currents at this height (Maple, Bowen and Singer 1950, Cahill 1959).

As mentioned in another article in this book, a dynamo effect due to a lunar tidal motion of the lower ionospheric atmosphere causes the lunar daily ionospheric current system. Other ionospheric currents are mainly caused by the sun. The solar daily quiet current system,  $S_q$ , is responsible

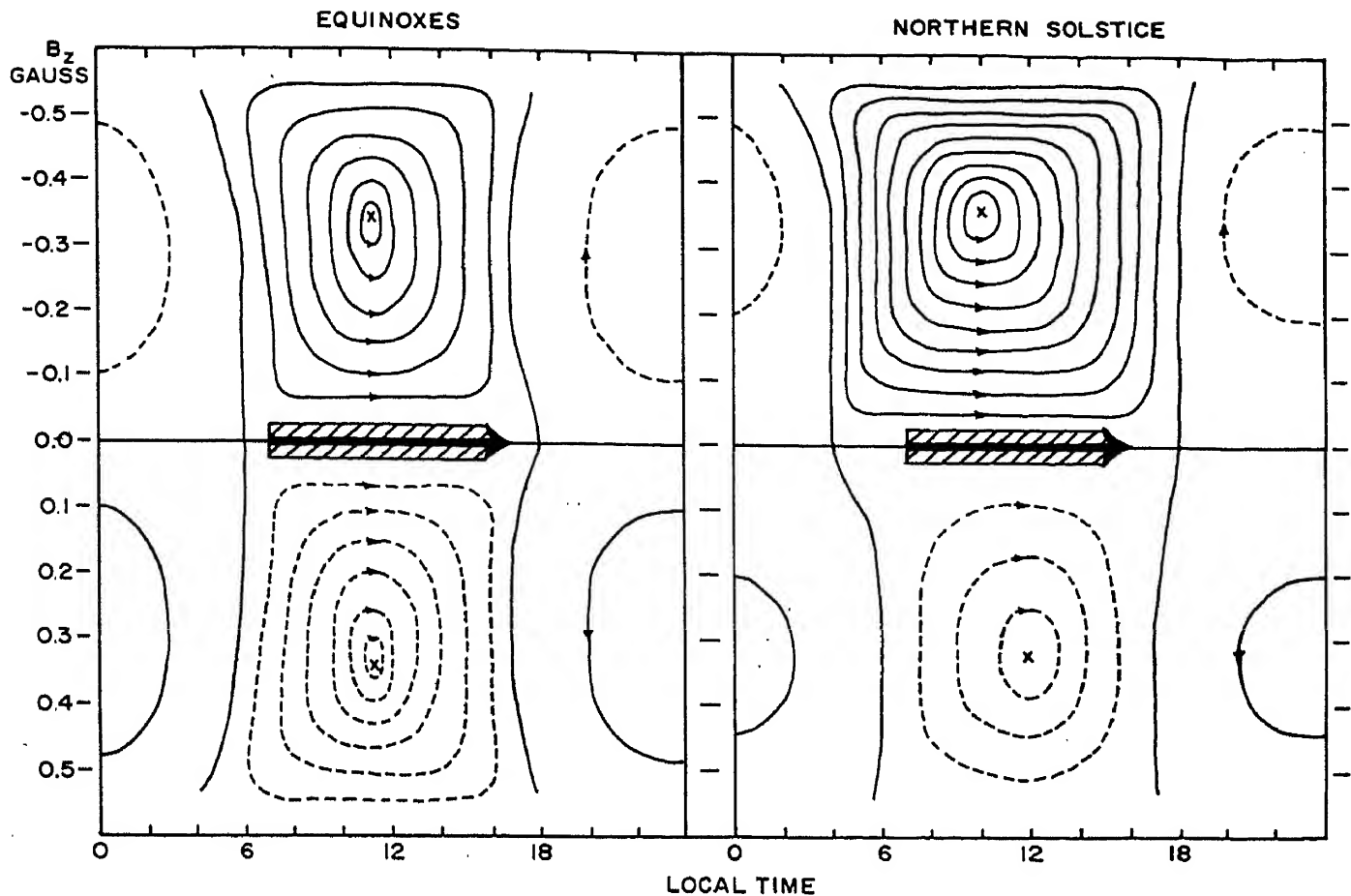


Fig. 1. Solar daily quiet electric current system and solar equatorial electrojet at about 100 km altitude in equinoxes (left) and northern solstice (right). About 10,000 amperes flow between each pair of adjacent current lines. The ordinate is shown by the vertical component of the earth's main magnetic field,  $B_z$ , which is the best parameter in order to avoid longitudinal inequalities of the current system. Seasonal changes of the location of the central positions (focus) of the daytime oval currents are quite different from Chapman and Bartels' current system. During the daytime the solar equatorial electrojet flows in the magnetic equatorial zone which is a region between approximately  $+0.03$  and  $-0.03$  gauss of  $B_z$ , and its intensity in equinoxes is about 1.5 times larger than that in solstices. The total current intensity in the entire equatorial zone is  $1.0 \times 10^5$  to  $1.5 \times 10^5$  amp.

for solar daily geomagnetic variations on quiet days, and is believed to be due to a dynamo effect in the lower ionosphere under the quiet solar radiation. Chapman and Bartels (1940) have shown the well-known diagrams of this current system. However, Matsushita (1960), using the IGY data, suggested that the current system should be revised. His current system, Fig. 1, shows that a strong eastward current named "equatorial electrojet" flows during daylight hours in a narrow zone centered on the magnetic equator. Here the magnetic dip angle is  $0^\circ$ , and the vertical component of the earth's main magnetic field is zero gauss. When solar flares occur, both the  $S_q$  current system and the equatorial electrojet are often intensified in the sunlit hemisphere due to the increased radiations

from the flares. This additional current can be called "flare current system" (Veldkamp and Van Sabben 1960, Van Sabben 1961, Rikitake and Yukutake 1962).

Ionospheric currents responsible for geomagnetic disturbances and storms have also been estimated, particularly in high latitudes. Matsushita (1960 a) has suggested three different ionospheric current systems for sudden commencements: eastward currents for the main impulse of sudden commencements, westward currents for the preceding negative impulse, and east and westward currents (depending on location) for the variation succeeding the main impulse. A current system for the disturbance daily variation during geomagnetic storms, such as  $D_s$  or  $S_D$ , has been studied by many workers (for example, Chapman and Bartels 1940, Vestine 1947, Fukushima 1949 and Matsushita 1953a). In auroral latitudes, however, this  $D_s$  ionospheric current simply represents an average current system obtained from a superposition of many bay-shaped variations which frequently occur in patchy distribution during geomagnetic storms. It is much more important to study the current due to individual bay-shaped variations, which was named "polar elementary storm" by Birkeland (1908), than the average current system in order to clarify the physical behavior involved in storms. Akasofu and Chapman (1961) have recently discussed this problem with regard to auroral phenomena.

Geomagnetic bays in auroral latitudes are similar to bay-shaped variations (polar elementary storms) but occur even on geomagnetically quiet days. The former have a more systematic and simple behavior than the latter, although both occur in patchy form. Since results obtained from the former can often apply to the latter, studies of bays are very useful for the investigation of complicated storm behavior. However, we should always be careful of certain differences involved with  $D_s$  (or  $S_D$ ), bay, and bay-shaped variation of polar elementary storm. Hatakeyama (1938) and Silsbee and Vestine (1942) obtained an average current system responsible for the bays.

Almost all of these ionospheric currents seem to correlate with different types of sporadic  $E$  ( $E_s$ ), although the mechanism involved in the correlation is not the same. This difference can be clearly seen in three separate zones: equatorial, temperate and auroral zones. Details of each zone are discussed in the following three sections.

## 2. EQUATORIAL $E_s$ AND THE SOLAR EQUATORIAL ELECTROJET

It has been well-known for many years that the daily amplitude of the geomagnetic horizontal variation field,  $H$ , at Huancayo is unusually large (Chapman and Bartels 1940). A similar enhancement has been observed at other equatorial stations as well. As is shown in the extreme left diagram of Fig. 2, the enhancement occurs in a narrow zone centered on the

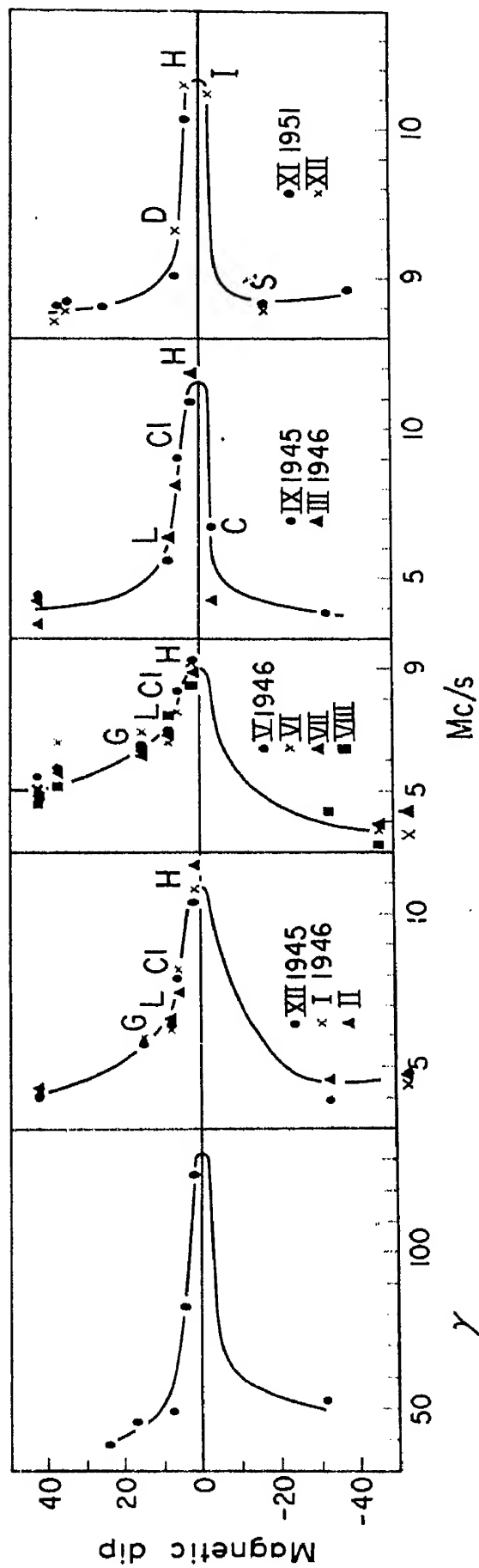


Fig. 2. Daily amplitude of the geomagnetic horizontal variation field, which is a good indication of the intensity of the solar equatorial electrojet, and  $f_oE_s$  values of the equatorial  $E_s$  (Matsushita 1953a).

magnetic equator (i.e. the earth's magnetic dip angle equals  $0^\circ$  and the vertical component of the earth's main magnetic field,  $B_z$ , is zero gauss). It can be easily understood that this enhancement results from a strong eastward electric current during daylight hours (see Fig. 1), which has been called the equatorial electrojet (Chapman 1951). The equatorial electrojet during the IGY has been studied in Peru by Forbush and Casaverde (1961), in Nigeria by Onwumechili (1959), and in Ghana by Osborne (1962). The actual cause of the electrojet is a high value of Cowling conductivity in the magnetic equatorial zone at about 100 km height combined with an electrostatic field caused by solar dynamo effects (for example, see Matsushita 1953a). In the same way the lunar dynamo effects can cause the lunar equatorial electrojet, as suggested by Matsushita (1953b, 1957, 1962a).

The daily amplitude of  $H$  is a good indication of the intensity of the equatorial electrojet, as will be discussed later. Average daily amplitudes of  $H$  at Huancayo on the ten quiet days in each month are plotted in Fig. 3 during the period from January 1922 through December 1959; these illustrate the variations of the intensity of the jet with solar activity and with season. Here the daily amplitude is taken as the difference between the average value of  $H$  during the period 09 00–14 00 hr and that during 21 00–02 00 hr, 75° W.M.T. As a parameter of the solar activity, monthly values of the Zürich sun-spot number are also plotted in Fig. 3. It is obvious in Fig. 3 that the daily amplitude, hence the intensity of the electrojet, varies with the 11 year solar cycle. Another remarkable result indicated in Fig. 3 is a seasonal variation of the jet-intensity; the maxima clearly occur in equinoctial months. This seasonal variation was also seen at other stations, such as Jarvis Is., Koror and Addis Ababa, in the magnetic equatorial zone during the International Geophysical Year.

As geomagnetic disturbances occur more frequently in equinoxes than in summer and winter, the ten quiet days in each month during equinoctial seasons have slightly higher values of geomagnetic index than those in solstitial seasons. However, this cannot be the cause of the maxima of the jet-intensity in equinoxes, because the daily amplitude in equinoxes is larger on more quiet days. The cause of the seasonal variation may be due to the fact that both the electric conductivity in the equatorial zone and the electrostatic field which is effective in the magnetic equatorial zone increase during the equinoxes.

As can be seen in Fig. 2, the equatorial  $E_s$  ( $E_s$ - $q$ ) appears in the same narrow zone as that in which the equatorial electrojet flows (Matsushita 1951; see also Knecht and McDuffie's article in this book). Also, an obvious correlation between the  $f_oE_s$ - $q$  and the daily amplitude of  $H$ , accordingly the jet-intensity, observed at the same station, can be obtained. Figure 4 shows examples of the correlation between the monthly averaged values of the two, and Fig. 5 shows the daily averaged values. However,

this correlation is not always good, since the  $f_oE_s-q$  values are influenced by sensitivities of different ionosondes and absorption in the lower ionosphere and also to some extent by scaling techniques in ionograms. Moreover, the  $f_oE_s-q$  value does not indicate the maximum electron density per  $\text{cm}^3$  which is usually given by

$$N_{\max} = 1.24 \times 10^4 f_o^2 \quad (f_o \text{ in Mc/s}),$$

but may depend upon the size and distribution of the nonhomogeneity in

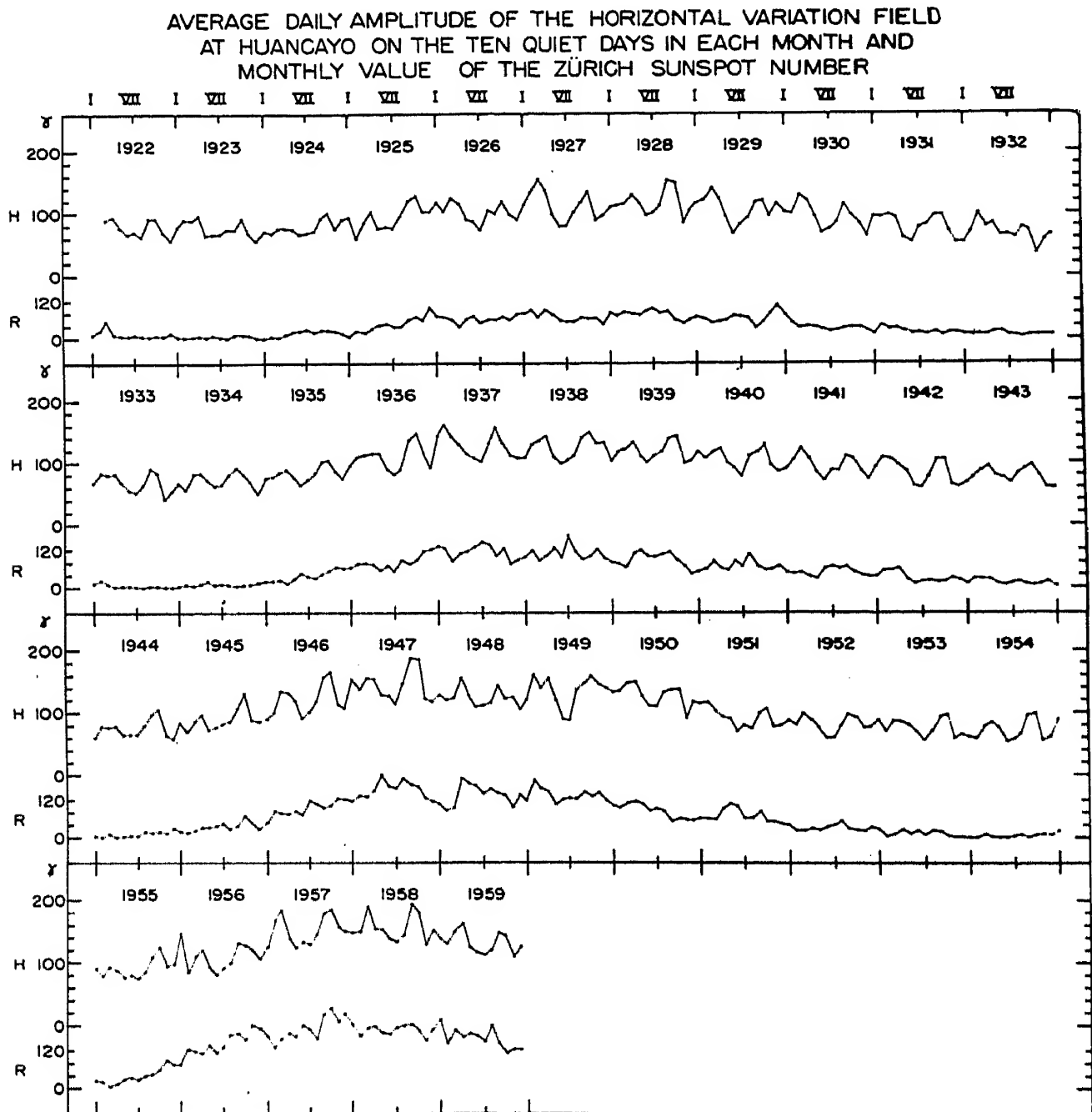


Fig. 3. Average daily amplitudes of  $H$  at Huancayo on the ten quiet days in each month and monthly values of the Zürich sunspot number during three and one-half solar cycles. The former shows an obvious seasonal change, which is the maxima in equinoctial months, with the 11 year solar cycle.



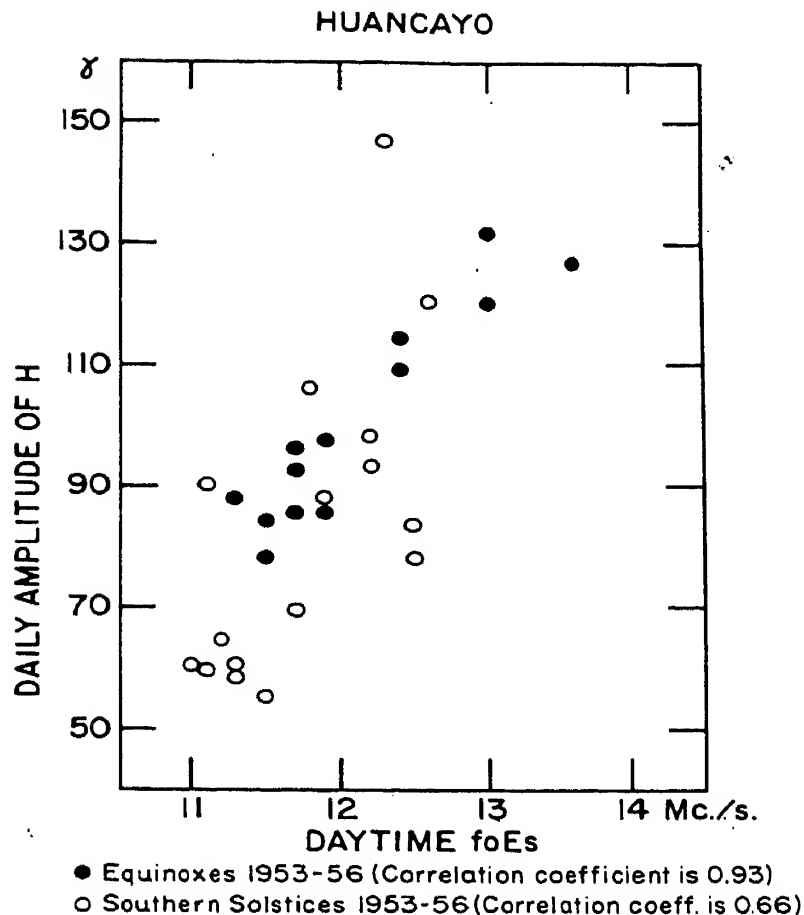


Fig. 4. Correlations between the monthly median value of  $f_oE_{s-q}$  averaged for the daytime (09 00–15 00 hr) and the daily amplitude of  $H$  averaged on the ten quiet days in each month at Huancayo in equinoctial and southern solstitial months of 1953–1956.

the  $E_{s-q}$ . Thus the  $f_oE_{s-q}$  must be considered as merely a parameter of approximate activity of the  $E_{s-q}$ . A different type of observation of the  $E_{s-q}$ , such as that taken by Bowles and Cohen (1960; also see their article in the present book), is more reliable for obtaining the correlation. In fact, Bowles and Cohen's observations in Peru during the IGY indicate a remarkable correlation between the field intensity due to the  $E_{s-q}$  and the  $H$  variation. In general we may safely conclude that the  $E_{s-q}$  has a close correlation with the  $H$ , hence the equatorial electrojet.

A further evidence of the correlation between the two can be obtained from lunar effects in the  $E_{s-q}$ ; the eastward lunar equatorial electrojet reinforces the  $E_{s-q}$ , but the westward lunar electrojet tends to cause a disappearance of the  $E_{s-q}$  (Matsushita 1957a, Knecht 1959, Egan 1960). This lunar effect indicates that the solar equatorial electrojet, which is an eastward current and is much larger than the eastward lunar electrojet, is

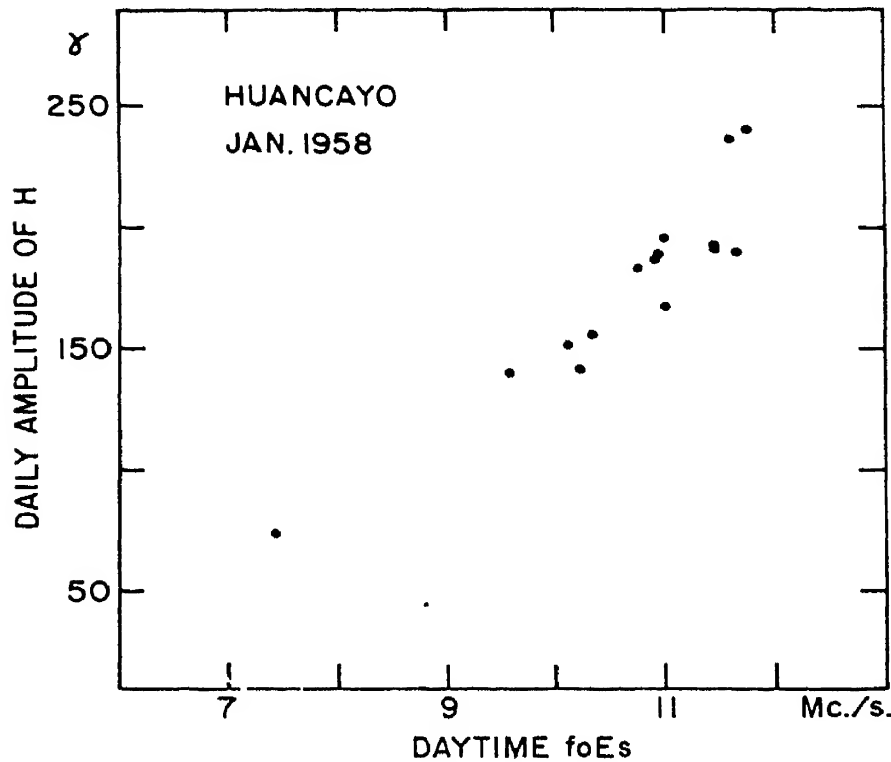


Fig. 5. Daytime  $f_oE_s-q$  value (average, 09 00–15 00 hr) plotted against daily amplitude of  $H$ , observed at Huancayo on each day in January 1958, excluding geomagnetically disturbed days and the three consecutive days near new and full moons. The correlation coefficient between the two is 0.95.

a major cause of the  $E_s-q$ . Results described earlier all support this conclusion. Details are omitted here since they are discussed in my other article on lunar tidal variation of  $E_s$  in this book. An essential conclusion of the discussion is that the  $E_s-q$  seems to consist of irregularities in the density of charged particles involved in the equatorial electrojet. The irregularity is due to a vertical upward drift motion of charged particles, whose drift speed  $W$  is proportional to the eastward jet-intensity  $I_y$ , as shown by

$$W = \{(q_r + e_r p_r \sigma_1 / \sigma_2) / \Sigma_3\} I_y. \quad (2.1)$$

$$\text{Here } \left. \begin{aligned} p_r &= (1/m_r \nu_r) \{ \nu_r^2 \cos^2 \phi / (\nu_r^2 + \omega_r^2) + \sin^2 \phi \}, \\ q_r &= (1/B) \{ \omega_r^2 / (\nu_r^2 + \omega_r^2) \} \cos \phi. \end{aligned} \right\} \quad (2.2)$$

$m_r$ ,  $e_r$ ,  $\nu_r$ , and  $\omega_r$  are the mass, charge (in e.m.u.), collision frequency with neutral particles, and gyrofrequency of particles of the  $r^{\text{th}}$  kind of gas (i.e. ions and electrons), respectively;  $\phi$  is the magnetic dip angle;  $\sigma_1$ ,  $\sigma_2$  and  $\Sigma_3$  are the Pedersen, Hall, and height-integrated Cowling conductivities;  $B$  is the intensity of the earth's main magnetic field. The formation of the irregularity due to this vertical drift may be by the mechanism Martyn (1953) discussed.

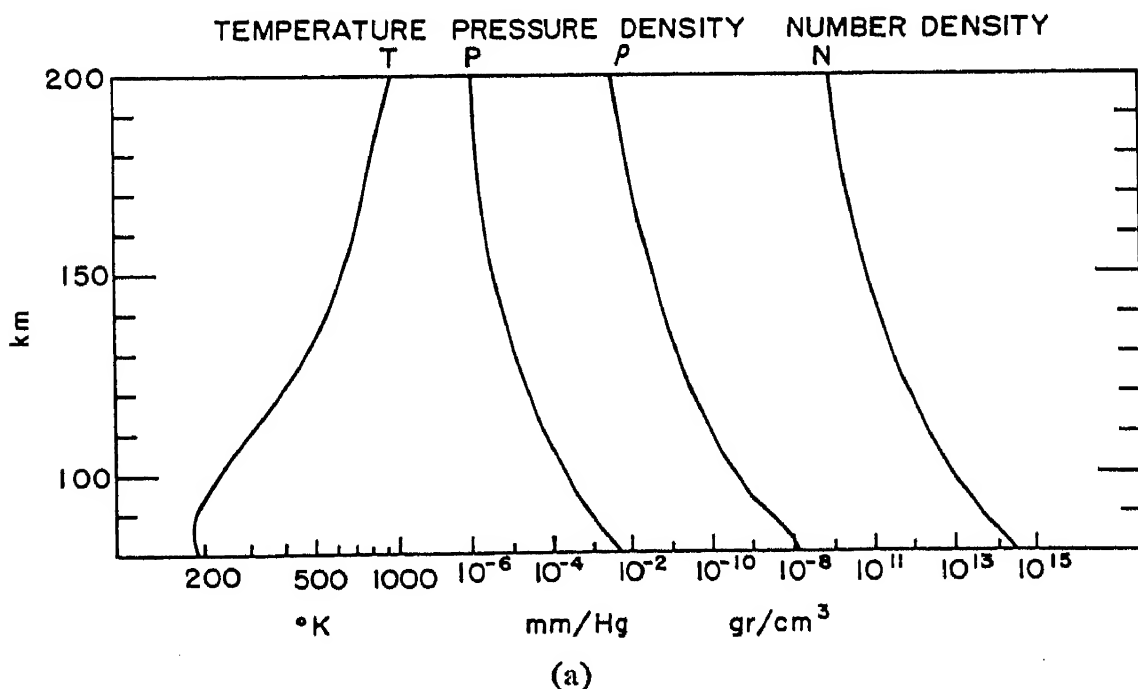
Let the northward component of the geomagnetic variation due to the external field caused by the solar equatorial electrojet be  $\Delta X$ . Then  $I_y$  can be approximated by  $\Delta X/2\pi$ .  $\Delta X$  is approximately equal to about  $\frac{2}{3}$  of the daily amplitude of  $H$ . When  $\Delta X$  is taken to be  $100 \gamma (=10^{-3}$  gauss),  $I_y$  becomes  $1.6 \times 10^{-4}$  e.m.u. or  $1.6 \times 10^{-3}$  amp. If the width of the equatorial electrojet zone is about 700 km as given by Knecht and McDuffie in their article in this book, the total intensity of the jet in the entire magnetic equatorial zone becomes  $111 \times 10^3$  amp. Here  $1.0 \times 10^5$  to  $1.5 \times 10^5$  amp may be a reasonable value of the total current intensity. Putting the above value of  $I_y$  into equation (2.1) leads to an evaluation of  $W$ , although the value of  $W$  also depends on an estimation of  $\nu_r$  and  $\omega_r$  in equation (2.2). A few meters per second seems to be a proper value of vertical drifts of the positive ions. In addition, the eastward component of the electric field,  $E_y$ , is approximately equal to  $I_y/\Sigma_3$ . Taking  $\Sigma_3 = 10^{-7}$  e.m.u. leads to  $E_y \simeq 1.6 \times 10^3$  e.m.u. (see Fig. 8). It should be noticed that this  $E_y$  on the magnetic equator is the electrostatic field.

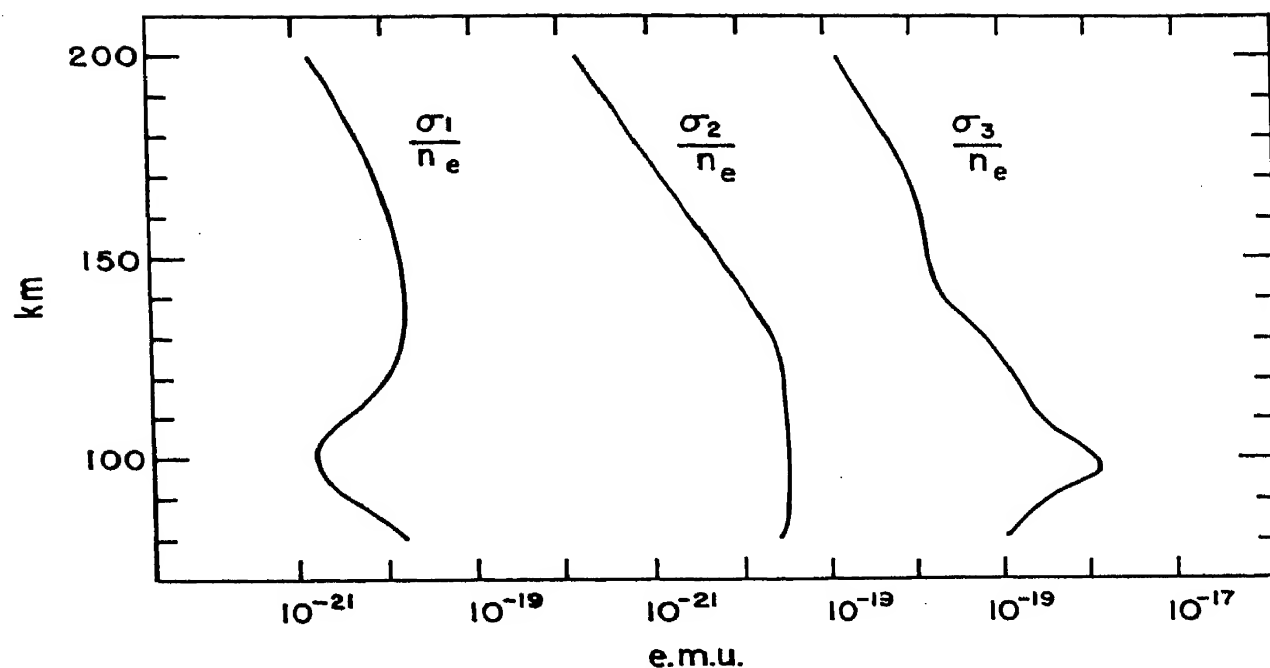
$I_y$  is the eastward current intensity per  $\text{cm}^2$  per column,  $h$  cm, which is the thickness of the jet flowing layer. If  $I_y/h$  is due to the westward horizontal motion of electrons having a number density per  $\text{cm}^3$  of  $N$ , neglecting the eastward motion of positive ions, the westward speed of electrons is 500 m/s assuming  $N$  is  $10^5$  and  $h$  is  $2 \times 10^6$  cm. This velocity compares favorably with the radio-determined westward movement of the  $E_s$ - $q$  with a speed of about 750 m/s, which has been observed by Bowles and Cohen (see their article in this book). If this value of the electron speed and the same values of  $I_y$  and  $N$  as above are taken,  $h$  becomes about 13 km, which is a reasonable thickness of the layer. Thus, what Bowles and Cohen have observed may be westward motions of electron clouds responsible for the electrojet, although they interpret it as a wave motion. Zmuda (1960) reached a conclusion similar to the present one. An overall model of the  $E_s$ - $q$  may now be estimated as follows:

- (1)  $I_y$  is produced by the eastward electrostatic field and the height-integrated Cowling conductivity.
- (2)  $W$  due to  $I_y$  causes irregularities in the density of charged particles in the electrojet.
- (3) These density irregularities of electrons move westward with other electrons at approximately the same speed, a few hundred meters per second.
- (4) This westward motion of electron irregularities and other electrons is the major part of the electrojet itself.
- (5) The  $E_s$ - $q$  on ionograms is due to radio echoes scattered by the irregularities in the jet.
- (6) Thus the  $E_s$ - $q$  has a close correlation with  $I_y$ .

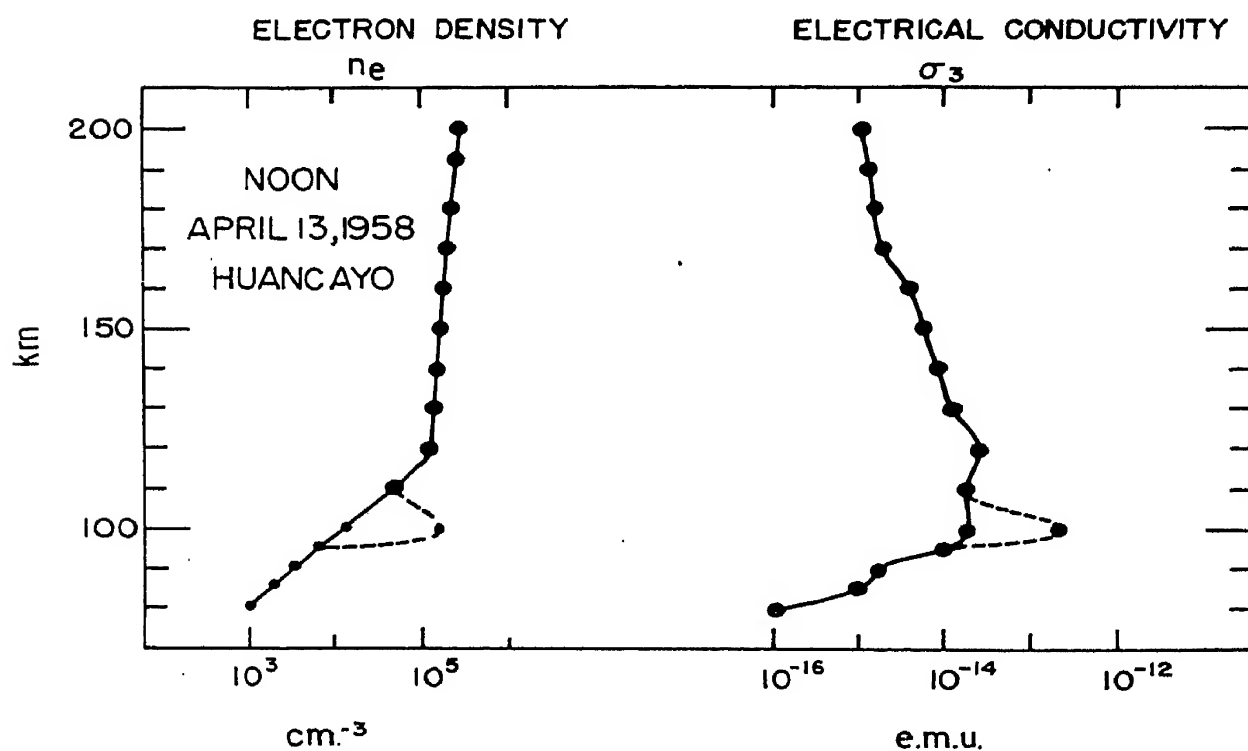
Since the solar equatorial electrojet shows a remarkable variation with season and solar activity, as is seen in Fig. 3, it can be expected from the above conclusion that the  $E_s$ - $q$  should also show similar variations with season and solar activity. This will be found only when a more quantitatively meaningful  $E_s$ - $q$  parameter is available. Simple statistics of the occurrence frequency of  $f_oE_s$ - $q$  can be misleading: this may be the reason why Chadwick (see his article in this book) did not obtain a correlation of the  $E_s$ - $q$  with the solar activity. Also, longitudinal inequality of the width and intensity of the  $E_s$ - $q$  belt should be studied in the future, because the intensity of the equatorial electrojet is not the same at different longitudes: during the IGY the jet intensity in South America (Huancayo) was slightly larger than that in the Pacific area (Koror and Jarvis Is.) and Africa (Addis Ababa and Ibadan).

In addition, the possibility of double layers of the electrojet should be mentioned because of Cahill's rocket observations (1959) of current peaks at altitudes of about 100 and 120 km. Figure 6a indicates estimated height distributions of temperature, pressure, density and number density (per  $\text{cm}^3$ ) of the atmosphere based on rocket observations. Using these values, height distributions of Pedersen, Hall and Cowling conductivities,  $\sigma_1$ ,  $\sigma_2$ , and  $\sigma_3$ , divided by electron number density, are obtained as shown in Fig. 6b. Huancayo vertical-incidence ionogram data obtained at noon on a quiet day (April 13, 1958) in an equinoctial period, are used for an estimation of the electron density distribution with height and are indicated by large dots in the left diagram of Fig. 6c: the density distribution lower than 110 km is based on an assumption and indicated by small dots in the diagram. Then a height distribution of  $\sigma_3$  can be obtained as is shown in the right diagram of Fig. 6c: two peaks at 100 and 120 km can be seen.





(b)



(c)

Fig. 6. (a) Estimated height distributions of temperature in  $^{\circ}\text{K}$ , pressure in mm/Hg, density in  $\text{gr}/\text{cm}^3$ , and number density per  $\text{cm}^3$  of the atmosphere based on rocket observations. (b) Height distributions of Pedersen, Hall, and Cowling conductivities,  $\sigma_1$ ,  $\sigma_2$ , and  $\sigma_3$ , divided by electron number density. (c) Left diagram indicates electron density distribution with height at noon on a typical quiet day in equinoctial season, April 13, 1958 (large dots). Small dots and a dotted curve show estimated density distributions. Right diagram represents a height distribution of Cowling conductivity,  $\sigma_3$ . Two peaks at 100 and 120 km can be seen.

If the electron density has a peak at about 100 km based on the already mentioned estimation of the  $E_s$ - $q$ ,  $\sigma_3$  shows a large peak at this height. This is indicated by dotted curves in Fig. 6c and seems to be more plausible. In fact, total  $\sigma_3$  integrated in this peaked layer,  $\Sigma_3$ , becomes about  $10^{-7}$  e.m.u. The main electrojet may be flowing in this layer. In the layer of a small peak of  $\sigma_3$ , at about 120 km height, it is possible for a weak jet current or a return current of the main jet to flow. The slant  $E_s$  in the equatorial zone (Smith 1957) might be due to a radio reflection mechanism among irregularities in these two layers (Cohen, Bowles and Calvert 1962). However, more observations of the jet layer by rocket are essential to support this argument of double jet layers.

### 3. $E_s$ IN THE TEMPERATE LATITUDES AND THE $S_q$ CURRENT SYSTEM

Heisler and Whitehead (1960a) recently suggested that the occurrence frequency of  $f_oE_s$  exceeding 5 Mc/s depends on the horizontal component of the earth's main magnetic field for stations situated in temperate latitudes; the occurrence frequency increases as the horizontal component increases. Based on this statistical result, Whitehead (1960, 1961) has given a theory of the formation of  $E_s$  in temperate latitudes. However, as can be seen in Fig. 7, the distribution of the occurrence frequency exceeding 5 Mc/s with respect to the horizontal component is not particularly better than that with the geomagnetic latitude. Moreover the distribution with respect to  $(0.65 - |B_z|)B_H$ , where  $B_z$  and  $B_H$  are the vertical and horizontal components of the earth's main magnetic field, seems to be better than others in Fig. 7; this may indicate that the  $E_s$  in temperate latitudes depends not only on  $B_H$  but also on  $B_z$ . However, the difference involved among the four diagrams in Fig. 7 is not very striking. This kind of statistical study is not really very strong evidence for the theory of the  $E_s$  formation that Whitehead puts forward.

Much more important evidence of  $E_s$  formation in temperate latitudes can be obtained from the lunar tidal variations of  $E_s$  in this zone. As is mentioned in my other article in this book,  $E_s$  shows obvious lunar variations in spite of a very small lunar effect in the  $E$ -layer. The main cause of the lunar variation in the ionosphere seems to be the vertical drift motions of charged particles resulting from a coupling of  $B_H$  and the horizontal electric fields caused by the lunar dynamo effect. Then the mechanism of formation of the  $E_s$ , whatever it is, should be very easily affected by the above mentioned vertical drift motions of charged particles. One possibility which satisfies this condition is that the  $E_s$  itself is formed by vertical drift motions of charged particles caused by other phenomena: probably wind shears, as suggested by Storey (private communication),

Dungey (1959), Whitehead (1960, 1961) and others. Artificially generated sodium clouds by rockets in the upper atmosphere indicate a strong vertical wind shear (vertical gradient in horizontal winds), typical speed gradients with height being 50 to 110 m/s per km at the level 104 to 109 km (Manring, Bedinger, Pettit and Moore 1959). Also, internal atmospheric gravity waves suggested by Hines (1960) may be a cause of the wind shear. Thus we may assume that strong vertical wind shears occur frequently at the level of the  $E_s$ .

Occurrence of  $fE_s > 5$  Mc/s, 0600-1800  
local time during equinoxes, 1948-1954,  
on different abscissae

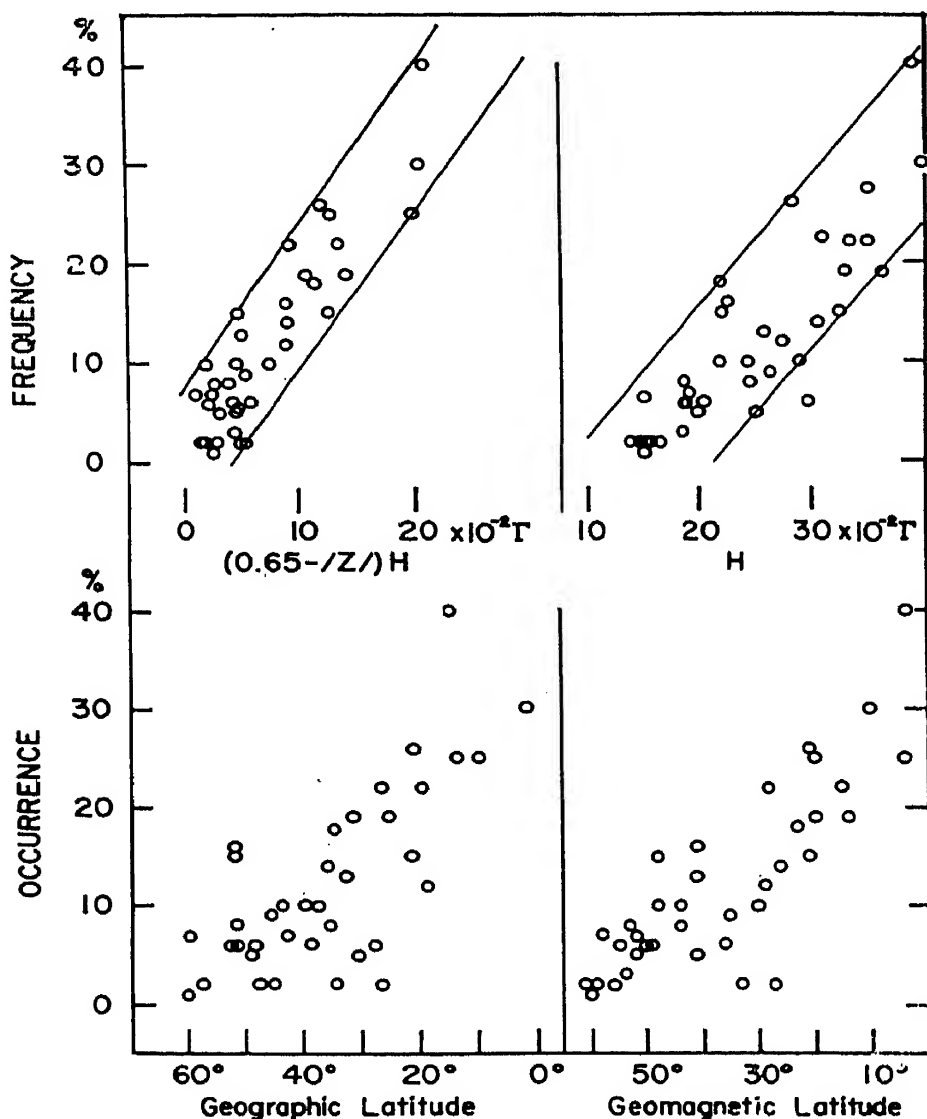


Fig. 7. Occurrence frequencies of  $f_oE_s$  exceeding 5 Mc/s in the day-time during equinoxes, 1948-1954 obtained by Smith (1957) are plotted with respect to four different abscissae: geographic and geomagnetic latitudes,  $B_H$ , and  $(0.65 - |B_z|) B_H$ , where  $B_H$  and  $B_z$  are the horizontal and vertical components of the earth's main magnetic field.  $0.65 - |B_z|$  is adopted in order to have a larger value in a lower latitude, where 0.65 is an approximate value of  $|B_z|$  at the magnetic north pole.  $H$  and  $Z$  in the figure should be read as  $B_H$  and  $B_z$ .

The wind shears produce electric fields due to the dynamo effect with the vertical component of the earth's main magnetic field,  $B_z$ . These horizontal electric fields and the horizontal component of the earth's main magnetic field,  $B_H$ , cause vertical drift motions of charged particles. Thus, the vertical drift motions are affected by both  $B_z$  and  $B_H$ , and if the  $E_s$  is due to these vertical drift motions, it is certainly influenced by both  $B_z$  and  $B_H$ .

Let the southward and eastward components of the electric fields be  $E_x$  and  $E_y$ , respectively. We assume that there is no vertical electric current. Then the vertical upward drift speed of electrons and ions,  $W$ , in moderate latitudes (Hirono 1953) can be represented by

$$W = -\cot \phi (e/m_i) \{ \nu_i / (\nu_i^2 + \omega_i^2) \} E_x + (q_i + q_e p_i / p_e) E_y. \quad (3.1)$$

All notations are the same as those in equations (2.1) and (2.2). At altitudes lower than about 120 km, the second term of the right side of equation (3.1) is much smaller than the first term. Thus we have

$$W = -\cot \phi (e/m_i) \{ \nu_i / (\nu_i^2 + \omega_i^2) \} E_x. \quad (3.2)$$

$E_x$  is the sum of  $V_y \times B_z$  and  $X$ , where  $V_y$  is the eastward horizontal wind speed, and  $X$  the southward component of the electrostatic field. If we ignore  $X$ , equation (3.2) becomes the same equation as Whitehead (1961) obtained. However,  $X$  cannot generally be neglected. Moreover, by including  $X$ , we can apply the same equation (3.2) to tidal effects of  $E_s$ .

If the horizontal wind is a shear,  $E_x$  (hence  $W$ ) has a sharp gradient with height. Then  $W$  can be represented by

$$W = W_0 e^{-\Gamma z} \sim W_0 (1 - \Gamma z), \quad \Gamma \ll 1$$

or

$$W = -W_0 \sin 2\pi z / \Gamma'.$$

The former equation has been treated by Matsushita (1962a) and the latter by Whitehead (1961; also his article in this book). In both cases, at a level where the upward decreasing  $W$  becomes zero an ionized layer, in which the electron density is three to ten times that in the normal  $E$  and the thickness is 300 to 1000 m, is obtained from these equations. This agrees with rocket observations of  $E_s$  (see Seddon's article in this book). Thus the main part of the  $E_s$  in temperate latitudes may be due to the drift motions caused by wind shears. Also it is possible by this mechanism of  $E_s$  formation to see that the lunar current would cause obvious lunar tidal variations in the  $E_s$ , as is mentioned in my other article in this book.

If the above estimation is correct, the  $S_q$  current system, such as shown in Fig. 1, should also cause a large effect of the  $E_s$  variation. The vertical upward drift speed caused by the  $S_q$  current system can also be deduced from equation (3.2), in which  $E_x$  may play an important rôle in the daily



variation of the drift speed. Fig. 8 is a distribution of the total electric field for the  $S_q$  current system in equinoctial months which was obtained by Maeda (1955). In the northern hemisphere the southward component begins to increase at about 17 00 hr in lower temperate latitudes and becomes negative at about 15 00 hr in higher latitudes, as can be seen in Fig. 8. Thus we can expect in the afternoon an increase of  $E_s$  in lower temperate latitudes and a decrease of the  $E_s$  ionization in higher temperate latitudes. This should hold in any season. A weak but positive evidence of the effect is indicated in Fig. 9; the lines in this figure show differences between

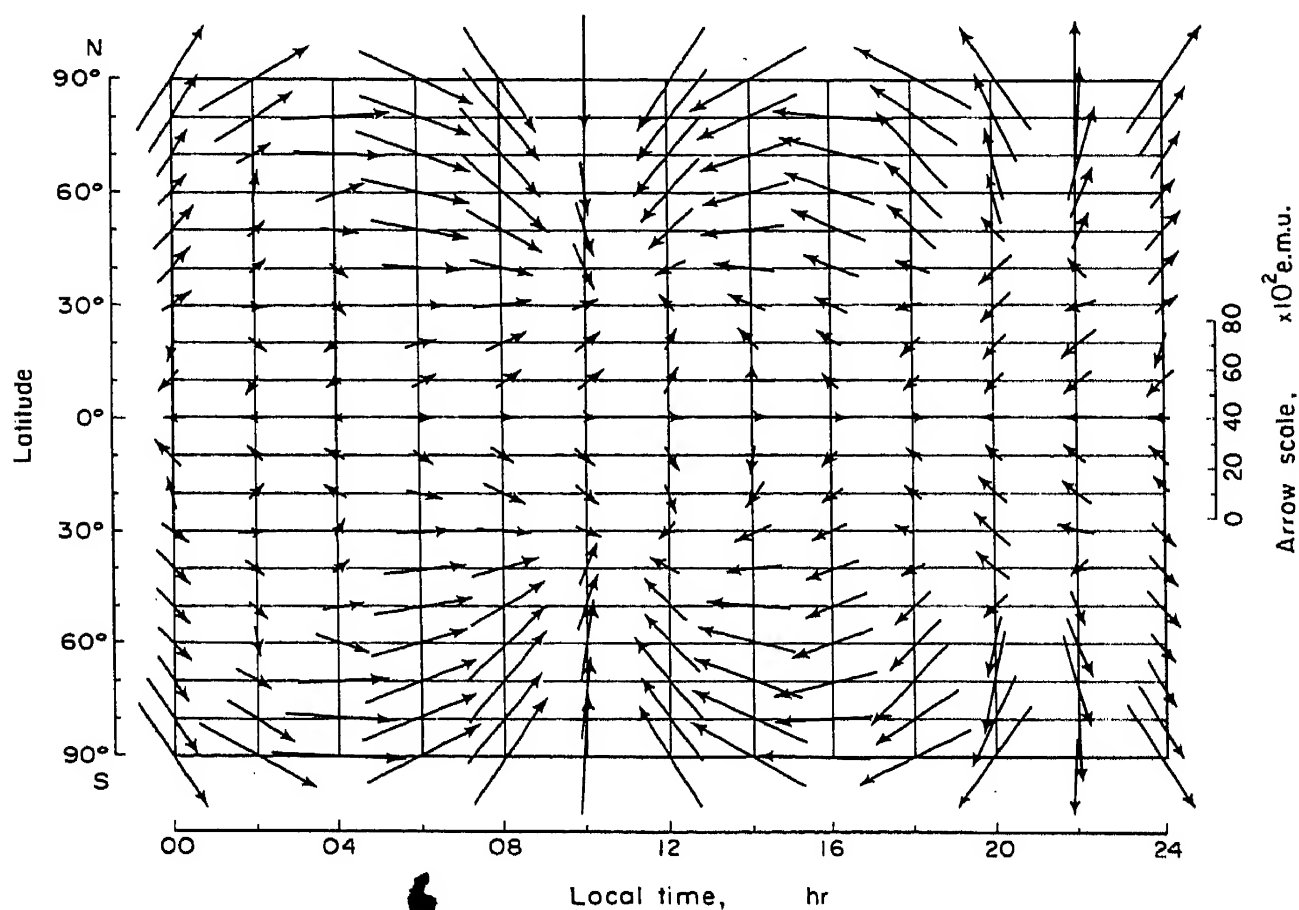


Fig. 8. Distribution of the total electric field for the  $S_q$  current system in equinoctial months (Maeda 1955).

monthly median hourly values of  $f_oE_s$  and those of  $f_oE$ , which have been obtained to show deviations of the daily variation of  $f_oE_s$  from that of  $f_oE$ . Since distributions of the occurrence of wind shears are not yet well-known, further studies of the effects of the  $S_q$  current on the  $E_s$  are not easy to make at the present stage.

Bibl (1960) obtained a correlation between an increase of  $E_s$  ionization and a rise of the  $F$  height. The vertical upward drift speed of charged particles in the  $F$ -region,  $W_F$ , can be represented by

$$W_F = (E_y^s/B) \cos \phi, \quad (3.3)$$

$B$  is the earth's main magnetic field,  $\phi$  is the magnetic dip angle,  $E_y^s$  is the eastward component of the electrostatic field which is formed at about 100 km altitude (see Matsushita 1962a). Thus  $E_y^s$  causes a rise in  $F$  height, and  $E_x$  causes an increase of  $E_s$  ionization as was already discussed (see equation (3.2)). Then the correlation obtained by Bibl can be explained if large  $E_y^s$  and  $E_x$  are both formed at about 100 km altitude. This is quite probable: for example, a large south-eastward electrostatic field due to winds or disturbed currents satisfies this condition. Bowman (1960) and Heisler and Whitehead (1960) reported an association between ionospheric travelling disturbances and  $E_s$  ionization. Thomas and Whitehead (1960) mention the association in their articles in this book. There is no

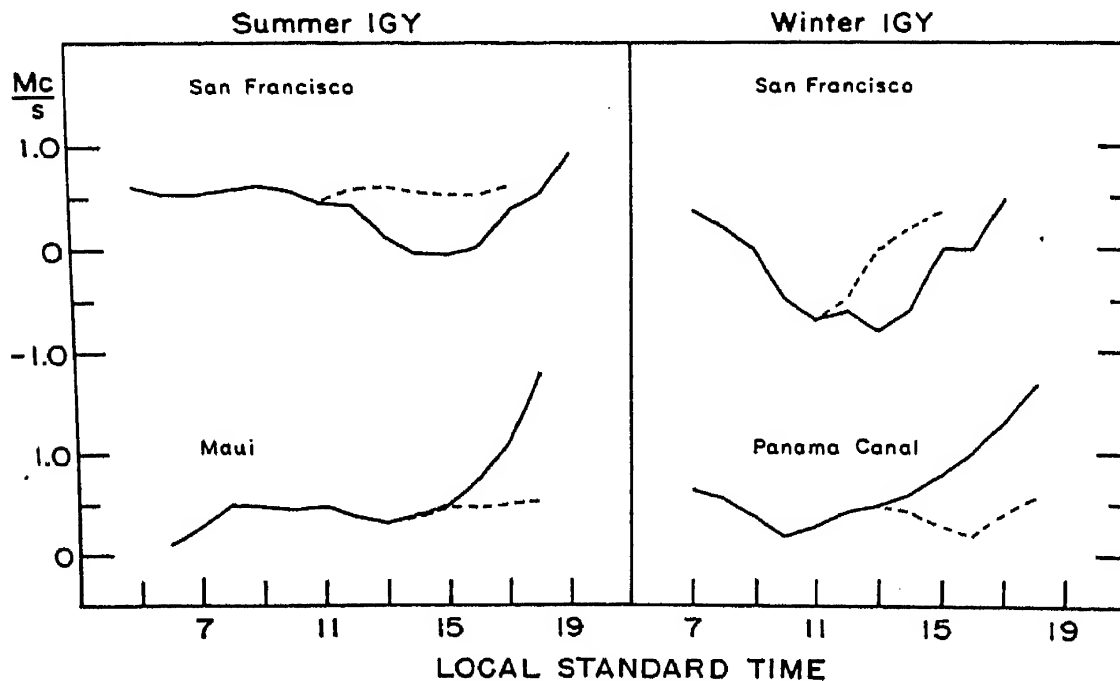


Fig. 9. Average of differences between monthly median hourly values of  $f_oE_s$  and those of  $f_oE$  in lower (Maui and Panama Canal) and higher (San Francisco) temperate latitudes in summer (left) and winter months (right) during the IGY. Dotted lines show symmetrical variations before and after 11 00 hr for San Francisco and before and after 13 00 hr for Maui and Panama Canal, at which times the eastward component of the total electric field becomes nearly zero.

It is noted that this association indicates descending (and sometimes ascending) ionization along the geomagnetic lines of force during ionospheric disturbances. The  $E_s$  structure formed by this mechanism seems to be a partially ionized cloud. This phenomenon is similar to the long lasting sequence of  $E_s$  which occurs frequently in temperate latitudes on quiet days, although its starting level and travelling times are different (Matsushita 1962a). All these seem to be either simple travellings of excess charges along

geomagnetic lines of force or drift motions along field lines. In the latter case the downward drift speed along field lines in the  $F$ -region is given by  $-(E_y^s/B) \cos \phi \cos(90^\circ - \phi)$  from equation (3.3), and the upward drift speed along field lines in the  $E$ -region is by  $-(e/m_i) \{v_i/(\nu_i^2 + \omega_i^2)\} E_x \cot \phi \cos(90^\circ - \phi)$  from equation (3.2). If  $E_y^s$  has a negative value, then a large westward electrostatic field is affected in the  $F$ -region, a downward drift along field lines from the  $F$ -region may occur. If the equator-ward electric field has an unusually large value in the  $E$ -region during storms an ascending ionization along field lines from the  $E$ -region might occur. Long lasting sequential  $E_s$  on quiet days begins to descend from 150–200 km altitude. A downward drift speed along field lines from this height is influenced by poleward and westward electrostatic field (see equation (3.1)). Due to the  $S_q$  dynamo effect, large poleward electrostatic fields are formed in the morning at lower temperate latitudes and large westward electrostatic fields are formed in the afternoon at higher temperate latitudes (see Fig. 4b, Maeda 1955). Thus a descending ionization along field lines may occur in the morning at lower temperate and in the afternoon at higher temperate latitudes. This agrees with the latitudinal distribution of beginning times of the occurrence of long-lasting sequential  $E_s$ , which has been obtained by Matsushita (1955). Even if the motion of sequential  $E_s$  is vertical instead of along field lines, the basic argument remains the same. However, another type of sequential  $E_s$ , which appears in the early morning and in the evening and lasts less than three hours, may be caused by a height variation of wind shear region due to sunrise and sunset. During storms a rapidly travelling sequential  $E_s$  occasionally appears; this can be due to hydromagnetic waves propagated along field lines, as Akasofu (1956) suggested.

Solar flares occasionally seem to cause a slight increase in  $f_oE_s$ . There are two possible explanation for this; one is that an increase of the intensity of the solar radiation responsible for the ionization of the  $E$ -level occurs, such as the solar X-rays, and the other is that a drift effect is created due to the flare current system, such as was obtained by Veldkamp and Van Sabben (1960).

Thus an overall model of the  $E_s$  in temperate latitudes is as follows:

- (1) A vertical gradient in horizontal winds (vertical wind shears) causes a sharp height gradient of vertical upward drift speeds of charged particles.
- (2) The above drift causes the formation of a thin patchy layer which is the predominant  $E_s$  in temperate latitudes.
- (3) Apparent horizontal (sometimes vertical) motions of the  $E_s$ , such as reported by Matsushita (1949) and by Dueño and Egan and Peterson in this book, may be mainly due to horizontal (sometimes vertical) change of wind shear region. As long as proper wind shears

exist, the  $E_s$  does not disappear; but once the shear ceases, the  $E_s$  soon decays.

- (4) A thick  $E_s$  cloud is occasionally formed by descending ionization from the upper ionosphere.
- (5) One cause of the descending ionization is the electrostatic field of the  $S_q$  current, as can be estimated for long-lasting sequential  $E_s$ .
- (6) Meteor bombardments and thunderstorm effects are ignored here, since they are apparently small.

#### 4. $E_s$ IN HIGH LATITUDES AND ELECTRIC CURRENTS DURING BAY DISTURBANCES AND GEOMAGNETIC STORMS

As shown in Fig. 10,  $f_oE_s$  monthly median values at night increase at latitudes higher than about geomagnetic  $60^\circ\text{N}$ , and reach a maximum at about  $69^\circ\text{N}$ , although  $f_oE_s$  in the daytime does not show such a distribution (Matsushita 1953, 1959). In fact, night- $E$  and special types of  $E_s$  which are named "auroral", "slant" and "retardation"  $E_s$  often appear at night in auroral latitudes (Penndorf and Coroniti 1958; also Leighton, Shapley and Smith for  $E_s$  and King for night- $E$  in this book). Correlations among auroras, geomagnetic disturbances and these types of  $E_s$  were studied by several workers (for example, Heppner, Byrne and Belon 1952, Heppner 1954, Knecht 1956; also see Thomas and Smith 1959). Using vertical incidence ionograms and magnetograms, both of which were obtained at College, Alaska, ( $64.9^\circ\text{N}$ ,  $147.8^\circ\text{W}$ ; gm. lat.  $64.5^\circ\text{N}$ ), during the period of one year starting from March 1955, Matsushita (1958, 1959) found a close correlation between  $E_s$  and geomagnetic bay disturbances.

The bay disturbance is one of the most remarkable geomagnetic phenomena in auroral latitudes, because it occurs there more frequently and with greater intensity than elsewhere. Large but patchy bays in auroral latitudes often occur at night, most frequently between 01 00 to 03 00 hr local time, even on small geomagnetic  $Ap$ -index days, particularly in equinoctial months. Average occurrence frequency of bays at College during equinoctial months is about 30 per cent (approximately 10 nights in a month) for negative bays, and about 15 per cent for positive bays. The time of change-over from positive bay to negative bay occurs between 22 00 and 23 00 hr local time, that is, approximately at geomagnetic midnight.\* The same time of change-over has recently been obtained in the southern hemisphere (Robertson 1960). These results suggest that the ionospheric current in auroral latitudes, which is responsible for the bay, flows eastward (hence

---

\* The term "geomagnetic midnight" was first introduced by Vegard (1917). Convenient diagrams for its calculation were obtained by McNish (1936) and Sugiura (1956).

causing positive bays) until geomagnetic midnight and westward (hence negative bays) after that time. This is illustrated in the top diagram of Fig. 12 and is consistent with observations of longitudinal motion of the aurora associated with bays (Nichols 1959, Davis 1960; also see Table 2 in Bond 1960), as is discussed later. Leakage currents of these main currents

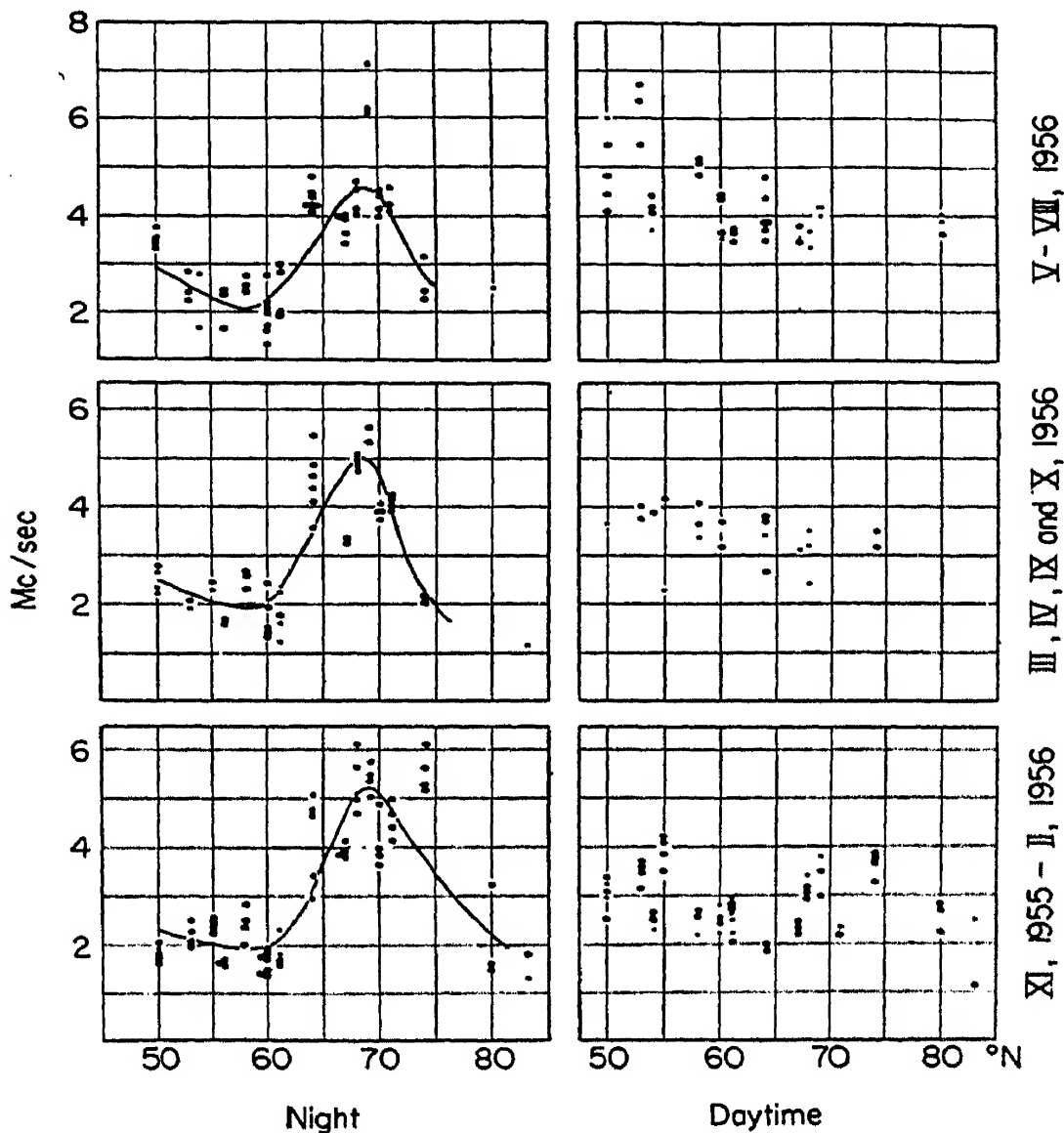


Fig. 10.  $f_oE_s$  distributions on geomagnetic latitudes at night (mean of monthly median values from 22 00 to 02 00 hr local time) and in the daylight hours (mean values from 1000 to 1400 hr) during three seasons. Small dots express less reliability than large dots (Matsushita 1959).

flow partly in middle latitudes and the polar cap. It should be emphasized here that the bay current system is formed in patchy distribution (Fukushima 1949).

Typical examples of ionospheric variations associated with bays at College are shown in Fig. 11. As can be seen in this figure,  $f_oE_s$  and  $f$ -min- $F$  (minimum radio frequency reflected by the  $F$ -region, perhaps a better

measure of  $E_s$  electron density) generally begin to increase at the onset of bay disturbances. At this initial stage, geomagnetic micropulsations are often associated with bays, and  $E_s$  is of the flat or retardation type (Campbell and Matsushita 1962). Following the increase of disturbances,  $f_oE_s$  further increases until the absorption in the  $D$ -region becomes very severe. At this stage auroral type of  $E_s$  and night- $E$  often occur. It can be assumed

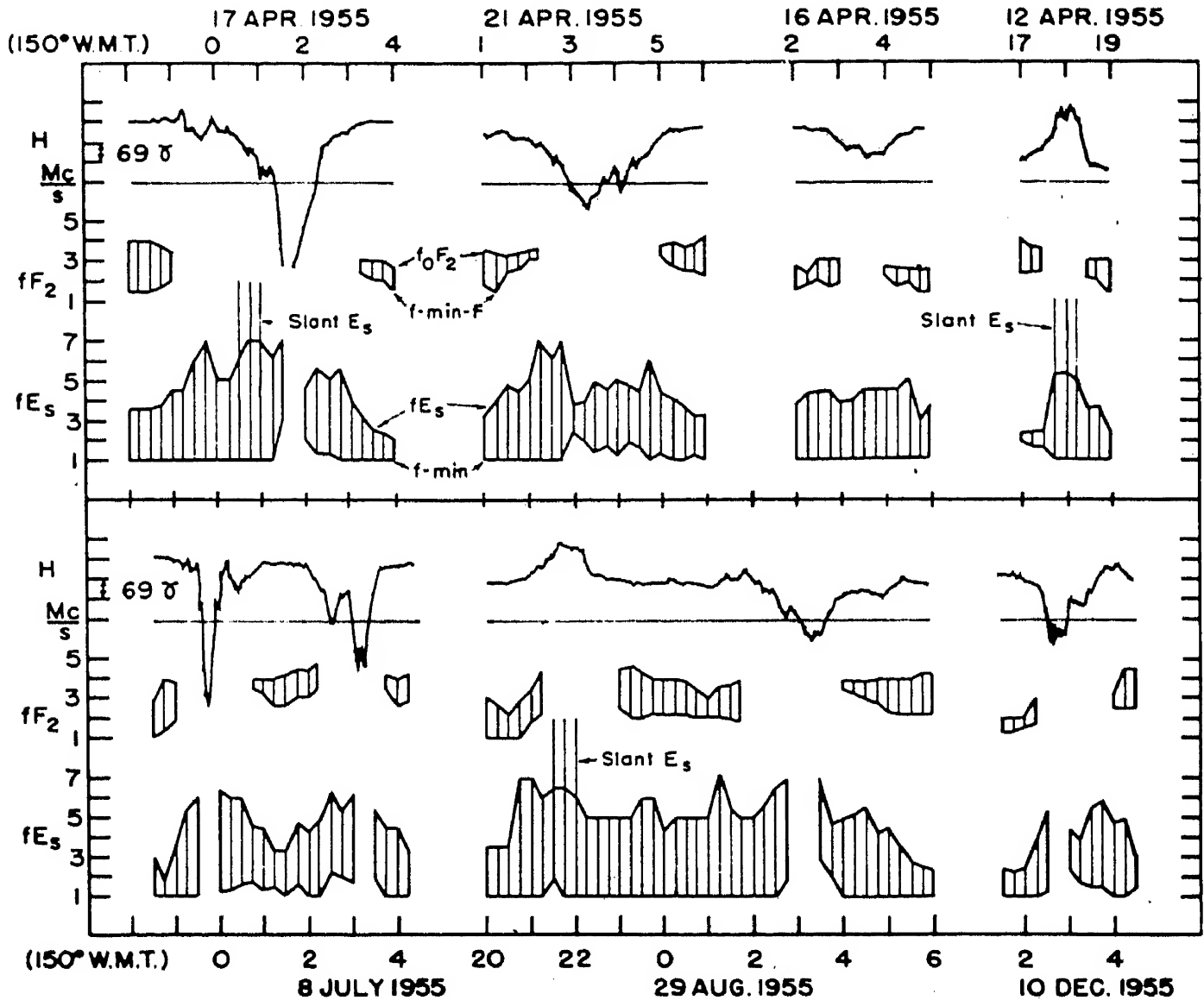


Fig. 11. Variations of  $f_oF_2$ ,  $f_{\min}-F$ ,  $f_oE_s$  and  $f_{\min}$ , every 15 minutes, and geomagnetic horizontal variations at College, Alaska, are compared on a common time scale. Complete blanketing of the  $F$ -region by the  $E_s$ , increase of  $E_s$  echo and  $f_{\min}$ , and occurrences of the slant  $E_s$  and blackout are associated with geomagnetic bays; these different variations consistently depend on the magnitude of the bay disturbance (Matsushita 1958).

that auroral type of  $E_s$  is formed by field-aligned clouds and retardation type of  $E_s$  is a thick ionized layer and that night- $E$  is a thicker layer than retardation type of  $E_s$ . Complete blanketing of the  $F$ -region by strong  $E_s$  and night- $E$  echoes almost always occurs when the range of the horizontal

component of the bay is moderate, namely, 100–200  $\gamma$  on internationally quiet days ( $Ap < 16$ ) and 200–300  $\gamma$  on disturbed days ( $Ap \geq 16$ ) for the positive bay, and about  $-200 \gamma$  (quiet days) and  $-300$  to  $-400 \gamma$  (disturbed days) for the negative bay. Since this intensity of bay most frequently occurs at night in auroral latitudes, the monthly median values of  $f_oE_s$  at night show large values: this can be seen on the distribution of  $f_oE_s$  at night in Fig. 10. When the range of the bay is larger than the above values, a blackout usually occurs near the maximum disturbance of the bay after an initial period of complete blanketing of the  $F$ -region, as is shown in Fig. 11. Matsushita (1958) called this a “gradual blackout”, as compared to another type of blackout named “sudden blackout”, which is mentioned later.

The ionospheric variations associated with moderate bays can be explained by the penetration of charged particles down to the level of about 100 km altitude, which causes the bay current systems and the  $E_s$  and night- $E$  ionization. Around the maximum disturbance of severe bays these particles and Bremsstrahlung X-rays penetrate deeply into the  $D$ -region and cause blackouts. Increased amount of ionization during the blackout can be roughly estimated by the following equation which represents the nondeviative absorption of the ordinary component of radio waves:

$$\int K \, dS \simeq \frac{1.17 \times 10^{-14}}{(f + f_L)^2} \int N_\nu \, dS,$$

where  $\int K \, dS$  is the absorption in decibels along the path through a stratum of  $S$ ,  $N$  is electron number density per  $\text{cm}^3$ ,  $\nu$  is the effective electron collision frequency per second, and  $f$  and  $f_L$  are the exploring radio frequency and longitudinal gyromagnetic frequency expressed in Mc/s. The calculated result indicates 10 to 100 times normal ionization assuming  $\nu$  does not change (Matsushita 1958). Accordingly, the electric conductivity may increase to the order of 10 times normal during blackouts.

In order to explain the bay current system and a similar system for the geomagnetic disturbance daily variations,  $D_s$  or  $S_D$ , a dynamo effect due to the increase of conductivity was studied by many workers (for example, Fukushima 1949, Matsushita 1953a, Obayashi and Jacobs 1957). However, these authors needed to assume an exceptionally enhanced conductivity. The wind system responsible for the bay and  $D_s$  disturbances, assuming a reasonable conductivity, was also studied by several workers, such as Vestine (1954), Maeda (1957) and Cole (1960). However, it is rather difficult to assume that the required wind system, which is quite different from that for the  $S_q$  field, can be easily set up, although a change of wind velocity may occur during disturbances. Bless, Gartlein, Kimball and Sprague (1959) suggested that instead of any dynamo action the bay might be caused by atmospheric winds operating on ionized particles

produced by incoming 50-keV solar protons. This suggestion was supported by Bernard (1960). However, as was pointed out by Cole and Bond (1961), these workers forgot to take into consideration the effect of electric polarization fields. Duncan (1960) unfortunately misinterpreted the bay current system, suggesting that protons and electrons cause counter clockwise and clockwise current loops, respectively.

The most plausible explanation of the bay current system seems to be that, in addition to increased conductivity, it is due to effects of longitudinal electrostatic fields caused by protons and electrons. Let the subscripts *x* and *y* indicate southward and eastward components respectively. Relations among the current intensity, *I*, electric field, *E*, and electric conductivity,  $\Sigma$ , all of which are height-integrated, are given by

$$I_x = \Sigma_{xx}E_x + \Sigma_{xy}E_y$$

$$I_y = \Sigma_{yx}E_x + \Sigma_{yy}E_y,$$

where  $\Sigma_{ij}$  is a tensor component of the height-integrated conductivity. In the low ionosphere at high latitudes,  $\Sigma_{xx} = \Sigma_1/\sin^2 \phi \simeq \Sigma_1$ ,  $\Sigma_{yy} = \Sigma_1$ , and  $\Sigma_{xy} = -\Sigma_{yx} = \Sigma_2/\sin \phi$ , where  $\phi$  is the magnetic dip angle, and  $\Sigma_1$  and  $\Sigma_2$  are height-integrated Pedersen and Hall conductivities. Then the eastward current intensity can be shown by  $I_y = -\Sigma_2 E_x/\sin \phi + \Sigma_1 E_y$ . Since  $|\sin \phi| \simeq 1$  and  $\Sigma_2 \gg \Sigma_1$  in auroral latitudes,

$$I_y \simeq -\Sigma_2 E_{x'}, \quad (4.1)$$

where  $E_{x'}$  is the equatorward electric field. In the same way as was discussed concerning the equatorial electrojet in Section 2,  $I_y$  can be approximated by  $\Delta X/2\pi$ , where  $\Delta X$  is the northward component of the geomagnetic variation due to the external field caused by the bay current. When  $\Delta X$  is taken to be  $-400 \gamma$  for a common negative bay accompanied by a blackout,  $I_y$  is  $-6.4 \times 10^{-4}$  e.m.u. or  $-6.4 \times 10^{-3}$  amp (the negative sign indicates a westward current). If this current flows in an area of 1000 km width, the total current becomes  $6.4 \times 10^5$  amp, which is a reasonable value. Then the product of the thickness of the current layer in cm and the speed of electrons in cm/sec becomes  $4 \times 10^{11}$ , assuming the average electron number density per  $\text{cm}^3$  is  $10^5$ . When the thickness of the layer is taken to be 40 km, the speed of electrons is 1 km/sec. If the average electron number density per  $\text{cm}^3$  is  $10^6$  and the thickness of the layer is 40 km, the speed of electrons decreases to 100 m/sec. These speeds agree well with observations of longitudinal motion of the aurora associated with bays (see Table 2 in Bond 1960). If  $\Sigma_2$  in equation (4.1) is 10 times normal,  $\Sigma_2 = (1.5 \times 10^{-8}) \times 10$  e.m.u. Putting these values of  $\Sigma_2$  and  $I_y$  in equation (4.1) gives

$$E_{x'} = 4.3 \times 10^3 \text{ e.m.u.}$$



If  $\Sigma_2$  is 100 times normal,  $E_{x'}$  decreases to  $4.3 \times 10^2$  e.m.u. In any case, we need an equatorward electric field in order to explain the negative bay which often occurs after geomagnetic midnight whether or not it is accompanied by a blackout. As is shown in Fig. 8, the electric field responsible for the  $S_q$  current in auroral latitudes around midnight is poleward; thus a simple increase of  $\Sigma_2$  apparently does not help to explain the negative bay current system unless an unlikely change of wind system is assumed, by which an equatorward electric field may be formed. However, there remains one possibility: if protons impact at higher latitudes than electrons after geomagnetic midnight, the required equatorward electric field can be set up (see Fig. 12). Following the same reasoning, the positive bay, which usually occurs before geomagnetic midnight, requires the poleward electric field (i.e.  $E_{x'}$  has a minus sign). Taking four times the normal  $\Sigma_2$ , based on  $E_s$  increase, and  $\Delta X = 200 \gamma$  in equation (4.1) gives  $E_{x'} = -5.3 \times 10^3$  e.m.u. The  $E_{x'}$  responsible for the  $S_q$  current in auroral latitudes before midnight is poleward, but its intensity is less than required (see Fig. 8). Thus we need an additional poleward electrostatic field: this is satisfied if electrons impact at higher latitudes than protons before geomagnetic midnight. Accordingly, as shown in Fig. 12, what we need is for the electron impact zone to change gradually from high to low latitudes during late evening and early morning and the proton impact zone to change from low to high latitudes. These two zones cross around geomagnetic midnight.

There are several observed results to support the above suggestion. Generally speaking, the electrons seem to be responsible for the  $E_s$  and the protons seem to be responsible for the  $D$ -region absorption or radio blackouts at night, although high-energy electrons and/or X-rays produced from them occasionally may cause radio blackouts. Hagg, Muldrew and Warren (1959) obtained a spiral occurrence of  $E_s$  with respect to local geomagnetic times and latitudes, which is similar to the electron impact zone in Fig. 12. A reversed sense of spiral occurrence of radio blackouts has been obtained by several workers (for example, Thomas and Piggott 1960, Bellchambers and Piggott 1960): this is similar to the proton impact zone in Fig. 12. Thus the formation of longitudinal electrostatic fields seems to be quite plausible. A similar mechanism may apply to the geomagnetic  $D_s$  variation. However, the origin of these charged particles and the cause of the above charge separations are not certain. Shaw (1959) suggested that electrons in the trapping region, which receive additional energy from disturbances on the day-side of the earth, travel around the region until they reach the point where the magnetic flux will no longer reflect them. However, positive particles also must penetrate and a mechanism for receiving additional energy needs to be found, since the bay disturbance occurs without any marked solar phenomena (Matsushita

current can be expected during bays. Fejer (1961) and Axford and Hines (1961) have recently introduced an interesting idea for the explanation of the bay and  $D_s$  current systems; they suggested that these currents are linked with magnetospheric motions. According to the latter authors, a viscous-like interaction between the magnetosphere and an assumed solar wind causes an eastward "driven flow" in the evening zone and a westward "driven flow" in the early morning zone in the outer part of the magnetosphere and reversed flows in the inner part. If this is the case, required electrostatic fields might be formed by these inner reversed flows, and the linked currents between the ionosphere and the magnetosphere suggested by these authors need not necessarily be assumed. In any case, more studies are needed.

Occurrences of blanketing  $F$  by  $E_s$  echoes and of gradual blackouts, associated with positive and negative bays, at College, Alaska, in three seasons are shown in Fig. 13. It is remarkable that bay disturbances occur even on internationally quiet days, particularly in equinoxes. Since geomagnetic storm periods are eliminated from the "disturbance" group, all these phenomena are associated with real bay disturbances (not bay-shaped variations during storms). Occurrence of the blanketing  $F$  indicates an increase of  $E_s$ , hence the electron impact, and occurrence of the blackout associated with negative bays indicates generally the proton impact. However, occasional blackouts associated with negative bays and all blackouts associated with positive bays may be due to high-energy electrons and/or X-rays produced by Bremsstrahlung from them. Thus Fig. 13 indicates that, at College, electrons begin to impact at 16 00–18 00 hr, and reach the maximum at about midnight (sometimes later), and that protons begin to impact at about midnight or slightly earlier, and reach the maximum at different times in different seasons. This is consistent with what is seen in Fig. 12.

In the daytime blackouts often occur suddenly without blanketing by  $E_s$ , both on quiet and disturbed (excluding storm periods) days; this is named "sudden blackout" in this study. These sudden blackouts are not usually accompanied by any remarkable geomagnetic variations. This should not be confused with daytime blackouts during storms which are associated with large geomagnetic variations. The most frequent occurrence of the sudden blackout is around noon on disturbed days, as is shown in Fig. 14. The PCA event (polar cap absorption due to high-energy protons) which occurred on February 23–25, 1956 (Collins, Jelly and Mathews 1961) is excluded from the present statistics. These sudden blackouts may be caused by ionization at a much lower altitude than the normal  $E$ -layer (hence no geomagnetic variations) due to X-rays generated by high-energy electrons (Matsushita 1958) which probably come from the trapped region in the sunlit side. The mechanism of their energy-gain may be due to the

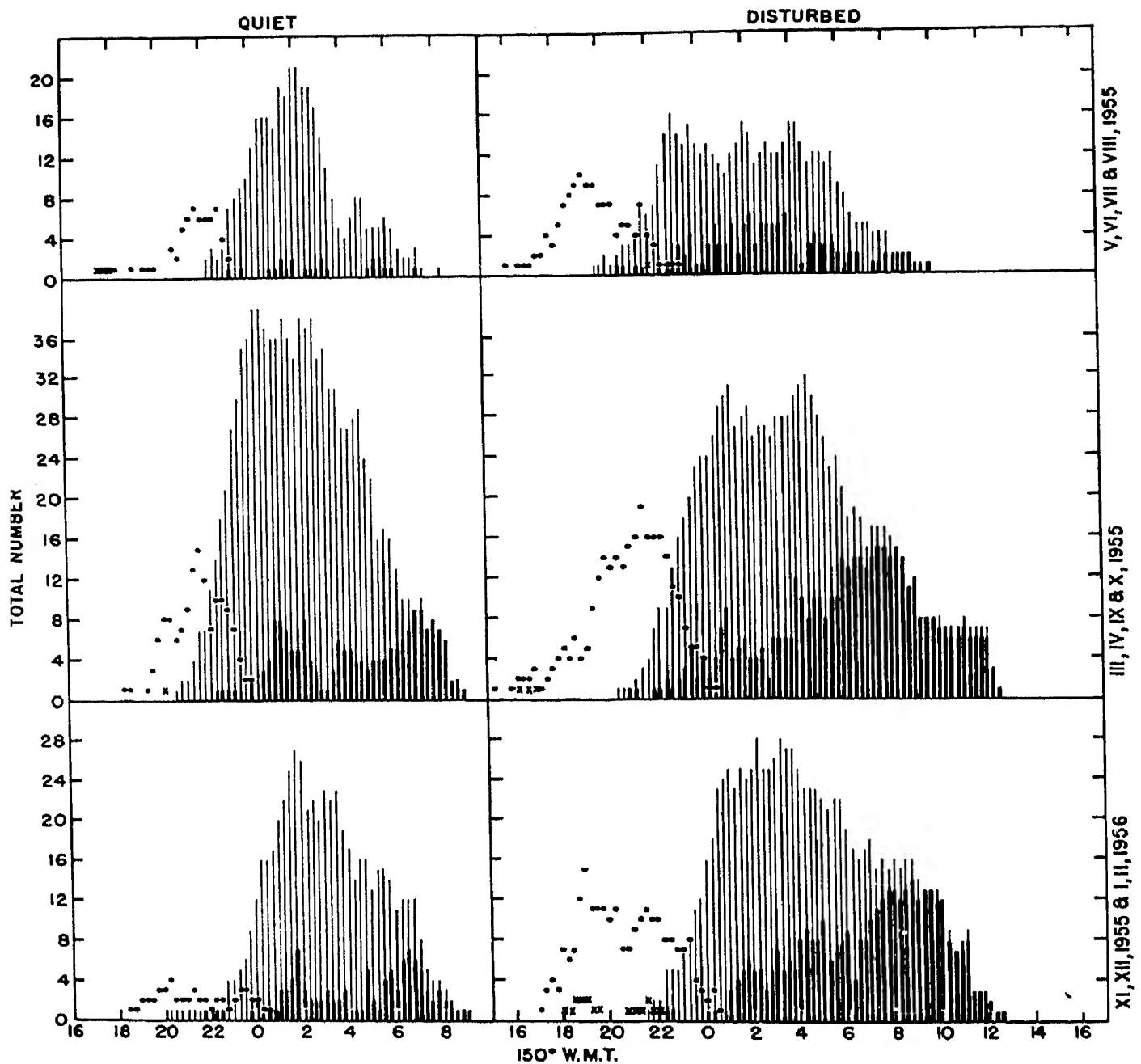


Fig. 13. Number of occurrences of blanketing  $F$  by  $E_s$  echoes and of gradual blackouts associated with geomagnetic bays at College every 15 minutes on quiet ( $A_p < 16$ ) and disturbed ( $A_p \geq 16$ ) days in three seasons. Storm periods are excluded in order to show effects due to real bays only. Dots and crosses are for blanketing  $F$  and blackout associated with positive bays, respectively, and thin and thick lines are of those associated with negative bays. Bay disturbances in auroral latitudes occur even on internationally quiet days.

effect of the solar wind or other solar agencies. When the temporal and geophysical distributions of polar blackouts are studied, it is essential to make a distinction among different types of blackouts, such as sudden and gradual blackouts associated with bays, PCA blackouts, flare and storm time blackouts: many previous workers unfortunately failed to do this.

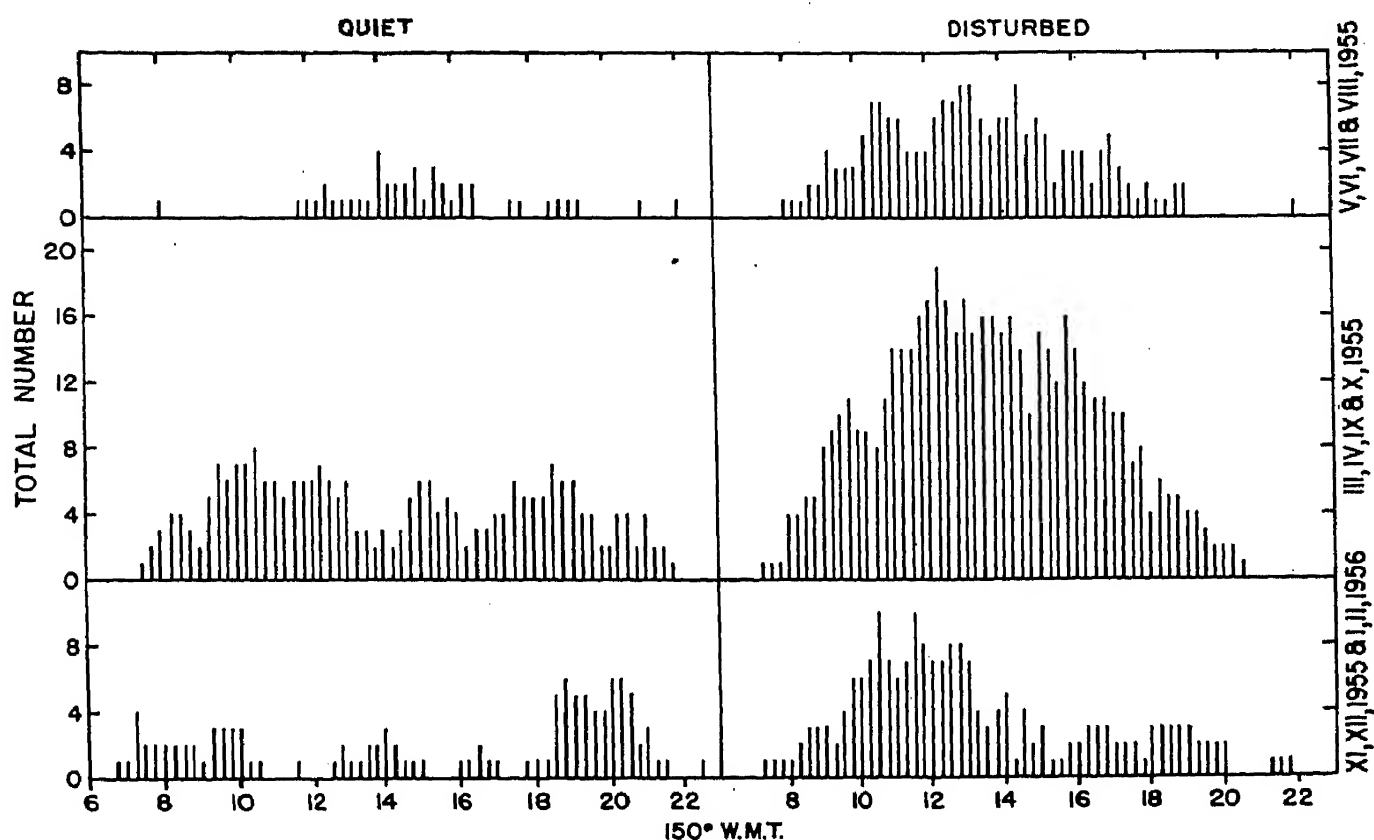


Fig. 14. Number of occurrences of sudden blackout at College every 15 minutes on quiet ( $A_p < 16$ ) and disturbed ( $A_p \geq 16$ ) days in three seasons. Storm periods and a PCA event on February 23–25, 1956 are excluded in these statistics. It must be noticed that blackouts suddenly occur without any remarkable geomagnetic variations on both internationally quiet and disturbed days and that they are not the PCA event.

As is indicated in Fig. 11, slant  $E_s$  occasionally appears during bays, particularly during positive bays (about half of the positive bays were accompanied by slant  $E_s$  at College), and it only occurs during bays and bay-shaped variations during storms. As is represented in Fig. 15, the time of the most frequent occurrence of slant  $E_s$  at College is 18 00–20 00 hr on disturbed days, indicating a frequent connection with the positive bay: this is a typical behavior of occurrence of slant  $E_s$  in auroral latitudes. In the polar cap, however, slant  $E_s$  occurs frequently during daylight hours, particularly around local noon, as shown by Olesen and Rybner (1958) at Godhavn (geographic  $69^\circ 15' \text{ N}$ ,  $53^\circ 30' \text{ W}$ ; geomagnetic  $79.8^\circ \text{ N}$ ). This is understandable because magnetic disturbances often occur at night in

auroral latitudes and in the daytime at the polar cap (Mayaud 1955). Heppner, Byrne and Belon (1952) reported that slant  $E_s$  at College is associated with auroras, Smith (1957) and Smith and Knecht (1957) suggested that the slant  $E_s$  echo is due to a mode of radio propagation between two ionospheric layers around the  $E$ -level, one reflecting and one scattering, and Bates (1961) described it as a scattering of radio waves by randomly distributed field-aligned irregularities. All of these indicate that slant  $E_s$  echoes are related to the impact of charged particles at night in auroral

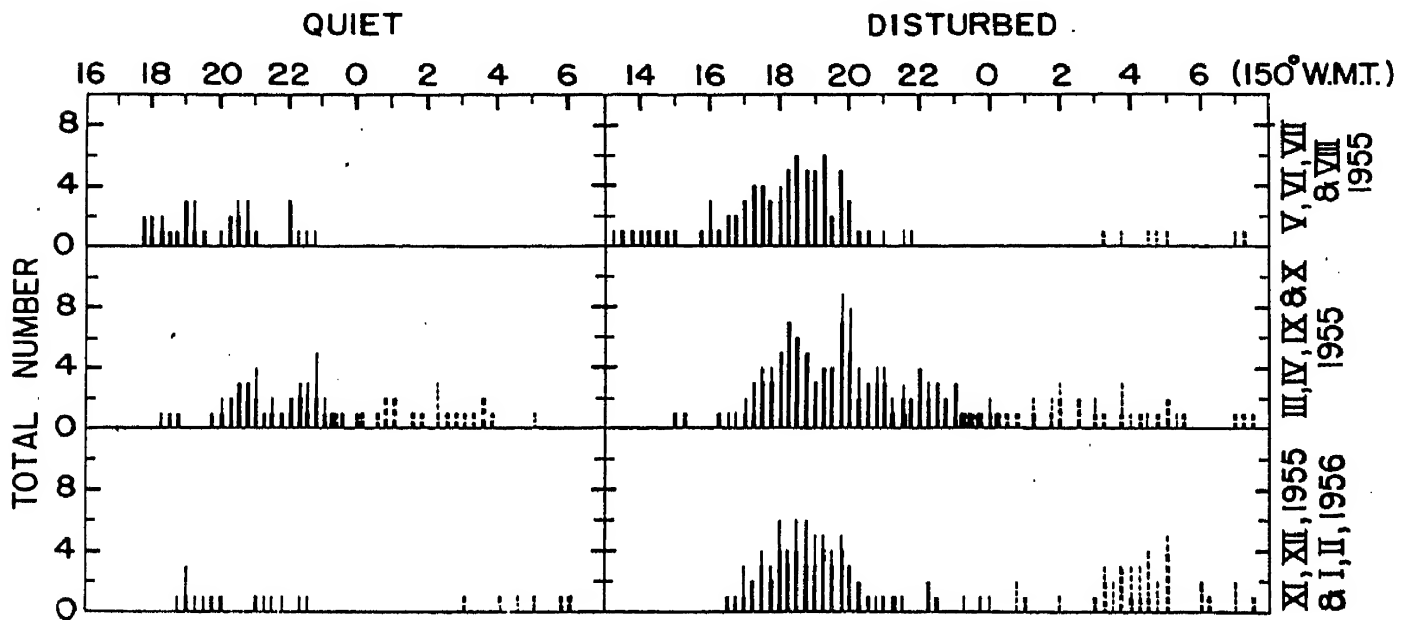


Fig. 15. Number of occurrences of slant  $E_s$  associated with positive (solid lines) and negative (broken lines) bays at College every 15 minutes on quiet ( $A_p < 16$ ) and disturbed ( $A_p \geq 16$ ) days in three seasons. Thin solid and broken lines indicate less reliability than thick lines. In auroral latitudes slant  $E_s$  occurs only during bays, particularly positive bays, and bay-shaped variations during geomagnetic storms.

latitudes and frequently in the daytime at the polar cap. Thus it can be concluded that electrons in the sunlit side of trapped zone which impact the polar cap cause slant  $E_s$  and magnetic disturbances in this region, and those which impact auroral latitudes cause sudden blackouts without any remarkable geomagnetic variation.

In auroral latitudes bay-shaped variations during geomagnetic storms (polar elementary storms) show a behavior similar to the negative bay, although they occur at almost any local time (of course most frequently at night). However, they have less systematic behavior with regard to  $E_s$  because their formation, particularly the mechanism of the charge separation, is different from the bay. One interesting interrelation between  $E_s$  and ionospheric currents during geomagnetic storms can be seen at sudden

commencements. Matsushita (1957b) classified the shape of sudden commencements in the horizontal geomagnetic variation field into three types:  $-SC$  is characterized by a small negative impulse preceding the main positive impulse,  $SC$  is a common main positive impulse alone, and  $SC^-$  is characterized by an increase lasting from 0 to about 6 minutes followed by a decrease to a level lower than the initial pre-sudden commencement level. These three different types depend on the location of observing stations and on the local time of sudden commencement at each station: in high latitudes  $-SC$  and  $SC^-$  occur much more frequently than  $SC$ , but in lower moderate latitudes sudden commencements are almost always of the  $SC$  type, and in higher moderate latitudes  $-SC$  often occurs in the afternoon and  $SC^-$  in the morning. Matsushita (1960a) suggested that the negative impulse of  $-SC$  and  $SC^-$  are due to westward electric currents at about 100 km altitude caused by charged particles from outside the earth's atmosphere and that the main impulse of sudden commencements is due to eastward ionospheric currents caused by hydromagnetic waves. When an  $SC$  shows a second positive impulse, the impulse is due to eastward currents caused by incoming charged particles. Ionograms obtained by vertical ionosondes soon after the occurrence of sudden commencements support the above suggestion of incoming charged particles, because the data often show the appearance of  $E_s$ , increase of  $f_oE_s$ , blanketing of the  $F$ -region by  $E_s$  echoes, increase of  $f$ -min, or beginning of blackout, all of which indicate an increase of ionization in the  $E$ -layer or an increase of radio absorption in the  $D$ -region (Matsushita 1957b). This is further supported by riometer observations of 27.6 Mc/s cosmic noise which often show an increase of absorption of 2 to 10 db starting at the same time as sudden commencements (Brown, Hartz, Landmark, Leinbach and Ortner 1961, Matsushita 1961, 1962 b). These indicate that charged particles (probably high-energy electrons) and/or X-rays produced by Bremsstrahlung from high-energy electrons, penetrate into the lower ionosphere and cause ionization; as a consequence, there occur ionospheric currents and  $E_s$  formation or increased absorption of radio waves and cosmic noise at the time of sudden commencements. The above process may result from hydromagnetic waves or electrostatic waves (Malville 1961), which propagate along the earth's magnetic lines of force and cause electrons in the outer Van Allen belt or the solar plasma responsible for storms to move down along the lines of force at the time of sudden commencement. Based on these observed results and hypothesis, it may be concluded that in auroral latitudes there is an interrelation of  $E_s$  and the ionospheric currents responsible for special features of sudden commencements.

Overall model of  $E_s$  formations in high latitudes is as follows:

(1) The retardation type  $E_s$  and auroral  $E_s$  are associated with geo-

magnetic bays and storms. The former is a thick layer and the latter is formed by field-aligned clouds, both of which are caused mainly by electron impact, probably from the trapped region.

- (2) Slant  $E_s$  echo in auroral latitudes and the polar cap is due to a mode of radio propagation between ionized layers, which are produced by electron impact.
- (3) Longitudinal electrostatic fields play an important rôle in the disturbed ionospheric current system in auroral latitudes at night.  $E_s$  associated with bays has a correlation with the static field.
- (4)  $E_s$  is occasionally associated with geomagnetic sudden commencements, probably due to electrons from the outer Van Allen belt or the solar plasma.

## 5. CONCLUSIONS

All ionospheric current systems, particularly certain new aspects of equatorial electrojets and  $S_q$ , bay and sudden commencement currents, are described, and their interrelation with different types of  $E_s$  and the mechanisms involved in the interrelation are discussed in this article, using statistical results on  $E_s$  which have been obtained by the present author during the past 12 years. It is already known that  $E_s$ - $q$  is due to the solar equatorial electrojet and that  $E_s$  in high latitudes is due to incoming charged particles. However, an attempt has been made to further clarify the mechanism of these  $E_s$  formations from the point of view of interrelations between  $E_s$  and the ionospheric currents. It is concluded that the  $E_s$ - $q$  echo is due to irregularities in the equatorial electrojet caused by vertical drifts and that retardation and auroral types of  $E_s$  are ionized layers mainly caused by electrons. Also it is suggested that the most common  $E_s$  in temperate latitudes is a thin patchy layer which is due to vertical drift effects caused by wind shears (namely, re-arrangement of pre-existing ionization), although occasionally  $E_s$  in temperate latitudes is formed by a descending thick cloud of ionization. Blanketing  $E_s$  does not occur in the vicinity of the magnetic equator, as is mentioned in the articles by Bowles and Cohen and by Knecht and McDuffie in this book, because neither  $E_s$ - $q$  nor equatorial slant  $E_s$  shows any blanketing; and neither the cause of thick  $E_s$ , which is responsible for blanketing upper layers, in temperate latitudes nor the cause in high latitudes can hold on the magnetic equator. Correlations between  $E_s$  and the lunar current system are not described in detail because they are mentioned in another article. Except for thunderstorms and meteor bombardments, the above mentioned mechanisms are suggested as the primary causes of the  $E_s$  ionization. This paper ignores those specialized echoes appearing on ionograms which are caused by the mode of radio wave propagation and which, although interesting from a



wave propagation standpoint (see Tao's, Layzer's and Rawer's articles in this book), do not provide much information on the main features of  $E_s$  structure. A question of the lifetime of  $E_s$  may be solved, since  $E_s$  does not disappear as long as the causing agency continues to act. Also, an apparent horizontal drift of  $E_s$  in temperate latitudes indicates a horizontal change of the causing agency, and that observed by radar in auroral latitudes and the magnetic equatorial zone indicates the ionospheric current flow.

*Acknowledgment*—I wish to express my gratitude to Dr. W. O. Roberts and Mr. A. H. Shapley for their kind help and to thank the Boulder Laboratories of the National Bureau of Standards for extending their facilities to me under appointment as a guest worker. The work reported here was supported by the National Academy of Sciences under grant NSF-G9427.

#### REFERENCES

- AKASOFU, S.-I. (1956) *Rep. Ionosph. Research Japan* **10**, 227.  
 AKASOFU, S.-I. and CHAPMAN, S. (1961) *Geophys. Inst., Univ. of Alaska, Scientific Report No. 7*.  
 AXFORD, W. I. and HINES, C. O. (1961) *Canadian J. Phys.* **39**, 1433.  
 BATES, H. F. (1961) *J. Geophys. Res.* **66**, 447.  
 BELLCHAMBERS, W. H. and PIGGOTT, W. R. (1960) *Proc. Roy. Soc. A* **256**, 200.  
 BERNARD, P. (1960) *J. Geophys. Res.* **65**, 785.  
 BIBL, K. (1960) *J. Geophys. Res.* **65**, 2333.  
 BIRKELAND, KR. (1908) *The Norwegian Aurora Polaris Expedition, 1902–1903*, Christiania, Norway.  
 BLESS, R. C., GARTLEIN, C. W., KIMBALL, D. S. and SPRAGUE G. (1959) *J. Geophys. Res.* **64**, 949.  
 BOND, F. R. (1960) *Aust. J. Phys.* **13**, 477.  
 BOWLES, K. L., COHEN, R., OCHS, G. R. and BALSLEY, B. B. (1960) *J. Geophys. Res.* **65**, 1853.  
 BOWMAN, G. G. (1960) *Planet, Space Sci.* **2**, 195.  
 BROWN, R. R., HARTZ, T. R., LANDMARK, B., LEINBACH, H. and ORTNER, J. (1961) *J. Geophys. Res.* **66**, 1035.  
 CAHILL, L. J., JR. (1959) *J. Geophys. Res.* **64**, 489.  
 CAMPBELL, W. H. and MATSUSHITA, S. (1962) *J. Geophys. Res.* **67**, 555.  
 CHAPMAN, S. (1951) *Arch. Meteor. Geophys. u. Bioklimatol. A* **4**, 368.  
 CHAPMAN, S. and BARTELS, J. (1940) *Geomagnetism*, Clarendon Press, Oxford.  
 COHEN, R., BOWLES, K. L. and CALVERT, W. (1962) *J. Geophys. Res.* **67**, 965.  
 COLE, K. D. (1960) *Aust. J. Phys.* **13**, 484.  
 COLE, K. D. and BOND, F. R. (1961) *J. Geophys. Res.* **66**, 327.  
 COLLINES, C., JELLY, D. and MATHEWS, A. G. (1961) *Canadian J. Phys.* **39**, 35.  
 DAVIS, T. N. (1960) *J. Geophys. Res.* **65**, 3497.  
 DUNCAN, R. A. (1960) *J. Geophys. Res.* **65**, 3589.  
 DUNGEY, J. W. (1959) *J. Geophys. Res.* **64**, 2188.  
 EGAN, R. D. (1960) *J. Geophys. Res.* **65**, 2343.  
 FEJER, J. A. (1961) *Canadian J. Phys.* **39**, 1409.  
 FORBUSH, S. E. and CASASVERDE, M. (1961) *Carnegie Insti. Washington Pub.* 620.  
 FUKUSHIMA, N. (1949) *Geophys. Notes*, Tokyo Univ. **2**, No. 21.  
 HAGG, E. L., MULDREW, D. and WARREN, E. (1959) *J. Atmosph. Terr. Phys.* **14**, 345.  
 HATAKEYAMA, H. (1938) *Geophys. Mag. Japan* **12**, 15 and 189.  
 HEISLER, L. H. and WHITEHEAD, J. D. (1960a) *Nature* **187**, 676.  
 HEISLER, L. H. and WHITEHEAD, J. D. (1960b) *J. Geophys. Res.* **65**, 2767.



- HEPPNER, J. P., BYRNE, E. C. and BELON, A. E. (1952) *J. Geophys. Res.* **57**, 121.  
HEPPNER, J. P. (1954) *J. Geophys. Res.* **59**, 329.  
HINES, C. O. (1960) *Canadian J. Phys.* **38**, 1441.  
HIRONO, M. (1953) *J. Geomag. Geoelect.* **5**, 22.  
KERN, J. W. (1961) *Rand Rep.*, RM-2753-NASA.  
KNECHT, R. W. (1956) *J. Geophys. Res.* **61**, 59.  
KNECHT, R. W. (1959) *J. Atmosph. Terr. Phys.* **14**, 348.  
MAEDA, H. (1955) *J. Geomag. Geoelect.* **7**, 121.  
MAEDA, H. (1957) *J. Geomag. Geoelect.* **9**, 119.  
MALVILLE, J. M. (1961) *Ph.D. Thesis*, Astro-Geophys. Dept., Univ. of Colo.  
MANRING, E., BEDINGER, J. F., PETTIT, H. B. and MOORE, G. B. (1959) *J. Geophys. Res.* **64**, 587.  
MAPLE, E., BOWEN, W. A. and SINGER, S. F. (1950) *J. Geophys. Res.* **55**, 115.  
MARTYN, D. F. (1953) *Phil. Trans. A* **246**, 306.  
MATSUSHITA, S. (1949) *J. Geomag. Geoelect.* **1**, 35.  
MATSUSHITA, S. (1951) *J. Geomag. Geoelect.* **3**, 44.  
MATSUSHITA, S. (1953a) *J. Geomag. Geoelect.* **5**, 109.  
MATSUSHITA, S. (1953b) *Rep. Ionosph. Research Japan* **7**, 45.  
MATSUSHITA, S. (1957a) *J. Atmosph. Terr. Phys.* **10**, 163.  
MATSUSHITA, S. (1957b) *J. Geophys. Res.* **62**, 162.  
MATSUSHITA, S. (1958) *Ann. de Géophys.* **14**, 483.  
MATSUSHITA, S. (1959) *J. Atmosph. Terr. Phys.* **15**, 68.  
MATSUSHITA, S. (1960a) *J. Geophys. Res.* **65**, 1423.  
MATSUSHITA, S. (1960b) *J. Geophys. Res.* **65**, 3835.  
MATSUSHITA, S. (1962) *J. Geophys. Res.* **66**, 3958.  
MATSUSHITA, S. (1962a) *Handbuch der Physik* **49** (in press).  
MATSUSHITA, S. (1962b) *J. Geophys. Res.* **67**, No. 10.  
MAYAUD, P. N. (1955) *Expéd. Polaires Françaises, Résult. Scientif.*, No. S. IV 2, Paris.  
MCNISH, A. G. (1936) *Terr. Mag. Atmosph. Elect.* **41**, 37.  
NICHOLS, B. (1959) *Proc. Inst. Radio Engrs.* **47**, 245.  
OBAYASHI, T. and JACOBS, J. A. (1957) *J. Geophys. Res.* **62**, 589.  
OLESEN, J. K. and RYBNER, J. (1958) *Danish National Committee U.R.S.I.*, Copenhagen.  
ONWUMECHILI, C. A. (1959) *J. Atmosph. Terr. Phys.* **13**, 222, 235.  
OSBORNE, D. G. (1962) *J. Atmosph. Terr. Phys.* **24**, 491.  
PENNDORF, R. and CORONITI, S. C. (1958) *J. Geophys. Res.* **63**, 789.  
RIKITAKE, T. and YUKUTAKE, T. (1962) *J. Atmosph. Terr. Phys.* **24**, 93.  
ROBERTSON, C. S. (1960) *Aust. J. Phys.* **13**, 470.  
SHAW, J. E. (1959) *Planet, Space Sci.* **2**, 56.  
SILSBEE, H. C. and VESTINE, E. H. (1942) *Terr. Mag. Atmosph. Elect.* **47**, 195.  
SMITH, E. K. (1957) *N.B.S. Circular* 582.  
SMITH, E. K. and KNECHT, R. W. (1957) *AGARD Polar Atmosph. Symp.*, part 2, Pergamon Press, p. 195.  
SUGIURA, M. (1956) *Scientific Rep. No. 2*, Geophys. Insti., Univ. of Alaska.  
THOMAS, J. A. and SMITH, E. K. (1959) *J. Atmosph. Terrest. Phys.* **13**, 295.  
THOMAS, L. and PIGGOTT, W. R. (1960) *Some Ionosph. Results IGY*, p. 61, Elsener, Amsterdam.  
VAN SABBEN, D. (1961) *J. Atmosph. Terr. Phys.* **22**, 32.  
VEGARD, L. (1917) *Jahrbuch der Radioaktivität und Elektronik*, **14**, 383.  
VELDKAMP, J. and VAN SABBEN, D. (1960) *J. Atmosph. Terr. Phys.* **18**, 192.  
VESTINE, E. H., LAPORTE, L., LANGE, I. and SCOTT, W. E. (1947) *Carnegie Institution of Washington Publication* 580.  
VESTINE, E. H. (1954) *J. Geophys. Res.* **59**, 93.  
WHITEHEAD, J. D. (1960) *Nature* **188**, 567.  
WHITEHEAD, J. D. (1961) *J. Atmosph. Terr. Phys.* **20**, 49.  
ZMUDA, A. J. (1960) *J. Geophys. Res.* **65**, 2247.

# Concluding Remarks

S. MATSUSHITA and E. K. SMITH, JR.

## 1. INTRODUCTION

The third contribution by Ratcliffe in the first chapter is a very fine survey presented at the conclusion of the Conference of Sporadic-*E* Ionization sponsored by AGARD at Cambridge in 1957. It is our aim in the concluding section of this text to use Ratcliffe's paper as a point of departure and, rather than review the entire field, to attempt to bring it up to date, particularly in the light of contributions to this volume. With this in mind, we are following a very similar outline to that used by Ratcliffe. His "facts" are covered in the second and third parts of our *Concluding Remarks* under the titles *Occurrence of Sporadic E* and *Sporadic-E Movements*. His section on electron distributions is largely paralleled by the fourth part of the conclusion entitled *Structure of Sporadic E*. Ratcliffe's following section, *The Ultimate Causes of  $E_s$* , is paralleled in this treatment by Section 5, *Discussion on the Cause of Sporadic E*. The final section in this chapter considers future research as does Ratcliffe's paper.

## 2. OCCURRENCE OF SPORADIC *E*

In the equatorial zone, considerable new information is now available. There are better measurements than before on the width of the equatorial sporadic-*E* belt in South America. Based on the close-spaced chain of ionosondes, Knecht and McDuffie find that the "half power points" of the sporadic-*E* belt lie at  $\pm 5\frac{1}{2}$  degrees in magnetic dip (approximately 700 km in width). In support of this finding, Bowles and Cohen find from their oblique-incidence circuits that the width of the belt must be at least  $\pm 5$  degrees in latitude. In addition, both Knecht and McDuffie, and Bowles and Cohen find that blanketing type of sporadic *E* is forbidden at the magnetic equator. The forbidden belt seems somewhat narrower than the belt pertinent to *q*-type  $E_s$  which is associated with the electrojet. Skinner and Wright have derived values for the frequency dependence of equatorial sporadic *E*. They suggest a value of 9.4 for the frequency exponent based on their measurements between 4 and 8 Mc/s at vertical incidence. If the 50 Mc/s radar measurements of Bowles and Cohen are considered as well, then the frequency exponent over the wider range of

frequencies appears to be more like 7. Using fixed-frequency backscatter techniques, Egan and Peterson find direct backscatter returns from the  $q$ -type sporadic  $E$  and postulate field-aligned ionization for this type of sporadic  $E$ . Bowles and Cohen suggest the height of  $q$ -type sporadic  $E$  to be between 100 and 107 km and find that slant  $E_s$ , as observed in the equatorial zone, also has the same height of origin.

In the temperate zone, we have substantial advances in the area of backscatter observations of sporadic  $E$ . The results of both Egan and Peterson and Dueño show surprising preferences for particular azimuths. Ocean paths are preferred both at Stanford and at Camden, Australia vs. the overland ones and the results also suggest that mountainous areas may have a strong effect on sporadic- $E$  occurrences. Dueño in his measurements from Puerto Rico finds a distinct preference for southerly azimuths (although in his case, he is surrounded by ocean on all sides). The Australian work reported by Thomas seems to be indicating very interesting relationships of sporadic  $E$  with  $F$ -region moving phenomena.

A sporadic- $E$  front, somewhat similar to the Australian type, was observed in the U.S. by DeGregorio *et al.* The variations of the different sporadic- $E$  types, as defined for the purposes of the IGY, have now become available (Leighton, Shapley, and Smith); but the interpretation of their significance largely remains for future researchers. A somewhat more comprehensive look at the problem of correlation of sporadic  $E$  as a whole with sun-spot number has been carried out by Chadwick who finds that a negative correlation exists for most hours at all his sample stations. The problem of interrelating the vast amount of vertical-incidence data to oblique-incidence circuits has been studied by DeGregorio *et al.* and appears much more complicated than was previously thought, with the result that no simple means of conversion appears possible.

It is interesting to consider night- $E$  in that it is part of the spectrum of  $E$ -region effects which is different from the regular  $E$ -region. In fact, it is difficult, and rather arbitrary, to call some of these effects sporadic  $E$  and not others. Night- $E$  is generally considered not to be sporadic  $E$ . King finds that in order to explain night- $E$  one must resort to either X-rays on the dark side of the earth or else ionization supplied from the  $F$ -region.

### 3. SPORADIC- $E$ MOVEMENTS

Movement of sporadic  $E$  in the equatorial zone is covered by Skinner and Wright and also Bowles and Cohen. The former find the order of a 60 meters per second steady component occurring along with a 30 meters per second random component. Bowles and Cohen find a westward movement with an apparent horizontal velocity of 750 meters per second for  $q$ -type sporadic  $E$  which they interpret as a wave motion rather than as a

real movement of ionization. A dichotomy in results between Doppler fading at 30 degrees and 60 degrees from the vertical leads Bowles and Cohen to hypothesize a spectrum of wave motions moving at different vertical azimuths.

Motions in the temperate zone are shown to be largely to the west. Egan and Peterson report that, although the majority of observed sporadic  $E$  appears stationary on backscatter equipment, of those that moved both Stanford and Camden observations show a largely westerly direction. Dueño finds a similar southwesterly direction for his observations for Puerto Rico with an average velocity of 150 meters per second. The analyses made to date on the great mass of Amateur sporadic- $E$  reports (mostly in the U.S.) accumulated at 50 Mc/s during the IGY show that all clouds appear to move, velocities in the westerly direction are preferred, and that clouds seem to have all conceivable sizes and shapes (Pfister, private communication).

Vertical movements are treated only in the lunar tide and sequential  $E_s$  by Matsushita.

#### 4. STRUCTURE OF SPORADIC $E$

In the equatorial zone, the dominant type of sporadic  $E$  is the so-called  $q$ -type which is a highly transparent belt formed on the daylight side of the earth with a width of approximately 700 km. The details of this type of sporadic  $E$  are covered in the previous section.

In temperate latitudes we now have quite a wealth of data on sporadic- $E$  structure, some of it conflicting. One gets a picture of large clouds of sporadic  $E$  approximately 200 km in diameter but subject to very wide variation in size. Seddon, in his discussion of rocket results, likes to think of sporadic  $E$  as a large flat platter. Tao has shown that strongly reflecting sporadic  $E$  looks very much like a thin layer whereas the weakly reflecting variety shows characteristics of a scattering mechanism. The problem of the maximum plasma density of  $E_s$  is still a worrisome one. The relatively meager rocket results do not favor very great intensification of daytime  $E$ -region intensity, although a many-fold increase of electron density at night-time is possible. However, the fading work reported in DeGregorio *et al.* best fits an explanation where plasma densities do exist which correspond to the observed  $E_s$  critical frequencies (frequently as high as 12 Mc/s) as is suggested by Rawer.

The rocket results do show evidence of steep gradients, but it is rather difficult to explain the intense sporadic  $E$  as seen at v.h.f. on the basis of gradients. Rawer points out that one can deduce from sporadic  $E$ , as seen on ionograms, that the thickness is less than 5 kilometers. Seddon suggests one-half to two kilometers from rocket results. Tao suggests that layers of the order of 300 meters to one kilometer provide a reasonable fit to the

data obtained and that, if a scattering model is assumed, a horizontal scale of 200 meters and a vertical scale of 50 meters is appropriate.

Sporadic  $E$  of the type found in the auroral zone or associated with auroral effects may take completely different forms than appear appropriate for the temperate zone. There is strong evidence of thick layers formed by incoming auroral particles. Similarly, in the equatorial zone, the  $q$ -type sporadic  $E$  associated with the equatorial electrojet is apparently quite distinct from the normal temperate latitude types.

## 5. DISCUSSION ON THE CAUSE OF SPORADIC $E$

$q$ -type sporadic  $E$  is intimately related with the equatorial electrojet as demonstrated by Bowles and Cohen, Matsushita and others. Certain details of the mechanism involved are still unclear, but it is certainly appropriate to specify the equatorial electrojet as the cause and  $q$ -type sporadic  $E$  as one of the consequences. One of the major problems in the understanding of  $q$ -type sporadic  $E$  is concerned with the fine structure of the reflecting mechanism. If Bowles and Cohen are to be believed, the reflections take place from a wave motion in the electron density. The velocity measurements of Bowles and Cohen, based on Doppler techniques, are approximately of an order of magnitude higher than the velocity obtained by Skinner and Wright using the MITRA method. The latter velocity would be acceptable in a cigar-shaped model, whereas the Bowles and Cohen velocity (which, according to Matsushita, is very similar to the expected electron velocity in the electrojets) requires that one considers a wave motion propagated in the direction of electron flow. In the temperate zone, as Rawer nicely catalogued, there is a good reason to suppose that most sporadic  $E$  must be explained on a terrestrial basis. Looking at the various terrestrial mechanisms available, the one described by Whitehead and also discussed by Matsushita is perhaps the most appealing. In this mechanism the vertical gradient of wind shear in the presence of the earth's magnetic field sets up drift motions which vary with height due to the gradient. If the wind shear mechanism is correct, then the distribution of sporadic  $E$  on a world-wide basis can be used to derive the wind shear pattern at these heights. The mechanism described by Layzer serves the useful purpose of deciding the limitations in intensification which can be derived from that mechanism. Sporadic  $E$ , explainable by turbulence, is probably very weakly reflecting by nature. Another interesting possibility is the effect of gravity waves as recently discussed by Hines, 1960 (see bibliography, Smith, Chap. I, Matsushita, Chap. II, part C), in the production or triggering of sporadic  $E$ . Despite exciting new possibilities, it must be admitted that there are several unanswered questions, such as the lack of information on the occurrence of wind shear, which block the

complete acceptance of any of the suggested mechanisms. The necessity for a terrestrial mechanism is perhaps primarily dictated by the strong seasonal variation with maxima six months out of phase in the Northern and Southern Hemispheres. In the auroral zone, it is quite logical to conceive of incoming particle bombardment being strongly influential and this, in fact, is fairly well established.

## 6. FUTURE RESEARCH

In order to complete our knowledge of  $q$ -type sporadic  $E$ , it is necessary to pursue the type of work which Bowles and Cohen have been carrying out and to bring more theoretical interpretation to bear on their experimental work. In particular, it is also necessary to resolve the difference in velocity observed by Bowles and Cohen and that observed by Skinner and Wright. There is no *a priori* reason for supposing that the electrojet is uniform around the world. It would therefore be very useful to get further geographical information of the type obtained by Knecht and McDuffie on the width and intensity of the sporadic- $E$  belt in other localities, perhaps West Africa. In the temperate zone, now that we have the benefit of the observations during the IGY on the typing system adopted for that period, there is a distinct need to modify some of the classifications. In particular, it would be useful to have a less artificial way of classifying sequential sporadic  $E$  and also of introducing some measure of transparency into the classification system. Due to our current lack of knowledge on vertical wind shear, it is important that in the future we obtain more information on wind shear, particularly coupled with direct observation of sporadic  $E$  and movements of the sporadic- $E$  patches. It still has not been determined by direct measurement of the integrated electron content whether or not sporadic  $E$  is due to new ionization or a redistribution of the existing ionization at temperate latitudes. It would be useful if this question could be resolved, perhaps using transmissions from a geostationary satellite.

# NAME INDEX

- ABE, G. 133, 134  
 AGY, V. 74  
 AIDA, K. 9  
 AIKIN, A. C. 278  
 AINSWORTH, J. A. 85  
 AKASOFU, S.-I. 346, 360, 367  
 ALBRECHT, H. J. 9  
 APPLETON, E. V. 31, 154, 183, 205, 314  
 ASCHENBRAND, L. M. 10  
 AXFORD, W. I. 368  
  
 BAILEY, D. K. 54, 55, 62, 132, 249  
 BALSLEY, B. B. 9, 99  
 BANDEEN, W. R. 85  
 BARTELS, J. 194, 207, 208, 345, 346  
 BARTMAN, F. L. 85  
 BATCHELOR, G. K. 263, 267  
 BATEMAN, R. 54, 55, 62, 132  
 BATES, D. R. 271, 341  
 BATES, H. F. 9, 91, 95, 371  
 BECKER, W. 9, 278  
 BEDINGER, J. F. 84, 356  
 BELLCHAMBERS, W. H. 6, 9, 170, 366  
 BELON, A. E. 361, 371  
 BENKOVA, N. P. 205  
 BENNINGTON, T. W. 9  
 BERG, O. E. 84  
 BERNARD, P. 365  
 BERRY, D. G. 64, 74  
 BESPROZVANNAYA, A. S. 182  
 BREYNON, W. J. G. 231  
 BIBL, K. 9, 152, 292, 295, 303, 322, 323, 326, 342, 358  
 BIRKELAND, K. 346  
 BLAIR, J. C. 251  
 BLAMONT, J. E. 84, 290  
 BLESS, R. C. 224, 229, 364  
 BOLGIANO, R. 19  
 BOND, F. R. 362, 365  
 BOOKER, H. G. 13, 19, 20, 24, 39, 40, 72, 73, 99, 236, 239, 241, 242, 243, 245, 249, 261  
 BOSSALASCO, M. 9  
 BOWEN, W. A. 344  
 BOWLES, K. L. 8, 9, 37, 45, 51-77, 99, 148, 211, 350, 352, 355, 373, 376, 377, 378, 379, 380  
 BOWMAN, G. G. 9, 123, 290, 359  
 BRAND, J. D. 314  
  
 BRAY, W. J. 249  
 BRIGGS, B. H. 29, 31, 70, 153, 206, 287, 323, 336  
 BROWN, G. M. 231  
 BROWN, J. N. 219  
 BROWN, R. R. 372  
 BUSCH, R. 152  
 BYRAM, E. T. 230  
 BYRNE, E. C. 361, 370  
  
 CAHILL, L. J., JR. 62, 344, 353  
 CALVERT, W. 75, 355  
 CAMPBELL, W. H. 363  
 CARPENTER, R. J. 143-148  
 CASAVARDE, M. 348  
 CHADWICK, W. B. 6, 8, 182-193, 353, 377  
 CHAPMAN, J. H. 205, 206  
 CHAPMAN, S. 194, 207, 208, 345, 346, 348, 367  
 CHATTERJEE, 29, 31  
 CHUBB, T. A. 230  
 CLARK, C. 103, 108, 117, 122  
 CLARK, N. 105  
 CLEMMOW, P. C. 73  
 COHEN, R. 8, 9, 37, 51-77, 99, 211, 350, 352, 355, 373, 376, 377, 378, 379, 380  
 COLE, K. D. 364, 365  
 COLLINES, C. 368  
 COOK, A. F. 271  
 CORONITI, S. C. 10, 361  
 CRAWFORD, A. B. 17, 236  
  
 DATARS, W. R. 205  
 DAVIDSON, D. 122, 182  
 DAVIES, F. T. 219  
 DAVIES, K. 172  
 DAVIS, L. R. 84  
 DAVIS, R. M. 9, 40, 132, 133, 134, 135, 249  
 DAVIS, T. N. 362  
 DEGREGORIO, J. F. 131-142, 377, 378  
 DIEMINGER, W. E. 9, 90, 91, 96  
 DUEÑO, B. 102, 103, 110-122, 360, 377, 378  
 DUHAMEL, R. H. 64, 74  
 DUNCAN, R. A. 365  
 DUNGEY, J. W. 9, 276, 355



- EGAN, R. D. 10, 45, 63, 75, 89-109, 350, 360, 377, 378  
ELENA, A. 9  
ELLIS, G. R. A. 9  
ELLISON, T. H. 261  
ELLYETT, C. D. 9, 40, 132, 133, 134, 135, 249  
  
FEJER, J. A. 368  
FINNEY, J. W. 5, 10, 131-142, 170  
FISHER, R. A. 296  
FOOKS, G. F. 9  
FORBUSH, S. 218, 348  
FOWLE, D. 219, 221  
FRIEDMAN, H. 230  
FRIIS, H. T. 17, 236  
FUKUSHIMA, N. 346, 362, 364  
  
GALLET, R. M. 19, 21, 23, 85, 243, 262  
GARTLEIN, C. W. 224, 229, 364  
GAUTIER, T. N. 11, 93, 134  
GAUZIT, J. 341  
GAZZARD, A. D. 9, 202  
GERSON, N. C. 9, 112  
GIESECKE, A. A., JR. 60  
GIPPS, G. DE V. 182, 314, 342  
GLADDEN, S. C. 178-181, 322  
GOLDSTEIN, S. 266  
GOODWIN, G. L. 9  
GORDON, W. E. 19, 20, 239, 242  
GREENHOW, J. S. 83, 270, 277  
GREENSTONE, R. 206  
GRINGAUZ, K. I. 83  
  
HAGG, E. L. 6, 9, 219, 221, 366  
HAGN, G. 105  
HANSON, G. H. 219, 221  
HARNISCHMACHER, E. 9, 203, 326  
HARTREE, D. R. 13, 236  
HARTZ, T. R. 372  
HARWOOD, J. 10, 111, 117, 122  
HATAKEYAMA, H. 346  
HATHERTON, T. 221  
HAUBERT, A. 228  
HAWKINS, G. S. 274  
HEISLER, L. H. 9, 170, 276, 288, 290, 355, 359  
HELLIWELL, R. A. 83, 202, 204  
HEPPNER, J. P. 84, 229, 361, 371  
HERLOFSON, N. 64  
HEYBORNE, R. L. 108  
HINES, C. O. 10, 105, 261, 278, 356, 368, 379  
HIRAI, M. 133, 134  
HIRONO, M. 357  
HÖCHTL, F. 298  
HOGG, D. C. 17, 236  
HOGG, D. E. 205  
  
HOJO, H. 126  
HOPE, J. 45  
HOUGH, W. S. 219  
  
ISHIKAWA, M. 10, 245  
  
JACKSON, J. E. 10, 79, 83, 86  
JACOBS, J. A. 364  
JACOBSEN, 263, 264  
JELLY, D. H. 205, 368  
JOUAUST, R. 341  
  
KAN, M. 292  
KASUYA, I. 10  
KERN, J. W. 367  
KILDAHL, K. 131-142  
KIMBALL, D. S. 224, 229, 364  
KING, G. A. M. 219-231, 361, 377  
KIRBY, R. C. 54, 55, 62, 132, 148  
KNAFLICH, H. 84  
KNECHT, R. W. 5, 8, 10, 58, 74, 98, 166, 172, 212, 215-218, 348, 350, 352, 361, 371, 373, 376, 380  
KONO, T. 133, 134  
KOSEKI, T. 9  
KOTADIA, K. M. 10  
KUPPERIAN, J. E. 230  
  
LANDMARK, B. 372  
LANGE, I. 375  
LAPORTE, L. 375  
LAYZER, D. 258-275, 379  
LEADABRAND, R. L. 95  
LEIGHTON, H. I. 6, 166-177, 361, 377  
LEINBACH, H. 372  
LIN, C. C. 264  
LINDQUIST, R. 220, 221  
LITTLEWOOD, C. A. 205  
LONG, R. R. 271  
LOVCOVA, V. A. 182  
LOVERA, G. 296  
LUSCOMBE, G. W. 249  
LYNCH, R. 84  
  
MAEDA, H. 360, 364  
MALVILLE, J. M. 372  
MANRING, E. 84, 270, 356  
MAPLE, E. 344  
MARMO, F. F. 10  
MARTYN, D. F. 10, 98, 99, 205, 275, 276, 341, 351  
MASON, R. F. 228  
MASSEY, H. S. W. 80, 341  
MATHEWS, A. G. 368  
MATSUSHITA, S. 10, 37, 52, 58, 98, 182, 194-214, 215, 218, 313, 315, 344-375, 376-380  
MAYAUD, P. N. 371



- McDUFFIE, R. E. 5, 8, 58, 166, 215-218, 348, 352, 373, 376, 380  
McNAMARA, A. G. 67  
McNICOL, R. W. E. 41, 46, 129, 182, 315, 342  
McNISH, A. G. 361  
MEEK, J. H. 219, 229  
MEGILL, L. R. 125  
MEREDITH, L. H. 84  
MIDWINTER, G. G. 221  
MILLER, J. C. P. 194  
MILLINGTON, G. 13, 15  
MILLMAN, P. M. 17, 83, 270, 277  
MITRA, A. P. 230  
MITRA, S. K. 291  
MIYA, K. 10, 245  
MOORE, C. B. 84, 356  
MUCHMORE, 23  
MULDREW, D. 6, 9, 366  
  
NAISMITH, R. 30, 154, 314, 340  
NAKATA, Y. 292  
NEUFELD, E. L. 84, 270, 277  
NICHOLS, B. 67, 362  
NICOLET, M. 10, 278  
NIELSON, D. 105  
NORDBERG, W. 85  
NORTON, K. A. 25, 239, 242, 253  
  
OBAYASHI, T. 364  
OCHS, G. R. 9, 99, 143-148  
OLESEN, J. K. 370  
OMHOLT, A. 222  
ONWUMECHILI, C. A. 348  
ORTNER, J. 372  
OSBORNE, D. G. 348  
  
PAUL, A. 9, 323  
PENNDORF, R. 10, 361  
PETERSON, A. M. 10, 89-109, 182, 360, 377, 378  
PETTIT, H. B. 84, 356  
PFISTER, W. H. 83, 287, 378  
PHILLIPS, G. J. 45, 48, 206  
PHILLIPS, M. L. 182  
PICKAR, A. D. 83, 86  
PIGGOTT, W. R. 9, 6, 38, 170, 183, 366  
PINEO, V. C. 340  
POINCELOT, P. 10  
PRANDTL, 261  
PRATT, D. S. 10, 91  
PRENATT, R. E. 83  
PRESSMAN, J. 10  
PULLEY, O. O. 341  
  
RAO, M. S. 10  
RATCLIFFE, J. A. 10, 28-33, 41, 73, 376  
  
RAWER, K. 9, 10, 13, 15, 151-165, 203, 236, 292-343, 378, 379  
RENAU, J. 243  
RICE, S. O. 41, 46  
RICHARDSON, L. F. 261, 266  
RIKITAKE, T. 346  
ROACH, F. E. 125  
ROBERTSON, C. S. 361  
ROBINSON, B. J. 129  
RORDEN, L. 105  
ROUGERIE, P. 205  
RYBNER, J. 370  
RYDBECK, O. E. H. 13, 14, 236  
  
SAKURAZAWA, A. 245, 257  
SALMON, K. J. 222  
SASAKI, T. 10, 245  
SATYANARAYANA, R. 10  
SAWAJI, K. 245  
SAXTON, J. A. 249  
SCHLICHTING, H. 270  
SCOTT, W. E. 375  
SEDDON, J. C. 10, 78-88, 323, 357, 378  
SHAPLEY, A. H. 6, 166-177, 361, 377  
SHAW, J. 10, 366  
SHEARMAN, E. D. R. 10, 111, 117, 122  
SHIMAZAKI, T. 10  
SHINN, D. H. 73  
SILBERSTEIN, R. 91, 92  
SILSBEE, H. C. 346  
SILVERMAN, R. A. 19, 23  
SINGER, S. F. 344  
SKINNER, N. J. 10, 11, 37-50, 67, 134, 196, 204, 376, 377, 379, 380  
SMITH, E. K., JR. 3-12, 28, 38, 40, 74, 91, 95, 96, 99, 103, 111, 112, 113, 131-142, 143-148, 166-177, 178, 182, 218, 249, 260, 355, 361, 371, 376-380  
SPENCER, M. 45, 48, 70, 206  
SPRAGUE, G. 224, 229, 364  
STARAS, H. 19, 243  
STOREY, L. R. O. 277, 278, 355  
STROUD, W. G. 85  
SUCHY, K. 152, 157  
SUGAR, G. R. 70  
SUGIURA, M. 361  
SVENSON, A. C. 202, 204  
SWARM, H. M. 202, 204  
  
TAMAOKA, M. 10  
TANDBERG-HANSEN, E. 125  
TAO, K. 13-27, 235-257, 338, 378  
TAYLOR, G. I. 261, 263, 264, 266  
THEISSEN, E. 228  
THOMAS, J. A. 3, 10, 28, 99, 123-130, 178, 202, 204, 276, 290, 359, 361, 366, 377

- THOMAS, L. 366  
TITUS, P. 88  
TOWNSEND, A. A. 261, 262, 263, 264,  
266 267, 268, 269, 270  
TSCHU, K. K. 194  
  
UCHIKURA, K. 9  
UESUGI, Y. 133, 134  
ULWICK, J. C. 88  
UPTON, E. 274  
UYEDA, H. 292  
  
VAN SABBEN, D. 346, 360  
VEGARD, L. 361  
VELDKAMP, J. 346, 360  
VENKATESWARLU, P. 10  
VESTINE, E. H. 346, 364  
VILLARS, F. 19, 20, 21, 22, 262  
  
WAIT, J. R. 17  
WARREN, E. 6, 9, 366  
  
WATTS, J. N. 219  
WEEKES, K. 205  
WEISSKOPF, V. F. 19, 20, 21, 22, 262  
WELLS, H. W. 182  
WHEELON, A. D. 19, 21, 23, 249  
WHITE, R. W. 249  
WHITEHEAD, J. D. 9, 10, 84, 129, 170,  
210, 276-291, 355, 357, 359, 379  
WRIGHT, J. W. 11, 134, 172, 192  
WRIGHT, R. W. 10, 11, 37-50, 93,  
134, 196, 204, 379, 380  
  
YAMAOKA, M. 17, 245, 253  
YONEZAWA, T. 126  
YUKUTAKE, T. 346  
  
ZAGULYAEVA, V. A. 205  
ZENNECK, J. 314  
ZHEKULIN, L. 11  
ZMUDA, A. J. 352

## SUBJECT INDEX

- Absorption, 156, 163
  - absence of, 163
  - D*-region, 363
  - effect of frequency parameters, 156
  - night-time, 163
- AGARD Conference on Sporadic-*E* Ionization, 11
- Airglow, 130
  - cells, 126
  - correlation with, 129, 130
- Amplitude distribution
  - Ibadan, 47-49
  - theory, 46, 47
- Amplitudes, 203, 332, 348
- Anisotropic electrical conductivity, 207
- Ap*-index, 361, 364
- Aspect sensitivity, 67, 73
- Aurora,
  - and night-*E* layer, 221, 222
- Auroral echoes, 73
- Auroral  $E_s$ , 361
  - observed by backscatter, 91, 93-95
- Auroral particles, 261
- Auroral zone, 8, 28, 331, 346
- Auto-correlation function, 297, 298
- Azimuthal variation in backscatter, Puerto Rico, 117
  
- Backscatter sounding, 89-109, 110-122
  - auroral  $E_s$ , 93-95
  - azimuthal extent of patches, 93
  - definition of echoes, 90, 91
  - direct backscattering, 92
  - equatorial  $E_s$ , 95-99
  - fixed frequency, swept azimuth, 89-109
  - ground backscattering, 92
  - identification of echoes, 90, 91
  - maximum range, 92
  - minimum range, 92
  - multi-channel, 110-122
  - Puerto Rico, 110-122
    - azimuthal variation, 112-116
    - motion of patches, 117-122
    - preferred direction, 117-122
    - seasonal variation, 112-116
  - sweep frequency, 89, 90
  - with high angular resolution, 129
- Bandwidth of fading, 61
- Bay disturbance, 361, 368
- Bay-shaped variation, 346
- Bifurcation of  $E_s$ -*q* layer, 62
- Blackout, 364, 366
  - gradual, 364, 368, 369
  - sudden, 364
- Blanketing,
  - during bay disturbances, 364, 369
- Blanketing  $E_s$ , 57, 218
  - equatorial, 37-50, 373
    - amplitude distribution, 47-49
    - drift velocity, 48, 49
    - fading characteristics, 48, 49
    - height, 38
    - reflection characteristics, 38, 48, 49
    - scale size, 49
  - exclusion zone, 57, 218
- Blanketing frequency, 152-165, 315-318
  - at Djibouti, 321
  - at Freiburg, 319, 320
  - seasonal behavior, 318
- Blanketing power, 329-332
- Bremsstrahlung X-rays, 364, 368
- Brisbane, 123-130, 195-205
  
- Cambridge, 205
- Camden, backscatter, 100-104
- Canberra, 203, 205
- Capetown,
  - median  $f_oE_s$ , 308
- Causes of  $E_s$ , 31, 32
  - changes in production rates, 31
  - redistribution of electrons, 31
- Charge transfer processes, 341
- Classification, 380
- Clouds with continuous gradations, 337
- Colatitude, 208
- Collisions with excited molecules, 341
- Conductivity, 351, 353
  - Cowling, 208, 209, 352, 353
  - Hall, 210, 353
  - Pedersen, 210, 353
- Corpuscular radiation, 340
- Correlation, 129
  - field strength and  $f_oE_s$ , 253
  - of signals, 70

- Correlation distance, 72
  - methods, 296
  - number, 297
  - range, 301
- Correlation with electrojet, 52, 55-57, 59-60, 350-352
  - zone, 57
- Cowling conductivity, 208, 209, 352, 353
- Critical frequency, 152, 154, 195
  - of equatorial sporadic  $E$ , 76, 349
- Cross-correlation function, 298-301
- $c$ -type, 136, 137, 156
  - virtual height, 180
- Current systems, 207, 345
  
- Dakar,
  - median values  $\overline{fE_s}$ , 310
  - sharpness of echoes, 324
- Decrease in  $H$ -component, 123
- Differential refraction, 80
- Diffraction pattern on the ground,
  - at low latitudes, 44-46, 48
- Diffusion,
  - coefficient, 283
  - effect on peak electron density, 286
- Dimensions of  $E_s$  patches, 30, 139, 140
  - clouds within patches, 30
- Dip equator, 313, 348
- Direct backscatter, 92
- Direction of arrival, 326
- Direction of motion
  - in Puerto Rico, 117-122
- Distance dependence,
  - $E_s$  propagation, 245-253
- Disturbance daily variation, 346, 364
- Diurnal effects (equatorial), 58-59
- Diurnal variations,
  - of backscatter echoes, 116
- Djibouti,
  - median values,  $\overline{fE_s}$ , 311
  - median values,  $f_b E_s$ , 321
  - sharpness of echoes, 325
- Doppler fading, 378
- Doppler shift, 67
- Drift motions,
  - vertical, 194, 209, 210, 351
- Drift speed, 360
- Drifting  $E_s$ , 107, 108
  - direction of motion, 107
- Dynamo effect, 344, 345
- Dynamo theory, 207
  
- Electrojet (*see* Equatorial electrojet)
- Electron density, 72
  - irregularities, 51
- Electron distributions, 30, 31
  - horizontally irregular, 30
  - horizontally stratified, 30, 31
  - steep gradients, 30, 31
  - thin layers, 31
- Energy balance, 338
- Enhanced ionization, 260
- Epstein Layer, 15
- Equatorial  $E$  layer, 75
- Equatorial electrojet, 52, 208, 215, 345, 348, 350, 351, 353, 379
  - caused by high value of Cowling conductivity, 348
  - intensity, 352
  - seasonal variation, 348
  - solar-cycle variation, 348
  - width, 352
  - zone, 352
- Equatorial ionosphere, 52
- Equatorial  $q$ -type  $E_s$  (*see*  $q$ -type)
- Equatorial scatter, 96
- Equatorial slant sporadic  $E$ , 52, 73-75
  - configuration, 73
  - description, 73
  - explanation, 74, 75
- Equatorial sporadic  $E$  (*see also specific types*), 51, 195, 215, 331, 346-355
  - and solar equatorial electrojet, 346-355
  - association with electrojet, 52-60
  - configuration, 76
  - frequency dependence, 64-67
  - frequency spectrum, 67
  - model, 72
  - nature of, 62-73
  - observed by backscattering, 91, 93-96
  - polarization studies, 64
  - radar echoes at 50 Mc/s, 60, 61
  - similarity with auroral echoes, 73
  - spaced antenna studies, 70-73
- Equatorial sporadic- $E$  layer, 75
  - bifurcation of, 62
- Equatorial studies, 51-77
  - correlation with electrojet, 52, 55-57, 59, 60
  - equatorial slant sporadic  $E$  ( $E_s$ - $s$ ), 73-75, 355
  - equatorial sporadic  $E$  ( $E_s$ - $q$ ), 51-77
- Equatorial zone, 8, 28, 376, 378, 379
- $E_s$ - $q$  (*see*  $q$ -type)
- $E_s$ - $s$  (*see* Equatorial slant sporadic  $E$ )
- $E2_s$ , 202
- Excitation mechanism, 72
  
- Earth's surface characteristics,
  - backscattering of  $E_s$ , 103-107

- Fading, 29
  - at three close-spaced receivers, 29
- Fading characteristics
  - of blanketing  $E_s$  at Ibadan, 47-49
  - of  $q$ -type  $E_s$  at Ibadan, 40-44
- Fading rate, 61, 138, 139
  - at vertical incidence, 138, 139
  - at v.h.f., 138, 139
- Fairbanks (College), 368, 369
  - correlation with sunspot number, 186, 187
  - diurnal variation, 189
  - seasonal variation, 191
  - yearly variation, 188
- Far East anomaly, 101
- Field-aligned clouds, 344, 372
- Field-aligned columns, 123
- Field-aligned echoes, 74, 129
- Field-aligned ionization, 129
- Field-aligned irregularities, 95, 96
- Fixed-frequency sounders, 89
- Flare current system, 346, 360
- Fluctuation range, 301
- Flux Richardson number, 266
- Formation of  $E_s$ , 288
  - from vertical gradient in horizontal wind, 276
- Forward-scatter signals, 55
- $F$ -region irregularities
  - correlated with  $E_s$ , 123-126
- $F$ -region storms,
  - and night- $E$ , 228
- $F$ -region travelling disturbances,
  - relation to  $E_s$ , 290
- Freiburg, 203, 205
  - median values  $f_b E_s$ , 319, 320
  - median values  $f E_s$ , 309
  - sharpness of echo, 324
- Frequency dependence of  $E_s$ - $q$  intensity, 64
- Frequency parameters, 151-165
  - blanketing frequency, 152-165
  - critical frequency, 152-165
  - effect of gyrofrequency, 158
  - o- and  $\alpha$ -components, 156
  - top frequency, 152-165
- Frequency spectrum of  $E_s$ - $q$  echoes, 67
- Frequency variation of transparency, 153
- $f$ -type, 136-138
  - virtual height, 179
- Geographical variations, 3-6, 166-177
  - equatorial belt, 5
  - maximum in Far East, 3, 5, 170
  - minimum in South Africa, 5, 170
  - principal zones, 8
  - Siberian minimum, 170
- Geomagnetic bay, 346
- Geomagnetic micropulsations, 363
- Geomagnetic midnight, 361, 366
- Geomagnetic storms, 361-371
- Geometry of reflecting area, 148
- Gradients, 82
  - deduced from rocket measurements, 79, 85, 86
- Gradual blackout, 364, 368, 369
- Ground backscatter, 92
- Gyrofrequency (or gyromagnetic frequency), 80, 86, 364
- Hall conductivity, 210, 353
- Hallett Station,
  - occurrence of night- $E$ , 220
- Harmonic dial, 195-200
- Height of irregularities (equatorial), 59
- Height of occurrence,
  - blanketing  $E_s$  at Ibadan, 38
- Height preference, 79-83
- Horizontal drift, 67, 373
- $h$ -type, 136, 137, 156
- Huancayo, 179, 195-199, 204, 209
  - correlation with sunspot number, 186, 187
  - diurnal variation, 190
  - seasonal variation, 190
  - temporal variations, 7
  - virtual heights, 179
  - yearly variation, 188
- Hydrodynamic stability, 264
- Hydromagnetic waves, 72, 372
- Ibadan, 37-50, 196, 200-204, 209
- Incoming auroral particles, 379
- Inhomogeneities, 87
  - (see also Irregularities)
- International Geophysical Year (IGY), 51, 201, 348, 349
- Ionization profile,
  - of night- $E$  layer, 226
- Ionosondes, 130, 195, 196
  - close spaced, 130
- Ionosonde sensitivity, 64
- Ionospheric currents, 344-373
- Ionospheric scattering, 51
- Ions,
  - vertical velocity, 278
- Irregularities,
  - instability of, 98
- Kokubunji, 195-199, 204

- Latitude distribution
  - by types, 176
- Latitudinal effects (equatorial), 58, 59
- Layer structure, 336
  - "holes", 336
- Least time focussing, 96
- Log-periodic antenna, 64
  - structures, 74
- Longitude variations, 170
- Longitudinal plasma waves, 72
- l*-type, 136, 137
  - virtual height, 179
- Lunar dynamo current, 210
- Lunar effect, 194, 315
- Lunar electrojet (*see* Lunar equatorial electrojet)
- Lunar equatorial electrojet, 212, 348
- Lunar geomagnetic current system, 194, 207
- Lunar tidal variations, 194-213
- Lunar tidal winds, 194, 203, 206-213
- Lunar tide, 378
- Lunar time, 194, 196, 201
- Lwiro,
  - sharpness of echoes, 325
- Lyman- $\alpha$  radiation,
  - scattered to night side, 230
- Magnetic activity,
  - and night-*E* layer, 223-226
  - correlation with, 28
- Magnetic correlation, 126-129
- Magnetic equator, 51, 345, 348
- Magnetic equatorial zone, 194, 196
- Magnetic field, 60, 195
  - affected by  $E_s$ , 290
  - height correlation with  $E_s$ , 84
- Magnetic field strength, 60
- Magnetograms, 59
- Magneto-ionic components, 80, 86, 87
  - distinction of, 156-165, 331
  - effect of gyrofrequency, 158
- Magnetometer, 84
- Magnetospheric motions, 368
- Maximum plasma density, 378
- Maximum plasma frequency, 305
- Mayaguez, (*see* Puerto Rico)
- Mechanisms for  $E_s$  reflections, 235-257
  - scattering model, 239-245
    - scattering cross-section, 242-244
    - generalized, 244
  - thin-layer model, 235-239
    - reflection coefficient, 237-239
- M*-echo, 323
- Meteor trails, 83
- Meteoric  $E_s$ -layer, 32
- Meteorological phenomenon, 343
- Meteors, 261, 340
- Micropulsations, 363
- Minimum plasma frequency, 305
- Minimum virtual height, 318
- Mixing-length theory, 266
- Models of layer structure, 336
  - clouds with continuous gradations, 337
  - layers with holes, 336
  - thin homogeneous layers, 336
- Monthly median results,
  - significance, 305
- Motion of patches, 139, 140
  - in Puerto Rico, 117-122
    - preferred directions, 117-122
- Movements, 377
- Movements of  $E_s$  echoes, 30
  - close-spaced receiver measurements, 30
- Multi-channel backscattering (*see* Back-scattering)
- Narsarssuak,
  - temporal variations, 7
- Nature of  $E_q S$ , 99
- Negative bay, 361, 366
- New ionization, 380
- Nha-trang,
  - median values,  $\overline{fE_s}$ , 312
- Night-*E*, 361, 377
- Night-*E* layer, 219-231
  - and *F*-region storms, 228
  - and travelling disturbances, 229
  - geographical occurrences of, 219-221
  - ionization profile, 226-229
  - occurrence at Hallett, 220
  - relation with aurora, 221-223
  - relation with magnetic activity, 223-226
- Night-time sporadic *E*, 129
- N*1 layer,
  - identified with night-*E*, 220
- North-south correlation distance, 73
- $N_2^+$  ions,
  - and night-*E* layer, 222
- Oblique scatter, 51
- Oblique scatter propagation, 76
- Origin of ionization, 338-342
  - charge transfer processes, 341
  - collisions with excited molecules, 341.
  - extraterrestrial radiation, 340
  - meteors, 340
  - rearrangement of existing ionization 341
  - shock waves, 341

- Ottawa, 203, 205
- Panama Canal, 201
- Partial correlation, 342
- Partial reflection, 323
- Patches, 380
  - azimuthal extent, 93
  - growth and decay, 130
  - motion, 117-122, 139, 140
  - shape and size, 129, 139, 140
- PCA blackouts, 370
- PCA event, 368
- Pederson conductivity, 210, 353
- Persistence of layer, 289
- Phase of  $E_s$  echo, 29
- Phase path measurement, 129
- Pitot-static measurements, 84
- Plane wave fronts, 72, 76
- Plasma frequency, 79, 86
- Plasma waves, 72
- Polar blackout (*see also* Blackouts), 370
- Polar elementary storm, 346
- Polarization of radar echoes, 64
- Positive bay, 361, 362
- Probable error circles, 195, 199
- Pulse broadening, 143-148
  - measurements at v.h.f., 143-148
  - theory of reflecting region, 147
    - geometry, 147
- TV-DX, 148
- Pulse measurements, 59
- Quartiles, 304
- Quiet day solar current system, 208, 344, 364
  - and temperate latitude  $E_s$ , 355-361
- $q$ -type, 37-49, 51, 215-218, 298 352, 377, 379, 380
  - amplitude distribution, 47, 48
  - critical frequency, 52
  - electrojet dependence, 37
  - fading characteristics, 40-46
  - irregularities
    - characteristics of, 62
    - dimensions and shape, 62
    - field alignment of, 62
    - magnetic-field-aligned, 62
    - radar echoes at 50 Mc/s, 62
  - reflection coefficient, 38-40
  - scale size, 40, 45
  - virtual height, 179
  - zone width, 217, 376
- Radio black-out (*see also* Blackout), 78
- Range of transparency, 333
- Rearrangement of ionization, 341, 380
- Recombination time in  $E$ -layer, 31
  - at night, 230
- Reflection coefficient, 28, 29, 37-50, 154, 323
  - Ibadan measurements, 37-50
    - blanketing  $E_s$ , 47-49
    - $q$ -type  $E_s$ , 38-48
  - thin layer theory, 13-19, 237-239
- Reflection function, 331-336
- Retardation, 323
  - in the normal  $E$ -layer, 156
- Retardation cusp, 151
- Retardation  $E_s$ , 361
- Reynolds number, 263
- Richardson number, 261
- Ring current, 367
- Rocket measurements, 78-88, 353
  - comparison with ionograms, 86
  - comparison with pulse techniques, 86
  - gradients observed, 79, 85
  - height preference, 83-85
  - uniformity of layer, 79-83
- Scale size of irregularities,
  - of blanketing  $E_s$  at Ibadan, 47-49
  - of  $q$ -type  $E_s$  at Ibadan, 40, 45
- Scatter theory, 19-26
  - (*see also* Scattering model)
- Scattering cross-section, 242-244
  - generalized for anisotropic case, 244
- Scattering layer, 338
  - thickness, 59
- Scattering mechanism, 378
- Scattering model, 19-26, 239-245
  - auto-correlation approach, 19-20
  - turbulent energy approach, 19-21
  - turbulent mixing approach, 21-26
- Scintillation of radio stars, 29
- Seasonal effect,
  - in top frequency, 306
- Seasonal effects (equatorial), 59, 348
- Seasonal variation of backscatter echoes, 102, 112-122
- Secular variation, 314
- Sensitivity of the ionosonde, 154
- Sequential  $E_s$ , 359, 360, 378
- Sharpness of echoes,
  - as classification criterion, 323
  - distributions according to, 324, 325
- Shock waves, 341
- SID effects (equatorial), 59
- Slant  $E_s$  (*see also* Equatorial slant  $E_s$ ), 96, 355, 361, 370-373
- Radar echoes, 64

- Slough, 196-199, 203-205  
 Sodium clouds, 84  
 Solar cycle,  
     variation of electrojet with, 348  
 Solar cycle correlation, 28  
 Solar daily geomagnetic variations, 345  
 Solar equatorial electrojet, 211, 352  
 Solar flares, 345  
 Solar wind, 370  
 Spaced antennas, 70  
 Spaced receiver experiments,  
     Ibadan, 44, 45, 48  
 Spectrum analysis, 67  
 Spherical function, 208  
 Spiral distributions, 6  
 Spiral occurrence of  $E_s$ , 366  
 Spread  $E_s$  echoes, 124  
 Spread  $F$ , 83  
 $Sq$  current, 208, 210, 358  
 Stanford, 202, 204  
     backscatter measurements, 102-108  
 Statistical behavior,  
     significance, 292-343  
 Steep-gradients, 378  
 Stratification, 259  
 Structure of irregularities, 72  
 Sudden blackout, 364, 368  
 Sudden commencement, 346, 371, 373  
 Summer preference, 306  
 Sunspot correlation, 182-193, 377  
     at Fairbanks (College), 182-193  
     at Huancayo, 182-193, 349  
     at Washington, 182-193  
     hourly, 187  
     monthly, 186  
     of  $f_b E_s$ , 322  
     of  $f E_s$ , 314, 315  
 Sunspot-cycle variation, 171  
 Sweep-frequency backscattering, 89, 90  
 Swept-azimuth backscattering, 89-109
- Temporal variations, 6-8  
     diurnal, 7, 8  
     Huancayo, 7  
     Narsarssuak, 7  
     seasonal, 7, 8  
     sunspot cycle, 8  
     Watheroo, 7  
     White Sands, 7  
 Terrestrial explanation, 379  
 Thickness, 323, 378  
     determined by partial reflections, 323  
     of scattering layer, 59  
     use of  $M$ -echo, 323  
 Thick layer, 379  
 Thin layer, 378  
 Thin layer model, 13-19, 235-239  
     reflection coefficients obtained by:  
         Friis, Crawford and Hogg, 17  
         Millington, 15, 16  
         Rawer, 15  
         Rydbeck, 13, 14  
         Tao, 17-19  
 Thunderstorm theory, 341  
 Tilts in layers,  
     effect on frequency parameters, 163  
 Top frequency, 152-165, 306-315  
 Total occurrence of  $E_s$ , 166-171  
     geographical variations, 166-171  
 Townsend's criterion, 266  
 Transient layer, 259  
 Transparency, 326-336, 380  
     classification by, 326  
     examples, 328, 329  
 Trapping, 341  
 Travelling disturbances,  
     and night- $E$ , 229  
 True height, 318  
 Turbulence, 85  
 Turbulence criterion, 262-270  
 Turbulent scattering, 55, 262  
 TV-DX, 148  
 Types of  $E_s$ , 28, 344  
     classification by World-Wide Sound-  
         ing Committee, 28, 172  
     illustrated by ionograms, 173-175  
     latitude distribution of, 176
- Uniformity of layer,  
     deduced from rocket measurements,  
         79-83  
 URSI World-Wide Sounding Com-  
     mittee, 178
- Valley between  $E$  and  $F$ , 227  
 Van Allen belt, 372  
 Velocity of flow, 61  
 Vertical drift, 209, 357  
 Vertical drift forces, 98  
 Vertical ionization redistribution, 123  
 Vertical movements, 378  
 Vertical-to-oblique relationship, 132-  
     136  
     by  $E_s$  type, 134-136  
 Vertical velocity of ions, 278  
 v.h.f. measurements, 131-139  
     dimension of patch, 139, 140  
     reflection characteristics by type,  
         136-138  
     vertical to oblique comparison, 132-  
         139  
 Virtual height, 178-181  
      $c$ -type, 180



- f*-type, 179
- l*-type, 179
- q*-type, 179
- Washington, D.C., 186-190, 196-199,  
204, 206
  - correlation with sunspot number, 186,  
187
  - diurnal variation, 190
  - seasonal variation, 191
  - yearly variation, 188
- Watheroo,
  - temporal variations, 7
- Wave radiation, 340
- White Sands
  - temporal variation, 7
- Wind shear, 83, 84, 85, 210, 258-262,  
343, 355, 356, 360, 373, 379,  
380
  - as cause of sporadic *E*, 276-291
- X-rays, 366, 368
- Z-mode, 80
- Zones of *E<sub>s</sub>*, 8, 28
  - auroral, 8, 28, 331, 361
  - equatorial, 8, 28, 352, 376, 378, 379
  - middle latitude, 28
  - temperate, 8, 355-361
- Zürich sunspot number, 349